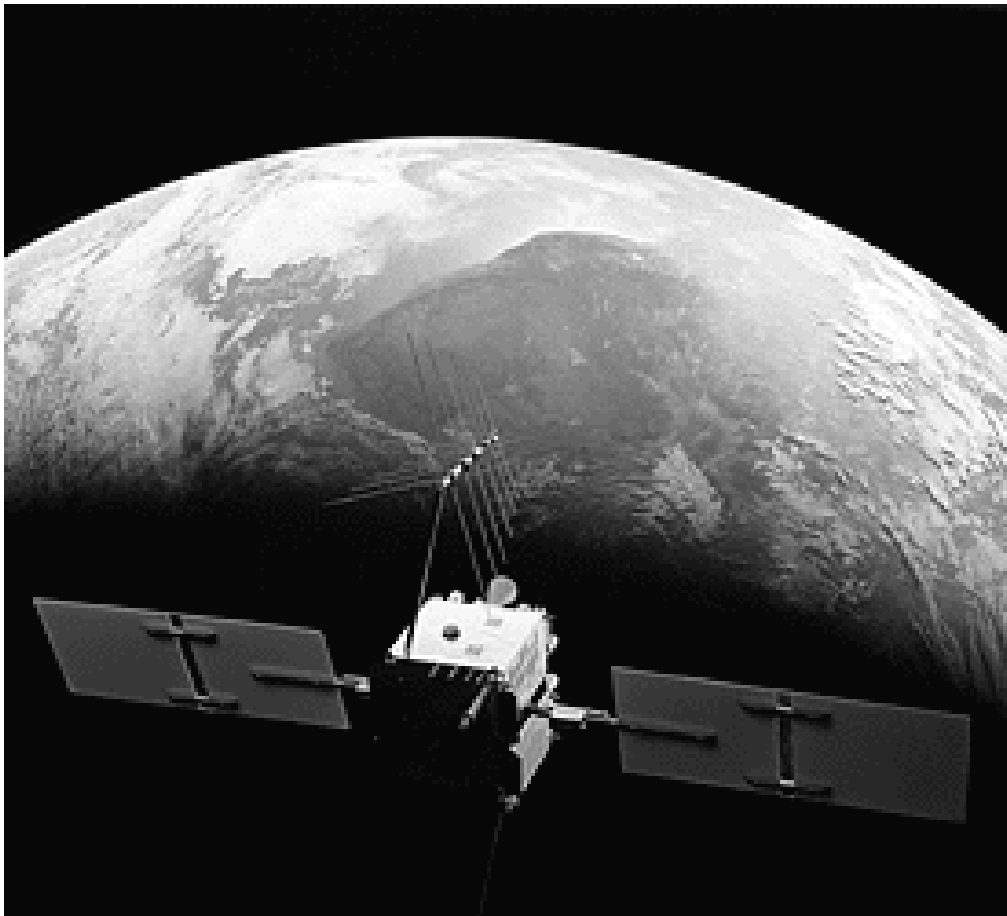


# Modeling and Extrapolation of Path Delays in GPS Signals



By

Philippe M. Herschke



GEODESY AND GEODYNAMICS LAB

# MODELING AND EXTRAPOLATION OF PATH DELAYS IN GPS SIGNALS

by

**Philippe M. Herschke**

March 2002

Master thesis submitted for the degree of Dipl. Phys. ETH at the Swiss Federal Institute of Technology, Zürich, Switzerland (ETHZ)

This work was supervised by Professors A.O. Benz and H.-G. Kahle

Department of Physics  
Swiss Federal Institute of Technology  
ETH Hoenggerberg  
CH-8093 Zurich  
Switzerland



## **EXECUTIVE SUMMARY**

### **Problem statement**

The United States Department of Defense's NAVSTAR (Navigation by Timing And Ranging) GPS (Global Positioning System) is nowadays the most widely used satellite system for navigation purposes. Already in the early stages of its development it has been recognized that its potential applications were enormous. Insufficient knowledge on the atmosphere above the receiver has always been one of the main limitations to the accuracy of the GPS system. The present study focuses on modeling the atmospheric effects on the GPS signal and eventually applying it to path delay forecasting. It is intended to evaluate the prediction feasibility and to determine the maximum extrapolation time for a given precision to achieve, thus answering the question: for a given error threshold how long can one predict a path delay at an arbitrary location without information at this site?

### **Work carried out**

First, a detailed description of the American Global Positioning System is covered. GPS is built around three segments. The space segment is a constellation of 21 operational and 3 spare satellites that emit on two frequencies,  $L_1 = 1575.42$  MHz and  $L_2 = 1227.60$  MHz. The United States armed forces manage the space vehicles and the ground control segment. The user segment gathers all receivers, both military and civilian. Intentional degradation of the GPS accuracy by the U.S. Department of Defense does influence the computation of path delays from the signal. By differential measurements, these effects can be mitigated. The errors induced by the outer layer of the atmosphere, the ionosphere can be removed to a great extent by linearly combining the GPS observables derived from both carrier phase measurements. Only the troposphere, spanning from the mean sea level to approximately 35 kilometers and where almost 90% of the atmospheric water vapor is concentrated, remains a major source of error.

Secondly an overview of the least-squares collocation technique also known as Kriging algorithm is presented. It is an efficient method for analyzing path delay computation problems. It has been first developed by geophysicists to interpolate and extrapolate data while minimizing possible errors. The mathematical and statistical methods deployed to study the refractivity field in the lower atmosphere, and thus the tropospheric path delay, are thoroughly treated. By opposition to the classical least-squares technique, signal and noise components are clearly separated and are assumed to be uncorrelated. The eventual knowledge of the physical processes taking place in the system to study is summarized in a functional model. To enable efficient data processing, this functional model is linearized.

In a third part a functional model for this Zenith Path Delays is conceived. Fermat's principle allows connecting the refractive index of a given atmospheric layer to the signal path. In atmospheric sciences, the refractivity is generally used instead of the refractive index. The different formulations for the refractivity field are taken into account. The Essen and Froome formula provides the relation between the refractivity and the three atmospheric fields, namely the atmospheric pressure  $p$ , the partial water vapor pressure  $e$  or its related relative humidity and the temperature  $T$ .

Spatial and temporal models for the three meteorological fields are derived which are then inserted in the Essen and Froome formula. This expression is then integrated along the GPS signal path and mapped to zenith at the GPS receiver's location, thus yielding to a compact Zenith Path Delay formula that depends on the reference pressure  $p_{ref}$ , the reference humidity  $e_{ref}$ , the reference temperature  $T_{ref}$ , the temperature at tropopause  $T_1$ , the tropospheric temperature gradient or lapse rate  $\gamma$ , the GPS receiver's altitude  $z_0$ , the tropopause height  $z_1$ , the upper limit of integration  $z'$ , the pressure scale height  $H_p$  and the humidity scale height  $H_e$ .

The last part concentrates on testing and validating the Zenith Path Delay (ZPD) model developed previously. The least-squares collocation technique requires the calculation of a design matrix  $A$ , which entries are all partial derivatives of the functional model with respect to each model parameter. The ZPD can be split into a Zenith Dry Delay (ZDD) and a Zenith Wet Delay (ZWD). Hence the ZPD partial derivative with respect to one parameter is the sum of the partial derivatives of the ZDD and ZWD with respect to the same parameter.

These ZPD partial derivatives are computed and then tested on the default parameter values. Both show very different patterns as one varies the GPS receiver's altitude  $z_0$ .  $\partial ZPD/\partial T_1$ ,  $\partial ZPD/\partial z_1$  and  $\partial ZPD/\partial z'$  do not depend on  $z_0$ . It is thus expected that they would introduce rank deficiencies in the design matrix, hindering the inversion of the normal matrix  $N$ . Constrains on seven parameters of the ZPD model have been applied in order to make possible the pseudo-inversion of the design matrix  $A$ .

The ZPD model is then implemented in the software package COMEDIE: Collocation of Meteorological Data for Interpolation and Estimation of Tropospheric Path Delays developed at the Geodesy and Geodynamics Lab at the Swiss Federal Institute of Technology at Zurich.

Further the ZPD model is validated on a regional campaign in Switzerland starting on Monday 22 May 2000 at 00:00:00 UTC and ending on Tuesday 30 May 2000 at 00:00:00 UTC. GPS data delivered by the Swiss Federal Office of Topography for this observation window and for eleven AGNES GPS permanent stations at Andermatt, Davos, EPF Lausanne, ETH Zurich, FHBB Muttenz, Jungfrauoch, Locarno-Monti, Neuchatel, Payerne, Pfänder and Zimmerwald has been used.

The differences between the COMEDIE ZPD estimates and the AGNES ZPD observations are evaluated when possible. Good agreements between estimates and observations are noted at all stations except Jungfrauoch and Locarno-Monti. This is probably due to the lack of data from stations at similar high altitudes for the former and due to its location South of the Swiss Alps for the latter. The Alps mountains represent a climatic barrier stopping wet and cold air masses arriving from a North-western direction. Hence Locarno-Monti has a very different climate than the rest of the AGNES stations surveyed. Further there appears to be no correlation between average, standard deviation and RMS of the ZPD differences with the altitude of the GPS receiver.

ZPD forecasts are performed at all eleven AGNES stations at disposals. The extrapolation starts on Saturday 27 May 2000 at 00:00:00 UTC and ends on Tuesday 30 May 2000 at 00:00:00 UTC. In the first 12 hours of the extrapolation time window some damped oscillations of the ZPD forecast are observed. Afterwards, the ZPD estimates seem to gradually stabilize around the ZPD value given by the functional model.

## **Conclusions**

COMEDIE forecast-AGNES observation ZPD differences are computed and their average, standard deviation and RMS are evaluated. For half of the AGNES stations surveyed it is possible to yield to a meaningful forecast during 9 hours after the last data were available. Both the standard deviation and RMS of the ZPD differences are less than 1 centimeter during the first 12 hours of the forecast. This implies that one can conduct a satisfactory prediction of the Zenith Path Delay twelve hours in advance! The ZPD extrapolation error evolves at an approximate velocity of half a millimeter per hour.

Navigation, i.e. the determination of one's position as function of time is the primary purpose of the NAVSTAR Global Positioning System. The 1-cm error in ZPD estimate implies nearly as much as 2.50 cm vertical error in the user's position. One cannot evaluate the horizontal position error due to the ZPD error with a single ZPD measurement at one's location. Multiple observations at different sites are required.



## **ACKNOWLEDGEMENTS**

The author would like to acknowledge the contribution of different scientists, without whom this project would have not been possible: Dr. Alain Geiger from the Geodesy and Geodynamics Laboratory (GGL), Institute of Geodesy and Photogrammetry at the Swiss Federal Institute of Technology (ETH) at Zurich, Switzerland coached the work of the author while challenging him along the development of the Zenith Path Delay model. His critical approach enhanced greatly the quality of this project.

Dr. Marc Cocard from the same laboratory instructed the author on the latest programming technique and jointly implemented the necessary routines in the COMEDIE software package. He stimulated the author for a continuous improvement of the functional model and supplied the author with judicious suggestions.

Mr. Marc Troller, also from the Geodesy and Geodynamics Laboratory, Institute of Geodesy and Photogrammetry at the Swiss Federal Institute of Technology at Zurich, Switzerland and currently performing his Ph.D. thesis on COMEDIE provided the author with numerous insights in the mystery of C and PERL programming while enlightening him on the beauty of COMEDIE.

Prof. Dr. A.O. Benz from the Institute of Astronomy in the Physics Department at Swiss Federal Institute of Technology at Zurich, Switzerland supervised this study along Prof. Dr. H.-G. Kahle, Head of the Geodesy and Geodynamics Laboratory, Institute of Geodesy and Photogrammetry at ETH Zurich. Prof. Dr. A.O. Benz constantly pushed the author gaining a better understanding of atmospheric modelling and mentored him on many critical issues. He should be warmly thanked for this. Prof. Dr. H.-G. Kahle made the fruitful completion of this study possible by allowing the author to enter the GPS scene inside GGL.

Many other persons deserved credit and thanks. Dr. Jérôme Verdun completely reviewed and commented parts of the M.Sc. thesis. Prof. Dr. Emile Klingelé always asked the author about the evolution of the study and showed great interest in the results. Thank you for your support.

To all those who might be forgotten, please accept my full apologizes.

Zurich, March 2002

P.M. Herschke

**Blank page**

# Contents

<b>EXECUTIVE SUMMARY .....</b>	<b>i</b>
<b>ACKNOWLEDGEMENTS .....</b>	<b>iii</b>
<b>CONTENTS .....</b>	<b>v</b>
<b>GLOSSARY .....</b>	<b>ix</b>
<b>LIST OF FIGURES.....</b>	<b>xiii</b>
<b>LIST OF TABLES.....</b>	<b>xvii</b>
<b>1. PATH DELAYS IN GPS SIGNAL .....</b>	<b>1</b>
1.1 NAVSTAR GPS .....	1
1.1.1 History .....	1
1.1.2 Segments and functionalities .....	1
1.1.2.1 Space segment .....	1
1.1.2.2 Ground Control Segment .....	3
1.1.2.3 User segment .....	3
1.1.3 GPS signal .....	3
1.1.3.1 Reference Systems .....	3
1.1.3.2 Ephemeris and calendar .....	3
1.1.3.3 Signal components.....	3
1.1.3.3.1 Frequency standards.....	4
1.1.3.3.2 Codes .....	4
1.1.3.3.3 Navigation message .....	5
1.1.4 Accuracy denial .....	5
1.1.4.1 Selective Availability.....	5
1.1.4.2 Anti-Spoofing .....	6
1.1.5 $L_1$ and $L_2$ frequency modeling.....	6
1.2 GPS OBSERVABLES .....	7
1.2.1 Code Pseudoranges .....	7
1.2.2 Phase Pseudoranges .....	8
1.2.3 Biases and error modelization .....	9
1.3 SINGLE AND DOUBLE DIFFERENCES .....	10
1.3.1 Ionospheric refraction.....	10
1.3.1.1 Modified Rayleigh Equation.....	10
1.3.1.2 Ionospheric path delay.....	12
1.3.2 Clock Errors.....	15
1.3.3 Single difference.....	15
1.3.4 Double difference .....	16
1.4 LINEAR COMBINATIONS.....	17
1.4.1 Ionosphere free LC $L_3$ .....	17
1.4.2 Geometry free LC $L_4$ .....	19
1.4.3 Wide lane LC $L_5$ .....	19
1.4.4 Melbourne-Wübbena LC $L_6$ .....	20
1.5 AMBIGUITY RESOLUTION .....	20
1.5.1 Combination of phase and code PRs .....	20
1.5.2 SEARCH algorithm.....	22
1.5.3 FARA algorithm.....	22
1.6 SUMMARY AND CONCLUSIONS .....	23
<b>2. LEAST-SQUARES COLLOCATION, PREDICTION AND EXTRAPOLATION.....</b>	<b>25</b>
2.1 MOTIVATION.....	25
2.2 COLLOCATION FUNDAMENTAL EQUATION – STOCHASTIC MODELING.....	27
2.3 INTERPOLATION VS. EXTRAPOLATION .....	30

2.4	COLLOCATION ACCURACY .....	31
2.4.1	Conventions .....	31
2.4.2	Collocation covariance matrix $C_{ll}$ .....	31
2.4.3	Unknown parameters error covariance matrix $Q_{xx}$ .....	32
2.4.4	Signal error covariance matrix $Q_{ss}$ .....	32
2.4.5	Prediction error covariance matrix $Q_{l'l'}$ .....	34
2.4.6	Accuracy summary .....	36
2.5	THE COVARIANCE FUNCTION $\Phi$ .....	36
2.6	SUMMARY AND CONCLUSIONS .....	37
<b>3.</b>	<b>PATH DELAYS AND ATMOSPHERE MODELING .....</b>	<b>39</b>
3.1.	MOTIVATION .....	39
3.2.	CLASSICAL MODELS .....	39
3.2.1.	Path delay and tropospheric delay .....	39
3.2.2.	Refractivity modeling .....	40
3.2.2.1.	Essen and Froome formula .....	40
3.2.2.2.	Smith and Weintraub formula .....	41
3.2.2.3.	Thayer model .....	43
3.2.3.	Hopfield model .....	44
3.2.3.1.	Normal Hopfield model .....	44
3.2.3.2.	Enhanced Hopfield model .....	44
3.2.3.3.	Modified Hopfield model .....	45
3.2.4.	Saastamoinen model .....	46
3.2.5.	Mapping function .....	48
3.2.5.1.	Marini mapping functions .....	48
3.2.5.2.	Herring mapping function .....	48
3.2.5.3.	Niell mapping function .....	49
3.3.	ATMOSPHERE MODELING .....	51
3.3.1.	Temperature field .....	51
3.3.1.1.	General description .....	51
3.3.1.2.	Temperature model .....	52
3.3.1.2.1.	Temperature profile .....	52
3.3.1.2.2.	Hydrostatic air gradient .....	52
3.3.1.2.3.	True temperature gradient .....	54
3.3.1.2.4.	Adopted temperature model .....	55
3.3.2.	Pressure model .....	55
3.3.3.	Atmospheric humidity model .....	58
3.3.3.1.	Clausius-Clapeyron equation .....	58
3.3.3.2.	Temperature dependence of the enthalpy of vaporization .....	59
3.3.3.3.	Temperature dependence of the saturation vapor pressure .....	60
3.3.3.4.	Water vapor pressure model .....	61
3.3.4.	Summary .....	62
3.4.	PATH DELAYS MODELING .....	63
3.4.1.	Motivation .....	63
3.4.2.	Mathematical background .....	66
3.4.3.	Integration .....	66
3.4.4.	Integration of $I_1$ .....	67
3.4.4.1.	Computation of $I_{11}$ .....	67
3.4.4.2.	Computation of $I_{12}$ .....	68
3.4.4.3.	Computation of $I_{13}$ .....	69
3.4.4.4.	Summary of $I_1$ .....	70
3.4.5.	Integration of $I_2$ .....	70
3.4.5.1.	Computation of $I_{21}$ .....	70
3.4.5.2.	Computation of $I_{22}$ .....	71
3.4.5.3.	Computation of $I_{23}$ .....	71
3.4.5.4.	Summary of $I_2$ .....	71
3.4.6.	Integration of $I_3$ .....	72
3.4.6.1.	Computation of $I_{31}$ .....	72
3.4.6.2.	Computation of $I_{32}$ .....	73

3.4.6.3.	Computation of $I_{33}$ .....	74
3.4.6.4.	Summary of $I_3$ .....	75
3.4.7.	Integration of $I_4$ .....	75
3.4.7.1.	Computation of $I_{41}$ .....	75
3.4.7.2.	Computation of $I_{42}$ .....	76
3.4.7.3.	Computation of $I_{43}$ .....	76
3.4.7.4.	Summary of $I_4$ .....	77
3.4.8.	Integration summary .....	77
3.4.9.	Path delay variables and zenith path delay .....	78
3.5.	SUMMARY .....	82
<b>4.</b>	<b>TEST AND EVALUATION .....</b>	<b>85</b>
4.1.	ZENITH PATH DELAY TESTING .....	85
4.1.1.	Parameter reference values .....	85
4.1.2.	Path Delay results .....	86
4.1.3.	Path Delays as function of $z_0$ .....	86
4.1.4.	Path Delays as function of $z'$ .....	88
4.1.5.	Path Delays as function of $z_1$ .....	91
4.1.6.	Path Delays as function of $H_p$ .....	94
4.1.7.	Path Delays as function of $H_e$ .....	94
4.1.8.	Path Delay testing summary .....	96
4.2.	PARTIAL DERIVATIVES TESTING .....	96
4.2.1.	ZDD partial derivatives results .....	98
4.2.2.	ZDD partial derivatives as function of $z_0$ .....	98
4.2.3.	ZWD partial derivatives results .....	101
4.2.4.	ZWD partial derivatives as function of $z_0$ .....	102
4.2.5.	ZPD partial derivatives results .....	105
4.2.6.	ZPD partial derivatives results as function of $z_0$ .....	106
4.2.7.	PARTIAL DERIVATIVES SUMMARY .....	110
4.3.	SWISS REGIONAL CAMPAIGN .....	110
4.3.1.	COMEDIE software .....	110
4.3.1.1.	Software structure .....	110
4.3.1.2.	Covariance function .....	110
4.3.2.	AGNES GPS stations .....	111
4.3.3.	AGNES station collocation .....	113
4.3.3.1.	Observation window .....	113
4.3.3.2.	Collocation parameters and covariance .....	113
4.3.3.3.	ZPD estimates .....	114
4.3.3.4.	COMEDIE quality assessment .....	121
4.3.3.5.	AGNES stations ZPD forecasts .....	129
4.3.3.6.	AGNES stations ZPD forecasts quality assessment .....	135
4.3.3.7.	AGNES stations ZPD forecasts operational quality assessment .....	141
4.3.3.8.	ZPD forecast and positioning .....	147
4.4.	SUMMARY .....	147
<b>5.</b>	<b>CONCLUSIONS.....</b>	<b>149</b>
5.1.	WORK SUMMARY .....	149
5.2.	RECOMMENDATIONS .....	150
	<b>BIBLIOGRAPHY .....</b>	<b>153</b>
	<b>APPENDICES .....</b>	<b>159</b>
	APPENDIX A. ESSEND AND FROOME FORMULA .....	159
	APPENDIX B. ZENITH PATH DELAY PARTIAL DERIVATIVES .....	163
B.1.	INTRODUCTION .....	163
B.2.	MATHEMATICAL BACKGROUND .....	163
B.3.	HELP FUNCTIONS .....	164

B.3.1.	Logarithm $\ln(T_{ref}, \gamma, z_0, z_1)$ .....	164
B.3.1.1.	$\partial \ln(T_{ref}, \gamma, z_0, z_1) / \partial T_{ref}$ .....	164
B.3.1.2.	$\partial \ln(T_{ref}, \gamma, z_0, z_1) / \partial \gamma$ .....	164
B.3.1.3.	$\partial \ln(T_{ref}, \gamma, z_0, z_1) / \partial z_0$ .....	165
B.3.1.4.	$\partial \ln(T_{ref}, \gamma, z_0, z_1) / \partial z_1$ .....	165
B.3.2.	$S_{11}$ .....	165
B.3.2.1.	$\partial S_{11} / \partial T_{ref}$ .....	165
B.3.2.2.	$\partial S_{11} / \partial \gamma$ .....	166
B.3.2.3.	$\partial S_{11} / \partial z_0$ .....	167
B.3.2.4.	$\partial S_{11} / \partial z_1$ .....	167
B.3.2.5.	$\partial S_{11} / \partial H_p$ .....	167
B.3.3.	$S_{12}$ .....	168
B.3.3.1.	$\partial S_{12} / \partial T_{ref}$ .....	168
B.3.3.2.	$\partial S_{12} / \partial \gamma$ .....	168
B.3.3.3.	$\partial S_{12} / \partial z_0$ .....	168
B.3.3.4.	$\partial S_{12} / \partial z_1$ .....	168
B.3.3.5.	$\partial S_{12} / \partial H_e$ .....	169
B.4.	ZENITH DRY DELAY PARTIAL DERIVATIVES .....	169
B.4.1.	$\partial ZDD / \partial p_{ref}$ .....	169
B.4.2.	$\partial ZDD / \partial e_{ref}$ .....	169
B.4.3.	$\partial ZDD / \partial T_{ref}$ .....	169
B.4.4.	$\partial ZDD / \partial T_1$ .....	170
B.4.5.	$\partial ZDD / \partial \gamma$ .....	170
B.4.6.	$\partial ZDD / \partial z_0$ .....	171
B.4.7.	$\partial ZDD / \partial z_1$ .....	172
B.4.8.	$\partial ZDD / \partial z'$ .....	173
B.4.9.	$\partial ZDD / \partial H_p$ .....	174
B.4.10.	$\partial ZDD / \partial H_e$ .....	175
B.5.	ZENITH WET DELAY PARTIAL DERIVATIVES .....	176
B.5.1.	$\partial ZWD / \partial e_{ref}$ .....	176
B.5.2.	$\partial ZWD / \partial T_{ref}$ .....	176
B.5.3.	$\partial ZWD / \partial T_1$ .....	178
B.5.4.	$\partial ZWD / \partial \gamma$ .....	179
B.5.5.	$\partial ZWD / \partial z_0$ .....	180
B.5.6.	$\partial ZWD / \partial z_1$ .....	181
B.5.7.	$\partial ZWD / \partial z'$ .....	183
B.5.8.	$\partial ZWD / \partial H_e$ .....	183
B.6.	PARAMETER DEPENDENCIES OF THE PARTIAL DERIVATIVES .....	187
APPENDIX C.	COMEDIE SOFTWARE .....	189
C.1.	M_HERSCHKE .....	189
C.2.	M_MODEL .....	191
C.3.	COLLOCATION AND PREDICTION PROGRAMS .....	199
C.4.	INPUT FILES .....	199

## Glossary

### A

AGL	Above Ground Level
AGNES	Automated GPS Network Switzerland
ANDE	Andermatt AGNES permanent station
ANETZ	Swiss Automated Weather Stations Network
AS	Anti-Spoofing

### C

C/A-code	Coarse/Acquisition code
CCIR	Consultative Committee of the International Telecommunication Union
CDMA	Code Division Multiple Access
cm	centimeter
CODE	Center for Orbit Determination in Europe
COMEDIE	Collocation of Meteorological Data for Interpolation and Estimation of Tropospheric Path delays
CONUS	CONTinental United States
Cs	Cesium

### D

DAVO	Davos AGNES permanent station
DMA	Defense Mapping Agency
DoD	U.S. Department of Defense

### E

EELV	Evolved Expendable Launch Vehicle
EGR	Error Growth Rate
EM	ElectroMagnetic
EPF	Ecole Polytechnique Fédérale – Swiss Federal Institute of Technology
EPFL	EPF Lausanne AGNES permanent station
ETH	Eidgenössische Technische Hochschule – Swiss Federal Institute of
Technology	
ETHZ	ETH Zurich or ETH Zurich AGNES permanent station

### F

FARA	Fast Ambiguity Resolution Approach
FHBB	FachHochschule Beider Basel
FOC	Full Operational Capability
FY	Fiscal Year

### G

GCS	Ground Control Station
GFZ Postdam	GeoForschungsZentrum Postdam
GGL	Geodesy and Geodynamics Lab
GPS	Global Positioning System

### H

HOW	Hand Over Word
hPa	hectopascal

### I

ICAO	International Civil Aviation Organization
ICD	Interface Control Document
IGS	International GPS Service
IOC	Initial Operational Capability
IR	InfraRed
ISA	International Standard Atmosphere

**J**

JPO Joint Program Office  
JUJO Jungfrauoch AGNES permanent station

**K**

K Kelvin

**L**

LC Linear Combination  
LHS Left Hand Side  
lin. linear  
LOMO Locarno-Monti AGNES permanent station  
LOS Line Of Sight  
L+T Bundesamt für Landestopography, Wabern, Schweiz – Swiss Federal Office of Topography, Wabern, Switzerland

**M**

M-code Military code  
MCS Master Control Station  
MEO Medium Earth Orbit  
MF Mapping Function  
MIT Massachusetts Institute of Technology  
mm millimeter  
MS Monitor Station  
MSL Mean Sea Level

**N**

NATO North Atlantic Treaty Organisation  
NAVCEN USCG NAVigation CENTER  
NAVSTAR NAVigation System by Timing And Ranging  
NEUC Neuchatel AGNES permanent station  
NIMA National Imagery & Mapping Agency  
NM Nautical Mile  
NRC National Research Council  
NSC National Security Council

**O**

OP Operational  
OPS Operations

**P**

P-code Precise code  
PAYE Payerne AGNES permanent station  
PD Path Delay  
PDD Presidential Decision Directive  
PDE Partial Differential Equation  
PDOP Precision Dilution Of Precision  
PFAN Pfänder AGNES permanent station  
PPS Precise Positioning Service  
PR PseudoRange  
PRN Pseudo Random Noise  
PTO Please Turn Over

**R**

Rb Rubidium  
RHS Right Hand Side  
RMS Root Mean Square  
RS RadioSonde



**S**

SA	Selective Availability
SANB	San Bernardino AGNES permanent station
Sigma	Standard deviation
SMA	Schweizer Meteorologische Anstalt – Swiss Meteorological Office
SMI	Swiss Meteorological Institute
SPS	Standard Positioning Service
STAB	Stabio AGNES permanent station
STDEV	Standartd Deviation
SV	Space Vehicle
SVN	Space Vehicle Number

**T**

TD	Total Delay
TEC	Total Electron Content
TFSR	Tapped Feedback Shift Receiver
TLM	Telemetry
TOA	Time Of Arrival
TVEC	Total Vertical Electron Content

**U**

US	United States of America
USAF	U.S. Air Force
USCG	U.S. Coast Guards
USNO	U.S. Naval Observatory
UTC	Universal Time Coordinated
UV	Ultra Violet

**W**

WGS84	World Geodetic System 1984
WRCC	World Radio Communications Conference
w.r.t.	With respect to
WV	Water Vapor

**Z**

ZDD	Zenith Dry Delay
ZHD	Zenith Hydrostatic Delay
ZIMM	Zimmerwald AGNES permanent station
ZPD	Zenith Path Delay
ZTD	Zenith Tropospheric Delay ( <i>sometimes</i> Zenith Total Delay)
ZWD	Zenith Wet Delay

**Blank page**

## LIST OF FIGURES

FIGURE 1. GPS CONSTELLATION .....	1
FIGURE 2. BLOCK IIF GPS VEHICLE .....	1
FIGURE 3. SIGNAL BENDING AND SLANT PATH DELAY .....	14
FIGURE 4. STRATEGIES TO DETERMINE THE ATMOSPHERIC SLANT PATH DELAY. AFTER [GEIGER ET AL., 1995] .....	26
FIGURE 5. LEAST-SQUARES COLLOCATION PRINCIPLE .....	27
FIGURE 6. ESSEN AND FROOME FORMULA. REFRACTIVITY FOR $e=10$ hPa .....	42
FIGURE 7. ESSEN AND FROOME FORMULA. DRY REFRACTIVITY FOR $p=1000$ hPa .....	42
FIGURE 8 ESSEN AND FROOME FORMULA. WET REFRACTIVITY .....	43
FIGURE 9. ENHANCED HOPFIELD MODEL. HYDROSTATIC PATH DELAY $HPD(T, \varepsilon)$ .....	45
FIGURE 10. SAASTAMOINEN FORMULA. ZENITH PATH DELAY $ZTD(p, T)$ .....	47
FIGURE 11. SAASTAMOINEN FORMULA. ZENITH PATH DELAY $ZTD(e, \varepsilon)$ .....	47
FIGURE 12. TEMPERATURE PROFILE AS FUNCTION OF ALTITUDE. AFTER [ROEDEL, 1992]. .....	51
FIGURE 13. PRESSURE OF A VOLUME ELEMENT .....	56
FIGURE 14. SATURATION WATER VAPOR PRESSURE AS A FUNCTION OF THE TEMPERATURE IN THE ATMOSPHERE, $e_s(T)$ .....	62
FIGURE 15. GPS SIGNAL PATH THROUGH THE ATMOSPHERE .....	64
FIGURE 16. ZPD, ZHD, ZDD AND ZWD RELATIONSHIP WITH THE ESSEN AND FROOME FORMULA .....	83
FIGURE 17. ZHD AND ZPD AS FUNCTION OF THE GPS RECEIVER'S ALTITUDE MSL $z_0$ .....	86
FIGURE 18. ZHD AND ZDD DIFFERENCE AS FUNCTION OF THE GPS RECEIVER'S ALTITUDE MSL $z_0$ .....	87
FIGURE 19. ZWD AS FUNCTION OF THE GPS RECEIVER'S ALTITUDE MSL $z_0$ .....	88
FIGURE 20. ZHD AND ZPD AS FUNCTION OF THE UPPER LIMIT OF INTEGRATION $z'$ FOR $z_0 = 905$ m MSL .....	88
FIGURE 21. ZHD AND ZDD DIFFERENCE AS FUNCTION OF THE UPPER LIMIT OF INTEGRATION $z'$ IN THE STRATOSPHERE .....	89
FIGURE 22. ZWD AS FUNCTION OF THE UPPER LIMIT OF INTEGRATION $z'$ IN THE STRATOSPHERE .....	90
FIGURE 23. RELATIVE CHANGE IN % OF THE ZHD, ZDD, ZWD AND ZPD WITH THE UPPER LIMIT OF INTEGRATION $z'$ IN THE STRATOSPHERE AND FOR $z_0 = 905$ m MSL .....	90
FIGURE 24. ZHD AND ZPD AS FUNCTION OF THE UPPER LIMIT OF INTEGRATION $z_1$ IN THE TROPOSPHERE AND FOR $z_0 = 905$ m MSL .....	91
FIGURE 25. ZHD AND ZDD DIFFERENCE AS FUNTION OF THE UPPER LIMIT OF INTEGRATION $z_1$ IN THE TROPOSPHERE AND FOR $z_0 = 905$ m MSL .....	92
FIGURE 26. ZWD AS FUNCTION OF THE UPPER LIMIT OF INTEGRATION $z_1$ IN THE TROPOSPHERE AND FOR $z_0 = 905$ m MSL .....	93
FIGURE 27. RELATIVE CHANGE IN % OF THE ZHD, ZDD, ZWD AND ZPD WITH THE UPPER LIMIT OF INTEGRATION $z_1$ IN THE TROPOSPHERE AND FOR $z_0 = 905$ m MSL .....	93
FIGURE 28. ZHD AND ZPD AS FUNCTION OF THE PRESSURE SCALE HEIGHT $H_p$ AND FOR $z_0 = 905$ m MSL .....	94
FIGURE 29. ZHD AND ZDD DIFFERENCE AS FUNCTION OF THE PRESSURE SCALE HEIGHT $H_p$ AND FOR $z_0 = 905$ m MSL .....	95
FIGURE 30. ZDD AND ZPD AS FUNCTION OF THE HUMIDITY SCALE HEIGHT $H_e$ AND FOR $z_0 = 905$ m MSL .....	95
FIGURE 31. ZWD AS FUNCTION OF THE HUMIDITY SCALE HEIGHT $H_e$ AND FOR $z_0 = 905$ m MSL .....	96
FIGURE 32. $\partial ZDD/\partial p_{ref}$ AND $\partial ZDD/\partial e_{ref}$ AS FUNCTION OF THE GPS RECEIVER'S ALTITUDE $z_0$ .....	98
FIGURE 33. $\partial ZDD/\partial T_{ref}$ AND $\partial ZDD/\partial z_0$ AS FUNCTION OF THE GPS RECEIVER'S ALTITUDE $z_0$ .....	99
FIGURE 34. $\partial ZDD/\partial \gamma$ AS FUNCTION OF THE GPS RECEIVER'S ALTITUDE $z_0$ .....	99
FIGURE 35. $\partial ZDD/\partial H_p$ AND $\partial ZDD/\partial H_e$ AS FUNCTION OF THE GPS RECEIVER'S ALTITUDE $z_0$ .....	100

FIGURE 36. RELATIVE CHANGE OF ZDD PARTIAL DERIVATIVES AS FUNCTION OF THE GPS RECEIVER'S ALTITUDE $z_0$ .....	101
FIGURE 37. $\partial ZWD/\partial e_{ref}$ AND $\partial ZWD/\partial T_{ref}$ AS FUNCTION OF THE GPS RECEIVER'S ALTITUDE $z_0$ .....	102
FIGURE 38. $\partial ZWD/\partial H_e$ AND $\partial ZWD/\partial z_0$ AS FUNCTION OF THE GPS RECEIVER'S ALTITUDE $z_0$ .....	103
FIGURE 39. $\partial ZWD/\partial \gamma$ AS FUNCTION OF THE GPS RECEIVER'S ALTITUDE $z_0$ .....	104
FIGURE 40. $\partial ZHD/\partial \gamma$ AS FUNCTION OF THE GPS RECEIVER'S ALTITUDE $z_0$ .....	104
FIGURE 41. RELATIVE CHANGE OF THE ZWD PARTIAL DERIVATIVES AS FUNCTION OF THE GPS RECEIVER'S ALTITUDE.....	105
FIGURE 42. $\partial ZPD/\partial e_{ref}$ AND $\partial ZPD/\partial p_{ref}$ AS FUNCTION OF THE GPS RECEIVER'S ALTITUDE $z_0$ .....	106
FIGURE 43. $\partial ZPD/\partial \gamma$ AND $\partial ZPD/\partial T_{ref}$ AS FUNCTION OF THE GPS RECEIVER'S ALTITUDE $z_0$ .....	107
FIGURE 44. $\partial ZPD/\partial H_p$ AND $\partial ZPD/\partial H_e$ AS FUNCTION OF THE GPS RECEIVER'S ALTITUDE $z_0$ .....	107
FIGURE 45. $\partial ZPD/\partial z_0$ AND $\partial ZPD/\partial z'$ AS FUNCTION OF THE GPS RECEIVER'S ALTITUDE $z_0$ .....	108
FIGURE 46. $\partial ZPD/\partial T_1$ AND $\partial ZPD/\partial z_1$ AS FUNCTION OF THE GPS RECEIVER'S ALTITUDE $z_0$ .....	108
FIGURE 47. RELATIVE CHANGE OF ZPD PARTIAL DERIVATIVES AS FUNCTION OF THE GPS OF THE GPS RECEIVER'S ALTITUDE $z_0$ .....	109
FIGURE 48. AGNES PERMANENT STATIONS USED, AFTER [L+T, 2002] .....	112
FIGURE 49. HEIGHT DISTRIBUTION IN WGS84 OF THE AGNES STATIONS. ....	112
FIGURE 50. ANDE, ETHZ, JUJO, LOMO AND DAVO AGNES STATIONS. CLOCKWISE FROM THE UPPER LEFT CORNER. © 2002 L+T. ....	113
FIGURE 51. COMEDIE ZPD ESTIMATES AT ANDE.....	115
FIGURE 52. COMEDIE ZPD ESTIMATES AT DAVO .....	115
FIGURE 53. COMEDIE ZPD ESTIMATES AT EPFL .....	116
FIGURE 54. COMEDIE ZPD ESTIMATES AT ETHZ.....	116
FIGURE 55. COMEDIE ZPD ESTIMATES AT FHBB .....	117
FIGURE 56. COMEDIE ZPD ESTIMATES AT JUJO.....	117
FIGURE 57. COMEDIE ZPD ESTIMATES AT LOMO .....	118
FIGURE 58. COMEDIE ZPD ESTIMATES AT NEUC .....	118
FIGURE 59. COMEDIE ZPD ESTIMATES AT PAYE .....	119
FIGURE 60. COMEDIE ZPD ESTIMATES AT PFAN.....	119
FIGURE 61. COMEDIE ZPD ESTIMATES AT ZIMM.....	120
FIGURE 62. COMEDIE-AGNES ZPD DIFFERENCES AT ANDE.....	121
FIGURE 63. COMEDIE-AGNES ZPD DIFFERENCES AT DAVO .....	122
FIGURE 64. COMEDIE-AGNES ZPD DIFFERENCES AT EPFL .....	122
FIGURE 65. COMEDIE-AGNES ZPD DIFFERENCES AT ETHZ.....	123
FIGURE 66. COMEDIE-AGNES ZPD DIFFERENCES AT FHBB .....	123
FIGURE 67. COMEDIE-AGNES ZPD DIFFERENCES AT JUJO.....	124
FIGURE 68. COMEDIE-AGNES ZPD DIFFERENCES AT LOMO .....	124
FIGURE 69. COMEDIE-AGNES ZPD DIFFERENCES AT NEUC .....	125
FIGURE 70. COMEDIE-AGNES ZPD DIFFERENCES AT PAYE .....	125
FIGURE 71. COMEDIE-AGNES ZPD DIFFERENCES AT PFAN.....	126
FIGURE 72. COMEDIE-AGNES ZPD DIFFERENCES AT ZIMM.....	126
FIGURE 73. AVERAGE COMEDIE-AGNES ZPD DIFFERENCE AS FUNCTION OF THE GPS STATIONS ALTITUDE .....	128
FIGURE 74. STANDARD DEVIATION OF COMEDIE-AGNES ZPD DIFFERENCE AS FUNCTION OF THE GPS STATIONS ALTITUDE .....	128
FIGURE 75. RMS OF COMEDIE-AGNES ZPD DIFFERENCE AS FUNCTION OF THE GPS STATIONS ALTITUDE.....	129
FIGURE 76. COMEDIE ZPD FORECAST AT ANDE.....	130
FIGURE 77. COMEDIE ZPD FORECAST AT DAVO .....	130
FIGURE 78. COMEDIE ZPD FORECAST AT EPFL.....	131
FIGURE 79. COMEDIE ZPD FORECAST AT ETHZ.....	131
FIGURE 80. COMEDIE ZPD FORECAST AT FHBB.....	132
FIGURE 81. COMEDIE ZPD FORECAST AT JUJO .....	132
FIGURE 82. COMEDIE ZPD FORECAST AT LOMO .....	133
FIGURE 83. COMEDIE ZPD FORECAST AT NEUC .....	133
FIGURE 84. COMEDIE ZPD FORECAST AT PAYE.....	134
FIGURE 85. COMEDIE ZPD FORECAST AT PFAN.....	134
FIGURE 86. COMEDIE ZPD FORECAST AT ZIMM .....	135
FIGURE 87. ZPD DIFFERENCES BETWEEN COMEDIE FORECASTS AND AGNES OBSERVATIONS, GROUP 1 .....	136

FIGURE 88. ZPD DIFFERENCES BETWEEN COMEDIE FORECASTS AND AGNES OBSERVATIONS, GROUP 2 .....	136
FIGURE 89. AVERAGE OF COMEDIE ZPD FORECAST – AGNES ZPD OBSERVATION.....	137
FIGURE 90. AVERAGE OF COMEDIE ZPD FORECAST – AGNES ZPD OBSERVATION.....	137
FIGURE 91. AVERAGE OF COMEDIE ZPD FORECAST – AGNES ZPD OBSERVATION.....	138
FIGURE 92. STANDARD DEVIATION OF COMEDIE ZPD FORECAST – AGNES ZPD OBSERVATION .....	138
FIGURE 93. RMS OF COMEDIE ZPD FORECAST – AGNES ZPD OBSERVATION.....	139
FIGURE 94. RMS OF COMEDIE ZPD FORECAST – AGNES ZPD OBSERVATION.....	139
FIGURE 95. RMS OF COMEDIE ZPD FORECAST – AGNES ZPD OBSERVATION.....	140
FIGURE 96. ZPD FORECAST QUALITY ASSESSMENT PRINCIPLES. ....	142
FIGURE 97. AVERAGE OF COMEDIE ZPD FORECAST – AGNES ZPD OBSERVATION.....	142
FIGURE 98. AVERAGE OF COMEDIE ZPD FORECAST – AGNES ZPD OBSERVATION.....	143
FIGURE 99. AVERAGE OF COMEDIE ZPD FORECAST – AGNES ZPD OBSERVATION.....	143
FIGURE 100. STANDARD DEVIATION OF COMEDIE ZPD FORECAST – AGNES ZPD OBSERVATION .....	144
FIGURE 101. RMS OF COMEDIE ZPD FORECAST – AGNES ZPD OBSERVATION.....	144
FIGURE 102. RMS OF COMEDIE ZPD FORECAST – AGNES ZPD OBSERVATION.....	145
FIGURE 103. RMS OF COMEDIE ZPD FORECAST – AGNES ZPD OBSERVATION.....	145
FIGURE A.1. ESSEN AND FROOME FORMULA. $N(p, T)$ FOR $E=0$ HPA.....	159
FIGURE A.2. ESSEN AND FROOME FORMULA. $N(p, T)$ FOR $E=5$ HPA.....	160
FIGURE A.3. ESSEN AND FROOME FORMULA. $N(p, T)$ FOR $E=10$ HPA.....	160
FIGURE A.4. ESSEN AND FROOME FORMULA. $N(p, T)$ FOR $E=15$ HPA.....	161

**Blank page**

## LIST OF TABLES

TABLE 1. GPS SVs STATUS AS OF 16 NOVEMBER 2001 AFTER [NAVCEN, 2001A] AND [NAVCEN, 2001B].....	2
TABLE 2. GPS CODES.....	6
TABLE 3. SYSTEMATIC ERRORS IN THE GPS SIGNAL.....	9
TABLE 4. CODE AND PHASE LINEAR COMBINATIONS, AFTER [FRIDEZ ET AL., 2001].....	20
TABLE 5. ESSEN AND FROOME FORMULA: COEFFICIENTS.....	41
TABLE 6. THAYER MODEL COEFFICIENTS.....	43
TABLE 7. NIELL HYDROSTATIC MAPPING FUNCTION COEFFICIENTS.....	50
TABLE 8. NIELL WET MAPPING FUNCTION COEFFICIENTS.....	50
TABLE 9. SATURATION VAPOR PRESSURE: CONSTANTS.....	61
TABLE 10. PARAMETERS REFERENCE VALUES.....	85
TABLE 11. ZENITH DELAYS EVALUATED AT ZIMMERWALD WITH PARAMETER REFERENCE VALUES.....	86
TABLE 12. 80% AND 90% LEVEL FOR PATH DELAYS AS FUNCTION OF ALTITUDE AND 15000 METERS MSL THRESHOLD.....	91
TABLE 13. 50% LEVEL FOR PATH DELAYS AS FUNCTION OF ALTITUDE, AND 11000 METERS MSL THRESHOLD.....	92
TABLE 14. PARAMETER DEPENDENCIES OF THE PARTIAL DERIVATIVES.....	97
TABLE 15. UNITS OF THE ZPD'S PARTIAL DERIVATIVES.....	97
TABLE 16. ZDD PARTIAL DERIVATIVES RESULTS FOR $z_0 = 905$ METERS MSL AND $z_0 = 0$ METERS MSL.....	98
TABLE 17. ZWD PARTIAL DERIVATIVES RESULTS FOR $z_0 = 905$ M MSL AND $z_0 = 0$ M MSL.....	101
TABLE 18. ZPD PARTIAL DERIVATIVES RESULTS FOR $z_0 = 905$ M MSL AND $z_0 = 0$ M MSL.....	105
TABLE 19. AGNES PERMANENT STATIONS USED.....	111
TABLE 20. ZPD PARAMETERS CONSTRAINED.....	114
TABLE 21. A-PRIORI COVARIANCE PARAMETERS.....	114
TABLE 22. COMEDIE-AGNES ZPD RESIDUALS STATISTICS.....	127
TABLE 23. TIME RESPONSE FOR 1CM ACCURACY LEVEL.....	135
TABLE 24. COMEDIE FORECAST-AGNES OBSERVATION RESIDUALS STATISTICS.....	140
TABLE 25. EXTRAPOLATION TIME PERIOD FOR OPERATIONAL PURPOSES.....	142
TABLE 26. COMEDIE FORECAST-AGNES OBSERVATION RESIDUALS STATISTICS FOR OPERATIONAL PURPOSES.....	146
TABLE B.1. PARAMETER DEPENDENCIES OF THE PARTIAL DERIVATIVES.....	187
TABLE C.1. M_HERSCHKE.H LIBRARY.....	189
TABLE C.2. M_HERSCHKE.C ROUTINE FOR ZPD FUNCTIONAL MODEL.....	191
TABLE C.3. M_MODEL.C ROUTINE CONTAINING THE COMEDIE FUNCTIONAL MODELS.....	199
TABLE C.4. EXAMPLE OF COLLOC_INPUT FILE.....	200
TABLE C.5. EXAMPLE OF INPUT_MAIN FILE FOR OBSERVATION WINDOW AND ROUTINE EXECUTION.....	201

**Blank page**



# 1 Path delays in GPS signal

The Earth's atmosphere strongly influences any signal incoming from space, as is the case with navigation satellites. In a first part, the NAVSTAR Global Positioning System is reviewed while the GPS observables are derived in a second part. The signal processing is then presented. It is intended to prove that the main residual error source is the troposphere.

## 1.1 NAVSTAR GPS

### 1.1.1 History

Starting in the 1960s, satellites were recognized as promising means of navigation guidance. At the beginning of the 1970s, the United States Department of Defense (DoD) needed to replace its ageing first generation space based navigation platforms constructed on the Defense Mapping agency (DMA) TRANSIT experiment. It required an all-weather, global satellite navigation system with unlimited number of suitably equipped users, which signal could be received independently of time and place. The NAVSTAR (NAVigation System by Timing And Ranging) GPS (Global Positioning System) was conceived in mid-1973 as a multi-service program.

In December 1973, the U.S. Air Force managed NAVSTAR GPS Joint Program Office (JPO) was directed by the DoD to "establish, develop, test, acquire and deploy a space borne positioning system" as mentioned by [Hofmann-Wellenhof, 1997].

### 1.1.2 Segments and functionalities

The system is built up around three segments: the space segment enveloping all satellites forming the constellation, the ground control segment maintaining the operational status of all the space vehicles (SV) and the user segment consisting of the receivers community.

#### 1.1.2.1 Space segment

The GPS satellites are evolving on a Medium Earth Orbit (MEO) at an altitude of approximately 10,858 nautical miles (NM) or 20200 km. Their orbit period is estimated to be 11 hours 57 minutes and 57.27 seconds. Hence each satellite rounds the Earth about twice a sidereal day.

As of November 2001, the constellation consists of 24 operational satellites, homogeneously distributed on six evenly spaced planes (A to F), inclined at 55° with respect to the Earth's equator as well as 4 spares as can be seen on Figure 1. It provides global coverage with a minimum of four space vehicles (SV) and up to eight satellites simultaneously visible above 15° elevation. Six generations of NAVSTAR GPS satellites are to date in orbit and reflect the evolution of military technologies. The GPS SVs are classified in Blocks and differentiated by their Pseudo Random Noise (PRN) code and Space Vehicle Number (SVN).



*Above:*  
Figure 1.  
GPS constellation

*Right side:*  
Figure 2. Block IIF  
GPS vehicle.

*Source:*  
[NAVSTAR-JPO, 2001]



The eleven Block I/IA satellites were launched from 22 February 1978 onwards until 9 October 1985. The last Block IA satellite, SVN11/PRN03 was deactivated on 14 April 1994 at 21:00 UT (Universal Time). The actual SV configuration consists of Block II/IIA and IIR SVs.

The eight Block II satellites, SVN 13 to 21, incorporate a denial system that restricts full signal reception to only certain DoD-approved users. Conversely to Block I satellites, Block II satellites employ two cesium (Cs) and two rubidium (Rb) atomic clocks as frequency standards. They were launched into space between 14 February 1989 and 6 November 1997.

The 15 Block IIA satellites carry advanced (therefore the “A”) radio systems, allowing a mutual communication capability. The first Block IIA satellite, SVN21/PRN23 was placed on 26 November 1990 on its E4 orbital plane. Their life expectancy was extended of 2 years to 10.68 years. The SVs were designed to implement both the Selective Availability (SA) and Anti-Spoofing (AS) capabilities to provide the adequate signal security. It is here referred to 1.1.4. for further explanation.

The Replenishment or Replacement Block IIR satellites, SVN 41 to 62 have their own on-board Hydrogen maser, one order of magnitude more precise than the conventionally used Cs and Rb atomic clocks aboard former blocks (c.f. [Fromm, 1998]). The first Block IIR satellite, SVN43/PRN13 was launched by the Space Shuttle on 23 July 1997 from Vandenberg AFB and activated on 31 January 1998. To date, six Block IIR satellites are on orbit. After [NATO, 2001], the last launch took place on 30 January 2001.

The United States Air Force intends to purchase (contract signed in 1996) 33 Follow-on Block IIF satellites (c.f. Figure 2), although 24 are operationally required, to ensure both military and civil navigation. All SVs are designed with a lifetime of more than ten years and should be launched between 2001 and 2004 with the Evolved Expandable Launch Vehicle (EELV) as booster on a launch-on-need basis to cut costs. The Block IIF satellites are intended to have an 11.5 years design life. It is referred to Table 1 for more details on the current GPS constellation.

SVN #	PRN #	Mission #	Launch Date	Slot	Operational Date	Month Operational	Clock
17	17	II-5	11-Dec-1989	D3	11-Jan-1990	132.6	Rb
18	18	II-6	24-Jan-1990	E4	14-Feb-1990	127.5	Rb
21	21	II-8	2-Aug-1990	E2	31-Aug-1990	125	Cs
15	15	II-9	1-Oct-1990	D5	20-Oct-1990	123.3	Cs
23	23	IIA-10	26-Nov-1990	E5	10-Dec-1990	121.3	Cs
24	24	IIA-11	3-Jul-1991	D1	30-Aug-1991	112	Cs
25	25	IIA-12	23-Feb-1992	A2	4-Mar-1992	106.2	Cs
26	26	IIA-14	23-Jul-1992	F2	23-Jul-1992	102.2	Rb
27	27	IIA-15	9-Sep-1992	A4	30-Sep-1992	100	Cs
32	1	IIA-16	22-Nov-1992	F4	11-Dec-1992	97.6	Cs
29	29	IIA-17	18-Dec-1992	F5	5-Jan-1993	96.8	Rb
22	22	IIA-18	2-Feb-1993	B1	4-Apr-1993	93.8	Rb
31	31	IIA-19	30-Mar-1993	C3	13-Apr-1993	93.5	Cs
37	7	IIA-20	13-May-1993	C4	12-Jun-1993	91.6	Rb
39	9	IIA-21	26-Jun-1993	A1	21-Jul-1993	90.3	Cs
35	5	IIA-22	30-Aug-1993	B4	20-Jul-1993	88.3	Cs
34	4	IIA-23	26-Oct-1993	D4	1-Dec-1993	85.9	Rb
36	6	IIA-24	10-Mar-1994	C1	24-Mar-1994	82	Cs
33	3	IIA-25	28-Mar-1993	C2	9-Apr-1996	57.7	Cs
40	10	IIA-26	16-Jul-1996	E3	15-Aug-1996	53.5	Cs
30	30	IIA-27	12-Sep-1996	B2	1-Oct-1996	51.9	Rb
38	8	IIA-28	6-Nov-1997	A3	18-Dec-1997	37.4	Rb
43	13	IIR-2	22-Jul-1997	F3	31-Jan-1998	36	Rb
46	11	IIR-3	6-Oct-1999	D2	3-Jan-2000	12.9	Rb
51	20	IIR-4	10-May-2000	E1	1-Jun-2000	7.9	Rb
44	28	IIR-5	16-Jul-2000	B5	17-Aug-2000	5.4	Rb
41	14	IIR-6	10-Nov-2000	F1	10-Dec-2000	1.6	Rb
54	2	IIR-7	30-Jan-2001	B3	-	-	Cs

Table 1. GPS SVs status as of 16 November 2001 after [NAVCEN, 2001a] and [NAVCEN, 2001b].

The Initial Operational Capability (IOC) was attained in July 1993 and declared by DoD on 8 December 1993 when 24 GPS space vehicles (Blocks I, II and IIA) were set in operation, available for navigation purposes and delivering full Standard Positioning Service (SPS).

The Full Operational Capability (FOC) was achieved in March 1994, when 24 Block II and IIA satellites were fully operational in the desired orbital planes and tested for operational military performances. The Office of the Assistant Secretary of Defense declared the FOC on 17 July 1995 (c.f. [DOD, 1995]).

### **1.1.2.2 Ground Control Segment**

The ground control segment is divided into three parts: the Master Control Station (MCS), the Monitor Stations (MS) and the Ground Control Stations (GCS). Its operational task is the tracking of all the SVs for orbit and clock determination, the prediction of time synchronization and the upload of data message to the satellites. It is also responsible for implementing the Selective Availability on the broadcast signal.

### **1.1.2.3 User segment**

Because NAVSTAR GPS is a Department of Defense program, two kinds of users should be distinguished: military and civilian users. The military users are the real or “true” users as invoked by the DoD. Civilian users are denied access to the full possibilities of the system when Selective Availability (SA) is deployed. However, SA has been turned following a Presidential Directive signed by President W. Clinton on 2 May 2000 at 04:07 Zulu, c.f. 1.1.4.1.

## **1.1.3 GPS signal**

The important part for the user is surely the GPS signal broadcasted by the satellite constellation. The receiver needs to know in which spatial and temporal reference systems it should consider the transmitted information. Then the signal should be separated in its different components and analyzed.

### **1.1.3.1 Reference Systems**

The equation of motion of the satellite on its orbit and of the receiver for dynamic positioning should be exactly computed. Therefore both a spatial co-ordinates system and a time system must be defined.

The World Geodetic System 1984 (WGS-84) is the system of reference for GPS measurements. It is defined by an important number (more than 100) of terrestrial reference stations. Belonging to WGS-84 is a geocentric equipotential ellipsoid of revolution. Its major and minor axes are defined by the fact that all reference stations must be located on the surface of the ellipsoid. Thus the height of a receiver can be deduced by knowing its height in the WGS-84 system and differentiating it with the satellite altitude, also given in the WGS-84 reference system. Transformations between the WGS-84 and other references systems are given in [NIMA, 1997].

The space vehicles are all equipped with a variable number of atomic clocks, defining a time standard. The Universal Time Coordinated (UTC) is based on the atomic second. However to reduce variations with the Universal Time (UT), an integer number of seconds was inserted at peculiar time epochs. The United States Naval Observatory (USNO) maintains the GPS time (see [USNO, 2001]) and it decided to relate it to UTC. Thus the GPS time is narrowly linked to UTC and it is counted in weeks, days, minutes, etc. It was set to zero on 6 January 1980 at 00.00 UTC. Thus the epoch 2000 of the Julian calendar corresponds to the GPS week 1042. Hence a rollover happened on midnight 21 to 22 August 1999. For further information regarding the rollover, refer to [USAF, 1999].

### **1.1.3.2 Ephemeris and calendar**

There are three kinds of data that are available to determine the pseudoranges and phase differences. All differ in accuracy and their utilization depends on the required precision as well as the processing time at disposal. These are the almanac data, the broadcast ephemeris and the precise ephemeris. As far as cinematic applications such as atmospheric sounding are concerned, only the last two are of interest.

### **1.1.3.3 Signal components**

It will be here referred to the official GPS signal description contained in the GPS Interface Control Document ICD-GPS-200, Revision C (see [DoD-USCG, 1993]).

### 1.1.3.3.1 Frequency standards

Due to military requirements, the actual carrier broadcast is spread over a large signal spectrum. Thus it is less subject to intentional or unintentional jamming. This is known as the Code Division Multiple Access (CDMA) and is a form of multiplexing where the transmitter encodes the signal using a characteristic pseudo-random sequence, as defined by [Tiemeyer, 1999]. This sequence is known from the receiver who then can use it to decode the received signal. Each random sequence corresponds to a different communication channel.

The key to the GPS accuracy is concealed in the control of all signal components by atomic clocks. The actual block II satellites are equipped with four on-board atomic clocks: two Rubidium (Rb) and two Cesium (Cs). Its long-term stability is approximately a few parts in  $10^{-13}$ . However the up-to date Block IIR SVs deploy as well a hydrogen maser. According to [Fromm, 1998], it produces “a state of the art ultra-stable atomic frequency standard based on a sapphire loaded miniature microwave cavity” and has an accuracy of a few parts in  $10^{-14}$  to  $10^{-15}$ . These highly accurate frequency standards are the heart of the GPS system and they produce a fundamental L-band frequency

$$f_0 = 10.23 \text{ MHz} \quad (1.1)$$

From this two signals are derived. The  $L_1$  and  $L_2$  carriers are generated by multiplying the fundamental frequency by respectively 154 and 120, yielding to

$$L_1 = 1575.42 \text{ MHz} \quad \text{and} \quad L_2 = 1227.60 \text{ MHz} \quad (1.2)$$

The need for two different signals originates from the necessity to eliminate the refraction effects of the ionosphere during the signal processing (c.f. 1.4.1., ionosphere-free pseudoranges), as it is the biggest error source.

A further  $L_3$  frequency is also extracted from the fundamental frequency, but is strictly reserved for military usage. By Presidential Directive, it is intended to generate an  $L_5$  frequency for civilian users, which will be implemented in Block IIF space vehicles.

### 1.1.3.3.2 Codes

The wave carriers  $L_1$  and  $L_2$  are biphase-modulated by codes, in order to broadcast information. This is achieved by addition of a code, a two-state time dependent sequence of 1 and  $-1$ , corresponding to binary values of 1 and 0. This code shifts the carrier phase by  $180^\circ$  whenever a change in code occurs. Tapped Feedback Shift Registers (TFSR) are used to generate the Pseudo Random Noise (PRN) sequence in the code. This technique is referred to as *spread spectrum technique* and limits the interference from other signals, c.f. [Forsell, 1991].

The outputs of two 10-bits TFSR (G1 and G2 codes) are binary added to form the linear Coarse/Acquisition code (C/A-code) or Controlled Access code with a frequency of

$$f_{C/A} = \frac{f_0}{10} = 1.023 \text{ MHz} \quad (1.3)$$

It is available to all users and officially designated as the Standard Positioning Service (SPS). It is modulated on the  $L_1$  carrier and intentionally not on  $L_2$ . This allows the JPO (Joint Program Office, see 1.1.1.) to control the information broadcast by the Space Vehicle.

The Precise code (P-code) or Protected code is generated in the same manner as the C/A-code at the original L-band fundamental frequency of

$$f_p = f_0 = 10.23 \text{ MHz} \quad (1.4)$$

but with a different bit sequence. The whole P-code lasts ca. 266.4 days. Its chip length is of about 30 meters intervals and each interval corresponds to a unique SV, thus defining its PRN number. Therefore, all satellites are identified through their PRN number. The P-code is available only to authorized users, i.e. U.S. military and is designated the Precise Positioning Service (PPS). Until the FOC (Full Operational Capability, c.f. 1.2.1.2) was achieved, they have unlimited access to PPS. The P-code is modulated on both the  $L_1$  and  $L_2$  carriers.

A Military code (M-code) will be allocated on the new civilian  $L_5$  carrier<sup>1</sup> as was approved during the World Radio Communications Conference on March 2000<sup>2</sup>. It was decided to set  $L_5$  carrier frequency as

<sup>1</sup> This is NOT the same  $L_5$  frequency as mentioned in 1.4.3.

$$L_5 = 1176.00 \text{ MHz} \quad (1.5)$$

It will be implemented on the first six Block IIR-M space vehicles and on the currently under development Block IIF SVs. It is intended to reach the IOC in 2012 and the FOC in 2014 according to [NATO, 2001].

Both the C/A-code and the P-code are not classified. However, in order to protect the transmitted signals from voluntary adverse spoofing, the P-code is encrypted by the Anti-Spoofing function (refer to 1.1.4.2.) to form the Y-code. The Y-code is defined as modulo two (mod-2) of the P-code with addition of the highly secret W-code. However, the P-code remains the main code of the GPS signal.

### 1.1.3.3.3 Navigation message

The navigation message is maybe the most important part of the signal for the users community. It contains all necessary information about the satellite, such as its health status, GPS time, etc. Principally no information concerning the receiver's position are transmitted but only raw data regarding the SV itself. Its frequency is

$$f_{NM} = \frac{f}{204600} = 50 \cdot 10^{-6} \text{ MHz} \quad (1.6)$$

It has a total length of 1500 bits spread homogeneously over 5 subframes, containing each 10 words of 30 bits. The first two word (TLM and HOW) are generated by the SV itself, while the eight others are created by the Ground Control Segment and uploaded to the satellite.

The TLM contains a synchronization pattern and basic diagnostic messages on the SV's health status. After [Fridez et al., 2001], the "HOW contains among others the so-called *Z-count* which gives the number of 1.5 s intervals since the beginning of the current GPS week. This number and the P-code give the reading of the satellite clock at signal transmission time. The first subframe contains various flags and the polynomial coefficients which define the satellite clock correction<sup>3</sup>".

The redundant processors-controlled data flux being of 50 bit per second, the word is broadcasted in 0.6 second and the full digital navigation message transmitted in 30 seconds. It is modulated with the PRN code sequence.

## 1.1.4 Accuracy denial

It exists principally two methods to prevent civilian users to have full access to the system's capability: Selective Availability (SA) and Anti-Spoofing (SA). Bias errors result from the application of the SA and are discussed hereunder.

### 1.1.4.1 Selective Availability

The navigation accuracy using the SPS is normally of approximately 15 to 40 meters in positioning and tenth of centimeters per second for velocity measurements. The final aim of SA is the accuracy denial. It consists of two processes: the delta process, which disturbs the satellite atomic clocks and the epsilon process that manipulates the ephemeris. The  $\delta$ -process corresponds to the intended disturbance of the fundamental frequency of the SV clock. The  $\epsilon$ -process corresponds to a partial truncation of the transmitted navigation message that is an ephemeris data manipulation.

According to the GPS SPS specifications [DoD-USCG, 1993] the U.S. Department of Defense decided to degrade the signal to 100 meters horizontally and 156 meters vertically. This implies a velocity error of  $0.3 \text{ m} \cdot \text{s}^{-1}$  at a 95% probability level and a transfer time of 340 nanoseconds in the UTC system. The National Research Council (NRC) along with the U.S. National Academy of Public Administration recommended in November 1995 to a presidential committee that SA should be reduced to zero after some years. On 24 March 1996, a Presidential Decision Directive (PDD) was released, declaring its intention to "discontinue the use of GPS Selective Availability within a decade, in a manner that allows adequate time and resources for [...] the U.S. armed forces to prepare fully for operation without SA", c.f. [NSC, 1996]. Indeed, this was achieved on 2 May 2000 at 04:07 Zulu following a PDD signed by President W. Clinton, c.f. [NSC, 2000].

<sup>2</sup> C.f. [WRC-2000, 2000].

<sup>3</sup> It is referred to eq. (1.78) in 1.3.2.

### 1.1.4.2 Anti-Spoofing

GPS was designed to include the possibility for the JPO (Joint Program Office) to install an encryption to the P-code to deny access to all but the allowed users. This is motivated by keeping adversaries from sending out false signals with the proper GPS markings and thus causing the users to miscalculate their position and more particularly misleading military receivers. It is accomplished by building the modulo two sum of the P-code and the  $L_1$  and  $L_2$  carriers and adding the encrypted W-code. The Y-code is generated in that way.

When the Anti-Spoofing (AS) is functioning, the unknown Y-code replaces the P-code on the  $L_1$  and  $L_2$  carriers. It should be noted that Anti-Spoofing has no variable influences, in opposition to SA. Further, when AS was activated on 31 January 1994, it was not meant to hinder the use of the P-code by unauthorized users, but it led exactly to this.

Finally, SA and AS are the major means for the U.S. DoD to control NAVSTAR GPS. Civilian users are still under the risk of a complete and sudden signal access denial.

### 1.1.5 $L_1$ and $L_2$ frequency modeling

It is intended to derive here a simple model for the GPS signal. Assume that the original carrier waves have a sine form:

$$S_{L_j}(t) = a_j \cdot \cos(f_j \cdot t), \quad j = 1, 2 \quad (1.7)$$

According to [Kayton, 1997] the 0's and 1's sequence of the navigation message is converted to a  $0^\circ$  and  $180^\circ$  phase shift. As this is simply a change in the sign of the carrier, "an equivalent representation is an amplitude modulation of  $\pm 1$ ".

Label the different time dependent codes as stated in the following table:

GPS code	Symbol
Coarse/Acquisition - C/A-code	$C_A(t)$
Precise code – P-code	$P(t)$
W-code	$W(t)$
Navigation Message or Data stream	$D_i(t)$

Table 2. GPS codes.

Both  $L_1$  and  $L_2$  carriers are modulated by the P-code. As mentioned earlier, the C/A-code is incorporated solely on  $L_1$  with a  $90^\circ$  shift in its phase. This technique is named *phase quadrature*. Then the modulated carrier signals take the form

$$\begin{aligned} S_{L_1}(t) &= a_1 \cdot \left[ P(t) \cdot W(t) \cdot D_i(t) \cdot \cos(f_1 \cdot t) + C_A(t) \cdot D_i(t) \cdot \cos\left(f_1 \cdot t + \frac{\pi}{2}\right) \right] \\ S_{L_2}(t) &= a_2 \cdot P(t) \cdot W(t) \cdot D_i(t) \cdot \cos(f_2 \cdot t) \end{aligned} \quad (1.8)$$

where the index  $i$  stands for the  $i$ -th GPS SV. Using now the relationship

$$\cos(a + b) = \cos a \cdot \cos b - \sin a \cdot \sin b \quad (1.9)$$

This yields to the classic equations for the modulated carriers

$$\begin{aligned} S_{L_1}(t) &= a_1 \cdot P(t) \cdot W(t) \cdot D_i(t) \cdot \cos(f_1 \cdot t) + a_1 \cdot C_A(t) \cdot N_M(t) \cdot \sin(f_1 \cdot t) \\ S_{L_2}(t) &= a_2 \cdot P(t) \cdot W(t) \cdot D_i(t) \cdot \cos(f_2 \cdot t) \end{aligned} \quad (1.10)$$

Due to this complex modulation, both carriers are spread over a large phase spectrum, therefore being extremely resistant to jamming. This fact is important for the integrity of the transmitted information. For more details on the GPS signal see, e.g. [Forsell, 1991].

## 1.2 GPS Observables

A GPS receiver measure the time needed for the signal to travel through the atmosphere. It synchronizes its simple crystal clock with the atomic clocks of the space vehicle with assistance of the Telemetry word. Further it reconstructs the original signal from the same algorithm as those employed by the satellite. Hence, by accurate comparison of the received signal with the receiver-generated signal, the phase difference corresponding to the travel time can be computed.

The observables are ranges computed from these phase differences. As these measurements are affected by clock errors on both sides (SV and receiver), one rather speaks of pseudoranges and distinguishes two kinds: code pseudorange and phase pseudorange.

### 1.2.1 Code Pseudoranges

At a fixed instant of time the knowledge of three coordinates is required to determine the position of a vehicle. Conventionally these are the latitude, the longitude and the elevation angle. In the ideal case the position is determined from the distance  $\rho_k^i$  measured between the receiver  $k$  and the space vehicle  $i$ :

$$\rho_k^i = \left| \mathbf{r}_k(t) - \mathbf{r}^i(t - \tau) \right| \quad (1.11)$$

where  $\tau$  is the signal traveling time,  $\mathbf{r}_k(t)$  the position of the receiver  $k$  at the signal reception time  $t$  and  $\mathbf{r}^i(t - \tau)$  the position of the satellite  $i$  at the signal emission time. The geometric distance for electromagnetic (EM) signals traveling in vacuum at the speed of light  $c$  is given by

$$\rho_k^i = c \cdot \tau \quad (1.12)$$

Now let  $t_{sat} := t - \tau$  be the time of signal emission by the SV in GPS time and  $t_{rec} := t$  be the signal reception time also in GPS time. Hence read the time difference  $\Delta t$  between the satellite atomic clock(s) time and the receiver time at reception of the signal

$$\Delta t = t_{sat} - t_{rec} = \tau \quad (1.13)$$

This can also be expressed as

$$\Delta t = t_{sat} - t_{rec} = \Delta t_{GPS} + \Delta \delta \quad (1.14)$$

This time difference is affected by both the satellite atomic clocks error  $\delta_{sat}$  and the receiver's crystal clock error  $\delta_{rec}$ . Therefore, the time error induced by the errors of the clocks with respect to the GPS time is given by

$$\Delta \delta = \delta_{sat} - \delta_{rec} = \delta_k - \delta^i \quad (1.15)$$

Combining (1.13), (1.14) and (1.15) yields to

$$\tau = \Delta t_{GPS} + \Delta \delta = \Delta t_{GPS} + \delta_k - \delta^i \quad (1.16)$$

Hence the observed quantities are affected by errors, e.g. time-related errors. The observed pseudorange (PR) from the space vehicle  $i$  and the receiver  $k$  is given by multiplying the speed of light  $c$  with the travel time  $\tau$  for the EM wave and adding a global error term  $\varepsilon$ :

$$PR_k^i = c \cdot \tau_k^i + \varepsilon_{PR_k^i} = c \cdot (\Delta t_{GPS} + \Delta \delta)_k^i + \varepsilon_{PR_k^i} \quad (1.17)$$

where (1.16) has been used. Further it holds

$$PR_k^i = c \cdot \left\{ (t + \delta_k) - (t - \tau + \delta^i) \right\} + \varepsilon_{PR_k^i} \quad (1.18)$$

Using expression (1.12) for the geometric distance, eq. (1.18) can be rewritten as

$$\boxed{PR_k^i = \rho_k^i + c \cdot \Delta \delta_k^i + \varepsilon_{PR_k^i} = \rho_k^i + \Delta \rho_k^i + \varepsilon_{PR_k^i}} \quad (1.19)$$

where

$$\Delta \rho_k^i = c \cdot \Delta \delta_k^i \quad (1.20)$$

is the error in geometric distance. Equation (1.19) is the so-called *code pseudorange*. It is obviously not linear. The effects of the atmosphere are contained along other errors in the global error term  $\varepsilon_{PR_k^i}$ .

## 1.2.2 Phase Pseudoranges

The instantaneous circular frequency  $f$  is defined as the time derivative in the GPS time frame of the phase

$$f = \frac{d\varphi}{dt} \quad (1.21)$$

Thus the phase generated by the  $L_1$  and  $L_2$  signals is given by

$$\varphi = \int_{t_0}^t f(t') dt' \quad (1.22)$$

As the four atomic clocks of the SV generate ultra-stable frequencies, assume that  $f = \text{const}$ . For convenience, put  $\varphi(t_0) = 0$ . Thus (1.22) becomes

$$\varphi = f \cdot (t - \tau) = f \cdot \left( t - \frac{\rho}{c} \right) \quad (1.23)$$

Using the method derived by [Hofmann-Wellenhof, 1997], the beat phase  $\Phi_{beat}$  is defined as

$$\Phi_{beat} = \varphi_{sat}(t) - \varphi_{rec}(t) = -f_{sat} \cdot t - f_{sat} \cdot \frac{\rho}{c} - \varphi_{sat}^0 - \left[ f_{rec} \cdot t + \varphi_{rec}^0 \right] \quad (1.24)$$

where  $\varphi_{rec}$  is the phase of the received signal,  $\varphi_{sat}$  is the phase of the reconstructed reference carrier by the receiver and  $\varphi_x^0$ ,  $x = rec, sat$  is the phase of the signal at epoch  $t_0 = 0$ .

The variations in frequency from the fundamental carrier frequency  $f_0$  can be neglected, as it is most of the time of an order of magnitude of a tenth of Hertz. Further, using (1.15) as in the case of the code pseudorange, one has

$$\Phi_{beat} = -f \cdot \frac{\rho}{c} - f \cdot \Delta\delta \quad (1.25)$$

where the definition of the frequency

$$f = 2\pi/T = c/\lambda \quad (1.26)$$

in cycles per second has been used.  $T$  is the period in seconds and  $\lambda$  the wavelength in meters per cycle.

Assume now that the receiver can track continuously a SV in the constellation. It then measures the instantaneous fractional beat phase in cycles from a given epoch  $t_0$  to the current epoch  $t$  in GPS time:

$$\Phi_{beat}(t) = \Delta\Phi_{beat} \Big|_{t_0}^t + N \quad (1.27)$$

where  $N$  is an integer corresponding to the number of cycles between the SV and the receiver since time  $t_0$ . The tracking continuity implies that  $N$  is constant in time for a short period of time as is the case between two observations. As done before, set  $\Phi_{beat}(t_0) = 0$  without loss of generality. Thus define the observed phase pseudorange by

$$\Phi := -\Delta\Phi_{beat}(t) \quad (1.28)$$

and by inserting (1.25) and (1.27) in (1.28), one obtains

$$\Phi = f \cdot \frac{\rho}{c} + f \cdot \Delta\delta + N \quad (1.29)$$

Combining eq. (1.26) and eq. (1.29), yields to

$$\Phi = \frac{\rho}{\lambda} + \frac{c}{\lambda} \cdot \Delta\delta + N \quad (1.30)$$



Finally the equation for the measured phase pseudorange between the space vehicle  $i$  and the receiver  $k$  is given by

$$\Phi_k^i = \frac{\rho_k^i}{\lambda_F} + \frac{c}{\lambda_F} \cdot (\delta_k - \delta^i) + N_{Fk}^i \quad (1.31)$$

where  $F = 1,2$  for both the  $L_1$  and  $L_2$  carriers and  $N_{Fk}^i$  the integer ambiguity number. Multiplying eq. (1.31) by the wavelength of the carrier  $\lambda_F$  gives the received phase

$$L_k^i := \Phi_k^i \cdot \lambda_F = \rho_k^i + c \cdot \Delta\delta_k^i + n_{Fk}^i \quad (1.32)$$

where  $n_{Fk}^i$  is the unknown integer number of cycles: the so-called *initial phase ambiguity*.

### 1.2.3 Biases and error modelization

Both the code and phase pseudoranges are affected by systematic errors or biases and random noises. These errors fall into three separate categories, namely the satellite related errors, propagation medium related errors and receiver related errors.

Some of these systematic errors can be modeled and thus give rise to additional terms in the observation equations (1.19) and (1.31) and/or (1.32). These will be explained in the rest of this study. Other effects can be eliminated by proceeding with an adequate combination of the observables.

The satellite related errors are the clock and orbital errors. As mentioned earlier, the clock errors are for instance the drift of the atomic clocks aboard each GPS SV. The orbital errors are essentially the oscillatory motion of the SV along its assigned orbit as well as its tendency of de-orbiting as it evolves in Medium Earth Orbit (MEO).

The presence of the atmosphere between the GPS satellite and the receiver induces propagation errors in the signal. These are classified accordingly to the different layers of the atmosphere. Only the ionosphere and the troposphere play a major role. This topic will be approached later in chapter 3 in further details.

The receiver related errors are made of the clock error, the antenna phase center variation and multipath. As is the case for the SV, the ground receiver shows also a drift of its crystal clock. The antenna phase center is the point to which the measurement is referred and does usually not correspond to the geometric antenna center. The antenna center variation results from this difference and is specific for each tracked satellite. This error can be accurately corrected.

Multipath is caused by the multiple reflections of the signal along its path, i.e. the interference between direct and reflected signals. This is thus a frequency dependent effect. Hence phase PRs are more affected than code PRs. It is particularly important in a mountainous or urban environment where the presence of mountains or buildings in the direct vicinity of the receiver represent an important treat to the measurement accuracy. By specific protection of the receiver's antenna the impact of multipath on the measurement can be greatly reduced. For further details refer to [Geiger, 1988].

The different major types of GPS errors are summarized in Table 3 below:

Class	Name
Space vehicle	Clock bias Orbital errors
Signal propagation	Ionospheric refraction Tropospheric refraction
Receiver	Antenna phase center variation Clock bias Multipath

Table 3. Systematic errors in the GPS signal

Consider now the signal propagation errors. These are implicitly contained in the formulation of equations (1.19), (1.31) and (1.32).

On one hand, one distinguishes the ionospheric refraction and on the other hand the tropospheric refraction. These two atmospheric layers induce the most errors in the signal and are characterized each by a specific error term. Errors emanating from the other layers of the atmosphere are put into the global error terms (c.f. hereunder).

The ionosphere is a dispersive medium for microwave signals. Hence the refractive index is frequency dependent for GPS signals. Let  $I_k^i$  be the effect of the ionosphere on the first carrier  $L_1$ . As will be shown in 1.3.1., the ionospheric effect is in second order inversely proportional to the square of the carrier frequency. Hence the effect of the ionosphere on the second carrier  $L_2$  is

$$\frac{f_1^2}{f_2^2} \cdot I_k^i \quad (1.33)$$

The ionosphere delays the GPS code pseudorange and advances the carrier phases. The effect of the ionosphere has the same absolute value for code and phase measurements but with opposite signs.

The troposphere is the neutral non-ionized part of the Earth's atmosphere and also its lower layer. By opposition to the ionospheric refractive index, the tropospheric refractive index does not depend on the frequency. Hence the troposphere effect is the same on the code and phase pseudoranges. Let denote it by  $\Delta_k^{tropo\ i}$ .

With the above consideration and equations (1.19), (1.31) and (1.32), one finally obtains

$$\begin{aligned} PR_{1k}^i &= \rho_k^i + c \cdot \Delta \delta_k^i + I_k^i + \Delta_k^{tropo\ i} + \tilde{\varepsilon}_{PR_k^i} \\ PR_{2k}^i &= \rho_k^i + c \cdot \Delta \delta_k^i + \frac{f_1^2}{f_2^2} \cdot I_k^i + \Delta_k^{tropo\ i} + \tilde{\varepsilon}_{PR_k^i} \end{aligned} \quad (1.34a,b)$$

for the code pseudorange. For the phase pseudorange it holds

$$\begin{aligned} L_{1k}^i &= \rho_k^i + c \cdot \Delta \delta_k^i + \lambda_1 \cdot n_{1k}^i - I_k^i + \Delta_k^{tropo\ i} + \tilde{\varepsilon}_{L_k^i} \\ L_{2k}^i &= \rho_k^i + c \cdot \Delta \delta_k^i + \lambda_2 \cdot n_{2k}^i - \frac{f_1^2}{f_2^2} \cdot I_k^i + \Delta_k^{tropo\ i} + \tilde{\varepsilon}_{L_k^i} \end{aligned} \quad (1.35a,b)$$

Where the effects of both the ionosphere and the troposphere are stated explicitly. The other error terms from Table 3 are respectively contained in  $\tilde{\varepsilon}_{PR_k^i}$  for the code PRs and in  $\tilde{\varepsilon}_{L_k^i}$  for the phase PRs. The phase pseudorange are as sensitive to the effects of the atmosphere as the code pseudorange. However, GPS has been designed so that the former are usually used for high accuracy measurements.

## 1.3 Single and double differences

### 1.3.1 Ionospheric refraction

The ionosphere stretches between approximately 50 km and 1000 km above the surface of the Earth. It is a dispersive medium for both GPS carriers  $L_1$  and  $L_2$ . In a first step it is intended to derive the modified Rayleigh equation for group velocities and in a second step the ionospheric error.

#### 1.3.1.1 Modified Rayleigh Equation

First consider a single EM wave of wavelength  $\lambda$  propagating through the 3-dimensional space  $\mathbb{R}^3$ . Its *phase velocity* is defined by

$$v_{ph} := \frac{\omega(k)}{k} \quad (1.36)$$

where  $\omega(k)$  is the circular frequency in  $[\text{rad} \cdot \text{s}^{-1}]$  and  $k$  the norm of the wave vector  $\mathbf{k}$  in  $[\text{rad} \cdot \text{m}^{-1}]$ . There are further two symmetries for waves: a periodicity in space and a periodicity in time:

$$\begin{aligned}\omega \cdot T &= 2\pi \\ k \cdot \lambda &= 2\pi\end{aligned}\tag{1.37a,b}$$

where  $T$  is the period in seconds and  $\lambda$  the wavelength in meters. Inserting (1.37a,b) in (1.36) gives

$$v_{ph} := \frac{\omega(k)}{k} = \frac{\lambda}{T} = \lambda \cdot f\tag{1.38}$$

This is the propagation velocity for both  $L_1$  and  $L_2$  carriers. For a group waves with slightly different frequencies, the *group velocity* is of significance. It defined as

$$v_{gr} := \frac{d\omega(k)}{dk}\tag{1.39}$$

and is a gauge for the propagation of the resulting energy. Only this velocity is important for GPS PRs measurements. Using the fact that

$$\omega = 2\pi \cdot f = k \cdot \lambda \cdot f = c \cdot k\tag{1.40}$$

It can be expressed as a function of the wavelength by deriving (1.40) with respect to  $\lambda$

$$v_{gr} := \frac{d\omega(k)}{dk} = -\frac{df}{d\lambda} \cdot \lambda^2\tag{1.41}$$

Building the derivative of the phase velocity with respect to the wavelength yields to

$$\frac{dv_{ph}}{d\lambda} = f + \lambda \cdot \frac{df}{d\lambda}\tag{1.42}$$

Hence

$$\frac{df}{d\lambda} = \frac{1}{\lambda} \cdot \frac{dv_{ph}}{d\lambda} - \frac{f}{\lambda}\tag{1.43}$$

Inserting eq. (1.43) in eq. (1.41) gives

$$v_{gr} = -\lambda \cdot \frac{dv_{ph}}{d\lambda} + f \cdot \lambda\tag{1.44}$$

Combining eq. (1.44) with eq. (1.38) one obtains

$$v_{gr} = v_{ph} - \lambda \cdot \frac{dv_{ph}}{d\lambda}\tag{1.45}$$

i.e. the known *Rayleigh equation* which contains the dispersion effects. For a non-dispersive medium such as the troposphere for GPS signals, it reduces to

$$v_{gr} = c = v_{ph}\tag{1.46}$$

Further introduce the refractive index  $n$  for refractive media. Hence the propagation velocity is given by

$$v = \frac{c}{n}\tag{1.47}$$

using the phase and group velocity concepts, one has in a similar way

$$v_{ph} = \frac{c}{n_{ph}} \quad \text{and} \quad v_{gr} = \frac{c}{n_{gr}}\tag{1.48a,b}$$

Differentiate eq. (1.48a) with respect to the wavelength

$$\frac{dv_{ph}}{d\lambda} = c \cdot \left[ -\frac{dn_{ph}}{d\lambda} \right] \cdot \frac{1}{n_{ph}^2} \quad (1.49)$$

Inserting this into the Rayleigh equation (1.45) gives

$$v_{gr} = \lambda \cdot c \cdot \frac{dn_{ph}}{d\lambda} \cdot \frac{1}{n_{ph}^2} + v_{ph} \stackrel{!}{=} \frac{c}{n_{gr}} \quad (1.50)$$

where eq (1.48b) has been set. Now, insert eq. (1.48a) into eq. (1.50) and obtain

$$\frac{1}{n_{gr}} = \frac{1}{n_{ph}} + \frac{\lambda}{n_{ph}^2} \cdot \frac{dn_{ph}}{d\lambda} = \frac{1}{n_{ph}} \cdot \left[ 1 + \frac{\lambda}{n_{ph}} \cdot \frac{dn_{ph}}{d\lambda} \right] \quad (1.51)$$

Inverting this gives

$$n_{gr} = n_{ph} \cdot \left[ 1 + \frac{\lambda}{n_{ph}} \cdot \frac{dn_{ph}}{d\lambda} \right]^{-1} \quad (1.52)$$

Proceed with a Taylor expansion for the term in square brackets accordingly to

$$[1 + \varepsilon]^{-1} = 1 - \varepsilon + O(\varepsilon^2) \quad (1.53)$$

Eq. (1.52) is thus reduced in first order to

$$n_{gr} \approx n_{ph} \cdot \left[ 1 - \frac{\lambda}{n_{ph}} \cdot \frac{dn_{ph}}{d\lambda} \right] = n_{ph} - \lambda \cdot \frac{dn_{ph}}{d\lambda} \quad (1.54)$$

Express it as a function of the frequency. Therefore derive the wavelength

$$\lambda = \frac{c}{f} \quad (1.55)$$

with respect to the frequency

$$\frac{d\lambda}{df} = -\frac{c}{f^2} \quad (1.56)$$

and insert it into eq. (1.54)

$$n_{gr} = n_{ph} - \frac{c}{f} \cdot \frac{dn_{ph}}{df} \cdot \frac{df}{d\lambda} = n_{ph} - \frac{c}{f} \cdot \frac{dn_{ph}}{df} \cdot \left( \frac{-f}{c^2} \right) \quad (1.57)$$

Finally one has

$$n_{gr} = n_{ph} + f \cdot \frac{dn_{ph}}{df} \quad (1.58)$$

Eq. (1.58) is the so-called *modified Rayleigh equation*.

### 1.3.1.2 Ionospheric path delay

According to [Davies, 1990] the index of refraction  $n$  for an ionized gas is derived from the *Appleton-Hartree equations*. It is given by the *formula of dispersion*

$$n^2 = 1 - \left( \frac{\omega}{\omega_p} \right)^2 = 1 - \frac{n_e}{\pi \cdot m_e} \cdot \left[ \frac{C \cdot e}{f} \right]^2 \quad (1.59)$$

where  $e$  is the electron charge,  $m_e$  the electron mass,  $n_e$  the electron density,  $f$  the frequency and  $C = 40.3$  [Hz<sup>2</sup>] a constant. Following [Seeber, 1993], the refraction coefficient accounting for the propagation of phases can be written as a power series

$$n_{ph} = 1 + \frac{c_2}{f^2} + \frac{c_3}{f^3} + \frac{c_4}{f^4} + \dots \quad (1.60)$$

Where the expansion coefficients  $c_i, i = 2, 3, 4, \dots$  do not depend on the frequency but on the electron density along the signal path. Proceeding with the expansion of eq. (1.55) up to the second order, one finds

$$n_{ph} \cong 1 + \frac{c_2}{f^2} \quad \text{where} \quad c_2 = -C \cdot n_e \quad (1.61)$$

Differentiating Eq. (1.61) with respect to the frequency yields to

$$\frac{dn_{ph}}{df} = -2 \cdot \frac{c_2}{f^3} \quad (1.62)$$

Inserting eq. (1.62) into eq. (1.58) gives

$$n_{gr} = 1 + \frac{c_2}{f^2} + f \cdot \left[ -\frac{2 \cdot c_2}{f^3} \right] \cong 1 - \frac{c_2}{f^2} \quad (1.63)$$

Hence the effect of the ionosphere on the group and phase velocities is nearly equal in magnitude but with opposite signs. Using eq. (1.61) and noting that it always holds  $n_e > 0$ , one can deduce that the group refractive index is bigger than the phase refractive index. Hence, it follows that

$$v_{gr} < v_{ph} \quad (1.64)$$

in the ionosphere. This has important consequences on the GPS signal propagation through this layer of the atmosphere, namely the code pseudoranges are delayed while the phase pseudoranges are advanced i.e. they are respectively measured too long and too short with respect to the geometric range  $\rho_k^i$ .

The *Fermat's principle* states that the measured range  $s$  is given by the integral over the whole ray path of the refractive index  $n$ , i.e. it holds

$$s = \int_{\text{ray path}} n(s') ds' \quad (1.65)$$

Furthermore the geometric path is given by the direct line or line of sight (LOS) between the space vehicle  $i$  and the receiver  $k$ . Thus  $n(s) = 1$  that is

$$s_0 = \int_{\text{straight line}} ds' \quad (1.66)$$

The influence of the ionospheric refraction is determined by the difference between the observed range and the geometric distance between SV and receiver. Hence one has

$$I_k^i = \Delta_k^{iono i} = \int n(s) ds - \int ds_0 \quad (1.67)$$

For the phase refractive index and with eq. (1.61) it follows that

$$\Delta_{ph k}^{iono i} = \int \left[ 1 + \frac{c_2}{f^2} \right] ds - \int ds_0 = \int \frac{c_2}{f^2} ds + \int ds - \int ds_0 \quad (1.68)$$

It is here referred to Figure 3 hereunder. In a first approximation integrate along a straight line, for instance the geometric path. Hence  $ds = ds_0$  and the difference of the two last integrals on the right hand side (RHS) of eq. (1.68) vanishes, i.e.

$$\Delta_{phk}^{iono} \approx \int \frac{c_2}{f^2} ds \quad (1.69)$$

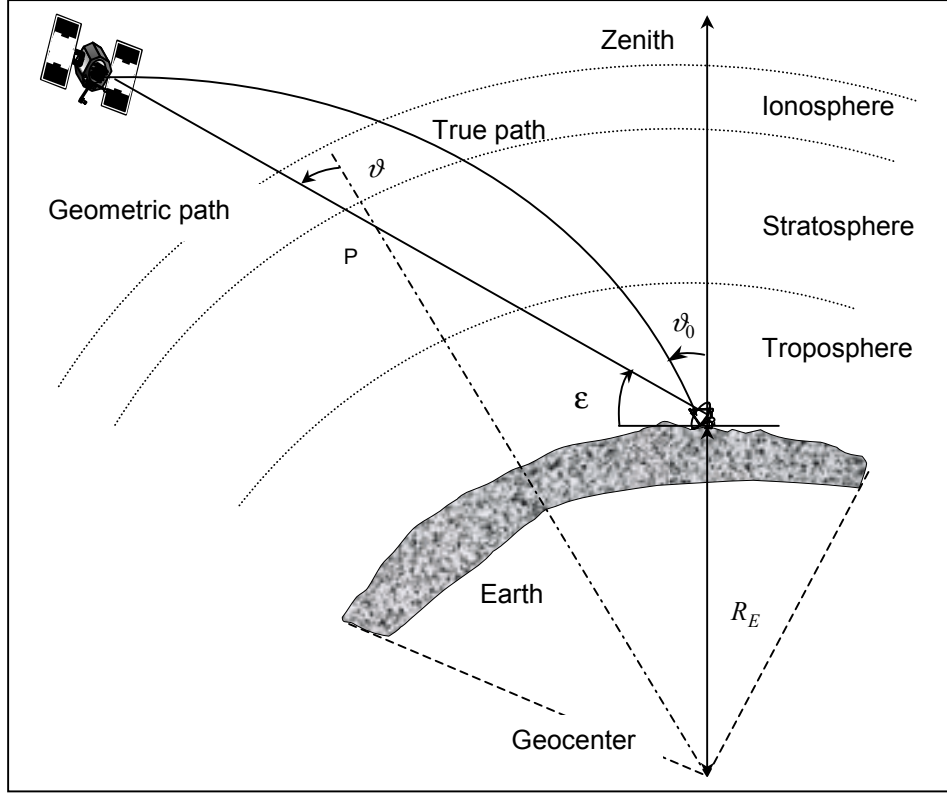


Figure 3. Signal bending and slant path delay

In a similar way, using eq. (1.63) it holds

$$\Delta_{grk}^{iono} \approx - \int \frac{c_2}{f^2} ds \quad (1.70)$$

Using the fact that  $f \neq f(s_0)$  and eq. (1.61), one obtains

$$\Delta_{ph,grk}^{iono} = \mp \frac{C}{f^2} \int n_e ds_0 \quad (1.71)$$

where the minus sign is for the phase ionospheric delay and the plus sign for the group ionospheric delay. Introduce now the notion of *total electron content* (TEC). It is defined as

$$TEC := \int n_e ds_0 \quad (1.72)$$

and corresponds to the amount of electrons present in a cylindrical column with base area  $1 \text{ m}^2$  stretching above the receiver up to the altitude of the GPS satellite. It is usually given in units of  $10^{16} \text{ e}^-/\text{m}^2$ . Inserting eq. (1.72) in eq. (1.71) gives the phase respectively group ionospheric delay in meters

$$\Delta_{phk}^{iono} = - \frac{C}{f^2} \cdot TEC = - \Delta_{grk}^{iono} \quad (1.73)$$

Usually the notion of Total Vertical Electron Content (TVEC) or Total Overhead Electron Content is rather used instead of the TEC. As the TEC depends on the position of the space vehicle and is computed in line of sight, it is

necessary to project it along the zenith direction in order to obtain a reference measure. Hence, for arbitrary LOS, the zenith angle of the satellite must be taken into account.

$$I(f) = \Delta^{iono} = \chi_j \cdot \frac{C}{\cos \vartheta'} \cdot \frac{TVEC}{f^2} \quad (1.74)$$

where

$$\chi_j = \begin{cases} +1 & , j = gr \\ -1 & , j = ph \end{cases} \quad (1.75)$$

and  $\vartheta'$  is the zenith angle of a infinitesimal volume element at altitude  $z$ . For code pseudorange measurements the formulation of equations (1.74) and (1.75) with respect to the group velocities sets the benchmark.

### 1.3.2 Clock Errors

As mentioned earlier, the SV's clocks show a tendency to drift over a long period of time. Although the 'Delta-V repositioning' maneuver which is performed once a year for each space vehicle is associated with an evacuation of the atomic clock's beam tubes, a residual error remains and must be modeled before partial removal.

A model derived by [Jorgensen, 1986], for geodetic uses, is presented here. The relativistic time correction term is given by

$$\Delta t_{rel} = \tilde{G} \cdot e \cdot \sqrt{A} \sin E_k \quad (1.76)$$

where  $e$  is the orbit eccentricity,  $A$  is the orbit's ellipse semi-major axis and  $E_k$  is the eccentric anomaly at time  $t_k$ . Further, it holds

$$\tilde{G} = \frac{-2\sqrt{\eta}}{c} \quad (1.77)$$

where  $\eta$  is the Earth's universal gravitational parameter. Thus the clock error of 1.2.1 is given by

$$\Delta \delta = a_0 + a_1 \cdot (t_{rec} - t_{cr}) + a_2 \cdot (t_{rec} - t_{cr})^2 + \Delta t_{rel} \quad (1.78)$$

where the three polynomial coefficients are taken from the navigation message,  $t_{rec}$  is the received time by the SV and  $t_{cr}$  is the atomic clock data reference time in seconds.

Further, this kind of correction is often not totally adequate and one wants to remove totally all the clock-related errors from the measurements. This is achieved by forming so-called single and then double differences.

### 1.3.3 Single difference

Consider the observation equation for the measured phase pseudorange  $\Phi$ , which expression in cycles (1.31) was derived in 1.2.2.

$$\Phi(t) = \frac{\rho(t)}{\lambda} + \frac{c}{\lambda} \cdot \Delta \delta(t) + N \quad (1.79)$$

where  $\lambda$  is the wavelength,  $N$  is the ambiguity phase number and  $\rho(t)$  the geometric range between the SV and the ground-based receiver. Split the bias term into two parts, one for the unknown receiver-related biases the other for the known SV-related errors [via equation (1.78)]. It holds with eq. (1.23)

$$\Delta \delta(t) = \delta_{sat}(t) - \delta_{rec}(t) \quad (1.80)$$

Using now the definition of the frequency

$$f = \frac{c}{\lambda} \quad (1.81)$$

and (1.80), equation (1.79) becomes

$$\Phi(t) - f \cdot \delta_{sat}(t) = \frac{\rho(t)}{\lambda} + N - f \cdot \delta_{rec}(t) \quad (1.82)$$

Consider now two different receivers  $k$  and  $l$  at two separate locations for instance but not necessarily on the ground and let – as usual –  $i$  be the SV number. Then it holds

$$\Phi_x^i(t) - f^i \cdot \delta_{sat}^i(t) = \frac{\rho_x^i(t)}{\lambda} + N_x^i - f^i \cdot \delta_{rec}^i(t) \Big|_x, \quad x = k, l \quad (1.83)$$

The clock errors related to the receiver being independent of the SV, these carry no subscript  $i$ . Build the difference now of (1.83) for each of the station.

$$\Phi_k^i(t) - \Phi_l^i(t) = \frac{1}{\lambda} \cdot [\rho_k^i(t) - \rho_l^i(t)] + N_k^i - N_l^i - f^i \cdot [\delta_{rec}^i(t) \Big|_k - \delta_{rec}^i(t) \Big|_l] \quad (1.84)$$

This is the *phase pseudorange single difference*. Similarly, using eq. (1.32) yields to

$$L_{Fkl}^i(t) := L_{Fk}^i(t) - L_{Fl}^i(t) \quad (1.85)$$

One should note that the SV-related clock errors have been removed thus eliminating errors due to clock dithering (c.f. [Rocken and Meertens, 1991]). However, the receiver-related clock errors remain. It is often suitable to remove them from the computation and thus completely eliminate clock errors. This is provided by performing the double differences.

From now onwards, to simplify the expressions, use the following conventions

$$Y_{kl}^i(t) := Y_k^i(t) - Y_l^i(t), \quad Y = \Phi, PR \quad Y_{kl}^i(t) := \rho_k^i(t) - \rho_l^i(t) \quad N_{kl}^i := N_k^i - N_l^i \quad (1.86)$$

### 1.3.4 Double difference

Consider two different SV labeled  $i$  and  $j$ . Setting (1.84) in (1.86) yields

$$\Phi_{kl}^m(t) = \frac{\rho_{kl}^m(t)}{\lambda} + N_{kl}^m - f^m \cdot \delta_{kl}^m(t), \quad m = i, j \quad (1.87)$$

Assume both stations are tracking different SV but on the same frequency, that is  $f^i = f^j$  and the wavelength is the same for both receivers  $\lambda^i = \lambda^j \equiv \lambda$ . Thus form the difference of (1.87) for each satellite

$$\Phi_{kl}^{ij}(t) := \Phi_{kl}^i(t) - \Phi_{kl}^j(t) = \frac{1}{\lambda} \cdot [\rho_{kl}^i(t) - \rho_{kl}^j(t)] + N_{kl}^i - N_{kl}^j \quad (1.88)$$

It is the *phase pseudorange double difference*. This equation shows no dependency of any kind on clock errors and is therefore widely used in combination with the ionosphere-free code pseudorange linear combination. However the carrier ambiguities  $N_{kl}^x, x = i, j$  are still there. It is possible to resolve these ambiguities by using filtering techniques. It is here referred to 1.5.

Now do the same for eq. (1.32) and get

$$\begin{aligned} L_{1kl}^{ij} &= \rho_{kl}^{ij} + \lambda_1 \cdot n_{1kl}^{ij} - I_{1kl}^{ij} + \Delta_{kl}^{tropo \ ij} \\ L_{2kl}^{ij} &= \rho_{kl}^{ij} + \lambda_2 \cdot n_{2kl}^{ij} - \frac{f_1^2}{f_2^2} I_{2kl}^{ij} + \Delta_{kl}^{tropo \ ij} \end{aligned} \quad (1.89)$$

In a similar way for the code pseudoranges (1.19) one obtains the *code pseudoranges double differences*

$$\begin{aligned} PR_{1kl}^{ij} &= \rho_{kl}^{ij} + I_{kl}^{ij} + \Delta_{kl}^{tropo \ ij} \\ PR_{2kl}^{ij} &= \rho_{kl}^{ij} + \frac{f_1^2}{f_2^2} \cdot I_{kl}^{ij} + \Delta_{kl}^{tropo \ ij} \end{aligned} \quad (1.90)$$

Again, no terms corresponding to the receiver and SV clock errors appear in the equations (1.89) and (1.90). It has been assumed that the receiver clock errors are known with enough accuracy in order to compute the geometric range with sufficient precision.



## 1.4 Linear combinations

Various errors influence the observed pseudoranges. In order to constrain their impact on the signal accuracy, it is often useful to form linear combinations (LC) of the code and phase pseudoranges. The most widely used are presented hereunder.

### 1.4.1 Ionosphere free LC $L_3$

Various derivation of the ionosphere-free pseudoranges exist, e.g. in [Botton, 1997], but all lead to the same aim, the cancellation of the ionospheric refraction from the measurements.

The ionospheric refraction  $\Delta^{iono}$  is given by eq. (1.74) and eq. (1.75). The measured code pseudorange to satellite  $i$  has been modeled in 1.2.1., eq. (1.19) as

$$PR_k^i = \rho_k^i + c \cdot \Delta\delta_k^i + \varepsilon_{PR_k^i} = \rho_k^i + \Delta\rho_k^i + \varepsilon_{PR_k^i} \quad (1.91)$$

where  $\Delta\delta_k^i$  is the clock error and  $\varepsilon_{PR_k^i}$  the global error balance. Thus replacing  $\varepsilon_{PR_k^i}$  by the corresponding ionospheric delay (ignore for the moment the other error sources) and letting aside the subscripts  $i$  and  $k$ , one obtains:

$$PR^F = \rho + c \cdot \Delta\delta + \Delta^{iono}(\lambda_F), \quad F = 1,2 \quad (1.92)$$

The standard procedure is to form now a linear combination of code pseudoranges, defined as

$$PR^{1,2} = m_1 \cdot PR^1 + m_2 \cdot PR^2 \quad (1.93)$$

where  $m_1$  and  $m_2$  are both integers that will be later determined. Setting (1.92) into (1.93) and reminding that one wants to eliminate the ionospheric refraction yields to

$$m_1 \cdot \Delta^{iono}(f_1) + m_2 \cdot \Delta^{iono}(f_2) = 0 \quad (1.94)$$

As the ionospheric refraction delays are nearly always not zero, one can divide by the first term:

$$m_2 = -\frac{\Delta^{iono}(f_2)}{\Delta^{iono}(f_1)} \cdot \frac{1}{m_1} \quad (1.95)$$

One can set the arbitrary coefficient  $m_1$  equal to 1 without loss of generality. Thus using the relationship (1.74) where the dependency of the ionospheric path delay on the frequency clearly appears, one has

$$m_2 = -\frac{\Delta^{iono}(f_2)}{\Delta^{iono}(f_1)} = -\frac{f_2^2}{f_1^2} \text{ and } m_1 = 1 \quad (1.96)$$

The ionosphere-free code pseudorange linear combination becomes then

$$PR^{1,2} = PR^1 - \frac{f_2^2}{f_1^2} \cdot PR^1 \quad (1.97)$$

In a similar way an ionosphere-free phase pseudorange formula can be derived except that there is now the ambiguity  $N$  to take into account. The carrier phase pseudoranges were expressed by eq. (1.31) in 1.2.2 for a single measurement as

$$\Phi = \frac{\rho}{\lambda} + \frac{c}{\lambda} \cdot \Delta\delta + N \quad (1.98)$$

Thus subtracting the ionosphere refraction term, it yields for each carrier to

$$\Phi_F = \frac{\rho}{\lambda_F} + \frac{c}{\lambda_F} \cdot \Delta\delta + N_F - \Delta^{iono}(f_F), \quad F = 1,2 \quad (1.99)$$

Using the definition of the frequency of a wave,  $f = c/\lambda$  one gets

$$\Phi_F = \frac{R}{\lambda_F} + f_F \cdot \Delta\delta + N_F - \Delta^{iono}(f_F), \quad F=1,2 \quad (1.100)$$

Proceeding as for the ionosphere-free code pseudorange, a linear combination of phase pseudorange is obtained

$$\Phi_{1,2} = u_1 \cdot \Phi_1 + u_2 \cdot \Phi_2 \quad (1.101)$$

where  $u_1$  and  $u_2$  are both arbitrary coefficients. Set then (1.100) in (1.101)

$$\Phi_{1,2} = R \cdot \left[ \frac{u_1}{\lambda_1} + \frac{u_2}{\lambda_2} \right] + [u_1 \cdot f_1 + u_2 \cdot f_2] \cdot \Delta\delta + u_1 \cdot N_1 + u_2 \cdot N_2 - Z \quad (1.102)$$

where  $Z$  is the quantity that must be set to zero

$$Z := \frac{u_1}{\lambda_1} \cdot \Delta^{iono}(f_1) - \frac{u_2}{\lambda_2} \cdot \Delta^{iono}(f_2) \stackrel{!}{=} 0 \quad (1.103)$$

The arbitrary coefficient  $u_1$  can be set equal to 1 for commonality but without any loss of generality, and it holds

$$u_2 = -\frac{\lambda_2}{\lambda_1} \cdot \frac{\Delta^{iono}(f_1)}{\Delta^{iono}(f_2)} \quad \text{and} \quad u_1 = 1 \quad (1.104)$$

The velocity of light can be expressed with respect to the frequency by using the definition of  $f$ ,  $c = \lambda \cdot f$  and using equation (1.74), one has

$$u_2 = -\frac{f_1}{f_2} \cdot \frac{f_2^2}{f_1^2} = -\frac{f_2}{f_1} \quad \text{and} \quad u_1 = 1 \quad (1.105)$$

Thus one obtains the classical ionosphere-free phase pseudorange linear combination

$$\Phi_{1,2} = \Phi_1 - \frac{f_2}{f_1} \Phi_2 \quad (1.106)$$

This model of ionosphere-free pseudorange is widely use in the dual frequency receivers in order to remove all delays due to the presence of the ionosphere in the atmosphere.

Another linear combination for the *ionosphere-free phase pseudorange* has been computed by [Spilker, 1978]. It is derived from the known dispersive behavior of the ionospheric electron plasma. Define the new 'combined' carrier as

$$L_3 := \frac{f_1^2 \cdot L_1 - f_2^2 \cdot L_2}{f_1^2 - f_2^2} \quad (1.107)$$

where  $L_1$  and  $L_2$  are defined by eq. (1.32). Hence it holds with the conventions introduced before

$$\Phi_{1,2} = \frac{f_1^2}{f_1^2 - f_2^2} \cdot \Phi_1 - \frac{f_2^2}{f_1^2 - f_2^2} \cdot \Phi_2 \equiv \Phi_3 \quad (1.108)$$

It is sometimes known as  $\Phi_3$  where the index 3 simply designates a linear combination of both carrier frequencies  $L_1$  and  $L_2$ . Hence, inserting the known frequencies of the carriers (1.2), equation (1.107) can be approximated as

$$\Phi_{1,2} \approx 2.5 \cdot \Phi_1 - 1.5 \cdot \Phi_2 \quad (1.109)$$

Further, the linear combination of the code pseudoranges yields to

$$PR_3 = \frac{1}{f_1^2 - f_2^2} [f_1^2 \cdot PR_1 - f_2^2 \cdot PR_2] \quad (1.110)$$

Looking at eq. (1.107) and eq. (1.101), one can see that of all the layers of the atmosphere, only residuals generated by the troposphere induce a large delay in the transmitted signal. This will be the main topic of Chapter 3.

Take now into account the double difference phase pseudorange (1.89) and continue to neglect the effect of the troposphere. It then holds

$$L_{3kl}^{ij} = \rho_{kl}^{ij} + B_{3kl}^{ij} \quad (1.111)$$

where the ionosphere free bias  $B_{3kl}^{ij}$  is given by

$$B_{3kl}^{ij} = \frac{1}{f_1^2 - f_2^2} \cdot \left[ f_1^2 \cdot \lambda_1 \cdot n_{1kl}^{ij} - f_2^2 \cdot \lambda_2 \cdot n_{2kl}^{ij} \right] \quad (1.112)$$

Equation (1.112) cannot be expressed as a linear function of the integer ambiguity  $n_{3kl}^{ij}$ , i.e.

$$B_{3kl}^{ij} \neq \text{const} \cdot \lambda_3 \cdot n_{3kl}^{ij} \quad (1.113)$$

where the wavelength of the combined carrier is

$$\lambda_3 = \frac{c}{\lambda_1 + \lambda_2} \quad (1.114)$$

If the wide lane combination  $L_5$  (c.f. 1.4.3.) is known, it is possible to write the ionosphere free bias as

$$B_{3kl}^{ij} = c \cdot \frac{f_2}{f_1^2 - f_2^2} \cdot n_{5kl}^{ij} + \frac{c}{\lambda_3} \cdot n_{1kl}^{ij} \quad (1.115)$$

where the first term on the right hand side is known and the so-called *narrow lane ambiguity*  $n_{1kl}^{ij}$  is unknown.

### 1.4.2 Geometry free LC $L_4$

The coefficients of the linear combination

$$L_4 = \alpha_1 \cdot L_1 + \alpha_2 \cdot L_2, \quad \alpha_1, \alpha_2 \in \mathbb{R} \quad (1.116)$$

are chosen in such a way that the geometric range  $\rho_k^i$  vanishes from the expression. Hence it holds

$$L_4 := L_1 - L_2 \quad (1.117)$$

The same is done with the code pseudoranges

$$PR_4 = PR_1 - PR_2 \quad (1.118)$$

combining eq. (1.35a,b) with eq. (1.117) yields to

$$L_4 = \lambda_1 \cdot n_1 - \lambda_2 \cdot n_2 + \left( \frac{f_1^2}{f_2^2} - 1 \right) \cdot I_k^i \quad (1.119)$$

and is a function of only the ionospheric path delay and the initial phase ambiguities. The main advantage of this combination is that the clock errors on both sides (SV and receiver) as well as the geometric range do not appear explicitly. However, the major issue with that linear combination consists in the fact that the resulting bias  $B_4$  is not an integer any more.

### 1.4.3 Wide lane LC $L_5$

The *wide lane linear combination* is used to fix eventual cycle slips and to resolve the ambiguity. Cycle slips occur when the receiver loses phase lock on the GPS satellite signal. It is defined as

$$L_5 := \frac{f_1 \cdot L_1 - f_2 \cdot L_2}{f_1^2 - f_2^2} \quad (1.120)$$

Neglecting the influence of both the ionosphere and the troposphere, one has

$$L_{5kl}^{ij} = \rho_{kl}^{ij} + \frac{c}{f_1 - f_2} \cdot (n_{1kl}^{ij} - n_{2kl}^{ij}) = \rho_{kl}^{ij} + \lambda_5 \cdot n_{5kl}^{ij} \quad (1.121)$$

Because the wavelength  $\lambda_5$  is approximately four times longer than the wavelength of the  $L_1$  and  $L_2$  carriers, the  $L_5$  linear combination is called wide lane. The wide lane ambiguity of eq. (1.121) is given by

$$n_{5kl}^i = n_{1kl}^i - n_{2kl}^i \quad (1.122)$$

For further details on the wide lane LC, refer to [Cocard and Geiger, 1992].

#### 1.4.4 Melbourne-Wübbena LC $L_6$

The idea of [Melbourne, 1985] and [Wübbena, 1985] is to linearly combine both the carrier phase and the P-code in order to eliminate the effects of the ionosphere and troposphere along the geometry and clock errors. The *Melbourne-Wübbena linear combination*  $L_6$  is defined as

$$L_6 \doteq \frac{1}{f_1 - f_2} \cdot [f_1 \cdot L_1 - f_2 \cdot L_2] - \frac{1}{f_1 + f_2} \cdot [f_1 \cdot PR_1 - f_2 \cdot PR_2] \quad (1.123)$$

After [Fridez et al., 2001], one obtains for double difference observations

$$L_{6kl}^i = \lambda_6 \cdot n_{6kl}^i \quad (1.124)$$

Although the advantages of this linear combination are clear, the systematic errors are here not constrained but vary proportionally to the wavelength. Hence a linear combination with a large wavelength does automatically have a strong ionospheric sensitivity.

The code and phase PRs linear combinations presented above are summarized along their wavelengths in Table 4 hereunder:

LC	Designation	Equation	Wavelength [cm]
$L_1$	Basic carrier	(1.2)	19.04
$L_2$	Basic carrier	(1.2)	24.45
$L_3$	Ionosphere free LC	(1.107)	10.70
$L_4$	Geometry free LC	(1.119)	$\infty$
$L_5$	Wide lane LC	(1.120)	86.20
$L_6$	Melbourne-Wübbena LC	(1.123)	86.20

Table 4. Code and phase linear combinations, after [Fridez et al., 2001]

The four last linear combinations of Table 4 allow for the elimination or partial removal of most of the GPS errors presented in Table 3. However, the remaining combined errors are increasing very rapidly with time. Hence, linear combinations are not entirely satisfactory but are commonly used while processing the GPS signal.

## 1.5 Ambiguity resolution

The ambiguity resolution consists in determining the number of integer cycles done by the phase when the signal arrives to the GPS receiver. It is a major task of the receiver to find these and to remove it. Indeed a small slip in phase, i.e. a small variation of the ambiguity term  $N$  would introduce a large uncertainty in the code pseudorange.  $N$  depends on both the tracked SV and the time at which the signal is emitted.

Unfortunately the Global Positioning System does not provide more than two basic carrier frequencies. Hence specific strategies were developed to solve the ambiguity issue. The main approaches are presented hereunder.

### 1.5.1 Combination of phase and code PRs

The procedure first formulated by [Remondi, 1990], where the ambiguities are resolved by combining the dual carrier frequencies code and phase pseudoranges, is presented here.

Reminding the navigation solution, i.e. the observables are the code and phase pseudoranges given by equations (1.11) and (1.23) where the subscript  $i$  indicates the tracked satellite,  $\varepsilon_{PR}$  is the global error term and  $N$  is the ambiguity number. The range  $\rho_i$  is measured simultaneously on both frequency channels and is thus the same for both  $L_1$  and  $L_2$ . Therefore no label  $i$  will be applied on it in the following. Multiplying  $\rho$  by the wavelength allows

to express it in terms of cycles<sup>4</sup>. Using the relationship (1.81) between frequency and wavelength and introducing the ionosphere contribution to the pseudoranges, equation (1.74)

$$\Delta^{iono}(f) = \frac{A}{f^2} \quad \text{where} \quad A := \chi_j \cdot \frac{C \cdot TVEC}{\cos \theta'} \equiv \text{const} \quad (1.125)$$

one has for (1.19) and (1.31) expressed in cycles of  $L_1$  and  $L_2$

$$\begin{aligned} \Phi_F &= \frac{\rho}{c} \cdot f_F - \frac{\kappa}{f_F} + N_F + f_F \cdot \Delta\delta, \quad F = 1,2 \\ PR_F &= \frac{R}{c} \cdot f_F + \frac{\kappa}{f_F} + f_F \cdot \Delta\delta, \quad F = 1,2 \end{aligned} \quad (1.126a,b)$$

where the constant kappa is defined as

$$\kappa := \frac{A}{c} \quad (1.127)$$

Subtracting (1.126a) and (1.126b) yields to

$$\Phi_F - PR_F = -\frac{2\kappa}{f_F} + N_F, \quad F = 1,2 \quad (1.128)$$

Difference (1.128) for each carrier  $L_1$  and  $L_2$

$$\Phi_1 - \Phi_2 - PR_1 + PR_2 = 2\kappa \cdot \left[ \frac{1}{f_2} - \frac{1}{f_1} \right] + N_1 - N_2 \quad (1.129)$$

Let the difference of phase pseudoranges in (1.129) be labeled by a capital delta, indicating a difference. This is similarly done each time such difference of the same parameters for each carrier arises. The code pseudoranges  $PR$  are the sole exception. Thus (1.129) is reformulated as

$$\Delta\Phi - PR_1 + PR_2 = 2\kappa \cdot \left[ \frac{1}{f_2} - \frac{1}{f_1} \right] + \Delta N \quad (1.130)$$

It is intended to express the relative ambiguity  $\Delta N$  in terms of the known parameters. Divide (1.126b) by the corresponding carrier frequency and subtract for each carrier yields

$$\frac{PR_1}{f_1} - \frac{PR_2}{f_2} = \kappa \cdot \left[ \frac{1}{f_2^2} - \frac{1}{f_1^2} \right] \quad (1.131)$$

Recombining this, using the perfect square laws and dividing by  $f_1 + f_2$ , one has

$$\frac{1}{f_2} - \frac{1}{f_1} = \frac{f_1 - f_2}{f_1 \cdot f_2} = \frac{1}{\kappa} \cdot \frac{f_2 \cdot PR_1 - f_1 \cdot PR_2}{f_1 + f_2} \quad (1.132)$$

Substitute (1.132) into (1.130) gives

$$N_5 = N_1 - N_2 = \Phi_1 - \Phi_2 - \frac{f_1 - f_2}{f_1 + f_2} \cdot [PR_1 + PR_2] \equiv N_w \quad (1.133)$$

Thus the difference in ambiguity parameters can be measured. Note that eq. (1.133) is the *wide lane ambiguity* and is therefore independent of the baseline length and of the ionospheric effects. Although all modeled systematic effects completely cancel out, the multipath effect<sup>5</sup> remains and strongly affects the wide lane ambiguity.

<sup>4</sup> C.f. equation (1.19).

<sup>5</sup> Multipath can intrinsically not be modeled due to its physical origin. It can solely be reduced for instance by protecting the receiver antenna from multiple reflections of the incoming space signal.

Further, [Hofmann-Wellenhof, 1997] shows that it is possible to determine the ambiguity parameter for each carrier by adequately combining equations (1.133) and (1.126a). These again demonstrate the important accuracy of the phase pseudorange. Multiply (1.126a) with  $\lambda_F$ ,  $F = 1, 2$  and divide for both carriers. This gives

$$f_2 \cdot \Phi_2 - f_1 \cdot \Phi_1 = \frac{\rho}{c} \cdot [f_2^2 - f_1^2] + \Delta\delta \cdot [f_2^2 - f_1^2] + f_2 \cdot N_2 - f_1 \cdot N_1 \quad (1.134)$$

Inserting eq. (1.133), i.e. eq. (1.122) into eq. (1.134) yields to

$$f_2 \cdot \Phi_2 - f_1 \cdot \Phi_1 = \left[ \frac{\rho}{c} + \Delta\delta \right] \cdot [f_2^2 - f_1^2] - f_2 \cdot N_5 + N_1 \cdot [f_2 - f_1] \quad (1.135)$$

Finally, one has

$$N_1 = \frac{f_1}{f_1 - f_2} \cdot \Phi_1 - \frac{f_2}{f_1 - f_2} \cdot [\Phi_2 + N_5] - \left[ \frac{\rho}{c} + \Delta\delta \right] \cdot [f_1 + f_2] \quad (1.136)$$

It should be remarked, that the true range  $\rho$  contains no subscripts, and is therefore the same for both carriers. This is due to the fact that the receiver tracks the same space vehicle simultaneously on both the  $L_1$  and  $L_2$  carriers. The technique presented above is well adapted for example for instantaneous ambiguity resolutions such as in navigation applications.

## 1.5.2 SEARCH algorithm

At least four GPS space vehicles are required to determine the exact location of the ground-based receiver. If one redundant satellite is available, the ambiguity can then be numerically resolved by proceeding with a least square adjustment. Thus, these are estimated as float numbers. For short baselines (less than 10 km) and for long observation windows (about an hour), these float numbers are approximately integers.

This least square search technique has been developed by R. Hatch. As a consequence of the linearization of the observation equations (1.19) and (1.31), the knowledge of the approximate position of the ground receiver is required. This can be obtained from a code range solution. The search range is limited to a cube of radius  $3 \cdot \sigma$ . Assume that the GPS receiver is tracking simultaneously more than four SVs of the constellation. The satellites are divided in two groups, the first containing four SVs. Based on these four SVs, which are assumed to have acceptable Position Dilution of Precision (PDOP), the possible ambiguities are determined using the method presented in 1.5.1. Consider now eq. (1.89) and move the ambiguities to the LHS as is they were known. One has

$$L_{Fkl}^j(t) - \lambda_F \cdot n_{Fkl}^j = \lambda_F \cdot \Phi_{Fkl}^j(t) - N_{Fkl}^j = \rho_{kl}^j(t) + noise \quad (1.137)$$

As far as the first group of satellites is concerned, one obtains three equations of the form of eq. (1.129). From this, the corresponding  $3 \times 3$  design matrix is build. The three unknown receiver coordinates are obtained by linearizing  $\rho_{kl}^j(t)$  and inverting the design matrix. By slightly varying the ambiguities a full set of solutions can be computed. The incorrect solutions are eliminated by running a least square adjustment with the information of the second group of SVs. Hence the solution with the smallest squared residual has to be chosen. This gives the selection criterion for selection of the right ambiguity. For more details, it is referred here to [Hatch, 1989 and 1991].

## 1.5.3 FARA algorithm

The Fast Ambiguity Resolution Approach (FARA) uses “statistical information from the initial adjustment to the select the search range, information of the variance/covariance matrix to reject ambiguity sets that are not acceptable from a statistical point of view and to apply statistical hypothesis testing to select the correct set of integer ambiguities”, according to [Hofmann-Wellenhof, 1997]. The main advantage of this technique is that it does only need data on the double difference phase pseudorange. Thus the knowledge of just few observables is required. Along the high processing velocity, this makes the FARA technique very attractive. For a complete review of the FARA algorithm refer to [Frei and Schubernigg, 1992] and [Chen and Lachapelle, 1994].

## 1.6 Summary and conclusions

Retake the phase pseudorange of eq. (1.35a), between SV  $i$  and GPS receiver  $k$ ,

$$L_{1k}^i = \underbrace{\rho_k^i}_1 + \underbrace{c \cdot \Delta \delta^i}_2 + \underbrace{\lambda_1 \cdot n_{1k}^i}_3 - \underbrace{I_k^i}_4 + \underbrace{\Delta_{tropo}^i}_5 + \underbrace{\tilde{\varepsilon}_{L_k^i}}_6 \quad (1.138)$$

and the systematic errors in the GPS signal summarized in Table 3. One could as well consider eq. (1.35b). Assume that other systematic errors are negligible when compared to these. The orbital errors are strongly diminished when inserting the precise orbits delivered by the International GPS Service (IGS) into the signal processing. Thus term (1) on the right hand side of eq. (1.138) can be determined very accurately.

By computing double differences of the incoming SV signal, the clock biases of the satellite and of the receiver (term (2)) are removed. Proceeding with the ambiguity resolution, for instance using the FARA algorithm, term (3) can be resolved up to 99%. Forming the ionosphere free linear combination eliminates the ionospheric refraction effects (term (4)). The antenna phase center and multipath are constrained by specific protection of the receiver (main errors in term (6)).

Finally one can see that the major residual error source left is the troposphere (term (5)). Therefore the rest of this study will concentrate on modeling the influence of the troposphere on the GPS signal.

**Blank page**



## 2 Least-squares collocation, prediction and extrapolation

This chapter concentrates on the mathematical and statistical methods that will be used to study the refractivity field in the lower atmosphere and thus the tropospheric path delay. Although the algorithms presented require heavy computation power, these are efficient for data post-processing. For real-time or nearly real-time evaluation of path delays, other techniques such as Kalman filters might prove to be more adequate.

### 2.1 Motivation

As stressed in the previous chapter, the tropospheric refraction is the main error source in the GPS signal that cannot be efficiently removed. This hinders achieving centimeter and eventually millimeter precision in GPS positioning.

In this study, it is therefore intended to develop models for partly eliminating the influence of the troposphere on the GPS signal. Three possible strategies can be adopted: the estimation of the total path delay, the modelization of the troposphere and the direct measurement of the delay induced by the atmosphere. These are summarized in Figure 4 on next page.

The *estimation* strategy is based on the assumption that the influence of the troposphere can be determined solely from GPS measurements. This impact of the troposphere in the GPS signal is accounted by estimating different correction terms that are then introduced in GPS software. The atmosphere is supposed to change so slowly that the corrections are taken as constants over short time windows. Look at Bernese, version 4.2, for a practical example. Refer to [Fridez et al., 2001] for further details. This strategy allows modeling the refraction field of the atmosphere in three dimensions. There are mostly two techniques that can be combined: parameter estimation in functional models and estimation based on tomographic departures.

The *modelization* strategy is based in meteorological models to compute the four-dimensional refractivity field of the atmosphere. This is then integrated along the signal path to deliver finally the path delay (PD). According to [Geiger et al., 1995], one should differentiate between the *standard model*, the *physical* and the *stochastic models*.

The *standard model* makes repeated use of assumptions on the refraction field and on the atmosphere in order to keep the computation as simple as possible. The path integrals are computed numerically and result in an expression of path delays as function of time and eventually the coordinates of the observation point. It is accounted for the International Standard Atmosphere<sup>6</sup> (ISA) by introducing meteorological data into the computation. The major formulas currently in use in GPS software are derived as stretched above. The known Saastamoinen formula often acts as reference for the hydrostatic slant path delay. A similar result has been deduced by Helen Hopfield. These differ from each other mainly by the choice of the so-called mapping function. Marini is considered as a pioneer in that field.

The *physical models* are better adapted to a realistic description of the physical phenomena taking place in the troposphere than the standard model where no local variability of the refractivity field is taken into account. As stated by [Hirter, 1998], the solutions of the exact partial differential equations (PDEs) and equations of state should lead to deterministic statements. These are based on extensive measurements of all dynamical variables. The solutions are characterized by instabilities and non-linearity. These models are currently used in weather forecasting and prove to be too complicated to implement during such a study. Hence there will not be further considered as such.

The *stochastic models* are derived from pure statistics based on the assumed behavior of the troposphere. Two categories are discerned: the stochastic PDEs and the correlation models. Stochastic PDEs are introduced to counter for inaccurate measurements or non-satisfactory information on the state of the atmosphere for a given location and a given period of time. Another approach consists in studying the correlation and covariance functions of stochastic relations derived from physical models of the atmosphere. The *Collocation method* or *Kriging technique* presented in the next paragraphs is a good representative of such models. It allows for computation of slant path delays via integration of the atmospheric refractivity field.

---

<sup>6</sup> For the exact definition, refer to [Lertes, 2000].

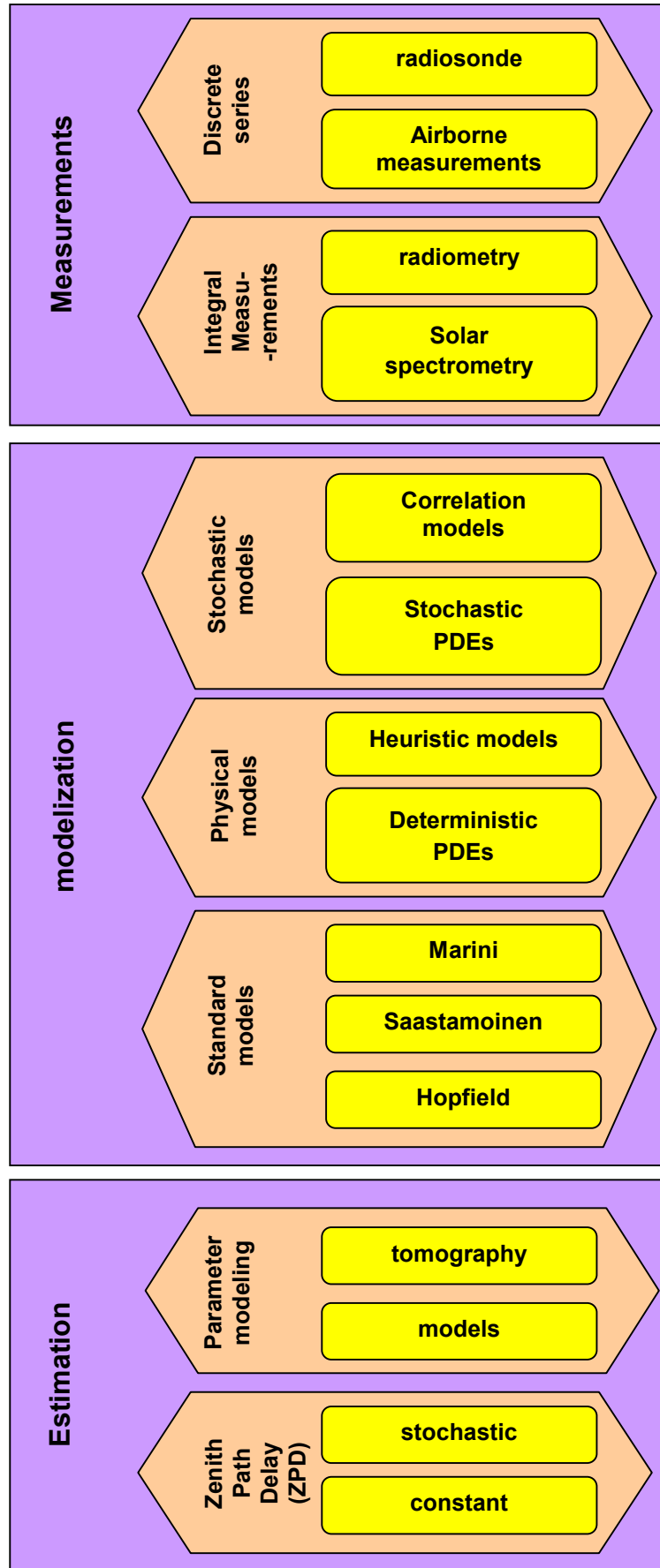


Figure 4. Strategies to determine the atmospheric slant path delay. After [Geiger et al., 1995].

The *measurements* are used to verify the accuracy of the models and techniques developed. Discrete time series are delivered by radiosonde or measurements on-board airborne platforms. The refractive index can be computed from measurements of temperature, relative humidity and atmospheric pressure. However this is valid only in small areas around the observation point. It is not possible without interpolation and extrapolation to conduct any global study of the refractivity field. Thus the domain of validity of the models will be investigated solely at specific locations.

## 2.2 Collocation fundamental equation – stochastic modeling

The collocation method is an extension of the classical least-squares technique on adjustment problems which is given by

$$\mathbf{l} = \mathbf{Ax} + \mathbf{v} \quad (2.2.1)$$

where  $\mathbf{l}$  is the measurement,  $\mathbf{A}$  is the design matrix,  $\mathbf{x}$  is the vector of unknowns and  $\mathbf{v}$  is the residual parameter.

According to [Christensen, 1991], the “methods of Kriging or best linear unbiased prediction were developed in France by Matheron<sup>7</sup>, who was originally inspired by the contributions of D.G. Krige to geostatistics. [...]. The French work was performed independently of Goldberger<sup>8</sup> who first derived the general best linear unbiased predictors for linear models”. However, one should mention the fundamental work of [Krarup, 1969] who set the modern basis of collocation theory.

The collocation method presents many advantages. Maybe the most important one concerns its application domain. Indeed, conversely to classical functional formulations (e.g. Hermite, Lagrange,...) there is no need for regular lattices. The inhomogeneous distribution of data is taken into account in the collocation algorithm through the covariance function. However this often implies that very large matrices must be inverted, slowing considerably the computation.

In the collocation technique, the observation vector or measurement  $\mathbf{l}$  is split into two parts: a functional part and a stochastic part. The functional part consist in a non-random parameter vector  $\mathbf{x}$  and a design matrix  $\mathbf{A}$  expressing the effect of the parameters on the measurement. It represents the systematic or parametric part of  $\mathbf{l}$ . In the current study, the troposphere models define the design matrix  $\mathbf{A}$ .

The stochastic part is build around a random measuring error or (white) *noise*  $\mathbf{n}$  and a *signal*  $\mathbf{s}$  at the measurement points (colored noise). Hence the least-squares collocation can be formulated as

$$\mathbf{l} = \mathbf{Ax} + \mathbf{s} + \mathbf{n} \quad (2.2.2)$$

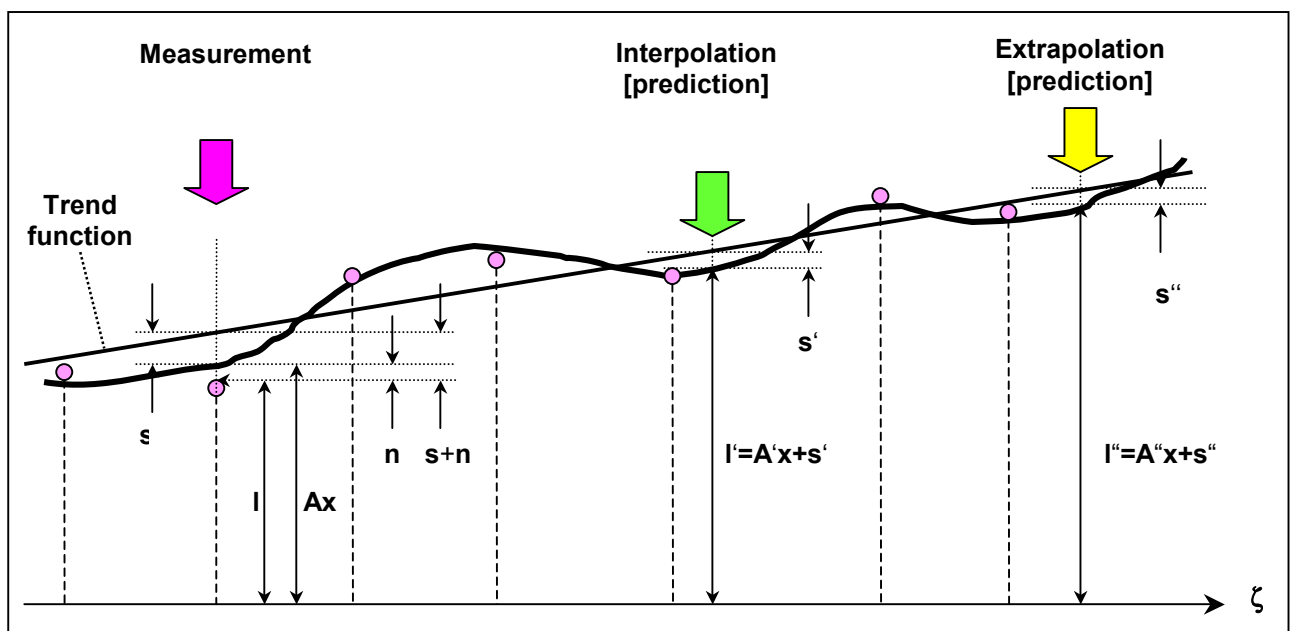


Figure 5. Least-squares collocation principle.

<sup>7</sup> It is referred to [Matheron, 1965 and 1969].

<sup>8</sup> Refer to [Goldberger, 1962].

Eq. (2.2.2) is sometimes also called *trend function*. In the words of [Moritz, 1989] “if we consider the determination of the parameter  $\mathbf{x}$  as *adjustment*, the removal of the noise as *filtering*, and the computation of the of  $\mathbf{s}$  at points other than the measuring points as *prediction*, we may say that the present model combines *adjustment*, *filtering* and *prediction*”. Refer now to Figure 5 on the previous page where  $\zeta = \zeta(\mathbf{x})$  is a random quantity:

It is now intended to derive the solution of eq. (2.2.2) using a minimization criterion for the white and colored noises as is usually done in the least-squares technique. For  $m$  measurements, one can rewrite eq. (2.2.2) as

$$\mathbf{Ax} + [\mathbf{I} \quad \mathbf{I}] \begin{bmatrix} \mathbf{n} \\ \mathbf{s} \end{bmatrix} - \mathbf{l} = \mathbf{0} \quad (2.2.3)$$

where  $\mathbf{I} \in \text{Mat}(m \times m, \mathbb{R})$  is the identity matrix and  $\mathbf{I} \in \text{Mat}(m \times 1, \mathbb{R})$ . Define the matrix  $\mathbf{B} \in \text{Mat}(m \times 2m, \mathbb{R})$  as

$$\mathbf{B} = [\mathbf{I} \quad \mathbf{I}] \quad (2.2.4)$$

and combine the signal and noise in the residual parameter  $\mathbf{v} \in \text{Mat}(2m \times m, \mathbb{R})$

$$\mathbf{v} = \begin{bmatrix} \mathbf{n} \\ \mathbf{s} \end{bmatrix} \quad (2.2.5)$$

Hence, one as

$$\mathbf{Ax} + \mathbf{Bv} - \mathbf{l} = \mathbf{0} \quad (2.2.6)$$

As is usually done for least-squares, one expects the following minimization condition

$$\mathbf{v}^T \mathbf{Pv} = \min \quad \text{Figure 6. Least square collocation principle.} \quad (2.2.7)$$

where  $T$  designates the transpose operation and

$$\mathbf{P} = \mathbf{Q}^{-1} \quad \text{with} \quad \mathbf{Q} = \begin{bmatrix} \mathbf{C}_{nn} & \mathbf{0} \\ \mathbf{0} & \mathbf{C}_{ss} \end{bmatrix} \quad (2.2.8a,b)$$

$\mathbf{P}$  is the cofactor matrix,  $\mathbf{Q}$  the global covariance matrix containing the auto covariance matrices of the signal  $\mathbf{C}_{ss}$  and the noise  $\mathbf{C}_{nn}$ . It has been assumed that signal and noise are random quantities that are normally distributed and not cross-correlated. Therefore, it holds

$$\mathbf{C}_{ns}^{-1} = \mathbf{0} = \mathbf{C}_{sn}^T \quad (2.2.9)$$

Inserting eq. (2.2.5) into eq. (2.2.7) and using eq. (2.2.8a,b), one has

$$\boxed{\mathbf{n}^T \mathbf{C}_{nn}^{-1} \mathbf{n} + \mathbf{s}^T \mathbf{C}_{ss}^{-1} \mathbf{s} = \min} \quad (2.2.10)$$

Eq. (2.2.10) is the *least-squares collocation minimum principle*.

Introduce the *Lagrange principal function*  $\Psi$  defined as

$$\Psi := \mathbf{v}^T \mathbf{Pv} - 2 \cdot \boldsymbol{\lambda}^T (\mathbf{Ax} + \mathbf{Bv} - \mathbf{l}) \quad (2.2.11)$$

where  $\boldsymbol{\lambda}^T$  is the transposed Lagrange multiplier vector. Hence determine  $\boldsymbol{\lambda}$  so that

$$\Psi = \min \quad (2.2.12)$$

This implies that all partial derivatives of  $\Psi$  vanish, i.e.

$$\begin{aligned} 0 &= \frac{\partial \Psi}{\partial \mathbf{v}} = \mathbf{Pv} - \boldsymbol{\lambda}^T \mathbf{B}^T \\ 0 &= \frac{\partial \Psi}{\partial \mathbf{x}} = \boldsymbol{\lambda}^T \mathbf{A} \\ 0 &= \frac{\partial \Psi}{\partial \boldsymbol{\lambda}} = \mathbf{Ax} + \mathbf{Bv} - \mathbf{l} \end{aligned} \quad (2.2.13a,b,c)$$

Using eq. (2.2.13a), the vector  $\mathbf{v}$  is given by

$$-\mathbf{P}\mathbf{v} + \mathbf{B}^T\boldsymbol{\lambda} = \mathbf{0} \quad \Rightarrow \quad \mathbf{v} = \mathbf{P}^{-1}\mathbf{B}^T\boldsymbol{\lambda} \quad (2.2.14)$$

Inserting (2.2.14) in (2.2.13c) gives

$$\mathbf{A}\mathbf{x} + \mathbf{B}\mathbf{P}^{-1}\mathbf{B}^T\boldsymbol{\lambda} - \mathbf{1} = \mathbf{0} \quad (2.2.15)$$

Hence, the Lagrange multiplier vector is

$$\boldsymbol{\lambda} = [\mathbf{B}\mathbf{P}^{-1}\mathbf{B}^T]^{-1}[\mathbf{1} - \mathbf{A}\mathbf{x}] \quad (2.2.16)$$

Taking (2.2.13b) into account yields to

$$\mathbf{0} = \mathbf{A}^T\boldsymbol{\lambda} \stackrel{(2.2.16)}{=} \mathbf{A}^T[\mathbf{B}\mathbf{P}^{-1}\mathbf{B}^T]^{-1}[\mathbf{1} - \mathbf{A}\mathbf{x}] \quad (2.2.17)$$

That is

$$\mathbf{A}^T[\mathbf{B}\mathbf{P}^{-1}\mathbf{B}^T]^{-1}\mathbf{1} = \mathbf{A}^T[\mathbf{B}\mathbf{P}^{-1}\mathbf{B}^T]^{-1}\mathbf{A}\mathbf{x} \quad (2.2.18)$$

Thus the unknown vector  $\mathbf{x}$  is

$$\mathbf{x} = [\mathbf{A}^T[\mathbf{B}\mathbf{P}^{-1}\mathbf{B}^T]^{-1}\mathbf{A}]^{-1} \cdot \mathbf{A}^T[\mathbf{B}\mathbf{P}^{-1}\mathbf{B}^T]^{-1} \cdot \mathbf{1} \quad (2.2.19)$$

This can be rewritten by computing each term separately. Using the definition of  $\mathbf{P}$ , one has

$$\mathbf{B}\mathbf{Q} \stackrel{(2.2.9a)}{=} \mathbf{B}\mathbf{P}^{-1} \stackrel{(2.2.9b)}{=} [\mathbf{I} \quad \mathbf{I}] \begin{bmatrix} \mathbf{C}_{nn} & \mathbf{0} \\ \mathbf{0} & \mathbf{C}_{ss} \end{bmatrix} = [\mathbf{C}_{nn} \quad \mathbf{C}_{ss}] \quad (2.2.20)$$

Hence

$$\mathbf{B}\mathbf{P}^{-1}\mathbf{B}^T \stackrel{(2.2.20)}{=} [\mathbf{C}_{nn} \quad \mathbf{C}_{ss}]\mathbf{B}^T \stackrel{(2.2.4)}{=} [\mathbf{C}_{nn} \quad \mathbf{C}_{ss}] \begin{bmatrix} \mathbf{I} \\ \mathbf{I} \end{bmatrix} = \mathbf{C}_{nn} + \mathbf{C}_{ss} := \mathbf{D} \quad (2.2.21)$$

Insert eq. (2.2.21) in eq. (2.2.19) and get

$$\mathbf{x} = [\mathbf{A}^T\mathbf{D}^{-1}\mathbf{A}]^{-1} \cdot \mathbf{A}^T\mathbf{D}^{-1}\mathbf{1} \quad (2.2.22)$$

while with eq. (2.2.16) one has

$$\boldsymbol{\lambda} = \mathbf{D}^{-1}[\mathbf{1} - \mathbf{A}\mathbf{x}] \quad (2.2.23)$$

Consider now eq. (2.2.14)

$$\mathbf{v} = \mathbf{P}^{-1}\mathbf{B}^T\boldsymbol{\lambda} = \mathbf{Q}\mathbf{B}^T\boldsymbol{\lambda} \stackrel{(2.2.23)}{=} \mathbf{P}^{-1}\mathbf{B}^T\mathbf{D}^{-1}[\mathbf{1} - \mathbf{A}\mathbf{x}] \quad (2.2.24)$$

But first compute  $\mathbf{P}^{-1}\mathbf{B}^T$ :

$$\mathbf{P}^{-1}\mathbf{B}^T \stackrel{(2.2.5/8)}{=} \begin{bmatrix} \mathbf{C}_{nn} & \mathbf{0} \\ \mathbf{0} & \mathbf{C}_{ss} \end{bmatrix} \begin{bmatrix} \mathbf{I} \\ \mathbf{I} \end{bmatrix} = \begin{bmatrix} \mathbf{C}_{nn} \\ \mathbf{C}_{ss} \end{bmatrix} \quad (2.2.25)$$

With the definition of  $\mathbf{v}$ , one has

$$\mathbf{v} \stackrel{(2.2.5)}{=} \begin{bmatrix} \mathbf{n} \\ \mathbf{s} \end{bmatrix} \stackrel{(2.2.24/25)}{=} \begin{bmatrix} \mathbf{C}_{nn}\mathbf{D}^{-1}[\mathbf{1} - \mathbf{A}\mathbf{x}] \\ \mathbf{C}_{ss}\mathbf{D}^{-1}[\mathbf{1} - \mathbf{A}\mathbf{x}] \end{bmatrix} \quad (2.2.26)$$

Finally, the solution of eq. (2.2.2) can be summarized as

$$\boxed{\begin{aligned} \mathbf{x} &= [\mathbf{A}^T \mathbf{D}^{-1} \mathbf{A}]^{-1} \cdot \mathbf{A}^T \mathbf{D}^{-1} \mathbf{l} \\ \mathbf{n} &= \mathbf{C}_{nn} \mathbf{D}^{-1} [\mathbf{l} - \mathbf{A} \mathbf{x}] \\ \mathbf{s} &= \mathbf{C}_{ss} \mathbf{D}^{-1} [\mathbf{l} - \mathbf{A} \mathbf{x}] \\ \mathbf{D} &= \mathbf{C}_{nn} + \mathbf{C}_{ss} \end{aligned}} \quad (2.2.27a,b,c,d)$$

According to [Kruse, 2000], these equations describe the ‘parameter solutions for the functional model  $\mathbf{x}$ , and signal and noise for every observation’. It should be noted that the covariance matrices for signal and noise are given by

$$\mathbf{C}_{ss} := E\{\mathbf{s}\mathbf{s}^T\} \quad \text{and} \quad \mathbf{C}_{nn} := E\{\mathbf{n}\mathbf{n}^T\} \quad (2.2.28)$$

Further one can assume according to [Wei, 1986] that the signal is a Gaussian random variable. Hence it is normally distributed, i.e.

$$\mathbf{s} \sim N(0, \mathbf{C}_{ss}) \quad (2.2.29)$$

In any case, this strongly holds for the noise. Therefore the noise  $\mathbf{n}$  is assumed to be a random variable following a normal distribution

$$\mathbf{n} \sim N(0, \mathbf{C}_{nn}) \quad (2.2.30)$$

Using the propagation law for covariance functions, it follows that the observations themselves are assumed to be normally distributed. Using the notation introduced above, one has

$$\mathbf{l} \sim N(\mathbf{A}\mathbf{x}, \mathbf{D}) \quad (2.2.31)$$

### 2.3 Interpolation vs. extrapolation

The interpolation and extrapolation of valued of interest at points where no measurements are available is done in the same manner as introduced above. It is given by the so-called *prediction* of the collocation. The reader is kindly advised to refer to Figure 4. Regarding the interpolated value  $\mathbf{l}'$ , one has

$$\mathbf{l}' = \mathbf{A}'\mathbf{x} + \mathbf{s}' \quad (2.3.1)$$

where the interpolated signal  $\mathbf{s}'$  is expressed as a function of the covariance matrix between the signals  $\mathbf{s}'_1$  and  $\mathbf{s}'_2$  at the points  $P_1$  and  $P_2$ .

$$\mathbf{s}' = \mathbf{C}_{s's'} \boldsymbol{\lambda} \stackrel{(2.2.23)}{=} \mathbf{C}_{s's'} \mathbf{D}^{-1} [\mathbf{l} - \mathbf{A}\mathbf{x}] \quad (2.3.2)$$

Hence the *interpolated values* are given by

$$\boxed{\mathbf{l}' = \mathbf{A}'\mathbf{x} + \mathbf{C}_{s's'} \mathbf{D}^{-1} [\mathbf{l} - \mathbf{A}\mathbf{x}]} \quad (2.3.3)$$

The extrapolated values  $\mathbf{l}''$  are obtained in an analogous way to the interpolated ones.

$$\mathbf{l}'' = \mathbf{A}''\mathbf{x} + \mathbf{s}'' \quad (2.3.4)$$

where the extrapolated signal  $\mathbf{s}''$  is given by

$$\mathbf{s}'' = \mathbf{C}_{s''s''} \boldsymbol{\lambda} \stackrel{(2.2.23)}{=} \mathbf{C}_{s''s''} \mathbf{D}^{-1} [\mathbf{l} - \mathbf{A}\mathbf{x}] \quad (2.3.5)$$

Finally, one obtains for the extrapolated values of interest

$$\boxed{\mathbf{l}'' = \mathbf{A}''\mathbf{x} + \mathbf{C}_{s''s''} \mathbf{D}^{-1} [\mathbf{l} - \mathbf{A}\mathbf{x}]} \quad (2.3.6)$$

Compare the signals respectively for the measurement points, the interpolation and the extrapolation. The three of them are linear combinations of the vector  $\mathbf{k}$  defined by

$$\mathbf{k} := \mathbf{D}^{-1} [\mathbf{l} - \mathbf{A}\mathbf{x}] \quad (2.3.7)$$

that is they are –as expected– linear combinations of the measurements themselves! Note that  $\mathbf{k}$  is constant. Therefore one only needs to compute it once and one can obtain the signals for all possible predictions.

## Collocation accuracy

The achievable accuracy of the least-squares collocation method plays an important role in the determination of the error in the Zenith Total Delay (ZTD). Therefore the subject of this paragraph is the computation of the error covariance matrices for the different parts of the measurement.

### 2.3.1 Conventions

Define the following help matrices from the solution (2.2.27a) and (2.2.27c):

$$\mathbf{G} := [\mathbf{A}^T \mathbf{D}^{-1} \mathbf{A}]^{-1} \cdot \mathbf{A}^T \mathbf{D}^{-1} \Rightarrow \mathbf{x} = \mathbf{G} \mathbf{l} \quad (2.4.1a,b)$$

hence

$$\mathbf{s} = \mathbf{C}_{ss} \mathbf{D}^{-1} [\mathbf{l} - \mathbf{A} \mathbf{x}] \stackrel{(2-4.1b)}{=} \mathbf{C}_{ss} \mathbf{D}^{-1} [\mathbf{l} - \mathbf{A} \mathbf{G} \mathbf{l}] = \mathbf{L} \mathbf{l} \Rightarrow \mathbf{L} := \mathbf{C}_{ss} \mathbf{D}^{-1} [\mathbf{l} - \mathbf{A} \mathbf{G}] \quad (2.4.2a,b)$$

For the predicted signal, e.g. the interpolated signal, one has

$$\mathbf{s}' = \mathbf{C}_{s's} \mathbf{D}^{-1} [\mathbf{l} - \mathbf{A} \mathbf{x}] \stackrel{(2.3.2)}{=} \mathbf{C}_{s's} \mathbf{D}^{-1} [\mathbf{l} - \mathbf{A} \mathbf{G} \mathbf{l}] = \mathbf{L}' \mathbf{l} \Rightarrow \mathbf{L}' := \mathbf{C}_{s's} \mathbf{D}^{-1} [\mathbf{l} - \mathbf{A} \mathbf{G}] \quad (2.4.3a,b)$$

Let denote the expectation value by the symbol  $E$ . Random errors such as the (white) noise  $\mathbf{n}$  have per definition zero expectation value. According to [Moritz, 1989], this holds as well for the signal  $\mathbf{s}$ . I.e., one has

$$\begin{aligned} E\{\mathbf{n}\} &= 0 \\ E\{\mathbf{s}\} &= 0 \end{aligned} \quad (2.4.4a,b)$$

### 2.3.2 Collocation covariance matrix $\mathbf{C}_{ll}$

Following [Wirth, 1990], it holds

$$E\{\mathbf{l}\} = \mathbf{A} \mathbf{x} \quad (2.4.5)$$

whereby

$$\mathbf{l} = \mathbf{A} \mathbf{x} + \mathbf{s} + \mathbf{n} = \mathbf{A} \bar{\mathbf{x}} + \bar{\mathbf{s}} + \bar{\mathbf{n}} \quad (2.4.6)$$

where the following convention is adopted: denote the *true values* by an over bar. Introduce the pure stochastic part  $\mathbf{z}$  of the measurement.

$$\mathbf{z} := \mathbf{l} - \mathbf{A} \mathbf{x} = \mathbf{s} + \mathbf{n} \quad (2.4.7a,b)$$

where  $\mathbf{A} \mathbf{x}$  is the functional part of the measurement. The covariance matrix of  $\mathbf{l}$  is defined

$$\mathbf{C}_{ll} := \text{cov}\{\mathbf{l}, \mathbf{l}\} = E\{[\mathbf{l} - E\{\mathbf{l}\}]^2\} = E\{[\mathbf{l} - E\{\mathbf{l}\}] \cdot [\mathbf{l} - E\{\mathbf{l}\}]^T\} = E\{[\mathbf{l} - E\{\mathbf{l}\}] \cdot [\mathbf{l}^T - E\{\mathbf{l}^T\}]\} \quad (2.4.8)$$

Using eq. (2.4.5), one gets

$$\mathbf{C}_{ll} \stackrel{(2.4.5)}{=} E\{[\mathbf{l} - \mathbf{A} \mathbf{x}] \cdot [\mathbf{l}^T - \mathbf{x}^T \mathbf{A}^T]\} \stackrel{(2.47a)}{=} E\{\mathbf{z} \cdot \mathbf{z}^T\} = \mathbf{C}_{zz} \quad (2.4.9)$$

Inserting eq. (2.4.7b), it follows that

$$\begin{aligned} \mathbf{C}_{ll} &= E\{[\mathbf{s} + \mathbf{n}] \cdot [\mathbf{s}^T + \mathbf{n}^T]\} \stackrel{(2.47a)}{=} E\{\mathbf{s} \mathbf{s}^T + \mathbf{s} \mathbf{n}^T + \mathbf{n} \mathbf{s}^T + \mathbf{n} \mathbf{n}^T\} \\ &= E\{\mathbf{s} \mathbf{s}^T\} + E\{\mathbf{s} \mathbf{n}^T\} + E\{\mathbf{n} \mathbf{s}^T\} + E\{\mathbf{n} \mathbf{n}^T\} \end{aligned} \quad (2.4.10)$$

However, one knows that signal and noise are uncorrelated. Therefore, one has with eq. (2.4.4a,b)

$$\begin{aligned} E\{\mathbf{s} \mathbf{s}^T\} &= \mathbf{C}_{ss} \quad , \quad E\{\mathbf{s} \mathbf{n}^T\} = 0 = E\{\mathbf{n} \mathbf{s}^T\} \\ E\{\mathbf{n} \mathbf{n}^T\} &= \mathbf{C}_{nn} \end{aligned} \quad (2.4.11a,b,c,d)$$

Thus

$$\mathbf{C}_{ll} \stackrel{(2.4.9)}{=} \mathbf{C}_{zz} \stackrel{(2.4.11)}{=} \mathbf{C}_{ss} + \mathbf{C}_{nn} \stackrel{(2.2.26d)}{=} \mathbf{D} \stackrel{(2.2.20)}{=} \mathbf{B} \mathbf{P}^{-1} \mathbf{B}^T \quad (2.4.12)$$

### 2.3.3 Unknown parameters error covariance matrix $\mathbf{Q}_{xx}$

As usual, it holds for the vector of the unknowns,

$$E\{\mathbf{x}\} = \bar{\mathbf{x}} \quad (2.4.13)$$

Consider now eq. (2.4.4b)

$$\mathbf{0} \stackrel{(2.4.4b)}{=} E\{\mathbf{s}\} \stackrel{(2.4.2a)}{=} E\{\mathbf{L}\mathbf{l}\} \stackrel{(2.4.7a)}{=} E\{\mathbf{L}(\mathbf{A}\mathbf{x} + \mathbf{z})\} \stackrel{(2.4.13)}{=} \mathbf{L}\mathbf{A}\bar{\mathbf{x}} + E\{\mathbf{z}\} \quad (2.4.14)$$

It follows that

$$\mathbf{L}\mathbf{A} = \mathbf{0} \quad \text{if} \quad \bar{\mathbf{x}} \neq \mathbf{0} \quad (2.4.15)$$

Furthermore,

$$E\{\mathbf{x}\} \stackrel{(2.4.1a)}{=} E\{\mathbf{G}\mathbf{l}\} \stackrel{(2.4.7a)}{=} E\{\mathbf{G}\mathbf{A}\mathbf{x} + \mathbf{G}\mathbf{z}\} = \mathbf{G}\mathbf{A} \cdot E\{\mathbf{x}\} + \mathbf{G} \cdot E\{\mathbf{z}\} = \mathbf{G}\mathbf{A}\bar{\mathbf{x}} + \mathbf{G} \cdot E\{\mathbf{z}\} \stackrel{(2.4.13)}{=} \bar{\mathbf{x}} \quad (2.4.16)$$

Combining eq. (2.4.7a) with eq. (2.4.4a,b), it holds

$$E\{\mathbf{z}\} = \mathbf{0} \quad (2.4.17)$$

Therefore, combining eq. (2.4.16) with (2.4.17) yields to

$$\mathbf{G}\mathbf{A} = \mathbf{I} \quad (2.4.18)$$

The true error  $\boldsymbol{\varepsilon}_x$  is given by building the difference between the true value  $\bar{\mathbf{x}}$  and the estimated value  $\mathbf{x}$

$$\boldsymbol{\varepsilon}_x := \bar{\mathbf{x}} - \mathbf{x} \stackrel{(2.4.1a)}{=} \bar{\mathbf{x}} - \mathbf{G}\mathbf{l} \stackrel{(2.4.6)}{=} \bar{\mathbf{x}} - \mathbf{G}\mathbf{A}\bar{\mathbf{x}} - \mathbf{G}\bar{\mathbf{z}} \stackrel{(2.4.18)}{=} -\mathbf{G}\bar{\mathbf{z}} \stackrel{(2.4.7b)}{=} -\mathbf{G} \cdot (\bar{\mathbf{s}} + \bar{\mathbf{n}}) \quad (2.4.19)$$

Thus

$$\boldsymbol{\varepsilon}_x \cdot \boldsymbol{\varepsilon}_x^T = \mathbf{G}\bar{\mathbf{z}} \cdot \bar{\mathbf{z}}\mathbf{G}^T = \mathbf{G} \cdot (\bar{\mathbf{s}} + \bar{\mathbf{n}}) \cdot (\bar{\mathbf{s}}^T + \bar{\mathbf{n}}^T) \cdot \bar{\mathbf{G}}^T \quad (2.4.20)$$

The *error covariance matrix* for the unknowns is then

$$\mathbf{Q}_{xx} := \text{cov}(\boldsymbol{\varepsilon}_x, \boldsymbol{\varepsilon}_x) = E\{\boldsymbol{\varepsilon}_x \cdot \boldsymbol{\varepsilon}_x^T\} \stackrel{(2.4.20)}{=} \mathbf{G}\mathbf{C}_{zz}\mathbf{G}^T \stackrel{(2.4.9)}{=} \mathbf{G}\mathbf{C}_{\bar{\ell}}\mathbf{G}^T \quad (2.4.21)$$

Further

$$\mathbf{Q}_{xx} \stackrel{(2.4.20)}{=} \mathbf{G} \cdot (\mathbf{C}_{mm} + \mathbf{C}_{ss}) \cdot \mathbf{G}^T \stackrel{(2.2.27d)}{=} \mathbf{G}\mathbf{D}\mathbf{G}^T \quad (2.4.22)$$

Inserting the definition of  $\mathbf{G}$  into eq. (2.4.21)

$$\mathbf{Q}_{xx} \stackrel{(2.4.1a)}{=} \left[ \mathbf{A}^T \mathbf{D}^{-1} \mathbf{A} \right]^{-1} \cdot \mathbf{A}^T \mathbf{D}^{-1} \mathbf{D} \left[ \mathbf{D}^{-1} \mathbf{A} \left[ \mathbf{A}^T \mathbf{D}^{-1} \mathbf{A} \right]^{-1} \right] \quad (2.4.23)$$

And taking in to account the fact that

$$\mathbf{D}\mathbf{D}^{-1} = \mathbf{D}^{-1}\mathbf{D} = \mathbf{I} \quad (2.4.24)$$

It follows that

$$\mathbf{Q}_{xx} = \left[ \mathbf{A}^T \mathbf{D}^{-1} \mathbf{A} \right]^{-1} \quad (2.4.25)$$

### 2.3.4 Signal error covariance matrix $\mathbf{Q}_{ss}$

For the signal, one has

$$\boldsymbol{\varepsilon}_s = \bar{\mathbf{s}} - \mathbf{s} \stackrel{(2.4.2a)}{=} \bar{\mathbf{s}} - \mathbf{L}\mathbf{l} \stackrel{(2.4.6)}{=} \bar{\mathbf{s}} - \mathbf{L}\mathbf{A}\bar{\mathbf{x}} - \mathbf{L}\bar{\mathbf{z}} \stackrel{(2.4.15)}{=} \bar{\mathbf{s}} - \mathbf{L}\bar{\mathbf{z}} \stackrel{(2.4.7b)}{=} \bar{\mathbf{s}} - \mathbf{L} \cdot (\bar{\mathbf{s}} + \bar{\mathbf{n}}) \quad (2.4.26)$$

and

$$\boldsymbol{\varepsilon}_s \cdot \boldsymbol{\varepsilon}_s^T = [\bar{\mathbf{s}} - \mathbf{L}\bar{\mathbf{z}}] \cdot [\bar{\mathbf{s}} - \mathbf{L}\bar{\mathbf{z}}]^T = [\bar{\mathbf{s}} - \mathbf{L}\bar{\mathbf{z}}] \cdot [\bar{\mathbf{s}}^T - \bar{\mathbf{z}}^T \mathbf{L}^T] = \bar{\mathbf{s}} \cdot \bar{\mathbf{s}}^T - \mathbf{L}\bar{\mathbf{z}} \cdot \bar{\mathbf{s}}^T - \bar{\mathbf{s}} \cdot \bar{\mathbf{z}}^T \mathbf{L}^T + \mathbf{L}\bar{\mathbf{z}} \cdot \bar{\mathbf{z}}^T \mathbf{L}^T \quad (2.4.27)$$



Hence the error covariance matrix of the signal is

$$\mathbf{Q}_{ss} := \text{cov}(\boldsymbol{\varepsilon}_s, \boldsymbol{\varepsilon}_s) = E(\boldsymbol{\varepsilon}_s \cdot \boldsymbol{\varepsilon}_s^T) = \mathbf{C}_{ss} - \mathbf{L}\mathbf{C}_{zs}^T - \mathbf{C}_{sz}\mathbf{L}^T + \mathbf{L}\mathbf{C}_{zz}\mathbf{L}^T \quad (2.4.28)$$

Let compute each term separately.

$$\mathbf{C}_{sz} = E\{\mathbf{s} \cdot \mathbf{z}^T\} \stackrel{(2.4.7a)}{=} E\{\mathbf{s} \cdot (\mathbf{s} + \mathbf{n})^T\} = E\{\mathbf{s} \cdot \mathbf{s}^T + \mathbf{s} \cdot \mathbf{n}^T\} = E\{\mathbf{s} \cdot \mathbf{s}^T\} + E\{\mathbf{s} \cdot \mathbf{n}^T\} = E\{\mathbf{s} \cdot \mathbf{s}^T\} = \mathbf{C}_{ss}, \quad (2.4.29)$$

because

$$E\{\mathbf{s} \cdot \mathbf{n}^T\} = 0 \quad (2.4.30)$$

as signal and noise are assumed to be uncorrelated. Hence with eq. (2.4.29), it holds

$$\mathbf{C}_{zs} = \mathbf{C}_{ss} = \mathbf{C}_{ss}^T \quad (2.4.31)$$

Therefore with eq. (2.4.9)

$$\mathbf{Q}_{ss} = \mathbf{C}_{ss} - \mathbf{L}\mathbf{C}_{ss}^T - \mathbf{C}_{ss}\mathbf{L}^T + \mathbf{L}\mathbf{C}_{zz}\mathbf{L}^T \quad (2.4.32)$$

Using eq. (2.4.7b), it holds

$$\mathbf{C}_{zz} \stackrel{(2.4.7b)}{=} \mathbf{C}_{ss} + \mathbf{C}_{nn} \stackrel{(2.2.27d)}{=} \mathbf{D} \quad (2.4.33)$$

Thus eq.(2.4.32) becomes

$$\mathbf{Q}_{ss} = \mathbf{C}_{ss} - \mathbf{L}\mathbf{C}_{ss}^T - \mathbf{C}_{ss}\mathbf{L}^T + \mathbf{L}\mathbf{D}\mathbf{L}^T \quad (2.4.34)$$

Now compute the  $\mathbf{L}$  terms. According to eq. (2.4.2b), one has

$$\mathbf{L} = \mathbf{C}_{ss}\mathbf{D}^{-1}[\mathbf{I} - \mathbf{A}\mathbf{G}] \quad (2.4.35)$$

Transpose eq. (2.4.35)

$$\mathbf{L}^T = [\mathbf{I} - \mathbf{G}^T\mathbf{A}^T]\mathbf{D}^{-1}\mathbf{C}_{ss}^T \quad (2.4.36)$$

as  $\mathbf{D}$  is a diagonal matrix. Using the definition of  $\mathbf{G}$ , eq. (2.4.1a) and multiplying term by term, one has

$$\begin{aligned} \mathbf{L}^T &= \left[ \mathbf{D}^{-1} - \mathbf{D}^{-1}\mathbf{A}(\mathbf{A}^T\mathbf{D}^{-1}\mathbf{A})^{-1}\mathbf{A}^T\mathbf{D}^{-1} \right] \mathbf{C}_{ss}^T = \mathbf{D}^{-1} \left[ \mathbf{I} - \mathbf{A}(\mathbf{A}^T\mathbf{D}^{-1}\mathbf{A})^{-1}\mathbf{A}^T\mathbf{D}^{-1} \right] \mathbf{C}_{ss}^T \\ &\stackrel{(2.4.1a)}{=} \mathbf{D}^{-1}[\mathbf{I} - \mathbf{A}\mathbf{G}]\mathbf{C}_{ss}^T \end{aligned} \quad (2.4.37)$$

This yields to

$$\mathbf{L}\mathbf{C}_{ss}^T = \mathbf{C}_{ss}\mathbf{L}^T \quad (2.4.38)$$

Furthermore

$$\mathbf{L}\mathbf{D}\mathbf{L}^T \stackrel{(2.4.35/37)}{=} \mathbf{C}_{ss}\mathbf{D}^{-1}[\mathbf{I} - \mathbf{A}\mathbf{G}]\mathbf{D}\mathbf{D}^{-1}[\mathbf{I} - \mathbf{A}\mathbf{G}]\mathbf{C}_{ss}^T = \mathbf{C}_{ss}\mathbf{D}^{-1}[\mathbf{I} - \mathbf{A}\mathbf{G}]^2\mathbf{C}_{ss}^T \quad (2.4.39)$$

One can see that  $\mathbf{I} - \mathbf{A}\mathbf{G}$  is idempotent, i.e.

$$[\mathbf{I} - \mathbf{A}\mathbf{G}]^2 = [\mathbf{I} - \mathbf{A}\mathbf{G}][\mathbf{I} - \mathbf{A}\mathbf{G}] = \mathbf{I} - 2\mathbf{A}\mathbf{G} + \mathbf{A}\mathbf{G}\mathbf{A}\mathbf{G} \stackrel{(2.4.18)}{=} \mathbf{I} - 2\mathbf{A}\mathbf{G} + \mathbf{A}\mathbf{I}\mathbf{G} = \mathbf{I} - \mathbf{A}\mathbf{G} \quad (2.4.40)$$

Thus

$$\mathbf{L}\mathbf{D}\mathbf{L}^T = \mathbf{C}_{ss}\mathbf{D}^{-1}[\mathbf{I} - \mathbf{A}\mathbf{G}]\mathbf{C}_{ss}^T \stackrel{(2.4.2b)}{=} \mathbf{L}\mathbf{C}_{ss}^T \quad (2.4.41)$$

Inserting eq. (2.4.38) and eq. (2.4.41) in eq. (2.4.34) gives

$$\mathbf{Q}_{ss} = \mathbf{C}_{ss} - \mathbf{L}\mathbf{C}_{ss}^T - \mathbf{C}_{ss}\mathbf{L}^T + \mathbf{L}\mathbf{C}_{ss}^T = \mathbf{C}_{ss} - \mathbf{L}\mathbf{C}_{ss}^T \stackrel{(2.4.35)}{=} \mathbf{C}_{ss} - \mathbf{C}_{ss}\mathbf{D}^{-1}[\mathbf{I} - \mathbf{A}\mathbf{G}]\mathbf{C}_{ss}^T \quad (2.4.42)$$

Insert the definition of  $\mathbf{G}$ , eq. (2.4.1a)

$$\begin{aligned}
\mathbf{Q}_{ss} &= \mathbf{C}_{ss} - \mathbf{C}_{ss} \mathbf{D}^{-1} \left[ \mathbf{I} - \mathbf{A} (\mathbf{A}^T \mathbf{D}^{-1} \mathbf{A})^{-1} \mathbf{A}^T \mathbf{D}^{-1} \right] \mathbf{C}_{ss}^T \\
&= \mathbf{C}_{ss} - \mathbf{C}_{ss} \mathbf{D}^{-1} \mathbf{C}_{ss}^T + \mathbf{C}_{ss} \mathbf{D}^{-1} \mathbf{A} (\mathbf{A}^T \mathbf{D}^{-1} \mathbf{A})^{-1} \mathbf{A}^T \mathbf{D}^{-1} \mathbf{C}_{ss}^T \\
&\stackrel{(2.4.25)}{=} \mathbf{C}_{ss} - \mathbf{C}_{ss} \mathbf{D}^{-1} \mathbf{C}_{ss}^T + \mathbf{C}_{ss} \mathbf{D}^{-1} \mathbf{A} \mathbf{Q}_{xx} \mathbf{A}^T \mathbf{D}^{-1} \mathbf{C}_{ss}^T
\end{aligned} \tag{2.4.43a,b,c}$$

Thus

$$\boxed{\mathbf{Q}_{ss} = \mathbf{C}_{ss} - \mathbf{C}_{ss} \mathbf{D}^{-1} \mathbf{C}_{ss}^T + \mathbf{C}_{ss} \mathbf{D}^{-1} \mathbf{A} \mathbf{Q}_{xx} \mathbf{A}^T \mathbf{D}^{-1} \mathbf{C}_{ss}^T} \tag{2.4.44}$$

### 2.3.5 Prediction error covariance matrix $\mathbf{Q}_{l'l'}$

It is now intended to concentrate on the prediction errors generated by extrapolation and interpolation. One follows the considerations of [Hirter, 1998]. Remind that the predicted measurement is given by eq. (2-3.1)

$$\mathbf{l}' = \mathbf{A}' \mathbf{x} + \mathbf{s}' \tag{2.4.45}$$

The error in the prediction is then

$$\boldsymbol{\varepsilon}_{l'} := \bar{\mathbf{l}}' - \mathbf{l}' = \mathbf{A}' \bar{\mathbf{x}} + \bar{\mathbf{s}}' - \mathbf{A}' \mathbf{x} - \mathbf{s}' \tag{2.4.46}$$

Further use the help matrices  $\mathbf{G}$  and  $\mathbf{L}'$  defined in eq. (2.4.1b) and in eq. (2.4.3b). Hence

$$\boldsymbol{\varepsilon}_{l'} = \mathbf{A}' \bar{\mathbf{x}} + \bar{\mathbf{s}}' - \mathbf{A}' \mathbf{G} \mathbf{l} - \mathbf{L}' \mathbf{l} \tag{2.4.47}$$

Recall that for a measurement it holds

$$\mathbf{l} = \mathbf{A} \mathbf{x} + \mathbf{s} + \mathbf{n} \tag{2.4.48}$$

Eq. (2.4.47) becomes then

$$\boldsymbol{\varepsilon}_{l'} = \mathbf{A}' \bar{\mathbf{x}} + \bar{\mathbf{s}}' - \mathbf{A}' \mathbf{G} \mathbf{A} \mathbf{x} - \mathbf{A}' \mathbf{G} (\mathbf{s} + \mathbf{n}) - \mathbf{L}' \mathbf{A} \bar{\mathbf{x}} - \mathbf{L}' (\bar{\mathbf{s}} + \bar{\mathbf{n}}) \tag{2.4.49}$$

Use eq. (2.4.15) and (2.4.18) applied to the prediction, i.e.

$$\begin{aligned}
\mathbf{A}' \mathbf{G} &= \mathbf{I} \\
\mathbf{L}' \mathbf{A} &= \mathbf{0}
\end{aligned} \tag{2.4.50}$$

and obtain

$$\boldsymbol{\varepsilon}_{l'} = \bar{\mathbf{s}}' - (\mathbf{A}' \mathbf{G} + \mathbf{L}') (\bar{\mathbf{s}} + \bar{\mathbf{n}}) = \bar{\mathbf{s}}' - \mathbf{K} (\bar{\mathbf{s}} + \bar{\mathbf{n}}) \tag{2.4.51}$$

where the matrix  $\mathbf{K}$  is defined as

$$\mathbf{K} := (\mathbf{A}' \mathbf{G} + \mathbf{L}') \tag{2.4.52}$$

The *error covariance matrix of the interpolated measurement* is thus

$$\mathbf{Q}_{l'l'} := \text{cov}(\mathbf{l}', \mathbf{l}') = E \left\{ (\mathbf{l}' - E\{\mathbf{l}'\})^2 \right\} \tag{2.4.53}$$

This can be expressed as a function of the prediction error

$$\mathbf{Q}_{l'l'} = \text{cov}(\boldsymbol{\varepsilon}_{l'}, \boldsymbol{\varepsilon}_{l'}) = E \left\{ [\bar{\mathbf{s}}' - \mathbf{K} (\bar{\mathbf{s}} + \bar{\mathbf{n}})] \cdot [\bar{\mathbf{s}}' - \mathbf{K} (\bar{\mathbf{s}} + \bar{\mathbf{n}})]^T \right\} \tag{2.4.54}$$

Multiplying term-by-term and executing the expectation value yields to

$$\mathbf{Q}_{l'l'} = \mathbf{C}_{s's'} - \mathbf{C}_{s's} \mathbf{K}^T - \mathbf{C}_{s'n} \mathbf{K}^T - \mathbf{K} \mathbf{C}_{s's}^T - \mathbf{K} \mathbf{C}_{s'n}^T + \mathbf{K} \mathbf{D} \mathbf{K}^T \tag{2.4.55}$$

where eq. (2.4.12) has been used. Again, recall that one has assumed that noise and signal are uncorrelated, i.e.

$$\mathbf{C}_{s'n} = \mathbf{0} \tag{2.4.56}$$

This gives

$$\mathbf{Q}_{l'l'} = \mathbf{C}_{s's'} - \mathbf{C}_{s's} \mathbf{K}^T - \mathbf{K} \mathbf{C}_{s's}^T + \mathbf{K} \mathbf{D} \mathbf{K}^T \tag{2.4.57}$$

As was done before, compute each term separately. It holds

$$\mathbf{K} \stackrel{(2.4.52)}{=} \mathbf{A}'\mathbf{G} + \mathbf{L}' \stackrel{(2.4.1a)}{=} \mathbf{A}'(\mathbf{A}^T\mathbf{D}^{-1}\mathbf{A})^{-1}\mathbf{A}^T\mathbf{D}^{-1} + \mathbf{L}' \stackrel{(2.4.25)}{=} \mathbf{A}'\mathbf{Q}_{xx}\mathbf{A}^T\mathbf{D}^{-1} + \mathbf{L}' \quad (2.4.58)$$

Multiplying from the right with  $\mathbf{C}_{s's}^T$  gives

$$\mathbf{K}\mathbf{C}_{s's}^T = \mathbf{A}'\mathbf{Q}_{xx}\mathbf{A}^T\mathbf{D}^{-1}\mathbf{C}_{s's}^T + \mathbf{L}'\mathbf{C}_{s's}^T \quad (2.4.59)$$

and from left and transposing

$$\mathbf{C}_{s's}'\mathbf{K}^T = \mathbf{C}_{s's}'(\mathbf{A}'\mathbf{Q}_{xx}\mathbf{A}^T\mathbf{D}^{-1})^T + \mathbf{C}_{s's}'\mathbf{L}'^T = \mathbf{C}_{s's}'\mathbf{D}^{-1}\mathbf{A}\mathbf{Q}_{xx}\mathbf{A}'^T + \mathbf{C}_{s's}'\mathbf{L}'^T \quad (2.4.60)$$

while taking into consideration the fact that  $\mathbf{Q}_{xx}$  is a diagonal matrix. This yields to

$$\mathbf{K}\mathbf{D}\mathbf{K}^T \stackrel{(2.4.52)}{=} (\mathbf{A}'\mathbf{G} + \mathbf{L}')\mathbf{D}(\mathbf{G}^T\mathbf{A}'^T + \mathbf{L}'^T) \quad (2.4.61)$$

Expanding it yields to

$$\mathbf{K}\mathbf{D}\mathbf{K}^T = \mathbf{A}'\mathbf{G}\mathbf{D}\mathbf{G}^T\mathbf{A}'^T + \mathbf{L}'\mathbf{D}\mathbf{G}^T\mathbf{A}'^T + \mathbf{A}'\mathbf{G}\mathbf{D}\mathbf{L}'^T + \mathbf{L}'\mathbf{D}\mathbf{L}'^T \quad (2.4.62)$$

Use the definitions of  $\mathbf{L}'$ ,  $\mathbf{D}$  and  $\mathbf{G}$  and obtain

$$\begin{aligned} \mathbf{L}'\mathbf{D} &\stackrel{(2.4.3b)}{=} \mathbf{C}_{s's}'\mathbf{D}^{-1}(\mathbf{I} - \mathbf{A}\mathbf{G})\mathbf{D} = \mathbf{C}_{s's}' - \mathbf{C}_{s's}'\mathbf{D}^{-1}\mathbf{A}\mathbf{G}\mathbf{D} \\ &\stackrel{(2.4.1a)}{=} \mathbf{C}_{s's}' - \mathbf{C}_{s's}'\mathbf{D}^{-1}\mathbf{A}(\mathbf{A}^T\mathbf{D}^{-1}\mathbf{A})^{-1}\mathbf{A}^T\mathbf{D}^{-1}\mathbf{D} \end{aligned} \quad (2.4.63)$$

This gives

$$\mathbf{L}'\mathbf{D} = \mathbf{C}_{s's}' - \mathbf{C}_{s's}'\mathbf{D}^{-1}\mathbf{A}(\mathbf{A}^T\mathbf{D}^{-1}\mathbf{A})^{-1}\mathbf{A}^T \quad (2.4.64)$$

Further, build the transpose of  $\mathbf{G}$  and multiply with  $\mathbf{A}'^T$

$$\mathbf{G}^T\mathbf{A}'^T \stackrel{(2.4.1a)}{=} \mathbf{D}^{-1}\mathbf{A}(\mathbf{A}^T\mathbf{D}^{-1}\mathbf{A})^{-1}\mathbf{A}'^T \quad (2.4.65)$$

Multiply eq. (2.4.62) with eq. (2.4.63)

$$\mathbf{L}'\mathbf{D}\mathbf{G}^T\mathbf{A}'^T = \mathbf{C}_{s's}'\mathbf{D}^{-1}\mathbf{A}(\mathbf{A}^T\mathbf{D}^{-1}\mathbf{A})^{-1}\mathbf{A}'^T - \mathbf{C}_{s's}'\mathbf{D}^{-1}\mathbf{A}(\mathbf{A}^T\mathbf{D}^{-1}\mathbf{A})^{-1}\mathbf{A}^T\mathbf{D}^{-1}\mathbf{A}(\mathbf{A}^T\mathbf{D}^{-1}\mathbf{A})^{-1}\mathbf{A}'^T \quad (2.4.66)$$

Note that for the second term on the right hand side (RHS) of eq. (2.4.66) it holds

$$\mathbf{A}^T\mathbf{D}^{-1}\mathbf{A}(\mathbf{A}^T\mathbf{D}^{-1}\mathbf{A})^{-1} = \mathbf{I} \quad (2.4.67)$$

Insert eq. (2.4.67) in eq. (2.4.66)

$$\mathbf{L}'\mathbf{D}\mathbf{G}^T\mathbf{A}'^T = \mathbf{C}_{s's}'\mathbf{D}^{-1}\mathbf{A}(\mathbf{A}^T\mathbf{D}^{-1}\mathbf{A})^{-1}\mathbf{A}'^T - \mathbf{C}_{s's}'\mathbf{D}^{-1}\mathbf{A}(\mathbf{A}^T\mathbf{D}^{-1}\mathbf{A})^{-1}\mathbf{A}'^T = \mathbf{0} \quad (2.4.68)$$

This holds under transposition. Hence

$$\mathbf{G}\mathbf{D}\mathbf{G}^T \stackrel{(2.4.1a)}{=} \left[ (\mathbf{A}^T\mathbf{D}^{-1}\mathbf{A})^{-1}\mathbf{A}^T\mathbf{D}^{-1} \right] \mathbf{D} \left[ \mathbf{D}^{-1}\mathbf{A}(\mathbf{A}^T\mathbf{D}^{-1}\mathbf{A})^{-1} \right] = (\mathbf{A}^T\mathbf{D}^{-1}\mathbf{A})^{-1} \quad (2.4.69)$$

Identify with eq. (2.4.25)

$$\mathbf{G}\mathbf{D}\mathbf{G}^T = \mathbf{Q}_{xx} \quad (2.4.70)$$

Combine eq. (2.4.66), (2.4.68), (2.4.69) and (2.4.62)

$$\mathbf{K}\mathbf{D}\mathbf{K}^T = \mathbf{A}'\mathbf{Q}_{xx}\mathbf{A}'^T + \mathbf{L}'\mathbf{D}\mathbf{L}'^T \quad (2.4.71)$$

With the current definition, remark that it holds

$$\mathbf{C}_{s's}' = \mathbf{C}_{ss} \quad (2.4.72)$$

Combine eq. (2.4.59), (2.4.60), (2.4.71) and (2.4.72) with eq. (2.4.57)

$$\begin{aligned} \mathbf{Q}_{l'l'} &\stackrel{(2.4.57)}{=} \mathbf{C}_{s's'} - \mathbf{C}_{s's} \mathbf{K}^T - \mathbf{K} \mathbf{C}_{s's}^T + \mathbf{K} \mathbf{D} \mathbf{K}^T \\ &= \mathbf{C}_{ss} - \mathbf{A}' \mathbf{Q}_{xx} \mathbf{A}^T \mathbf{D}^{-1} \mathbf{C}_{s's}^T - \mathbf{L}' \mathbf{C}_{s's}^T - \mathbf{C}_{s's} \mathbf{D}^{-1} \mathbf{A} \mathbf{Q}_{xx} \mathbf{A}'^T - \mathbf{C}_{s's} \mathbf{L}'^T + \mathbf{A}' \mathbf{Q}_{xx} \mathbf{A}'^T + \mathbf{L}' \mathbf{D} \mathbf{L}'^T \end{aligned} \quad (2.4.73)$$

Reorganize the right hand side of eq. (2.4.73)

$$\mathbf{Q}_{l'l'} = \mathbf{C}_{ss} - \mathbf{L}' \mathbf{C}_{s's}^T - \mathbf{C}_{s's} \mathbf{L}'^T + \mathbf{L}' \mathbf{D} \mathbf{L}'^T - \mathbf{A}' \mathbf{Q}_{xx} \mathbf{A}^T \mathbf{D}^{-1} \mathbf{C}_{s's}^T - \mathbf{C}_{s's} \mathbf{D}^{-1} \mathbf{A} \mathbf{Q}_{xx} \mathbf{A}'^T + \mathbf{A}' \mathbf{Q}_{xx} \mathbf{A}'^T \quad (2.4.74)$$

Remind the definition of  $\mathbf{L}'$ , eq. (2.4.2b), and repeat the steps from eq. (2.4.35) to eq. (2.4.41) this time for the predicted measurement and obtain

$$\begin{aligned} \mathbf{L}' &\stackrel{(2.4.2b)}{=} \mathbf{C}_{s's} \mathbf{D}^{-1} [\mathbf{I} - \mathbf{A} \mathbf{G}] \\ \mathbf{L}' \mathbf{C}_{s's}^T &= \mathbf{C}_{s's} \mathbf{L}'^T \\ \mathbf{L}' \mathbf{D} \mathbf{L}'^T &= \mathbf{L}' \mathbf{C}_{s's}^T \end{aligned} \quad (2.4.75a,b,c)$$

Insert eq. (2.4.75b,c) in eq. (2.4.74) and obtain

$$\mathbf{Q}_{l'l'} = \mathbf{C}_{ss} - \mathbf{L}' \mathbf{C}_{s's}^T - \mathbf{A}' \mathbf{Q}_{xx} \mathbf{A}^T \mathbf{D}^{-1} \mathbf{C}_{s's}^T - \mathbf{C}_{s's} \mathbf{D}^{-1} \mathbf{A} \mathbf{Q}_{xx} \mathbf{A}'^T + \mathbf{A}' \mathbf{Q}_{xx} \mathbf{A}'^T \quad (2.4.76)$$

Use eq. (2.4.75a)

$$\mathbf{Q}_{l'l'} = \mathbf{C}_{ss} - \mathbf{C}_{s's} \mathbf{D}^{-1} \mathbf{C}_{s's}^T + \mathbf{C}_{s's} \mathbf{D}^{-1} \mathbf{A} \mathbf{G} \mathbf{C}_{s's}^T - \mathbf{A}' \mathbf{Q}_{xx} \mathbf{A}^T \mathbf{D}^{-1} \mathbf{C}_{s's}^T - \mathbf{C}_{s's} \mathbf{D}^{-1} \mathbf{A} \mathbf{Q}_{xx} \mathbf{A}'^T + \mathbf{A}' \mathbf{Q}_{xx} \mathbf{A}'^T \quad (2.4.77)$$

From eq. (2.4.18), one knows that

$$\mathbf{A} = \mathbf{G}^{-1} \quad (2.4.78)$$

and with eq. (2.4.25) get

$$\mathbf{Q}_{xx} = [\mathbf{A}^T \mathbf{D}^{-1} \mathbf{A}]^{-1} = \mathbf{G} \mathbf{D} \mathbf{G}^T = \mathbf{G} \mathbf{D} (\mathbf{A}^{-1})^T \Rightarrow \mathbf{G} = \mathbf{Q}_{xx} \mathbf{A}^T \mathbf{D}^{-1} \quad (2.4.79)$$

Insert eq. (2.4.79) in the third term on the RHS of eq. (2.4.77) and get

$$\mathbf{Q}_{l'l'} = \mathbf{C}_{ss} - \mathbf{C}_{s's} \mathbf{D}^{-1} \mathbf{C}_{s's}^T + \mathbf{C}_{s's} \mathbf{D}^{-1} \mathbf{A} \mathbf{Q}_{xx} \mathbf{A}^T \mathbf{D}^{-1} \mathbf{C}_{s's}^T - \mathbf{A}' \mathbf{Q}_{xx} \mathbf{A}^T \mathbf{D}^{-1} \mathbf{C}_{s's}^T - \mathbf{C}_{s's} \mathbf{D}^{-1} \mathbf{A} \mathbf{Q}_{xx} \mathbf{A}'^T + \mathbf{A}' \mathbf{Q}_{xx} \mathbf{A}'^T \quad (2.4.80)$$

This can be rewritten as

$$\boxed{\mathbf{Q}_{l'l'} = \mathbf{C}_{ss} - \mathbf{C}_{s's} \mathbf{D}^{-1} \mathbf{C}_{s's}^T + (\mathbf{C}_{s's} \mathbf{D}^{-1} \mathbf{A} - \mathbf{A}') \mathbf{Q}_{xx} (\mathbf{A}^T \mathbf{D}^{-1} \mathbf{C}_{s's}^T - \mathbf{A}'^T)} \quad (2.4.81)$$

## 2.4.6 Accuracy summary

For simplicity, the accuracy results for the measurements  $\mathbf{l}$ , the unknown parameters  $\mathbf{x}$ , the signal  $\mathbf{s}$  and the prediction  $\mathbf{l}'$  are summarized hereunder:

$$\boxed{\begin{aligned} \mathbf{C}_{ll} &= \mathbf{C}_{zz} = \mathbf{C}_{ss} + \mathbf{C}_{nn} = \mathbf{D} = \mathbf{B} \mathbf{P}^{-1} \mathbf{B}^T \\ \mathbf{Q}_{xx} &= [\mathbf{A}^T \mathbf{D}^{-1} \mathbf{A}]^{-1} \\ \mathbf{Q}_{ss} &= \mathbf{C}_{ss} - \mathbf{C}_{ss} \mathbf{D}^{-1} \mathbf{C}_{ss}^T + \mathbf{C}_{ss} \mathbf{D}^{-1} \mathbf{A} \mathbf{Q}_{xx} \mathbf{A}^T \mathbf{D}^{-1} \mathbf{C}_{ss}^T \\ \mathbf{Q}_{l'l'} &= \mathbf{C}_{ss} - \mathbf{C}_{s's} \mathbf{D}^{-1} \mathbf{C}_{s's}^T + (\mathbf{C}_{s's} \mathbf{D}^{-1} \mathbf{A} - \mathbf{A}') \mathbf{Q}_{xx} (\mathbf{A}^T \mathbf{D}^{-1} \mathbf{C}_{s's}^T - \mathbf{A}'^T) \end{aligned}} \quad (2.4.82a,b,c,d)$$

As stressed by [Moritz, 1989], the error covariance matrices for the unknowns  $\mathbf{x}$ , the signal and the prediction can be a-priori computed. No explicit measurements are required to perform this. Only the covariance matrices from both signal and noise as well as the position of the measurements in the matrices  $\mathbf{A}$  and  $\mathbf{A}'$  (or  $\mathbf{A}''$ ) are required. This is a common fact from both the least-squares theory and the least-squares collocation technique.

## 2.5 The covariance function $\Phi$

The error covariance matrices from the above paragraph allow for a computation of the accuracy with which the measurements and the prediction are performed. On the other hand the covariance function  $\Phi$ , respectively the

covariance matrix  $C_{ss}$  gives the covariance between two signals  $s_i$  and  $s_j$  at two different points  $P_i$  and  $P_j$ . The influence of the measurements on the predicted values is determined by the covariance function. Hence, the strength of the smoothing on the prediction is controlled by  $\Phi$ . The covariance function is not exactly known and its shape is based on the assumptions taken.

Independently of its exact formulation, the covariance function  $\Phi$  has the following properties:

- i. It reaches its maximum at the origin, i.e. when  $P_i = P_j$ ,
- ii. Its norm decreases with the distance,
- iii. It vanishes at infinity.

This can be expressed in a more mathematical way as

$$\Phi(\mathbf{0}) = \max \quad \text{i.e.} \quad \left. \frac{\partial \Phi}{\partial \mathbf{r}} \right|_{\mathbf{r}=\mathbf{0}} = \mathbf{0} \quad \text{and} \quad \left. \frac{\partial^2 \Phi}{\partial^2 \mathbf{r}} \right|_{\mathbf{r}=\mathbf{0}} < \mathbf{0} \quad (2.5.1)$$

$$\left. \frac{\partial |\Phi|}{\partial \mathbf{r}} \right|_{\mathbf{r}=\mathbf{0}} < \mathbf{0} \quad (2.5.2)$$

$$\lim_{r \rightarrow +\infty} \Phi(r) = 0, \quad |\mathbf{r}| = r \quad (2.5.3)$$

This topic will be studied in details in the next chapter. Meanwhile another approach to the extrapolation is taken into consideration hereunder.

## 2.6 Summary and conclusions

The least-squares collocation method or Kriging technique is an efficient mathematical tool first developed by geophysicists to interpolate and extrapolate data while minimizing possible errors. Its apparent resemblance to least-squares is limited. Indeed, by opposition to the classical least-squares technique, signal and noise components are clearly separated and are assumed to be uncorrelated. The eventual knowledge of the physical processes taking place in the system to study are summarized in a functional model. To enable efficient data processing, this functional model is linearized.

One of the major advantage of the collocation technique consists in the ability to predict data at other locations and other times from a given observation data set. The smoothness of the extrapolation is insured by the correlation function, which vanishes at infinity. The errors are computed through error covariance matrices both for the signal and for the unknown parameters vector. Indeed, it is possible starting from *a priori* values to determine adjusted parameters, which is an additional advantage of Kriging.

However, the least-squares collocation method is complicated to implement and require an important computation time, thus limiting its general usage.

**Blank page**

## 3. Path delays and atmosphere modeling

### 3.1. Motivation

That atmosphere is classified into different layers with respect to their altitude above ground. Only some of them play an important role regarding the behavior of the GPS signal carriers.

As already stated in 1.3.1.2., the ionosphere is a dispersive medium with respect to radio waves with frequencies up to 15 GHz. Hence the delay induced by the ionosphere or, for short, the ionospheric delay is frequency dependent. However it can be fully removed if dual frequency GPS receivers of the same network are deployed. Using the known dispersion relations for the ionosphere, the phase pseudoranges (PR) of both  $L_1$  and  $L_2$  carriers are linearly combined according to the method presented in 1.4.1. Hence ionosphere-free PRs are obtained.

The neutral atmosphere comprises both the stratosphere and the troposphere. The water vapor (WV) introduces a significant delay because it is the only atmospheric constituent in sufficient quantity that possesses a dipole moment. This dipole moment is generated by an asymmetric charge distribution in the water molecule. The hydrogen bond between water molecules of liquid water greatly diminishes the effect of the dipole moment on the GPS signal. Therefore the presence of cloud and ice therein does not actively affect the GPS measurements.

The majority of the atmospheric WV is located in the lower part of the atmosphere: the troposphere. Different studies have empirically shown that it is reasonable to assume that 90% of the atmospheric WV can be found between sea level and an average altitude of 5000 meters. Therefore, the stratospheric delay is always neglected by comparison to the tropospheric delay. Concluding, the troposphere is the only layer that causes important delays to the GPS signal.

Reminding some results from the first chapter, GPS SVs transmit in the microwave frequency range. The Time of Arrival (TOA) of the GPS signal is delayed because of the refractive bending and slowing of the signal due to the presence of the atmosphere between satellite and ground-based receiver. Thus a shift in the phase of the  $L_1$  and  $L_2$  carrier waves is observed and can be accurately determined. Conventionally this phase shift is stated in the additional distance traveled by the signal or excess path and is often denoted as the Total Delay (TD) or slant path delay as it is compared with the geometric path. This geometric path corresponds to the path the signal would follow if there were no atmosphere. Hence the models established as standards in the last years are presented hereunder.

### 3.2. Classical models

As the neutral atmosphere is a non-dispersive medium, the delays cannot be calibrated and estimated in the same way as for the ionosphere. Different models were developed in order to estimate this tropospheric delay. It is intended here to present only the most significant models for the current study.

#### 3.2.1. Path delay and tropospheric delay

The increase in the travel path length  $L$  or path delay (PD) is given by

$$\Delta L = \int_L n(s) ds - G \quad (3.2.1.1)$$

where  $G$  is the straight-line distance between the SV and the receiver and  $n$  is the refractive index of the air. The path delay for a given atmospheric layer is defined with respect to the refractive index  $n$  of the air as

$$\Delta s|_{layer} = \int (n-1) ds \equiv \Delta^{layer} \quad (3.2.1.2)$$

where the integral is performed along the geometric path. Generally, the *refractivity*  $N$  is used instead of the refractive index. The dimensionless refractivity is given by

$$N := 10^6 \cdot (n-1) \quad (3.2.1.3)$$

Accordingly to paragraph 3.1., concentrate now on the troposphere. Inserting (3.2.1.3) in (3.2.1.2) yields to the classical formulation of the tropospheric delay

$$\Delta^{trop} = 10^{-6} \cdot \int N ds = \Delta^{trop}(\varepsilon, \phi) \equiv \Delta^{trop}(\varepsilon) \quad (3.2.1.4)$$

where  $\varepsilon$  is the elevation angle and  $\phi$  is the direction of the path as seen from the GPS receiver's location. The last equality was proven by [Elósegui et al., 1999]. According to [Bevis et al., 1992], the path delay is then

$$\Delta L = \Delta^{trop} + S - G = 10^{-6} \cdot \int N ds + S - G \quad (3.2.1.5)$$

where  $S$  is the geometric path length along the ray. The  $S-G$  term corresponds to bending of the signal path.

The troposphere is a mixture of gas and WV. As stated above, the WV is the only constituent that has a dipole moment. [Hopfield, 1969] showed that the dipole component of the refractivity has an intensity of approximately 20 times the non-dipole component. Therefore it is possible to treat the “dry” and “wet” components of the refractivity separately. In practice one should not use the label of *dry* component but rather of hydrostatic component. It is introduced here only for the reader to get used to that widely used notation. Thus

$$N^{trop} = N_h^{trop} + N_w^{trop} \quad (3.2.1.6)$$

where  $N_h^{trop}$  is the hydrostatic component of the refractivity and  $N_w^{trop}$  is the wet component of the refractivity. All the gases except WV generate the hydrostatic component of the refractivity, which in turn is responsible for the wet component. Hence, with (3.2.1.4), one has for the tropospheric path delay

$$\Delta^{trop} = \Delta_h^{trop} + \Delta_w^{trop} = 10^{-6} \cdot \int N_h^{trop} ds + 10^{-6} \cdot \int N_w^{trop} ds \quad (3.2.1.7)$$

About 90% of the tropospheric delay is produced by the hydrostatic part that can be very accurately modeled. Conversely, this is not the case for the highly variable wet component.

## 3.2.2. Refractivity modeling

As can be seen from eq. (3.2.1.5), the refractivity plays a major role in the accurate determination of the path delay. Starting in the early 1950s and with the rapid development of radio transmissions and their broad public usage increasing, many scientists developed models for the refractivity.

### 3.2.2.1. Essen and Froome formula

In 1951, L. Essen and K.D. Froome used a microwave interferometer to study the refractive indices of the air and its principal constituents. Using the method of Pound (1947), they set both cavities of the interferometer in resonance. They evacuated them and replaced the vacuum by the gas to study at different temperatures. The refractive index of air is then obtained by an extrapolation formula.

Hereby they have taken the following assumptions: the refractive index varies proportionally to the density (1), the dry air or hydrostatic air follows the ideal gas law for any temperature (2) and the water vapor follows a simple Debye equation (3).

Indeed, the water vapor is a polar gas with an electric dipole moment and therefore obeys *Debye's equation* (1929) of the form

$$\varepsilon - 1 = p' \cdot \left[ \frac{A}{T} + \frac{B}{T^2} \right] \quad (3.2.2.1)$$

where  $\varepsilon$  is the dielectric constant,  $p'$  is the pressure the water vapor would exert on the system if assumption (2) holds and  $T$  is the temperature in the cavity. The  $A$  term represents the contribution of the atomic and electronic polarization to  $\varepsilon$  while the  $B$  term represents the contribution of the dipole moment to  $\varepsilon$ . For refractivity measurements, [Barell and Sears, 1939] proved that both constants are given by

$$\begin{aligned} A &= (1.725 \pm 0.005) \times 10^{-4} \\ B &= 0.9913 \end{aligned} \quad (3.2.2.2a,b)$$

where  $B$  was experimentally determined only on average. Barell and Sears also proved that

$$p' = p \cdot (1 + 2.4 \times 10^{-5} \cdot p) \quad (3.2.2.3)$$



where  $p$  is the atmospheric pressure. Thus, combining eq. (3.2.2.1) to (3.2.2.3) and the optical dispersion formula applied to different mixture of gases, Essen and Froome showed that it holds for the refractive index of air

$$(n_{t,p} - 1) \times 10^6 = 103.49 \cdot \frac{p_1}{T} + 177.40 \cdot \frac{p_2}{T} + \frac{86.26}{T} \cdot \left( 1 + \frac{5748}{T} \right) \cdot p_3 + \dots \quad (3.2.2.4)$$

and

$$p = p_1 + p_2 + p_3 \quad (3.2.2.5)$$

where  $p_1$  is the pressure of the air,  $p_2$  is the partial pressure of  $\text{CO}_2$ ,  $p_3$  is the water vapor partial pressure, all three in Hectopascal and  $T$  is the temperature in Kelvin. Eq. (3.2.2.4) holds for the following conditions as stated by [Essen and Froome, 1951]

- i.  $-20^\circ\text{C} \leq T \leq +60^\circ\text{C}$
- ii. Unsaturated water vapor pressure  $p_3 \leq 100 \text{ mm Hg} \approx 133.3 \text{ hPa}$
- iii. All wavelength  $\lambda > 7 \times 10^{-3} \text{ m}$

Furthermore, one can neglect the effect of carbon dioxide for most purposes since its percentage in open air is less than 0.03 by volume. Hence one can set

$$p_2 = 0 \quad (3.2.2.6)$$

Generally the *partial pressure of water vapor* is labeled by  $e$  and the *atmospheric pressure* by  $p$ . Using these conventions, setting eq. (3.2.2.6) in eq. (3.2.2.4) and neglecting higher order temperature terms, one obtains

$$N(p, T, e) = (n - 1) \times 10^6 = \frac{77.64}{T} \cdot (p - e) + \frac{64.68}{T} \cdot \left( 1 + \frac{5748}{T} \right) \cdot e \quad (3.2.2.7)$$

This is the classical *Essen and Froome formula*. Both the atmospheric pressure  $p$  and the water vapor pressure  $e$  are in hectopascal [hPa] and the atmospheric temperature  $T$  is in Kelvin [K]. The coefficients and their units are summarized in Table 5 below.

Coefficient	Unit
77.64	$\text{K} \cdot \text{hPa}^{-1}$
64.68	$\text{K} \cdot \text{hPa}^{-1}$
5748	K

Table 5. Essen and Froome formula: coefficients.

The first term is the so-called *hydrostatic refractivity* or *dry refractivity* and the second term is labeled as the *wet refractivity*. For further details, refer to [Essen and Froome, 1951].

The refractivity  $N$ , given by the Essen and Froome formula is plotted on Figure 6 on next page as function of the temperature  $T$  in the range  $200 \text{ K} \leq T \leq 325 \text{ K}$  and the pressure  $p$  in the range  $0 \text{ hPa} \leq p \leq 1000 \text{ hPa}$ . A pressure of 0 hPa is encountered in outer space. It is assumed that the GPS space vehicles are evolving in an environment with little pressure. For European latitudes the partial water vapor pressure varies between 5 hPa in summer and 15 hPa in winter. Therefore a mean value of  $e = 10 \text{ hPa}$  has been chosen. It is referred to appendix A for further computations.

On Figure 6, the linear dependence of the refractivity on the pressure and its inverse proportionality to the temperature can be clearly seen. The hydrostatic refractivity  $N_{dry}$  is plotted on Figure 7 on next page. It shows the same features as the refractivity  $N$  of Figure 6. On the contrary, the wet refractivity  $N_{wet}$ , plotted as a function of  $T$  and  $e$ , does not depend on the atmospheric pressure. This is a major property of the wet refractivity.

### 3.2.2.2. Smith and Weintraub formula

In 1953, E.K. Smith and S. Weintraub suggested the relationship

$$N = 77.6 \cdot \frac{p}{T} + 3.73 \times 10^5 \cdot \frac{e}{T^2} \quad (3.2.2.8)$$

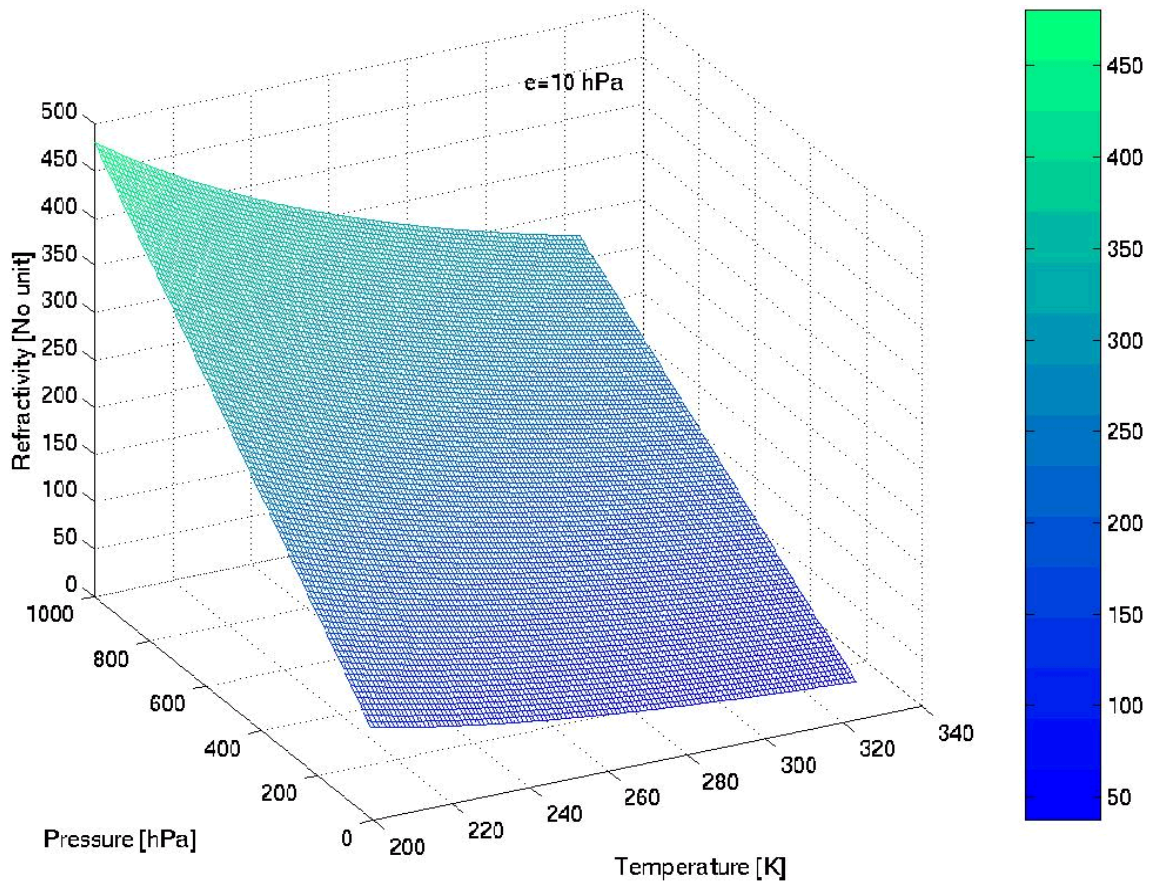


Figure 6. Essen and Froome formula. Refractivity for  $e=10$  hPa.

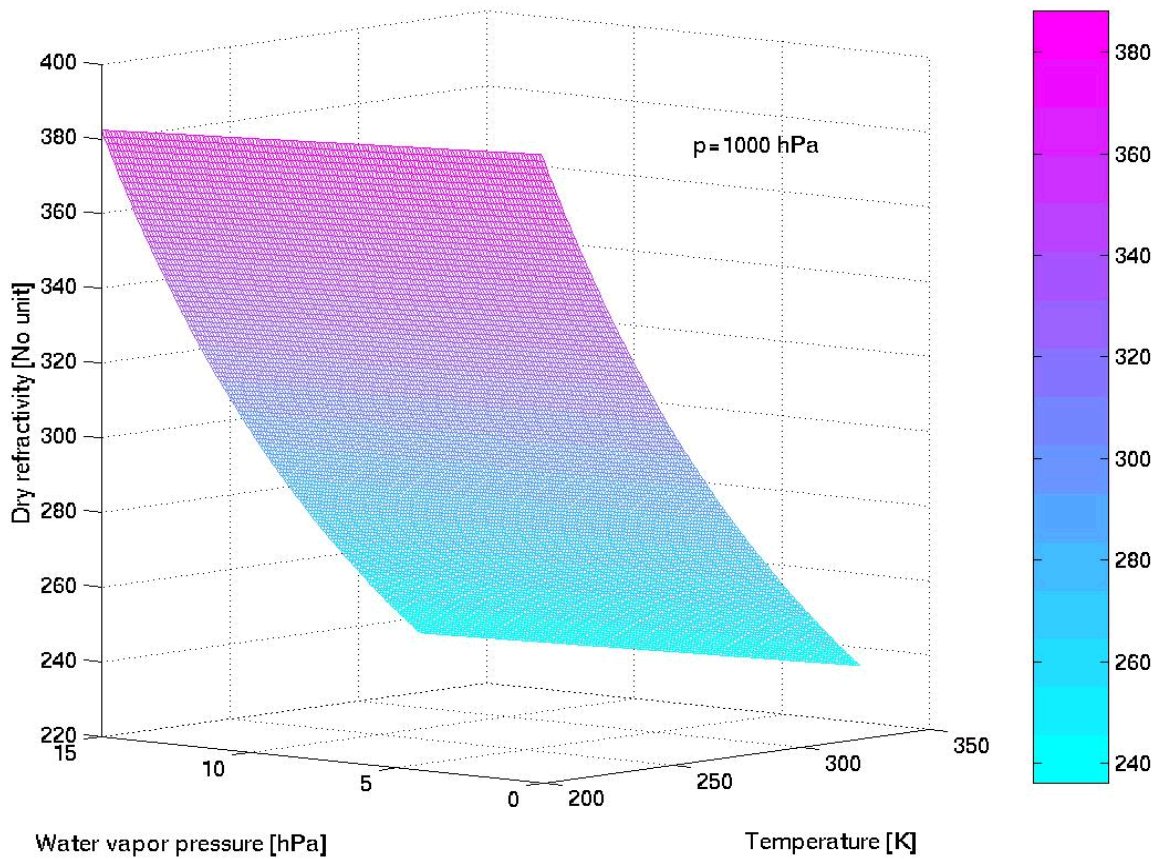


Figure 7. Essen and Froome formula. Dry refractivity for  $p=1000$  hPa.

where  $p$  is the total atmospheric pressure in hectopascal,  $T$  the surface temperature in Kelvin and  $e$  the partial water vapor pressure in hectopascal. Equation (3.2.2.8) is accurate to about 0.5%. For further details, refer to [Smith and Weintraub, 1953].

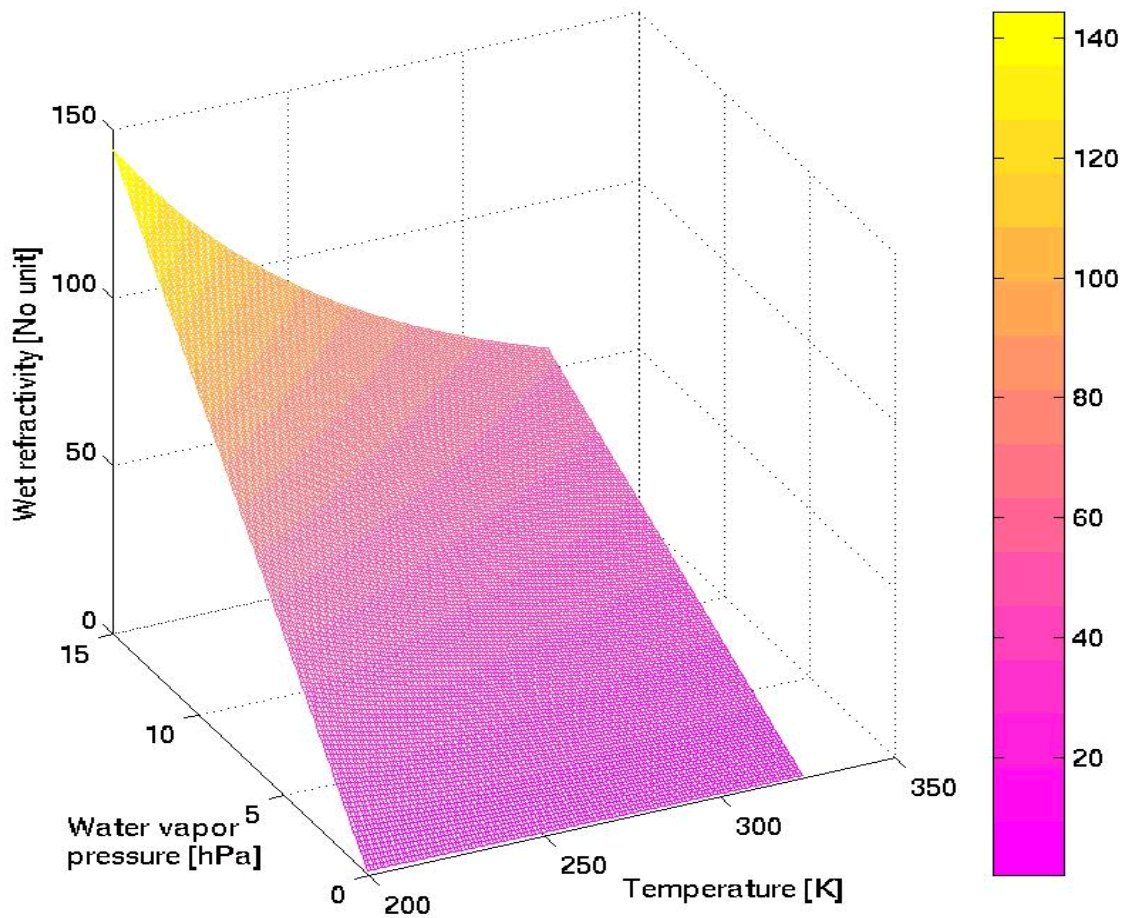


Figure 8. Essen and Froome formula. Wet refractivity.

### 3.2.2.3. Thayer model

In 1974, G. Thayer showed that the refractivity was directly proportional to the atmospheric surface pressure  $p$  in hectopascal and inversely proportional to the surface temperature  $T$  in Kelvin.

$$N = k_1 \cdot \left( \frac{p_h}{T} \right) \cdot \frac{1}{Z_h} + k_2 \cdot \left( \frac{e}{T} \right) \cdot \frac{1}{Z_{wv}} + k_3 \cdot \left( \frac{e}{T^2} \right) \cdot \frac{1}{Z_{wv}} \quad (3.2.2.9)$$

where  $p_h$  is the pressure of the dry air in hectopascal, and  $Z_h$  and  $Z_{wv}$  are respectively the compressibility factors of the dry or “hydrostatic” air and atmospheric water vapor. The three constants are summarized in Table 6 hereunder:

Constant	Value	Error	Unit
$k_1$	77.604	0.014	$\text{K} \cdot \text{hPa}^{-1}$
$k_2$	64.79	0.08	$\text{K} \cdot \text{hPa}^{-1}$
$k_3$	$3.776 \times 10^5$	$0.004 \times 10^5$	$\text{K}^2 \cdot \text{hPa}^{-1}$

Table 6. Thayer model coefficients

After [Davis et al., 1985] the accuracy of the Thayer model is about 0.02%. For the derivation of eq. (3.2.2.9), refer to [Thayer, 1974].

### 3.2.3. Hopfield model

In the late 1960s, the British scientist Dr. Helen Hopfield based her study of the atmosphere in numerous experiments around the globe and gained then a profound understanding of the atmospheric mass movements. From 1969 onwards she devised three successively improved models for the atmospheric refractivity.

#### 3.2.3.1. Normal Hopfield model

She assumed that the troposphere could be separated into isotropic layers. Thus she empirically derived a model for the hydrostatic refractivity

$$N_h^{trop}(z) = N_h^{trop}(0) \cdot \left[ \frac{z_h - z}{z_h} \right]^4 \quad (3.2.3.1)$$

where  $z$  is the altitude above the surface and  $z_h$  is the thickness of the troposphere, given in meters by

$$z_h = 40136 + 148.72 \cdot [T - 273.15] \quad (3.2.3.2)$$

where  $T$  is the surface temperature in Kelvins. Setting (3.2.3.1) in (3.2.1.7) for the hydrostatic delay and integrating, one obtains

$$N_h^{trop} = \frac{10^{-6}}{5} \cdot N_h^{trop}(0) \cdot z_h \quad (3.2.3.3)$$

This is the hydrostatic refractivity of the normal Hopfield model. For further details, refer to [Hopfield, 1969].

#### 3.2.3.2. Enhanced Hopfield model

Both the hydrostatic and wet delays are often not “measured” at the same elevation angle as one single receiver tracks many SVs at the same time and as these are evolving along their assigned orbits. It is therefore convenient to define a reference direction: the *zenith direction*. Hence the path delay is projected on the zenith axis, which is normal to the tangent plane of the GPS receiver. This projection or elevation angle dependency is described by so-called *mapping functions*  $m$ . For further details regarding these, it is referred to paragraph 3.2.5. With equation (3.2.1.7) and by analogy to (3.2.3.3), one has

$$\Delta^{trop} = \frac{10^{-6}}{5} \cdot [N_h^{trop}(0) \cdot z_h \cdot m_h(\varepsilon) + N_w^{trop}(0) \cdot z_w \cdot m_w(\varepsilon)] \quad (3.2.3.4)$$

where  $\varepsilon$  is the elevation angle,  $m_h$  and  $m_w$  are respectively the hydrostatic and wet Hopfield mapping functions,  $z_h$  is from equation (3.2.3.2) and  $z_w$  is the mean scale height for water vapor (c.f. eq. (3.3.2.25) and paragraph 3.3.3.4). The first term is usually called the *hydrostatic delay* and the second term the *wet delay*. The Hopfield mapping functions are given by

$$m_h(\varepsilon) = \left[ \sin \sqrt{\varepsilon^2 + 6.25} \right]^{-1} \quad \text{and} \quad m_w(\varepsilon) = \left[ \sin \sqrt{\varepsilon^2 + 2.25} \right]^{-1} \quad (3.2.3.5)$$

Thus, the hydrostatic component of the tropospheric delay is

$$\Delta_h^{trop}(\varepsilon) = \frac{10^{-6}}{5} \cdot \left[ \frac{N_h^{trop}(0) \cdot z_h}{\sin \sqrt{\varepsilon^2 + 6.25}} \right] \quad (3.2.3.6)$$

Furthermore insert for instance the formula of [Essen and Froome, 1951] for the hydrostatic refractivity, i.e. the first term in eq. (3.2.2.7):

$$N_h^{trop}(0) = a \cdot \frac{p}{T}, \quad a = 77.64 \text{ K} \cdot \text{hPa}^{-1} \quad (3.2.3.7)$$

where  $p$  is the surface atmospheric pressure in hectopascal [hPa] and  $T$  the surface temperature in Kelvin [K] in eq. (3.2.3.6). These are obtained from ground meteorological data. Combining (3.2.3.2.), (3.2.3.6) and (3.2.3.7) yields to

$$\Delta_h^{trop}(\varepsilon) = \frac{10^{-6}}{5} \cdot \frac{40136 + 148.72 \cdot [T - 273.15]}{\sin \sqrt{\varepsilon^2 + 6.25}} \cdot 77.64 \cdot \frac{p}{T} \quad (3.2.3.8)$$



where  $\Delta_h^{trop}$  is expressed in meters. Eq. (3.2.3.8) is plotted on Figure 9 below. By opposition to the Saastamoinen model, eq. (3.2.4.5), there is no divergence at very low elevation angles.

### 3.2.3.3. Modified Hopfield model

Some years later, Dr. Helen Hopfield modified her model by taking into account the curvature of the atmosphere, thus using the modulus of the position vector  $r$  rather the altitude  $z$  of the considered volume element. Considering eq. (3.2.3.1) but introducing the radius of the Earth  $R_E$ , one has

$$N_h^{trop}(r) = N_h^{trop}(0) \cdot \left[ \frac{r_h - r}{r_h - R_E} \right]^4 \quad (3.2.3.9)$$

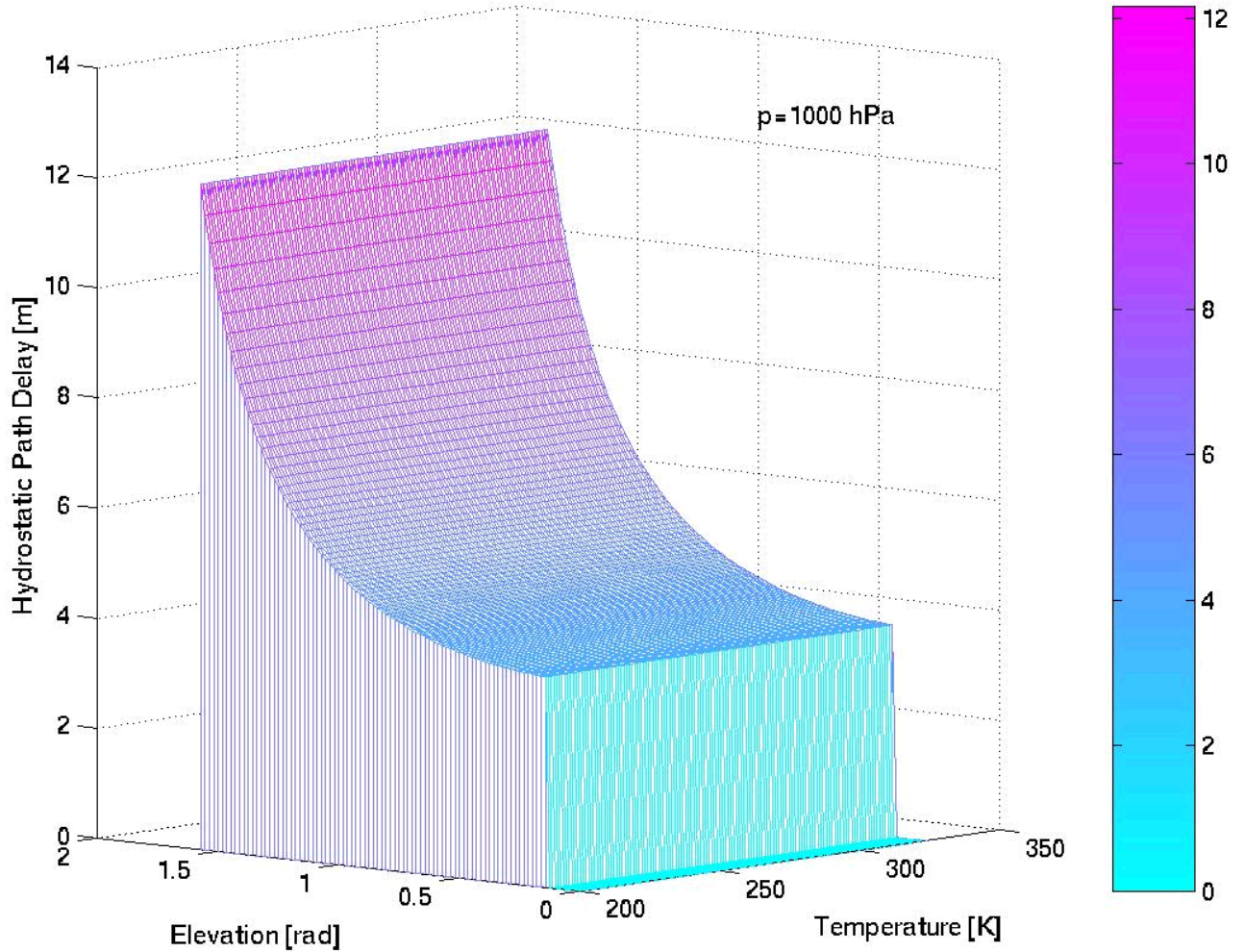


Figure 9. Enhanced Hopfield model. Hydrostatic Path Delay  $HPD(T, \varepsilon)$  in meters.

where  $r_h = R_E + z_h$  and  $r = R_E + z$  are respectively the total height of the troposphere, where zero is set at the geocenter of the Earth, and the position vector. Thus the modified hydrostatic component of the tropospheric delay is given by

$$\Delta_h^{trop}(\vartheta) = 10^{-6} \cdot \int_{R_E}^{r_h} \frac{N_h^{trop}(r)}{\cos \vartheta(r)} dr \quad (3.2.3.10)$$

where  $\vartheta$  is the zenith angle and depends on the location  $r$ . Consider the zenith angle  $\vartheta_0$  at the observation station where the GPS receiver is located, and apply the cosine law. One has

$$\cos \vartheta(r) = \frac{1}{r} \cdot \left[ r^2 - R_E^2 \sin^2 \vartheta_0 \right]^{1/2} \quad (3.2.3.11)$$

Combining (3.2.3.9), (3.2.3.10) and (3.2.3.11), one obtains

$$\Delta_h^{trop}(\vartheta) = \frac{10^{-6} \cdot N_h^{trop}(0)}{[r_h - R_E]^4} \cdot \int_{R_E}^{r_h} \frac{r \cdot [r_h - r]^4}{\sqrt{r^2 - R_E^2 \sin^2 \vartheta_0}} dr \quad (3.2.3.12)$$

This is the corresponding formula for the hydrostatic component of the tropospheric delay of the modified Hopfield model. It is sometimes useful to express the zenith angle  $\vartheta$  with respect to the elevation angle  $\varepsilon$ . It holds

$$\vartheta = 90^\circ - \varepsilon \quad (3.2.3.13)$$

A complete derivation of the computations can be found for example in [Hofmann-Wellenhof, 1997].

### 3.2.4. Saastamoinen model

The Canadian meteorologist J. Saastamoinen derived in 1971 and 1972 a model for the tropospheric delay from the gas laws. He used the *law of Goldstone and Dale* for the pressure distribution in the atmosphere and assumed a hydrostatic equilibrium. Hence the atmospheric refractivity is proportional to the ground pressure. He started from the path delay in eq. (3.2.1.1)

$$\Delta s|_{trop} = \int_{radio\ path} (n-1) ds \equiv \Delta^{trop} \quad (3.2.4.1)$$

and he mapped this delay along the zenith direction. As referred to Figure 3, the simplest mapping function relating any elevation angle with the zenith is given by the secant of the zenith angle  $\vartheta$ . Thus one has

$$\Delta^{trop} = \int_{radio\ path} (n-1) \cdot \sec \vartheta ds \quad (3.2.4.2)$$

[Saastamoinen, 1972] showed that the path delay can be expressed as a function of the available surface meteorological data where he used the [Essen and Froome, 1951] formula for the tropospheric refractivity, eq. (3.2.2.7)

$$N^{trop} = 10^6 \cdot (n-1) = 77.624 \frac{p}{T} - 12.92 \frac{e}{T} + 371900 \frac{e}{T^2} \quad (3.2.4.3)$$

where  $p$  is the total surface pressure,  $e$  the partial water vapor pressure, both in hectopascal and  $T$  is the absolute temperature in Kelvin. Reminding the relationship between refractive index and refractivity, equation (3.2.1.3), and for applied computations, the numerical form of equation (3.2.4.1) is

$$\Delta^{trop} = 0.002277 \cdot \sec \vartheta \cdot \left[ p + \left( \frac{1255}{T} + 0.05 \right) \cdot e - 1.16 \cdot \tan^2 \vartheta \right] + \delta \quad (3.2.4.4)$$

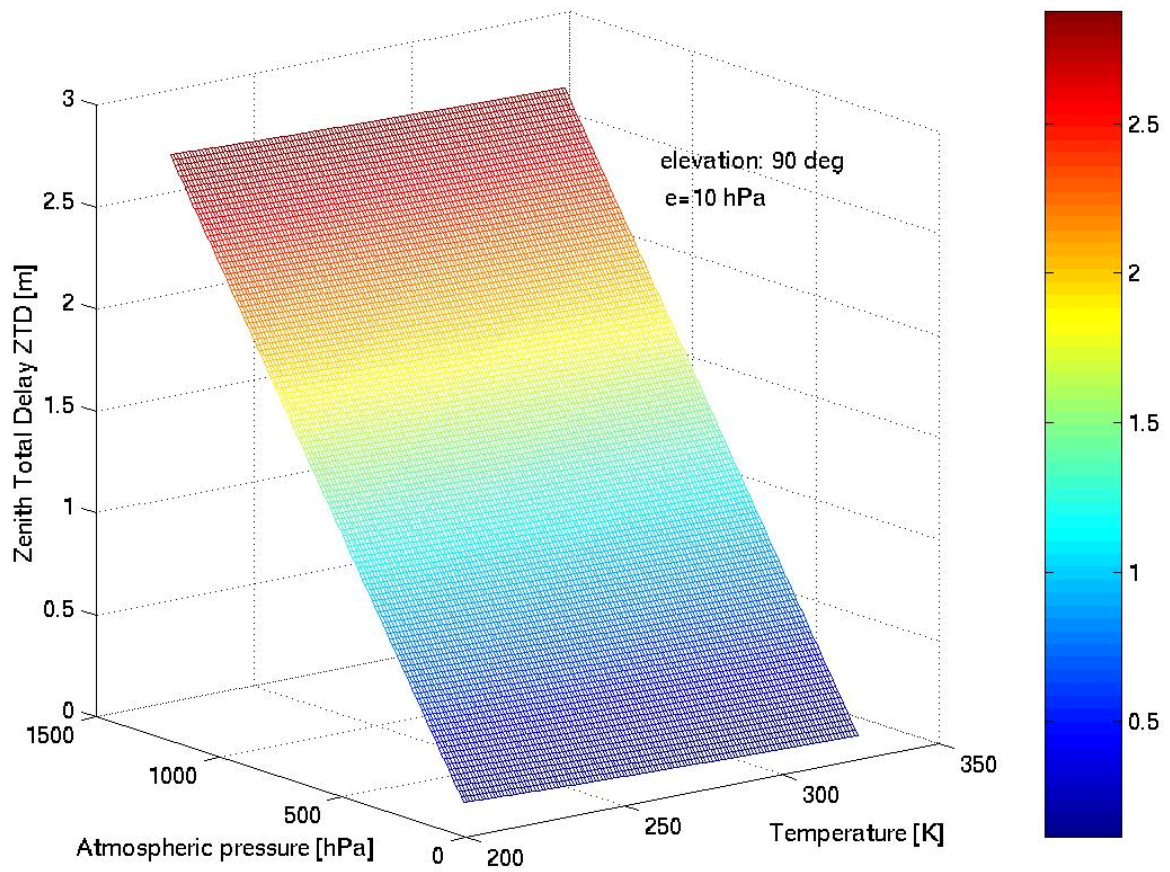
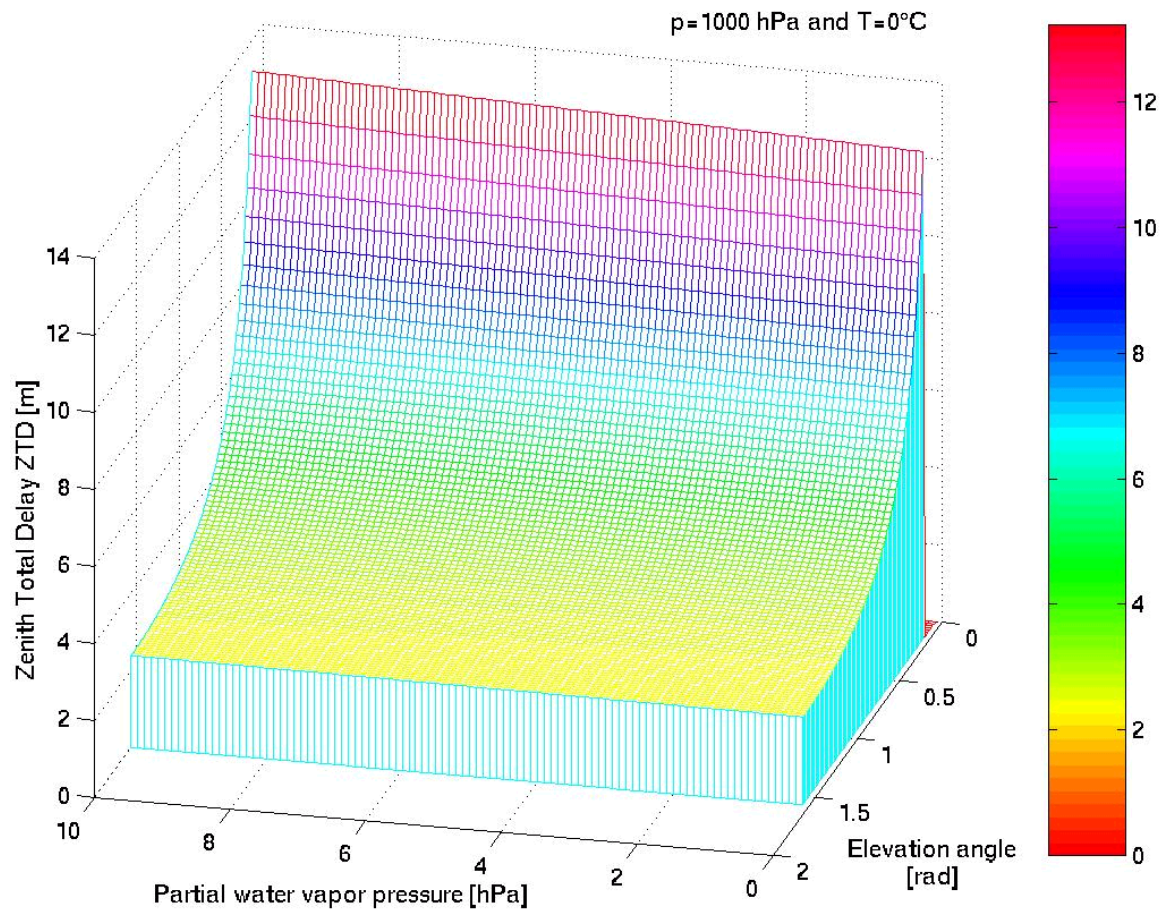
where  $\delta$  is a small correction term depending on the altitude of the observation point. [Saastamoinen, 1971 and 1972] computed this for different locations. One can formulate this as function of the sine of the elevation angle with (3.2.3.13) and obtains

$$\Delta^{trop} = \frac{0.002277}{\sin \varepsilon} \cdot \left[ p + \left( \frac{1255}{T} + 0.05 \right) \cdot e - \frac{1.16}{\tan^2 \varepsilon} \right] + \delta \quad (3.2.4.5)$$

in meters, since

$$\sec \vartheta = \frac{1}{\cos \vartheta} = \frac{1}{\sin \varepsilon} \quad \text{and} \quad \tan \vartheta = \frac{1}{\tan \varepsilon} \quad (3.2.4.6)$$

Eq. (3.2.4.5) is the known *Saastamoinen formula* for the tropospheric delay. Note that the total delay (TD) and the tropospheric delay are nearly similar. For further details refer to [Saastamoinen, 1971 and 1972]. The path delay of Eq. (3.2.4.6) is plotted at zenith on Figure 10 on next page, as function of the temperature  $T$  and the atmospheric pressure  $p$ . For a standard ground pressure of  $p = 1013.25$  hPa, it is of the order of magnitude of  $ZTD \approx 2.40$  m for

Figure 10. Saastamoinen formula. Zenith Path Delay  $ZPD(p, T)$  in meters.Figure 11. Saastamoinen formula. Zenith Path Delay  $ZPD(e, \varepsilon)$  in meters.

a partial water vapor pressure of  $e = 10$  hPa . It matches with independent measurements obtained with water vapor radiometers (WVR). The linearity of the Zenith Total Delay (ZTD) with the pressure can be clearly seen. The term in eq. (3.2.4.5) containing the inverse proportionality to the temperature is strongly constrained. It contributes to the ZTD to only 10 cm.

The ZTD as function of the partial water vapor pressure and of the elevation angle for  $10 \text{ deg} \leq \varepsilon \leq 90 \text{ deg}$  is plotted on Figure 11 on previous page. As can be guessed from eq. (3.2.4.5), the ZTD increases approximately as  $1/\varepsilon$  at very low elevation angle and thus diverges for  $\varepsilon = 0 \text{ deg}$  . Therefore a cut-off angle of 10 degrees is generally set. Hence the ZTD has been computed for  $10 \text{ deg} \leq \varepsilon \leq 90 \text{ deg}$  . The ZTD varies slowly with the water vapor partial pressure which term contributes to about 5% to the total delay.

### 3.2.5. Mapping function

The role of a mapping function is to describe the dependency of the total delay on different geodetic and meteorological parameters. These are generally the observation station coordinates, where the GPS receivers are located, the surface temperature, the surface atmospheric pressure, the relative humidity and the water vapor partial pressure.

#### 3.2.5.1. Marini mapping functions

In 1972, J.W. Marini basing his model on the work of Helen Hopfield, assumed that one could separate the atmosphere in different layers where the refractive index was approximately constant, c.f. [Marini, 1972]. Further he supposed that the troposphere was horizontally stratified. As stated above, the basic mapping function is just given by

$$m(\varepsilon) = \frac{1}{\sin \varepsilon} =: \text{cosec } \varepsilon \quad (3.2.5.1)$$

J.W. Marini expands this in a truncature of a continuous fraction with the sine of the elevation angle as parameter.

$$m(\varepsilon) = \frac{1}{\sin \varepsilon + \frac{a}{\sin \varepsilon + \frac{b}{\sin \varepsilon + \frac{c}{\sin \varepsilon + \dots}}}} \quad (3.2.5.2)$$

where  $\varepsilon$  varies from the horizon or  $0^\circ$  to the zenith or  $90^\circ$  and  $a, b, c, \dots$  are dimensionless coefficients. This mapping function known as the Marini function constitutes the basis for almost all later derived tropospheric models. Actually, using only the two first terms  $a$  and  $b$  in (3.2.5.1), Marini has found great agreement with ray traces of a model atmosphere to better than 3%, after [Niell, 1996]. In 1973, C.W. Murray and J.W. Marini included a correction term for the variation of gravity with latitude and height.

[Davis et al., 1985] based his research on Marini and Murray's work. He introduced the third coefficient  $c$  and also normalized the Marini function to the zenith. Therefore he changed the second parameter  $b$  to a tangent to ensure that the mapping function takes the value 1 at zenith.

$$m(\varepsilon) = \frac{1}{\sin \varepsilon + \frac{a}{\tan \varepsilon + \frac{b}{\sin \varepsilon + c}}} \quad (3.2.5.3)$$

A sub-centimeter accuracy in Zenith TD (ZTD) was thus ensured down to elevation angles of  $5^\circ$ . The parameters  $a$  and  $b$  linearly depend on the surface meteorological data (usually the surface pressure, the relative humidity and ground temperature) and on the height of the troposphere.

#### 3.2.5.2. Herring mapping function

In 1992 T.A. Herring from Delft University in the Netherlands, c.f. [Herring, 1992], developed a model by integrating radiosonde data from continental United States (CONUS) stations in the mapping function. He introduced for the first time a dependency of the mapping function on the geographic coordinates of the observation



site as well as the surface temperature. This was aimed at compensating for the varying upper air layer temperatures at different latitudes.

He obtained for elevation angles down to 3° and latitudes between 27° and 65° North

$$m_x(\varepsilon, \varphi, h, T) = \frac{\frac{1}{1 + \frac{a_x}{1 + \frac{b_x}{1 + c_x}}}}{\sin \varepsilon + \frac{a_x}{\sin \varepsilon + \frac{b_x}{\sin \varepsilon + c_x}}}, \quad x = h, w \quad (3.2.5.4)$$

where the three coefficients depend linearly on the cosine of the latitude  $\varphi$ , on the height  $h$  above the WGS-84 geoid and on the surface temperature  $T$  in Kelvin of the station. For the hydrostatic component of the refractivity, these are given by

$$\begin{aligned} a_h &= 10^{-3} \cdot [1.2320 + 0.0139 \cdot \cos \varphi - 0.0209 \cdot h + 2.15 \cdot 10^{-3} \cdot (T - 283)] \\ b_h &= 10^{-3} \cdot [3.1612 + 0.1600 \cdot \cos \varphi - 0.0331 \cdot h + 2.06 \cdot 10^{-3} \cdot (T - 283)] \\ c_h &= 10^{-3} \cdot [71.2440 + 4.2930 \cdot \cos \varphi - 0.1490 \cdot h + 2.10 \cdot 10^{-3} \cdot (T - 283)] \end{aligned} \quad (3.2.5.5)$$

For the wet component of the refractivity, one has

$$\begin{aligned} a_w &= 10^{-3} \cdot [0.583 + 0.011 \cdot \cos \varphi - 0.052 \cdot h + 1.4 \cdot 10^{-3} \cdot (T - 283)] \\ b_w &= 10^{-3} \cdot [1.402 + 0.102 \cdot \cos \varphi - 0.101 \cdot h + 2.0 \cdot 10^{-3} \cdot (T - 283)] \\ c_w &= 10^{-3} \cdot [45.85 + 1.91 \cdot \cos \varphi - 1.290 \cdot h + 1.5 \cdot 10^{-3} \cdot (T - 283)] \end{aligned} \quad (3.2.5.6)$$

### 3.2.5.3. Niell mapping function

A few years later, 1996 to be exact, A.E. Niell from the Massachusetts Institute of Technology (MIT) detected many limitations in the mapping functions of Herring. The only real variable in both (3.2.5.4), (3.2.5.5) and (3.2.5.6) is the surface temperature  $T$ . All the other parameters are fixed by the location of the observation station. This does not take into account the temporal variability of the temperature due to the variation of troposphere thickness with time. The temperature strongly varies from sea level up to circa 2000 meters and then gradually becomes constant, indicating the presence of a boundary layer. This phenomenon limits the accuracy of the former mapping functions. A.E. Niell corrected this. For further details, refer to [Niell, 1996].

His mapping function is formed by a combination of a 3-terms Marini function and a normalization to unity at zenith, as was done by Herring. However the coefficients are profoundly modified. These are linearly interpolated from nine sets of radiosonde profiles.

He assumed that “(1) the Southern and Northern hemispheres are antisymmetric in time; that is, the seasonal behavior is the same, (2) the equatorial region is described by the 15° north latitude profile, and (3) the polar regions are described by the 75° north latitude profiles. Then the nine sets of coefficients provide mapping functions near the two extrema of the annual variation spanning all latitudes”. Thus mapping functions for any latitude and epoch are obtained by linear interpolation (in latitude) of the sets of coefficients.

Regarding the mapping function, the coefficients are modeled at each latitude  $\lambda_i$  as sinusoids in time with period of a year (in UT time). For complete information on this modeling, refer to [Emardson et al., 1998a to d]. The coefficients are then given by

$$x(\lambda_i, t) = x_{avg}(\lambda_i) + x_{amp}(\lambda_i) \cdot \cos \left[ 2\pi \cdot \left( \frac{t - T_0}{326.25} \right) \right], \quad x = a, b, c \quad i = 1, \dots, N \quad (3.2.5.7)$$

where  $T_0$  is the phase given by the time at Day of Year (DOY) 28, starting from January 0.0, in UT days. The average and amplitude coefficients are given in Table 7. An analytic height correction was introduced in the model

$$\Delta m(\varepsilon) = \left[ \frac{1}{\sin \varepsilon} - m(\varepsilon, a_{ht}, b_{ht}, c_{ht}) \right] \cdot H \quad (3.2.5.8)$$

where  $H$  is the height of the observation station above the WGS-84 geoid, the mapping function  $m$  is the one of (3.2.5.3) and the coefficients  $x_{ht}$ ,  $x = a, b, c$  ( $ht = \text{height}$ ) are also given in Table 7. Thus one obtains a hydrostatic mapping function of type

$$m_h(\varepsilon) = \frac{\frac{1}{1 + \frac{a_h}{1 + \frac{b_h}{1 + c_h}}} + \Delta m(\varepsilon)}{\sin \varepsilon + \frac{a_h}{\sin \varepsilon + \frac{b_h}{\sin \varepsilon + c_h}}} \quad (3.2.5.9)$$

The error in height being relatively small, the Niell model assumes a single height correction for all latitudes. Further the wet mapping function has no temporal dependence. The wet mapping function of Niell is thus given by equation (3.2.5.4) and the height correction is also applied.

Finally, one has for the hydrostatic mapping function coefficients the results of Table 7 hereunder:

coefficients	latitude	
	45°	60°
$a_{avg}$	$1.2465 \cdot 10^{-3}$	$1.2196 \cdot 10^{-3}$
$b_{avg}$	$2.9288 \cdot 10^{-3}$	$2.9022 \cdot 10^{-3}$
$c_{avg}$	$63.7217 \cdot 10^{-3}$	$63.8242 \cdot 10^{-3}$
$a_{amp}$	$2.6523 \cdot 10^{-5}$	$3.4000 \cdot 10^{-5}$
$b_{amp}$	$3.0160 \cdot 10^{-5}$	$7.2562 \cdot 10^{-5}$
$c_{amp}$	$4.3497 \cdot 10^{-5}$	$84.7953 \cdot 10^{-5}$
$a_{ht}$	$2.53 \cdot 10^{-5}$	$2.53 \cdot 10^{-5}$
$b_{ht}$	$5.49 \cdot 10^{-3}$	$5.49 \cdot 10^{-3}$
$c_{ht}$	$1.14 \cdot 10^{-3}$	$1.14 \cdot 10^{-3}$

Table 7. Niell hydrostatic mapping function coefficients

Combining the parameter values of Table 7, eqs. (3.2.5.7), (3.2.5.8) and (3.2.5.9) and linearly extrapolating for any given latitude (with the given coefficients of Table 7 for European stations), the hydrostatic mapping function of Niell is fully defined.

For the wet mapping function, it holds Table 8 below.

coefficients	latitude	
	45°	60°
$a_w$	$5.8118 \cdot 10^{-4}$	$5.9725 \cdot 10^{-4}$
$b_w$	$1.45727 \cdot 10^{-3}$	$1.50074 \cdot 10^{-3}$
$c_w$	$4.390893 \cdot 10^{-2}$	$4.462698 \cdot 10^{-2}$

Table 8. Niell wet mapping function coefficients

As it was already done for the hydrostatic mapping function coefficients, the wet mapping function of Niell is obtained by linear extrapolation.

The Niell mapping function presents huge advantages compared to other mapping functions. First of all it is totally independent of any surface meteorological data, thus being very robust with variations in experiment design and abrupt changes in the meteorological conditions. The sudden changes cannot be modeled very accurately. Secondly,

it holds up to low elevation angles: up to 3 degree. Hence the mapping functions biases are quasi-negligible. This was not the case for all mapping functions presented until then, except the Herring mapping function. Further, the troposphere becomes azimuthally asymmetric at very low elevation angles. Niell proved that his model could augment the accuracy of the Zenith Tropospheric Delay (ZTD) above the observation site and yield to a GPS signal sensitivity in ZTD in the centimeter range. To date, the Niell mapping function is without doubt one of the most precise functions for determining the hydrostatic delay in the GPS signal.

The choice of the mapping function depends essentially on the information one has at disposal. Indeed, if no ground meteorological data is available for the location of the GPS receivers, the Niell mapping functions seems to be well adapted. However, this is rarely the case and thus other mapping functions are used, e.g. the Herring mapping functions. As new mapping functions might be proposed, this decision will become more difficult and might reveal itself as not the most judicious.

### 3.3. Atmosphere modeling

The major issue for the determination of the tropospheric path delay and more generally path delays remains the availability or not of ground meteorological data. Usually one understands under meteorological data a set of temperature measurements, atmospheric pressure and partial water vapor pressure or its related relative humidity observations. Hereunder a spatial and temporal model is presented for each of the meteorological observables.

#### 3.3.1. Temperature field

##### 3.3.1.1. General description

The atmosphere is separated into four main regions depending on their altitude above the mean sea level (MSL). The temperature profile of these layers is summarized on Figure 12. The marks on the left side of Figure 12 represent the amount of gases left above that height.

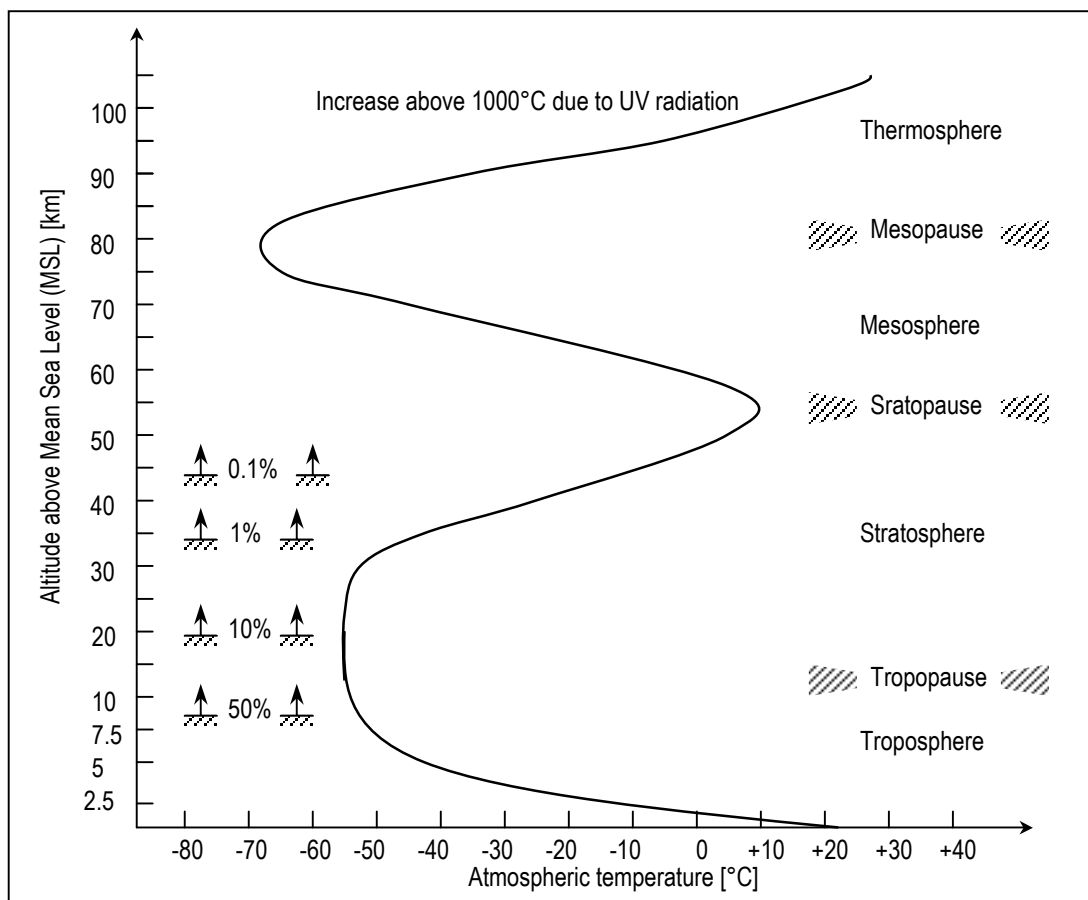


Figure 12. Temperature profile as function of altitude. After [Rödel, 2000].

The lowest layer is the so-called *troposphere*. It stretches from the MSL to approximately 8 to 10 km depending of the latitude of the observation site. The sole exceptions are the poles where a temperature inversion already takes

place at 2 to 3 km above ground level (AGL). As stated in paragraph 3.1, the troposphere contains the majority of the atmospheric water vapor. There, the temperature decreases with the altitude with an approximate constant rate varying between  $-0.5^\circ\text{C}/100\text{ m}$  and  $-1^\circ\text{C}/100\text{ m}$ . The adiabatic expansion of the hydrostatic and humidity fields, i.e. the compression or expansion of the air masses are the main processes for the formation of a temperature profile in the troposphere. Beneath those, radiative processes also take place.

The second lowest layer is the *tropopause* where the temperature is nearly constant with increasing altitude. Climbing from the MSL upwards, the temperature minimum is attained between 8 km and 10 km in Northern latitudes and between 17 km and 18 km in the tropics. This temperature minimum marks the beginning of the tropopause. According to the International Standard Atmosphere (ISA) model, c.f. [Lertes, 2000] regulated by the International Civil Aviation Organization (ICAO), the tropopause shows a temperature minimum of  $-56.51^\circ\text{C}$ . The physical processes are characterized by low heating due to solar radiation and slight cooling through thermal radiation.

In the *stratosphere*, which stretches between 18 km and 55 km MSL, the mixing ratios of these two effects are inverted. The radiation cooling through the water vapor in the upper troposphere and in the tropopause as well as the absorption of solar radiation in the upper stratosphere lead to a convection layer with little thermal exchanges. Therefore, the thermal profile of the stratosphere is determined by radiation equilibrium between heating through solarization and cooling through radiation in the infrared (IR) spectral range. The lower stratosphere can be seen as an isothermal layer while the upper stratosphere can be modeled with a constant and positive temperature gradient. The upper stratosphere starts at about 32 km MSL.

The *stratopause* marks a temperature inversion at an altitude MSL of approximately 55 km. The further upper layer is the *mesosphere*. It shows a similar behavior to the troposphere as far as the temperature is concerned. Above it comes the *mesopause*, i.e. between 75 km and 80 km MSL. There the atmosphere is heated by absorption of the solar ultraviolet (UV) radiation by the hydrogen molecules  $\text{H}_2$ . The temperature increases strongly with altitude in the fourth layer, the *thermosphere*. It shows strong diurnal variations in temperature and reaches  $1200^\circ\text{C}$ - $1500^\circ\text{C}$ . At the same time, the ion density strongly decreases.

### 3.3.1.2. Temperature model

The main issue as far as the temperature profile is concerned is the determination of the temperature gradients for all infinitesimal atmospheric layers. This is the topic of the coming paragraphs.

#### 3.3.1.2.1. Temperature profile

Retaking the observation form the previous paragraph and referring to Figure 12, one can model the altitude dependence of temperature as either a linear function or a constant. Hence, it is of the type

$$T(z) = \begin{cases} T_0 + \gamma \cdot z, & z_0 \leq z \leq z_1 \\ T_1, & z > z_1 \end{cases} \quad (3.3.1.1)$$

where  $z$  is the altitude MSL,  $z_0$  is the altitude of the reference point MSL and  $z_1$  is the altitude of the tropopause. Eq. (3.3.1.1) can be extended to the upper layers of the atmosphere by inserting different layers with linear temperature profile. Now one has to compute the temperature gradient  $\gamma$ .

#### 3.3.1.2.2. Hydrostatic air gradient

The first law of thermodynamic states

$$dU = \delta Q + \delta W \quad (3.3.1.2)$$

where  $U$  is the internal energy of the gas,  $Q$  the heating rate or simply heating and  $W$  is the work applied to the system. Now for a *closed system* it holds

$$\delta W = - p \cdot dV \quad (3.3.1.3)$$

Thus, introducing eq. (3.3.1.3) in eq. (3.3.1.2) gives

$$dU = \delta Q - p \cdot dV \quad (3.3.1.4)$$

Assume that the *dry air* is an *ideal gas*. Then the internal energy is only a function of the temperature  $T$ :

$$dU = n \cdot C_V \cdot dT \quad (3.3.1.5)$$

where  $n$  is the number of mol of the gas in the system and

$$C_V := \left( \frac{\partial U}{\partial T} \right)_V \quad (3.3.1.6)$$

is the heat capacity at constant volume. Because  $C_V$  is an extensive variable, and hence depends on the mass  $M$  of the system, one often deals with the heat capacity per unit mass or specific heat capacity:

$$c_V := \frac{C_V}{M} \quad (3.3.1.7)$$

Inserting eq. (3.3.1.5) in eq. (3.3.1.4) yields to

$$\delta Q = p \cdot dV + n \cdot C_V \cdot dT \quad (3.3.1.8)$$

The *ideal gas law* is

$$p \cdot V = n \cdot R \cdot T \quad (3.3.1.9)$$

where

$$R = 8.314510 \text{ J} \cdot \text{mol}^{-1} \cdot \text{K}^{-1} \quad (3.3.1.10)$$

is the universal gas constant. Build the differential of eq. (3.3.1.9) for  $n=1$  mol

$$p \cdot dV + V \cdot dp = R \cdot dT \quad (3.3.1.11)$$

Combine eq. (3.3.1.8) and eq. (3.3.1.11) again for  $n=1$  mol,

$$\delta Q = -V \cdot dp + (R + C_V) \cdot dT \quad (3.3.1.12)$$

The specific heat at constant pressure is defined as

$$C_p := \left( \frac{\partial H}{\partial T} \right)_p \quad (3.3.1.13)$$

where

$$H := U + p \cdot V \quad (3.3.1.14)$$

is the enthalpy of the gas. Similarly to eq. (3.3.1.7), one defines the specific heat at constant temperature as

$$c_p := \frac{C_p}{M} \quad (3.3.1.15)$$

Further, it holds

$$C_p = C_V + R \quad (3.3.1.16)$$

Insert eq. (3.3.1.16) in eq. (3.3.1.12)

$$\delta Q = -V \cdot dp + C_p \cdot dT \quad (3.3.1.17)$$

Now use the ideal gas law, eq. (3.3.1.9) to obtain

$$\delta Q = -\frac{RT}{p} \cdot dp + C_p \cdot dT \quad (3.3.1.18)$$

An *adiabatic process* is defined as a process where there is no exchange of heat with the environment. Thus it holds

$$\delta Q = 0 \quad (3.3.1.19)$$

Assume that the processes that take place in the troposphere are adiabatic. One has then with eq. (3.3.1.18),

$$0 = -\frac{RT}{p} \cdot dp + C_p \cdot dT \quad (3.3.1.20)$$

Furthermore, the barometric formula (c.f. paragraph 3.3.2.) states that

$$\frac{dp}{p} = \frac{-Mg}{RT} \cdot dz \quad (3.3.1.21)$$

Insert eq. (3.3.1.21) in eq. (3.3.1.20). This yields to

$$0 = Mg \cdot dz + C_p \cdot dT \quad (3.3.1.22)$$

That is

$$\frac{dT}{dz} = \frac{-Mg}{C_p} \stackrel{(3.3.1.14)}{=} \frac{-g}{c_p} \quad (3.3.1.23)$$

This adiabatic temperature gradient is often labeled as

$$\Gamma := \left( \frac{dT}{dz} \right)_{adia} \quad (3.3.1.24)$$

### 3.3.1.2.3. True temperature gradient

However it exists water vapor in the air. This water vapor is concentrated mostly in the troposphere. Hence defined a true temperature gradient to take into account the effects of the water vapor on the temperature variations with altitude.

$$\gamma := \left( \frac{dT}{dz} \right)_{true} \quad (3.3.1.25)$$

Assume now that there is *no condensation* taking place. Then replace the specific heat at constant pressure  $c_p$  by the weighed specific heats for wet and hydrostatic air. Define the *specific humidity* as

$$s := \frac{\rho_w}{\rho_w + \rho_h} \quad (3.3.1.26)$$

where  $\rho$  is the density and the indices  $w$  stand for wet and  $h$  for hydrostatic, i.e. for respectively the contribution of the water vapor and of the dry air. Inserting eq. (3.3.1.26) in eq. (3.3.1.23), it holds then for humid air

$$\left( \frac{dT}{dz} \right)_{wet|no\ condensation} = \frac{-g}{c_{p,w} \cdot s + c_{p,h} \cdot (1-s)} \quad (3.3.1.27)$$

If the atmospheric water vapor condensates, then eq. (3.3.1.27) does not hold. In order to derive the *humid adiabatic temperature gradient*, one has to consider again the first law of thermodynamics, the energy conservation law. Insert eq. (3.3.1.21) in eq. (3.3.1.18) for  $n=1$  mol,

$$\delta Q = C_p \cdot dT + Mg \cdot dz \quad (3.3.1.28)$$

Because the saturation of air with water vapor is only a question of absolute humidity, i.e. of water vapor content per unit volume, express all quantities as a function of the volume  $V$ . Thus using the ideal gas law, multiply the right hand side (RHS) of eq. (3.3.1.28) with

$$\frac{n}{V} = \frac{p}{RT} \quad (3.3.1.29)$$

Hence the left hand side (LHS) of eq. (3.3.1.28) is the heating per volume unit. This yields to

$$\delta Q = \frac{C_p \cdot p}{R \cdot T} \cdot dT + \frac{M \cdot g \cdot p}{R \cdot T} \cdot dz \quad (3.3.1.30)$$

As condensation has been assumed, there is a phase transfer of gaseous water vapor into liquid water (droplets) for saturated air as it cools down. Labeling the vaporization latent heat per water mass unit by  $L_{vap}$ , one has

$$\delta Q = -L_{vap} \cdot d\rho_{w,sat} \quad (3.3.1.31)$$

The minus sign stands for the decrease in the amount of water vapor molecules present in the air. The index *sat* stands for the saturated air<sup>9</sup>. Equating (3.3.1.30) and (3.3.1.31) yields to

$$-L_{vap} \cdot \frac{d\rho_{w,sat}}{dT} \cdot dT = \frac{C_p \cdot p}{R \cdot T} \cdot dT + \frac{M \cdot g \cdot p}{R \cdot T} \cdot dz \quad (3.3.1.32)$$

Reorganizing eq. (3.3.1.32),

$$\left( \frac{dT}{dz} \right)_{wet} \Big|_{with\ condensation} = \frac{-M \cdot p \cdot g}{C_p \cdot p + R \cdot T \cdot L_{vap} \cdot \frac{d\rho_{w,sat}}{dT}} \quad (3.3.1.33)$$

This is the humid adiabatic temperature gradient. It contains the hydrostatic adiabatic temperature gradient as limit for

$$\frac{d\rho_{w,sat}}{dT} = 0 \quad (3.3.1.34)$$

### 3.3.1.2.4. Adopted temperature model

Combining the results of the three previous paragraphs, and using the Heavyside function defined as

$$\Theta(z) := \begin{cases} 1, & z \geq 0 \\ 0, & z < 0 \end{cases} \quad (3.3.1.35)$$

one has for the altitude dependence of the temperature

$$T(z) = [T_0 + \gamma \cdot z] \cdot [1 - \Theta(z - z_1)] + T_1 \cdot \Theta(z - z_1) \quad (3.3.1.36)$$

For numerical applications, the following expression,

$$\Theta(z - z_1) \approx \frac{1}{\pi} \cdot [\arctan(z - z_1)] + \frac{1}{2} \quad (3.3.1.37)$$

is a good approximation of the Heavyside function. In order to take into account the local variations of temperature with the direction, one can insert a two dimensional horizontal gradient in eq. (3.3.1.36). This gives

$$T(x, y, z) = [T_0 + \gamma \cdot z] \cdot [1 - \Theta(z - z_1)] + T_1 \cdot \Theta(z - z_1) + a_T \cdot (x - x_0) + b_T \cdot (y - y_0) \quad (3.3.1.38)$$

where the index 0 labels the reference point. Another indexing will be introduced later. Furthermore assume that the temperature varies slowly with time but nonetheless varies. Hence add also a time gradient. This yields to the four dimensional (4D) temperature model:

$$T(\mathbf{x}, t) = T(x, y, z, t) = [T_0 + \gamma \cdot z] \cdot [1 - \Theta(z - z_1)] + a_T \cdot (x - x_0) + b_T \cdot (y - y_0) + c_T \cdot (t - t_0) + T_1 \cdot \Theta(z - z_1) \quad (3.3.1.39)$$

where the index *T* in the three coefficients is set to differentiate them from simple constants.

## 3.3.2. Pressure model

Consider an infinitesimal volume element  $dV$  of unit area. Then  $dV = dz$ . Refer to Figure 13 left on next page. According to Newton's law of mechanics, it holds

$$dp = -\rho \cdot g \cdot dz \quad (3.3.2.1)$$

for the pressure differential  $dp$ .  $\rho$  is the air density and  $g$  is the gravity constant. The universal gas law states

$$\frac{p}{\rho} = R \cdot \frac{T}{m} \quad (3.3.2.2)$$

<sup>9</sup> Do not confound it with the index for the GPS satellites !

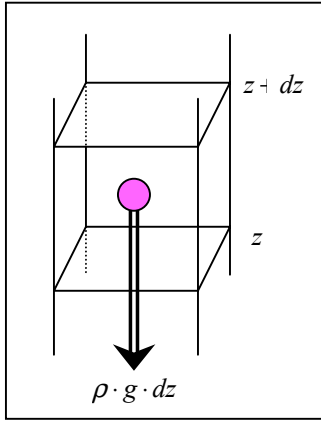


Figure 13. Pressure of a volume element.

where  $p$  is the pressure in  $\text{N} \cdot \text{m}^{-2}$ ,  $R$  is the universal gas constant defined in eq. (3.3.1.10),  $T$  is the temperature in K,  $\rho$  is the density in  $\text{kg} \cdot \text{m}^{-3}$  and  $m$  is the molecular mass of the considered gas, in  $\text{kg} \cdot \text{mol}^{-1}$ .

Following [Hopfield, 1969], assume one can separate the wet air from the hydrostatic air. Then one has two relative gas constants:

$$R_h := \frac{R}{m_h} \quad \text{and} \quad R_w := \frac{R}{m_w} \quad (3.3.2.3a,b)$$

Further, it holds

$$\frac{R_h}{R_w} = \frac{m_w}{m_h} \cong 0.622 \quad (3.3.2.4)$$

Extract now the density for wet air from the partial water vapor pressure and the universal gas law.

$$\rho_w = \frac{e}{R_w \cdot T} \quad (3.3.2.5)$$

With the specific humidity from eq. (3.3.1.26), one has

$$s := \frac{\rho_w}{\rho} \quad \text{where} \quad \rho := \rho_w + \rho_h \quad (3.3.2.6a,b)$$

Assuming the air is mostly dry, i.e.  $m \approx m_h$ , and using (3.3.2.3a) to express the unity

$$\frac{R_h}{R} \cdot m = 1 \quad (3.3.2.7)$$

the specific humidity becomes

$$s = \frac{\rho_w}{\rho} \cdot 1 = \frac{\rho_w}{\rho} \cdot \frac{R_h}{R} \cdot m = R_h \cdot \left[ \frac{m}{\rho \cdot R} \right] \cdot \rho_w \quad (3.3.2.8)$$

Insert eq. (3.3.2.2) in eq. (3.3.2.8)

$$s = \frac{R_h \cdot \rho_w \cdot T}{p} = \frac{R_h}{R_w} \cdot \frac{R_w \cdot \rho_w \cdot T}{p} \quad (3.3.2.9)$$

and introduce eq. (3.3.2.5)

$$s = \frac{R_h}{R_w} \cdot \frac{e}{p} \quad (3.3.2.10)$$

According to [Höflinger, 1993], and inserting  $R_h$ ,  $R_w$ ,  $\rho_h$  and  $\rho_w$  in the universal gas law gives for the pressure

$$p = T \cdot R_h \cdot \rho \cdot (1 + 0.608 \cdot s) \quad (3.3.2.11)$$

Recombine eq. (3.3.2.11) by introducing the virtual temperature defined by

$$T_v := T \cdot (1 + 0.608 \cdot s) \quad (3.3.2.12)$$

This gives a modified gas law:

$$\frac{p}{\rho} = R_h \cdot T_v \quad (3.3.2.13)$$

where the total density is given by eq. (3.3.2.6.b). From eq. (3.3.2.13) get

$$\rho = \frac{p}{R_h \cdot T_v} \quad (3.3.2.14)$$



and insert this eq. (3.3.2.1) to obtain

$$dp = -p \cdot \frac{g}{R_h \cdot T_v} \cdot dz \quad (3.3.2.15)$$

Take now the model for the temperature as a function of the altitude, eq. (3.3.1.1). There are two cases to consider. First assume that the virtual temperature is constant, i.e.  $T_v \neq T_v(z)$  and integrate eq. (3.3.2.15)

$$\int_{z_1}^z \frac{dp}{p} = - \int_{z_1}^z \frac{g}{R_h \cdot T_v} dz' \quad (3.3.2.16)$$

This results in

$$\ln\left(\frac{p(z)}{p(z_1)}\right) = -\frac{g}{R_h \cdot T_v} \cdot (z - z_1) \quad (3.3.2.17)$$

Thus one has

$$p(z) = p(z_1) \cdot \exp\left\{-\frac{g}{R_h \cdot T_v} \cdot (z - z_1)\right\} \quad (3.3.2.18)$$

Assume now that the virtual temperature depends on the altitude  $z$ , i.e.  $T_v = T_v(z)$ . Again integrate eq. (3.3.2.15)

$$\int_{z_0}^{z_1} \frac{dp}{p} = -\frac{g}{R_h} \cdot \int_{z_0}^{z_1} \frac{dz'}{T_v(z')} \quad (3.3.2.19)$$

and use the harmonic mean for the virtual temperature, defined as

$$\left(\overline{\frac{1}{T_v}}\right) := \frac{1}{z} \cdot \int_0^z \frac{dz'}{T_v(z')} \quad (3.3.2.20)$$

Approximate eq. (3.3.2.19) with eq. (3.3.2.20),

$$\ln\left(\frac{p(z_1)}{p(z_0)}\right) = -\frac{g}{R_h} \cdot \left(\overline{\frac{1}{T_v}}\right) \cdot (z_1 - z_0) \quad (3.3.2.21)$$

This leads to

$$p(z_1) = p(z_0) \cdot \exp\left\{-\frac{g}{R_h} \cdot \left(\overline{\frac{1}{T_v}}\right) \cdot (z_1 - z_0)\right\} \quad (3.3.2.22)$$

Now define a scale height  $H_p$  by

$$H_p := \frac{R_h}{g} \cdot \left[\left(\overline{\frac{1}{T_v}}\right)\right]^{-1} \quad (3.3.2.23)$$

Insert eq. (3.3.2.23) in eq. (3.3.2.22) and index it with  $p$  for pressure

$$\boxed{p(z_1) = p(z_0) \cdot \exp\left\{-\frac{(z_1 - z_0)}{H_p}\right\}} \quad (3.3.2.24)$$

Note that in general the scale height<sup>10</sup>, usually labeled as  $z_0$  is defined in the following way

$$\frac{\text{total ensemble}}{\text{area}} = \int_0^{+\infty} c(z) dz = c_0 \cdot z_0 \quad (3.3.2.25)$$

<sup>10</sup> This notation is not used here in order to prevent any confusion with the ground altitude MSL, i.e. with the GPS's receiver altitude.

where  $c(z)$  is the concentration at altitude  $z$  of the quantity of interest. Thus the scale height is

$$z_0 = \frac{1}{c_0} \cdot \int_0^{+\infty} c(z) dz \quad (3.3.2.26)$$

As was done with eq. (3.3.1.36) for the temperature dependence on altitude, one can introduce a 2D horizontal gradient as well as a temporal gradient in both eq. (3.3.2.18) and eq. (3.3.2.24) in order to obtain a 4D pressure model. Hence one obtains

$$p(\mathbf{x}, t) = p(x, y, z, t) = \left[ p_0 + a_p \cdot (x - x_0) + b_p \cdot (y - y_0) + c_p \cdot (t - t_0) \right] \cdot e^{-\frac{(z-z_0)}{H_p}} \quad (3.3.2.27)$$

where the index 0 indicates the GPS's receiver position,  $H_p$  is the pressure scaling height and  $a$ ,  $b$  and  $c$  are the gradient coefficients.

### 3.3.3. Atmospheric humidity model

The atmospheric humidity  $e$  is the most volatile of the three quantities considered. Indeed its high temporal and spatial variability often limits the accuracy of the meteorological models. It is intended here to derive a basic model for  $e$ .

#### 3.3.3.1. Clausius-Clapeyron equation

From thermodynamics it is known that for a reversible process it holds

$$\frac{d}{dt} S(V, T) = \frac{1}{T} \cdot \frac{dU}{dt} + \frac{p}{T} \cdot \frac{dV}{dt} \quad (3.3.3.1)$$

where  $S$  is the entropy of the system. Further it holds

$$\frac{d}{dt} S(V, T) = \frac{\partial S}{\partial T} \cdot \frac{dT}{dt} + \frac{\partial S}{\partial V} \cdot \frac{dV}{dt} \quad (3.3.3.2)$$

Using the chain rule and comparing term by term eq. (3.3.3.1) with eq. (3.3.3.2), one has

$$\begin{aligned} \frac{\partial S}{\partial T} &= \frac{1}{T} \cdot \frac{\partial U}{\partial T} \\ \frac{\partial S}{\partial V} &= \frac{1}{T} \cdot \left( \frac{\partial U}{\partial V} + p \right) \end{aligned} \quad (3.3.3.3a,b)$$

where the temperature  $T$  and the volume  $V$  are independent variables. Combine both equations to build the second order partial differential of the entropy by first proceeding with (3.3.3.3a),

$$\frac{\partial^2 S}{\partial V \partial T} = \frac{1}{T} \cdot \frac{\partial^2 U}{\partial V \partial T} \quad (3.3.3.4)$$

However one can first proceed with eq. (3.3.3.3b). This gives

$$\frac{\partial^2 S}{\partial T \partial V} = \frac{1}{T} \cdot \left( \frac{\partial^2 U}{\partial T \partial V} + \frac{\partial p}{\partial T} \right) - \frac{1}{T^2} \cdot \left( \frac{\partial U}{\partial V} + p \right) \quad (3.3.3.5)$$

Using Schwarz's law to equate eq. 3.3.3.4) and eq. (3.3.3.5) yields to

$$\frac{\partial U}{\partial V} = T \cdot \frac{\partial p}{\partial T} - p \quad (3.3.3.6)$$

Eq. (3.3.3.6) holds for any system: for liquids and for gases or for a mixture of both as it is in the case of humid air. Especially for an ideal gas it holds

$$\frac{\partial U}{\partial V} = 0 \quad (3.3.3.7)$$

However the mixture of hydrostatic air and water vapor is *not* an ideal gas. During a phase transformation from gas to liquid, nothing changes except the relative amount of each component. Therefore it holds

$$U = \tau \cdot U_w + (1 - \tau) \cdot U_v, \quad 0 \leq \tau \leq 1 \quad (3.3.3.8)$$

where  $U_v$  is the internal energy of the system at the beginning of the phase change where there is only water vapor and  $U_w$  is the internal energy of the system at the end of the phase change where there the water vapor is entirely present in under liquid form (pure water). In a similar way one has with the corresponding quantities for the volume  $V$

$$V = \tau \cdot V_w + (1 - \tau) \cdot V_v, \quad 0 \leq \tau \leq 1 \quad (3.3.3.9)$$

Combine eq. (3.3.3.8) and eq. (3.3.3.9) to get

$$\frac{\partial U}{\partial V} = \frac{\partial U}{\partial \tau} \cdot \left[ \frac{\partial \tau}{\partial V} \right]^{-1} = \frac{U_v - U_w}{V_v - V_w} \quad (3.3.3.10)$$

Define the enthalpy of vaporization  $L_v$  as

$$L_v := H_v - H_w = U_v - U_w + p \cdot (V_v - V_w) \quad (3.3.3.11)$$

where the definition of the enthalpy, eq. (3.3.1.14) has been used. Combine eq. (3.3.3.6), eq. (3.3.3.10) and eq. (3.3.3.11) to obtain

$$\frac{U_v - U_w}{V_v - V_w} = \frac{H_v - H_w}{V_v - V_w} - p \stackrel{(3.3.3.10)}{=} \frac{\partial U}{\partial V} \stackrel{(3.3.3.11)}{=} T \cdot \frac{\partial p}{\partial T} - p \quad (3.3.3.12)$$

Again using eq. (3.3.3.11), it follows

$$T \cdot \frac{\partial p}{\partial T} = \frac{L_v}{V_v - V_w} \quad (3.3.3.13)$$

According to [Bohren and Albrecht, 1998], one should note that the pressure  $p$  here is just the saturation vapor pressure  $e_s$  and that  $e_s = e_s(T)$  for pure water. Hence one has ordinary derivatives in eq. (3.3.3.13) instead of partial derivatives. Thus eq. (3.3.3.13) becomes

$$\frac{de_s}{dT} = \frac{1}{T} \cdot \frac{L_v}{V_v - V_w} \quad (3.3.3.14)$$

It is of interest to work with intensive variables such as the specific quantities. Hence divide the RHS of eq. (3.3.3.14) by the total mass of water to obtain

$$\frac{de_s}{dT} = \frac{1}{T} \cdot \frac{l_v}{v_v - v_w} \quad (3.3.3.15)$$

where

$$l_v = \frac{L_v}{M} \quad \text{and} \quad v = \frac{V}{M} \quad (3.3.3.16a,b)$$

Eq. (3.3.3.16a) is the enthalpy of vaporization per mass unit and eq. (3.3.3.16b) is the specific volume, sometimes called inverse density. Eq. (3.3.3.15) is the *Clausius-Clapeyron equation*.

### 3.3.3.2. Temperature dependence of the enthalpy of vaporization

Recall that the enthalpy is defined by eq. (3.3.1.14) as

$$H := U + p \cdot V \quad (3.3.3.17)$$

and the enthalpy of vaporization  $L_v$  was defined by eq. (3.3.3.11) as

$$L_v := H_v - H_w = U_v - U_w + p \cdot (V_v - V_w) \quad (3.3.3.18)$$

as the enthalpy difference between gaseous (vapor) and liquid phase at their common equilibrium pressure, which depends only on the temperature  $T$ . Hence  $L_v$  depends also only on the temperature  $T$ . Differentiate eq. (3.3.3.18) with respect to  $T$ ,

$$\frac{\partial L_v}{\partial T} = \frac{\partial H_v}{\partial T} - \frac{\partial H_w}{\partial T} = C_{pv} - C_{pw} \quad (3.3.3.19)$$

where the definition of the heat capacity at constant pressure has been used. Because  $L_v$  depends also only on the temperature, one has ordinary derivatives in eq. (3.3.3.19). Therefore

$$\frac{dL_v}{dT} = C_{pv} - C_{pw} = \text{const} \quad (3.3.3.20)$$

The specific heats decrease monotonically and very slowly with the temperature. Hence by assuming  $C_p \neq C_p(T)$ , one introduces only a small error into the computation. Integrate eq. (3.3.3.20)

$$L_v(T) = L_{v0} + (C_{pv} - C_{pw}) \cdot (T - T_0) \quad (3.3.3.21)$$

where  $T_0$  is the reference temperature. Again multiply the RHS by  $1/M$  to obtain

$$l_v(T) = l_{v0} + (c_{pv} - c_{pw}) \cdot (T - T_0) \quad (3.3.3.22)$$

This is the enthalpy of vaporization of water. It is linear in the temperature. According to [Bohren and Albrecht, 1998], eq. (3.3.3.22) agrees up to 1% with measurements in the range  $-20^\circ\text{C} \leq T \leq +30^\circ\text{C}$  for a reference temperature  $T_0 = 0^\circ\text{C}$ .

### 3.3.3.3. Temperature dependence of the saturation vapor pressure

Assume that the specific volume of vapor is much larger than the specific volume of liquid, i.e. it is such that

$$v_v \gg v_w \quad (3.3.3.23)$$

Retake the Clausius-Clapeyron equation, eq. (3.3.3.15) and use the previous assumption

$$\frac{de_s}{dT} \approx \frac{1}{T} \cdot \frac{l_v}{v_v} \quad (3.3.3.24)$$

Furthermore water vapor can be considered as an ideal gas to a good approximation. Using the ideal gas law, it follows that

$$e_s = R_v \cdot \frac{T}{v_v} \quad (3.3.3.25)$$

Combine eq. (3.3.3.24) and eq. (3.3.3.25)

$$\frac{1}{e_s} \cdot \frac{de_s}{dT} = \frac{l_v}{R_v \cdot T^2} \quad (3.3.3.26)$$

Insert eq. (3.3.3.22) in eq. (3.3.3.26)

$$\frac{1}{e_s} \cdot \frac{de_s}{dT} = \frac{l_{v0} + (c_{pw} - c_{pv}) \cdot T_0}{R_v \cdot T^2} - \frac{c_{pw} - c_{pv}}{R_v \cdot T} \quad (3.3.3.27)$$

Integrating eq. (3.3.3.27) yields to

$$\ln\left(\frac{e_s}{e_{s0}}\right) = \frac{l_{v0} + (c_{pw} - c_{pv}) \cdot T_0}{R_v} \cdot \left(1 - \frac{T_0}{T}\right) - \left(\frac{c_{pw} - c_{pv}}{R_v}\right) \cdot \ln\left(\frac{T}{T_0}\right) \quad (3.3.3.28)$$

where the constants of integration (reference temperature) for the enthalpy of vaporization and for the saturation vapor pressure have been assumed identical. For  $T_0 = 0^\circ\text{C}$ , the constants in eq. (3.3.3.28) are given by Table 9.

Constant	Value	Unit
$T_0$	273.15	K
$l_{v0}$	$2.5 \times 10^6$	$\text{J} \cdot \text{kg}^{-1}$
$c_{pw}$	4200	$\text{J} \cdot \text{kg}^{-1} \cdot \text{K}^{-1}$
$c_{pv}$	1850	$\text{J} \cdot \text{kg}^{-1} \cdot \text{K}^{-1}$
$R_v$	461.763	$\text{J} \cdot \text{mol}^{-1} \cdot \text{K}^{-1}$
$e_{s0}$	6.107	hPa

Table 9. Saturation vapor pressure: constants

With the values of Table 9, eq. (3.3.3.28) becomes

$$\ln\left(\frac{e_s}{e_{s0}}\right) = 6804.14 \cdot \left(\frac{1}{T_0} - \frac{1}{T}\right) - 5.09 \cdot \ln\left(\frac{T}{T_0}\right) \quad (3.3.3.29)$$

This can be further simplified if one assumes that  $l_v$  is independent of the temperature. Take this fact into account and integrate eq. (3.3.3.26). This yields to

$$e_s = e_{s0} \cdot \exp\left(\frac{l_v}{R_v \cdot T_0}\right) \cdot \exp\left(-\frac{l_v}{R_v \cdot T}\right) \quad (3.3.3.30)$$

With the values of Table 9, eq. (3.3.3.30) becomes

$$\ln\left(\frac{e_s}{e_{s0}}\right) = 19.82 - \frac{5414.03}{T} \quad (3.3.3.31)$$

The saturation water vapor pressure from eq. (3.3.3.29) and eq. (3.3.3.31) are compared and plotted on Figure 14 on next page as a function of the atmospheric temperature in the range  $200 \text{ K} \leq T \leq 325 \text{ K}$ , i.e.  $-73.15^\circ\text{C} \leq T \leq 52.15^\circ\text{C}$ . One can see that eq. (3.3.3.31), in red on Figure 14, although much simpler than eq. (3.3.3.29), in green, does not deviate much from the more exact curve. Hence consider only eq. (3.3.3.31) in the following.

It is intended now to develop the link between the saturation water vapor pressure and the water vapor pressure as a function of the temperature in the atmosphere and then as a function of the three dimensional position in space and, of course, of the time  $t$ .

### 3.3.3.4. Water vapor pressure model

The relative humidity, expressed in %, is defined as

$$rH := 100 \cdot \frac{e_s}{e} \quad (3.3.3.32)$$

where  $e_s$  is the saturation water vapor pressure and  $e$  is the water vapor pressure, both at temperature  $T$ . Insert eq. (3.3.3.30) in eq. (3.3.3.32),

$$e(T) = \frac{rH}{100} \cdot e_s(T) = \frac{rH}{100} \cdot e_{s0} \cdot e^{\frac{l_v}{R_v \cdot T_0}} \cdot e^{-\frac{l_v}{R_v \cdot T}} \quad (3.3.3.33)$$

In numerical form, eq. (3.3.3.33) is

$$e(T) = \frac{rH}{100} \cdot 6.107 \cdot \exp\left[\frac{19.82 \cdot T - 5414.03}{T}\right] \quad (3.3.3.34)$$

Following [Troller et al., 2001 & 2002] linearize the exponent w.r.t. the altitude  $z$  and recall the temperature model of paragraph 3.3.1.2.4. Remind that  $\gamma$  is negative in the troposphere. Thus with eq. (3.3.3.34) one has

$$e(z) = e(z_0) \cdot e^{\frac{-(z-z_0)}{H_e}} \quad (3.3.3.35)$$

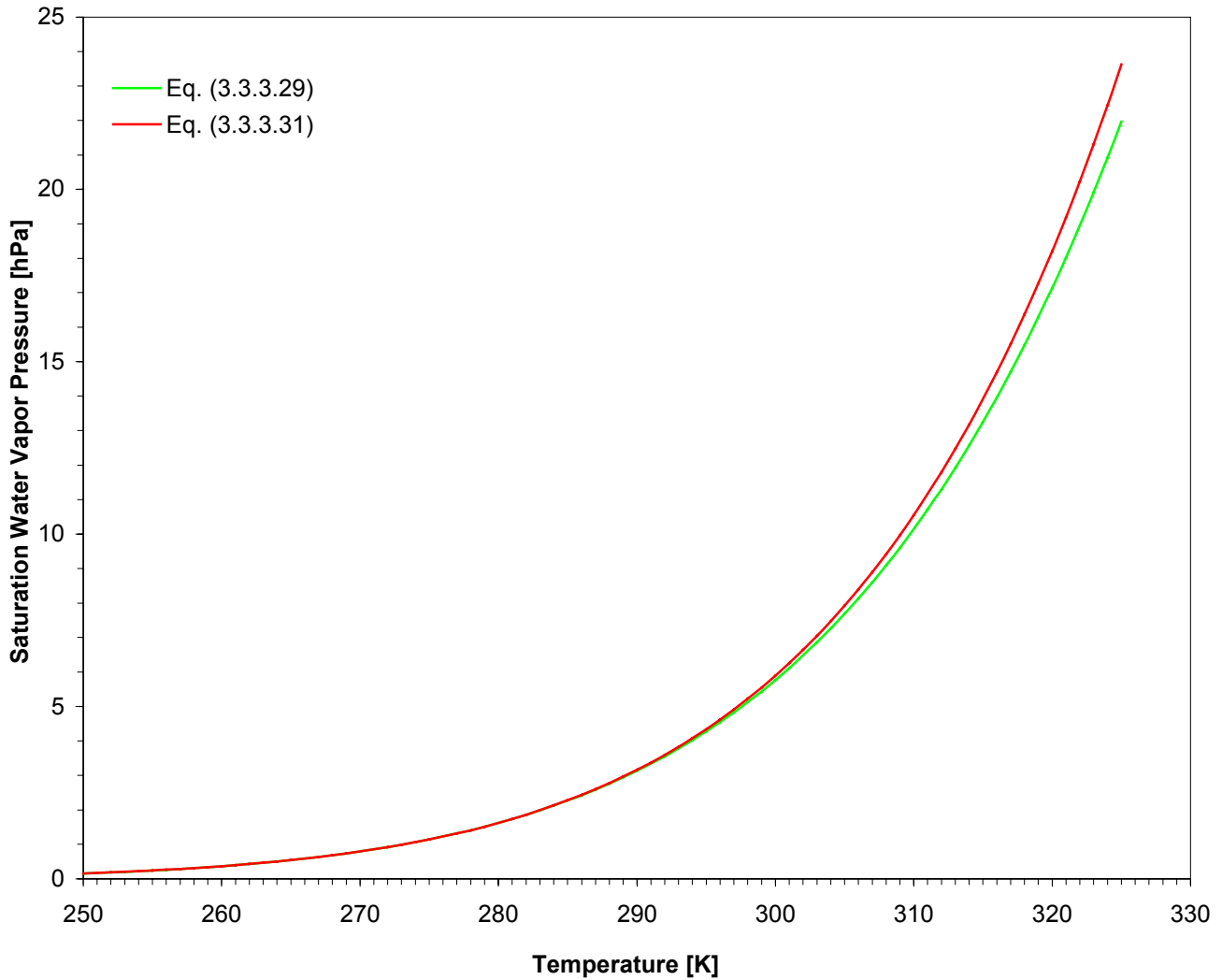


Figure 14. Saturation water vapor pressure as a function of the temperature in the atmosphere,  $e_s(T)$ .

where the scaling height  $H_e$  is different from the one for the pressure model! This is the one-dimensional model for the variation of the water vapor pressure with the altitude. It depends on the surroundings of the observation point: plain, mountain, sea... However a model with global validity is required. Therefore introduce a horizontal gradient as well as a temporal gradient. Finally this leads to the following 4D functional model for the water vapor pressure:

$$e(\mathbf{x}, t) = e(x, y, z, t) = [e_0 + a_e \cdot (x - x_0) + b_e \cdot (y - y_0) + c_e \cdot (t - t_0)] \cdot e^{-\frac{(z - z_0)}{H_e}} \quad (3.3.3.36)$$

### 3.3.4. Summary

Two kinds of functional models for the atmospheric temperature  $T$ , the atmospheric pressure  $p$  and the water vapor pressure  $e$  have been derived in the previous paragraphs. The first set depends only on the altitude  $z$ . It is

$$T(z) = [T_0 + \gamma \cdot z] \cdot [1 - \epsilon(z - z_1)] + T_1 \cdot \epsilon(z - z_1) \quad (3.3.4.1)$$

$$p(z) = p(z_0) \cdot \exp\left\{-\frac{(z - z_0)}{H_p}\right\} \quad (3.3.4.2)$$

$$e(z) = e(z_0) \cdot \exp\left\{-\frac{(z - z_0)}{H_e}\right\} \quad (3.3.4.3)$$

The second set consists in 4D functional models with an explicit dependence on space and time:

$$T(\mathbf{x}, t) = T(x, y, z, t) = [T_0 + \gamma \cdot z] \cdot [1 - \Theta(z - z_1)] \\ + a_T \cdot (x - x_0) + b_T \cdot (y - y_0) + c_T \cdot (t - t_0) \\ + T_1 \cdot \Theta(z - z_1) \quad (3.3.4.4)$$

$$p(\mathbf{x}, t) = p(x, y, z, t) = [p(z_0) + a_p \cdot (x - x_0) + b_p \cdot (y - y_0) + c_p \cdot (t - t_0)] \cdot e^{-\frac{(z-z_0)}{H_p}} \quad (3.3.4.5)$$

$$e(\mathbf{x}, t) = e(x, y, z, t) = [e(z_0) + a_e \cdot (x - x_0) + b_e \cdot (y - y_0) + c_e \cdot (t - t_0)] \cdot e^{-\frac{(z-z_0)}{H_e}} \quad (3.3.4.6)$$

### 3.4. Path delays modeling

In the following, a model for the path delay of the GPS signal is derived. It takes into account the altitude of the different atmospheric layers.

#### 3.4.1. Motivation

As discussed previously, the atmosphere can be separated into different layers of constant refractive index. Experimentally, the main variations of path delays are observed along the radial axis, i.e. in the zenith direction. Hence assume that the atmosphere shows an azimuthal symmetry around the ground receiver location. The atmosphere might be inclined with respect of the normal plane to the zenith direction.

According to Chapter 1, the troposphere represents the main concern for the evaluation of path delays. In order to accurately take it into account, the two sets of models presented above will be introduced in the computation. Referring to paragraph 3.3.1. and especially Figure 12, only 1% of the gaseous atmosphere is situated above 35 km MSL. The mass ratio is set as the selective criterion. Therefore a two layer model can be assumed to sufficiently and accurately represent the reality.

Label the GPS space vehicle's location by  $P'$  and the ground receiver's location by  $P_0$  with respective altitude  $z'$  and  $z_0$ . It is referred to Figure 15 on next page. The altitude of the tropopause is  $z_1$ . The zenith angle of the ground receiver is  $\theta_0$ . Consider an infinitesimal path element  $ds$  of the GPS signal path, stretching to point  $P$ . Let  $\theta$  be the zenith angle of  $P$ , i.e. at altitude  $z$ .

Retaking the computation of paragraph 3.2.1, the path delay is given by

$$\Delta L = \int_{P_0}^{P'} [n(s) - 1] ds \quad (3.4.1.1)$$

This can be projected along the zenith direction for each point  $P$  along the signal path. Hence eq. (3.4.1.1) becomes

$$\Delta L = \int_{z_0}^{z'} [n(z) - 1] \cdot \sec \theta ds \quad (3.4.1.2)$$

The zenith angle  $\theta$  depends on the refractive index  $n$ . One intends to find an expression for  $\sec \theta$  so that eq. (3.4.1.2) is integrable. The secant and cosecant are defined as

$$\sec x := \frac{1}{\cos x} \quad \text{and} \quad \operatorname{cosec} x := \frac{1}{\sin x} \quad (3.4.1.3a,b)$$

The *refraction law* gives

$$n \cdot z \cdot \sin \theta = n_0 \cdot z_0 \cdot \sin \theta_0 = \text{const} \quad (3.4.1.4)$$

It is useful to define the following quantity

$$y := \frac{n \cdot z}{n_0 \cdot z_0} \quad (3.4.1.5)$$

Combining eq. (3.4.1.4) and eq. (3.4.1.5) yields to

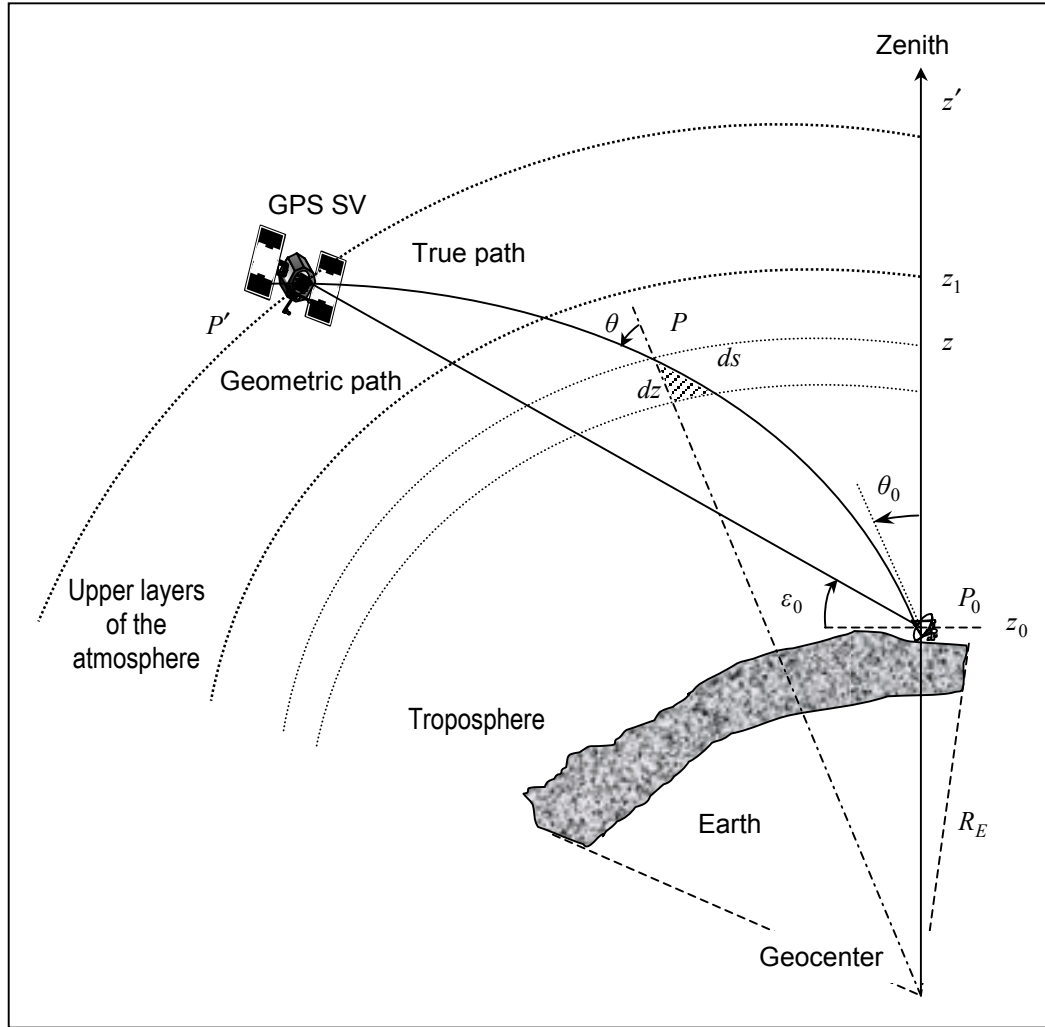


Figure 15. GPS signal path through the atmosphere

$$\sin^2 \theta = \frac{\sin^2 \theta_0}{y^2} = \frac{1 - \cos^2 \theta_0}{y^2} \stackrel{(3.4.1.3a)}{=} \frac{1}{y^2} \cdot \left[ \frac{\sec^2 \theta_0 - 1}{\sec^2 \theta_0} \right] \quad (3.4.1.6)$$

Thus

$$\cos^2 \theta = 1 - \sin^2 \theta = \frac{y^2 \cdot \sec^2 \theta_0 - \sec^2 \theta_0 + 1}{y^2 \cdot \sec^2 \theta_0} \quad (3.4.1.7)$$

With eq. (3.4.1.3a), one has

$$\sec \theta = y \cdot \sec \theta_0 \cdot \left[ (y^2 - 1) \cdot \sec^2 \theta_0 + 1 \right]^{1/2} \quad (3.4.1.8)$$

For small values of  $x$ , the Taylor expansion of  $(1+x)^s$ ,  $s \in \mathbb{R}$ , is

$$(1+x)^s = 1 + s \cdot x + \frac{s \cdot (s-1)}{2!} \cdot x^2 + O(x^3) \quad (3.4.1.9)$$

Using the definition of the refractivity, it holds

$$\frac{n}{n_0} = \frac{1 + N \cdot 10^{-6}}{1 + N_0 \cdot 10^{-6}} \approx (1 + N \cdot 10^{-6}) \cdot (1 + N_0 \cdot 10^{-6})^{-1} = 1 - (N - N_0) \cdot 10^{-6} - N \cdot N_0 \cdot 10^{-12} \quad (3.4.1.10)$$



According to [CCIR, 1986], it holds  $0 \leq N \leq 350$  and  $N_0 \approx 315$  for Switzerland. Hence one can assume with eq. (3.4.1.10) that

$$\frac{n}{n_0} \approx 1 \quad (3.4.1.9)$$

Therefore one has with eq. (3.4.1.8) and eq. (3.4.1.9)

$$\sec \theta = y \cdot \sec \theta_0 - \frac{1}{2} \cdot y \cdot (y^2 - 1) \cdot \sec^3 \theta_0 + O(y^5 \cdot \sec^5 \theta_0) \quad (3.4.1.10)$$

Eq. (3.4.1.11) further implies that

$$y \approx \frac{z}{z_0} = 1 + \frac{1}{z_0} \cdot (z - z_0) \quad (3.4.1.11)$$

Similarly

$$y \cdot (y^2 - 1) \approx \frac{2}{z_0} \cdot (z - z_0) \quad (3.4.1.12)$$

Combining eq. (3.4.1.12), eq. (3.4.1.13) and eq. (3.4.1.14) gives

$$\sec \theta = \sec \theta_0 - \frac{z - z_0}{z_0} \cdot [\sec^3 \theta_0 - \sec \theta_0] = \sec \theta_0 - \frac{z - z_0}{z_0} \cdot [\sec^2 \theta_0 - 1] \cdot \sec \theta_0 \quad (3.4.1.13)$$

Using the fact that

$$\sec^2 \theta_0 - 1 = \frac{1}{\tan^2 \theta_0} \quad (3.4.1.14)$$

One has

$$\sec \theta = \sec \theta_0 - \frac{z - z_0}{z_0} \cdot \sec \theta_0 \cdot \tan^2 \theta_0 \quad (3.4.1.15)$$

This implies that the atmosphere is considered as isotropic. Insert eq. (3.4.1.17) in eq. (3.4.1.2),

$$PD \equiv \Delta L = \sec \theta_0 \cdot \int_{z_0}^{z'} [n(z) - 1] dz - \frac{\sec \theta_0 \cdot \tan^2 \theta_0}{z_0} \cdot \int_{z_0}^{z'} [n(z) - 1] \cdot (z - z_0) dz \quad (3.4.1.16)$$

Regroup eq. (3.4.1.18)

$$PD = \left( \sec \theta_0 + \sec \theta_0 \cdot \tan^2 \theta_0 \right) \cdot \int_{z_0}^{z'} [n(z) - 1] dz - \frac{\sec \theta_0 \cdot \tan^2 \theta_0}{z_0} \cdot \int_{z_0}^{z'} [n(z) - 1] \cdot z dz \quad (3.4.1.17)$$

Develop eq. (3.4.1.19) and taking the temperature models (3.3.3.37) or (3.3.3.40) into account, one has

$$\begin{aligned} PD &= \left( \sec \theta_0 + \sec \theta_0 \cdot \tan^2 \theta_0 \right) \cdot \int_{z_0}^{z_1} [n(z) - 1] dz \\ &\quad + \left( \sec \theta_0 + \sec \theta_0 \cdot \tan^2 \theta_0 \right) \cdot \int_{z_1}^{z'} [n(z) - 1] dz \\ &\quad - \frac{\sec \theta_0 \cdot \tan^2 \theta_0}{z_0} \cdot \int_{z_0}^{z_1} [n(z) - 1] \cdot z dz \\ &\quad - \frac{\sec \theta_0 \cdot \tan^2 \theta_0}{z_0} \cdot \int_{z_1}^{z'} [n(z) - 1] \cdot z dz \\ &= : I_1 + I_2 + I_3 + I_4 \end{aligned} \quad (3.4.1.18)$$

Eq. (3.4.1.18) holds under the assumption that the atmosphere is isotropic.

### 3.4.2. Mathematical background

In order to evaluate the four integrals of eq. (3.4.1.20), forming the path delay, some mathematical theorems and laws are required. Thus a short mathematical background is provided hereunder.

**Law 1.** For all  $a \in \mathbb{R}$  and  $x \in ]0, +\infty[$ , it holds

$$\int \frac{e^{ax}}{x} dx = \ln x + \sum_{n \geq 1} \frac{(ax)^n}{n \cdot n!} \quad (3.4.2.1)$$

**Law 2.** For all  $a \in \mathbb{R}$ ,  $x \in ]0, +\infty[$  and  $n > 1$ , it holds

$$\int \frac{e^{ax}}{x^n} dx = \frac{1}{n-1} \cdot \left[ -\frac{e^{ax}}{x^{n-1}} + a \cdot \int \frac{e^{ax}}{x^{n-1}} dx \right], \quad n > 1 \quad (3.4.2.2)$$

Combining Law 1 and Law 2, one obtains the following

**Corollary 1.** In the specific case of  $n=2$ , for all  $a \in \mathbb{R}$ ,  $x \in ]0, +\infty[$  one has

$$\int \frac{e^{ax}}{x^2} dx = -\frac{e^{ax}}{x} + a \cdot \ln x + a \cdot \sum_{n \geq 1} \frac{(ax)^n}{n \cdot n!} \quad (3.4.2.3)$$

**Law 3. (Binomial theorem)** For all  $a, b, x \in \mathbb{R}$  and  $n \in \mathbb{N}$ , it holds

$$(a + b \cdot x)^n = \sum_{k=0}^n \binom{n}{k} \cdot a^{n-k} \cdot (b \cdot x)^k \quad (3.4.2.4)$$

**Law 4.** For all  $n \in \mathbb{N} \setminus \{0\}$ ,  $a \in \mathbb{R}$  and  $x \in [0, +\infty[$ , it holds

$$\int x^n \cdot e^{ax} dx = \frac{x^n}{a} \cdot e^{ax} - \frac{n}{a} \cdot \int x^{n-1} \cdot e^{ax} dx \quad (3.4.2.5)$$

Two specific cases are derived from Law 4, namely

**Corollary 2. ( $n=2$ )** For all  $a \in \mathbb{R}$  and  $x \in [0, +\infty[$ , it holds

$$\int x^2 \cdot e^{ax} dx = \left[ \frac{x^2}{a} - \frac{2x}{a^2} + \frac{2}{a^3} \right] \cdot e^{ax} \quad (3.4.2.6)$$

**Corollary 3. ( $n=1$ )** For all  $a \in \mathbb{R}$  and  $x \in [0, +\infty[$ , it holds

$$\int x \cdot e^{ax} dx = \frac{e^{ax}}{a^2} \cdot (ax - 1) \quad (3.4.2.7)$$

### 3.4.3. Integration

Insert the Essen and Froome formula, eq. (3.2.2.7) of paragraph 3.2.2.1, i.e.

$$N(p, T, e) = (n-1) \times 10^6 = \frac{77.64}{T} \cdot (p - e) + \frac{64.68}{T} \cdot \left( 1 + \frac{5748}{T} \right) \cdot e \quad (3.4.3.1)$$

into eq. (3.4.1.20) and use the atmospheric models of paragraph 3.3. In a first step, consider the simplest set of models where only altitude and ground data dependence appears, i.e.

$$T(z) = [T_0 + \gamma \cdot z] \cdot [1 - \epsilon(z - z_1)] + T_1 \cdot \epsilon(z - z_1) \quad (3.4.3.2)$$

$$p(z) = p_0 \cdot \exp\left\{-\frac{(z - z_0)}{H_p}\right\} \quad (3.4.3.3)$$

$$e(z) = e_0 \cdot \exp\left\{-\frac{(z - z_0)}{H_e}\right\} \quad (3.4.3.4)$$

According to the chosen models, eq. (3.3.4.1) to eq. (3.3.4.3), in eq. (3.4.3.2),  $T_0$  is the reference temperature while in eq. (3.4.3.3) resp. eq. (3.4.3.4),  $p_0$  and  $e_0$  are the pressure and the humidity at the GPS receiver's location! The procedure now consists in inserting eq. (3.4.3.1) in the different terms of eq. (3.4.1.20) and evaluating each of them.

### 3.4.4. Integration of $I_1$

The first integral of eq. (3.4.1.20),  $I_1$ , is

$$I_1 := \left(\sec\theta_0 + \sec\theta_0 \cdot \tan^2\theta_0\right) \cdot \int_{z_0}^{z_1} [n(z) - 1] dz = \left(\sec\theta_0 + \sec\theta_0 \cdot \tan^2\theta\right) \cdot 10^{-6} \cdot \int_{z_0}^{z_1} N(z) dz \quad (3.4.4.1)$$

Insert eq. (3.4.3.1) in eq. (3.4.4.1)

$$\begin{aligned} I_1 &= \left(\sec\theta_0 + \sec\theta_0 \cdot \tan^2\theta_0\right) \cdot 10^{-6} \cdot 77.64 \cdot e^{\frac{z_0}{H_p}} \cdot \int_{z_0}^{z_1} \frac{p_0}{T_0 + \gamma \cdot z} \cdot e^{\frac{-z}{H_p}} dz \\ &\quad - \left(\sec\theta_0 + \sec\theta_0 \cdot \tan^2\theta_0\right) \cdot 10^{-6} \cdot 12.96 \cdot e^{\frac{z_0}{H_e}} \cdot \int_{z_0}^{z_1} \frac{e_0}{T_0 + \gamma \cdot z} \cdot e^{\frac{-z}{H_e}} dz \\ &\quad + \left(\sec\theta_0 + \sec\theta_0 \cdot \tan^2\theta_0\right) \cdot 10^{-6} \cdot 5748 \cdot 64.68 \cdot e^{\frac{z_0}{H_e}} \cdot \int_{z_0}^{z_1} \frac{e_0}{(T_0 + \gamma \cdot z)^2} \cdot e^{\frac{-z}{H_e}} dz \\ &=: I_{11} + I_{12} + I_{13} \end{aligned} \quad (3.4.4.2)$$

#### 3.4.4.1. Computation of $I_{11}$

$I_{11}$  is defined as

$$I_{11} := \underbrace{\left(\sec\theta_0 + \sec\theta_0 \cdot \tan^2\theta_0\right) \cdot 10^{-6} \cdot 77.64 \cdot e^{\frac{z_0}{H_p}}}_{=: C_{11}} \cdot \int_{z_0}^{z_1} \frac{p_0}{T_0 + \gamma \cdot z} \cdot e^{\frac{-z}{H_p}} dz \quad (3.4.4.1.1)$$

Proceed with the following variable transformation

$$u := T_0 + \gamma \cdot z \quad (3.4.4.1.2)$$

that is

$$z = \frac{u - T_0}{\gamma} \quad \text{and} \quad dz = \frac{1}{\gamma} \cdot du \quad (3.4.4.1.3a,b)$$

Insert eq. (3.4.4.1.2) and eq. (3.4.4.1.3) in eq. (3.4.4.1.1),

$$I_{11} = C_{11} \cdot p_0 \cdot \int_{T_0 + \gamma \cdot z_0}^{T_0 + \gamma \cdot z_1} \frac{1}{u} \cdot e^{\left(\frac{u - T_0}{\gamma}\right) \frac{1}{H_p}} \cdot \frac{du}{\gamma} \quad (3.4.4.1.4)$$

Regroup

$$I_{11} = \underbrace{C_{111} \cdot p_0 \cdot \frac{1}{\gamma} \cdot e^{\frac{T_0}{\gamma \cdot H_p}}}_{=C_{111}} \cdot \int_{T_0+\gamma \cdot z_0}^{T_0+\gamma \cdot z_1} \frac{e^{\frac{-u}{\gamma \cdot H_p}}}{u} du \quad (3.4.4.1.5)$$

Use now Law 1 of paragraph 3.4.2 to evaluate the integral of eq. (3.4.4.1.5)

$$I_{11} = C_{111} \cdot \left[ \ln(T_0 + \gamma \cdot z_1) - \ln(T_0 + \gamma \cdot z_0) + \sum_{n \geq 1} \left( \frac{-1}{\gamma \cdot H_p} \right)^n \cdot \frac{1}{n \cdot n!} \cdot \left[ (T_0 + \gamma \cdot z_1)^n - (T_0 + \gamma \cdot z_0)^n \right] \right] \quad (3.4.4.1.6)$$

Use the *Binomial law*, Law 4

$$I_{11} = C_{111} \cdot \left[ \ln \left( \frac{T_0 + \gamma \cdot z_1}{T_0 + \gamma \cdot z_0} \right) + \sum_{n \geq 1} \left( \frac{-1}{\gamma \cdot H_p} \right)^n \cdot \frac{1}{n \cdot n!} \cdot \sum_{k=0}^n \binom{n}{k} \cdot T_0^{n-k} \cdot \gamma^k \cdot \left[ z_1^k - z_0^k \right] \right] \quad (3.4.4.1.7)$$

For simplicity, define the following series

$$S_{11} := \sum_{n \geq 1} \left( \frac{-1}{\gamma \cdot H_p} \right)^n \cdot \frac{1}{n \cdot n!} \cdot \sum_{k=0}^n \binom{n}{k} \cdot T_0^{n-k} \cdot \gamma^k \cdot \left[ z_1^k - z_0^k \right] \quad (3.4.4.1.8)$$

Thus eq. (3.4.4.1.7) reduces to

$$I_{11} = C_{111} \cdot \left[ \ln \left( \frac{T_0 + \gamma \cdot z_1}{T_0 + \gamma \cdot z_0} \right) + S_{11} \right] \quad (3.4.4.1.9)$$

### 3.4.4.2. Computation of $I_{12}$

$I_{12}$  is defined as

$$I_{12} := - \underbrace{\left( \sec \theta_0 + \sec \theta_0 \cdot \tan^2 \theta_0 \right) \cdot 10^{-6} \cdot 12.96 \cdot e^{\frac{z_0}{H_e}}}_{=C_{12}} \cdot \int_{z_0}^{z_1} \frac{e_0}{T_0 + \gamma \cdot z} \cdot e^{\frac{-z}{H_e}} dz \quad (3.4.4.2.1)$$

Use the same variable transformation as before, i.e. eq. (3.4.4.1.2). This leads to

$$I_{12} = -C_{12} \cdot e_0 \cdot \int_{T_0+\gamma \cdot z_0}^{T_0+\gamma \cdot z_1} \frac{1}{u} \cdot e^{\frac{-1}{\gamma \cdot H_e} \left( \frac{u-T_0}{\gamma} \right)} \cdot \frac{du}{\gamma} \quad (3.4.4.2.2)$$

Developing the integral yields to

$$I_{12} = -C_{12} \cdot e_0 \cdot \underbrace{\frac{1}{\gamma} \cdot e^{\frac{T_0}{\gamma \cdot H_e}}}_{=C_{121}} \cdot \int_{T_0+\gamma \cdot z_0}^{T_0+\gamma \cdot z_1} \frac{e^{\frac{-u}{\gamma \cdot H_e}}}{u} du \quad (3.4.4.2.3)$$

i.e.,

$$I_{12} = -C_{121} \cdot \int_{T_0+\gamma \cdot z_0}^{T_0+\gamma \cdot z_1} \frac{e^{-u \cdot \left( \frac{1}{\gamma \cdot H_e} \right)}}{u} du \quad (3.4.4.2.4)$$

Again use law 1 to evaluate the integral

$$I_{12} = -C_{121} \cdot \left[ \ln(T_0 + \gamma \cdot z_1) - \ln(T_0 + \gamma \cdot z_0) + \sum_{n \geq 1} \left( \frac{-1}{\gamma \cdot H_e} \right)^n \cdot \frac{1}{n \cdot n!} \cdot \left[ (T_0 + \gamma \cdot z_1)^n - (T_0 + \gamma \cdot z_0)^n \right] \right] \quad (3.4.4.2.5)$$

Rewrite eq. (3.4.4.2.5) using the *Binomial law*, law 4

$$I_{12} = -C_{121} \cdot \left[ \ln \left( \frac{T_0 + \gamma \cdot z_1}{T_0 + \gamma \cdot z_0} \right) + \sum_{n \geq 1} \left( \frac{-1}{\gamma \cdot H_e} \right)^n \cdot \frac{1}{n \cdot n!} \cdot \sum_{k=0}^n \binom{n}{k} \cdot T_0^{n-k} \cdot \gamma^k \cdot \left[ z_1^k - z_0^k \right] \right] \quad (3.4.4.2.6)$$

It is useful to define the series

$$S_{12} := \sum_{n \geq 1} \left( \frac{-1}{\gamma \cdot H_e} \right)^n \cdot \frac{1}{n \cdot n!} \cdot \sum_{k=0}^n \binom{n}{k} \cdot T_0^{n-k} \cdot \gamma^k \cdot \left[ z_1^k - z_0^k \right] \quad (3.4.4.2.7)$$

Thus eq. (3.4.4.2.7) simplifies to

$$I_{12} = -C_{121} \cdot \left[ \ln \left( \frac{T_0 + \gamma \cdot z_1}{T_0 + \gamma \cdot z_0} \right) + S_{12} \right] \quad (3.4.4.2.8)$$

### 3.4.4.3. Computation of $I_{13}$

$I_{13}$  has been defined as

$$I_{13} := \underbrace{\left( \sec \theta_0 + \sec \theta_0 \cdot \tan^2 \theta_0 \right) \cdot 10^{-6} \cdot 5748 \cdot 64.68 \cdot e^{\frac{z_0}{H_e}}}_{=: C_{13}} \cdot \int_{z_0}^{z_1} \frac{e_0}{(T_0 + \gamma \cdot z)^2} \cdot e^{\frac{-z}{H_e}} dz \quad (3.4.4.3.1)$$

Proceed with the variable transformation of eq. (3.4.4.1.2), i.e.

$$u := T_0 + \gamma \cdot z \quad (3.4.4.3.2)$$

that is

$$z = \frac{u - T_0}{\gamma} \quad \text{and} \quad dz = \frac{1}{\gamma} \cdot du \quad (3.4.4.3.3a,b)$$

Insert eq. (3.4.4.3.1) in eq. (3.4.4.3.2) and obtain

$$I_{13} = C_{13} \cdot e_0 \cdot \int_{T_0 + \gamma \cdot z_0}^{T_0 + \gamma \cdot z_1} \frac{1}{u^2} \cdot e^{\frac{-1}{\gamma \cdot H_e} \left( \frac{u - T_0}{\gamma} \right)} \cdot \frac{du}{\gamma} \quad (3.4.4.3.4)$$

i.e.,

$$I_{13} = \underbrace{C_{13} \cdot e_0 \cdot \frac{1}{\gamma} \cdot e^{\frac{T_0}{\gamma \cdot H_e}}}_{=: C_{131}} \cdot \int_{T_0 + \gamma \cdot z_0}^{T_0 + \gamma \cdot z_1} \frac{e^{-u \left( \frac{1}{\gamma \cdot H_e} \right)}}{u^2} du \quad (3.4.4.3.5)$$

Use Law 2 or Corollary 1 to compute the integral

$$I_{13} = C_{131} \cdot \left[ \frac{-\frac{1}{\gamma \cdot H_e} (T_0 + \gamma \cdot z_1)}{T_0 + \gamma \cdot z_1} + \frac{-\frac{1}{\gamma \cdot H_e} (T_0 + \gamma \cdot z_0)}{T_0 + \gamma \cdot z_0} - \frac{1}{\gamma \cdot H_e} \cdot \underbrace{\int_{T_0 + \gamma \cdot z_0}^{T_0 + \gamma \cdot z_1} \frac{e^{-u \left( \frac{1}{\gamma \cdot H_e} \right)}}{u} du}_{=: I_{131}} \right] \quad (3.4.4.3.6)$$

Note that  $I_{13}$  is linearly proportional to  $I_{12}$ , that is using eq. (3.4.4.2.4),

$$I_{13} = \frac{-I_{12}}{C_{121}} \quad (3.4.4.3.7)$$

Therefore,  $I_{13}$  is completely known. Thus introducing the previous results for  $I_{12}$ , one has

$$I_{13} = C_{131} \cdot \left[ \frac{-e^{-\frac{(T_0 + \gamma \cdot z_1)}{\gamma \cdot H_e}}}{T_0 + \gamma \cdot z_1} + \frac{e^{-\frac{(T_0 + \gamma \cdot z_0)}{\gamma \cdot H_e}}}{T_0 + \gamma \cdot z_0} - \frac{1}{\gamma \cdot H_e} \cdot \left[ \ln \left( \frac{T_0 + \gamma \cdot z_1}{T_0 + \gamma \cdot z_0} \right) + S_{12} \right] \right] \quad (3.4.4.3.8)$$

#### 3.4.4.4. Summary of $I_1$

Sampling eq. (3.4.4.2), eq. (3.4.4.1.9), eq. (3.4.4.2.8) and eq. (3.4.4.3.8), it follows that

$$I_1 = C_{111} \cdot \left[ \ln \left( \frac{T_0 + \gamma \cdot z_1}{T_0 + \gamma \cdot z_0} \right) + S_{11} \right] - C_{121} \cdot \left[ \ln \left( \frac{T_0 + \gamma \cdot z_1}{T_0 + \gamma \cdot z_0} \right) + S_{12} \right] + C_{131} \cdot \left[ \frac{-e^{-\frac{(T_0 + \gamma \cdot z_1)}{\gamma \cdot H_e}}}{T_0 + \gamma \cdot z_1} + \frac{e^{-\frac{(T_0 + \gamma \cdot z_0)}{\gamma \cdot H_e}}}{T_0 + \gamma \cdot z_0} - \frac{1}{\gamma \cdot H_e} \cdot \left[ \ln \left( \frac{T_0 + \gamma \cdot z_1}{T_0 + \gamma \cdot z_0} \right) + S_{12} \right] \right] \quad (3.4.4.4.1)$$

This means that  $I_1$  is a function of

$$I_1 = I_1(\theta_0, p_0, e_0, T_0, T_1, \gamma, z_0, z_1, H_p, H_e) \quad (3.4.4.4.2)$$

### 3.4.5. Integration of $I_2$

The second integral of eq. (3.4.1.20),  $I_2$ , is

$$I_2 := \left( \sec \theta_0 + \sec \theta_0 \cdot \tan^2 \theta_0 \right) \cdot \int_{z_1}^{z'} [n(z) - 1] dz \quad (3.4.5.1)$$

Follow the same idea as was done in paragraph 3.4.4., and introduce the Essen and Froome formula, eq. (3.4.3.1) in eq. (3.4.5.1)

$$\begin{aligned} I_2 &= \left( \sec \theta_0 + \sec \theta_0 \cdot \tan^2 \theta_0 \right) \cdot 10^{-6} \cdot 77.64 \cdot e^{\frac{z_0}{H_p}} \cdot \int_{z_1}^{z'} \frac{p_0}{T_1} \cdot e^{\frac{-z}{H_p}} dz \\ &\quad - \left( \sec \theta_0 + \sec \theta_0 \cdot \tan^2 \theta_0 \right) \cdot 10^{-6} \cdot 12.96 \cdot e^{\frac{z_0}{H_e}} \cdot \int_{z_1}^{z'} \frac{e_0}{T_1} \cdot e^{\frac{-z}{H_e}} dz \\ &\quad + \left( \sec \theta_0 + \sec \theta_0 \cdot \tan^2 \theta_0 \right) \cdot 10^{-6} \cdot 5748 \cdot 64.68 \cdot e^{\frac{z_0}{H_e}} \cdot \int_{z_1}^{z'} \frac{e_0}{T_1^2} \cdot e^{\frac{-z}{H_e}} dz \\ &=: I_{21} + I_{22} + I_{23} \end{aligned} \quad (3.4.5.2)$$

#### 3.4.5.1. Computation of $I_{21}$

$I_{21}$  is defined as

$$I_{21} := \underbrace{\left( \sec \theta_0 + \sec \theta_0 \cdot \tan^2 \theta_0 \right) \cdot 10^{-6} \cdot 77.64 \cdot e^{\frac{z_0}{H_p}}}_{=: C_{21}} \cdot \int_{z_1}^{z'} \frac{p_0}{T_1} \cdot e^{\frac{-z}{H_p}} dz \quad (3.4.5.1.1)$$

The integral on the right hand side of eq. (3.4.5.1.1) is a simple integral. It can be directly integrated. One has

$$I_{21} = C_{21} \cdot \frac{p_0}{T_1} \cdot (-H_p) \cdot \left[ e^{\frac{-z'}{H_p}} - e^{\frac{-z_1}{H_p}} \right] = C_{21} \cdot \frac{p_0}{T_1} \cdot H_p \cdot \left[ e^{\frac{-z_1}{H_p}} - e^{\frac{-z'}{H_p}} \right] \quad (3.4.5.1.2)$$

### 3.4.5.2. Computation of $I_{22}$

$I_{22}$  is defined as

$$I_{22} := - \underbrace{(\sec \theta_0 + \sec \theta_0 \cdot \tan^2 \theta_0)}_{=: C_{22}} \cdot 10^{-6} \cdot 12.96 \cdot e^{\frac{z_0}{H_e}} \cdot \int_{z_1}^{z'} \frac{e_0}{T_1} \cdot e^{\frac{-z}{H_e}} dz \quad (3.4.5.2.1)$$

that is

$$I_{22} = -C_{22} \cdot \frac{e_0}{T_1} \cdot \int_{z_1}^{z'} e^{\left(\frac{1}{H_e}\right)^z} dz \quad (3.4.5.2.2)$$

Eq. (3.4.5.2.2) is also a simple integral, namely

$$I_{22} = -C_{22} \cdot \frac{e_0}{T_1} \cdot (-H_e) \cdot \left[ e^{\left(\frac{1}{H_e}\right)^{z'}} - e^{\left(\frac{1}{H_e}\right)^{z_1}} \right] = C_{22} \cdot \frac{e_0}{T_1} \cdot H_e \cdot \left[ e^{\frac{-z'}{H_e}} - e^{\frac{-z_1}{H_e}} \right] \quad (3.4.5.2.3)$$

### 3.4.5.3. Computation of $I_{23}$

$I_{23}$  is defined as

$$I_{23} := \underbrace{(\sec \theta_0 + \sec \theta_0 \cdot \tan^2 \theta_0)}_{=: C_{23}} \cdot 10^{-6} \cdot 5748 \cdot 64.68 \cdot e^{\frac{z_0}{H_e}} \cdot \int_{z_1}^{z'} \frac{e_0}{T_1^2} \cdot e^{\frac{-z}{H_e}} dz \quad (3.4.5.3.1)$$

i.e.

$$I_{23} = C_{23} \cdot \frac{e_0}{T_1^2} \cdot \int_{z_1}^{z'} e^{\left(\frac{1}{H_e}\right)^z} dz \quad (3.4.5.3.2)$$

and integrate

$$I_{23} = C_{23} \cdot \frac{e_0}{T_1^2} \cdot (-H_e) \cdot \left[ e^{\left(\frac{1}{H_e}\right)^{z'}} - e^{\left(\frac{1}{H_e}\right)^{z_1}} \right] = -C_{23} \cdot \frac{e_0}{T_1^2} \cdot H_e \cdot \left[ e^{\frac{-z'}{H_e}} - e^{\frac{-z_1}{H_e}} \right] \quad (3.4.5.3.3)$$

### 3.4.5.4. Summary of $I_2$

Insert eq. (3.4.5.1.2), eq. (3.4.5.2.3) and eq. (3.4.5.3.3) in eq. (3.4.5.2). This results in

$$I_2 = C_{21} \cdot \frac{p_0}{T_1} \cdot H_p \cdot \left[ e^{\frac{-z_1}{H_p}} - e^{\frac{-z'}{H_p}} \right] + C_{22} \cdot \frac{e_0}{T_1} \cdot H_e \cdot \left[ e^{\frac{-z'}{H_e}} - e^{\frac{-z_1}{H_e}} \right] - C_{23} \cdot \frac{e_0}{T_1^2} \cdot H_e \cdot \left[ e^{\frac{-z'}{H_e}} - e^{\frac{-z_1}{H_e}} \right] \quad (3.4.5.4.1)$$

Thus  $I_2$  is a function of

$$I_2 = I_2(\theta_0, p_0, e_0, T_1, z_0, z_1, z', H_p, H_e) \quad (3.4.5.4.2)$$

The difference in the variables between  $I_1$  and  $I_2$  lies in the fact that  $I_2$  depends on  $z'$  while  $I_1$  does not. Conversely  $I_1$  depends on  $T_0$  and  $\gamma$  while  $I_2$  does not.

### 3.4.6. Integration of $I_3$

The third integral of eq. (3.4.1.20),  $I_3$ , is

$$I_3 := -\frac{\sec\theta_0 \cdot \tan^2\theta_0}{z_0} \cdot \int_{z_0}^{z_1} [n(z) - 1] \cdot z \, dz = -\frac{\sec\theta_0 \cdot \tan^2\theta_0}{z_0} \cdot 10^{-6} \cdot \int_{z_0}^{z_1} N(z) \cdot z \, dz \quad (3.4.6.1)$$

Insert the Essen and Froome formula, eq. (3.4.3.1) in eq. (3.4.6.1)

$$\begin{aligned} I_3 &= -\frac{\sec\theta_0 \cdot \tan^2\theta_0}{z_0} \cdot 10^{-6} \cdot 77.64 \cdot e^{\frac{z_0}{H_p}} \cdot \int_{z_0}^{z_1} \frac{p_0 \cdot z}{T_0 + \gamma \cdot z} \cdot e^{\frac{-z}{H_p}} \, dz \\ &\quad + \frac{\sec\theta_0 \cdot \tan^2\theta_0}{z_0} \cdot 10^{-6} \cdot 12.96 \cdot e^{\frac{z_0}{H_e}} \cdot \int_{z_0}^{z_1} \frac{e_0 \cdot z}{T_0 + \gamma \cdot z} \cdot e^{\frac{-z}{H_e}} \, dz \\ &\quad - \frac{\sec\theta_0 \cdot \tan^2\theta_0}{z_0} \cdot 10^{-6} \cdot 5748 \cdot 64.68 \cdot e^{\frac{z_0}{H_e}} \cdot \int_{z_0}^{z_1} \frac{e_0 \cdot z}{(T_0 + \gamma \cdot z)^2} \cdot e^{\frac{-z}{H_e}} \, dz \\ &=: I_{31} + I_{32} + I_{33} \end{aligned} \quad (3.4.6.2)$$

#### 3.4.6.1. Computation of $I_{31}$

$I_{31}$  is defined as

$$I_{31} := -\underbrace{\frac{\sec\theta_0 \cdot \tan^2\theta_0}{z_0} \cdot 10^{-6} \cdot 77.64 \cdot e^{\frac{z_0}{H_p}}}_{=: C_{31}} \cdot \int_{z_0}^{z_1} \frac{p_0 \cdot z}{T_0 + \gamma \cdot z} \cdot e^{\frac{-z}{H_p}} \, dz \quad (3.4.6.1.1)$$

Rewrite in a simpler form

$$I_{31} = -C_{31} \cdot p_0 \cdot \int_{z_0}^{z_1} \frac{z}{T_0 + \gamma \cdot z} \cdot e^{\frac{-z}{H_p}} \, dz \quad (3.4.6.1.2)$$

Retake the variable transformation used till then

$$u := T_0 + \gamma \cdot z \quad (3.4.6.1.3)$$

that is

$$z = \frac{u - T_0}{\gamma} \quad \text{and} \quad dz = \frac{1}{\gamma} \cdot du \quad (3.4.6.1.4a,b)$$

Insert eq. (3.4.6.1.3) and eq. (3.4.6.1.3) in eq. (3.4.6.1.1) and obtain

$$I_{31} = -C_{31} \cdot p_0 \cdot \int_{T_0 + \gamma \cdot z_0}^{T_0 + \gamma \cdot z_1} \left( \frac{u - T_0}{\gamma} \right) \cdot \frac{1}{u} \cdot e^{\left( \frac{u - T_0}{\gamma \cdot H_p} \right)} \cdot \frac{du}{\gamma} \quad (3.4.6.1.5)$$

It follows that



$$I_{31} = \underbrace{-C_{311} \cdot p_0 \cdot \frac{1}{\gamma^2} \cdot e^{\frac{T_0}{\gamma H_p}}}_{=C_{311}} \cdot \left[ \int_{T_0+\gamma \cdot z_0}^{T_0+\gamma \cdot z_1} e^{\gamma H_p \cdot \frac{-u}{\gamma}} du - T_0 \cdot \int_{T_0+\gamma \cdot z_0}^{T_0+\gamma \cdot z_1} \frac{e^{\gamma H_p \cdot \frac{-u}{\gamma}}}{u} du \right] \quad (3.4.6.1.6)$$

The first integral on the right hand side of eq. (3.4.6.1.6) can be directly computed while one needs Law 1 and Law 3 to perform the second integral. This yields to

$$I_{31} = -C_{311} \cdot \left[ -\gamma \cdot H_p \cdot \left[ e^{\frac{-(T_0+\gamma \cdot z_0)}{\gamma H_p}} - e^{\frac{-(T_0+\gamma \cdot z_1)}{\gamma H_p}} \right] \right] \\ - C_{311} \cdot \left[ -T_0 \cdot \left( \ln \left( \frac{T_0 + \gamma \cdot z_1}{T_0 + \gamma \cdot z_0} \right) + \sum_{n \geq 1} \left( \frac{-1}{\gamma \cdot H_p} \right)^n \cdot \frac{1}{n \cdot n!} \cdot \sum_{k=0}^n \binom{n}{k} \cdot T_0^{n-k} \cdot \gamma^k \cdot [z_1^k - z_0^k] \right) \right] \quad (3.4.6.1.7)$$

Remark that the series in the second term on the RHS of eq. (3.4.6.1.7) is nothing else than  $S_{11}$ ! Hence eq. (3.4.6.1.7) can be written simply as

$$I_{31} = C_{311} \cdot \left[ \gamma \cdot H_p \cdot \left[ e^{\frac{-(T_0+\gamma \cdot z_0)}{\gamma H_p}} - e^{\frac{-(T_0+\gamma \cdot z_1)}{\gamma H_p}} \right] + T_0 \cdot \left[ \ln \left( \frac{T_0 + \gamma \cdot z_1}{T_0 + \gamma \cdot z_0} \right) - S_{11} \right] \right] \quad (3.4.6.1.8)$$

### 3.4.6.2. Computation of $I_{32}$

$I_{32}$  is defined as

$$I_{32} := \underbrace{\frac{\sec \theta_0 \cdot \tan^2 \theta_0 \cdot 10^{-6} \cdot 12.96 \cdot e^{\frac{z_0}{H_e}}}{z_0}}_{=C_{32}} \cdot \int_{z_0}^{z_1} \frac{e_0 \cdot z}{T_0 + \gamma \cdot z} \cdot e^{\frac{-z}{H_e}} dz \quad (3.4.6.2.1)$$

that is

$$I_{32} = C_{32} \cdot e_0 \cdot \int_{z_0}^{z_1} \frac{z}{T_0 + \gamma \cdot z} \cdot e^{\frac{-1}{H_e} \cdot z} dz \quad (3.4.6.2.2)$$

Proceed with the now known variable transformation, eq. (3.4.6.1.3),

$$I_{32} = C_{32} \cdot e_0 \cdot \int_{T_0+\gamma \cdot z_0}^{T_0+\gamma \cdot z_1} \left( \frac{u-T_0}{\gamma} \right) \cdot \frac{1}{u} \cdot e^{\left( \frac{u-T_0}{\gamma} \right) \frac{1}{H_e}} \cdot \frac{du}{\gamma} \quad (3.4.6.2.3)$$

Separate Eq. (3.4.6.2.3) in two terms

$$I_{32} = C_{32} \cdot e_0 \cdot \frac{1}{\gamma^2} \cdot e^{\frac{T_0}{\gamma H_e}} \cdot \left[ \int_{T_0+\gamma \cdot z_0}^{T_0+\gamma \cdot z_1} e^{\gamma H_e \cdot \frac{-u}{\gamma}} du - T_0 \cdot \int_{T_0+\gamma \cdot z_0}^{T_0+\gamma \cdot z_1} \frac{e^{\gamma H_e \cdot \frac{-u}{\gamma}}}{u} du \right] \quad (3.4.6.2.4)$$

Compute directly the first integral and use Law 1 and Law 3 to perform the second.

$$I_{32} = C_{321} \cdot \left[ -\gamma \cdot H_e \cdot \left[ e^{\frac{-(T_0+\gamma \cdot z_1)}{\gamma H_e}} - e^{\frac{-(T_0+\gamma \cdot z_0)}{\gamma H_e}} \right] \right] \\ + C_{321} \cdot \left[ -T_0 \cdot \left( \ln \left( \frac{T_0 + \gamma \cdot z_1}{T_0 + \gamma \cdot z_0} \right) + \sum_{n \geq 1} \left( \frac{-1}{\gamma \cdot H_e} \right)^n \cdot \frac{1}{n \cdot n!} \cdot \sum_{k=0}^n \binom{n}{k} \cdot T_0^{n-k} \cdot \gamma^k \cdot [z_1^k - z_0^k] \right) \right] \quad (3.4.6.2.5)$$

Note that the series of eq. (3.4.6.2.5) is just  $S_{12}$  ! Further, rewrite  $I_{32}$  in order to simplify the expression.

$$I_{32} = -C_{321} \cdot \left[ \gamma \cdot H_e \cdot \left[ e^{\frac{-(T_0 + \gamma \cdot z_1)}{\gamma \cdot H_e}} - e^{\frac{-(T_0 + \gamma \cdot z_0)}{\gamma \cdot H_e}} \right] + T_0 \cdot \left( \ln \left( \frac{T_0 + \gamma \cdot z_1}{T_0 + \gamma \cdot z_0} \right) + S_{12} \right) \right] \quad (3.4.6.2.6)$$

### 3.4.6.3. Computation of $I_{33}$

$I_{33}$  is defined as

$$I_{33} = - \underbrace{\frac{\sec \theta_0 \cdot \tan^2 \theta_0}{z_0} \cdot 10^{-6} \cdot 5478 \cdot 64.68 \cdot e^{\frac{z_0}{H_e}}}_{=: C_{33}} \cdot \int_{z_0}^{z_1} \frac{e_0 \cdot z}{(T_0 + \gamma \cdot z)^2} \cdot e^{\frac{-z}{H_e}} dz \quad (3.4.6.3.1)$$

i.e.

$$I_{33} = -C_{33} \cdot e_0 \cdot \int_{z_0}^{z_1} \frac{z}{(T_0 + \gamma \cdot z)^2} \cdot e^{\frac{-z}{H_e}} dz \quad (3.4.6.3.2)$$

Proceed with the now known variable transformation, eq. (3.4.6.1.3),

$$I_{33} = -C_{33} \cdot e_0 \cdot \int_{T_0 + \gamma \cdot z_0}^{T_0 + \gamma \cdot z_1} \left( \frac{u - T_0}{\gamma} \right) \cdot \frac{1}{u^2} \cdot e^{\frac{-1}{H_e} \cdot \left( \frac{u - T_0}{\gamma} \right)} \cdot \frac{du}{\gamma} \quad (3.4.6.3.3)$$

Separate the integral in two terms

$$I_{33} = -C_{331} \cdot \underbrace{\frac{1}{\gamma^2} \cdot e^{\frac{T_0}{\gamma \cdot H_e}}}_{=: C_{331}} \cdot \left[ \int_{T_0 + \gamma \cdot z_0}^{T_0 + \gamma \cdot z_1} \frac{e^{\frac{-u}{\gamma \cdot H_e}}}{u} du - T_0 \cdot \int_{T_0 + \gamma \cdot z_0}^{T_0 + \gamma \cdot z_1} \frac{e^{\frac{-u}{\gamma \cdot H_e}}}{u^2} du \right] \quad (3.4.6.3.4)$$

Use Law 1 and Law 3 to perform the first integral and use Law 2 for  $n=2$ , i.e. Corollary 1 to compute the second. This gives

$$\begin{aligned} I_{33} = & -C_{331} \cdot \left( \ln \left( \frac{T_0 + \gamma \cdot z_1}{T_0 + \gamma \cdot z_0} \right) + \sum_{n \geq 1} \left( \frac{-1}{\gamma \cdot H_e} \right)^n \cdot \frac{1}{n \cdot n!} \cdot \sum_{k=0}^n \binom{n}{k} \cdot T_0^{n-k} \cdot \gamma^k \cdot [z_1^n - z_0^n] \right) \\ & - C_{331} \cdot \left[ -T_0 \cdot \left[ \frac{e^{\frac{-(T_0 + \gamma \cdot z_1)}{\gamma \cdot H_e}}}{T_0 + \gamma \cdot z_1} - \frac{e^{\frac{-(T_0 + \gamma \cdot z_0)}{\gamma \cdot H_e}}}{T_0 + \gamma \cdot z_0} \right] \right] \\ & - C_{331} \cdot \left[ -T_0 \cdot \left( -\frac{1}{\gamma \cdot H_e} \right) \cdot \left( \ln \left( \frac{T_0 + \gamma \cdot z_1}{T_0 + \gamma \cdot z_0} \right) + \sum_{n \geq 1} \left( \frac{-1}{\gamma \cdot H_e} \right)^n \cdot \frac{1}{n \cdot n!} \cdot \sum_{k=0}^n \binom{n}{k} \cdot T_0^{n-k} \cdot \gamma^k \cdot [z_1^k - z_0^k] \right) \right] \end{aligned} \quad (3.4.6.3.5)$$

Note that the series is again  $S_{12}$  . Thus Eq. (3.4.6.3.5) can be simplified to

$$I_{33} = -C_{331} \cdot \left[ \ln \left( \frac{T_0 + \gamma \cdot z_1}{T_0 + \gamma \cdot z_0} \right) + S_{12} + T_0 \cdot \left[ \frac{e^{\frac{-(T_0 + \gamma \cdot z_1)}{\gamma \cdot H_e}}}{T_0 + \gamma \cdot z_1} - \frac{e^{\frac{-(T_0 + \gamma \cdot z_0)}{\gamma \cdot H_e}}}{T_0 + \gamma \cdot z_0} \right] + T_0 \cdot \left( \frac{1}{\gamma \cdot H_e} \right) \cdot \left( \ln \left( \frac{T_0 + \gamma \cdot z_1}{T_0 + \gamma \cdot z_0} \right) + S_{12} \right) \right] \quad (3.4.6.3.6)$$

### 3.4.6.4. Summary of $I_3$

Insert eq. (3.4.6.1.8), eq. (3.4.6.2.6) and eq. (3.4.6.3.6) in eq. (3.4.6.2). This yields to

$$\begin{aligned}
 I_3 = & C_{311} \cdot \left[ \gamma \cdot H_p \cdot \left[ e^{\frac{-(T_0 + \gamma \cdot z_0)}{\gamma \cdot H_p}} - e^{\frac{-(T_0 + \gamma \cdot z_1)}{\gamma \cdot H_p}} \right] + T_0 \cdot \ln \left( \frac{T_0 + \gamma \cdot z_1}{T_0 + \gamma \cdot z_0} \right) - S_{11} \right] \\
 & - C_{321} \cdot \left[ \gamma \cdot H_e \cdot \left[ e^{\frac{-(T_0 + \gamma \cdot z_1)}{\gamma \cdot H_e}} - e^{\frac{-(T_0 + \gamma \cdot z_0)}{\gamma \cdot H_e}} \right] + T_0 \cdot \left( \ln \left( \frac{T_0 + \gamma \cdot z_1}{T_0 + \gamma \cdot z_0} \right) + S_{12} \right) \right] \\
 & - C_{331} \cdot \left[ \ln \left( \frac{T_0 + \gamma \cdot z_1}{T_0 + \gamma \cdot z_0} \right) + S_{12} + T_0 \cdot \left[ \frac{e^{\frac{-(T_0 + \gamma \cdot z_1)}{\gamma \cdot H_e}}}{T_0 + \gamma \cdot z_1} - \frac{e^{\frac{-(T_0 + \gamma \cdot z_0)}{\gamma \cdot H_e}}}{T_0 + \gamma \cdot z_0} \right] + T_0 \cdot \left( \frac{1}{\gamma \cdot H_e} \right) \cdot \left( \ln \left( \frac{T_0 + \gamma \cdot z_1}{T_0 + \gamma \cdot z_0} \right) + S_{12} \right) \right]
 \end{aligned} \tag{3.4.6.4.1}$$

Hence  $I_3$  depends on the following variables

$$I_3 = I_3(\theta_0, p_0, e_0, T_1, \gamma, z_0, z_1, H_p, H_e) \tag{3.4.6.4.2}$$

Therefore,  $I_3$  and  $I_1$  have exactly the same variables. This was to be expected.

### 3.4.7. Integration of $I_4$

The fourth integral of eq. (3.4.1.20),  $I_4$ , is

$$I_4 := -\frac{\sec \theta_0 \cdot \tan^2 \theta_0}{z_0} \cdot \int_{z_1}^{z'} [n(z) - 1] \cdot z \, dz = -\frac{\sec \theta_0 \cdot \tan^2 \theta_0}{z_0} \cdot 10^{-6} \cdot \int_{z_1}^{z'} N(z) \cdot z \, dz \tag{3.4.7.1}$$

Insert the Essen and Froome formula, eq. (3.4.3.1) in eq. (3.4.7.1)

$$\begin{aligned}
 I_4 = & -\frac{\sec \theta_0 \cdot \tan^2 \theta_0}{z_0} \cdot 10^{-6} \cdot 77.64 \cdot e^{\frac{z_0}{H_p}} \cdot \int_{z_1}^{z'} \frac{p_0 \cdot z}{T_1} \cdot e^{\frac{-z}{H_p}} \, dz \\
 & + \frac{\sec \theta_0 \cdot \tan^2 \theta_0}{z_0} \cdot 10^{-6} \cdot 12.96 \cdot e^{\frac{z_0}{H_e}} \cdot \int_{z_1}^{z'} \frac{e_0 \cdot z}{T_1} \cdot e^{\frac{-z}{H_e}} \, dz \\
 & - \frac{\sec \theta_0 \cdot \tan^2 \theta_0}{z_0} \cdot 10^{-6} \cdot 5748 \cdot 64.68 \cdot e^{\frac{z_0}{H_e}} \cdot \int_{z_1}^{z'} \frac{e_0 \cdot z}{T_1^2} \cdot e^{\frac{-z}{H_e}} \, dz \\
 =: & I_{41} + I_{42} + I_{43}
 \end{aligned} \tag{3.4.7.2}$$

#### 3.4.7.1. Computation of $I_{41}$

$I_{41}$  is defined as

$$I_{41} := \underbrace{-\frac{\sec \theta_0 \cdot \tan^2 \theta_0}{z_0} \cdot 10^{-6} \cdot 77.64 \cdot e^{\frac{z_0}{H_p}}}_{=: C_{41}} \cdot \int_{z_1}^{z'} \frac{p_0 \cdot z}{T_1} \cdot e^{\frac{-z}{H_p}} \, dz \tag{3.4.7.1.1}$$

that is

$$I_{41} = -C_{41} \cdot \frac{p_0}{T_1} \cdot \int_{z_1}^{z'} z \cdot e^{\frac{-z}{H_p}} \, dz \tag{3.4.7.1.2}$$

Integrate eq. (3.4.7.1.2) by part or use Corollary 3 to compute the integral

$$I_{41} = -C_{41} \cdot \frac{p_0}{T_1} \cdot \left[ \left( -\frac{z'}{H_p} - 1 \right) \cdot e^{\frac{-z'}{H_p}} \cdot \left( -\frac{1}{H_p} \right)^{-2} - \left( -\frac{z_1}{H_p} - 1 \right) \cdot e^{\frac{-z_1}{H_p}} \cdot \left( -\frac{1}{H_p} \right)^{-2} \right] \quad (3.4.7.1.3)$$

Eq. (3.4.7.1.3) can be rewritten as

$$I_{41} = -C_{41} \cdot \frac{p_0}{T_1} \cdot H_p^2 \cdot \left[ \left( \frac{z_1}{H_p} + 1 \right) \cdot e^{\frac{-z_1}{H_p}} - \left( \frac{z'}{H_p} + 1 \right) \cdot e^{\frac{-z'}{H_p}} \right] \quad (3.4.7.1.4)$$

### 3.4.7.2. Computation of $I_{42}$

$I_{42}$  is defined as

$$I_{42} := \underbrace{\frac{\sec \theta_0 \cdot \tan^2 \theta_0}{z_0} \cdot 10^{-6} \cdot 12.96 \cdot e^{\frac{z_0}{H_e}}}_{=: C_{42}} \cdot \int_{z_1}^{z'} \frac{e_0 \cdot z}{T_1} \cdot e^{\frac{-z}{H_e}} dz \quad (3.4.7.2.1)$$

i.e.

$$I_{42} = C_{42} \cdot \frac{e_0}{T_1} \cdot \int_{z_1}^{z'} z \cdot e^{\frac{-1}{H_e} \cdot z} dz \quad (3.4.7.2.2)$$

Eq. (3.4.7.2.2) can be either integrated by part or evaluated by using Corollary 3. This gives

$$I_{42} = C_{42} \cdot \frac{e_0}{T_1} \cdot \left[ \left( -\frac{z'}{H_e} - 1 \right) \cdot e^{\frac{-z'}{H_e}} \cdot \left( -\frac{1}{H_e} \right)^{-2} - \left( -\frac{z_1}{H_e} - 1 \right) \cdot e^{\frac{-z_1}{H_e}} \cdot \left( -\frac{1}{H_e} \right)^{-2} \right] \quad (3.4.7.2.3)$$

In turn, this can be rewritten as

$$I_{42} = C_{42} \cdot \frac{e_0}{T_1} \cdot (H_e)^2 \cdot \left[ \left( \frac{z_1}{H_e} + 1 \right) \cdot e^{\frac{-z_1}{H_e}} - \left( \frac{z'}{H_e} + 1 \right) \cdot e^{\frac{-z'}{H_e}} \right] \quad (3.4.7.2.4)$$

### 3.4.7.3. Computation of $I_{43}$

$I_{43}$  is defined as

$$I_{43} := \underbrace{-\frac{\sec \theta_0 \cdot \tan^2 \theta_0}{z_0} \cdot 10^{-6} \cdot 5748 \cdot 64.68 \cdot e^{\frac{z_0}{H_e}}}_{=: C_{43}} \cdot \int_{z_1}^{z'} \frac{e_0 \cdot z}{T_1^2} \cdot e^{\frac{-z}{H_e}} dz \quad (3.4.7.3.1)$$

That is

$$I_{43} = -C_{43} \cdot \frac{e_0}{T_1^2} \cdot \int_{z_1}^{z'} z \cdot e^{\frac{-1}{H_e} \cdot z} dz \quad (3.4.7.3.2)$$

Remark that the integral in eq. (3.4.7.3.2) is just  $I_{42}$  up to a constant. Using the results from the previous paragraph, one obtains directly

$$I_{43} = -C_{32} \cdot \frac{e_0}{T_1^2} \cdot (H_e)^2 \cdot \left[ \left( \frac{z_1}{H_e} + 1 \right) \cdot e^{\frac{-z_1}{H_e}} - \left( \frac{z'}{H_e} + 1 \right) \cdot e^{\frac{-z'}{H_e}} \right] \quad (3.4.7.3.3)$$

### 3.4.7.4. Summary of $I_4$

Insert eq. (3.4.7.1.4), eq. (3.4.7.2.4) and eq. (3.4.7.3.3) in eq. (3.4.7.2). This yields to

$$\begin{aligned}
 I_4 = & -C_{41} \cdot \frac{p_0}{T_1} \cdot H_p^2 \cdot \left[ \left( \frac{z_1}{H_p} + 1 \right) \cdot e^{\frac{-z_1}{H_p}} - \left( \frac{z'}{H_p} + 1 \right) \cdot e^{\frac{-z'}{H_p}} \right] \\
 & + C_{42} \cdot \frac{e_0}{T_1} \cdot (H_e)^2 \cdot \left[ \left( \frac{z_1}{H_e} + 1 \right) \cdot e^{\frac{-z_1}{H_e}} - \left( \frac{z'}{H_e} + 1 \right) \cdot e^{\frac{-z'}{H_e}} \right] \\
 & - C_{43} \cdot \frac{e_0}{T_1^2} \cdot (H_e)^2 \cdot \left[ \left( \frac{z_1}{H_e} + 1 \right) \cdot e^{\frac{-z_1}{H_e}} - \left( \frac{z'}{H_e} + 1 \right) \cdot e^{\frac{-z'}{H_e}} \right]
 \end{aligned} \tag{3.4.7.4.1}$$

One can see that  $I_4$  depends on the following variables

$$I_4 = I_4(\theta_0, p_0, e_0, T_1, z_0, z_1, z', H_p, H_e) \tag{3.4.7.4.2}$$

Remark that  $I_2$  and  $I_4$  are functions of the same variables.

### 3.4.8. Integration summary

Retake eq. (3.4.1.20) and insert the results from paragraphs 3.4.3 to 3.4.7. The path delay is thus

$$\begin{aligned}
PD = & C_{111} \cdot \left[ \ln \left( \frac{T_0 + \gamma \cdot z_1}{T_0 + \gamma \cdot z_0} \right) + S_{11} \right] - C_{121} \cdot \left[ \ln \left( \frac{T_0 + \gamma \cdot z_1}{T_0 + \gamma \cdot z_0} \right) + S_{12} \right] \\
& + C_{131} \cdot \left[ \frac{-e^{-\frac{(T_0 + \gamma \cdot z_1)}{\gamma \cdot H_e}}}{T_0 + \gamma \cdot z_1} + \frac{e^{-\frac{(T_0 + \gamma \cdot z_0)}{\gamma \cdot H_e}}}{T_0 + \gamma \cdot z_0} - \frac{1}{\gamma \cdot H_e} \cdot \left[ \ln \left( \frac{T_0 + \gamma \cdot z_1}{T_0 + \gamma \cdot z_0} \right) + S_{12} \right] \right] \\
& - C_{21} \cdot \frac{p_0}{T_1} \cdot H_p \cdot \left[ e^{\frac{-z'}{H_p}} - e^{\frac{-z_1}{H_p}} \right] + C_{22} \cdot \frac{e_0}{T_1} \cdot H_e \cdot \left[ e^{\frac{-z'}{H_e}} - e^{\frac{-z_1}{H_e}} \right] \\
& - C_{23} \cdot \frac{e_0}{T_1^2} \cdot H_e \cdot \left[ e^{\frac{-z'}{H_e}} - e^{\frac{-z_1}{H_e}} \right] \\
& + C_{311} \cdot \left[ \gamma \cdot H_p \cdot \left[ e^{\frac{-(T_0 + \gamma \cdot z_0)}{\gamma \cdot H_p}} - e^{\frac{-(T_0 + \gamma \cdot z_1)}{\gamma \cdot H_p}} \right] + T_0 \cdot \ln \left( \frac{T_0 + \gamma \cdot z_1}{T_0 + \gamma \cdot z_0} \right) - S_{11} \right] \\
& - C_{321} \cdot \left[ \gamma \cdot H_e \cdot \left[ e^{\frac{-(T_0 + \gamma \cdot z_1)}{\gamma \cdot H_e}} - e^{\frac{-(T_0 + \gamma \cdot z_0)}{\gamma \cdot H_e}} \right] + T_0 \cdot \left( \ln \left( \frac{T_0 + \gamma \cdot z_1}{T_0 + \gamma \cdot z_0} \right) + S_{12} \right) \right] \\
& - C_{331} \cdot \left[ \ln \left( \frac{T_0 + \gamma \cdot z_1}{T_0 + \gamma \cdot z_0} \right) + S_{12} + T_0 \cdot \left[ \frac{e^{-\frac{(T_0 + \gamma \cdot z_1)}{\gamma \cdot H_e}}}{T_0 + \gamma \cdot z_1} - \frac{e^{-\frac{(T_0 + \gamma \cdot z_0)}{\gamma \cdot H_e}}}{T_0 + \gamma \cdot z_0} \right] + T_0 \cdot \left( \frac{1}{\gamma \cdot H_e} \right) \cdot \left[ \ln \left( \frac{T_0 + \gamma \cdot z_1}{T_0 + \gamma \cdot z_0} \right) + S_{12} \right] \right] \\
& - C_{41} \cdot \frac{p_0}{T_1} \cdot H_p^2 \cdot \left[ \left( \frac{z_1}{H_p} + 1 \right) \cdot e^{\frac{-z_1}{H_p}} - \left( \frac{z'}{H_p} + 1 \right) \cdot e^{\frac{-z'}{H_p}} \right] \\
& + C_{42} \cdot \frac{e_0}{T_1} \cdot (H_e)^2 \cdot \left[ \left( \frac{z_1}{H_e} + 1 \right) \cdot e^{\frac{-z_1}{H_e}} - \left( \frac{z'}{H_e} + 1 \right) \cdot e^{\frac{-z'}{H_e}} \right] \\
& - C_{43} \cdot \frac{e_0}{T_1^2} \cdot (H_e)^2 \cdot \left[ \left( \frac{z_1}{H_e} + 1 \right) \cdot e^{\frac{-z_1}{H_e}} - \left( \frac{z'}{H_e} + 1 \right) \cdot e^{\frac{-z'}{H_e}} \right]
\end{aligned} \tag{3.4.8.1}$$

### 3.4.9. Path delay variables and zenith path delay

Combining eq. (3.4.4.4.2), eq. (3.4.5.4.2), eq. (3.4.6.4.2) and eq. (3.4.7.4.2), one can conclude that the path delay of eq. (3.4.8.1) depends on the following variables

$$PD = PD(\theta_0, p_0, e_0, T_0, T_1, \gamma, z_0, z_1, z', H_p, H_e) \tag{3.4.9.1}$$

However, the above formulation implies that the path delay depends on the temperature  $T_0$ . One should note that with the chosen temperature model, eq. (3.3.4.1),  $T_0$  is the temperature at the altitude of reference and not the temperature at the GPS receiver's location, i.e. at altitude  $z_0$ ! That is

$$T_0 \neq T(z_0) \tag{3.4.9.2}$$

Indeed, it holds

$$T_0 = T_{ref} = T(z_0) - \gamma \cdot z_0 \quad (3.4.9.3)$$

However, with the adopted pressure model, eq. (3.3.4.2), it holds

$$p_0 = p_{ref} \cdot e^{\frac{-z_0}{H_p}} \quad (3.4.9.4)$$

and with the adopted atmospheric humidity model, eq. (3.3.4.3), one has

$$e_0 = e_{ref} \cdot e^{\frac{-z_0}{H_e}} \quad (3.4.9.5)$$

Hence the path delay depends on the variables

$$PD = PD(\theta_0, p_{ref}, e_{ref}, T_{ref}, T_1, \gamma, z_0, z_1, z', H_p, H_e) \quad (3.4.9.6)$$

A GPS receiver tracks simultaneously up to 12 GPS satellites at the same time. However for positioning only 4 GPS space vehicles (SV) are required. Usually the GPS receiver computes the path delays for each SV and then projects them to zenith with the mapping functions of paragraph 3.2.5. Hence only path delays projected to zenith are of interest. Therefore consider the special case where

$$\theta_0 = 0 \text{ deg at zenith} \quad (3.4.9.7)$$

It holds then

$$\sec \theta_0 = 1 \quad \text{and} \quad \tan \theta_0 = 0 \quad (3.4.9.8)$$

Insert eq. (3.4.9.5) in eq. (3.4.1.20). Remark that  $I_3$  and  $I_4$  vanish, i.e.

$$I_3 = 0 \quad \text{and} \quad I_4 = 0 \quad (3.4.9.9)$$

because the corresponding mapping function itself vanishes. Furthermore the coefficients of  $I_1$  are

$$C_{111} = 10^{-6} \cdot 77.64 \cdot e^{\frac{z_0}{H_p}} \cdot p_0 \cdot \frac{1}{\gamma} \cdot e^{\frac{T_{ref}}{\gamma \cdot H_p}} = 10^{-6} \cdot 77.64 \cdot \frac{p_{ref}}{\gamma} \cdot e^{\frac{T_{ref}}{\gamma \cdot H_p}} \quad (3.4.9.10)$$

$$C_{121} = 10^{-6} \cdot 12.96 \cdot 10^{\frac{z_0}{H_e}} \cdot e_0 \cdot \frac{1}{\gamma} \cdot e^{\frac{T_{ref}}{\gamma \cdot H_e}} = 10^{-6} \cdot 12.96 \cdot \frac{e_{ref}}{\gamma} \cdot e^{\frac{T_{ref}}{\gamma \cdot H_e}} \quad (3.4.9.11)$$

$$C_{131} = 10^{-6} \cdot 5748 \cdot 64.68 \cdot 10^{\frac{z_0}{H_e}} \cdot e_0 \cdot \frac{1}{\gamma} \cdot e^{\frac{T_{ref}}{\gamma \cdot H_e}} = 10^{-6} \cdot 5748 \cdot 64.68 \cdot \frac{e_{ref}}{\gamma} \cdot e^{\frac{T_{ref}}{\gamma \cdot H_e}} \quad (3.4.9.12)$$

and of  $I_2$  are

$$C_{21} = 10^{-6} \cdot 77.64 \cdot e^{\frac{z_0}{H_p}} \quad (3.4.9.13)$$

$$C_{22} = 10^{-6} \cdot 12.96 \cdot e^{\frac{z_0}{H_e}} \quad (3.4.9.14)$$

$$C_{23} = 10^{-6} \cdot 5748 \cdot 64.68 \cdot e^{\frac{z_0}{H_e}} \quad (3.4.9.15)$$

Instead of directly inserting this in eq. (3.4.8.1), one intends to rewrite eq. (3.4.8.1) in such a form that its physical origin is clear. Remind the Essen and Froome formula. It is composed of three terms respectively proportional to  $p/T$ ,  $e/T$  and  $e/T^2$ . The term proportional to  $p/T$  does not depend on the water vapor content of the atmosphere and thus depends only on the so-called hydrostatic air. Conversely, the two other terms depend on the water vapor

present in the atmosphere and thus contribute to the so-called ‘wet’ path delay. Some scientists rather consider the term  $(p - e)/T$  in the formula of Essen and Froome, eq. (3.2.2.7) and call it the ‘dry’ refractivity.

In the present case where the path delay is evaluated at zenith, the path delay is known as the Zenith Path Delay (ZPD) or Zenith Total Delay (ZTD)<sup>11</sup>. It is split in two terms corresponding to the contributions of the ‘dry’ air and of the ‘wet’ air to the path delay, i.e.

$$ZPD := ZDD + ZWD \quad (3.4.9.16)$$

Thus define the Zenith Hydrostatic Delay (ZHD) as

$$ZHD := I_{11}(\theta_0 = 0) + I_{21}(\theta_0 = 0) \quad (3.4.9.17)$$

and the Zenith Wet Delay (ZWD) as

$$ZWD := \frac{64.68}{12.96} \cdot I_{12}(\theta_0 = 0) + I_{13}(\theta_0 = 0) + \frac{64.68}{12.96} \cdot I_{22}(\theta_0 = 0) + I_{23}(\theta_0 = 0) \quad (3.4.9.18)$$

The Zenith Dry Delay (ZDD) is then defined as

$$ZDD := I_{11}(\theta_0 = 0) + \frac{77.64}{12.96} \cdot I_{12}(\theta_0 = 0) + I_{21}(\theta_0 = 0) + \frac{77.64}{12.96} \cdot I_{22}(\theta_0 = 0) \quad (3.4.9.19)$$

Combine eq. (3.4.9.7) to eq. (3.4.9.12) and eq. (3.4.8.1) to obtain for the ZHD

$$\boxed{ZHD = 10^{-6} \cdot 77.64 \cdot \frac{p_{ref}}{\gamma} \cdot e^{\frac{T_{ref}}{\gamma \cdot H_p}} \cdot \left[ \ln \left( \frac{T_{ref} + \gamma \cdot z_1}{T_{ref} + \gamma \cdot z_0} \right) + S_{11} \right] + 10^{-6} \cdot 77.64 \cdot \frac{p_{ref}}{T_1} \cdot H_p \cdot \left[ e^{\frac{-z_1}{H_p}} - e^{\frac{-z'}{H_p}} \right]} \quad (3.4.9.20)$$

The Zenith Wet Delay is

$$\begin{aligned} ZWD = & -10^{-6} \cdot 64.68 \cdot \frac{e_0}{\gamma} \cdot e^{\frac{1}{H_e} \left( z_0 + \frac{T_0}{\gamma} \right)} \cdot \left[ \ln \left( \frac{T_0 + \gamma \cdot z_1}{T_0 + \gamma \cdot z_0} \right) + S_{12} \right] \\ & + 10^{-6} \cdot 5748 \cdot 64.68 \cdot \frac{e_0}{\gamma} \cdot e^{\frac{1}{H_e} \left( z_0 + \frac{T_0}{\gamma} \right)} \cdot \left[ \frac{-e^{\frac{-(T_0 + \gamma \cdot z_1)}{\gamma \cdot H_e}}}{T_0 + \gamma \cdot z_1} + \frac{e^{\frac{-(T_0 + \gamma \cdot z_0)}{\gamma \cdot H_e}}}{T_0 + \gamma \cdot z_0} - \frac{1}{\gamma \cdot H_e} \cdot \left[ \ln \left( \frac{T_0 + \gamma \cdot z_1}{T_0 + \gamma \cdot z_0} \right) + S_{12} \right] \right] \\ & + 10^{-6} \cdot 64.68 \cdot e^{\frac{z_0}{H_e}} \cdot \frac{e_0}{T_1} \cdot H_e \cdot \left[ e^{\frac{-z'}{H_e}} - e^{\frac{-z_1}{H_e}} \right] \\ & - 10^{-6} \cdot 5748 \cdot 64.68 \cdot e^{\frac{z_0}{H_e}} \cdot \frac{e_0}{T_1^2} \cdot H_e \cdot \left[ e^{\frac{-z'}{H_e}} - e^{\frac{-z_1}{H_e}} \right] \end{aligned} \quad (3.4.9.21)$$

Insert for the GPS receiver’s temperature, pressure and relative humidity respectively eq. (3.4.9.3), eq. (3.4.9.4) and eq. (3.4.9.5) in eq. (3.4.9.21). It holds

<sup>11</sup> Do not confond the Zenith Total Delay with the Zenith Tropospheric Delay that takes only the influence of the lower part of the atmosphere, namely the troposphere, into account.



$$\begin{aligned}
ZWD = & -10^{-6} \cdot 64.68 \cdot \frac{e_{ref}}{\gamma} \cdot e^{\frac{T_{ref}}{\gamma \cdot H_e}} \cdot \left[ \ln \left( \frac{T_{ref} + \gamma \cdot z_1}{T_{ref} + \gamma \cdot z_0} \right) + S_{12} \right] \\
& + 10^{-6} \cdot 5748 \cdot 64.68 \cdot \frac{e_{ref}}{\gamma} \cdot e^{\frac{T_{ref}}{\gamma \cdot H_e}} \cdot \left[ \frac{-e^{\frac{-(T_{ref} + \gamma \cdot z_1)}{\gamma \cdot H_e}}}{T_{ref} + \gamma \cdot z_1} + \frac{e^{\frac{-(T_{ref} + \gamma \cdot z_0)}{\gamma \cdot H_e}}}{T_{ref} + \gamma \cdot z_0} - \frac{1}{\gamma \cdot H_e} \cdot \left[ \ln \left( \frac{T_{ref} + \gamma \cdot z_1}{T_{ref} + \gamma \cdot z_0} \right) + S_{12} \right] \right] \\
& + 10^{-6} \cdot 64.68 \cdot \frac{e_{ref}}{T_1} \cdot H_e \cdot \left[ e^{\frac{-z'}{H_e}} - e^{\frac{-z_1}{H_e}} \right] \\
& - 10^{-6} \cdot 5748 \cdot 64.68 \cdot \frac{e_{ref}}{T_1^2} \cdot H_e \cdot \left[ e^{\frac{-z'}{H_e}} - e^{\frac{-z_1}{H_e}} \right]
\end{aligned} \tag{3.4.9.22}$$

Combine eq. (3.4.9.19), eq. (3.4.9.20) and eq. (3.4.9.22) to compute the ZDD

$$\begin{aligned}
ZDD = & 10^{-6} \cdot 77.64 \cdot \frac{p_{ref}}{\gamma} \cdot e^{\frac{T_{ref}}{\gamma \cdot H_p}} \cdot \left[ \ln \left( \frac{T_{ref} + \gamma \cdot z_1}{T_{ref} + \gamma \cdot z_0} \right) + S_{11} \right] \\
& - 10^{-6} \cdot 77.64 \cdot \frac{e_{ref}}{\gamma} \cdot e^{\frac{T_{ref}}{\gamma \cdot H_e}} \cdot \left[ \ln \left( \frac{T_{ref} + \gamma \cdot z_1}{T_{ref} + \gamma \cdot z_0} \right) + S_{12} \right] \\
& + 10^{-6} \cdot 77.64 \cdot \frac{p_{ref}}{T_1} \cdot H_p \cdot \left[ e^{\frac{-z_1}{H_p}} - e^{\frac{-z'}{H_p}} \right] \\
& - 10^{-6} \cdot 77.64 \cdot \frac{e_{ref}}{T_1} \cdot H_e \cdot \left[ e^{\frac{-z'}{H_e}} - e^{\frac{-z_1}{H_e}} \right]
\end{aligned} \tag{3.4.9.23}$$

Recall that eq. (3.4.9.16) holds, i.e.

$$\boxed{ZTD := ZDD + ZWD} \tag{3.4.9.24}$$

With eq. (3.4.4.1.8) and eq. (3.4.9.3), the series  $S_{11}$  is thus

$$S_{11} = \sum_{n \geq 1} \left( \frac{-1}{\gamma \cdot H_p} \right)^n \cdot \frac{1}{n \cdot n!} \cdot \left[ (T_{ref} + \gamma \cdot z_1)^n - (T_{ref} + \gamma \cdot z_0)^n \right] \tag{3.4.9.25}$$

i.e. with Law 3

$$S_{11} = \sum_{n \geq 1} \left( \frac{-1}{\gamma \cdot H_p} \right)^n \cdot \frac{1}{n \cdot n!} \cdot \sum_{k=0}^n \binom{n}{k} \cdot T_{ref}^{n-k} \cdot \gamma^k \cdot [z_1^k - z_0^k] \tag{3.4.9.26}$$

and with eq. (3.4.4.2.7) and eq. (3.4.9.3), the series  $S_{12}$  is

$$S_{12} = \sum_{n \geq 1} \left( \frac{-1}{\gamma \cdot H_e} \right)^n \cdot \frac{1}{n \cdot n!} \cdot \left[ (T_{ref} + \gamma \cdot z_1)^n - (T_{ref} + \gamma \cdot z_0)^n \right] \tag{3.4.9.27}$$

With the *Binomial law*, Law 3, eq. (3.4.9.27) can be rewritten as

$$S_{12} = \sum_{n \geq 1} \left( \frac{-1}{\gamma \cdot H_e} \right)^n \cdot \frac{1}{n \cdot n!} \cdot \sum_{k=0}^n \binom{n}{k} \cdot T_{ref}^{n-k} \cdot \gamma^k \cdot [z_1^k - z_0^k] \quad (3.4.9.28)$$

Hence the ZHD is a function of

$$ZHD = ZHD(p_{ref}, T_{ref}, T_1, \gamma, z_0, z_1, z', H_p) \quad (3.4.9.29)$$

the ZWD depends on

$$ZWD = ZWD(e_{ref}, T_{ref}, T_1, \gamma, z_0, z_1, z', H_e) \quad (3.4.9.30)$$

and the ZDD on

$$ZDD = ZDD(p_{ref}, e_{ref}, T_{ref}, T_1, \gamma, z_0, z_1, z', H_p, H_e) \quad (3.4.9.31)$$

Therefore the ZTD is a function of

$$ZTD = ZTD(p_{ref}, e_{ref}, T_{ref}, T_1, \gamma, z_0, z_1, z', H_p, H_e) \quad (3.4.9.32)$$

### 3.5. Summary

The path delay (PD) calculations are based on the Fermat's principle. The PD is given by the integral of the refractivity along the signal path through the atmosphere. The standard models of Essen and Froome (1951), Smith and Weintraub (1953) and Thayer (1974) compute the refractivity as function of the atmospheric temperature  $T$ , the atmospheric pressure  $p$ , and the partial water vapor  $e$ . Both the Hopfield and Saastamoinen models provide direct formulas for the path delay that can be used for comparison.

Three distinct models have been derived for the atmospheric variables  $T$ ,  $p$  and  $e$ . They are split into two sets, the first one being only one-dimensional (1D) with the altitude  $z$  as position variable. The second set is four-dimensional (4D), depending on the horizontal position, altitude and time.

The temperature model takes into account the possible condensation of water vapor. It represents a linear decrease of the temperature from the GPS's receiver altitude up to the tropopause. From the tropopause up to the upper limit of integration, generally in the lower stratosphere, the temperature is assumed to be constant.

The atmospheric pressure model consists in an exponential law based on the known barometric formula. It contains a scaling height. The partial water vapor pressure follows also an exponential law, derived from the Clausius-Clapeyron equation. It takes into account the vaporization through the saturation water vapor.

The path delay is computed via the integration of the refractivity through the spherical symmetric atmosphere between the GPS's receiver location and the GPS space vehicle. The refractivity is modeled with the Essen and Froome formula where the temperature model, pressure model and the partial water vapor model previously generated have been inserted.

The resulting path delay is calculated at zenith and then split in two terms in order to ease its physical interpretation. The Zenith Path Delay (ZPD) – also called the Zenith Total Delay (ZTD) - is made up of a dry term, the Zenith Dry Delay (ZDD) and of a wet term, the Zenith Wet Delay (ZWD). The Zenith Hydrostatic Delay (ZHD) has also been computed, as it is often a quantity of interest. The relationship between the ZPD, ZPD, ZHD, ZHD, ZWD and the Essen and Froome formula is outlined on Figure 16 on next page.

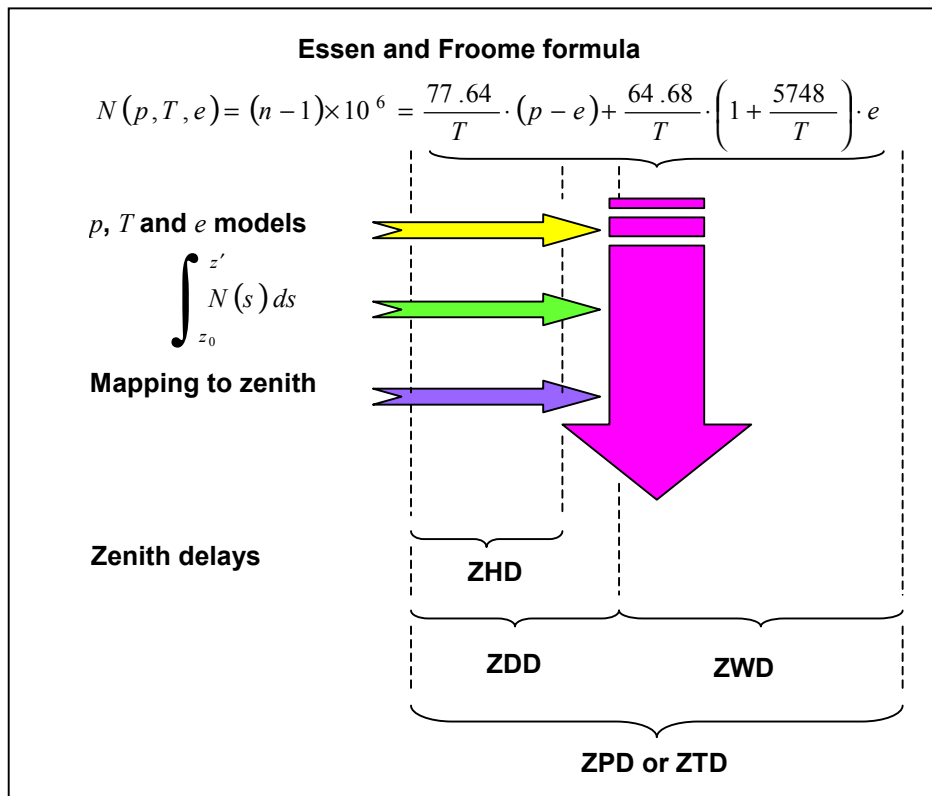


Figure 16. ZPD, ZHD, ZDD and ZWD relationship with the Essen and Froome formula

The three zenith delays depend on a set of 10 parameters: the reference pressure, the reference humidity, the reference temperature, the temperature at the tropopause, the tropospheric temperature gradient (lapse rate), the GPS's receiver altitude, the tropopause height, the upper limit of integration, the pressure scale height and the humidity scale height.

**Blank page**

## 4. Test and evaluation

The path delay (PD) models of Chapter 3 are used to generate path delay charts and predictions over the Swiss territory. In a first step these PD models are tested on reference values for each of the ten parameters in order to evaluate their plausibility. In a second step the partial derivatives that fill the design matrix of the system are computed and tested. Finally the model is implemented in collocation software and evaluated on a Swiss regional campaign.

### 4.1. Zenith Path Delay testing

The Zenith Hydrostatic Delay (ZHD), the Zenith Dry Delay (ZDD) and Zenith Wet Delay (ZWD) have been derived in Chapter 3. These are eq. (3.4.9.20), eq. (3.4.9.23) and eq. (3.4.9.22). They are tested here on reference values for the different parameters.

#### 4.1.1. Parameter reference values

The International Standard Atmosphere (ISA) defines reference equations and values for the behavior of the different layers of the atmosphere. For detailed information on ISA refer to [Lertes, 2000]. The reference pressure, humidity and temperature at MSL are set by ISA. It is the same of the temperature at tropopause and of the lapse rate.

The GPS receiver's location has been chosen at the Zimmerwald Observatory, a few miles South of the Swiss capital of Berne. This site presents many advantages. Among others it is assumed to be the best determined point in Switzerland with an altitude of 905 m Mean Sea Level (MSL). It is also part of the International GPS Service (IGS) and harbors a permanent GPS reference station.

The tropopause height varies usually between 8000 m and 12000 m for European latitudes. According to [Troller et al., 2002], the tropopause is situated at around 11000 m MSL over the Swiss territory, although seasonal variations are observed.

The upper limit of integration was set at 15000 m MSL as increasing it during preliminary studies didn't improved significantly the results. It is referred to paragraph 1.4.5. The pressure scale height normally stretches between 8000 m and 11000 m MSL. In Switzerland, it is known to vary few and observations have shown that it is centered on 9000 m MSL. The humidity scale height spans over the 1500 m to 5000 m MSL range. It depends strongly on the location. It was arbitrary set at 3000 m MSL.

These ten parameters are summarized in Table 10 hereunder:

Symbol	Value	Unit [SI]	Parameters	
			Identification	Remark
$p_{ref}$	1013.25	hPa	Reference pressure	ISA reference value
$e_{ref}$	10	hPa	Reference humidity	ISA reference value
$T_{ref}$	288.15	K	Reference temperature	$T_{ref} = 15^{\circ}\text{C}$ at MSL (0 m) as ISA reference value
$T_1$	216.64	K	Temperature at tropopause	$T_1 = -56.51^{\circ}\text{C}$ at $z_1 = 11000$ m as ISA reference value
$\gamma$	$-6.501 \cdot 10^{-3}$	$\text{K} \cdot \text{m}^{-1}$	Tropospheric temperature gradient (Lapse rate)	ISA reference value
$z_0$	905	m	GPS's receiver altitude	Zimmerwald altitude MSL
$z_1$	11000	m	Tropopause height	w.r.t. MSL
$z'$	15000	m	Upper limit of integration	w.r.t. MSL
$H_p$	9000	m	Pressure scale height	w.r.t. MSL
$H_e$	3000	m	Humidity scale height	w.r.t. MSL

Table 10. Parameters reference values.

### 4.1.2. Path Delay results

The Zenith Hydrostatic Delay (ZHD), Zenith Dry Delay (ZDD), Zenith Wet Delay (ZWD), and Zenith Path Delay (ZPD) have been computed for the parameter values of Table 10. As summarized in Table 11, the following results were obtained.

Symbol	Value	Unit [SI]	Identification
ZHD	2.0445	m	Zenith Hydrostatic Delay
ZDD	2.0384	m	Zenith Dry Delay
ZWD	0.1240	m	Zenith Wet Delay
ZPD	2.1624	m	Zenith Path Delay

Table 11. Zenith Delays evaluated at Zimmerwald with parameter reference values.

The values obtained for the ZHD, ZDD, ZWD and ZPD are in good agreement with observations made at Zimmerwald. Indeed the ZHD was expected to be around 2 meters. The ZDD should be slightly less than the ZHD as the term corresponding to the first  $e/T$  term in the Essen and Froome formula, eq. (3.2.2.7), has been subtracted.

The Zenith Wet Delay is generally observed in the centimeter range for European latitudes. Independent studies such as the Geodesy and Geodynamics Lab at the Swiss Federal Institute of Technology and the Federal Office of Topography's COMEDIE (Collocation of Meteorological Data for Interpolation and Estimation of Tropospheric Path delays) have found ZWD in the 20-25 centimeters range for the Zimmerwald site. For further information on COMEDIE, refer to [Troller et al, 2001].

The Zenith Path Delay should be slightly more than the Zenith Hydrostatic Delay while being less than the sum of the ZHD and ZWD. According to the International GPS Service's Geoforschungszentrum Postdam (GFZ Postdam), Germany, the ZPD observed at Zimmerwald are in the 2.15-2.20 meters range for the year 2001. For full data, refer to [Gendt, 2002].

It is now of interest to study the variations of the Zenith Delays with respect to some of the parameters of Table 10.

### 4.1.3. Path Delays as function of $z_0$

The ZHD, ZDD, ZWD and ZPD have been computed for the parameter reference values of Table 10. The whole Swiss territory is comprised between 195 meters MSL and 4554 meters MSL. The lowest point is located in Tessin near the city of Locarno, the highest point is the Monte Rosa, South of Zermatt in Wallis. Therefore, the GPS's receiver altitude  $z_0$  has been varied over the range.

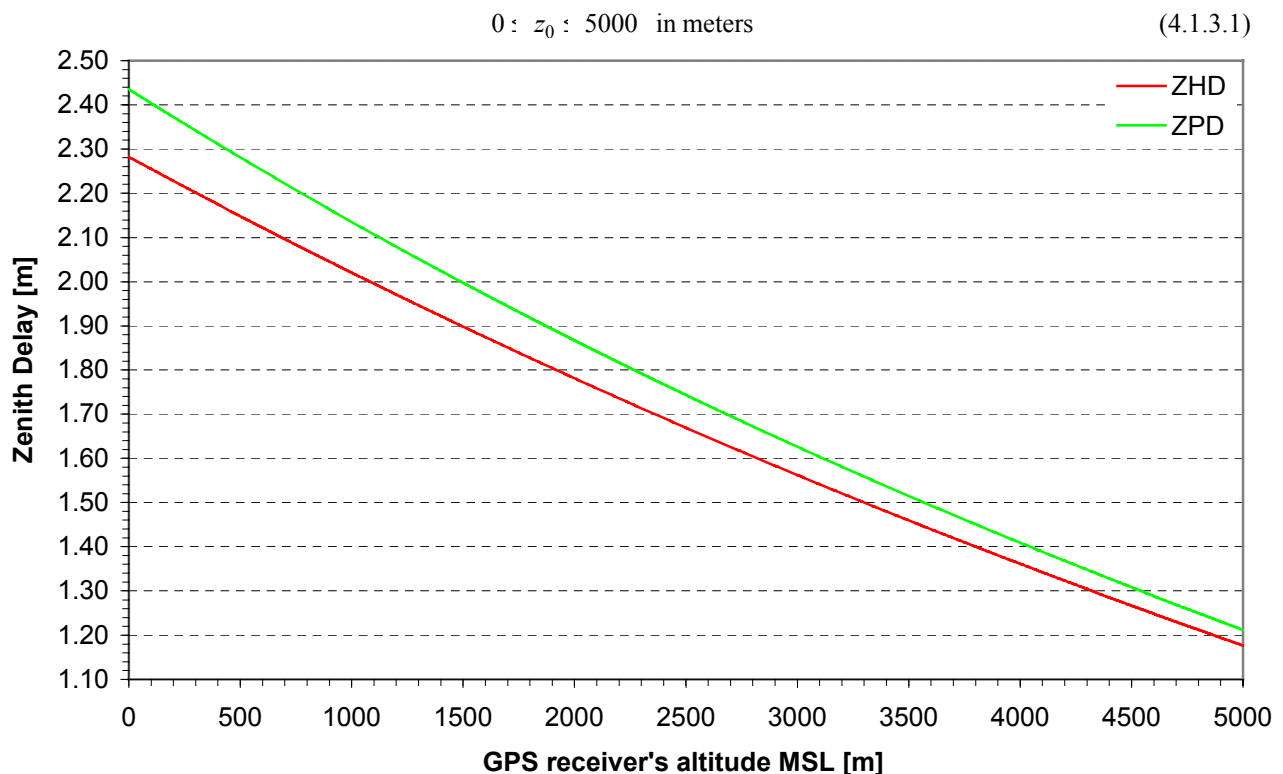


Figure 17. ZHD and ZPD as function of the GPS receiver's altitude MSL  $z_0$

The ZHD and ZPD are plotted together on Figure 17 on the previous page.

As expected, both the ZPD and ZHD decrease with  $z_0$ . Indeed, the higher one locates the GPS receiver, the shorter is the atmosphere thickness, and the less distance should the signal travel through the atmosphere. Further, the higher the less water vapor there is left above the GPS receiver's location. Indeed, the water vapor is mostly found in lower altitudes.

The variation of the ZPD with  $z_0$  is similar to the variation of the ZHD. This can be explained as follows. The main difference between the ZHD and ZPD originates from the partial water vapor terms, the  $e$ -terms, in the Essen and Froome formula. Refer to Figure 16. Thus the difference is due to the presence of water vapor in the atmosphere. However, one should remark that the pressure in the first term of the Essen and Froome formula is the total atmospheric pressure and hence partly accounts for the humidity of the atmosphere.

The ZHD and ZDD should have a similar behavior with respect to  $z_0$ . Thence their difference is plotted on Figure 18.

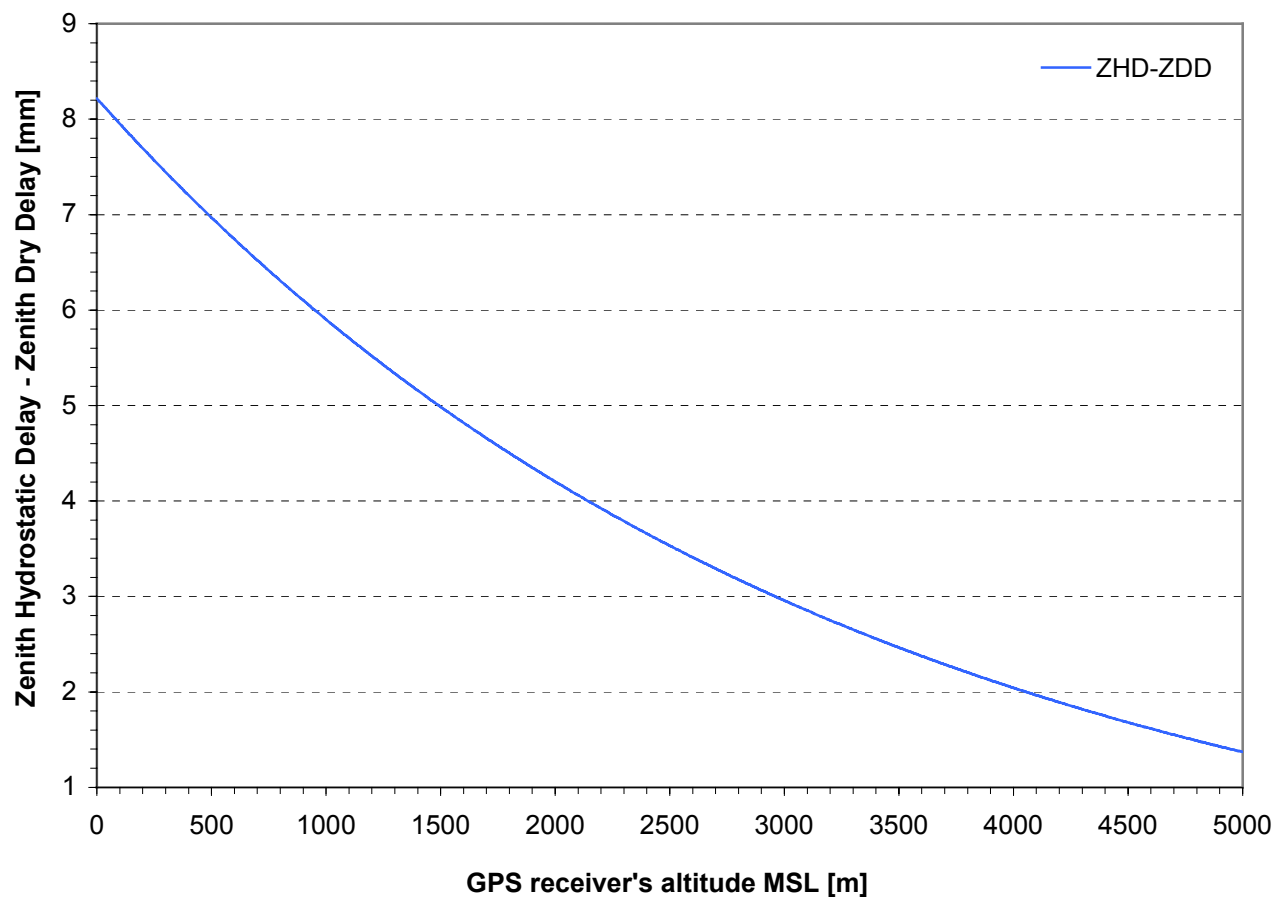


Figure 18. ZHD and ZDD difference as function of the GPS receiver's altitude MSL  $z_0$

The difference is in the millimeter range thus confirming the matching between both quantities. It diminishes with the altitude of the GPS receiver as the GPS signal has fewer atmospheric layers to cross. At that point, one should concentrate on the water vapor present in the air. The ZWD as function of  $z_0$  is plotted on Figure 19 on next page.

The majority of the atmospheric water vapor is situated in the lower troposphere. Indeed up to 50% is commonly encountered at altitude less than 4000 meters MSL. Compare with the data of Table 13. The ZWD is proportional to the partial water vapor pressure and thus a very good measure of the water vapor content of the atmosphere. It is used as basic observable in GPS Meteorology. Refer to [Rocken et al., 1993], [Niell, 1996], [Businger et al., 1996], [Rocken et al., 1997], and [Davis et al. 1998] for a review of the main features of GPS Meteorology.

In the next paragraph, one is interested in varying the upper limit of integration  $z'$  in order to determine whether or not one should consider the lower and mid-stratosphere.

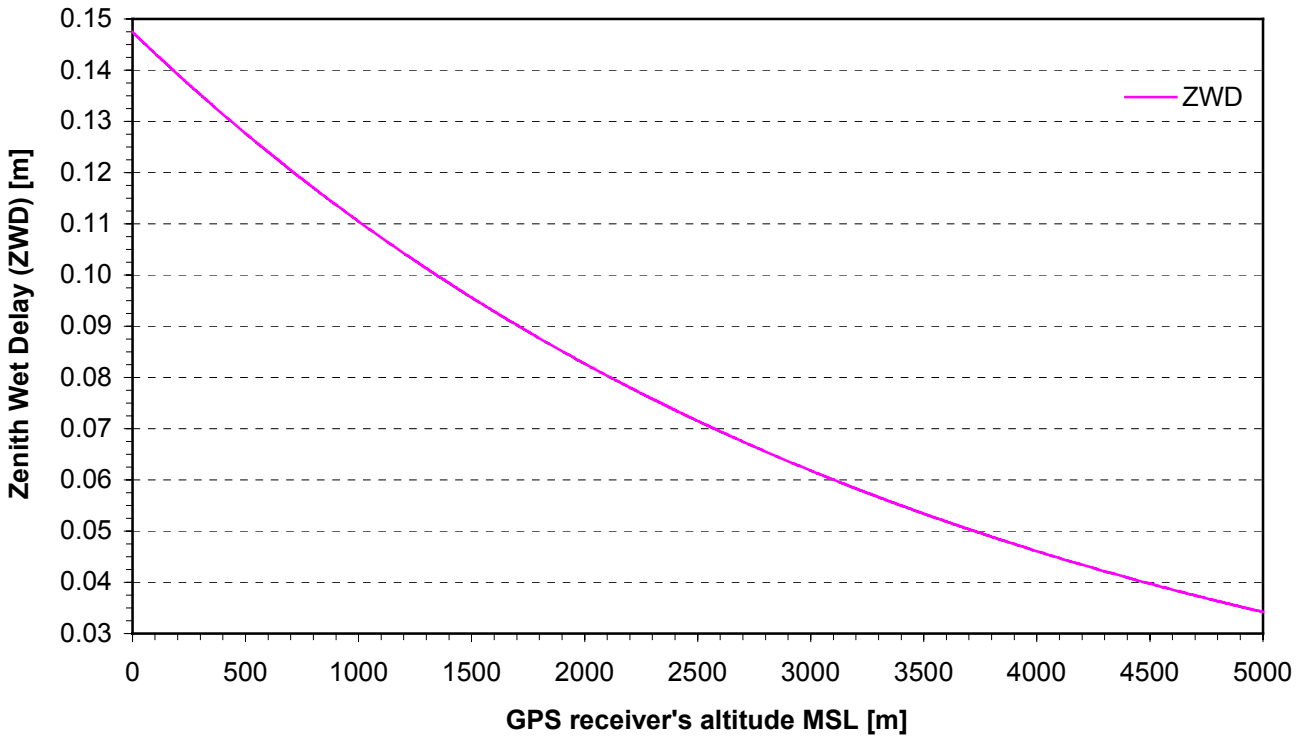


Figure 19. ZWD as function of the GPS receiver's altitude MSL  $z_0$

#### 4.1.4. Path Delays as function of $z'$

As was done in the previous paragraph for the GPS receiver's altitude  $z_0$ , vary the upper limit of integration  $z'$ . Referring to Table 10, the tropopause height has been a priori set to  $z_1 = 11000$  meters MSL. Therefore the lower limit for  $z'$  is 11000 meters MSL. As can be seen on Figure 12, the temperature of the atmosphere remains approximately stable and constant up to 35000 meters MSL. This will be the maximum limit for  $z'$ . Thus one let  $z'$  vary in the altitude range of

$$11000 \leq z' \leq 35000 \text{ in meters} \tag{4.1.4.1}$$

The ZHD and ZPD are plotted on Figure 20 hereunder.

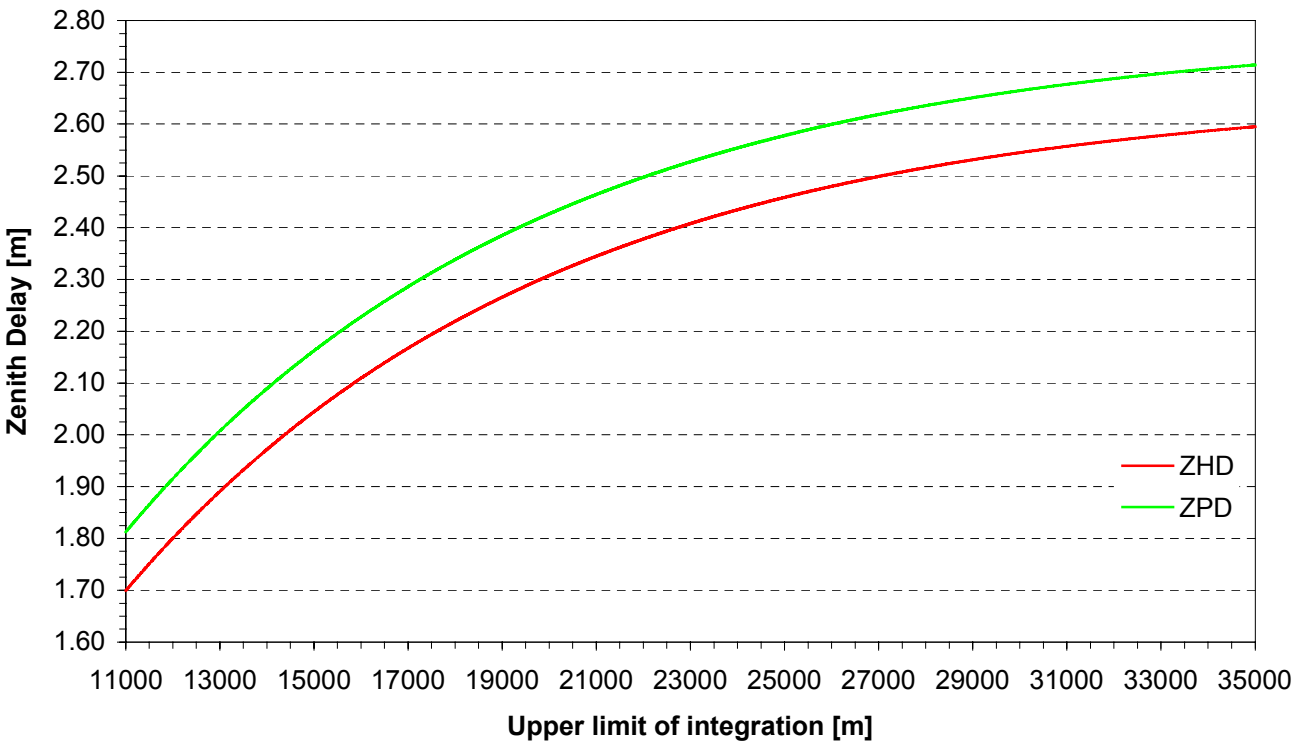


Figure 20. ZHD and ZPD as function of the upper limit of integration  $z'$  for  $z_0 = 905$  m MSL



It can be seen on Figure 20 that both the ZHD and the ZPD increase with the upper limit of integration. Apparently they seem to grow at the same rate. This is due to the fact that the third and fourth terms of the ZWD, i.e. the seventh and height terms of the ZPD are small and vary few with  $z'$ . This is also observed on Figure 22. The decision to take 15000 meters MSL as default value for the upper limit of integration is motivated by the fact that more than 90% of the atmospheric water vapor is below that altitude and nearly 80% of path delay is induced by layers spanned between the mean sea level and that altitude. This problem will be approached in more details later.

The ZHD and ZDD are compared on Figure 21. Their difference decreases of 0.3 millimeters if the upper limit of integration is increased. This means that there is less influence of the water vapor above the stratopause. This is in good agreement with the presence of the WV mostly in the lower atmosphere, namely the troposphere.

The ZWD as function of  $z'$  is plotted on Figure 22, also on next page. It increases with  $z'$  in the range of eq. (4.1.4.1) only of 6.5 mm, that is only by approximately 5%. This implies that the ZWD is already stable at 11000 meters MSL. Indeed, as it is a direct measure of the WV content of the atmosphere, it is proportional to  $e_{ref}$ . Most of the WV is below that altitude. Therefore the ZWD shouldn't be very sensitive to variations of the upper limit of integration.

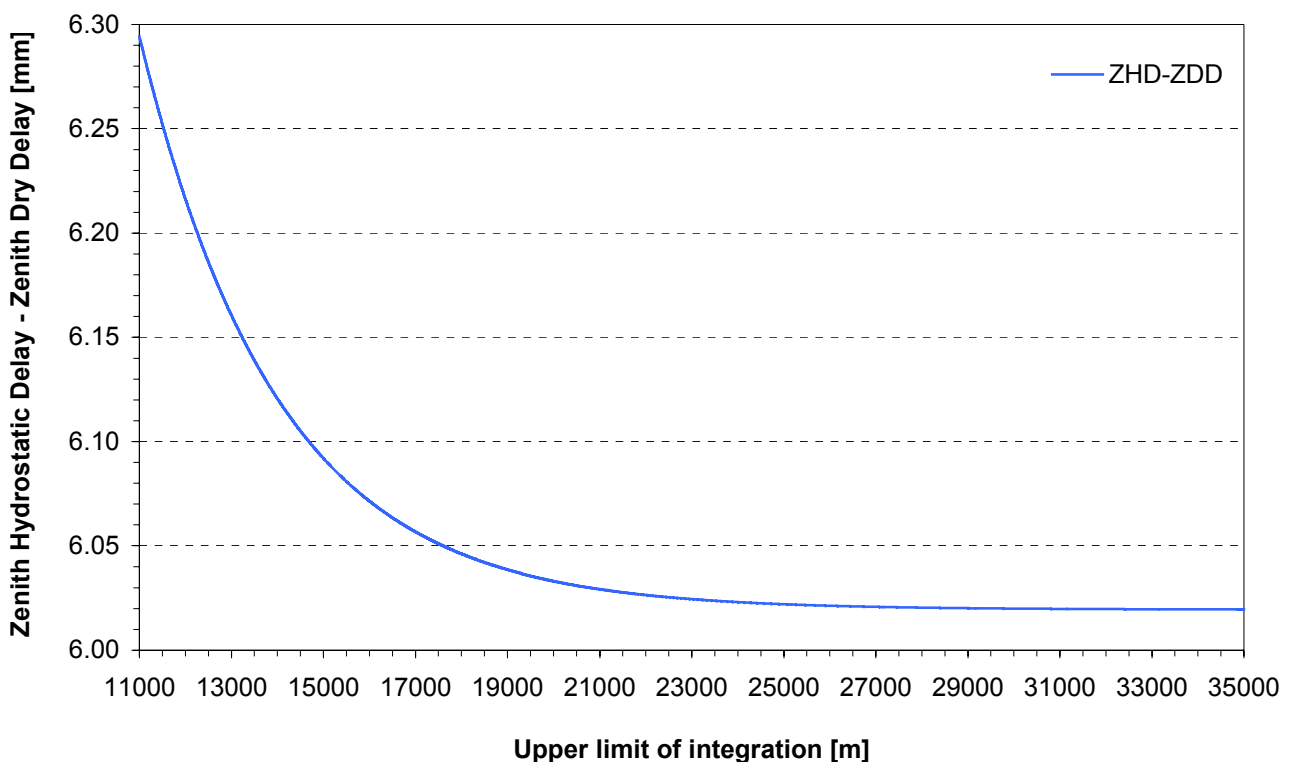


Figure 21. ZHD and ZDD difference as function of the upper limit of integration  $z'$  in the stratosphere and for  $z_0 = 905$  m MSL

As mentioned above, one is interested in determining the relative influence of the upper limit of integration  $z'$  on the different path delays at zenith. The relative change of the ZHD, ZDD, ZWD and ZPD with  $z'$  is plotted on Figure 23 on next page. The reference (100%) value is set at 35000 meters MSL. The 90% limit for the ZPD is achieved at about 20420 meters for all zenith delays and for ZHD and ZDD at approximately 20750 meters. At that altitude, one has already nearly 100% of the wet delay. As one could foresee, the 90% ZWD limit is much lower. It is at 8870 meters MSL. On the other side, at a threshold altitude of 15000 meters, just 79% of the ZHD and ZDD are obtained while 80% of the ZPD is achieved. However, one has already 98.5% of the ZWD! For this reason, it has been decided to set the default value of the upper limit of integration at 15000 meters MSL. Note that the ZHD and ZDD are almost superposed.

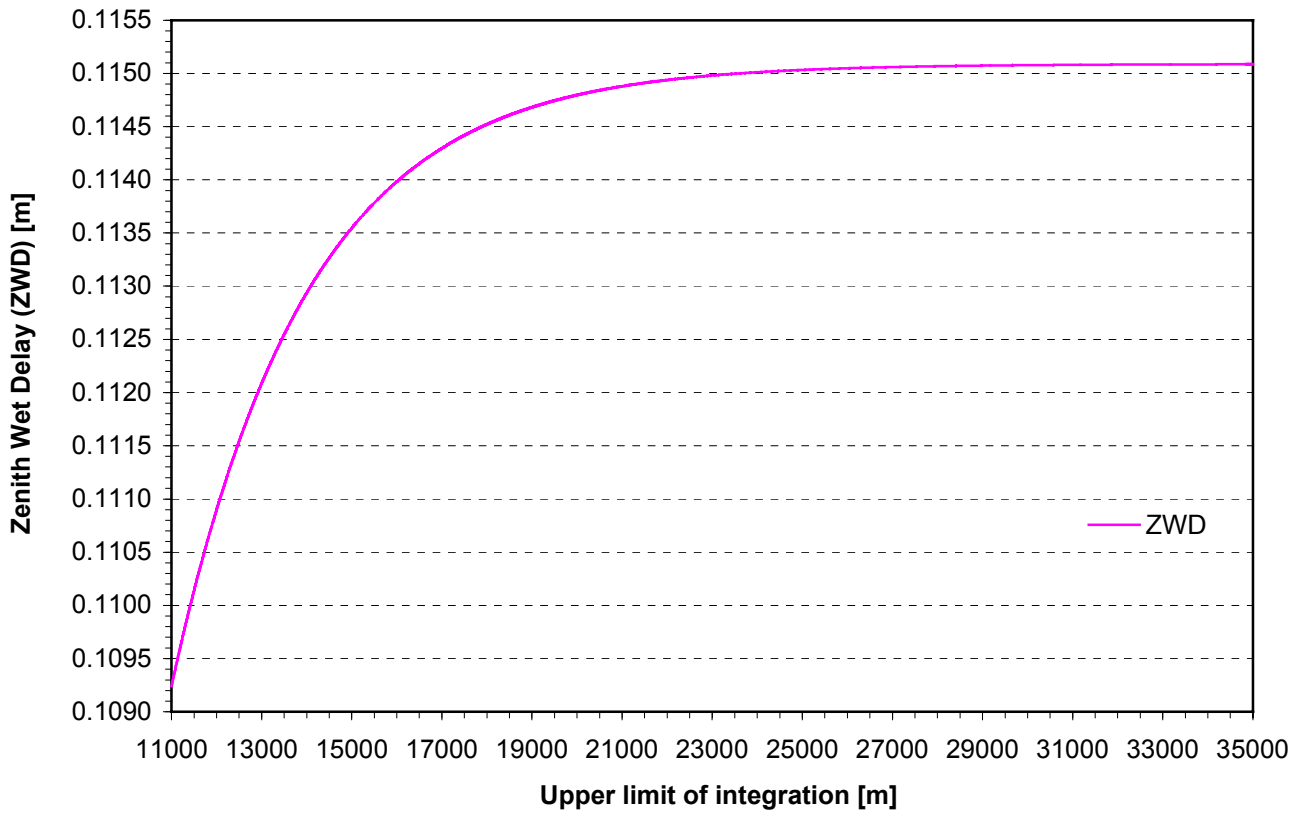


Figure 22. ZWD as function of the upper limit of integration  $z'$  in the stratosphere and for  $z_0 = 905$  m MSL

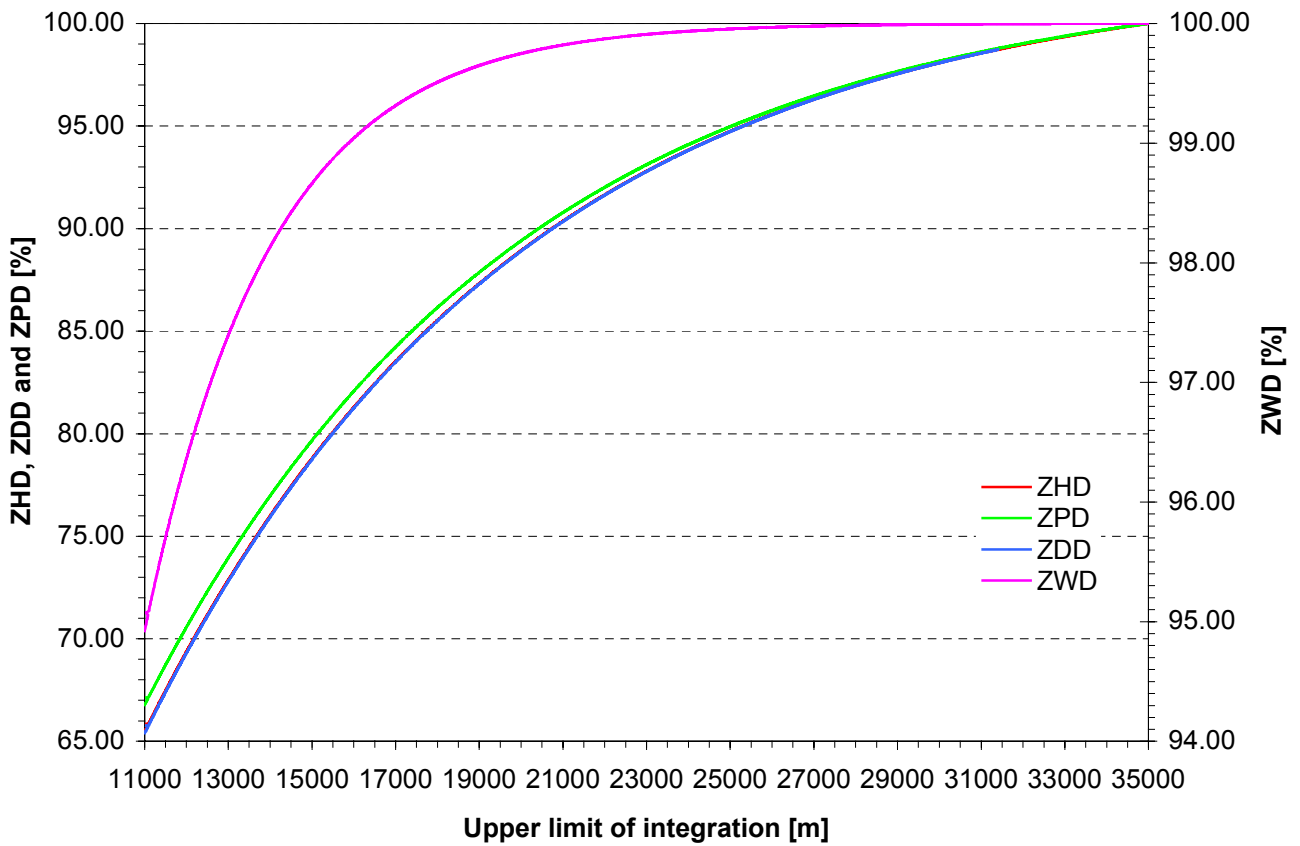


Figure 23. Relative change in % of the ZHD, ZDD, ZWD and ZPD with the upper limit of integration  $z'$  in the stratosphere and for  $z_0 = 905$  m MSL

The results obtained are summarized in Table 12 hereunder. The 80 % and 90% level are explicitly stated as these often are good indicators for the spatial distribution of the path delay sources.

Criterion	Observable			
	ZHD	ZDD	ZWD	ZPD
80% level	15480 m	15140 m	6530 m <sup>12</sup>	15490 m
90% level	20740 m	20760 m	8870 m <sup>13</sup>	20420 m
15000 m MSL	78.79 %	78.74 %	98.66 %	79.66 %

Table 12. 80% and 90% level for path delays as function of altitude, and 15000 m MSL threshold

#### 4.1.5. Path Delays as function of $z_1$

On one side one wants to know the influence of the tropopause on the various path delays at zenith, and on the other the influence of the upper limit of integration *in the troposphere*. Therefore the evolution of PDs as function of the upper limit of integration  $z_1$  (identical to the tropopause height if 8000 :  $z_1$  : 11000 meters MSL) is investigated in this paragraph.

From Table 10, one knows that the default altitude for the GPS receiver is the altitude of Zimmerwald, i.e. at 905 meters MSL. Hence the lower limit for the variation of  $z_1$  is taken at 1000 meters MSL. The upper limit is set at the default value for the tropopause height. Thus one has

$$1000 : z_1 : 11000 \quad \text{in meters} \quad (4.1.5.1)$$

The ZHD and ZPD are plotted together on Figure 24. At European latitudes, the tropopause is usually observed at an altitude varying between 8000 meters MSL and 12000 meters MSL. With respect to this fact, one is interested only in the right part of Figure 24, starting with a tropopause height  $z_1$  of 8000 meters MSL. The ZHD and ZPD

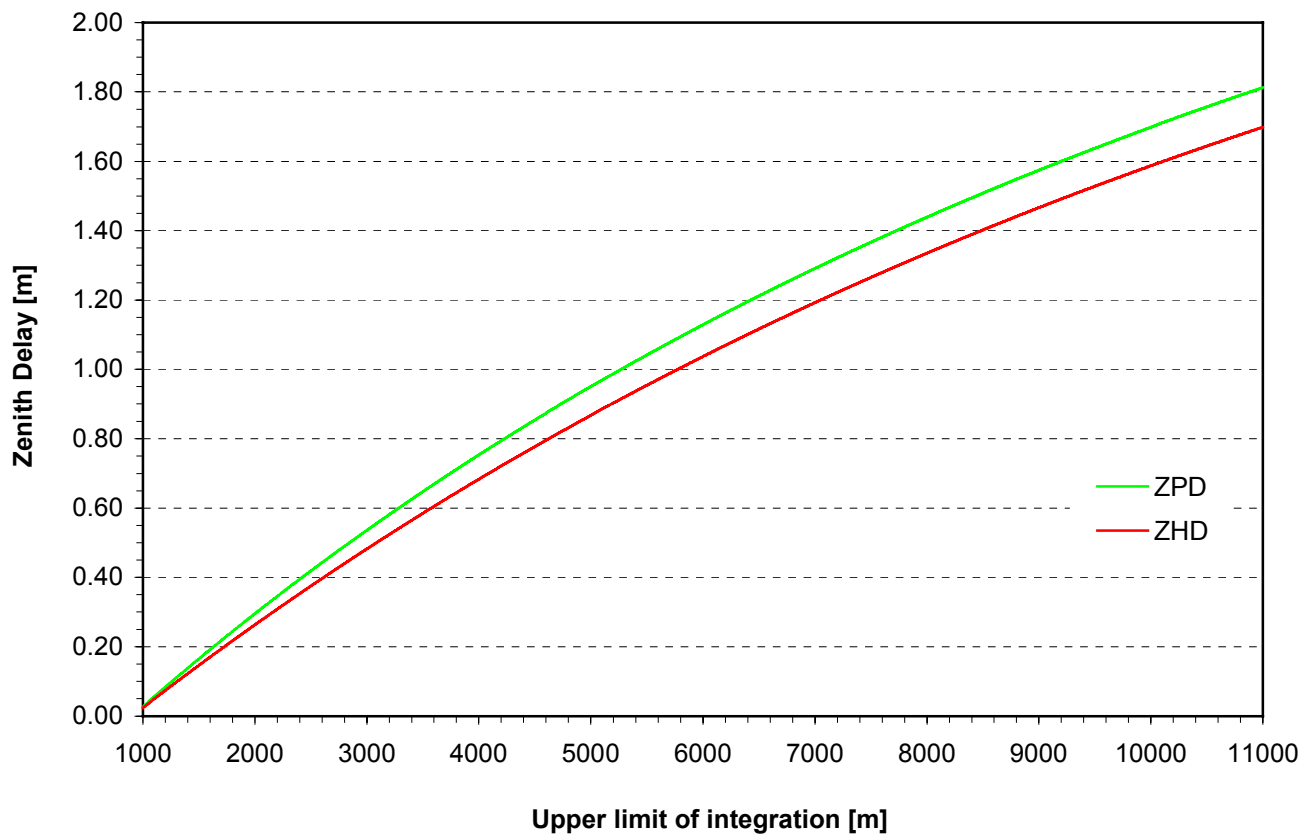


Figure 24. ZHD and ZPD as function of the upper limit of integration  $z_1$  in the troposphere and for  $z_0 = 905$  m MSL

<sup>12</sup>To obtain this value, refer to paragraph 4.1.5, Figure 27.

<sup>13</sup>Analogous to <sup>12</sup>.

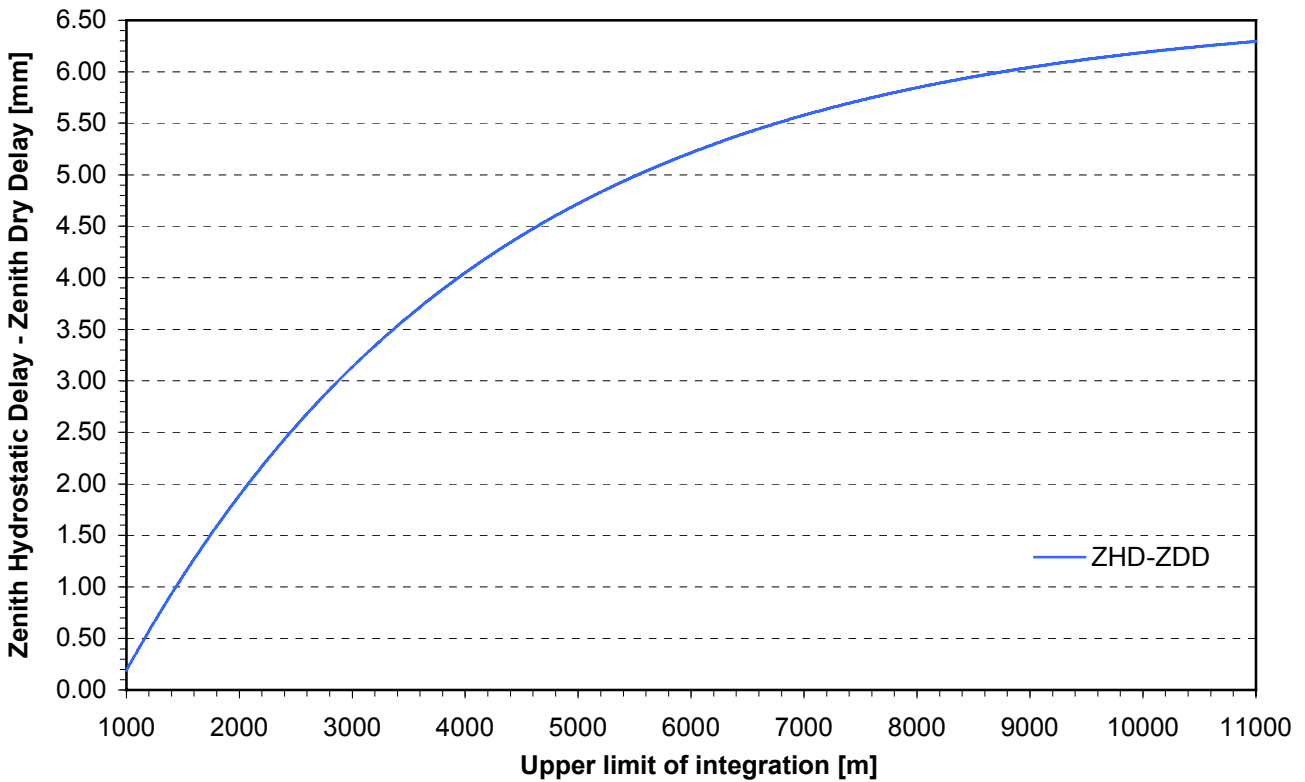


Figure 25. ZHD and ZDD difference as function of upper limit of integration  $z_1$  in the troposphere and for  $z_0 = 905$  m MSL

have a like wise attitude toward  $z_1$ . The slight offset of the ZPD is due to the water vapor present in the atmosphere

As it was the case for the GPS receiver’s altitude  $z_0$ , the ZHD and ZDD should perform in the same way with respect to  $z_1$ . Refer to Figure 25 above. Their increase seems to be of a logarithm type although it is not solely due to that. Both the  $S_{11}$  and  $S_{12}$  series generate this offset as can be guessed when comparing eq. (3.4.9.20) and eq. (3.4.9.23).

The Zenith Wet Delay as function of the tropopause height  $z_1$  is sketched on Figure 26. It increases rapidly for low values of  $z_1$  and then seems to stabilize itself. The 10 centimeters threshold is reached at 7970 meters MSL. This appears reasonable as one usually measures ZWD of that magnitude in the field while the tropopause is observed near its approximate lower limit of 8000 meters MSL.

As follow-on of Figure 23, the relative change of the ZHD, ZDD, ZWD and ZPD with the tropopause height is investigated with Figure 27 on next page. The value of the observable with a default tropopause height of meters MSL and a maximum upper limit of integration of meters MSL serves as reference for the scaling.

The 50% threshold for all path delays is achieved at around 7750 meters MSL for the ZPD while the ZHD is slightly lower. However, the ZDD, which does not contain any humidity terms, is reached 300 meters below. On the other hand, half of the ZWD is already taken into account at altitudes above 3500 meters MSL! This indeed very low for a mountainous country such as Switzerland where high peaks are usually above 4000 meters.

The percentage of path delays generated for the default tropopause height of 11000 meters MSL is also stated in Table 13. At that height one has approximately computed 65% of the Zenith Total Delay. Hence one absolutely needs a two-step temperature model as this shows that the influence of the lower stratosphere is not negligible!

Criterion	Observable			
	ZHD	ZDD	ZWD	ZPD
50% level	7730 m	7440 m	3340 m	7750 m
11000 m MSL	65.48 %	66.77 %	94.92 %	65.39 %

Table 13. 50% level for path delays as function of altitude, and 11000 m MSL threshold

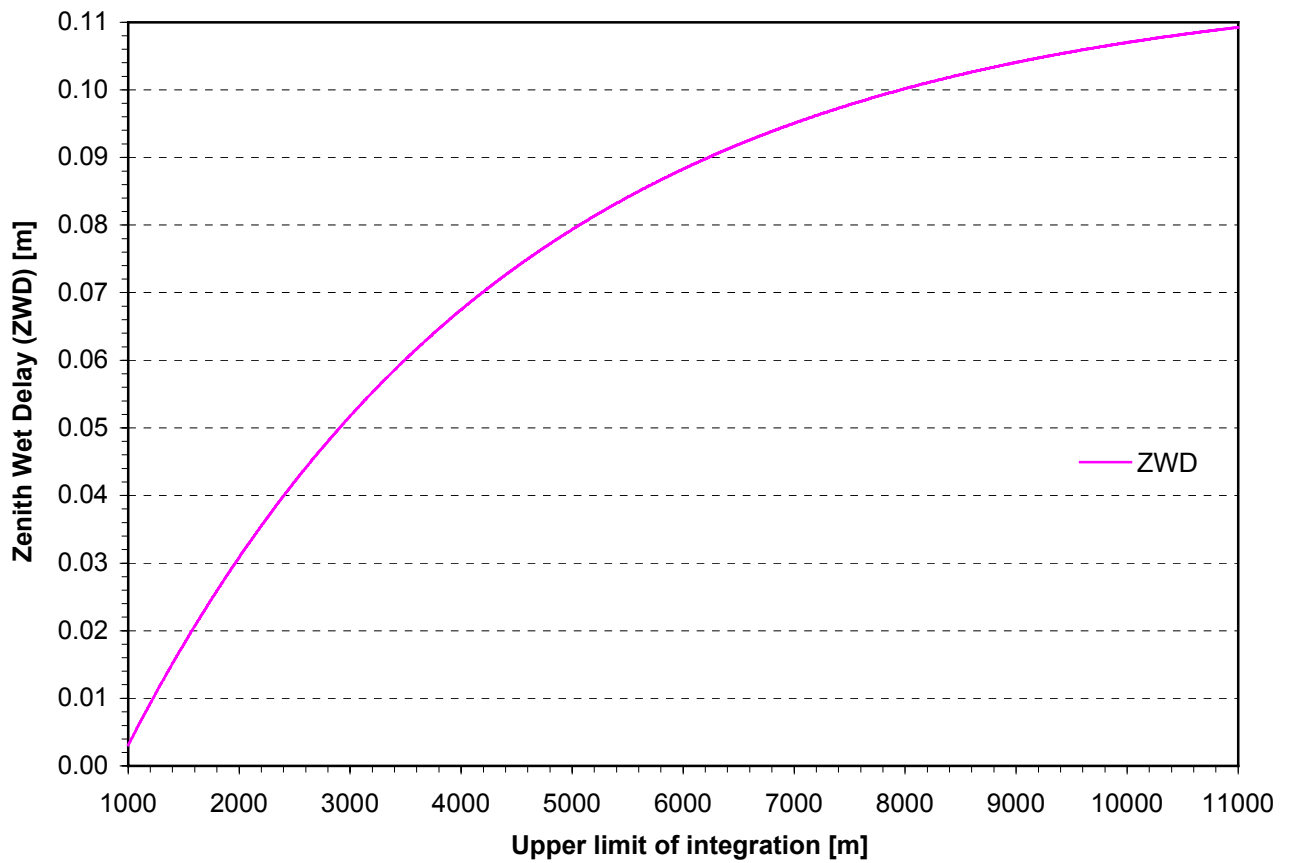


Figure 26. ZWD as function of the upper limit of integration  $z_1$  in the troposphere and for  $z_0 = 905$  m MSL

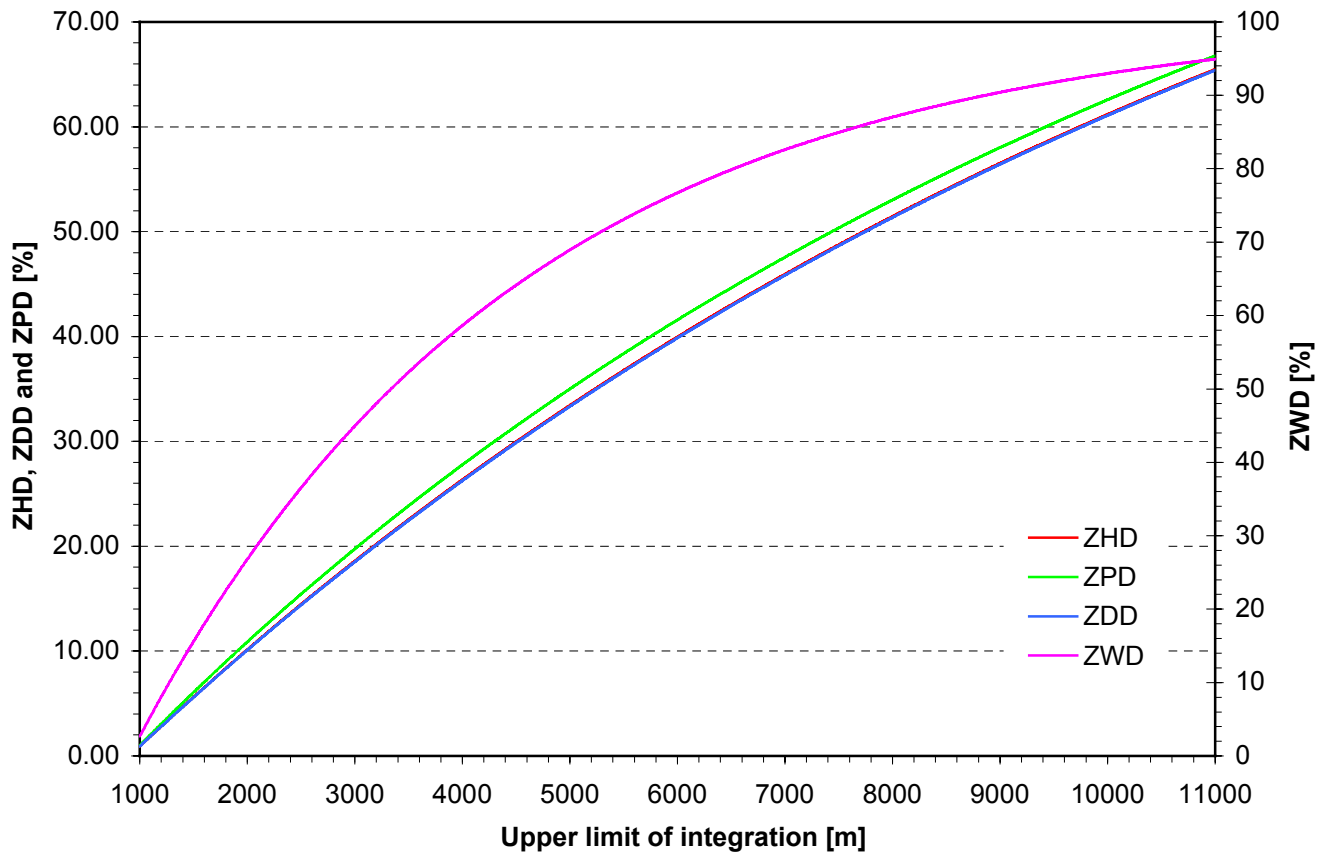


Figure 27. Relative change in % of the ZHD, ZDD, ZWD and ZPD with the upper limit of integration  $z_1$  in the troposphere and for  $z_0 = 905$  m MSL

### 4.1.6. Path Delays as function of $H_p$

The pressure scale height  $H_p$  is an important parameter. The ZHD, ZDD and ZPD are very sensitive to its variation. According to observations from the Swiss network of automatic stations ANETZ operated by the Swiss Meteorological Institute (SMA - Schweizer Meteorologische Anstalt), the pressure scale height is located on average at about 9000 meters MSL for Switzerland. Therefore this has been chosen as the default value. Refer to [Troller et al, 2001] for further details on ANETZ.

Meteorological observations show that the pressure scale height is normally situated between 7000 meters MSL and 12000 meters MSL for European latitudes, depending on the season. Thus, it has been varied over the range

$$7000 \leq H_p \leq 12000 \text{ in meters} \tag{4.1.6.1}$$

The ZHD and ZPD are plotted on Figure 28 on next page. Their increase is homogeneous over the whole pressure scale height range. Indeed they grow at exactly the same rate. This is absolutely normal! Indeed one should note that the Zenith Wet Delay does *not* depend on the pressure and thus on  $H_p$ . This fact is again explicitly stated on Figure 29. The difference between the ZHD and ZDD is constant. It corresponds exactly to the second term of the Essen and Froome formula, which is a constant with respect to  $H_p$ . The ZWD does not depend on  $H_p$ . It is therefore not plotted.

### 4.1.7. Path Delays as function of $H_e$

As was done in the previous paragraph above for the pressure scale height, one computes now the path delays as function of the partial water vapor scale height – or humidity scale height for short -  $H_e$ . Observations from the ANETZ network show that it varies between

$$1000 \leq H_e \leq 6000 \text{ in meters} \tag{4.1.7.1}$$

It is always lower as  $H_p$ . This is due to the fact that the humidity is expressed in terms of partial water vapor pressure. The latter is less than the sum of all partial pressures, according to Dalton’s law, and thus less than the total pressure.

The ZDD and ZPD are plotted on Figure 30 on next page.

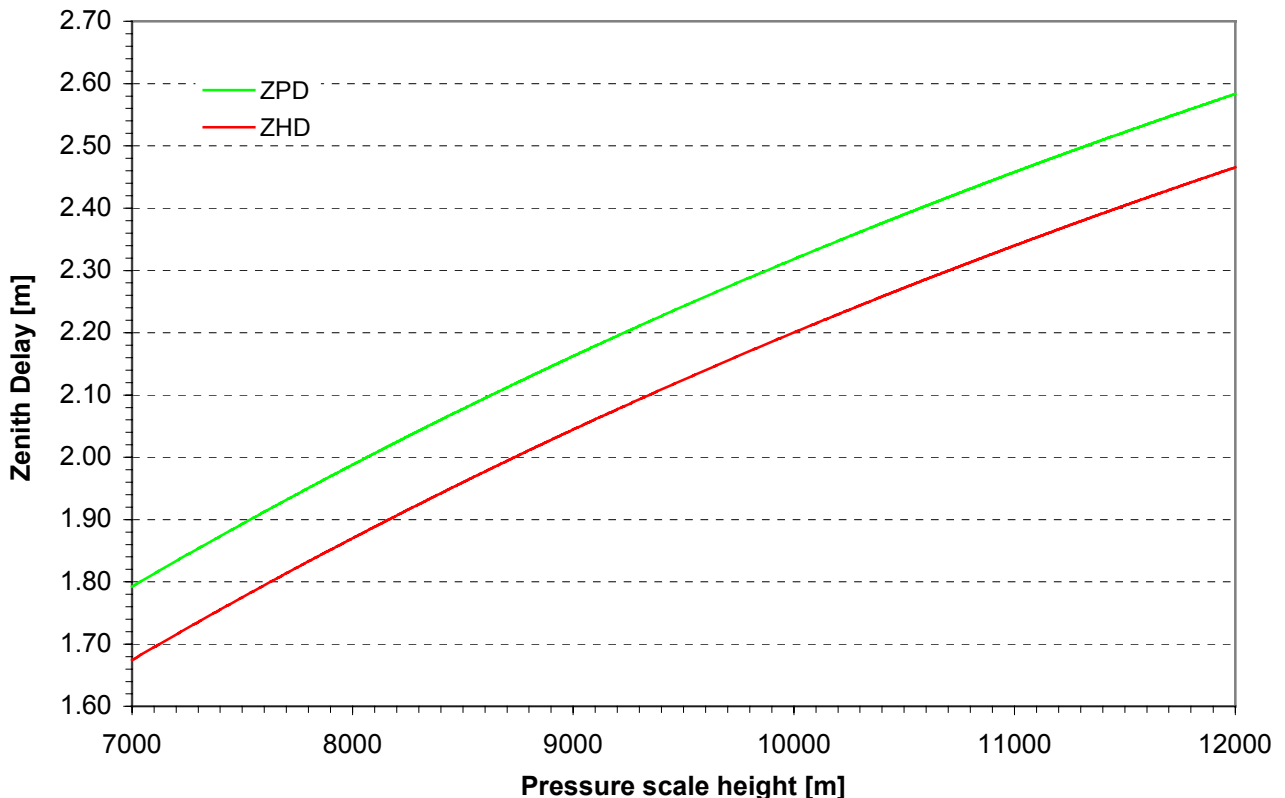


Figure 28. ZHD and ZPD as function of the pressure scale height  $H_p$  and for  $z_0 = 905$  m MSL

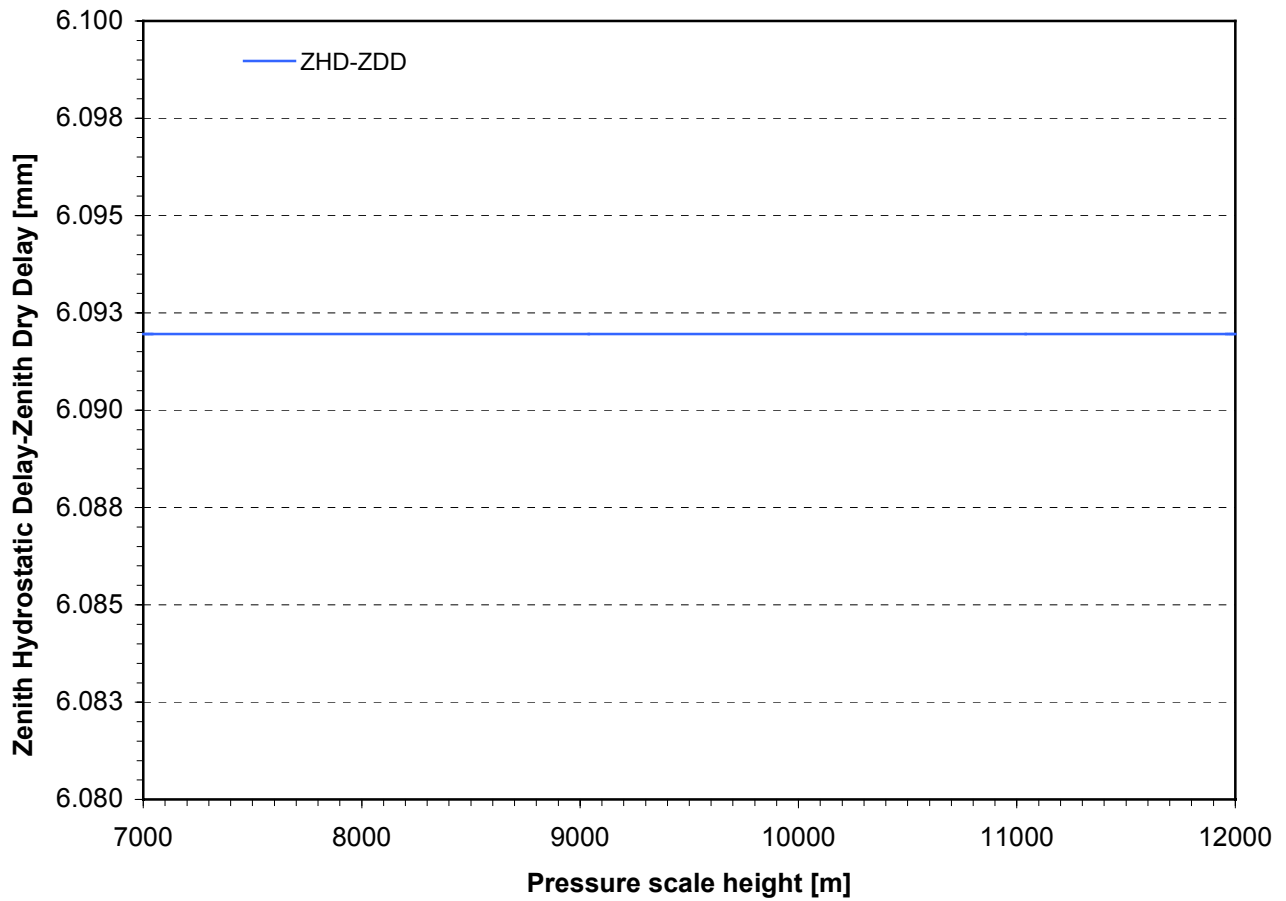


Figure 29. ZHD and ZDD difference as function of the pressure scale height  $H_p$  and for  $z_0 = 905$  m MSL

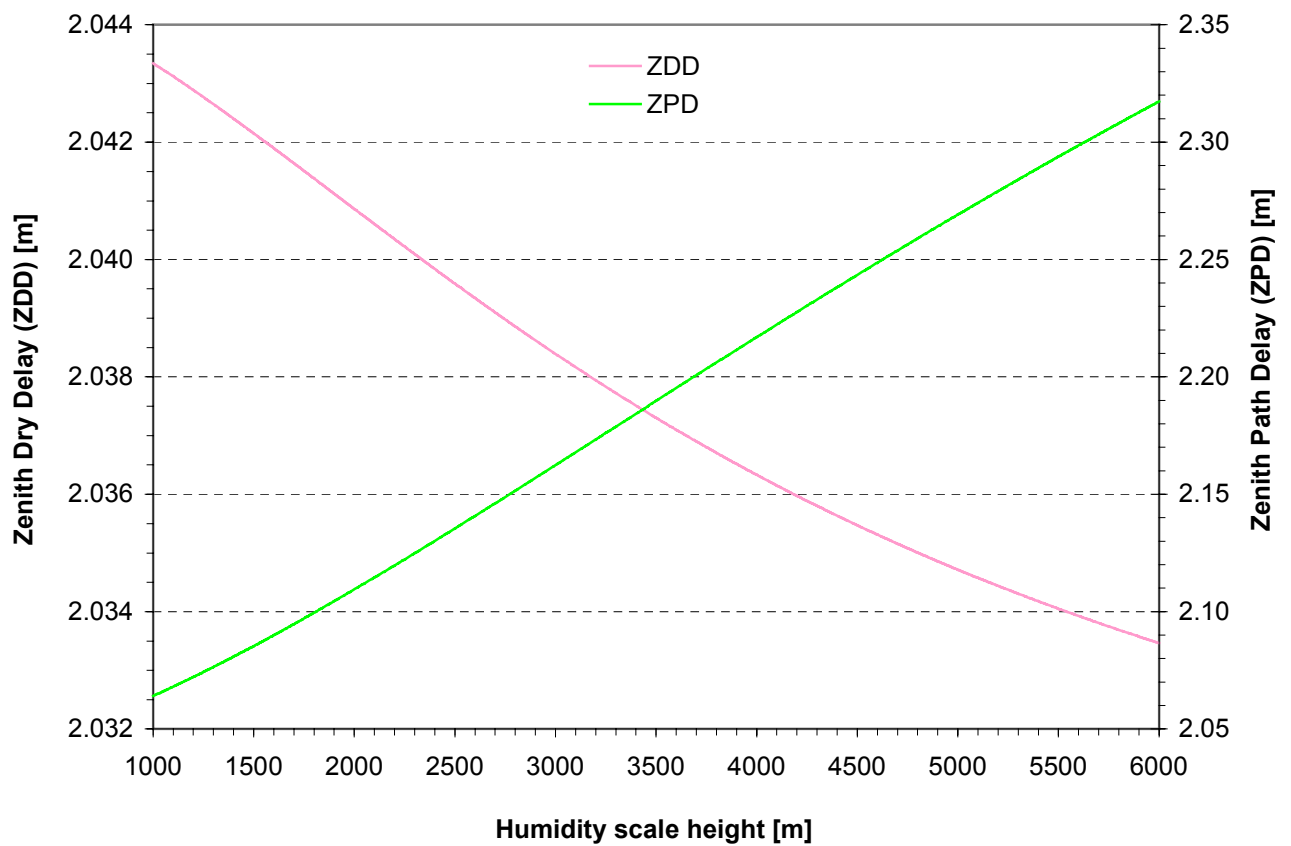


Figure 30. ZDD and ZPD as function of the humidity scale height  $H_e$  and for  $z_0 = 905$  m MSL

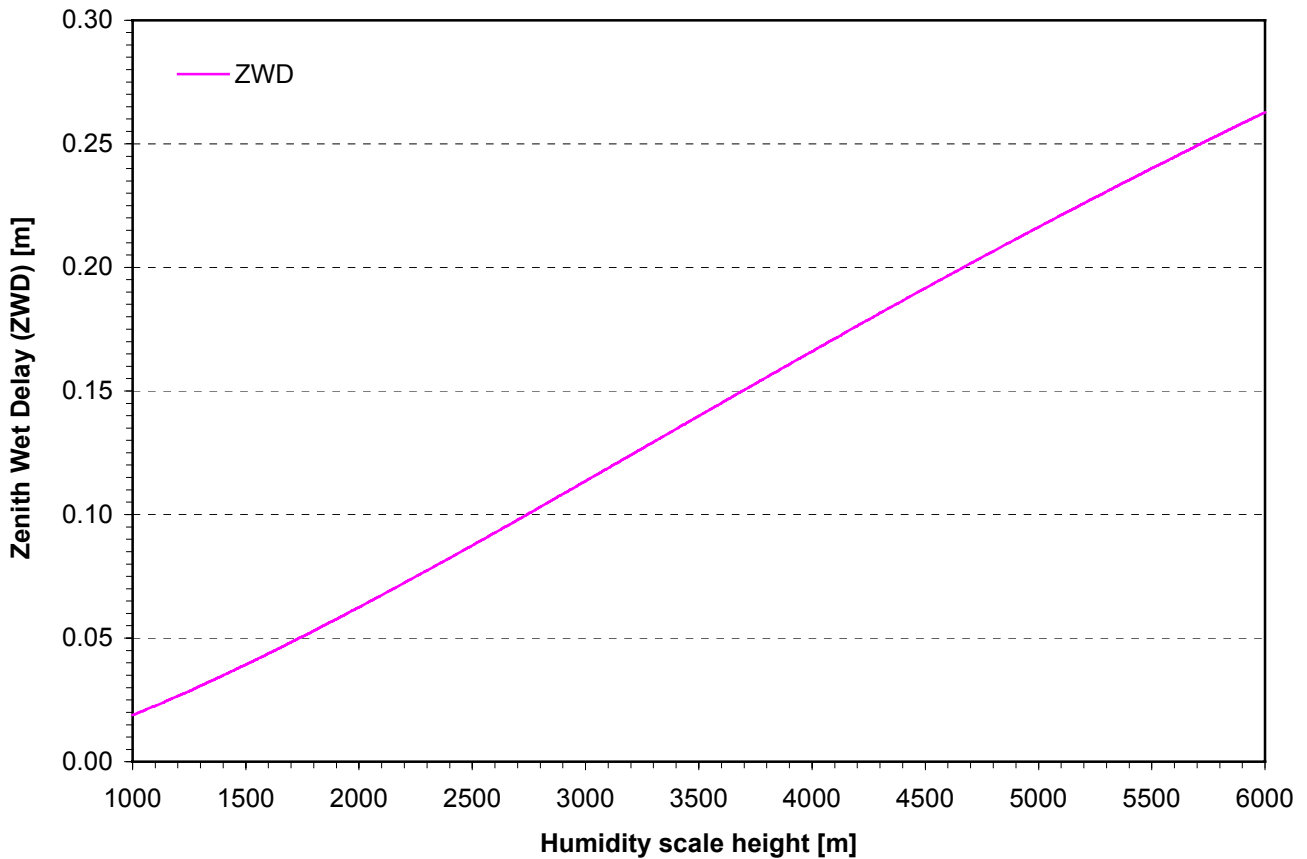


Figure 31. ZWD as function of the humidity scale height  $H_e$  and for  $z_0 = 905$  m MSL

As can be seen on Figure 30, the ZDD diminishes as the humidity scale height increases while it is the opposite for the ZPD! Indeed the path delay due to the atmospheric water vapor, i.e. the ZWD of Figure 31, increases with  $H_e$ . The ZDD corresponds to the two first terms of the Essen and Froome formula, c.f. Figure 16, and hence to the *difference* between the atmospheric pressure and the first partial water vapor pressure term. This  $e$ -term being negative, it let the ZDD decreases with  $H_e$ . On the other hand, the ZWD is directly proportional to an exponential of the inverse of  $H_e$  and thus increases with it. Therefore the ZPD increases with  $H_e$ . Note that the ZHD does not depend on  $H_e$ .

#### 4.1.8. Path Delay testing summary

The Zenith Hydrostatic Delay (ZHD), the Zenith Dry Delay (ZDD) and Zenith Wet Delay (ZWD) have been derived in Chapter 3 via eq. (3.4.9.20), eq. (3.4.9.23) and eq. (3.4.9.22). They have been tested on reference values for the ten different parameters. These reference values are summarized in Table 10. From a point of view of the order of magnitude, the results obtained are in good agreement with observations made by the Automated GPS Network Switzerland (AGNES) operated by the Swiss Federal Office of Topography (L+T).

In view of these encouraging results, the partial derivatives of the ZDD and ZWD with respect to the parameters of Table 10 are computed and evaluated in the coming paragraph.

### 4.2. Partial derivatives testing

The path delay partial derivatives were computed in Appendix B following a step-by-step approach. The main results are restated here. It is referred to Appendix B for more details.

The dependency of the different partial derivatives of the Zenith Dry Delay and of the Zenith Wet Delay with respect to the ten parameters is summarized in Table 14.



Function	Parameters										Eq. Nr.
	$p_{ref}$	$e_{ref}$	$T_{ref}$	$T_1$	$\gamma$	$z_0$	$z_1$	$z'$	$H_p$	$H_e$	
ZDD	×	×	×	×	×	×	×	×	×	×	(3.4.9.23)
ZWD		×	×	×	×	×	×	×		×	(3.4.9.22)
$\partial ZDD/\partial p_{ref}$			×	×	×	×	×	×	×		(B.4.1.1)
$\partial ZDD/\partial e_{ref}$			×		×	×	×	×		×	(B.4.2.1)
$\partial ZDD/\partial T_{ref}$	×	×	×		×	×	×		×	×	(B.4.3.2)
$\partial ZDD/\partial T_1$	×	×		×			×	×	×	×	(B.4.4.2)
$\partial ZDD/\partial \gamma$	×	×	×		×	×	×		×	×	(B.4.5.3)
$\partial ZDD/\partial z_0$	×	×	×		×	×			×	×	(B.4.6.5)
$\partial ZDD/\partial z_1$	×	×	×		×		×		×	×	(B.4.7.4)
$\partial ZDD/\partial z'$				×				×	×	×	(B.4.8.3)
$\partial ZDD/\partial H_p$	×		×	×	×	×	×		×		(B.4.9.5)
$\partial ZDD/\partial H_e$		×	×	×	×	×	×	×		×	(B.4.10.5)
$\partial ZWD/\partial p_{ref}$											—
$\partial ZWD/\partial e_{ref}$			×	×	×	×	×	×		×	(B.5.1.1)
$\partial ZWD/\partial T_{ref}$		×	×		×	×	×			×	(B.5.2.3)
$\partial ZWD/\partial T_1$		×		×			×	×		×	(B.5.3.3)
$\partial ZWD/\partial \gamma$		×	×	×	×	×	×			×	(B.5.4.6)
$\partial ZWD/\partial z_0$		×	×		×	×				×	(B.5.5.5)
$\partial ZWD/\partial z_1$		×	×	×	×		×			×	(B.5.6.4)
$\partial ZWD/\partial z'$		×		×				×		×	(B.5.7.2)
$\partial ZWD/\partial H_p$											—
$\partial ZWD/\partial H_e$		×	×	×	×	×	×			×	(B.5.8.6)

Table 14. Parameter dependencies of the partial derivatives

Due to the linearity of the derivation operations, the partial derivative of the Zenith Path Delay with respect to one of the ten parameters is just the sum of the partial derivatives of the ZDD and ZWD with respect to that very same parameter. Therefore one has to add the results for the ZDD and ZWD and one obtains the behavior of the ZPD.

The units of the partial derivatives of the ZPD are given in Table 15. These are the same for the ZWD.

Partial derivative	Unit
$\partial ZPD/\partial p_{ref}$	$\text{m} \cdot \text{hPa}^{-1}$
$\partial ZPD/\partial e_{ref}$	$\text{m} \cdot \text{hPa}^{-1}$
$\partial ZPD/\partial T_{ref}$	$\text{m} \cdot \text{K}^{-1}$
$\partial ZPD/\partial T_1$	$\text{m} \cdot \text{K}^{-1}$
$\partial ZPD/\partial \gamma$	$\text{m}^2 \cdot \text{K}^{-1}$
$\partial ZPD/\partial z_0$	No unit
$\partial ZPD/\partial z_1$	No unit
$\partial ZPD/\partial z'$	No unit
$\partial ZPD/\partial H_p$	No unit
$\partial ZPD/\partial H_e$	No unit

Table 15. Units of the ZPD's partial derivatives

### 4.2.1. ZDD partial derivatives results

For the default parameter values of Table 10, one has obtained the results of Table 16 for the ZDD partial derivatives. Note that in the second column, the results are stated for  $z_0 = 905$  meters MSL, i.e. for a GPS receiver located at Zimmerwald, while in the last column the results are given for  $z_0 = 0$  meters MSL, i.e. for a GPS receiver located at the Mean Sea Level.

Partial derivative	Value	
	$z_0 = 905$ m MSL	$z_0 = 0$ m MSL
$\partial ZDD/\partial p_{ref}$	$2.01775 \cdot 10^{-3} \text{ m} \cdot \text{hPa}^{-1}$	$2.2521 \cdot 10^{-3} \text{ m} \cdot \text{hPa}^{-1}$
$\partial ZDD/\partial e_{ref}$	$6.09196 \cdot 10^{-4} \text{ m} \cdot \text{hPa}^{-1}$	$-8.21766 \cdot 10^{-4} \text{ m} \cdot \text{hPa}^{-1}$
$\partial ZDD/\partial T_{ref}$	$-6.69976 \cdot 10^{-3} \text{ m} \cdot \text{K}^{-1}$	$-7.52478 \cdot 10^{-3} \text{ m} \cdot \text{K}^{-1}$
$\partial ZDD/\partial T_1$	$-1.59549 \cdot 10^{-3} \text{ m} \cdot \text{K}^{-1}$	$-1.59549 \cdot 10^{-3} \text{ m} \cdot \text{K}^{-1}$
$\partial ZDD/\partial \gamma$	$-22.9908 \text{ m}^2 \cdot \text{K}^{-1}$	$-18.5765 \text{ m}^2 \cdot \text{K}^{-1}$
$\partial ZDD/\partial z_0$	$-2.50007 \cdot 10^{-4}$	$-2.70319 \cdot 10^{-4}$
$\partial ZDD/\partial z_1$	$-1.82723 \cdot 10^{-7}$	$-1.82723 \cdot 10^{-7}$
$\partial ZDD/\partial z'$	$6.86108 \cdot 10^{-5}$	$6.86108 \cdot 10^{-5}$
$\partial ZDD/\partial H_p$	$1.64685 \cdot 10^{-4}$	$1.65993 \cdot 10^{-4}$
$\partial ZDD/\partial H_e$	$-2.29156 \cdot 10^{-6}$	$-2.39344 \cdot 10^{-6}$

Table 16. ZDD partial derivatives results for  $z_0 = 905$  m MSL and  $z_0 = 0$  m MSL

Remark that  $\partial ZDD/\partial T_1$ ,  $\partial ZDD/\partial z_1$  and  $\partial ZDD/\partial z'$  remain unchanged as one varies  $z_0$  as they do *not* depend on the GPS receiver's altitude. This can be clearly seen in Table 14 on the previous page. The values are relatively low. As this might present a singularity during the inversion of the design matrix **A**, it is required to study the dependence on  $z_0$  of each of the partial derivatives.

### 4.2.2. ZDD partial derivatives as function of $z_0$

Each of the ten ZDD partial derivatives have been evaluated for the GPS receiver's altitude varying in the range

$$0 \leq z_0 \leq 5000 \text{ in meters} \tag{4.2.2.1}$$

The ZDD partial derivatives with respect to the reference pressure and reference humidity are plotted on Figure 32.

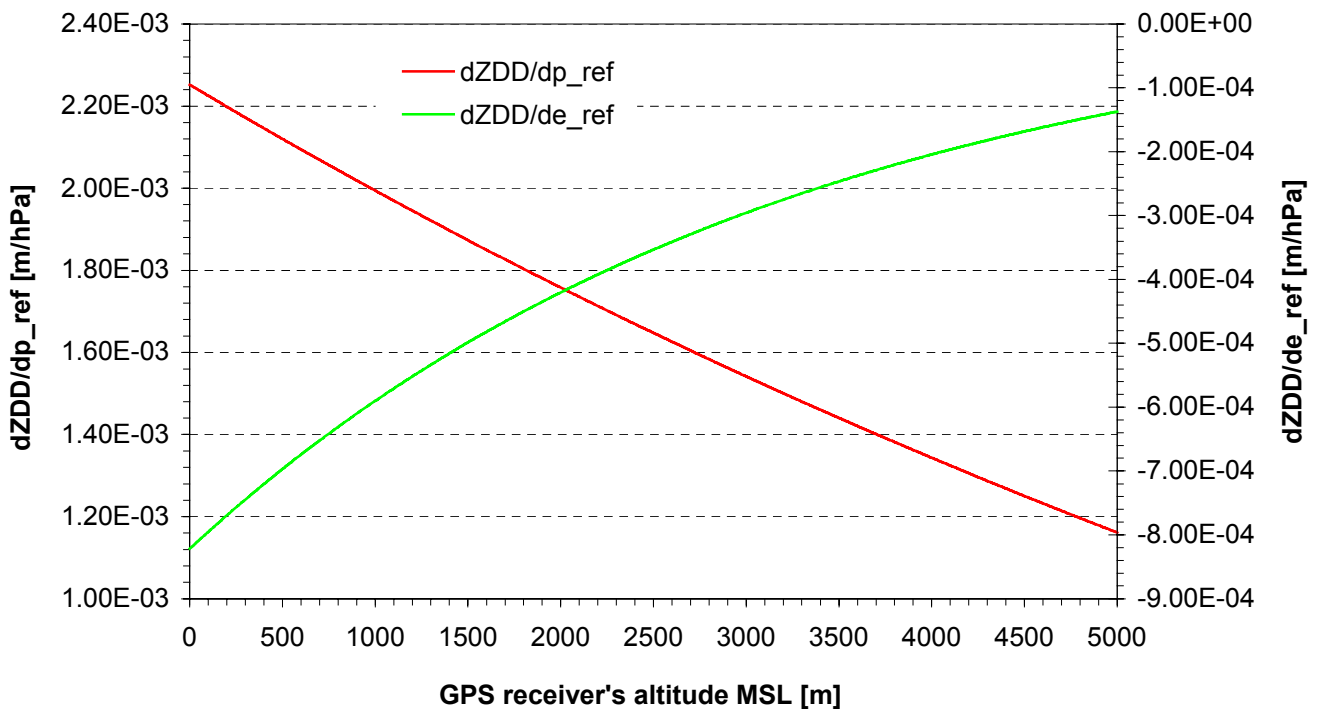


Figure 32.  $\partial ZDD/\partial p_{ref}$  and  $\partial ZDD/\partial e_{ref}$  as function of the GPS receiver's altitude  $z_0$

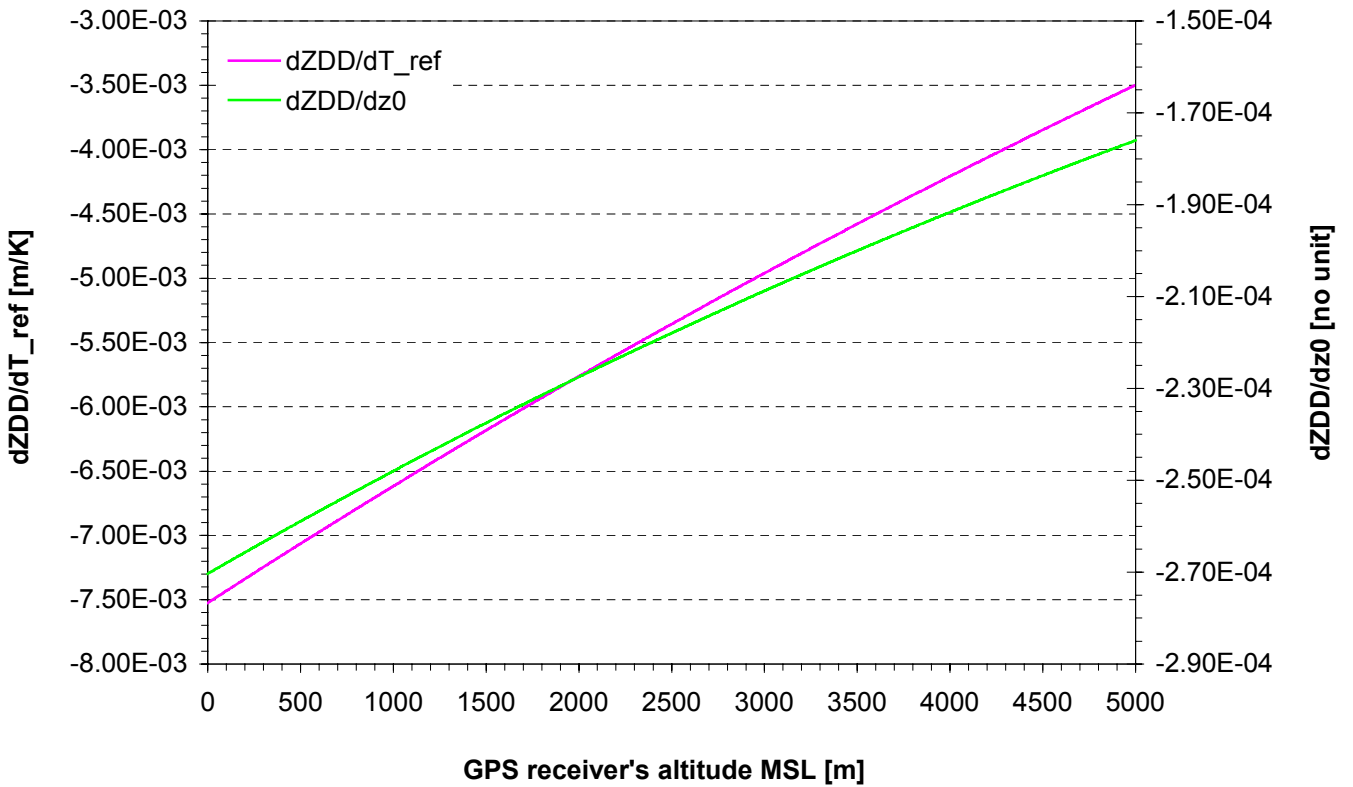


Figure 33.  $\partial ZDD/\partial T_{ref}$  and  $\partial ZDD/\partial z_0$  as function of the GPS receiver's altitude  $z_0$

Although the pressure  $p$  and the partial water vapor pressure  $e$  decrease with the altitude and with the GPS receiver's altitude, both partial derivatives of Figure 32 show an opposite behavior with respect to  $z_0$ . This is due to the fact that both series  $S_{11}$  and  $S_{12}$  react differently to variations of  $z_0$ . Indeed,  $S_{12}$  is bigger than  $S_{11}$  and also negative. It decreases sharply with  $z_0$  and thus let  $\partial ZDD/\partial e_{ref}$  increase while this is not the case for  $\partial ZDD/\partial p_{ref}$ . C.f. eq. (B.4.1.1) and eq. (B.4.2.1).

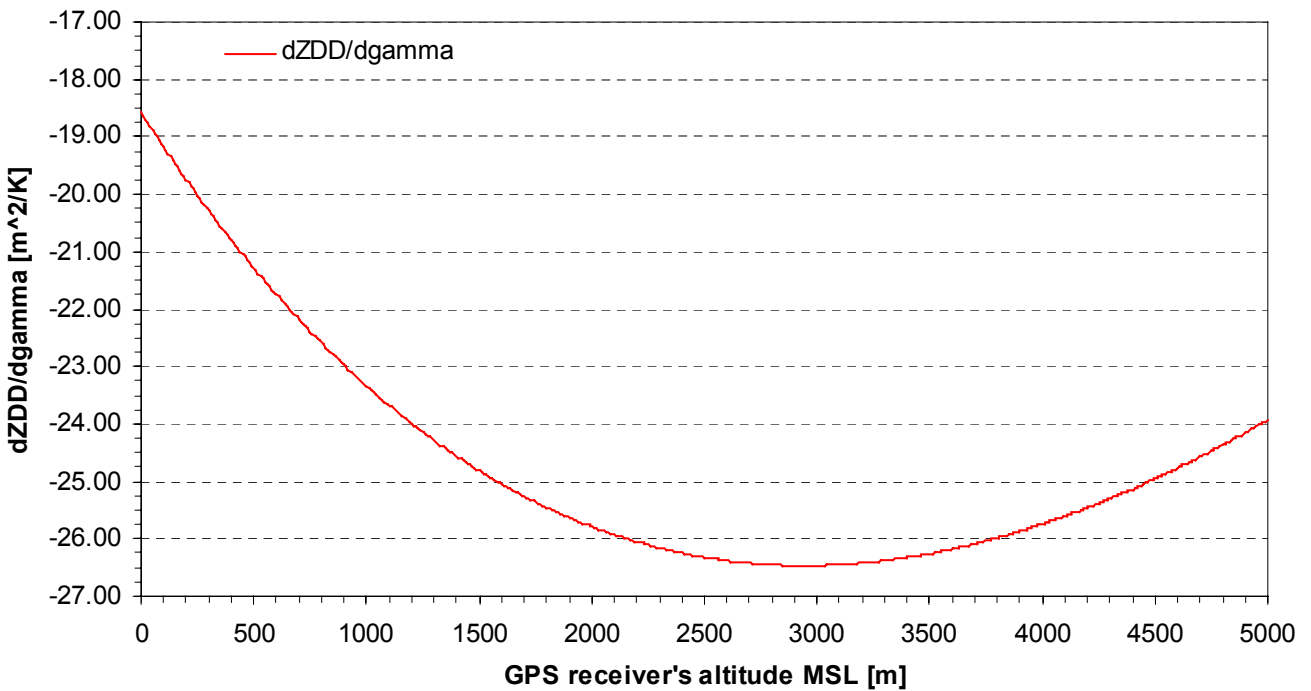


Figure 34.  $\partial ZDD/\partial \gamma$  as function of the GPS receiver's altitude  $z_0$

Figure 33 represents the bearing of  $\partial ZDD/\partial T_{ref}$  and  $\partial ZDD/\partial z_0$  as function of  $z_0$ . Both have a very small curvature and thus increase almost linearly with the GPS receiver's altitude, although the former grows faster. Their amplitudes stretch over a restrained range of order of magnitude of  $10^{-3} \text{ m} \cdot \text{K}^{-1}$  respectively  $10^{-4}$ .  $\partial ZDD/\partial T_{ref}$  is approximately 40 times larger than  $\partial ZDD/\partial z_0$ .

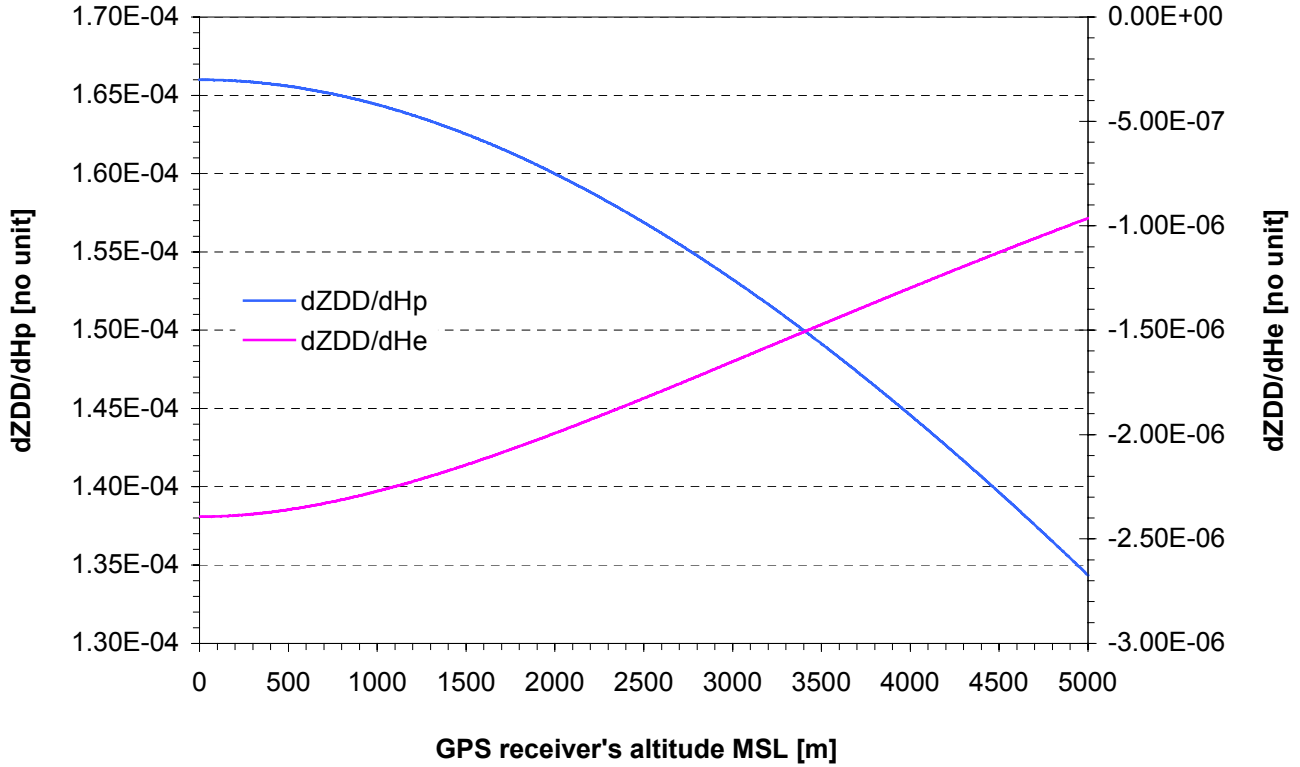


Figure 35.  $\partial ZDD/\partial H_p$  and  $\partial ZDD/\partial H_e$  as function of the GPS receiver's altitude  $z_0$

Figure 34 gives the variation of  $\partial ZDD/\partial \gamma$  with  $z_0$ . It has the largest amplitude of all partial derivatives and is rather sensible to  $z_0$ . This convex curve reaches its minimum for  $z_0 = 2940$  meters MSL. It therefore should not hinder the inversion of the design matrix.

$\partial ZDD/\partial H_p$  and  $\partial ZDD/\partial H_e$  as function of the GPS receiver's altitude  $z_0$  are plotted on Figure 35. The former is nearly 300 times larger than the latter while showing an opposite behavior with respect to  $z_0$ . There seems to be an axis of symmetry but a careful approach demonstrates that it is not the case. The order of magnitude of  $\partial ZDD/\partial H_e$  is  $10^{-7}$  and thus very small. This is of concern for the inversion of the design matrix **A**.

Remark that  $\partial ZDD/\partial T_1$ ,  $\partial ZDD/\partial z_1$  and  $\partial ZDD/\partial z'$  do *not* depend on the GPS receiver's altitude  $z_0$  and therefore are constants with respect to this parameter. As a matter of fact, there are not plotted here for this very reason. Their values can be obtained from Table 16.

Finally the relative change of the ZDD partial derivatives with  $z_0$  discussed above is plotted on Figure 36.

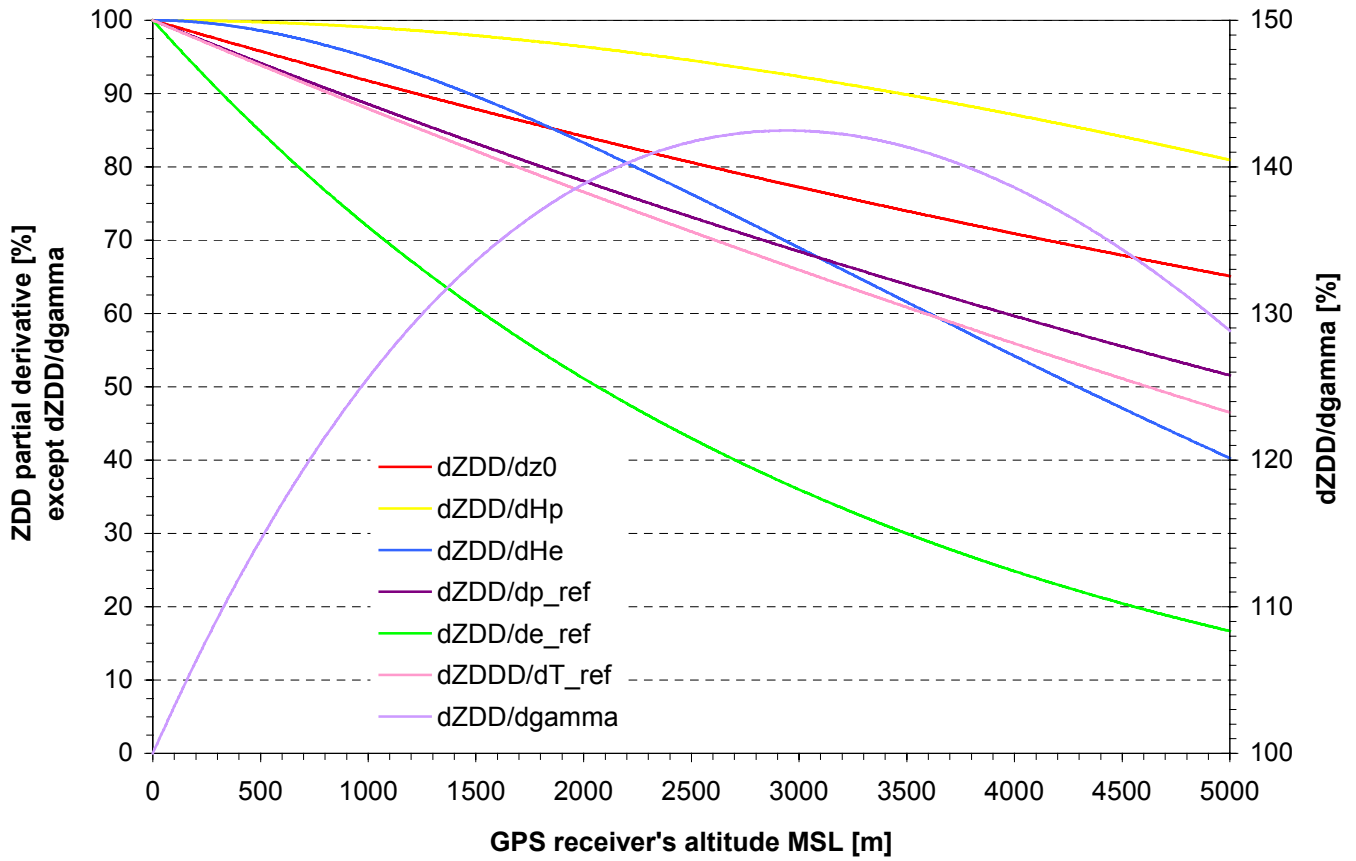


Figure 36. Relative change of ZDD partial derivatives as function of the GPS receiver's altitude  $z_0$

The partial derivatives reference values (100%) have been taken at the mean sea level, i.e. at 0 meters MSL. The GPS receiver's default altitude is still  $z_0 = 905$  meters MSL.  $\partial ZDD/\partial \gamma$  has its own scale on the right hand side of Figure 36 as it relatively increases with  $z_0$  up to 2940 meters MSL. When referring to Figure 34, one should take great care with the sign of the function of consideration.

It is now intended to study the variations of the different Zenith Wet Delay partial derivatives with  $z_0$ .

### 4.2.3. ZWD partial derivatives results

For the default parameter values of Table 10, one has obtained the results of Table 17 for the ZWD partial derivatives. As was done for the ZDD, the results in the second column are stated for  $z_0 = 905$  meters MSL, i.e. for a GPS receiver located at Zimmerwald, while in the last column the results are given for  $z_0 = 0$  meters MSL, i.e. for a GPS receiver located at the Mean Sea Level.

Partial derivative	Value	
	$z_0 = 905$ m MSL	$z_0 = 0$ m MSL
$\partial ZWD/\partial e_{ref}$	$1.13547 \cdot 10^{-2} \text{ m} \cdot \text{hPa}^{-1}$	$1.4745 \cdot 10^{-2} \text{ m} \cdot \text{hPa}^{-1}$
$\partial ZWD/\partial T_{ref}$	$7.06688 \cdot 10^{-2} \text{ m} \cdot \text{K}^{-1}$	$9.37776 \cdot 10^{-2} \text{ m} \cdot \text{K}^{-1}$
$\partial ZWD/\partial T_1$	$-4.05193 \cdot 10^{-3} \text{ m} \cdot \text{K}^{-1}$	$-4.05193 \cdot 10^{-5} \text{ m} \cdot \text{K}^{-1}$
$\partial ZWD/\partial \gamma$	$-3339.3003 \text{ m}^2 \cdot \text{K}^{-1}$	$-4514.0110 \text{ m}^2 \cdot \text{K}^{-1}$
$\partial ZWD/\partial z_0$	$-3.28161 \cdot 10^{-5}$	$-4.25318 \cdot 10^{-5}$
$\partial ZWD/\partial z_1$	$1.83412 \cdot 10^{-11}$	$1.83412 \cdot 10^{-11}$
$\partial ZWD/\partial z'$	$5.13632 \cdot 10^{-7}$	$5.13632 \cdot 10^{-7}$
$\partial ZWD/\partial H_e$	$5.25515 \cdot 10^{-5}$	$5.41825 \cdot 10^{-5}$

Table 17. ZWD partial derivatives results for  $z_0 = 905$  m MSL and  $z_0 = 0$  m MSL

Remark that  $\partial ZWD/\partial T_1$ ,  $\partial ZWD/\partial z_1$  and  $\partial ZWD/\partial z'$  remain unchanged as one varies  $z_0$  as they do *not* depend on the GPS receiver's altitude. The same partial derivatives for the ZDD showed a similar behavior. This can be clearly seen in Table 14. The values of the different ZWD partial derivatives are generally low with  $\partial ZWD/\partial \gamma$  as sole exception. Following the procedure used for the ZDD partial derivatives, study now the dependence on  $z_0$  of each of the partial derivatives.

#### 4.2.4. ZWD partial derivatives as function of $z_0$

First of all note that the ZWD does depend neither on  $p_{ref}$  nor on  $H_p$ . Refer to Table 14. There are hence two partial derivatives less to compute than for the ZDD. Each of the 8 ZWD partial derivatives have been evaluated for the GPS receiver's altitude varying in the range

$$0 \leq z_0 \leq 5000 \text{ in meters} \tag{4.2.2.1}$$

The ZWD partial derivatives with respect to the reference humidity and reference temperature are plotted on Figure 37.

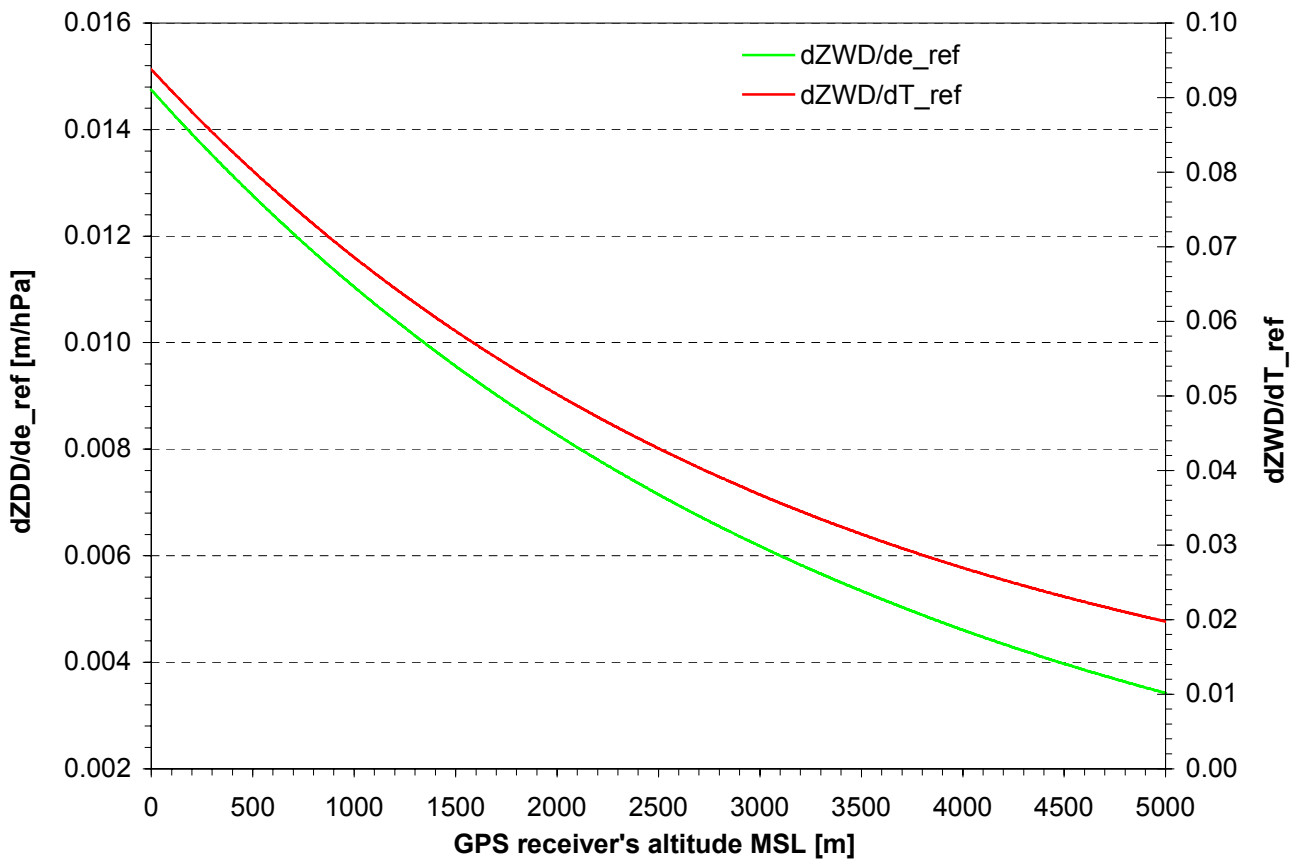


Figure 37.  $\partial ZWD/\partial e_{ref}$  and  $\partial ZWD/\partial T_{ref}$  as function of the GPS receiver's altitude  $z_0$

The behavior of  $\partial ZWD/\partial e_{ref}$  and  $\partial ZWD/\partial T_{ref}$  is identical with respect to the GPS receiver's altitude  $z_0$ . The amplitude of the former is one time and half larger than the latter. Both decrease with  $z_0$  and tend to zero for large  $z_0$ . However  $\partial ZWD/\partial T_{ref}$  tends certainly to zero for values of  $z_0$  less than 11000 meters MSL. Indeed, at  $z_0 = z_1 = 11000$  meters MSL, i.e. at tropopause height, the temperature becomes constant and thus  $\partial ZWD/\partial T_{ref}$  vanishes. In the case of  $\partial ZWD/\partial e_{ref}$ , it becomes a constant equal to  $4.30475 \cdot 10^{-4} \text{ m} \cdot \text{hPa}^{-1}$ .

Figure 38 represents the bearing of  $\partial ZWD/\partial H_e$  and  $\partial ZWD/\partial z_0$  with the GPS receiver's altitude  $z_0$ .

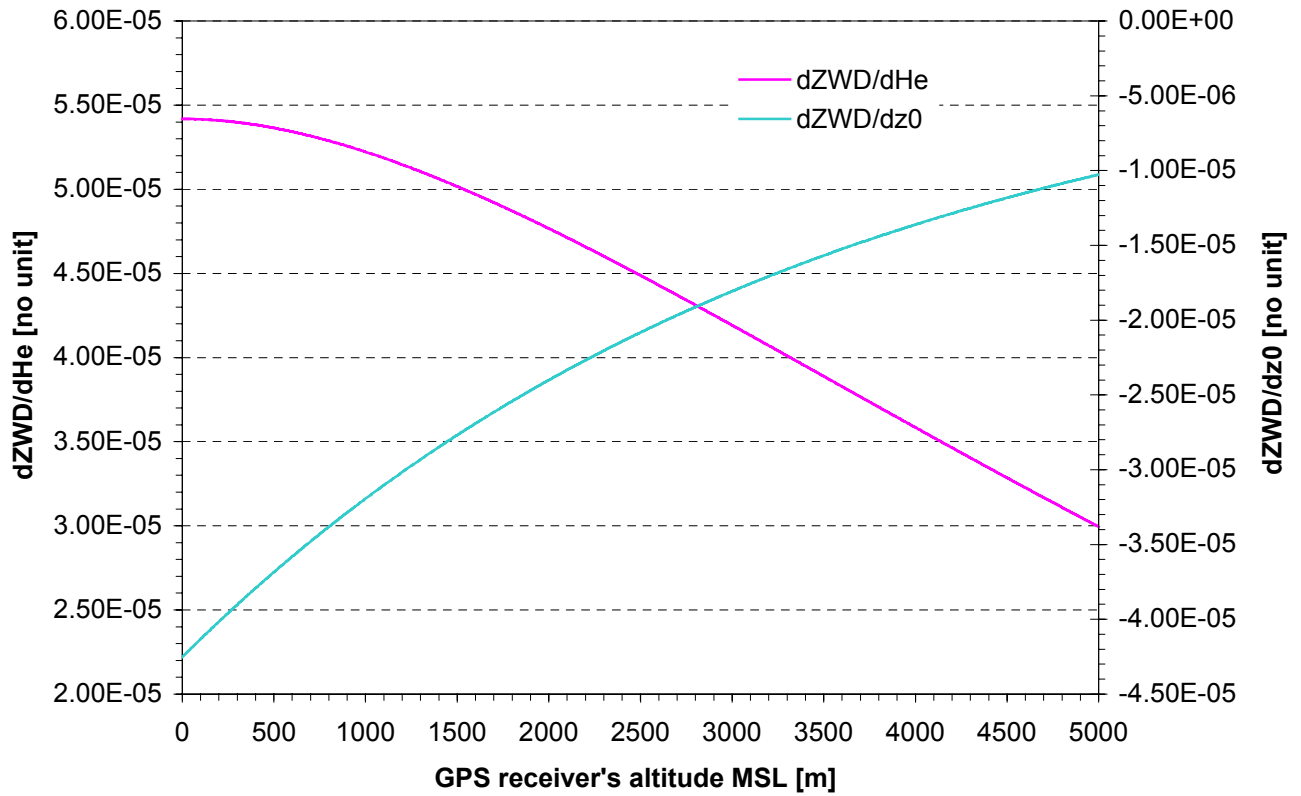


Figure 38.  $\partial ZWD/\partial H_e$  and  $\partial ZWD/\partial z_0$  as function of the GPS receiver's altitude  $z_0$

While  $\partial ZWD/\partial H_e$  is positive and decreases with  $z_0$ ,  $\partial ZWD/\partial z_0$  is negative and increases. But both tend to zero for large values of  $z_0$ . This is due to the fact that the integration path becomes shorter and eventually vanishes. Both partial derivatives have amplitudes of similar order of magnitude.

The variation of the ZWD partial derivatives with respect to the tropospheric temperature gradient  $\gamma$  is plotted on Figure 39 on next page. It is negative and decreases as the GPS receiver's altitude  $z_0$  increases. As one could expect, the maximum amplitude is encountered at the Mean Sea Level (MSL) as the integration path is maximum at that altitude and the atmospheric water vapor is mainly located in the troposphere.  $\partial ZWD/\partial \gamma$  has a completely different aspect than  $\partial ZDD/\partial \gamma$ . It is probably due to the fact that it contains only terms proportional to  $e_{ref}$  and is not a function of the reference pressure  $p_{ref}$ . In order to check this,  $\partial ZHD/\partial \gamma$  is plotted on Figure 40, also on next page.

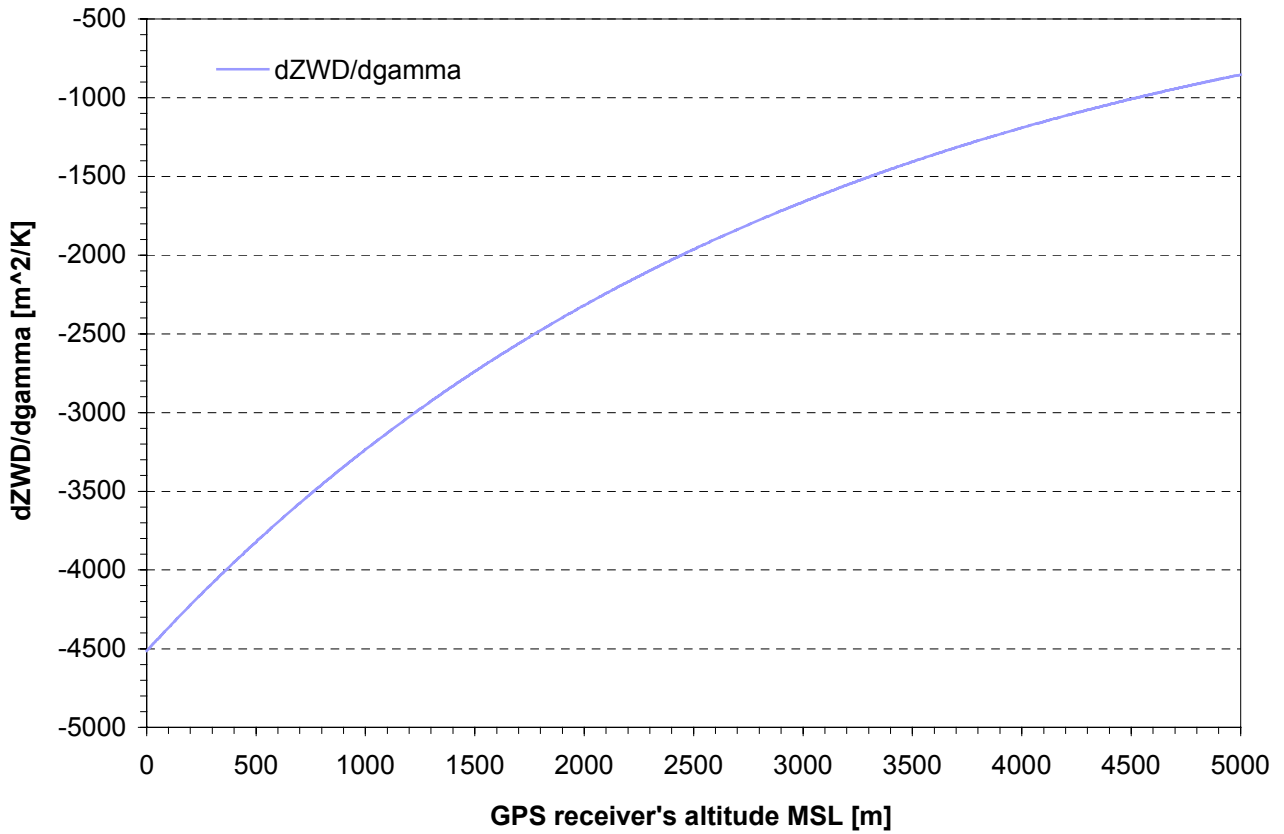


Figure 39.  $\partial ZWD/\partial\gamma$  as function of the GPS receiver's altitude  $z_0$

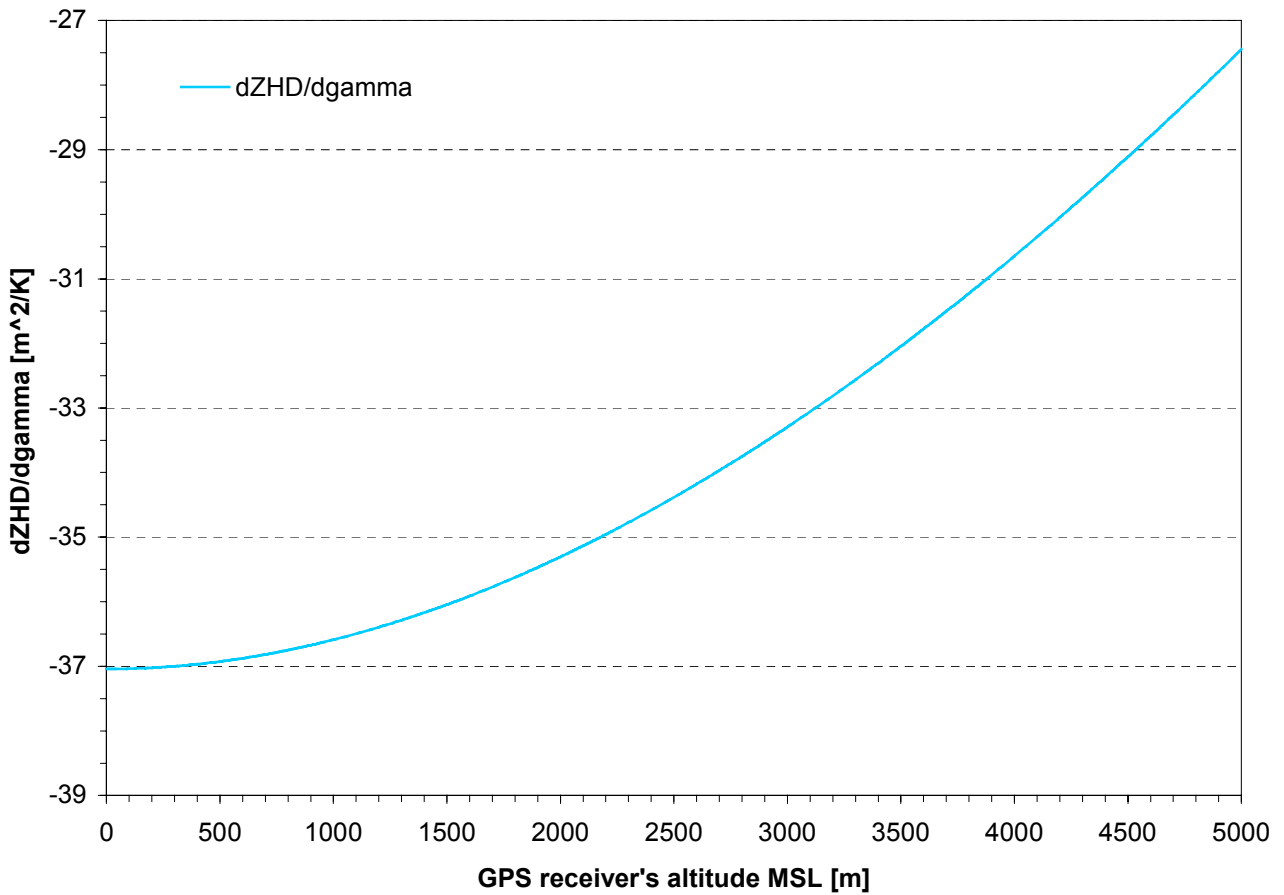


Figure 40.  $\partial ZHD/\partial\gamma$  as function of the GPS receiver's altitude  $z_0$



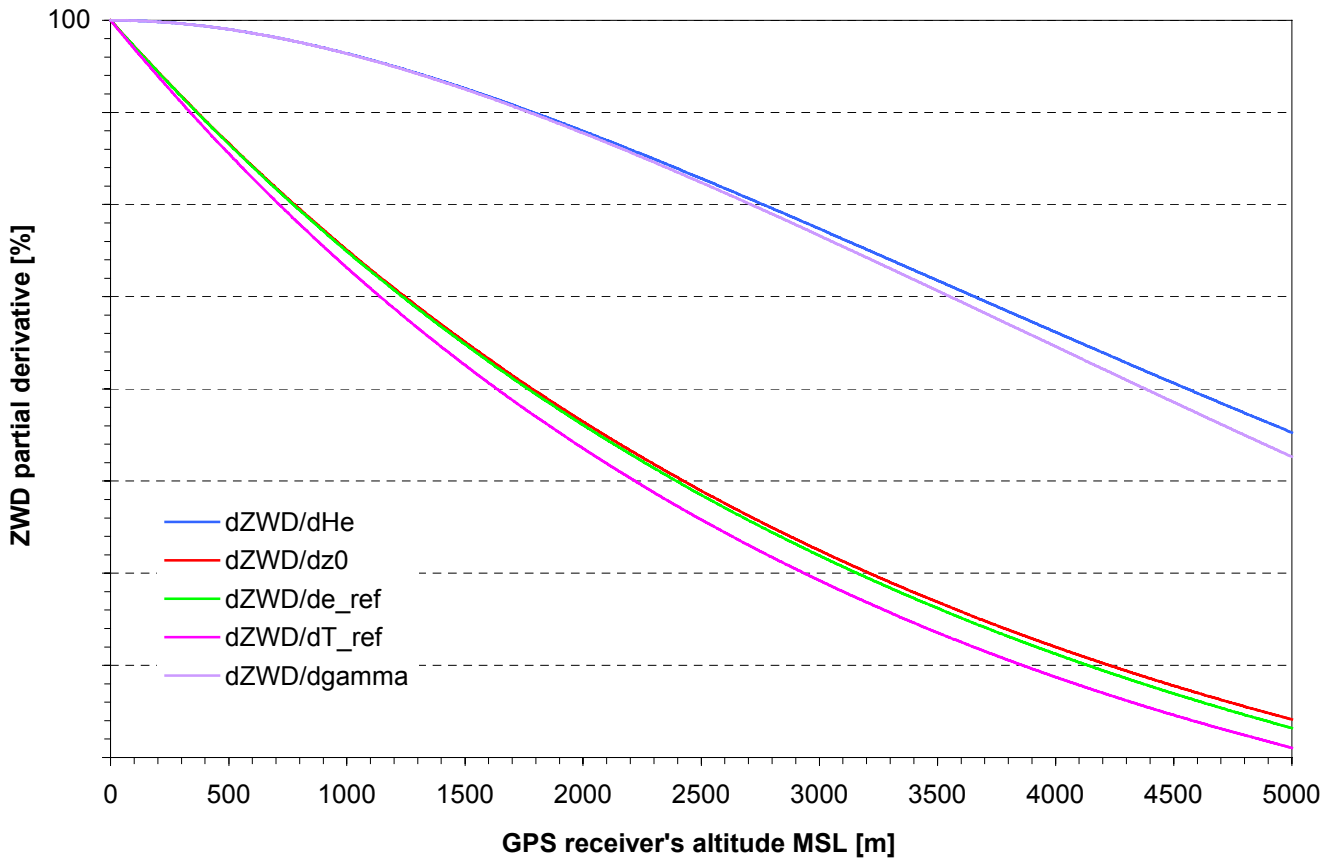


Figure 41. Relative change of the ZWD partial derivatives as function of the GPS receiver's altitude

The relative change of the ZWD partial derivatives is spread in two amplitude groups.  $\partial ZWD/\partial H_e$  and  $\partial ZWD/\partial \gamma$  are less sensitive to a small shift in  $z_0$  at low altitudes than the three others which are concentrated in the same bundle. Due to the fact that their variation is almost identical, singularities in the inversion of the design matrix  $\mathbf{A}$  should be expected with high probability.  $\partial ZWD/\partial T_1$ ,  $\partial ZWD/\partial z_1$  and  $\partial ZWD/\partial z'$  are not plotted on Figure 41 as they do not depend on  $z_0$ .

#### 4.2.5. ZPD partial derivatives results

Recall that the Zenith Path Delay (ZPD) is just the sum of the ZDD and the ZWD, according to eq. (3.4.9.16). Hence one just has to sum the contributions of both the dry and wet part of the zenith delay partial derivatives. For all ten parameters of Table 10, the results of Table 18 have been obtained.

Partial derivative	Value	
	$z_0 = 905$ m MSL	$z_0 = 0$ m MSL
$\partial ZPD/\partial p_{ref}$	$2.01775 \cdot 10^{-3} \text{ m} \cdot \text{hPa}^{-1}$	$2.2521 \cdot 10^{-3} \text{ m} \cdot \text{hPa}^{-1}$
$\partial ZPD/\partial e_{ref}$	$1.07455 \cdot 10^{-2} \text{ m} \cdot \text{hPa}^{-1}$	$-1.39232 \cdot 10^{-2} \text{ m} \cdot \text{hPa}^{-1}$
$\partial ZPD/\partial T_{ref}$	$-6.69976 \cdot 10^{-3} \text{ m} \cdot \text{K}^{-1}$	$-7.52478 \cdot 10^{-3} \text{ m} \cdot \text{K}^{-1}$
$\partial ZPD/\partial T_1$	$-1.63601 \cdot 10^{-3} \text{ m} \cdot \text{K}^{-1}$	$-1.63601 \cdot 10^{-3} \text{ m} \cdot \text{K}^{-1}$
$\partial ZPD/\partial \gamma$	$-26.3924 \text{ m}^2 \cdot \text{K}^{-1}$	$-22.0841 \text{ m}^2 \cdot \text{K}^{-1}$
$\partial ZPD/\partial z_0$	$-2.82823 \cdot 10^{-4}$	$-3.1285 \cdot 10^{-4}$
$\partial ZPD/\partial z_1$	$-1.82704 \cdot 10^{-7}$	$-1.82704 \cdot 10^{-7}$
$\partial ZPD/\partial z'$	$6.91244 \cdot 10^{-5}$	$6.91244 \cdot 10^{-5}$
$\partial ZPD/\partial H_p$	$1.64685 \cdot 10^{-4}$	$1.65993 \cdot 10^{-4}$
$\partial ZPD/\partial H_e$	$-5.0260 \cdot 10^{-5}$	$5.1789 \cdot 10^{-5}$

Table 18. ZPD partial derivatives results for  $z_0 = 905$  m MSL and  $z_0 = 0$  m MSL

Remark that  $\partial ZPD/\partial T_1$ ,  $\partial ZPD/\partial z_1$  and  $\partial ZPD/\partial z'$  remain unchanged as one varies the GPS receiver's altitude  $z_0$ . This is a real hindrance to a smooth inversion of the design matrix **A**. Indeed **A** is filled with all partial derivatives as the system is linearized. The influence of the ZWD on the ZPD partial derivatives is clearly marked when one derives with respect to  $e_{ref}$ ,  $T_{ref}$ ,  $T_1$ ,  $\gamma$ ,  $z_0$ ,  $z'$  and  $H_e$ .

The ZPD partial derivatives are now computed as a function of the GPS receiver's altitude  $z_0$ .

### 4.2.6. ZPD partial derivatives results as function of $z_0$

Each of the ten ZPD partial derivatives have been evaluated for the GPS receiver's altitude varying in the range

$$0 \leq z_0 \leq 5000 \text{ in meters} \tag{4.2.6.1}$$

The ZPD partial derivatives with respect to the reference pressure and reference humidity are plotted on Figure 42.

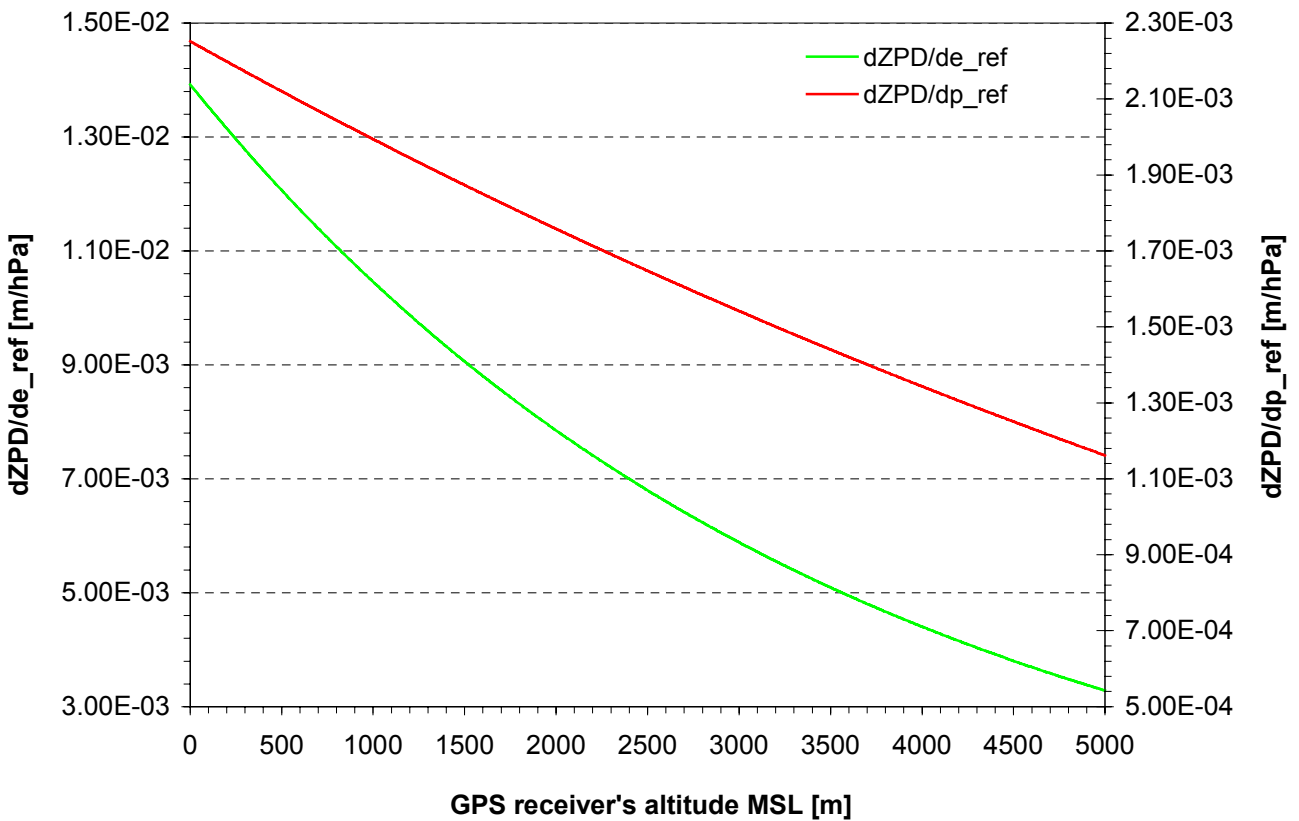


Figure 42.  $\partial ZPD/\partial e_{ref}$  and  $\partial ZPD/\partial p_{ref}$  as function of the GPS receiver's altitude  $z_0$

Both decrease as the GPS receiver's altitude  $z_0$  increase. However,  $\partial ZPD/\partial e_{ref}$  is almost five times larger than  $\partial ZPD/\partial p_{ref}$ . The former also has a well-marked curvature while it is the opposite for the latter. Compare with Figure 32 and note that  $\partial ZDD/\partial e_{ref}$  adopted a completely different pattern. This demonstrates the influence of the atmospheric water vapor on the GPS signal: it induces a non-negligible path delay, i.e. a non-negligible retardation.

Consider now the derivatives of the ZPD with respect to the reference temperature and the tropospheric temperature gradient. They are plotted on Figure 43 on next page. The ZWD shifts downwards the ZPD. Thus  $\partial ZPD/\partial \gamma$  is a convex curve with minimum for  $z_0 = 2670$  meters MSL.  $\partial ZPD/\partial T_{ref}$  is almost proportional to GPS receiver's altitude and therefore increases almost linearly with  $z_0$ . It shows the same pattern as  $\partial ZDD/\partial T_{ref}$ .

The attitude of  $\partial ZPD/\partial H_p$  and  $\partial ZPD/\partial H_e$  toward the GPS receiver's altitude  $z_0$  is sketched on Figure 43 on next page. For low valued of  $z_0$ , both decrease slowly. They then diminish more rapidly until their decrease rate

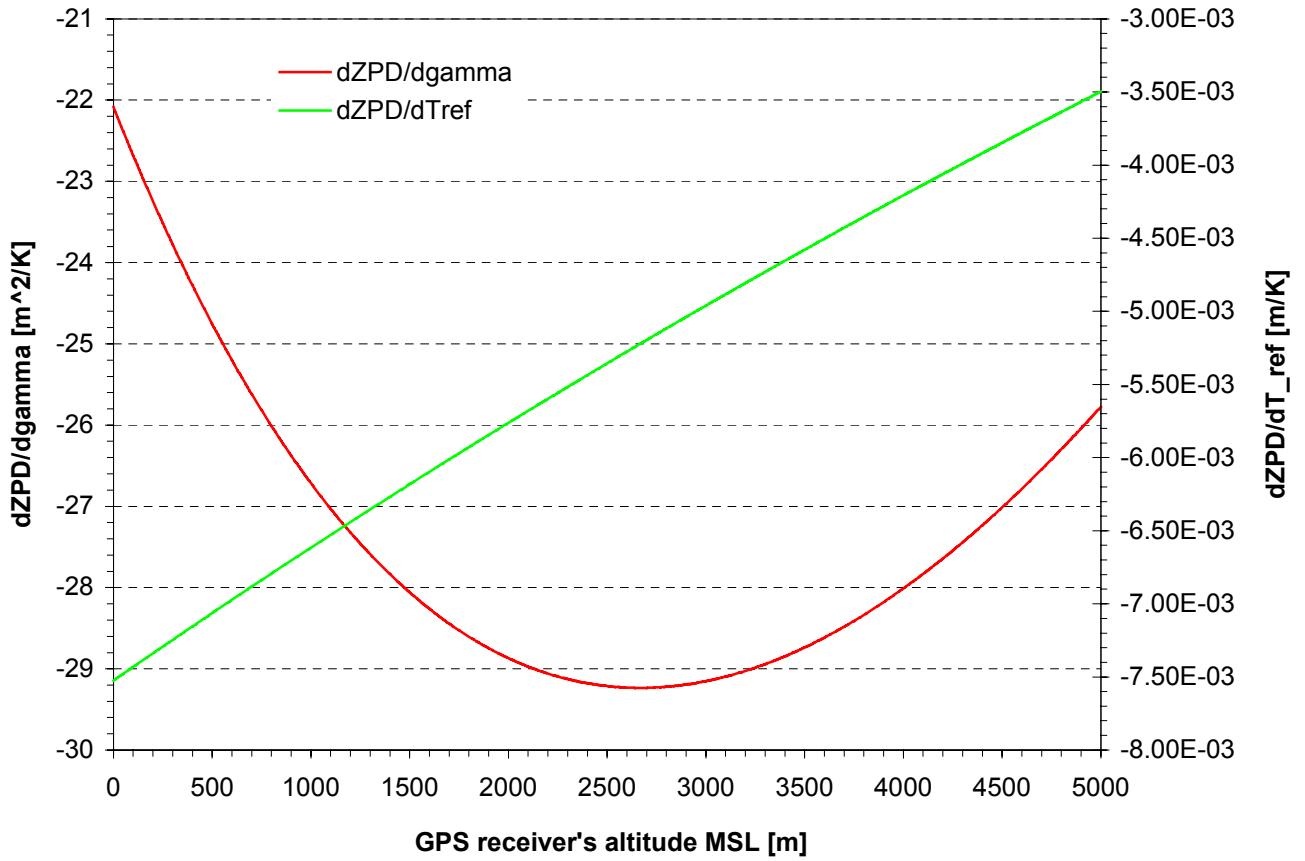


Figure 43.  $\partial ZPD/\partial\gamma$  and  $\partial ZPD/\partial T_{ref}$  as function of the GPS receiver's altitude  $z_0$

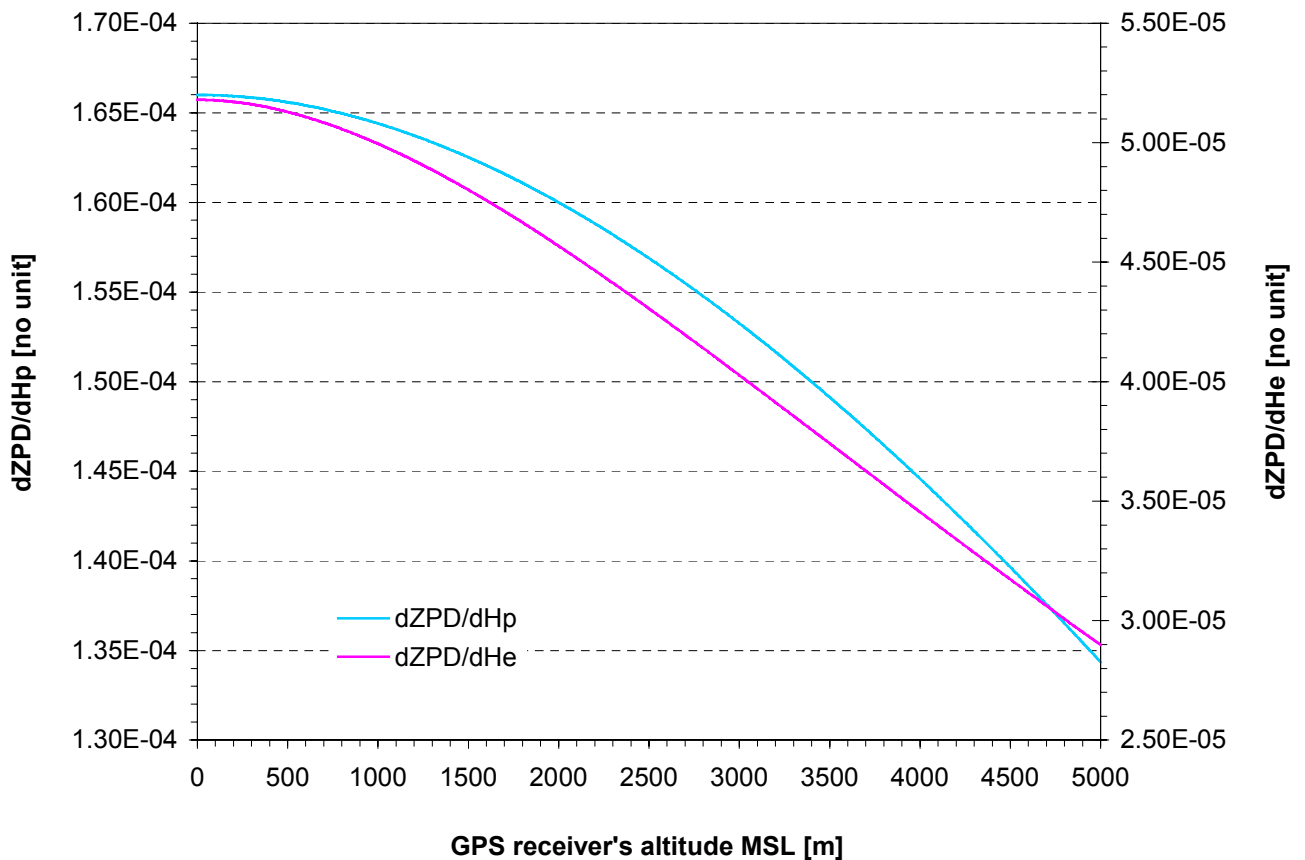


Figure 44.  $\partial ZPD/\partial H_p$  and  $\partial ZPD/\partial H_e$  as function of the GPS receiver's altitude  $z_0$

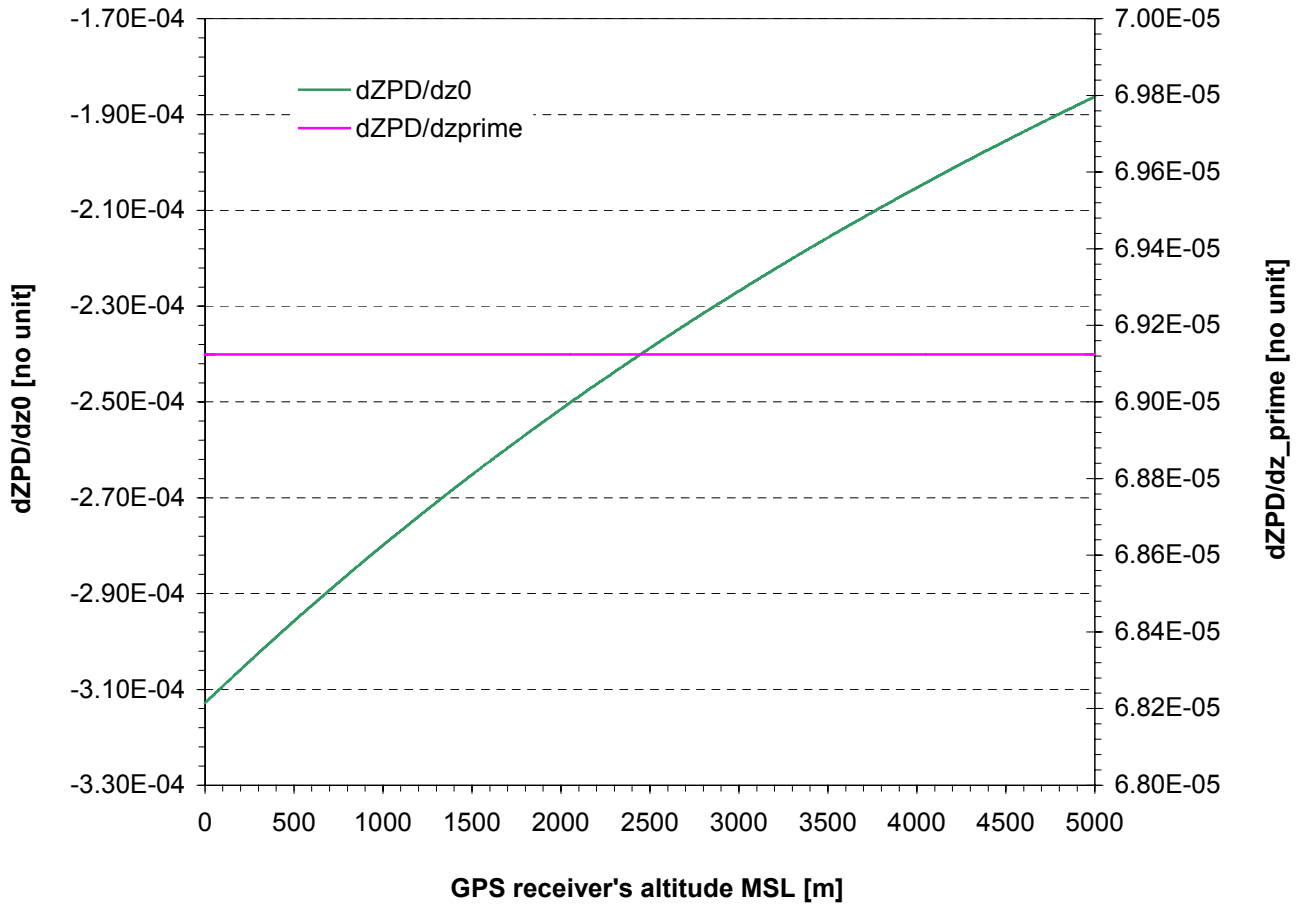


Figure 45.  $\partial ZPD/\partial z_0$  and  $\partial ZPD/\partial z'$  as function of the GPS receiver's altitude  $z_0$

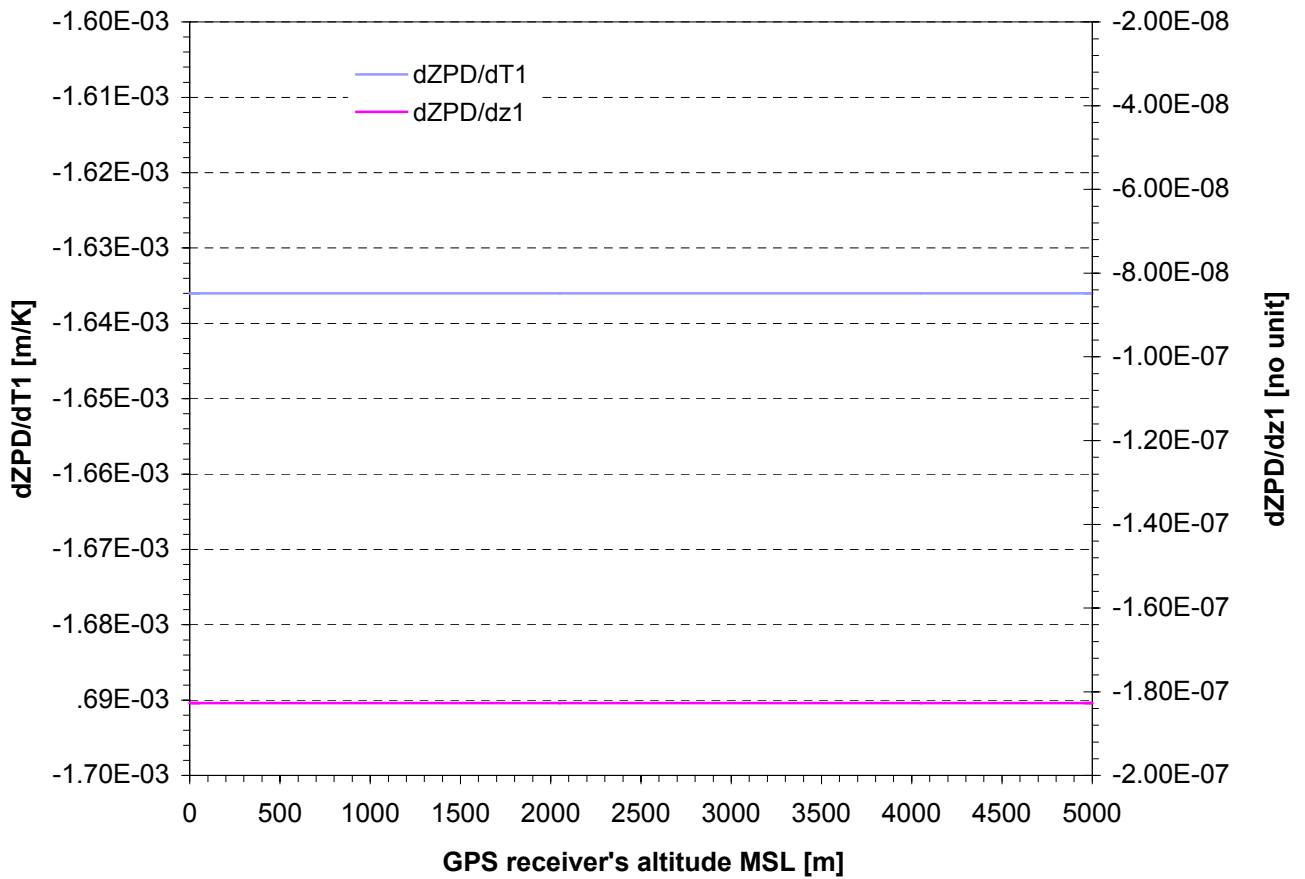


Figure 46.  $\partial ZPD/\partial T_1$  and  $\partial ZPD/\partial z_1$  as function of the GPS receiver's altitude  $z_0$

stabilizes. This was already the case for  $\partial ZDD/\partial H_p$  as the ZWD does not depend on the humidity reference scale. However  $\partial ZPD/\partial H_e$  behaves differently than  $\partial ZDD/\partial H_e$ . This is due to proportional relationship that links  $\partial ZWD/\partial H_e$  with the humidity scale height.

The dependence of the ZPD on the GPS receiver's altitude  $z_0$  and on the upper limit of integration is represented on Figure 45 on the previous page.  $\partial ZPD/\partial z_0$  increases with  $z_0$  but not largely. Its amplitude is still in the  $10^{-4}$  range! This is indeed quite small.  $\partial ZPD/\partial z'$  as well as  $\partial ZPD/\partial T_1$  and  $\partial ZPD/\partial z_1$ , that are plotted on Figure 46, do not depend on the GPS receiver's altitude  $z_0$ . Therefore they do not vary with  $z_0$ .  $\partial ZPD/\partial z_1$  is 400 times smaller than  $\partial ZPD/\partial z'$ . It is also  $10^4$  times smaller than  $\partial ZPD/\partial T_1$ !

It is now intended to study the relative change of the ZPD partial derivatives. These are plotted on Figure 47.

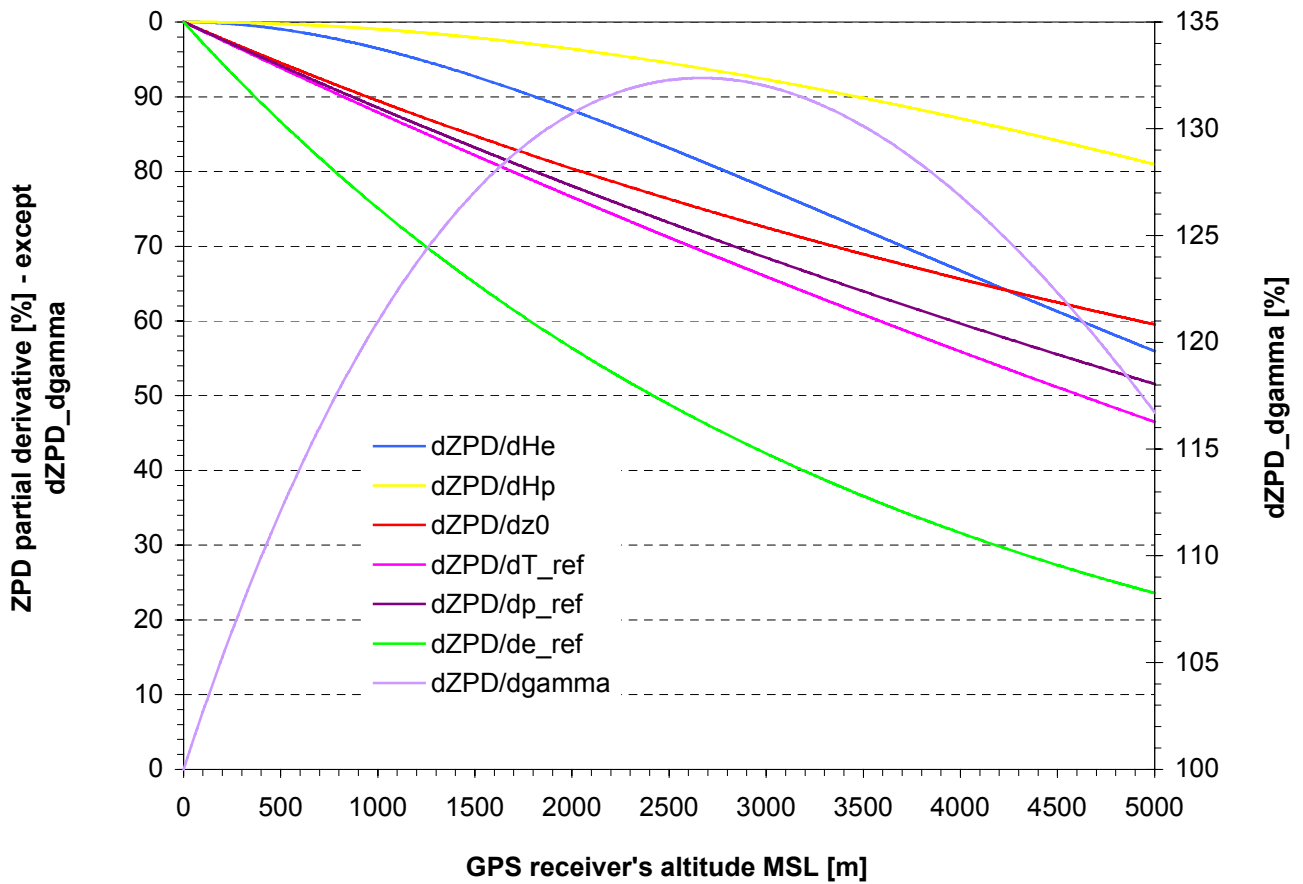


Figure 47. Relative change of ZPD partial derivatives as function of the GPS receiver's altitude  $z_0$

The partial derivatives reference values (100%) have been taken at the mean sea level, i.e. at 0 meters MSL. The GPS receiver's default altitude is still  $z_0 = 905$  meters MSL.  $\partial ZPD/\partial \gamma$  is still a convex curve with large amplitude. Hence it should not represent a problem while inverting the design matrix **A**.

This is also the case for  $\partial ZPD/\partial e_{ref}$ ,  $\partial ZPD/\partial H_p$  and  $\partial ZPD/\partial H_e$ . Although the latter two show a similar behavior, and because their curvature is opposite to the other partial derivatives, it seems probable that they would induce only small singularities that may be hindered. This is however not the case of  $\partial ZPD/\partial z_0$ ,  $\partial ZPD/\partial p_{ref}$  and  $\partial ZPD/\partial T_{ref}$ . These three partial derivatives showing an almost identical pattern are expected to generate problems during the inversion of **A**.

Note that  $\partial ZPD/\partial T_1$ ,  $\partial ZPD/\partial z_1$  and  $\partial ZPD/\partial z'$  have not been plotted on Figure 47, as they do not depend on  $z_0$ .

### 4.2.7. Partial derivatives summary

The partial derivatives of the Zenith Dry Delay (ZDD) and of the Zenith Wet Delay (ZWD) with respect to ten parameters of Table 10 have been integrally derived in Appendix B. The parameter dependency of the partial derivatives is summarized in Table 14. The ZDD and ZWD partial derivatives show very different patterns as one varies the GPS receiver's altitude  $z_0$ .

The Zenith Path Delay (ZPD) is just the sum of the ZDD and ZWD. Hence its partial derivative with respect to one parameter is the sum of the partial derivatives of the ZDD and ZWD with respect to the same parameter.  $\partial ZPD/\partial T_1$ ,  $\partial ZPD/\partial z_1$  and  $\partial ZPD/\partial z'$  do not depend on  $z_0$ . It is thus expected that they would introduce singularities in the design matrix, hindering its inversion. This is the source of concern as one intends to perform collocations with the system. It should be however possible to constrain  $\mathbf{A}$  in such a way so that one can go around this problem.

## 4.3. Swiss regional campaign

The Zenith Path Delay (ZPD) model developed in Chapter 3 has been tested in the previous paragraph. It is now intended to validate it on a virtual regional campaign in Switzerland. But first a few words are attributed to the software development.

### 4.3.1. COMEDIE software

The software package COMEDIE: Collocation of Meteorological Data for Interpolation and Estimation of Tropospheric Path Delays has been developed by Dipl. Ing. Marc Troller, Dr. Marc Cocard and Dr. Alain Geiger at the Geodynamics and Geodesy Lab. (GGL) at the Swiss Federal Institute of Technology Zurich (ETHZ). It is based on the work of [Eckert et al., 1992] and [Hirter, 1998]. The current version is release 1.1 as of 18 January 2002.

#### 4.3.1.1. Software structure

The main computation routines are written in C while the data import/extraction and structure scripts are written in PERL. For the purpose of this study, the calculation routines are centered around two sub-programs, namely `m_colcprep.c` and `m_interpol.c`. Those have been expanded by the author in order to insert the Zenith Path Delay (ZPD) model developed in Chapter 3. These are printed in Appendix C.

The `m_model.c` program manages the functional models implemented. To each model corresponds one case. The serial number 1000 has been attributed to the ZPD model. An external routine called `m_herschke.c` has been written by the author and corresponds to the ZPD functional model: it contains eq. (3.4.9.22) and eq. (3.4.9.23) for the Zenith Wet Delay and Zenith Dry Delay.

External option files serve as user interface. Indeed the choice of the model to use as well as the options are stated in the `input_main` file and the `colloc_input` file. The options chosen will be described in details in the coming paragraphs.

For further details on the COMEDIE software, it is referred to [Troller et al., 2002].

#### 4.3.1.2. Covariance function

As already stated in paragraph 2.5, the choice of the covariance function is important. It gives the dependency of different computations points on each other. Imagine one has the AGNES GPS network at his disposal. At the GPS stations locations, one obtains information on the ZPD above the GPS receiver. However one is interested in knowing the ZPD at a different position and a different (future) time. It is thus required to make assumptions on the correlation between the four dimensional points. This is achieved in providing a covariance function.

Two different covariance functions  $\Phi(\mathbf{x}, t)$  have been used for the ZPD collocation. These functions must obey eq. (4.3.1.2.1) to eq. (4.3.1.2.3), i.e.

$$\Phi(\mathbf{0}) \stackrel{!}{=} \max \quad \text{i.e.} \quad \left. \frac{\partial \Phi}{\partial \mathbf{x}} \right|_{\mathbf{x}=\mathbf{0}} = \mathbf{0} \quad \text{and} \quad \left. \frac{\partial^2 \Phi}{\partial^2 \mathbf{x}} \right|_{\mathbf{x}=\mathbf{0}} < \mathbf{0} \quad (4.3.1.2.1)$$

$$\left. \frac{\partial |\Phi|}{\partial \mathbf{x}} \right|_{\mathbf{x}=\mathbf{0}} < \mathbf{0} \quad (4.3.1.2.2)$$

$$\lim_{r \rightarrow +\infty} \Phi(r) = 0, \quad |\mathbf{x}| = r \quad (4.3.1.2.3)$$

It describes the covariance between two signals and depends on the location of both points  $i$  and  $j$ . It reaches its maximum when the displacement is nil and it decreases if the displacement increases.

Therefore the first covariance function considered is

$$\Phi_{ij} := \frac{\sigma_0^2}{1 + \left[ \left( \frac{x_i - x_j}{\Delta x_0} \right)^2 + \left( \frac{y_i - y_j}{\Delta y_0} \right)^2 + \left( \frac{z_i - z_j}{\Delta z_0} \right)^2 + \left( \frac{t_i - t_j}{\Delta t_0} \right)^2 \right]} \quad (4.3.1.2.4)$$

It contains five parameters:  $\sigma_0$ ,  $\Delta x_0$ ,  $\Delta y_0$ ,  $\Delta z_0$  and  $\Delta t_0$ . As usually one has a lack of information in the higher regions, c.f. paragraph 4.3.2., another covariance function has been considered. A damping factor is implemented to take this fact into account. Thus the second covariance function is

$$\Phi_{ij} := \frac{\sigma_0^2}{1 + \left[ \left( \frac{x_i - x_j}{\Delta x_0} \right)^2 + \left( \frac{y_i - y_j}{\Delta y_0} \right)^2 + \left( \frac{z_i - z_j}{\Delta z_0} \right)^2 + \left( \frac{t_i - t_j}{\Delta t_0} \right)^2 \right]} \cdot e^{-\frac{(z_i + z_j)}{2 \cdot z_0}} \quad (4.3.1.2.5)$$

It contains one parameter more than the first covariance function, namely  $z_0$ . Do not confound this with the altitude of the GPS receiver. It is here an altitude of reference.

### 4.3.2. AGNES GPS stations

The GPS data was delivered by the Swiss Federal Office of Topography ([www.swisstopo.ch](http://www.swisstopo.ch)), located at Wabern near Bern, the Swiss capital, and by the Geodesy and Geodynamics Lab (GGL) at the Swiss Federal Institute of Technology, Zurich. Eleven permanent stations from the Automated GPS Network Switzerland (AGNES) have been taken into consideration for the computation. These are summarized in Table 19 hereunder. Their coordinates in the World Geodetic System 1984 (WGS84) are also stated.

Station ID	Northing			Easting			Altitude	Name
	[deg]	[min]	[sec]	[deg]	[min]	[sec]	[m]	
ANDE	46	39	11.86	08	36	57.18	2366.388	Andermatt
DAVO	46	48	46.49	09	50	36.65	1645.582	Davos
EPFL	46	31	17.27	06	34	04.42	460.487	EPF <sup>14</sup> Lausanne
ETHZ	47	24	25.44	08	30	37.91	594.832	ETH <sup>15</sup> Zurich
FHBB	47	32	01.91	07	38	18.97	377.734	FHBB <sup>16</sup> Muttenz
JUJO	46	32	50.95	07	59	05.65	3634.584	Jungfrauoch
LOMO	46	32	50.95	07	59	05.65	438.011	Locarno - Monti
NEUC	46	59	37.78	06	56	25.73	504.674	Neuchatel
PAYE	46	48	43.70	06	56	38.183	548.707	Payerne
PFAN	47	30	55.17	09	47	04.78	1090.266	Pfänder
ZIMM	46	52	37.54	07	27	54.98	956.338	Zimmerwald

Table 19. AGNES permanent stations used

The AGNES stations are also plotted on Figure 48 on next page. As of January 1, 2002, all 29 GPS stations are fully operational. The stations represented with red triangles were already in service before 2002 or were installed during fiscal year 2001 and 2002 (FY01-02) by the Swiss Federal Office of Topography (L+T). Of all stations

<sup>14</sup> EPF: Ecole Polytechnique Fédérale – Swiss Federal Institute of Technology

<sup>15</sup> ETH: Eidgenössische Technische Hochschule – Swiss Federal Institute of Technology

<sup>16</sup> FachHochschule Beider Basel

shown on Figure 48, only the GPS stations in green were used during this study. This decision is motivated by the significance of those and by the reduction of data quantity that must be processed.

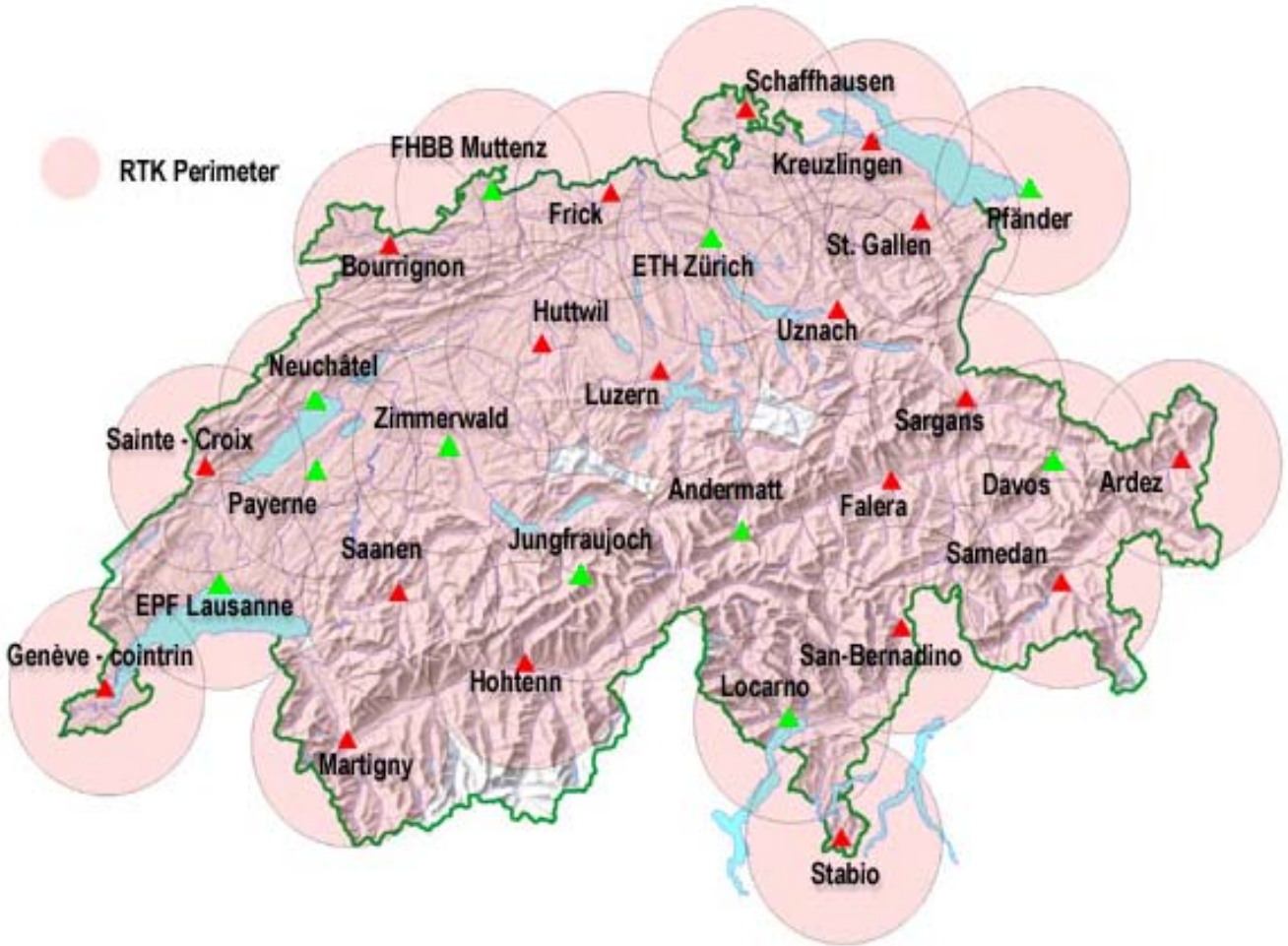


Figure 48. AGNES permanent stations used, after [L+T, 2002]

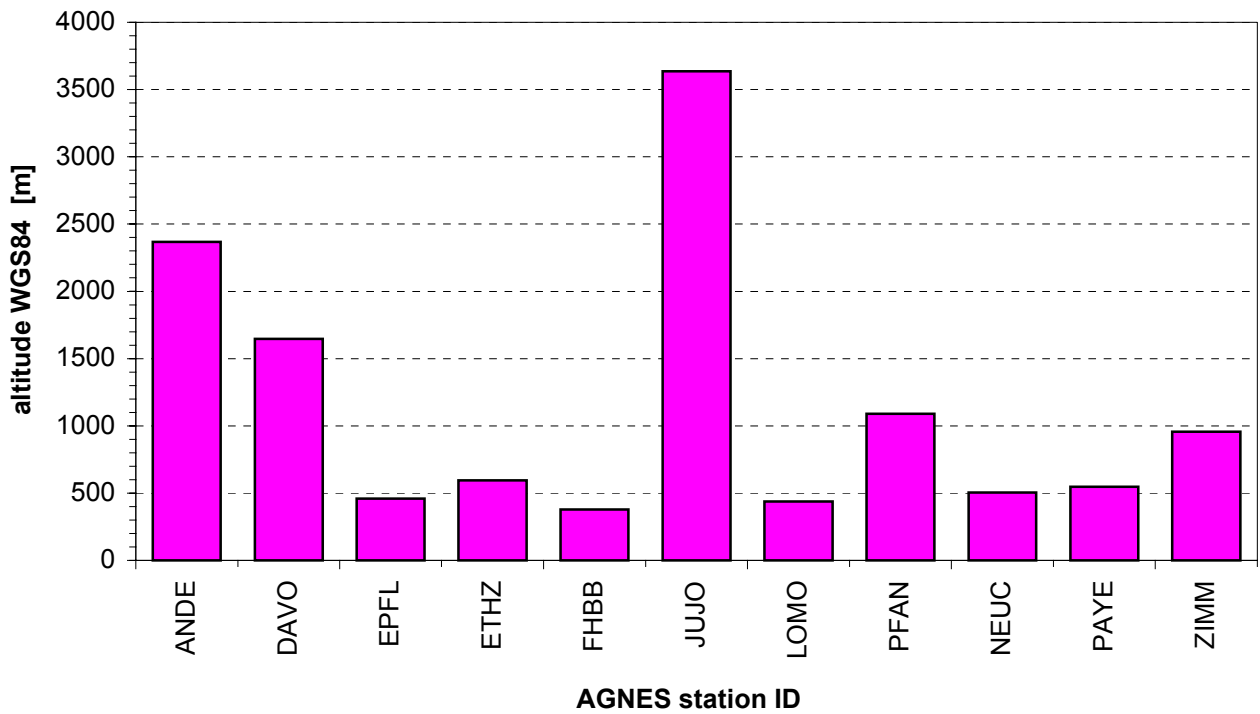


Figure 49. Height distribution in WGS84 of the AGNES stations



With respect to the models developed in Chapter 3, the vertical coordinate or height of the GPS station has the major influence on the collocation procedure. Hence the altitude distribution with respect to the World Geodetic System 1984 of the AGNES stations of Table 19 is plotted on Figure 49. Remark that most stations are located at an altitude below 1000 meters.

The AGNES stations of ANDE, ETHZ, JUJO, LOMO and DAVO are plotted on Figure 50 below, clockwise from the upper left corner.

For further technical information and a detailed description of AGNES, the interested reader should refer to [Brockmann et al., 2001 & 2002].



Figure 50. ANDE, ETHZ, JUJO, LOMO and DAVO AGNES GPS stations. Clockwise from the upper left corner. © 2002 L+T.

### 4.3.3. AGNES station collocation

In a first step the collocation technique is applied to the eleven AGNES permanent GPS of Table 19. The collocation itself yields to a set of estimated parameters that are recursively determined. These are then reinserted in the computation in order to proceed with the prediction. The data is then processed and evaluated.

The different assumptions taken as well as the options chosen are described in the coming paragraphs.

#### 4.3.3.1. Observation window

It has been decided to proceed with a survey of the eleven AGNES GPS stations of Table 19. It has been continuously observed during a time period starting on Monday 22 May 2000 at 00:00:00 UTC and ending on Tuesday 30 May 2000 at 00:00:00 UTC. The time counter has been set to zero at the start of the observation window. The time lag is two hours.

#### 4.3.3.2. Collocation parameters and covariance

Numerical instabilities were experienced during the implementation of the ZPD functional model. Therefore, of the ten original parameters of eq. (3.4.9.22) and eq. (3.4.9.23), seven have been constrained. Indeed, their determinations via collocation yield to important errors masking the significance of the result. Hence they have been blocked around their default value. These are stated in Table 20 on next page.

Parameters			
Symbol	Value	Unit [SI]	Identification
$T_1$	216.64	K	Temperature at tropopause
$\gamma$	$-6.501 \cdot 10^{-3}$	$K \cdot m^{-1}$	Tropospheric temperature gradient (Lapse rate)
$z_0$	905	m	GPS's receiver altitude
$z_1$	11000	m	Tropopause height
$z'$	15000	m	Upper limit of integration
$H_p$	9000	m	Pressure scale height
$H_e$	3000	m	Humidity scale height

Table 20. ZPD parameters constrained.

Thus only  $p_{ref}$ ,  $e_{ref}$  and  $T_{ref}$  were let free to vary. One can shadow this assumption by asking why constrain so many parameters and thus limit so much the model? The answer is well known to scientists working in an entrepreneurial environment. Due to the important time investment that the leveraging of the numerical instabilities implies, to the time limitations imposed on that study and the fact that the author is not a professional programmer, it has been decided to let this issue for further study.

According to eq. (4.3.1.2.4), the *a-priori* covariance parameters for the first covariance function introduced previously were set as stated in Table 21 below.

Parameters		
Symbol	Value	Unit
$c_0$	2	No unit
$\Delta x_0$	100	km
$\Delta y_0$	100	km
$\Delta z_0$	1	km
$\Delta t_0$	6	hrs

Table 21. A-priori covariance parameters

These have been determined by judicious guessing, and fine tuned by trial and error. One should note that the collocation technique intrinsically allows for an approximate knowledge of the parameters. Indeed these are re-determined as by-products as part of the collocation procedure.

### 4.3.3.3.ZPD estimates

Assume one wants to know the ZPD for instance at Andermatt (ANDE), during the whole survey period without knowing anything about the atmosphere above the station and with no observations being made. From the eleven AGNES permanent GPS stations from which data is available, one has been set aside. Here it is Andermatt. The data from the ten other stations has been introduced in the COMEDIE software, which generates an estimation of the ZPD at a given point, here ANDE. This is then compared to observations that have been actually performed at ANDE. One proceeds alternatively for the other stations in the same way. This enables to test the quality of the solution and thus validate the ZPD model and COMEDIE software.

The ZPD estimates for the eleven stations are plotted on Figure 51 to 61. The stations are designed by their four-digit code (refer to the first column of Table 19).



Figure 51. COMEDIE ZPD estimates at ANDE

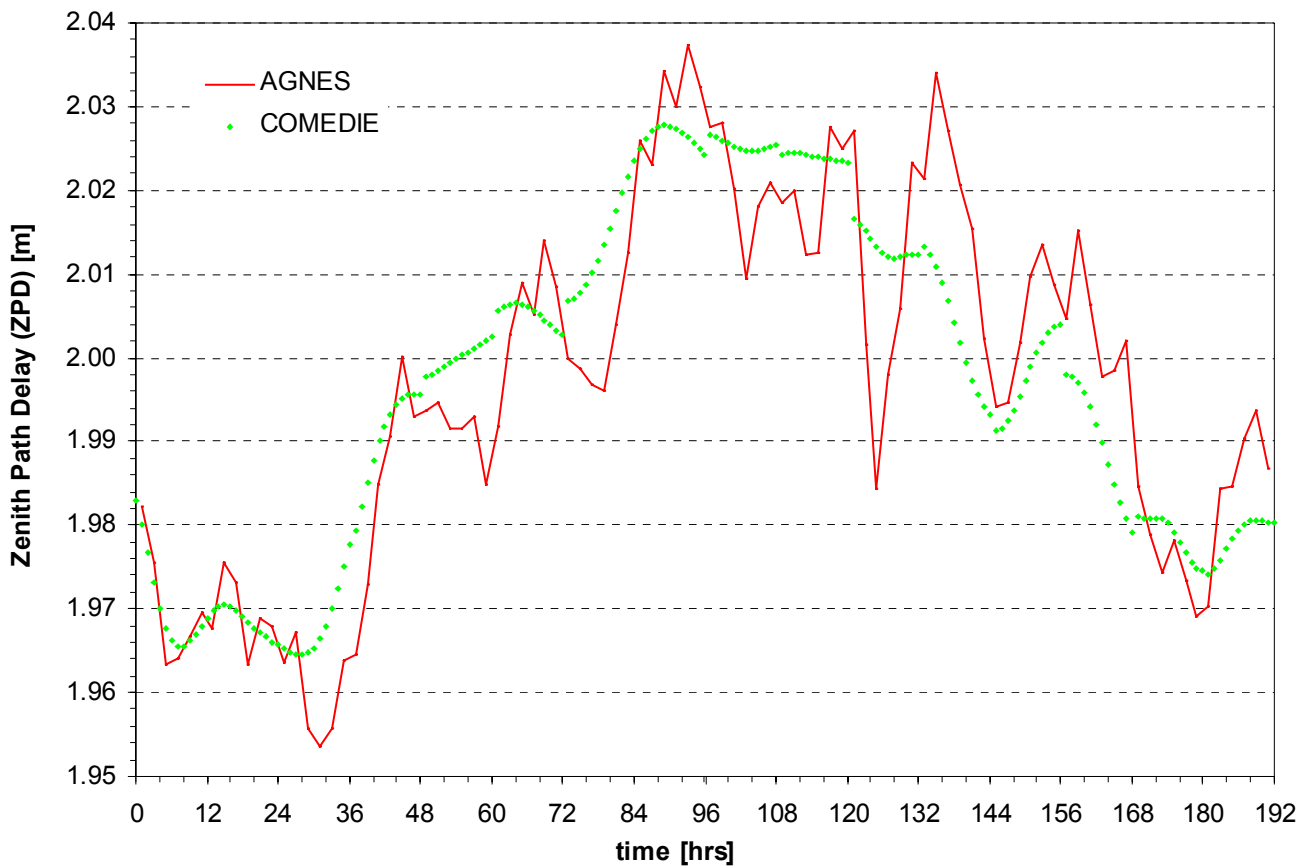


Figure 52. COMEDIE ZPD estimates at DAVO

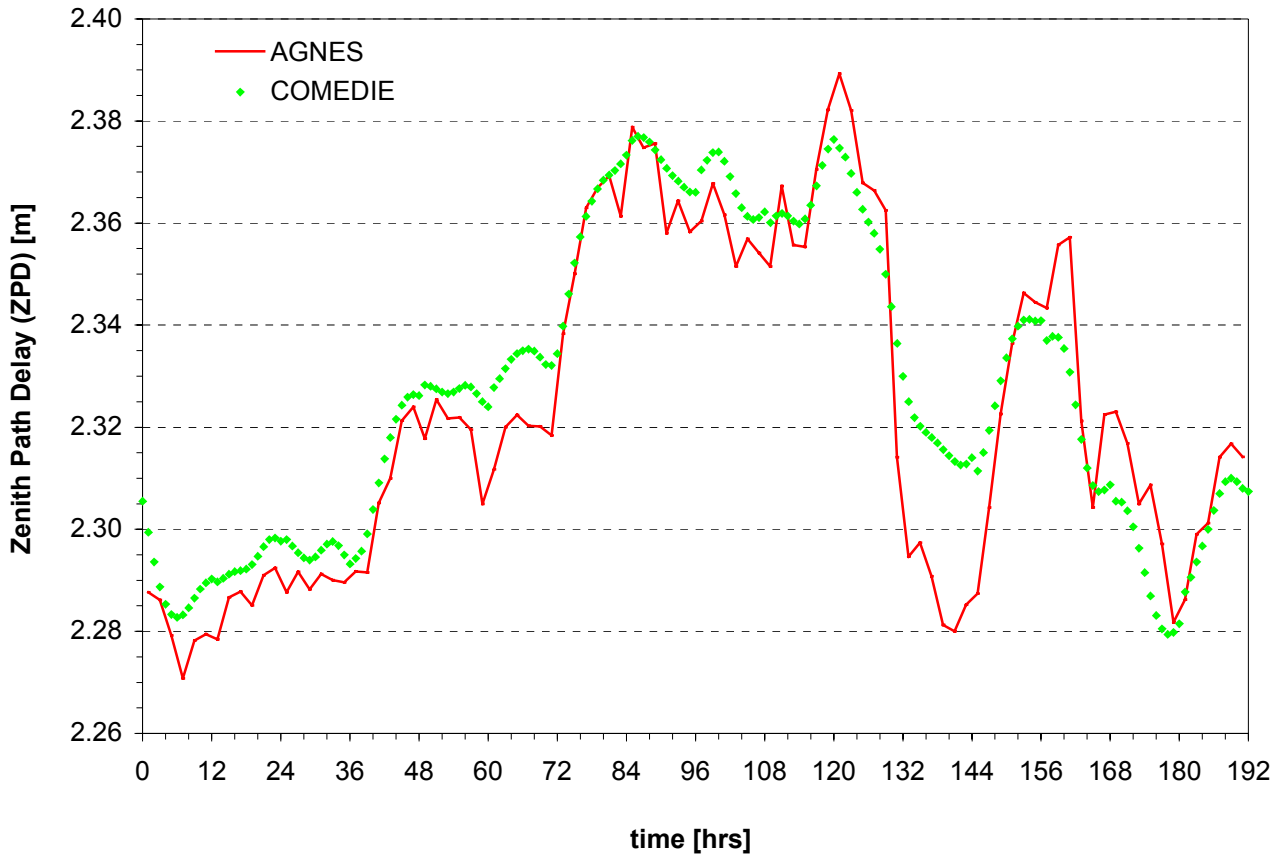


Figure 53. COMEDIE ZPD estimates at EPFL

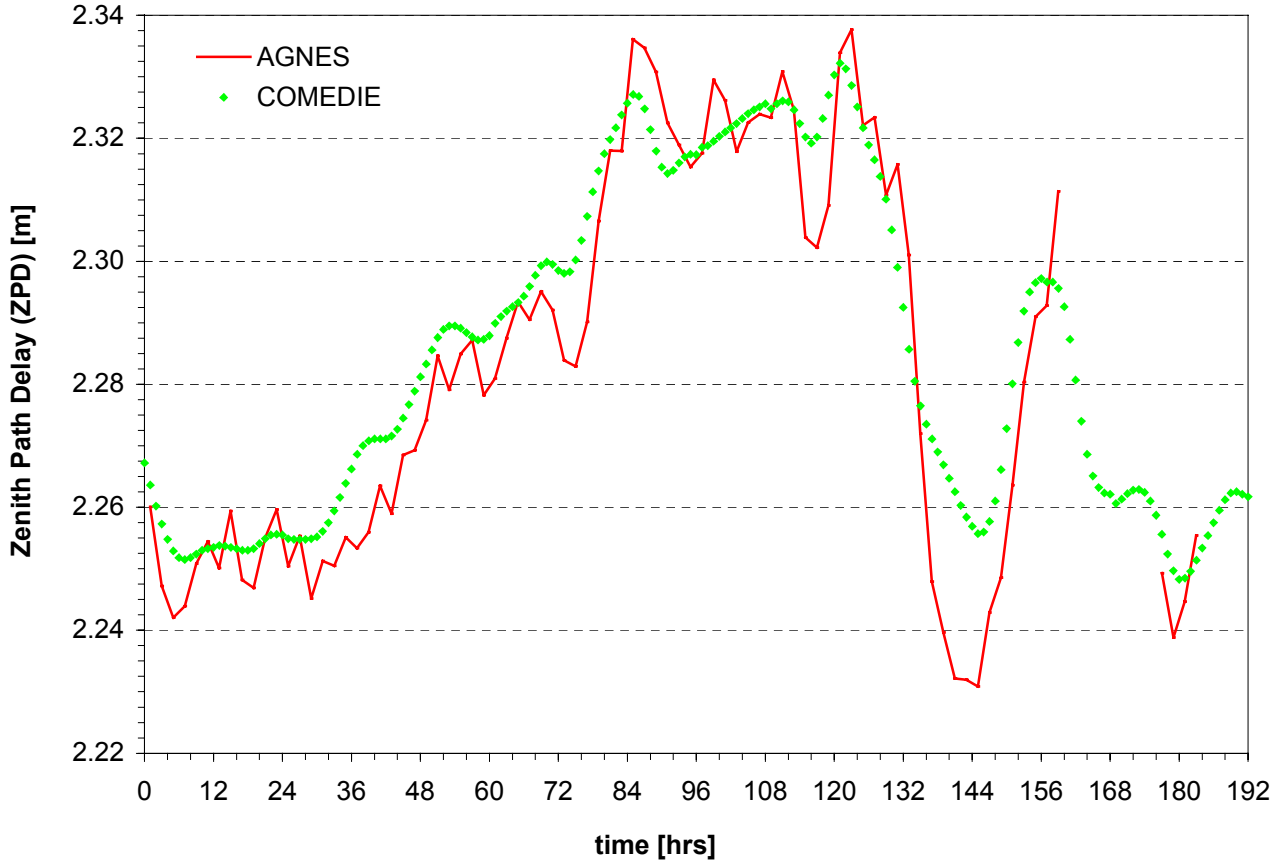


Figure 54. COMEDIE ZPD estimates at ETHZ

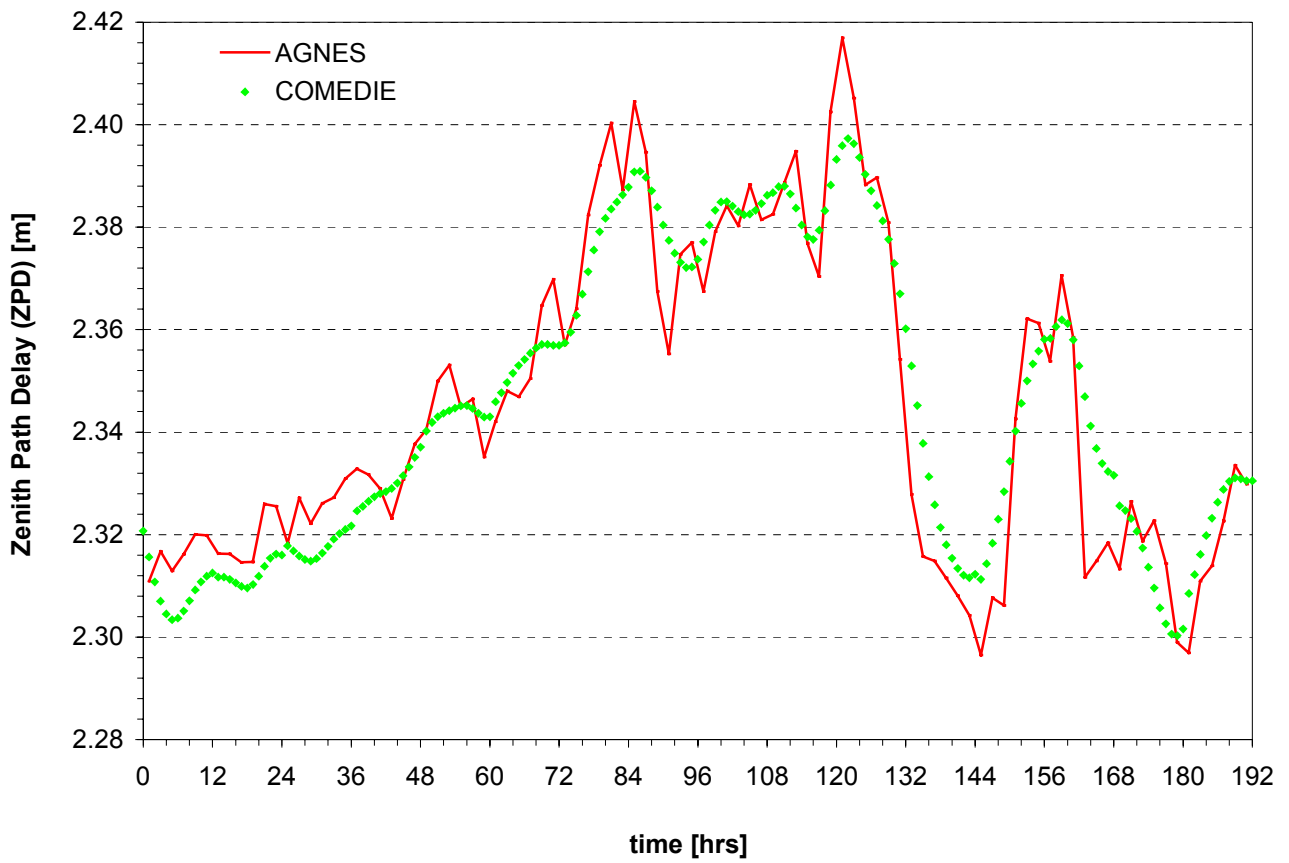


Figure 55. COMEDIE ZPD estimates at FHBB

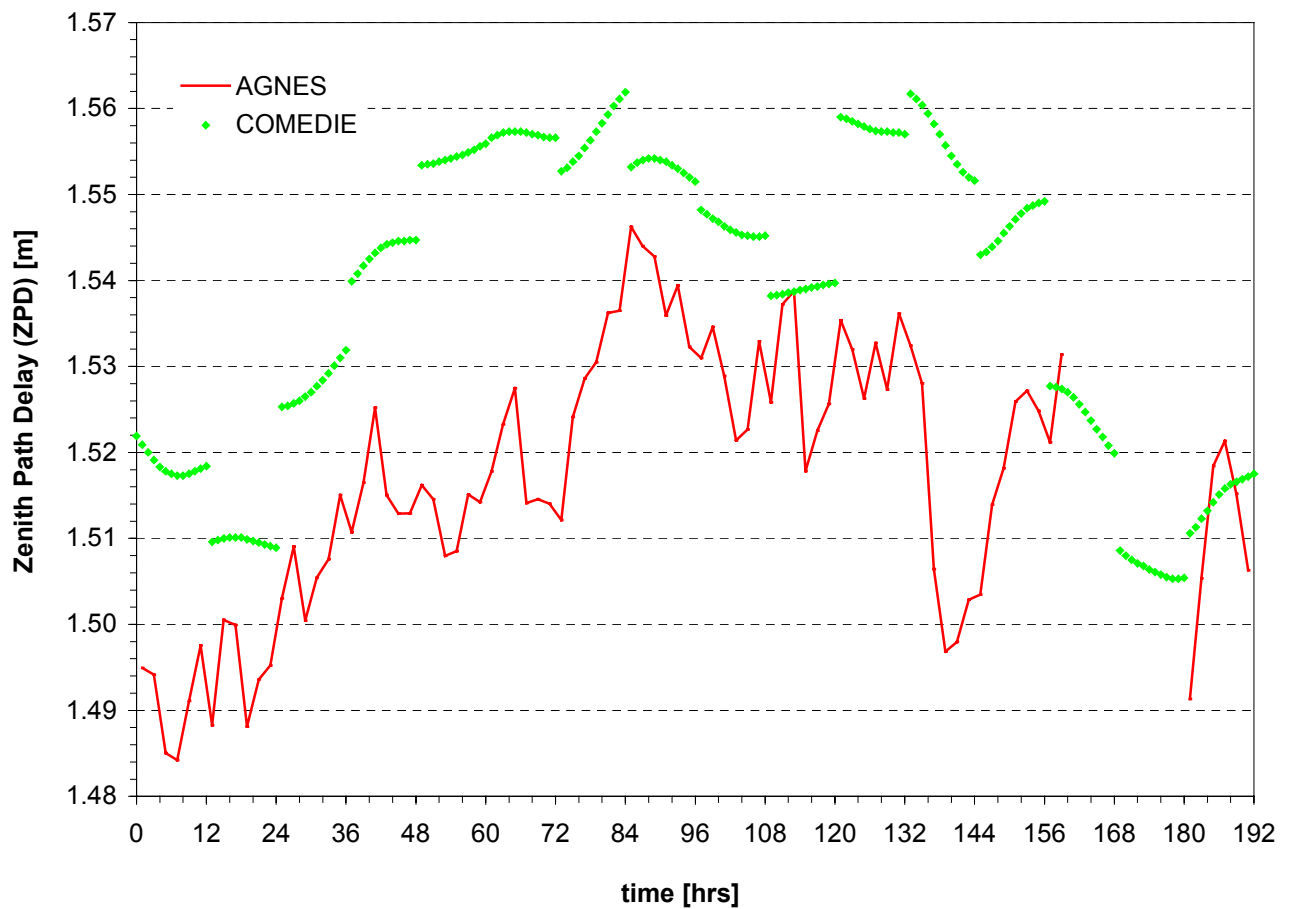


Figure 56. COMEDIE ZPD estimates at JUJO

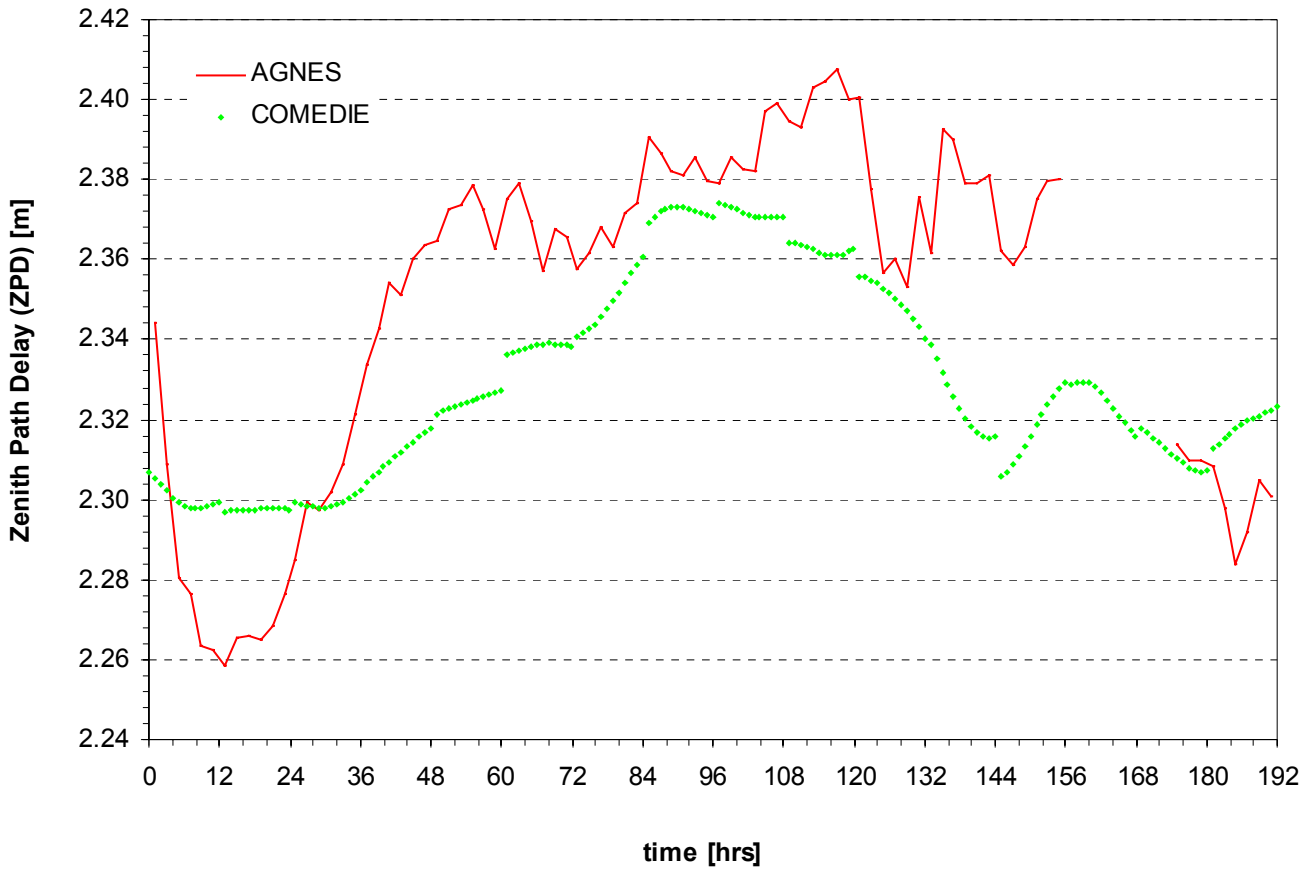


Figure 57. COMEDIE ZPD estimates at LOMO



Figure 58. COMEDIE ZPD estimates at NEUC



Figure 59. COMEDIE ZPD estimates at PAYE

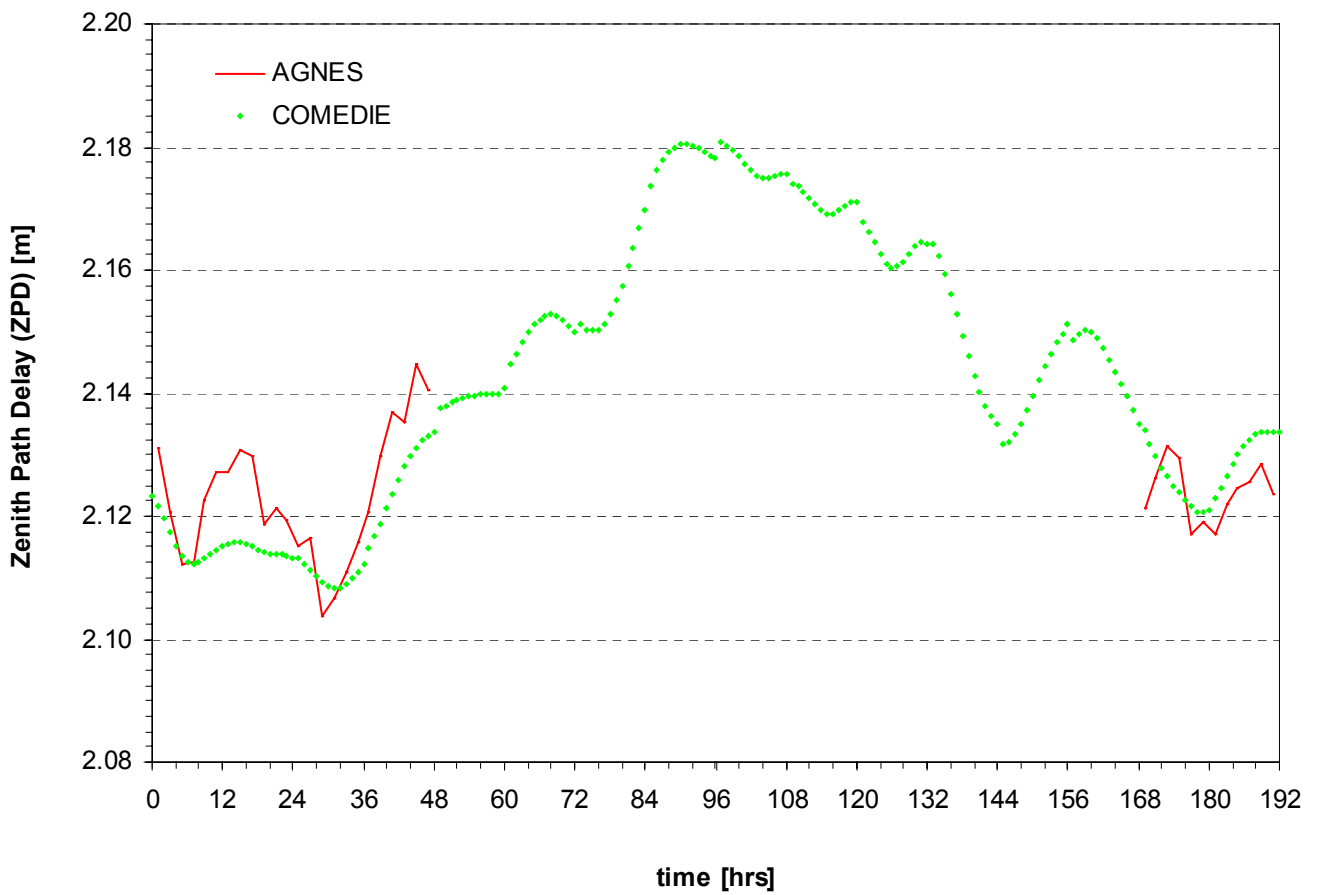


Figure 60. COMEDIE ZPD estimates at PFAN

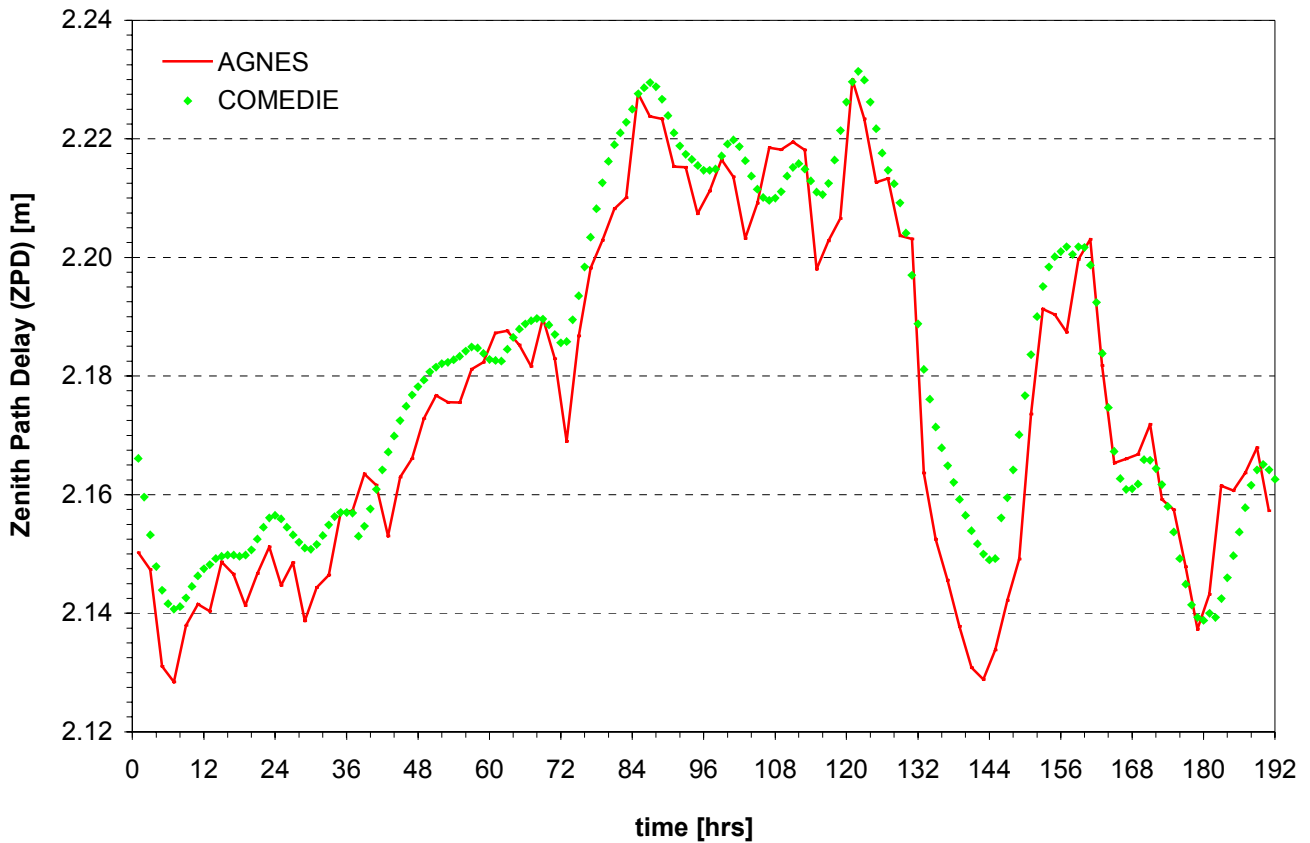


Figure 61. COMEDIE ZPD estimates at ZIMM

The ZPD estimates obtained with COMEDIE are plotted with green squares while a red line represents the AGNES observations.

It should be first noted that half of the plots are not continuous in time. Indeed it has not been possible to obtain continuously GPS data during the observation window. This is probably due to faulty GPS space vehicles, malfunctioning GPS receivers and leaky data transfer. This is clearly observed at ETHZ (figure 54), Jungfrauoch (Figure 56), Locarno-Monti (Figure 57), Payerne (Figure 59) and Pfänder (figure 60).

The data density is asymmetric. Observations have been performed at the AGNES permanent GPS stations with a time leg of two hours. To be exact, it is observed every 30 seconds and then averaged on a period of two hours in order to improve reliability of the data. However, it has been interpolated hourly. Thus one obtains more estimates than actual observations, c.f. Figure 60 between  $t_1 = 47.00$  hours and  $t_2 = 169.00$  hours. This corresponds to the period between Tuesday 23 May 2000 at 23:00 hours UTC and Sunday 29 May 2000 at 01:00 hours UTC. The possibility to choose the time interval for the prediction is one of the numerous advantages of the collocation technique.

Fortunately, the general aspect of both AGNES and COMEDIE are similar. The Zenith Path Delay is usually found to be between 2.10 meters and 2.42 meters. There is no large disagreement between estimates and observation with the exception of the Jungfrauoch (JUJO).

Indeed, JUJO is by far the highest station and one has a lack of data at equivalent altitudes to cross-validate the solution. One should note that the GPS signal has fewer atmosphere to cross at JUJO than at the other AGNES stations. Further it is established that the atmospheric water vapor (WV) causes most of the ZPD. This WV is located in the lower troposphere. The humidity scaling height has been set at 3000 meters. However, comparing with the information of Table 19, one can see that JUJO is above the scaling height!

Further, the collocation estimates obtained with COMEDIE are discontinuous. Refer to Figure 56. The COMEDIE solution is stacked in time segments of 12 hours length. This stacking has been voluntarily performed in order to ease the computations. For the final solution, each block is added to a global estimates file. The discontinuities might be explained by strong and different RHS and LHS gradients at the beginning and end of a time stack.



The Locarno-Monti (LOMO) station, Figure 57, presents some peculiar behavior. The COMEDIE solution seems to be offset with the actual AGNES observations, that vary stronger and faster. This is a known phenomenon already observed during previous campaigns. It is due to two main factors. First, LOMO is situated in Tessin, South of the Alps mountain arc and has its own microclimate. Indeed, the Alps are a mountainous barrier that stops cold and wet fronts arriving from a Northwest direction to continue on their way East. Thus LOMO is located in a warmer and dryer area than the rest of the AGNES stations used during this study. Second the geometry of the AGNES network is of importance. As can be seen on Figure 48, LOMO is set aside of the rest of the stations. Hence it is nearly impossible to correlate its ZPD estimates with results from other parts of the AGNES network. It is assumed that the COMEDIE solution would strongly improve if one would insert the Stabio (STAB) and San Bernardino (SANB) AGNES stations in the computation. This is one reason why the Swiss Federal Office of Topography has installed the latter two stations during FY01-02.

One intends now to evaluate the exact quality of matching between the COMEDIE Zenith Path Delay estimates and the AGNES ZPD observations.

#### 4.3.3.4.COMEDIE quality assessment

A short reminder of the statistic formulas used is given hereunder.

**Definition 1.** (Standard deviation) The standard deviation of a sample of  $n$  measurements  $x_i$  is defined as

$$STDEV := \sqrt{\frac{n \cdot \sum_{i=1}^n x_i^2 - \left(\sum_{i=1}^n x_i\right)^2}{n \cdot (n-1)}} \quad (4.3.3.4.1)$$

**Definition 2.** (RMS) The Root Mean Square of a sample of  $n$  measurements  $x_i$  and  $n$  observations  $x_i^{true}$  is defined as

$$RMS := \sqrt{\frac{1}{n} \cdot \sum_{i=1}^n (x_i - x_i^{true})^2} \quad (4.3.3.4.2)$$

The COMEDIE ZPD estimates AGNES observations differences are plotted for all AGNES GPS stations of Table 19 on Figure 62 to 72.

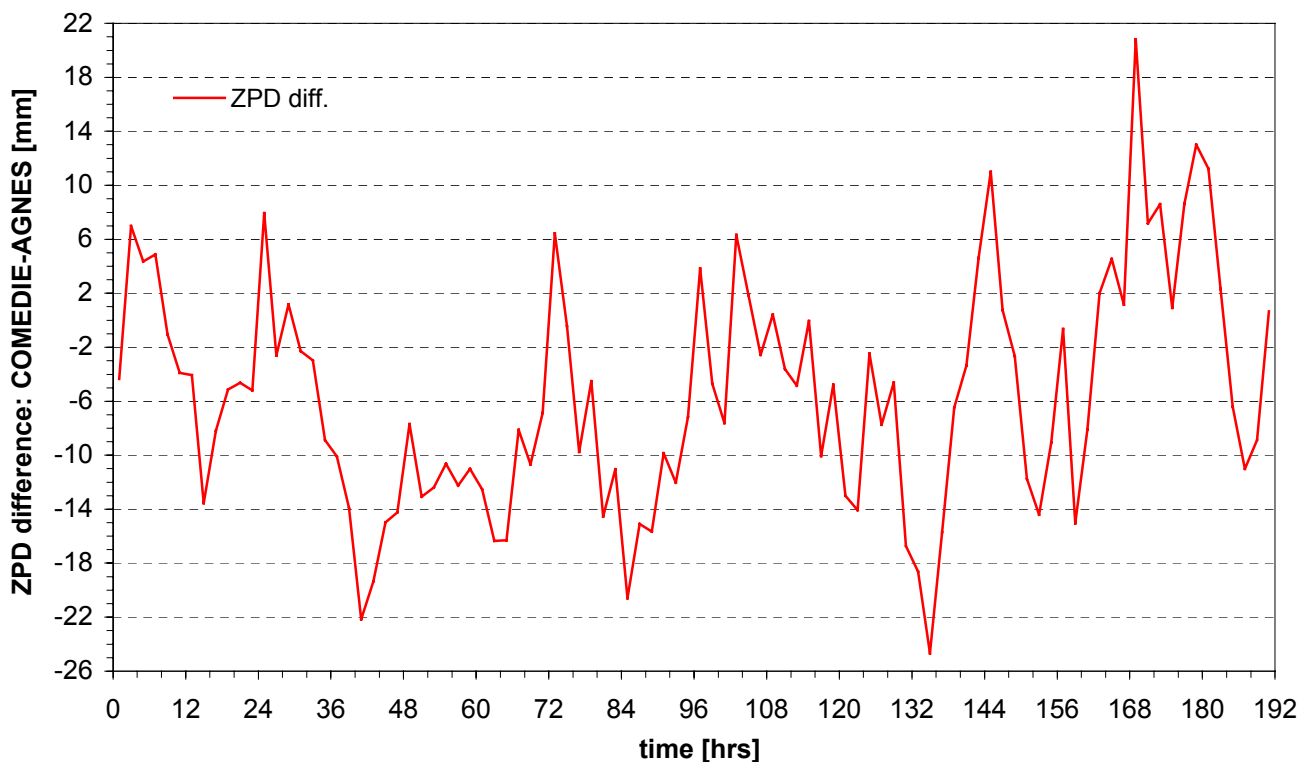


Figure 62. COMEDIE-AGNES ZPD differences at ANDE

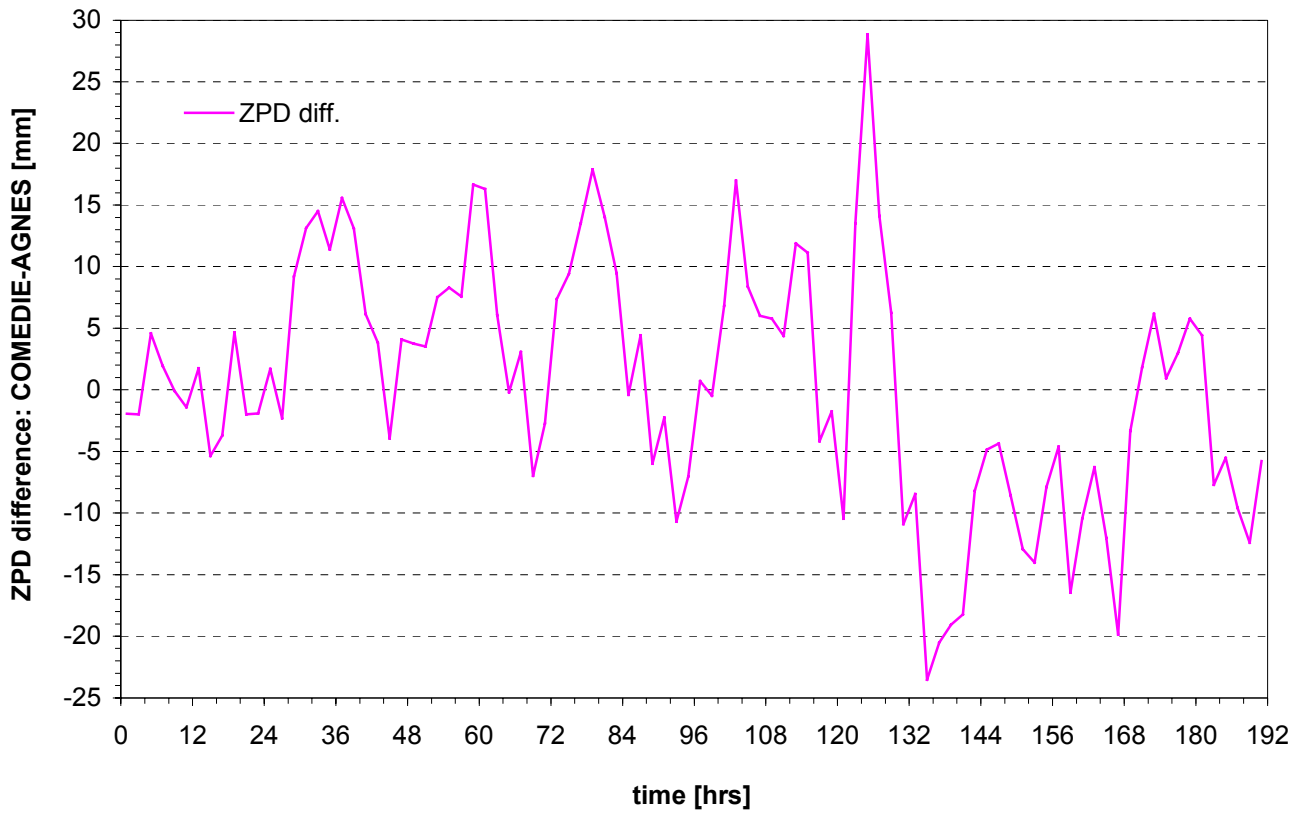


Figure 63. COMEDIE-AGNES ZPD differences at DAVO

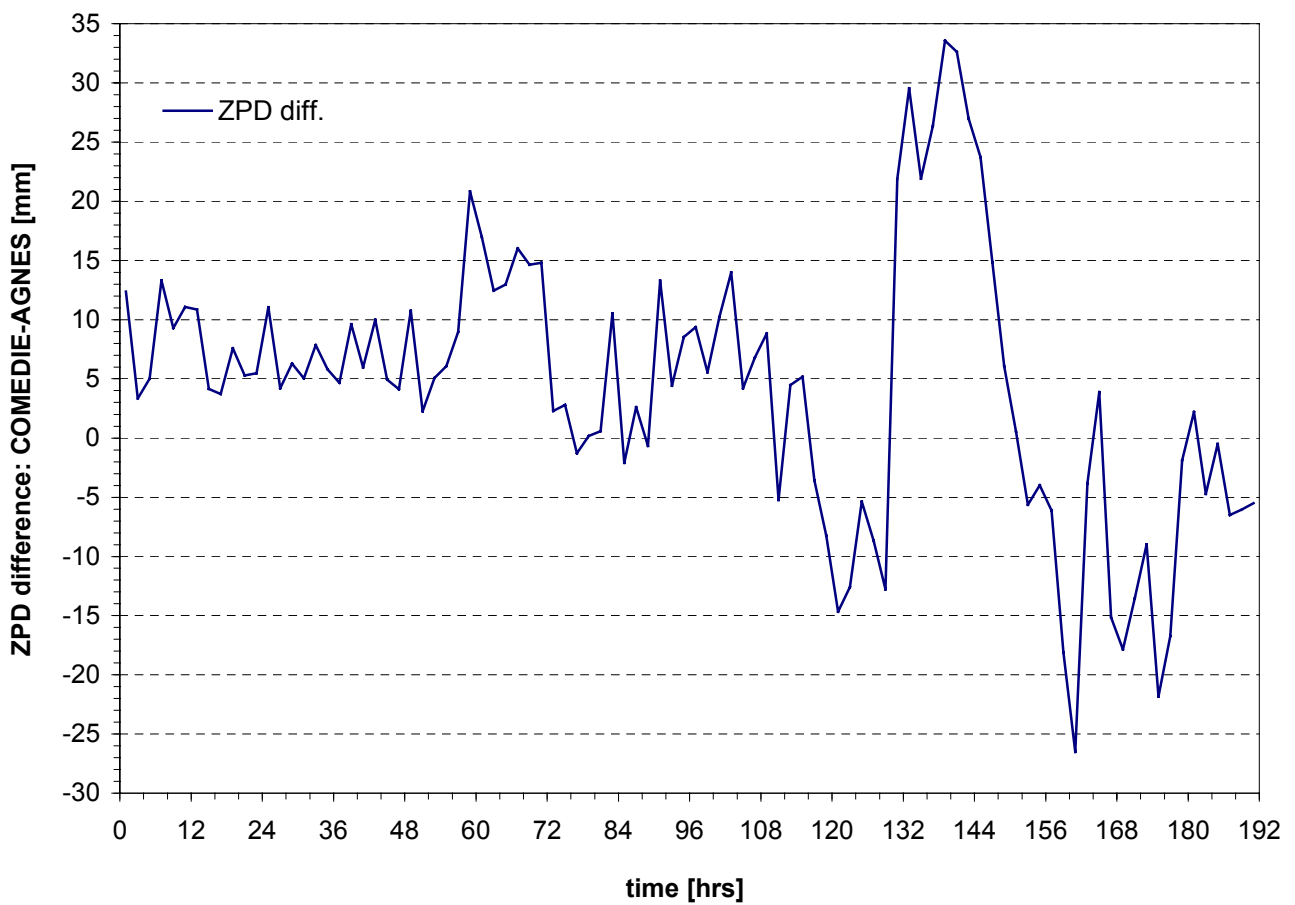


Figure 64. COMEDIE-AGNES ZPD differences at EPFL

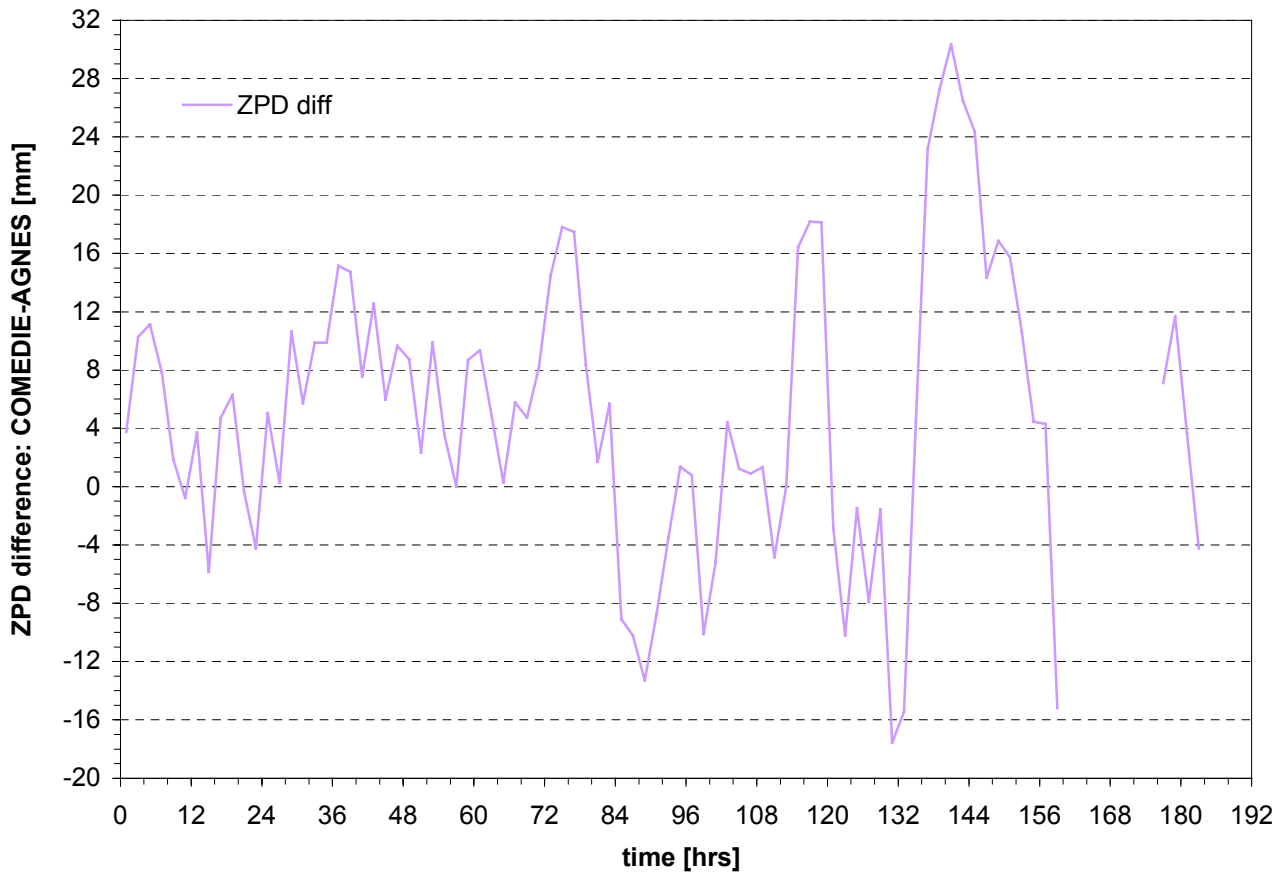


Figure 65. COMEDIE-AGNES ZPD differences at ETHZ

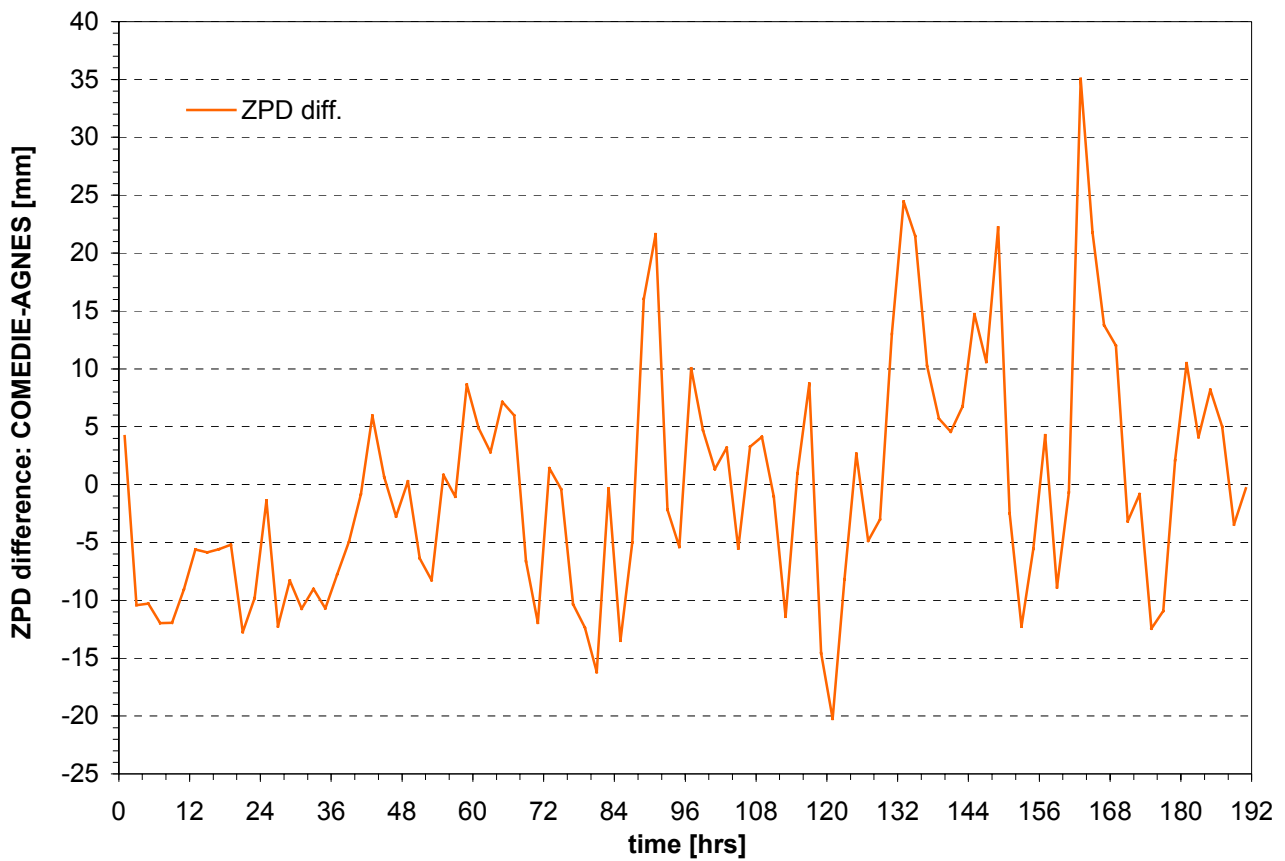


Figure 66. COMEDIE-AGNES ZPD differences at FHBB

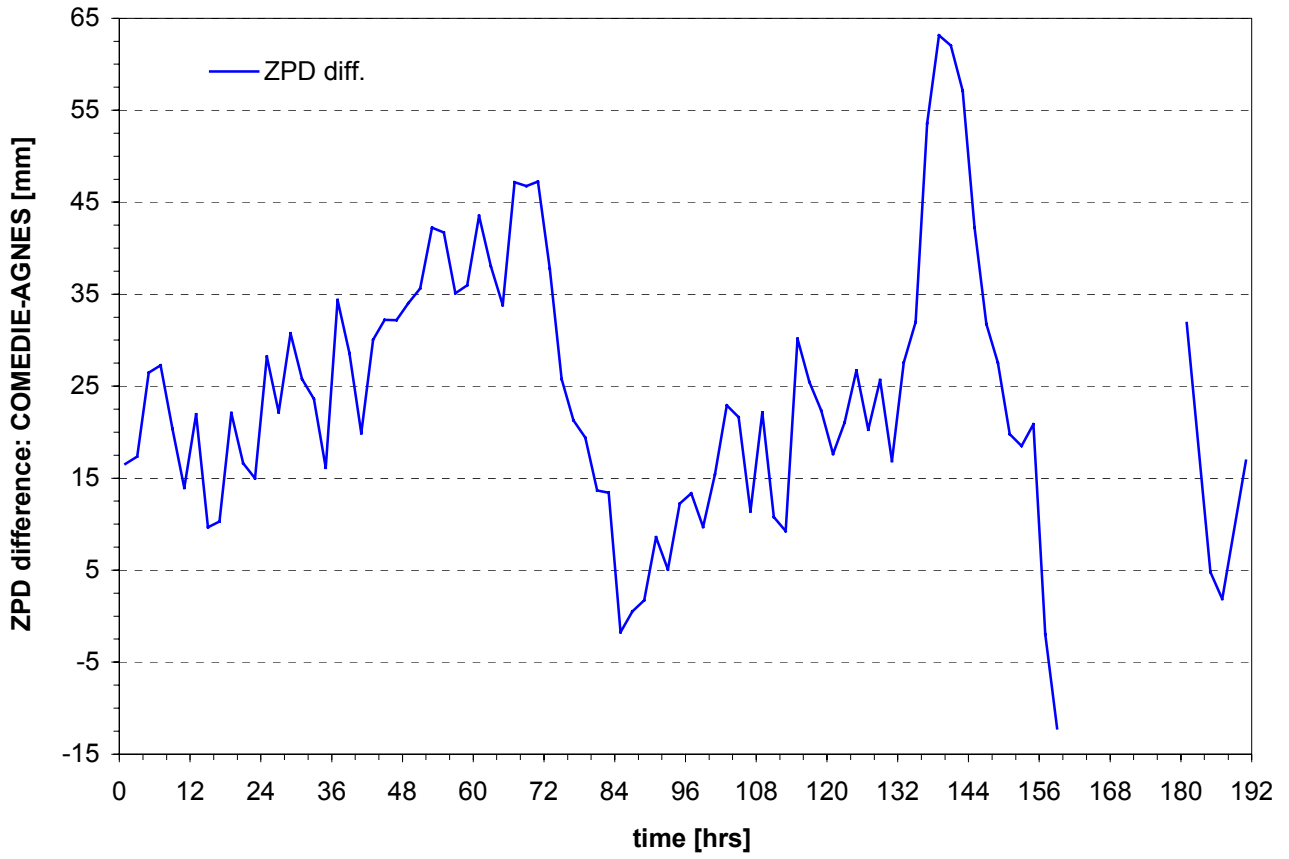


Figure 67. COMEDIE-AGNES ZPD differences at JUJO



Figure 68. COMEDIE-AGNES ZPD differences at LOMO

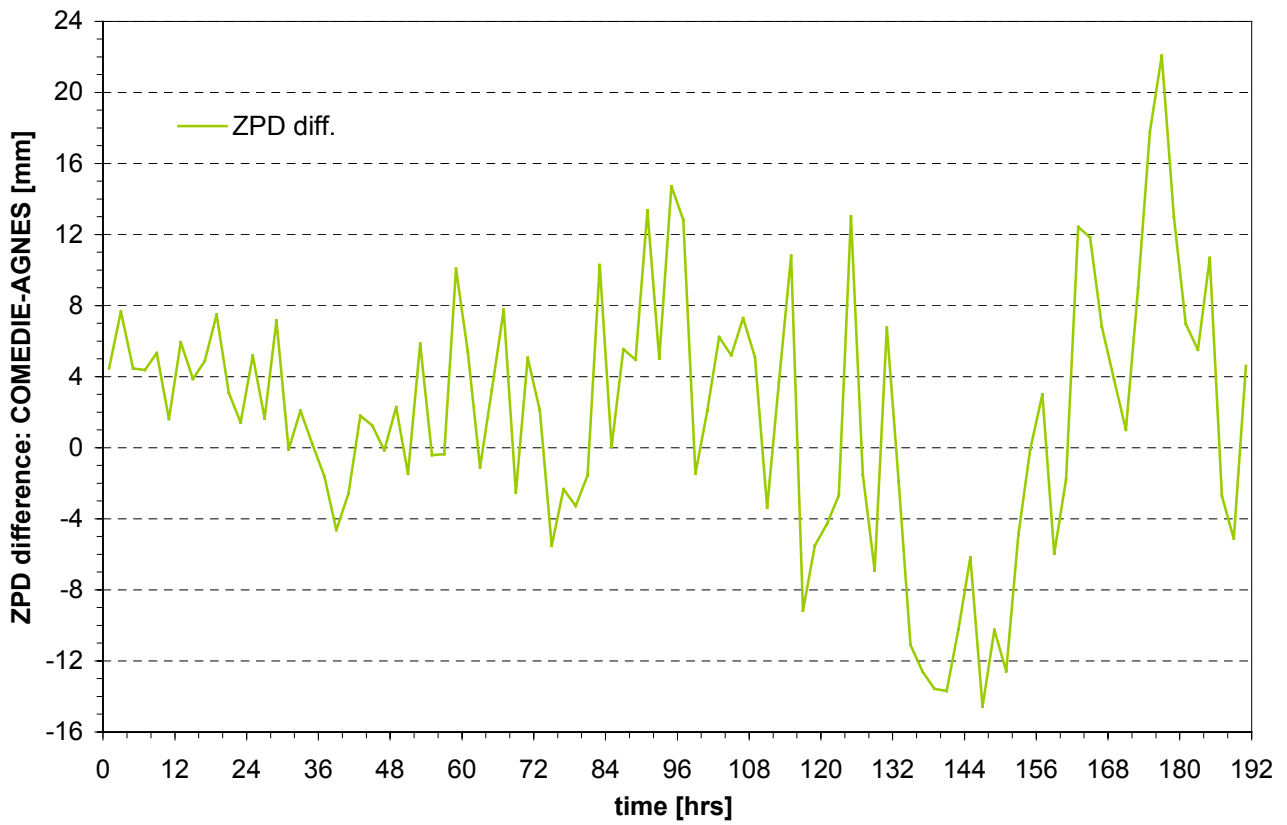


Figure 69. COMEDIE-AGNES ZPD differences at NEUC

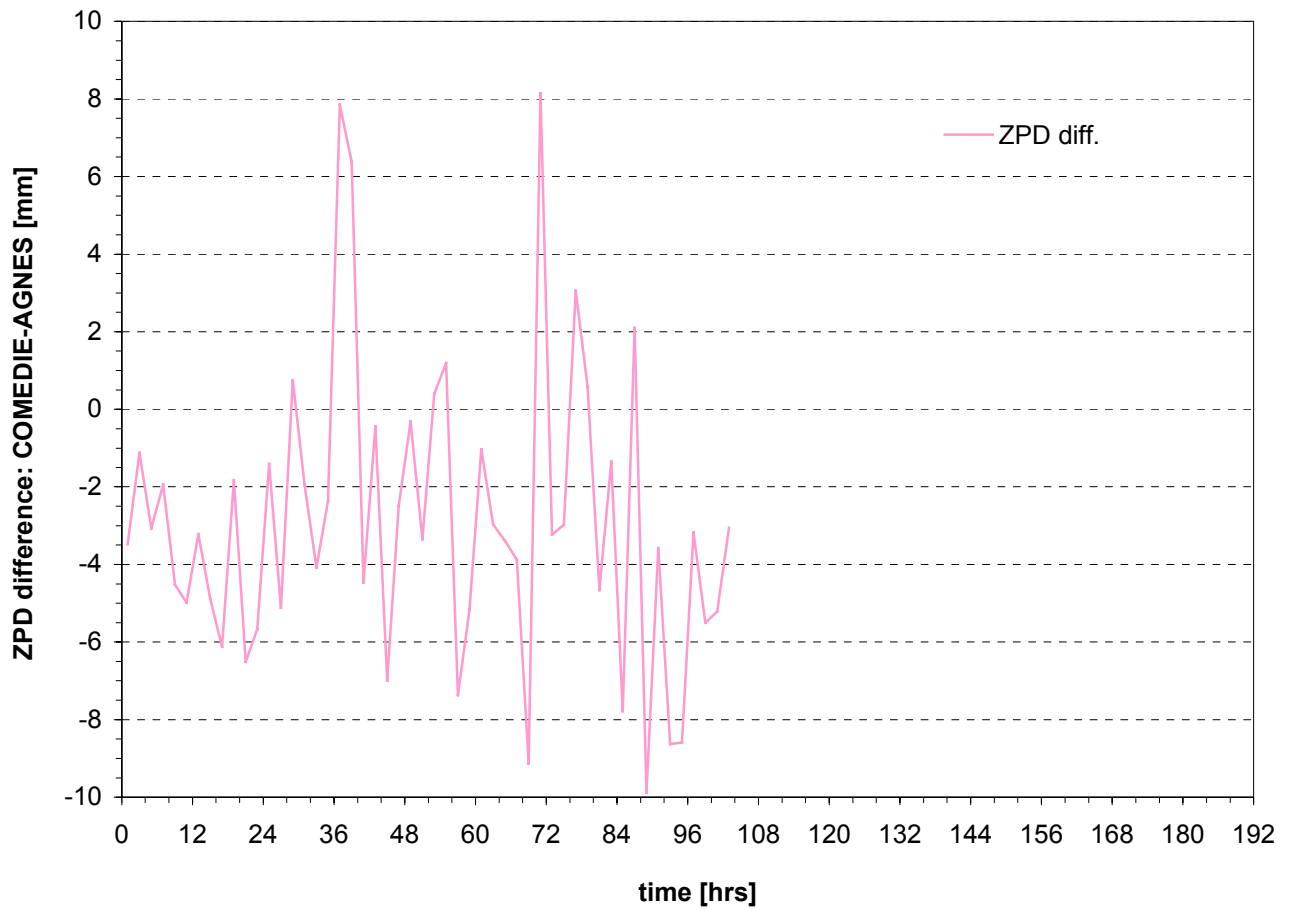


Figure 70. COMEDIE-AGNES ZPD differences at PAYE

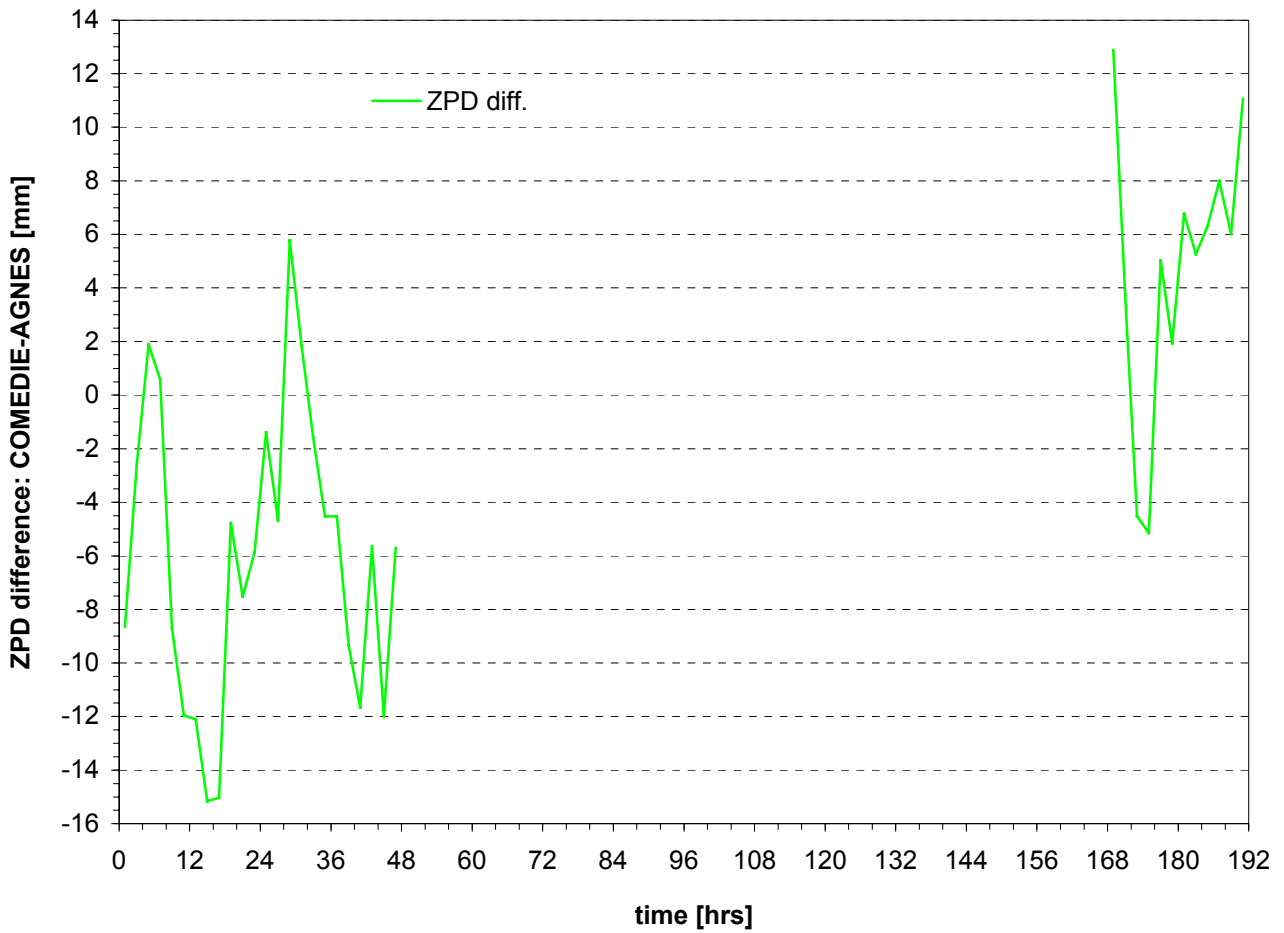


Figure 71. COMEDIE-AGNES ZPD differences at PFAN

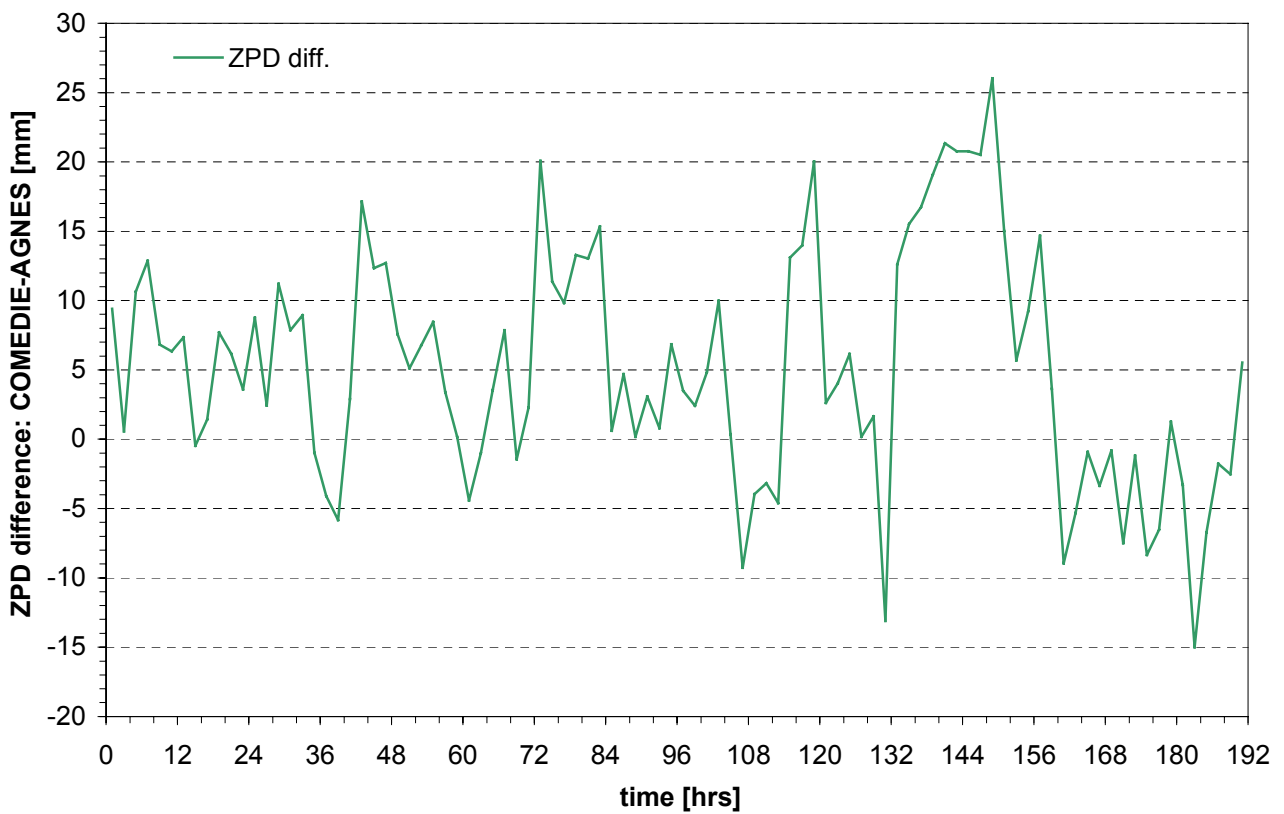


Figure 72. COMEDIE-AGNES ZPD differences at ZIMM

The COMEDIE-AGNES differences can be considered as ZPD residuals. They are a measure of the error between prediction and observation. In order to evaluate their accuracy, the Root Mean Square (RMS) and standard deviation have been computed for each AGNES station during the whole observation window and when data was available. The minimum, maximum and average ZPD residuals are also stated in Table 22 below.

The following statistics have been obtained:

AGNES Station ID	Statistical measure				
	Minimum [mm]	Maximum [mm]	Average [mm]	RMS [mm]	Stand. Deviation [mm]
ANDE	-24.68	20.82	-5.54	10.24	8.59
DAVO	-23.52	28.85	0.61	9.90	9.88
EPFL	-26.53	33.57	4.30	12.28	11.49
ETHZ	-17.57	30.35	5.04	11.07	9.84
FHBB	-20.25	35.03	-0.28	10.18	10.18
JUJO	-12.18	63.15	24.05	28.13	14.35
LOMO	-66.60	39.31	-18.31	33.62	28.12
NEUC	-14.58	22.06	1.89	7.39	7.14
PAYE	-9.89	8.14	-2.89	4.82	3.84
PFAN	-15.16	12.87	-2.39	7.83	7.45
ZIMM	-15.01	26.04	5.08	9.82	8.39

Table 22. COMEDIE-AGNES ZPD residuals statistics

Large discrepancies between the different AGNES stations used can be observed. Indeed the most Southeastern stations do have larger COMEDIE-AGNES ZPD difference variations. For instance, it is the case of Locarno-Monti (LOMO). This is supposedly due to the presence of the Alps mountains acting as climatic barrier. Further the wet air masses generally arrive over the zone of interest from the West and take time to cross the Swiss territory. This is taken into account via the signal part. The Jungfraujoch (JUJO) station has the largest mean difference. Due to lack of data from GPS stations at similar altitude, one should act with caution as far as the interpretation of the results from LOMO and JUJO is concerned.

The mean Root Mean Square (RMS) of all eleven AGNES stations is 13.85 mm and thus just above 1 centimeter. This is good when compared to other techniques of ZPD estimation. The RMS is a fairly constant value with, again, the exception of JUJO and LOMO. The standard deviation of JUJO is only 14.35 mm while its RMS is 28.13 mm, almost two times larger! This implies that the reliability of the JUJO ZPD estimates is low. One should consider discarding JUJO from further evaluations.

The mean standard deviation of the eleven AGNES GPS stations is evaluated at 10.84 mm. This is almost 3 mm less than the average RMS. Payerne (PAYE) has the lowest sigma level. This was already the case with the RMS. Thus the PAYE location seems to deliver good and reliable ZPD estimates. However one should remark that it has been observed only during the first four days.

In order to determine the possible correlation between average, standard deviation and RMS of the COMEDIE-AGNES ZPD differences with the altitude of the GPS stations, these have been plotted on Figures 73 to 75.

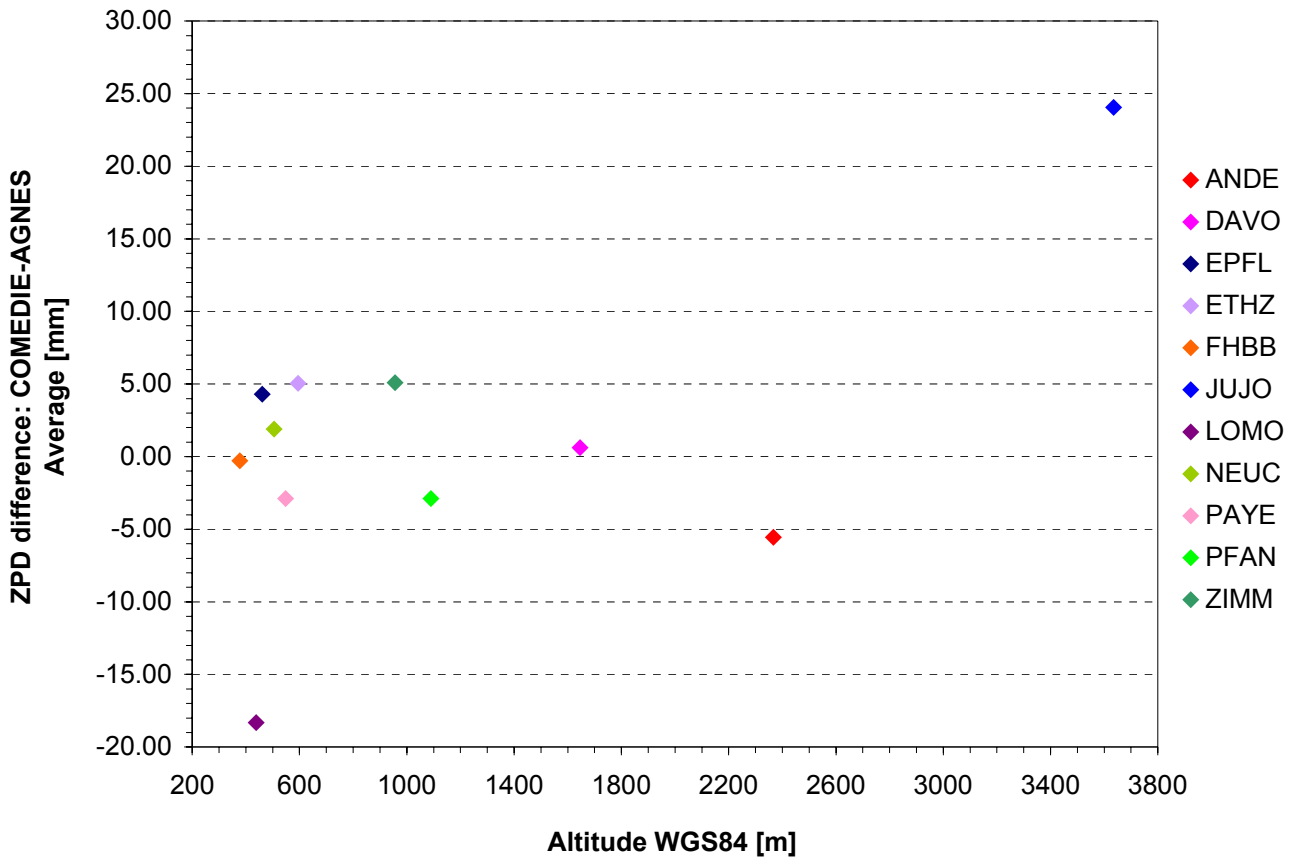


Figure 73. Average COMEDIE-AGNES ZPD difference as function of the GPS stations altitude

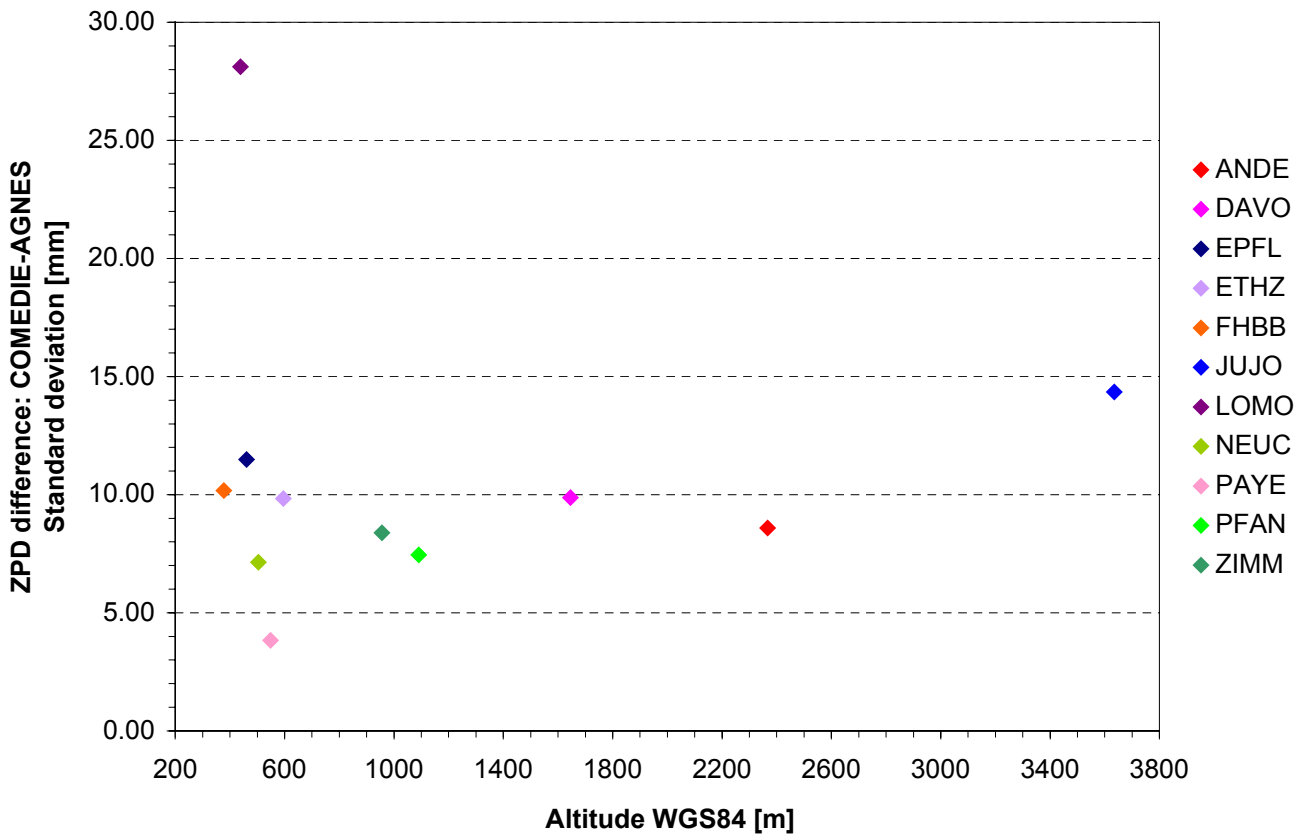


Figure 74. Standard deviation of COMEDIE-AGNES ZPD difference as function of the GPS stations altitude



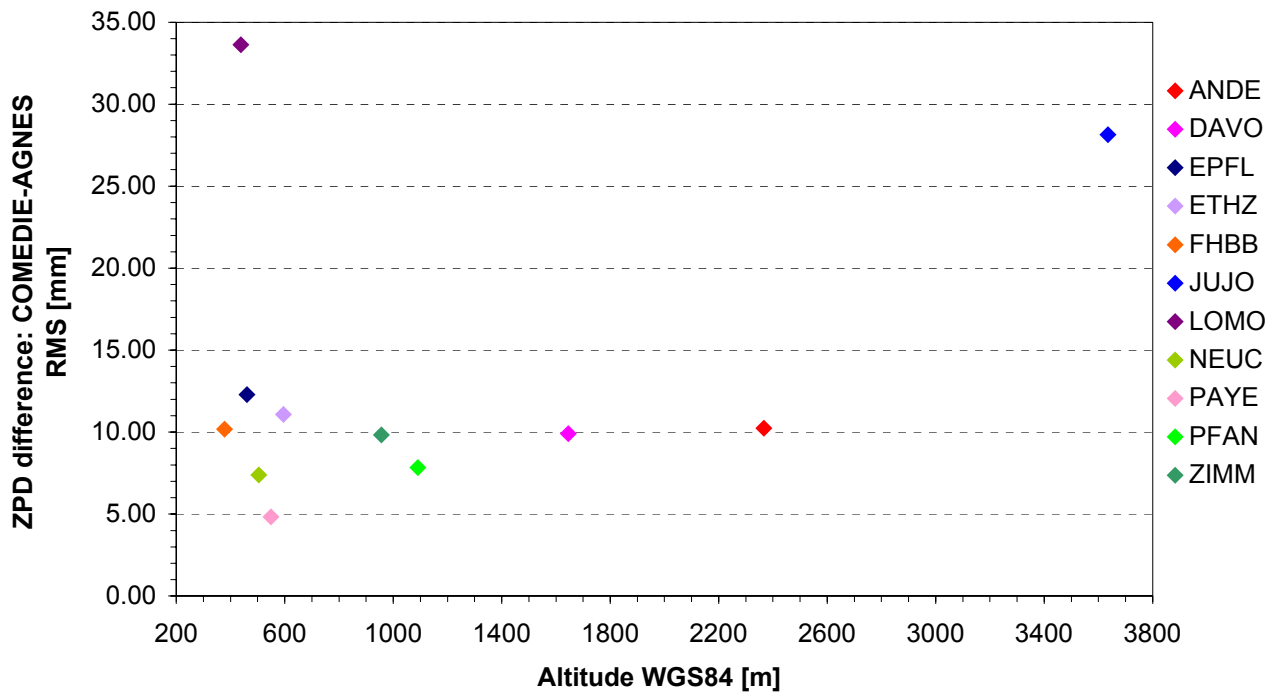


Figure 75. RMS of COMEDIE-AGNES ZPD difference as function of the GPS stations altitude

If one discards the JUJO and LOMO GPS stations, there appear to be no correlation between altitudes of the GPS receivers and average, RMS and standard deviation of the COMEDIE-AGNES ZPD differences. Note that variations of approximately 2 cm on the network are expected. The RMS and standard deviations are below 15 mm while the average varies between  $\pm 5$  mm. Therefore the results obtained and plotted on Figures 73 to 75 lead to the conclusion that the functional model used is relatively accurate.

#### 4.3.3.5. AGNES stations ZPD forecasts

In the previous paragraph, it has been seen that one could gain important knowledge about an AGNES permanent GPS station without knowing anything about it except its location. This was a first success. It is now intended to investigate whether or not one can also predict the ZPD at this very same station for a future epoch. The certainty and accuracy of the forecast are also determined.

The observation window is again starting on Monday 22 May 2000 at 00:00:00 UTC and ending on Tuesday 30 May 2000 at 00:00:00 UTC. The time counter has been set to zero at the start of the observation window. The time lag is two hours.

The collocation is performed between Monday 22 May 2000, 00:00:00 UTC and Friday 26 May 2000, 00:00:00 UTC. The parameters determined in the *last* 12 hours<sup>17</sup>, i.e. between Thursday 25 May 2000 12:00:00 UTC and Friday 26 May 2000, 00:00:00 UTC, are inserted in the extrapolation algorithm to produce ZPD estimates (forecasts) between Friday 26 May 2000, 00:00:00 UTC and Tuesday 30 May 2000, 00:00:00 UTC. The time threshold is thus on Friday 26 May 2000 at 00:00:00 UTC for the transition period (blue vertical line on the figures) and on Saturday 27 May 2000 at 00:00:00 UTC for the extrapolation (pink vertical line on the figures). This corresponds respectively to 96.00 hours and 108.00 hours since the time counter starts. The extrapolation time step is approximately 1 minute (exactly 0.017 hours).

The ZPD forecasts for all eleven AGNES stations of Table 19 are plotted on Figures 76 to 86. As the collocation procedure is the same one as in paragraph 4.3.3.3, the results are similar in the time period stretching from Monday 22 May 2000 at 00:00:00 UTC to Friday 26 May 2000 at 00:00:00 UTC. In the first 12 hours of the extrapolation time window ( $t = 108.00$ - $120.00$  hours), some damped oscillations of the ZPD forecast are observed. Afterwards, the ZPD estimates seem to gradually stabilize around a nearly constant value. However, the ZPD values obtained from observations made at the AGNES station continue to strongly vary. There are hence large discrepancies between the ZPD forecast and the future ZPD observation. Note that JUJO provides as before no meaningful results due to lack of data from other AGNES stations at similar altitude.

<sup>17</sup> The parameters are determined over a central period of 12 hours and with the injection of data from 12 hours before and after it. Therefore they correspond to a 36 hours time period but with validity only for the central period.

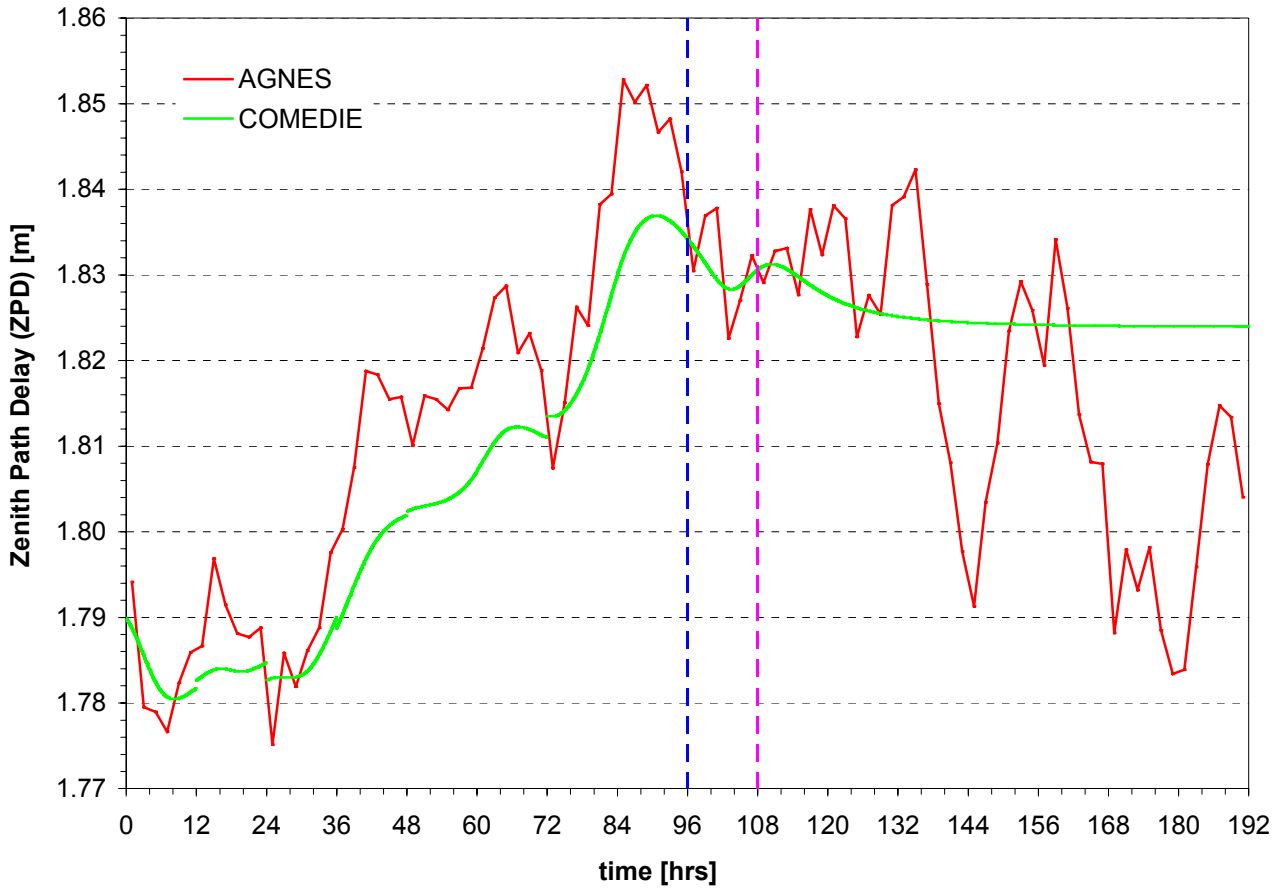


Figure 76. COMEDIE ZPD forecast at ANDE

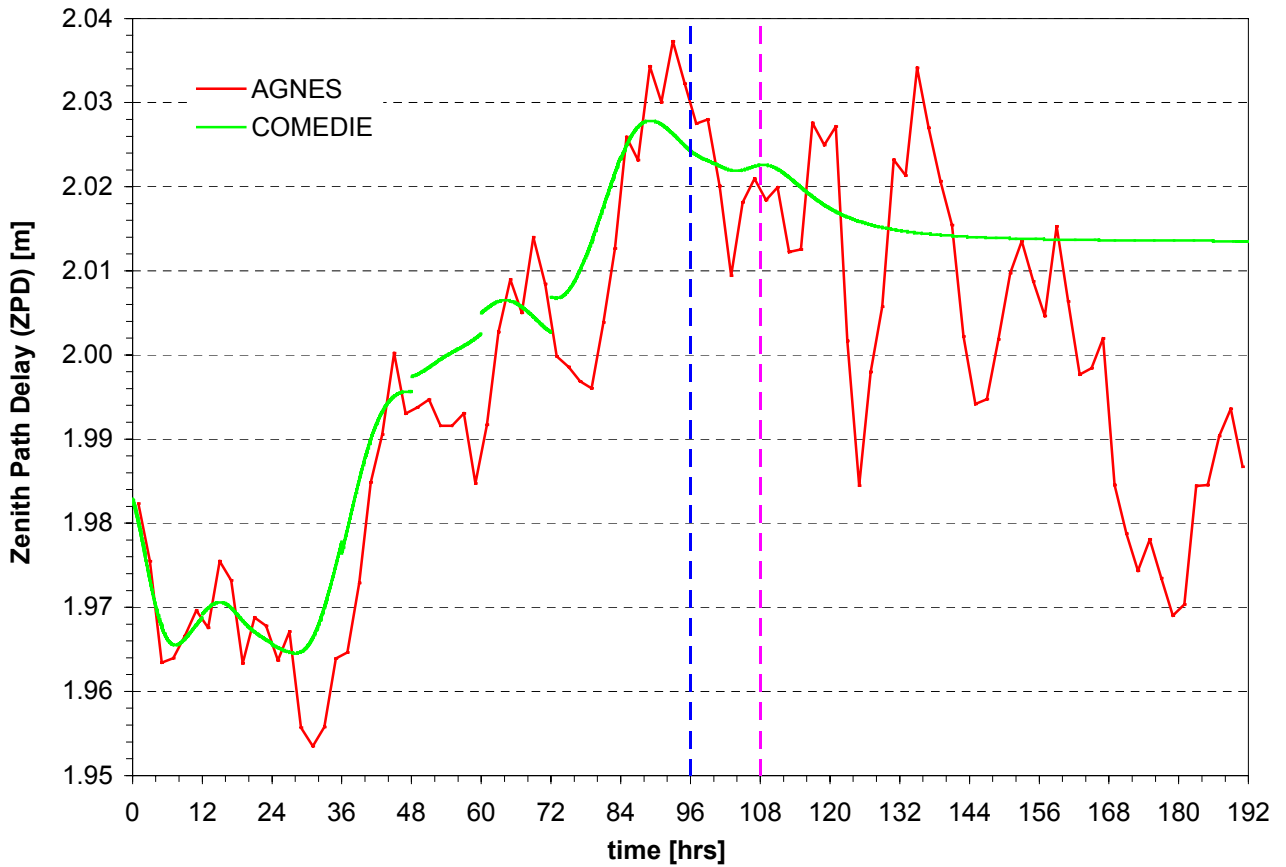


Figure 77. COMEDIE ZPD forecast at DAVO

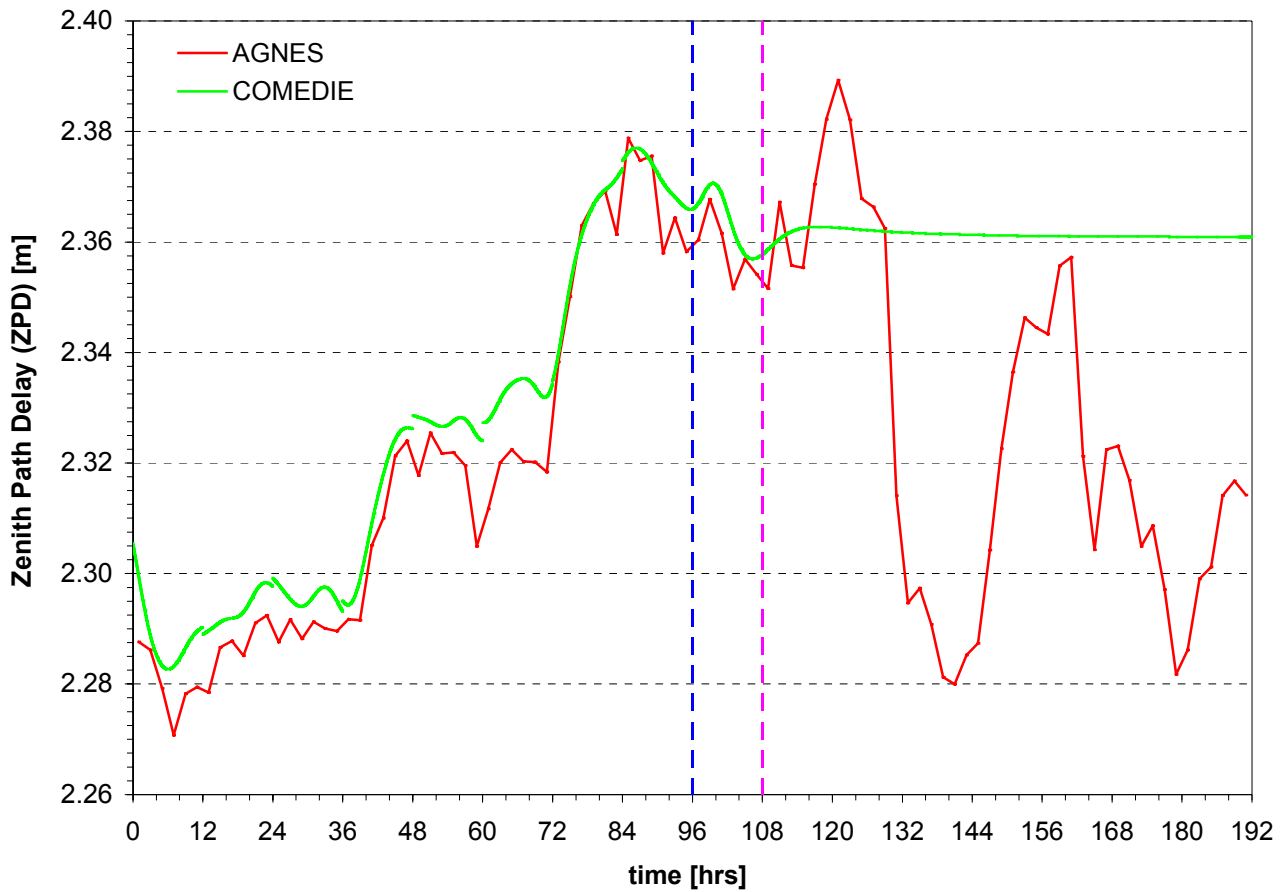


Figure 78. COMEDIE ZPD forecast at EPFL

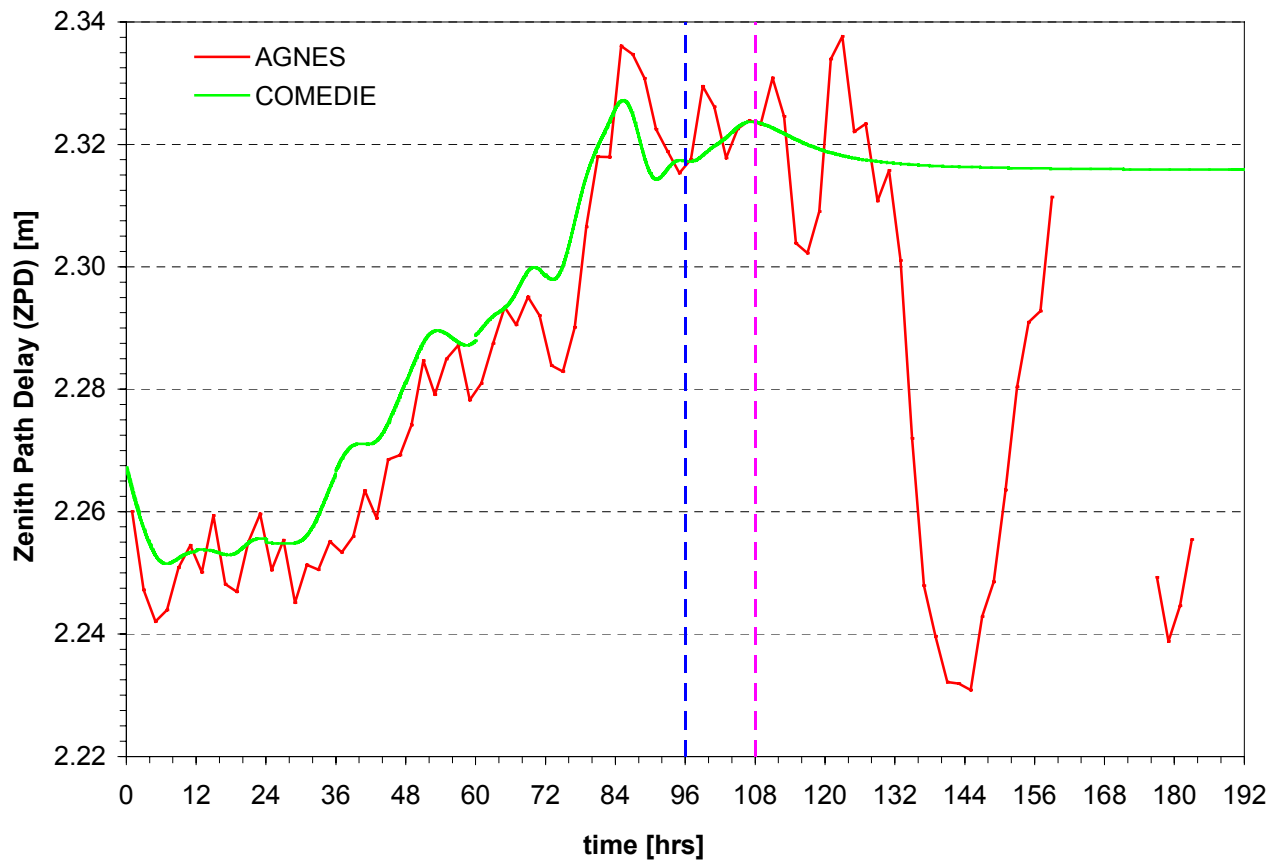


Figure 79. COMEDIE ZPD forecast at ETHZ

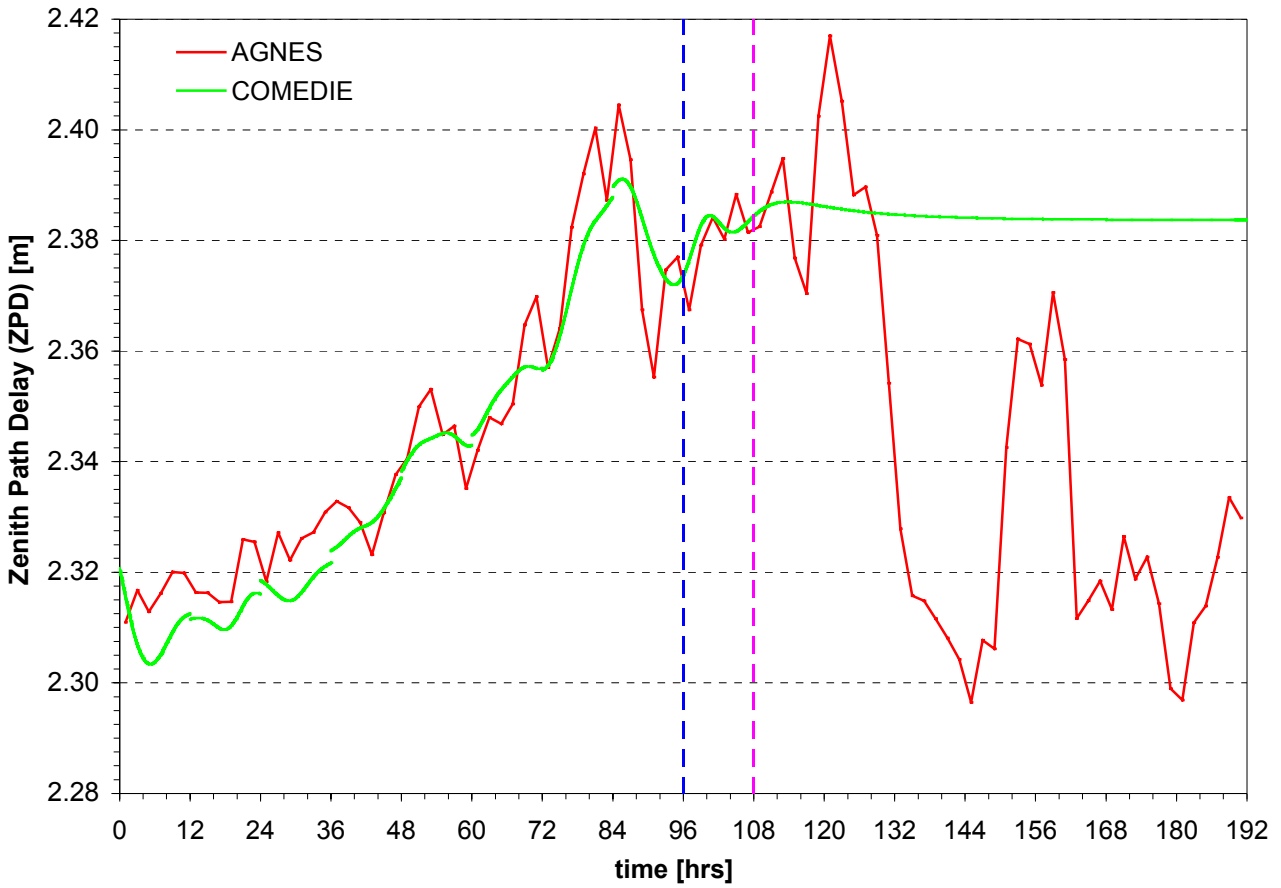


Figure 80. COMEDIE ZPD forecast at FHBB

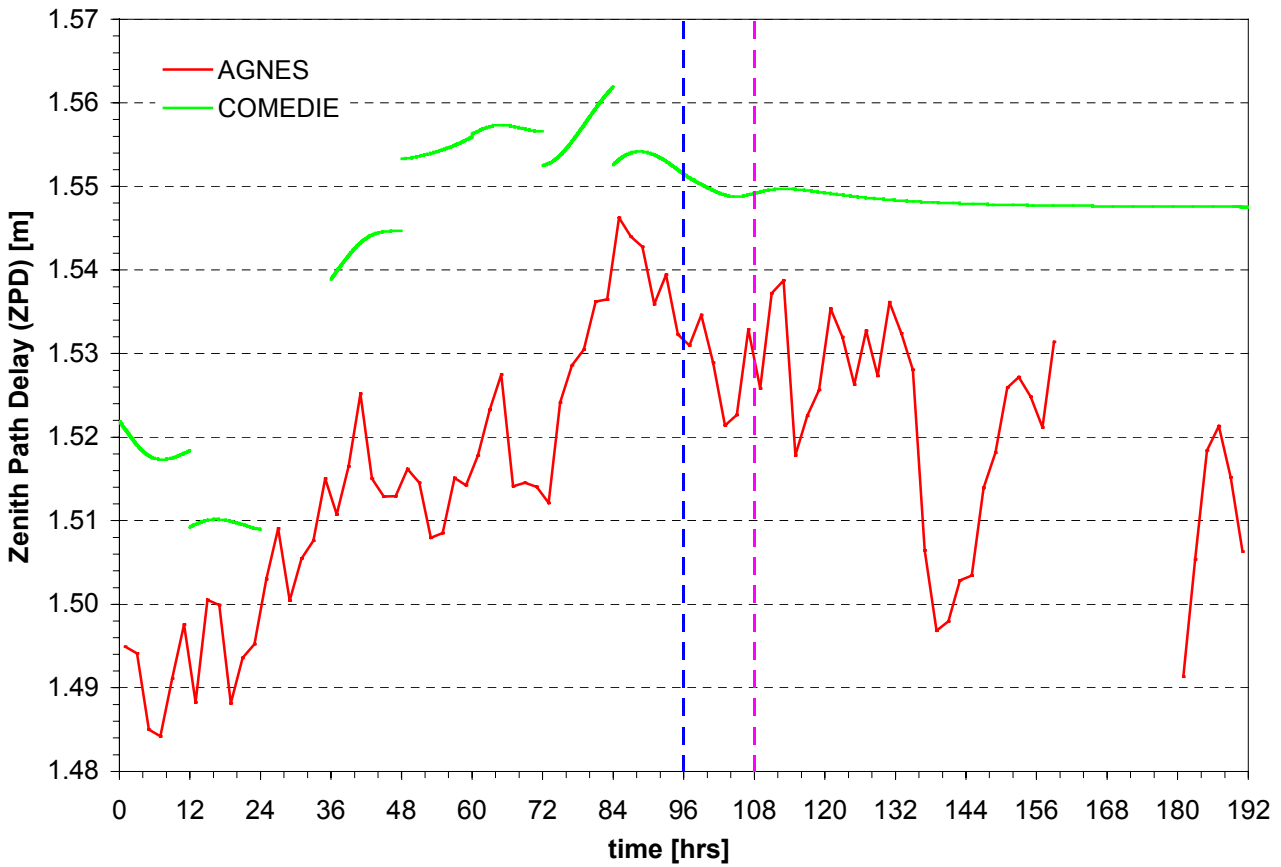


Figure 81. COMEDIE ZPD forecast at JUJO

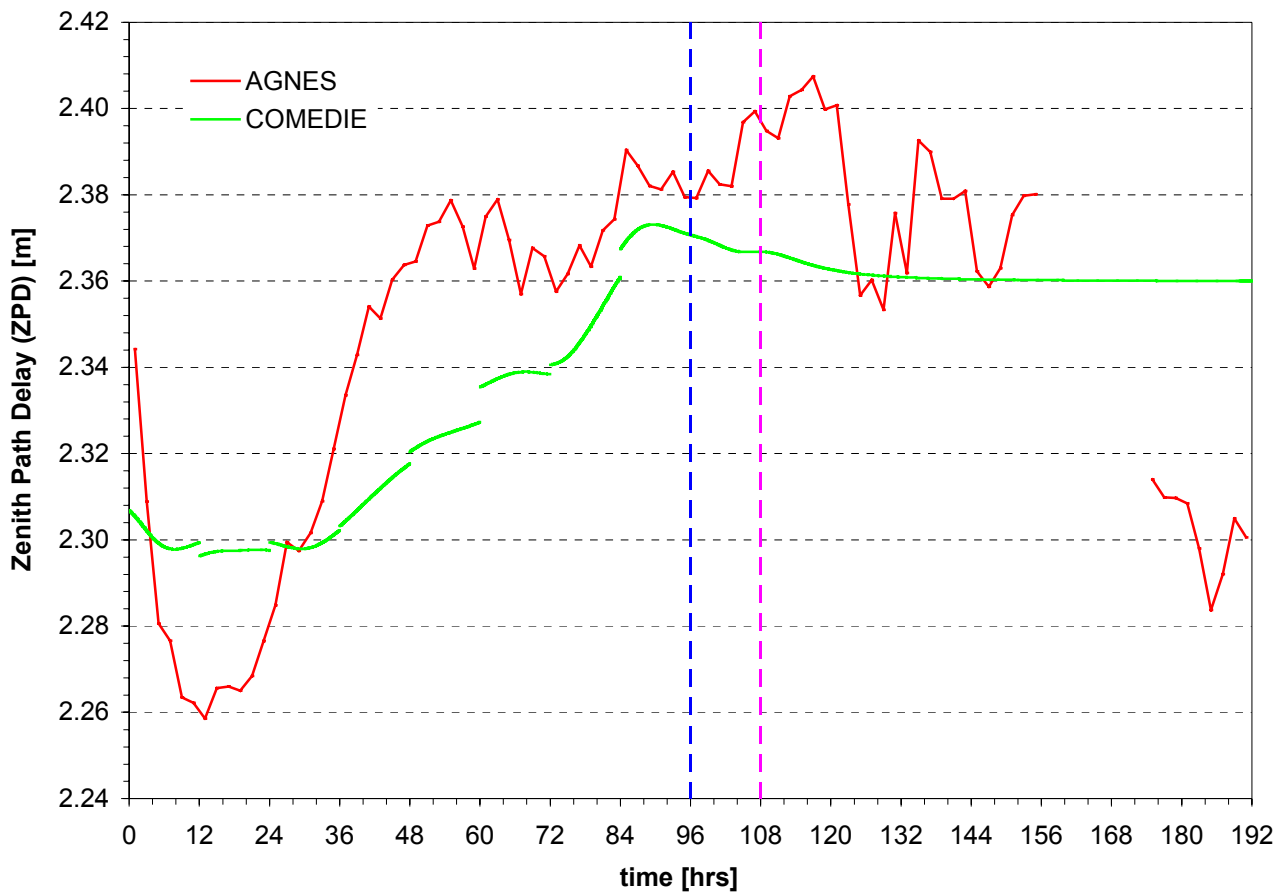


Figure 82. COMEDIE ZPD forecast at LOMO

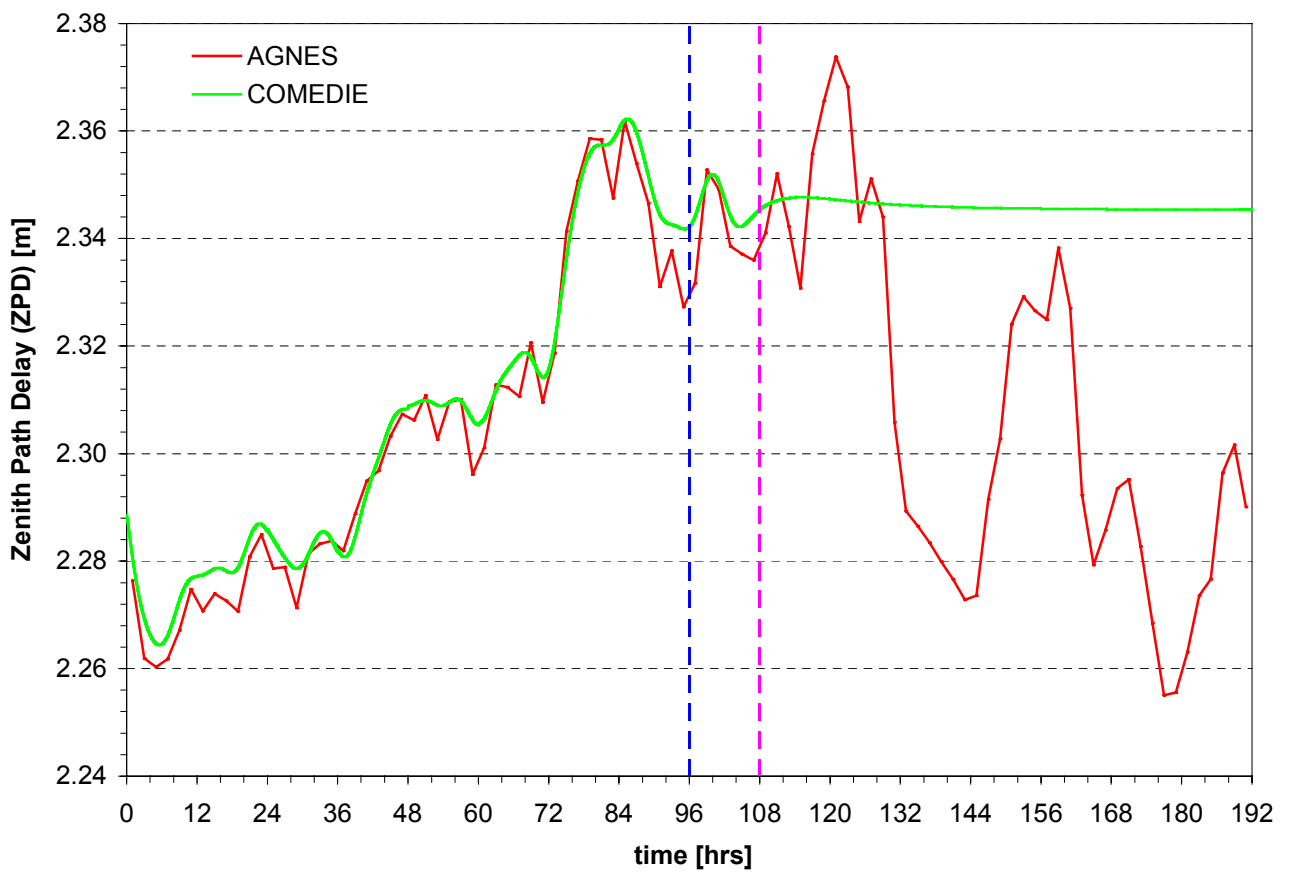


Figure 83. COMEDIE ZPD forecast at NEUC

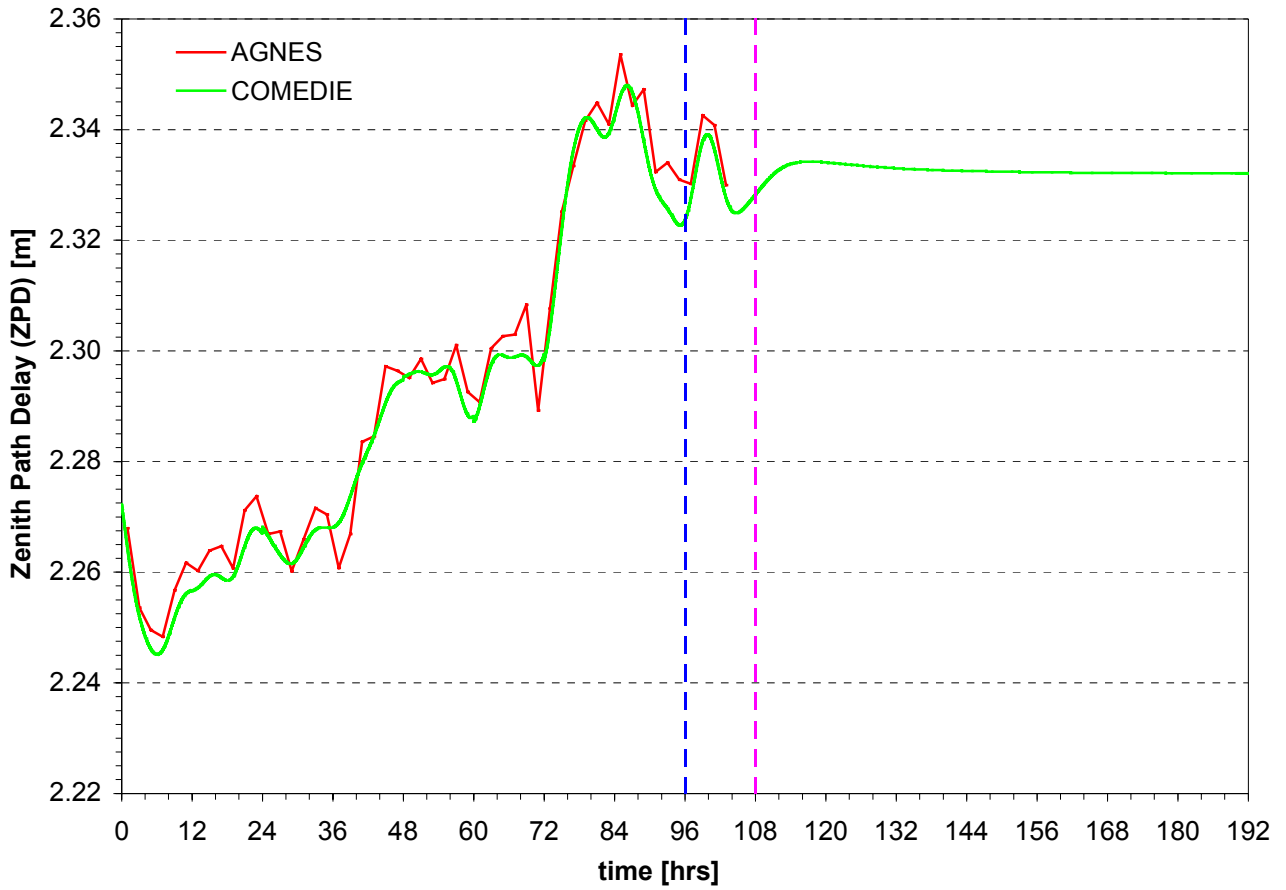


Figure 84. COMEDIE ZPD forecast at PAYE

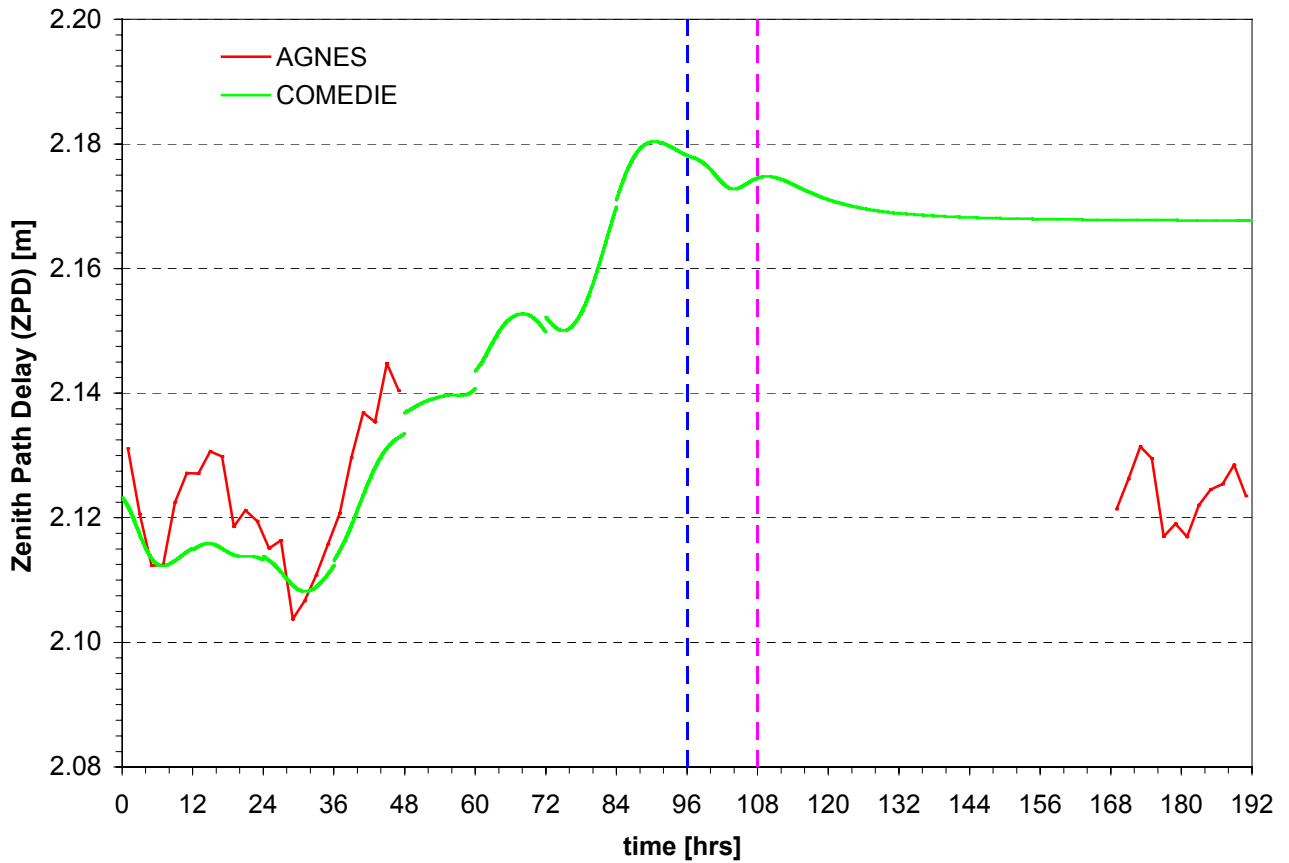


Figure 85. COMEDIE ZPD forecast at PFAN

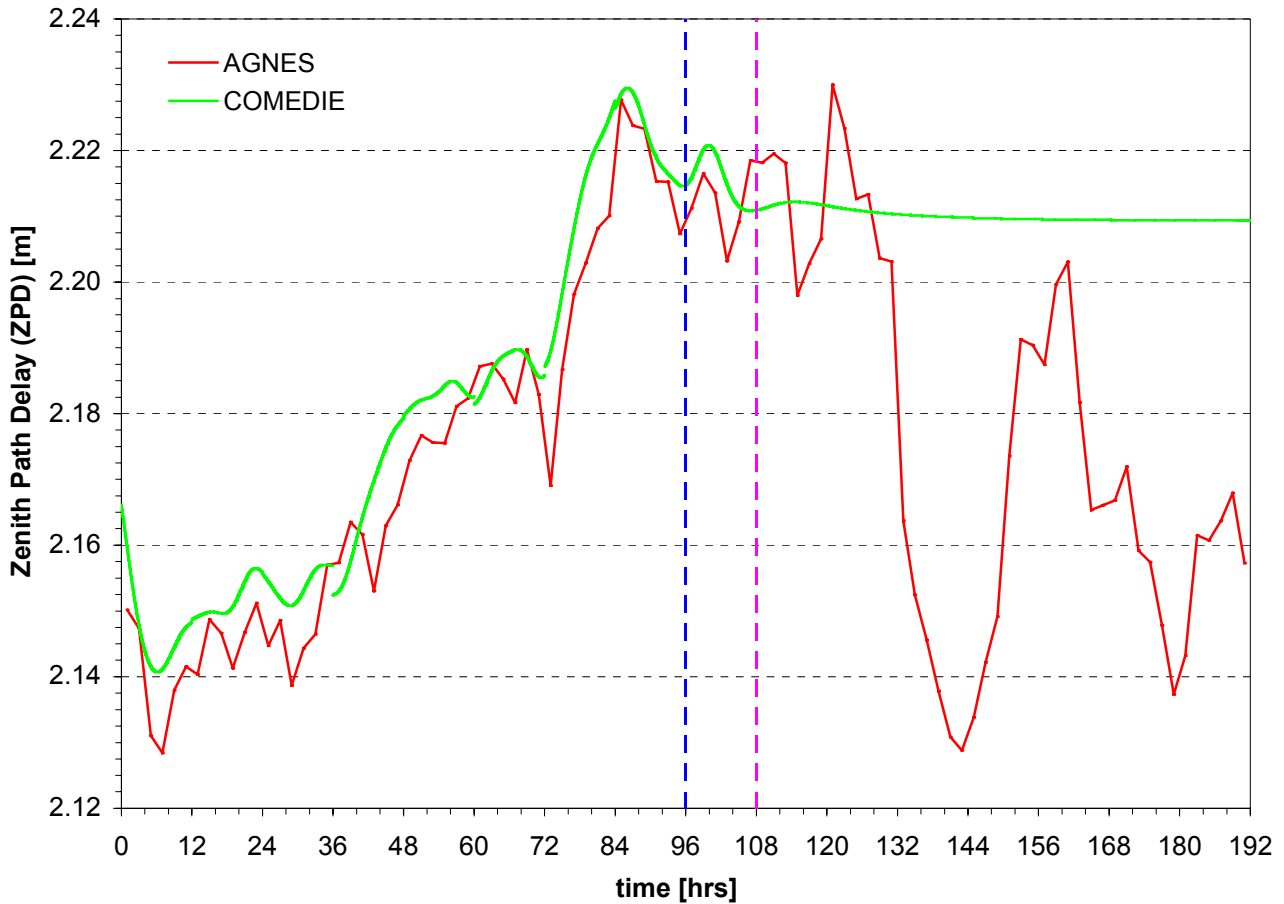


Figure 86. COMEDIE ZPD forecast at ZIMM

#### 4.3.3.6. AGNES stations ZPD forecasts quality assessment

In order to evaluate the quality and certainty of the ZPD forecast, the COMEDIE-AGNES ZPD differences are computed for the first few hours after the start of the extrapolation. The time leg for comparison is determined by the AGNES ZPD observations frequency as one has fewer observations than ZPD estimates from COMEDIE. Thus one can compare data only every two hours.

The COMEDIE ZPD forecasts and AGNES ZPD observations allow gaining an approximate knowledge on the certainty of the prediction that has been made. One discerns two groups of stations. The classification is derived from the amplitude of the ZPD forecasts differences. Note that it has not been possible to evaluate those differences at Pfänder (PFAN) as it could not be observed during that time period. The two groups are plotted on Figures 87 and 88.

According to Figures 87 and 88, the results are surprisingly good. Indeed the variations are all centered in a stream of radius 40 mm. Remark that LOMO diverges during the whole transition and extrapolation time window. From  $t = 118.00$  hours onwards, the COMEDIE forecast-AGNES observation ZPD differences tend to increase rapidly. Table 23 gives the number of hours during which the 1-centimeter accuracy level is maintained.

Time [hrs]	Time length extrapolation [hrs]	AGNES station
113	5	ETHZ, NEUC, ZIMM
115	7	DAVO
117	9	ETHZ, FHBB
119	11	ANDE
-	-	JUJO, LOMO, PAYE, PFAN

Table 23. Time response for 1cm accuracy level

One can see that for half of the AGNES stations surveyed it is possible to yield to a *meaningful forecast during 9 hours after the last data were available*. The average, standard deviation and RMS of the differences are plotted as

function of the extrapolation time on Figures 89 to 95. The time counter is set to zero at 96.00 hours. The extrapolation time threshold is again set at 108.00 hours and represented by a pink vertical line. For clarity purposes two groups are distinguished.

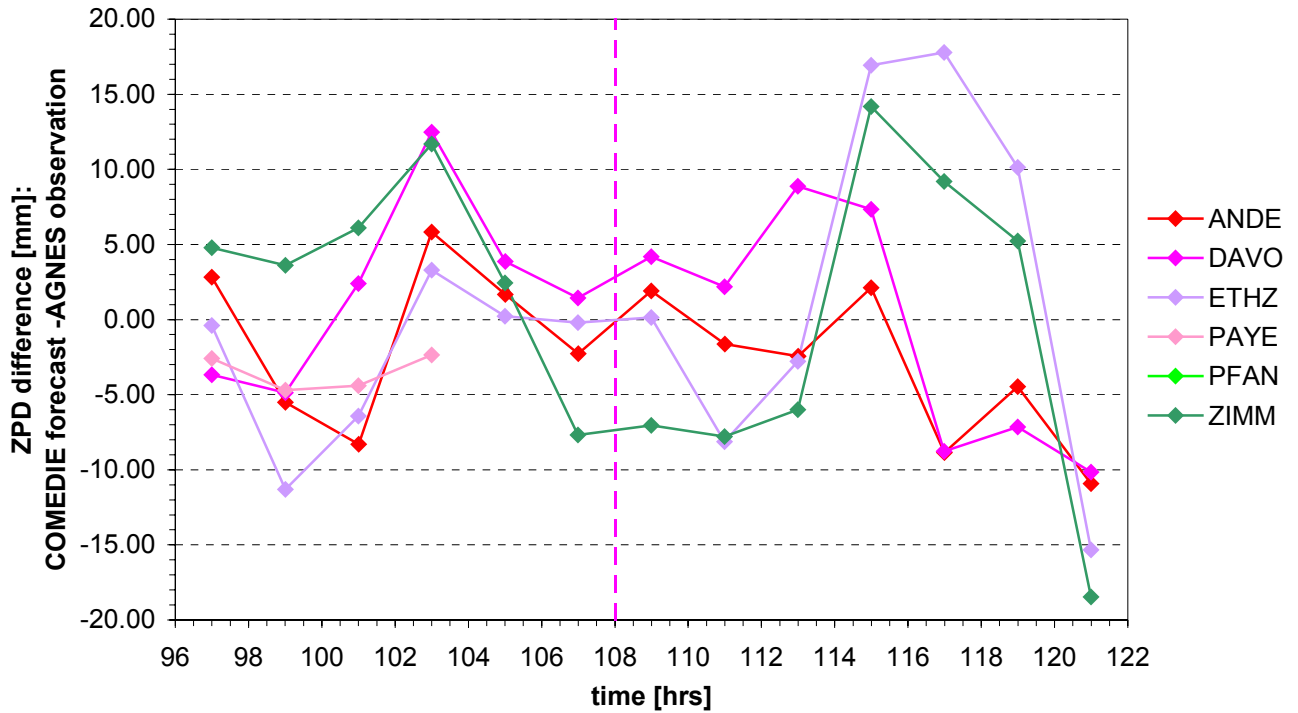


Figure 87. ZPD differences between COMEDIE forecasts and AGNES observations, Group 1

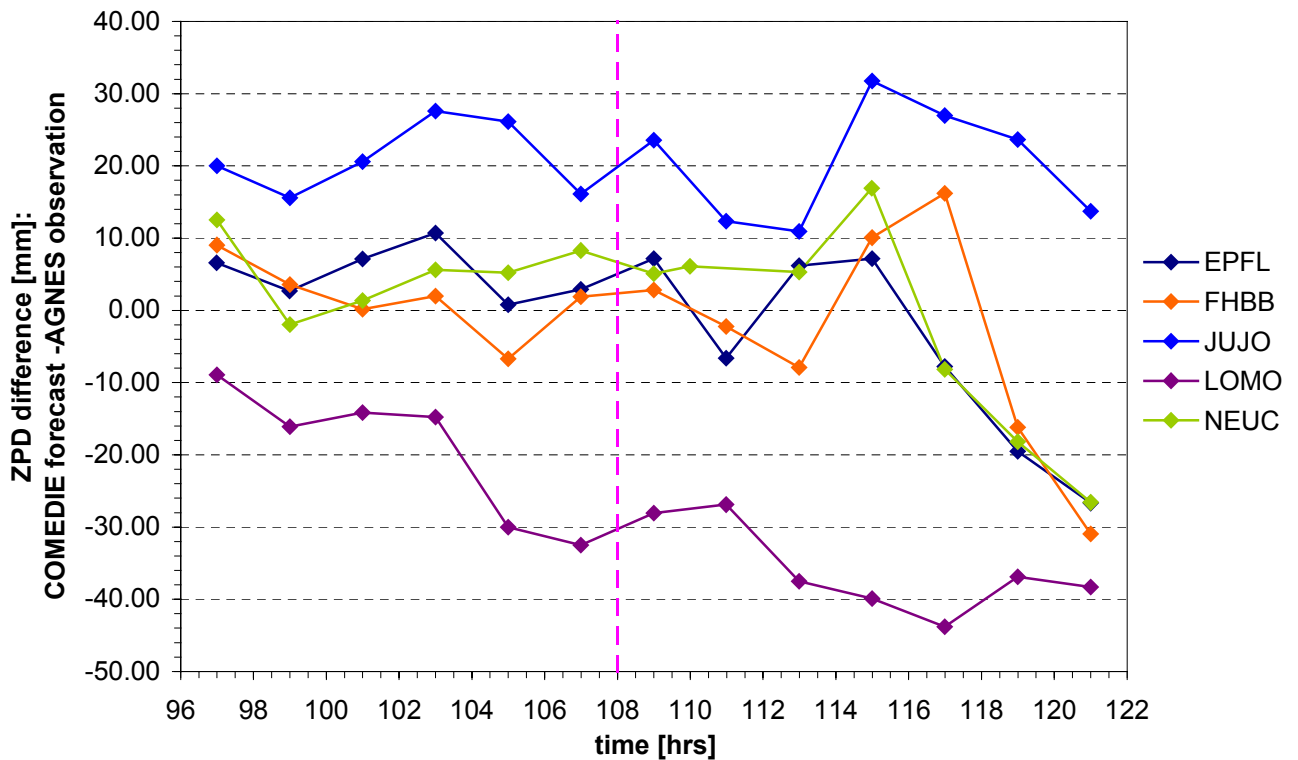


Figure 88. ZPD differences between COMEDIE forecasts and AGNES observations, Group 2

The mean of the average ZPD differences, standard deviation and RMS is plotted in a red dashed line.

The averages of the ZPD differences seem to converge against zero, as one can see on Figures 89 and 91. The influence of the last collocation diminishes rapidly with the extrapolation time. Indeed the longer one extrapolates the less information one has from the signal share. The ZPD is then fully given by the functional model. Hence



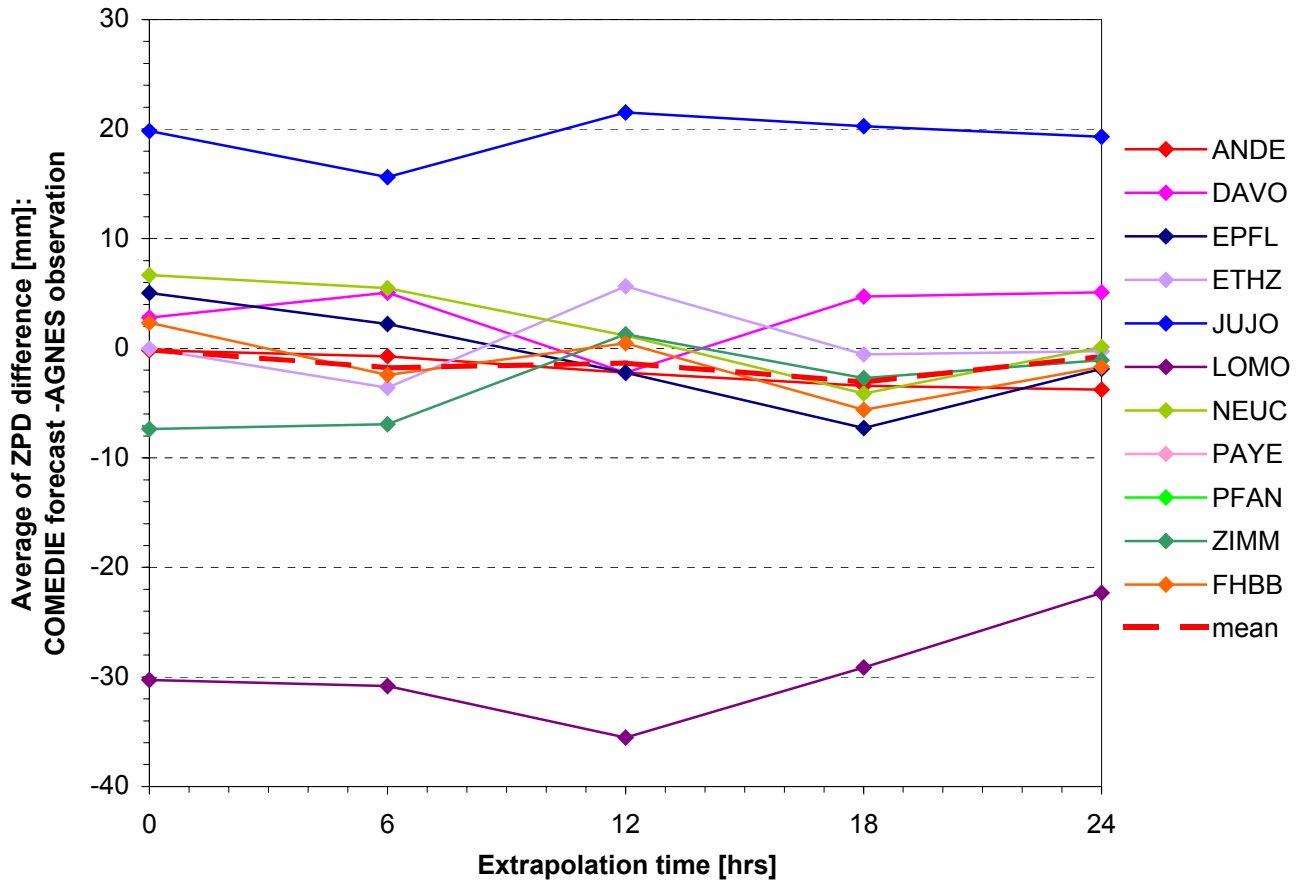


Figure 89. Average of COMEDIE ZPD forecast – AGNES ZPD observation as function of the extrapolation time

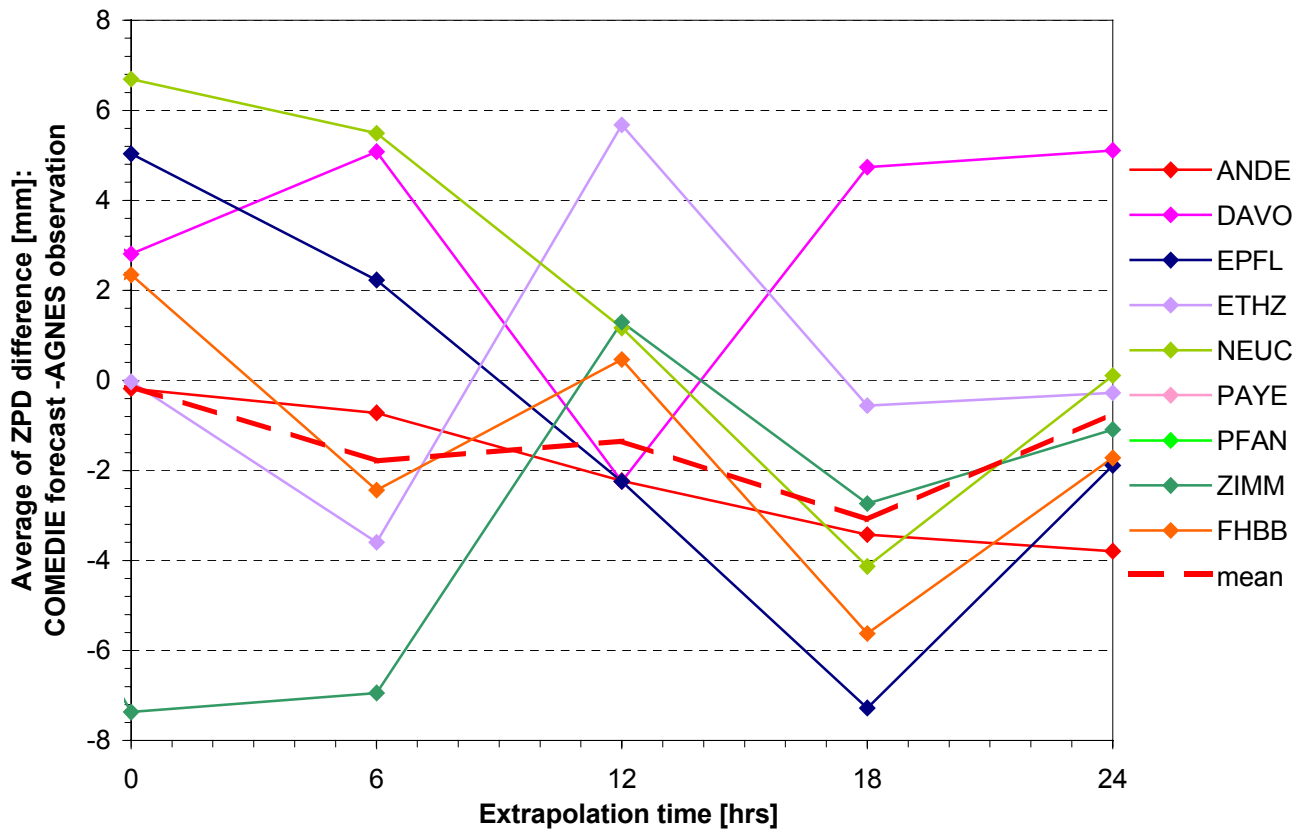


Figure 90. Average of COMEDIE ZPD forecast – AGNES ZPD observation as function of the extrapolation time. Group 1

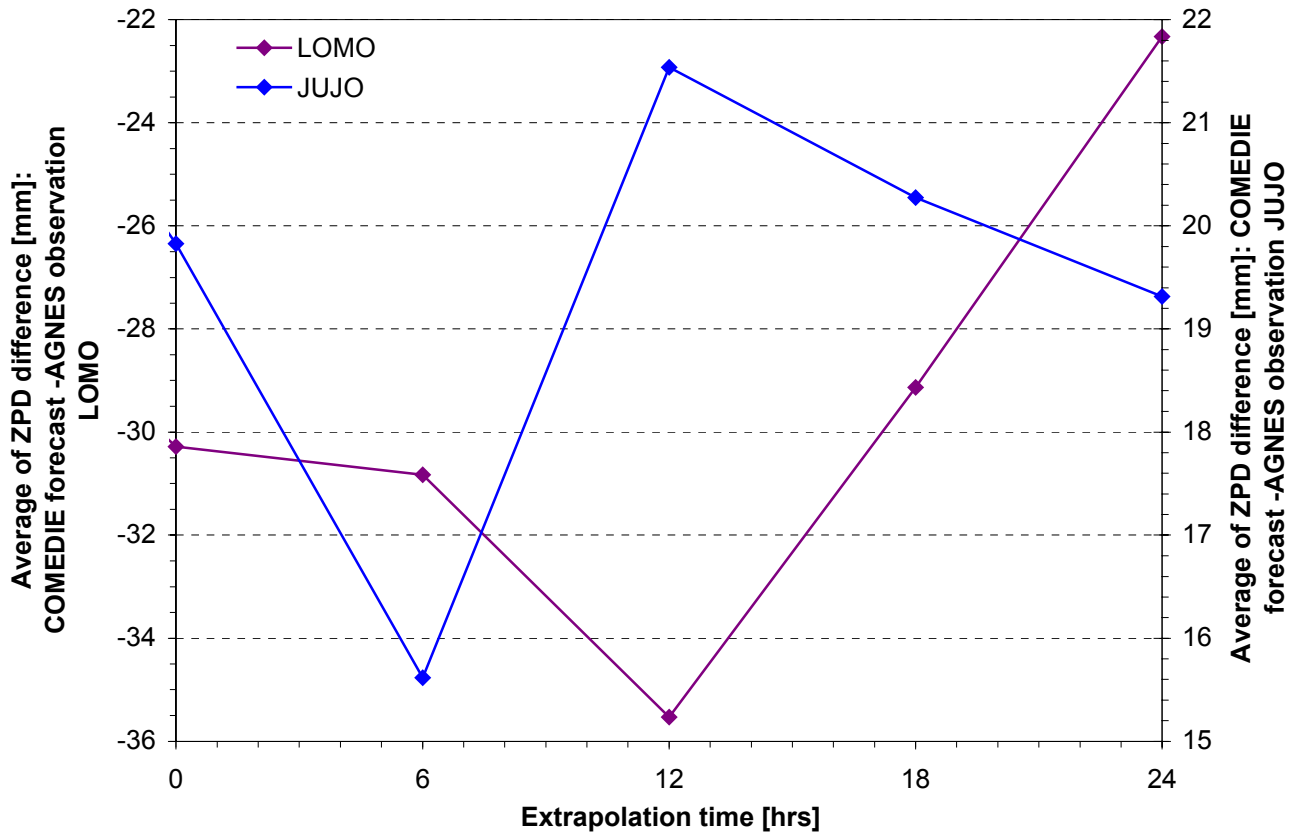


Figure 91. Average of COMEDIE ZPD forecast – AGNES ZPD observation as function of the extrapolation time. Group 2

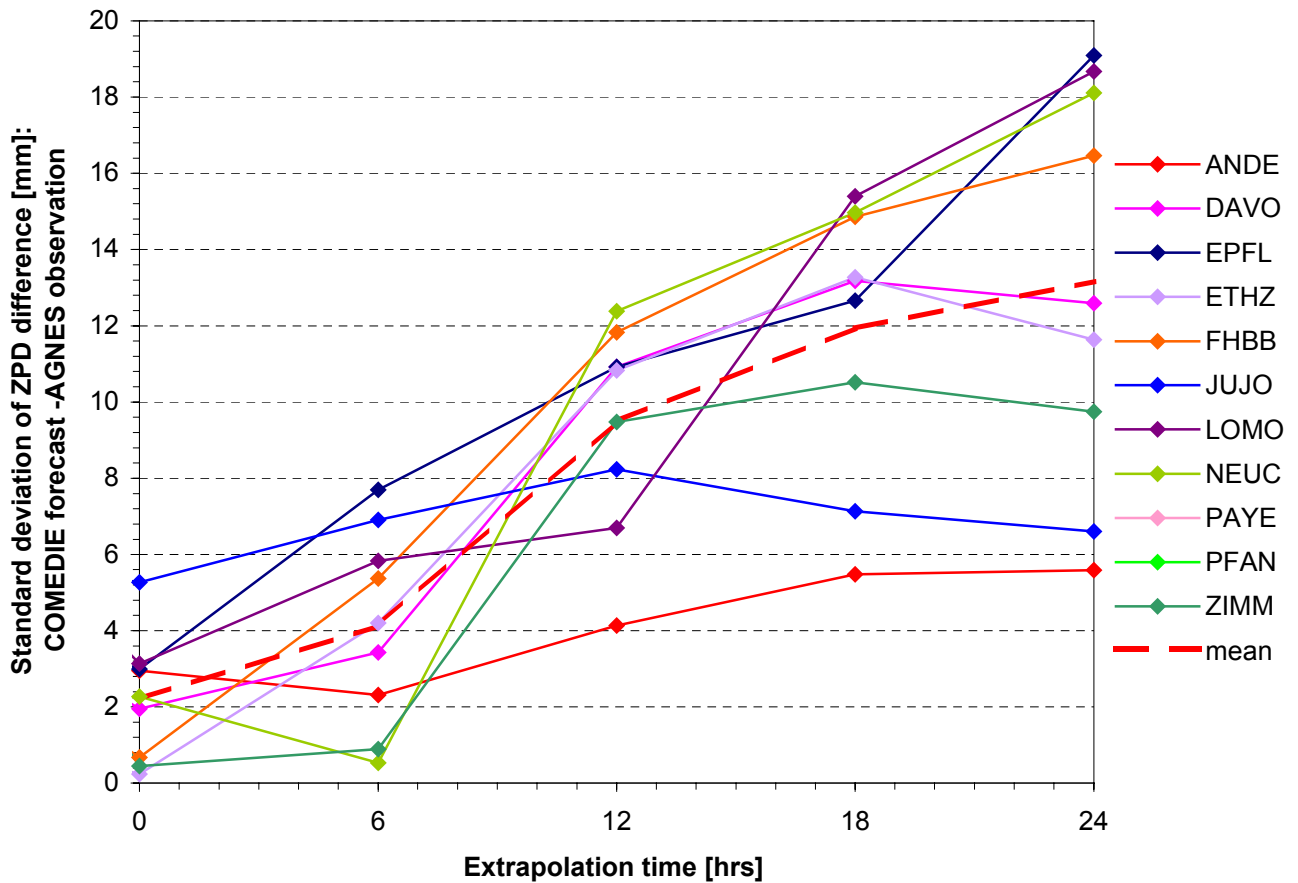


Figure 92. Standard deviation of COMEDIE ZPD forecast – AGNES ZPD observation as function of the extrapolation time

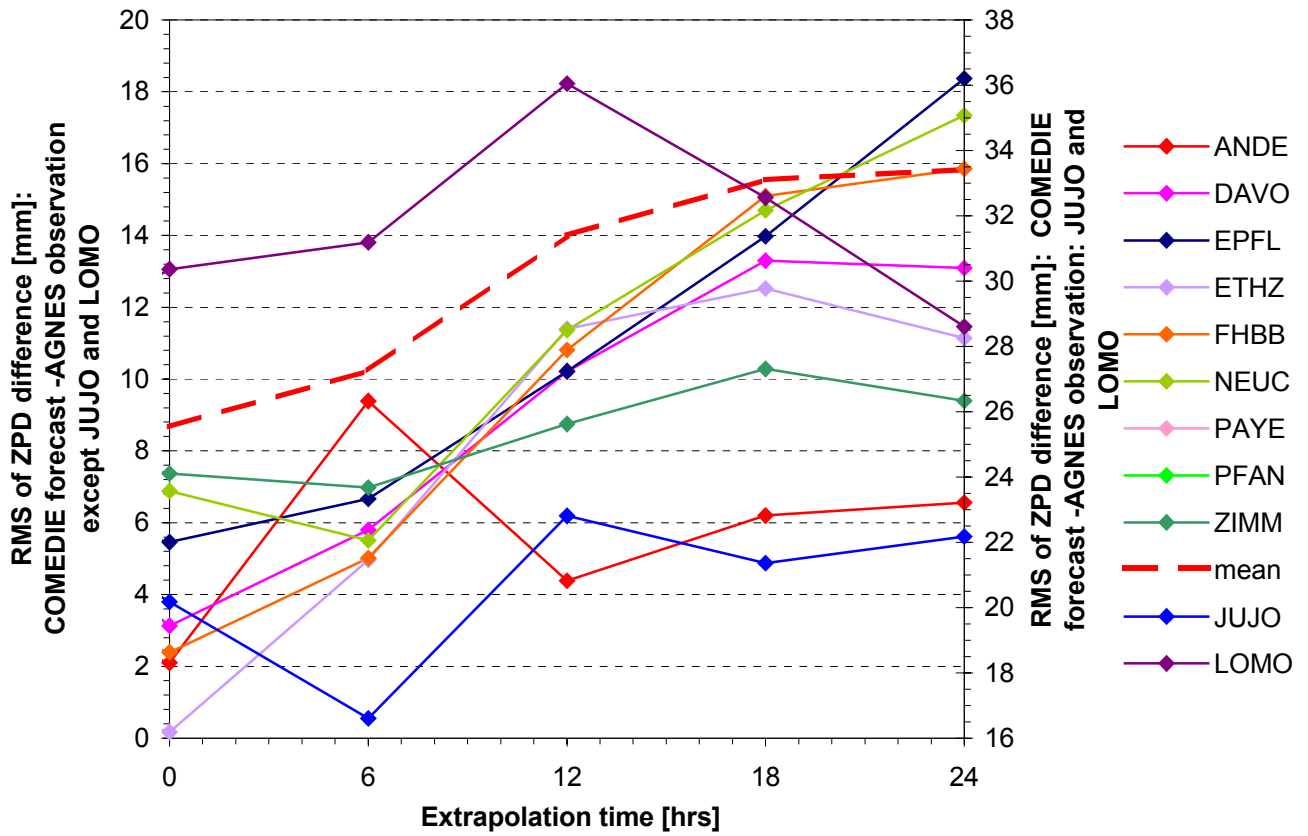


Figure 93. RMS of COMEDIE ZPD forecast – AGNES ZPD observation as function of the extrapolation time

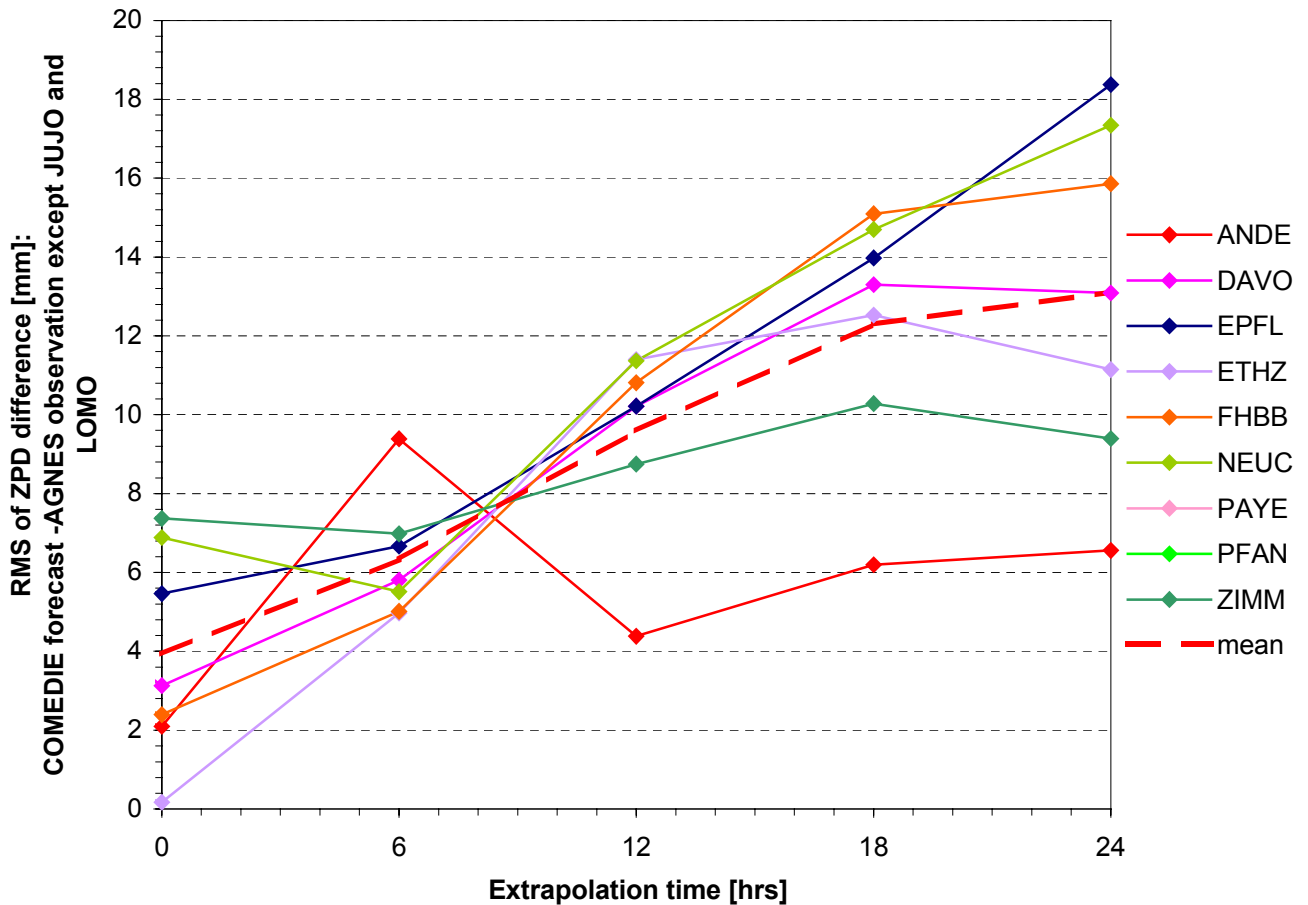


Figure 94. RMS of COMEDIE ZPD forecast – AGNES ZPD observation as function of the extrapolation time. Group 1

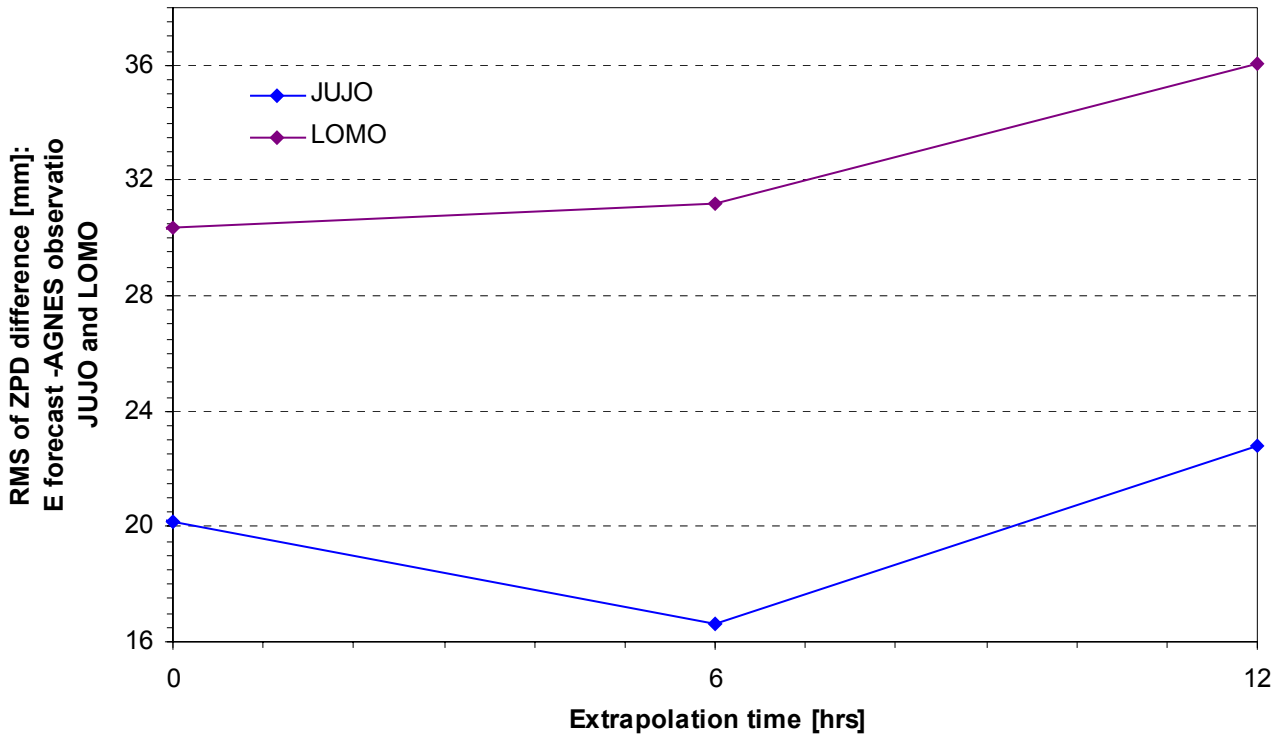


Figure 95. RMS of COMEDIE ZPD forecast – AGNES ZPD observation as function of the extrapolation time. Group2

should one intend to know the convergence value of the ZPD, he or she should compute the value of the ZPD of the functional model using the last set of parameters determined by the collocation just before starting the extrapolation. Note that JUJO and LOMO are offset. The reason for this behavior is probably the one assumed until then: lack of data at similar altitude (JUJO) and in the same region (LOMO) due to the presence of a microclimate (presence of the Alps mountains as climatic barrier).

It can be noted on Figure 92 that the standard deviation increases with the extrapolation time and thus the quality of the prediction itself. Except for Davos (DAVO) and Andermatt (ANDE), it is less than 1 centimeter during the first 6 hours of the extrapolation. It seems to diverge for long extrapolation periods, i.e. for predictions far in the future.

The RMS of Figures 93 to 95 has a similar behavior to the standard deviation. However the amplitude of the RMS is larger than of the standard deviation. It is less than 1 centimeter for all AGNES stations of consideration, during the first 6 hours of the forecast except for LOMO. It does not diverge for all AGNES stations surveyed, for instance ANDE. As Andermatt is quite isolated and relatively high compared to the rest of the network, this might explain the - somewhat - unexpected behavior. This needs however to be further investigated. On the other hand, EPFL grows rapidly and does not seem to increase slower with the extrapolation time. It shows that one cannot predict with accuracy over a long time.

The mean of the average, standard deviation and RMS of the ZPD differences are calculated. The statistical results are summarized in Table 24 hereunder:

Time [hrs]	Extrapolation time [hrs]	Statistical quantity		
		Average [mm]	Standard deviation [mm]	RMS [mm]
108.00	0	-0.13	2.21	8.67
114.00	6	-1.79	4.13	10.24
120.00	12	-1.34	9.49	14.00
126.00	18	-3.10	11.94	15.55
132.00	24	-0.73	13.17	15.84

Table 24. COMEDIE forecast-AGNES observation residuals statistics

According to Table 24, the average standard deviation for all 11 AGNES stations of Table 19 during the first 6 hours of the forecast is 4.13 mm. However, the RMS for the very same time period has already reached the 1-centimeter threshold. On the other hand, *the average is still inferior to the 1 cm threshold during the first 12 hours of the prediction*. This implies that one can perform a satisfactory prediction of the Zenith Path Delay twelve hours in advance!

Furthermore it has been proceeded with a linear regression of the mean of the standard deviation of the COMEDIE forecast-AGNES observation ZPD differences. The equation gives the approximate numerical extrapolation error law. It enables to determine the average growth rate of extrapolation error. The same has been performed for the envelope, i.e. for the maximal value of the standard deviation as it is plotted on Figure 92. The time  $t$  is stated in hours since the beginning of the extrapolation. For the linear regression of the mean of the standard deviation, this yields to

$$\sigma_{mean} = 0.4953 \cdot t + 2.2454 \quad (4.3.3.6.1)$$

with an R-squared ( $R^2$ ) value of

$$R_{mean}^2 = 0.9523 \quad (4.3.3.6.2)$$

The R-squared value measures the proportion of the total variance in  $\sigma$  that can be explained by time shifts. Thus the mean extrapolation error growth rate (EGR) is

$$mean \text{ extrapolation } EGR = 0.4953 \text{ mm} \cdot \text{hr}^{-1} \quad (4.3.3.6.3)$$

The offset at the start of the extrapolation i.e. at  $t = 108.00$  hours (on Friday 26 May 2000 at 00:00:00 UTC) since the beginning of the observation window is 2.2454 millimeters. It not equal to zero as the standard deviation at  $t = 0.00$  hours<sup>18</sup> is computed from data for the time period between  $t = -1.00$  hours and  $t = 1.00$  hours. The computation of the standard deviation at  $t = 0.00$  hours is considered as the weak point of this error analysis.

As far as the linear regression of the maximum of the standard deviation is concerned, one obtains

$$\sigma_{max} = 0.5891 \cdot t + 4.8987 \quad (4.3.3.6.4)$$

and an R-squared value of

$$R_{max}^2 = 0.9931 \quad (4.3.3.6.5)$$

Therefore the maximum extrapolation error growth rate is

$$max. \text{ extrapolation } EGR = 0.5891 \text{ mm} \cdot \text{hr}^{-1} \quad (4.3.3.6.6)$$

which is almost 20 % larger than the average extrapolation error growth rate!

#### 4.3.3.7. AGNES stations ZPD forecasts operational quality assessment

It is now intended to answer the following question: “What is the extrapolation error of the ZPD difference between COMEDIE forecast and AGNES observation for a given survey time ?” For instance, one observes ZPDs at one AGNES station, say Zimmerwald (ZIMM). For one reason or other, one cannot further survey at ZIMM. And one is interested to know what error should be expected if one measures in 15.00 hours from now.

Conversely to paragraph 4.3.3.6. where the statistics are computed over an extrapolation time period stretching from  $t = 0.00$  hours to  $t = t_{threshold}$  in hours, this time,  $t$  varies in 6.00 hours steps. This can be schematically represented as on Figure 96 on next page. The main advantage to this operational quality assessment is that one can directly compare the extrapolation error with the error one obtains when surveying 15.00 hours later. Should one take the extrapolation error from the previous paragraph, one would compare the ‘survey’ error with an error determined over an extrapolation period possibly stretching far away from the time of interest, thus making no real sense.

Hence one obtains the four following time periods of Table 25.

<sup>18</sup> In the extrapolation time system where the time is reinitialized at the point where no observation data is available. In the present study, this means that  $t_{extrapolation} = 0.00$  hours at  $t_{obs} = 108.00$  hours.

Time period number	Time [hrs]		Extrapolation time [hrs]
	Start	End	
1	108.00	114.00	6
2	114.00	120.00	12
3	120.00	126.00	18
4	126.00	132.00	24

Table 25. Extrapolation time period for operational purposes

The average, standard deviation and RMS of the COMEDIE forecast-AGNES observation ZPD differences have been computed for the extrapolation time periods of Table 25. These are plotted on Figures 97 to 103.

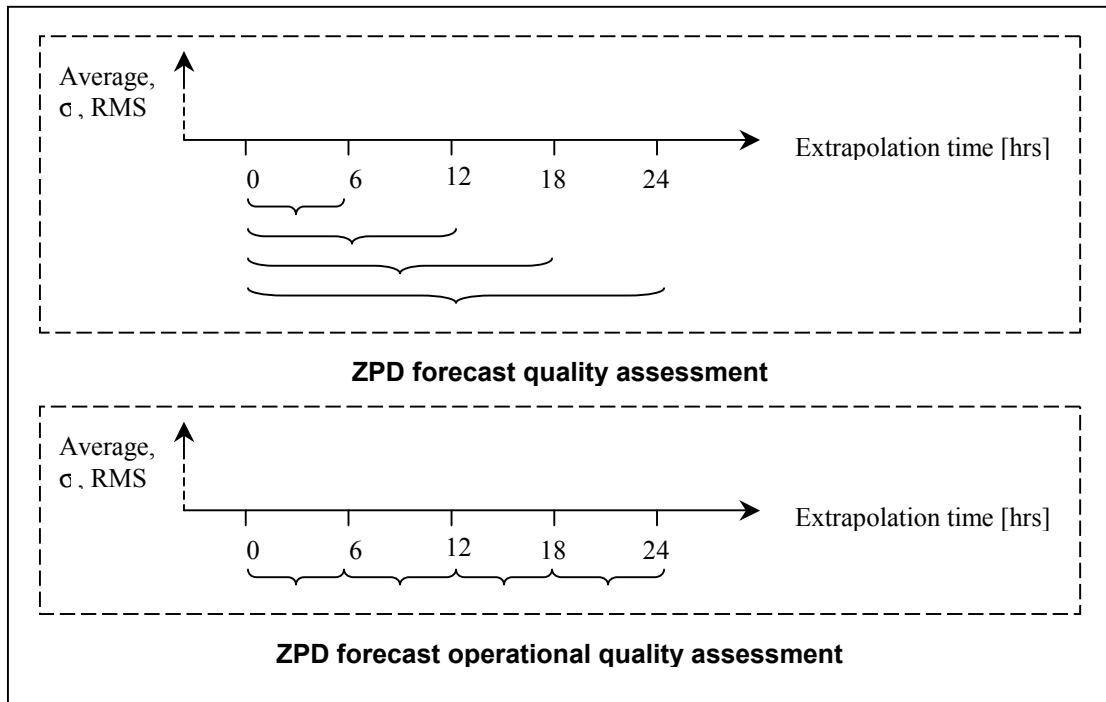


Figure 96. ZPD forecast quality assessment principles.

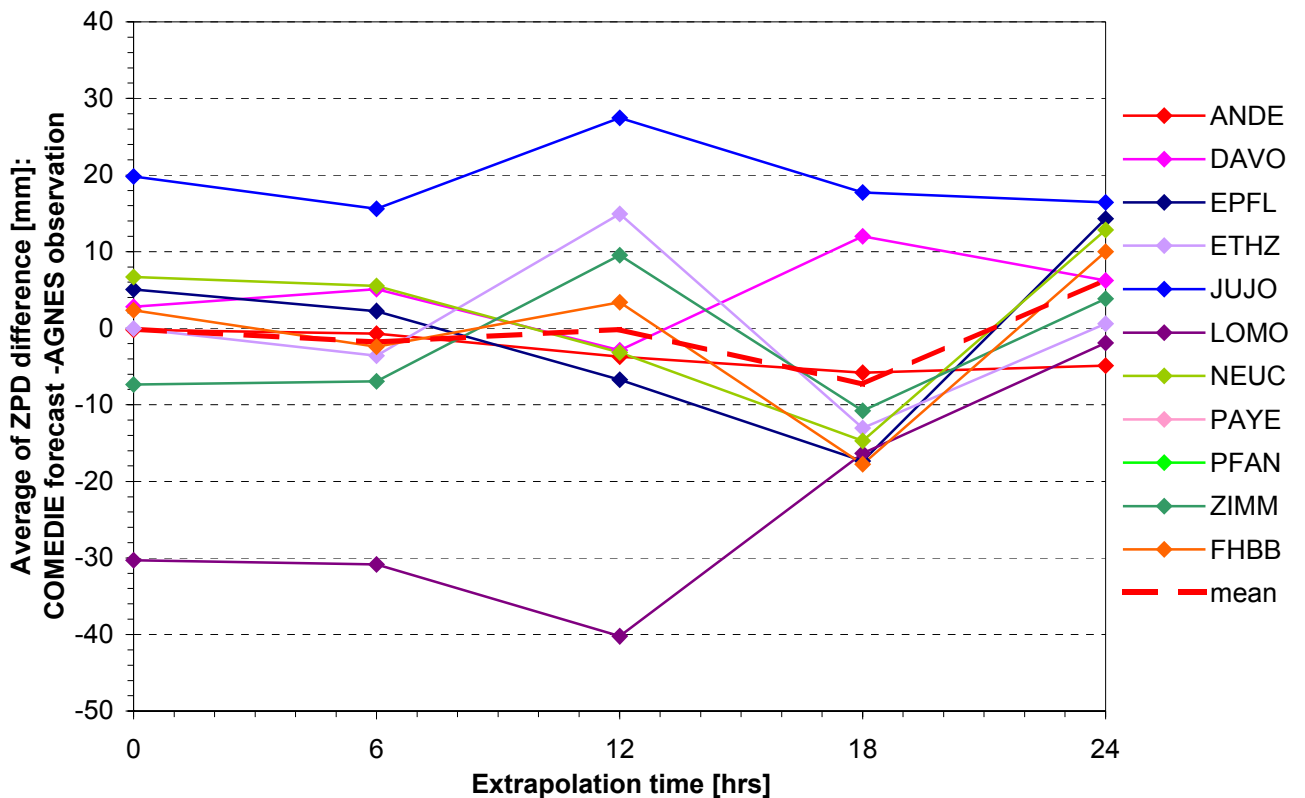


Figure 97. Average of COMEDIE ZPD forecast – AGNES ZPD observation as function of the extrapolation time for operational purposes

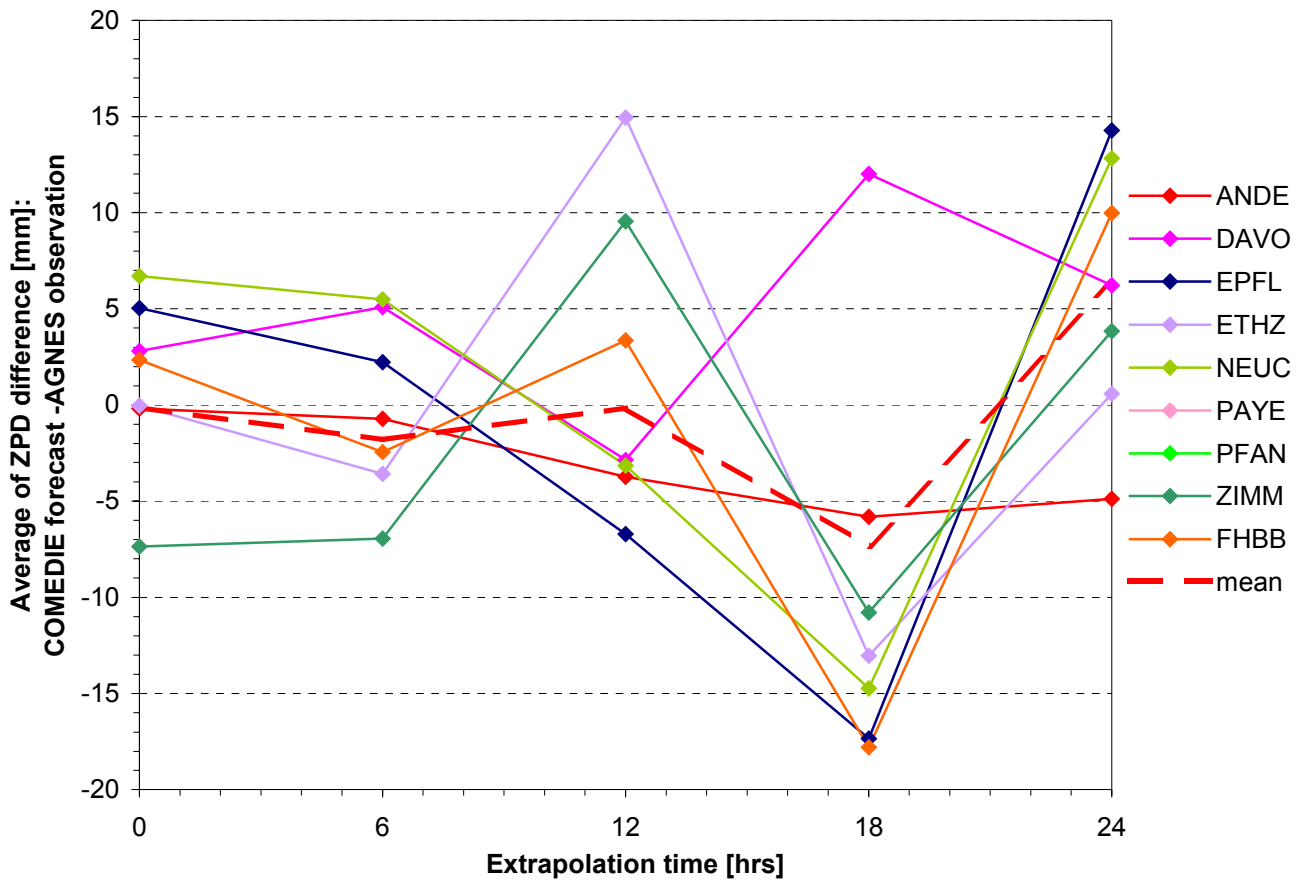


Figure 98. Average of COMEDIE ZPD forecast – AGNES ZPD observation as function of the extrapolation time for operational purposes. Group 1

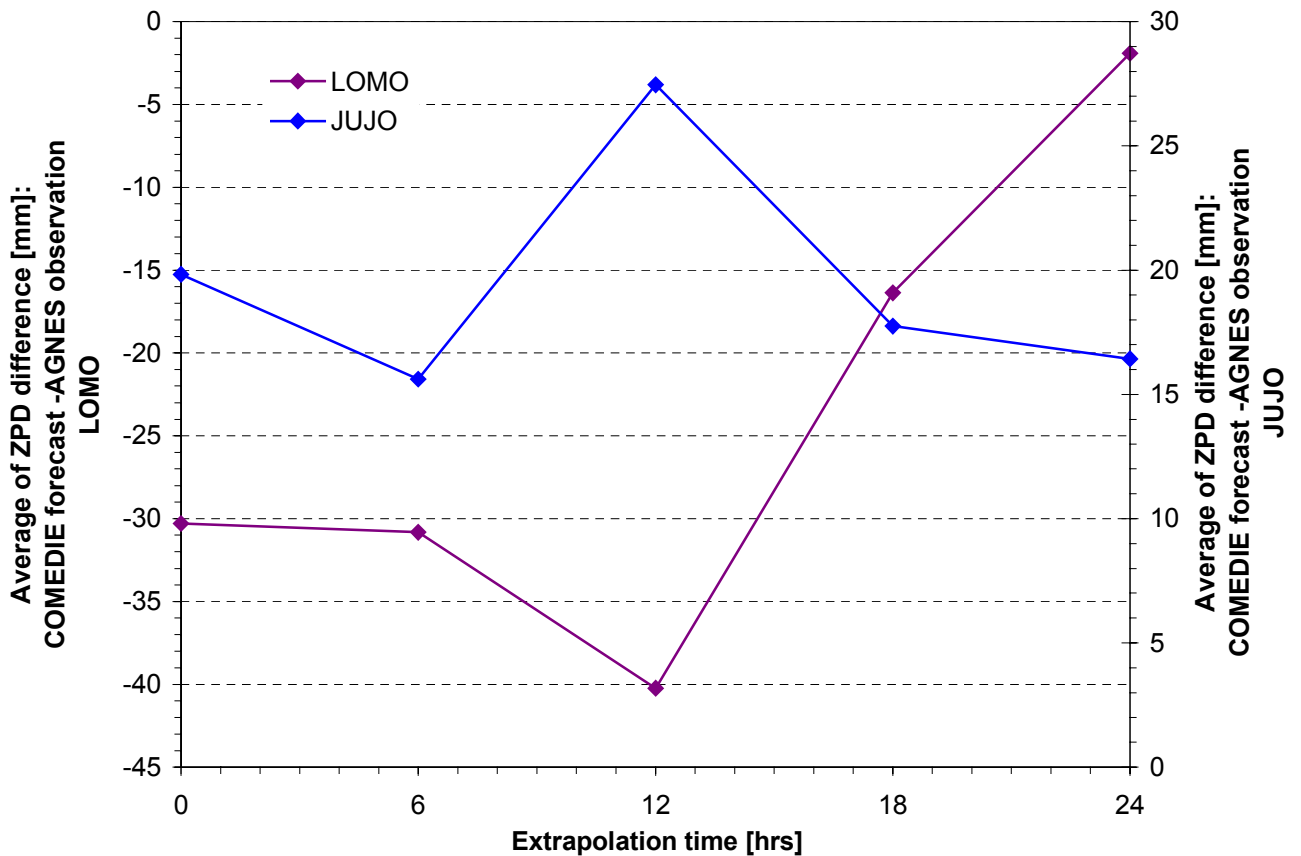


Figure 99. Average of COMEDIE ZPD forecast – AGNES ZPD observation as function of the extrapolation time for operational purposes. Group 2

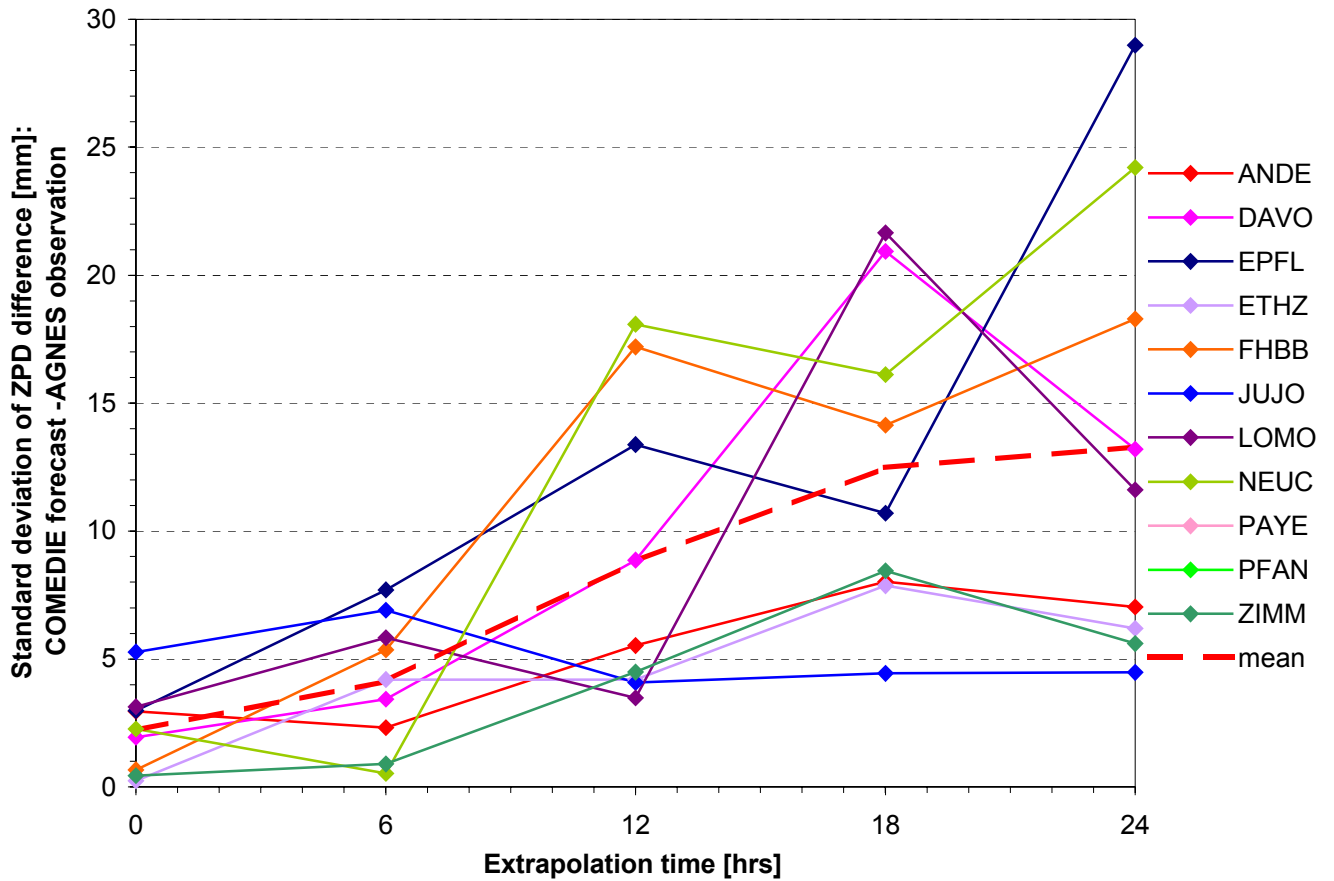


Figure 100. Standard deviation of COMEDIE ZPD forecast – AGNES ZPD observation as function of the extrapolation time for operational purposes

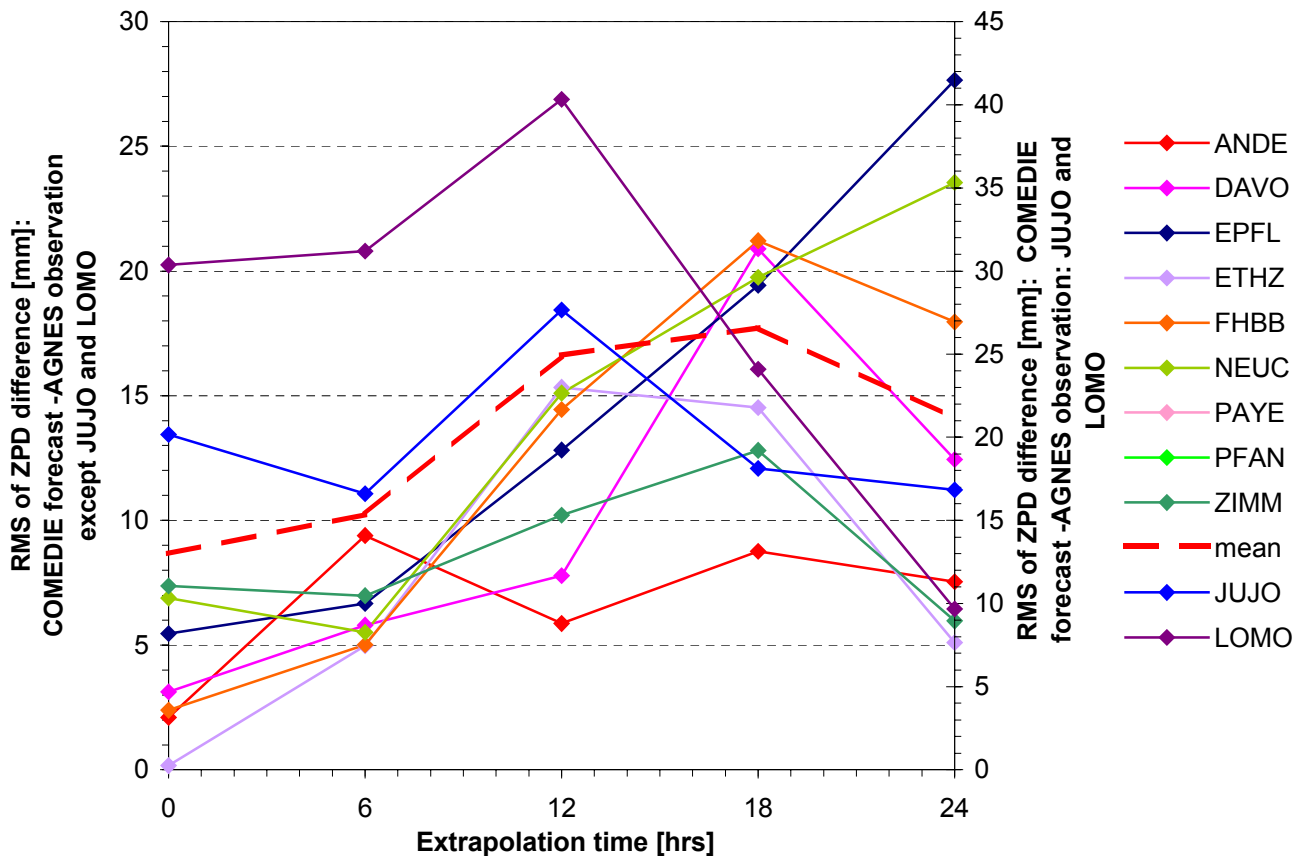


Figure 101. RMS of COMEDIE ZPD forecast – AGNES ZPD observation as function of the extrapolation time for operational purposes



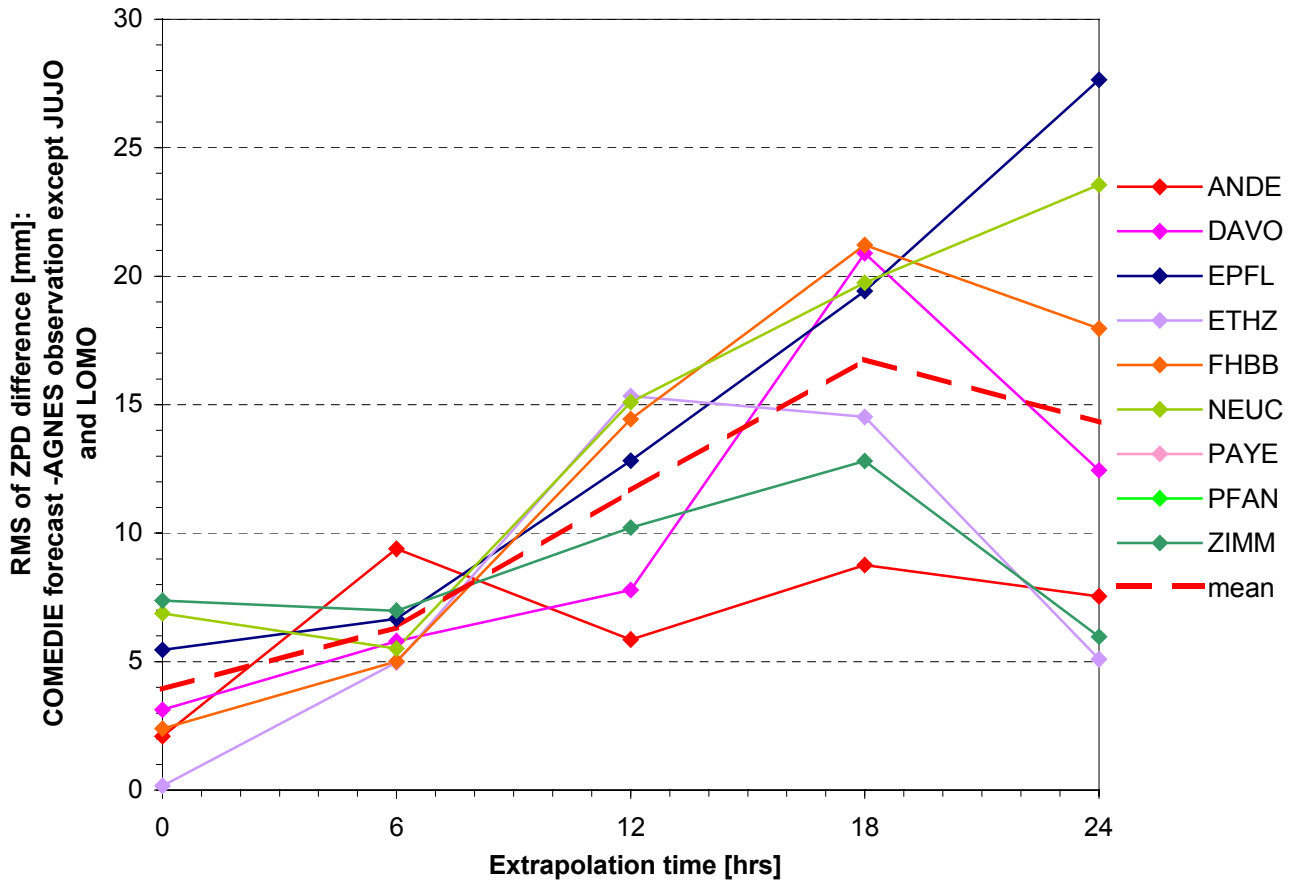


Figure 102. RMS of COMEDIE ZPD forecast – AGNES ZPD observation as function of the extrapolation time for operational purposes. Group 1

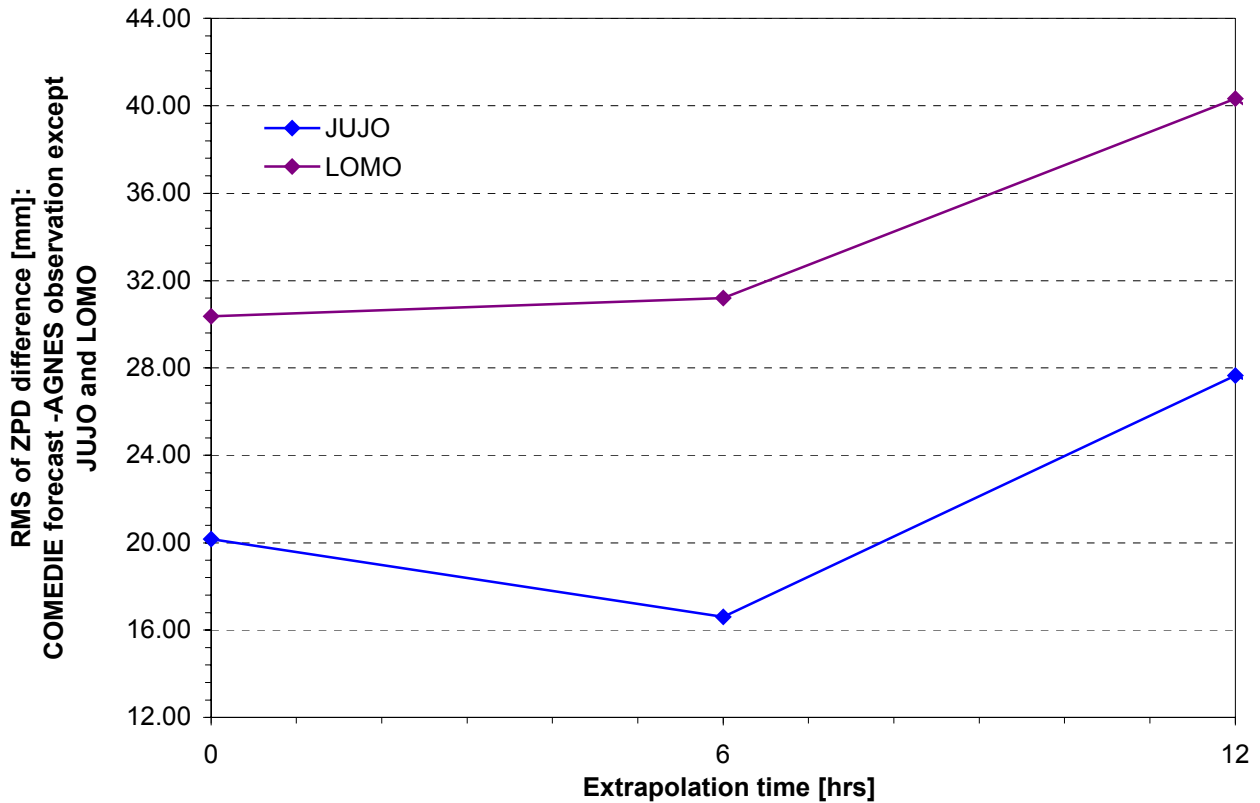


Figure 103. RMS of COMEDIE ZPD forecast – AGNES ZPD observation as function of the extrapolation time for operational purposes. Group 2

Compare the average of the COMEDIE ZPD forecast –AGNES ZPD observation of Figures 89 and 97. For operational purposes, the average is slightly larger than for prediction purposes, although the variations during the first six hours of extrapolation are similar. The volatility of the average significantly increases for an extrapolation of more than 12 hours. Especially the outcomes for a one-day forecast are very different.

The spread of the outcome for the first group of AGNES GPS permanent stations is as much as 2 centimeters for operational purposes while being only of 8 mm for prediction purposes. From a statistical point of view, the average should however converge to zero for large extrapolation time on Figure 89, due to the perfect adequacy between forecast and observation. This might not be the case, i.e. presence of an offset, if the starting average is far out centered or if there are systematic effects inducing a residual error.

On Figure 97, the averages are equivalent from a statistical point of view. They are distributed over a larger domain. If one builds the statistics over a year observation, one should see seasonal variations. It is here not the case due to the limited and arbitrary observation window chosen.

The average shows a flatter timely development on Figure 89 than on Figure 97. This suggests that the forecast is worse when one considers future operations. That fact is corroborated on Figures 90 and 98 for the first group of stations. The general pattern of the prediction time series for both purposes at LOMO and JUJO are similar. However variations of up to 4 cm against 1.2 cm previously are established. Thus one has lower confidence in the accuracy of the forecast at LOMO and JUJO for operational purposes.

The standard deviations of the ZPD differences vary faster and more frequently on Figure 100 than on Figure 92. This is due to the computation procedure applied. While the behavior of the standard deviations during the first 12 hours of extrapolation is comparable, it is not the case later. The mean sigma appears to stabilize itself between 18 and 24 hours prediction time. It will stabilize at a higher value in the second case than in the first. The observed sharp bend on Figure 100 is assumed to be there by mere chance. One cannot absolutely conclude about its origin.

Usually the RMS is larger than the standard deviation. In the way it is defined, the RMS forms some kind of deviation from the true value, while the variance is the deviation squared to the mean. Hence RMSs have generally larger variations than sigmas. This can be seen on Figures 93 and 101. As shown on Figures 101 and 103, LOMO and JUJO have the largest RMS. In the case of LOMO, this might be reduced by the introduction in the study of data from the Stabio (STAB) and San Bernardino (SANB) AGNES GPS permanent stations in Tessin. However, JUJO is still the highest permanent station among the whole AGNES network. It is therefore not possible to greatly reduce the shortcomings of the collocation at this site. It will be the same for all GPS receiver's locations situated at high altitudes such as at the top of mountains (e.g. Monte Rosa in Wallis).

As was done before, the mean of the average, standard deviation and RMS of the ZPD differences are calculated. The statistical results are summarized in Table 26 hereunder:

Time [hrs]	Extrapolation time [hrs]	Statistical quantity		
		Average [mm]	Standard deviation [mm]	RMS [mm]
108.00	0	-0.13	2.21	8.67
114.00	6	-1.79	4.13	10.24
120.00	12	-0.15	<b>8.81</b>	16.62
126.00	18	7.35	12.48	17.73
132.00	24	6.37	13.29	14.08

Table 26. COMEDIE forecast-AGNES observation residuals statistics for operational purposes

The first two rows of Table 24 and 26 are identical. This was to be expected as they are derived from the same computation. According to Table 26, the average standard deviation for the 11 AGNES GPS stations at 12 hours after the start of the extrapolation is of 8.81 mm. Therefore, the 1-centimeter threshold for the forecast accuracy is again reached at 12 hours. This means that *one can predict the ZPD for 12 hours in advance with an accuracy of less than 1 centimeter!*

Now proceed with a linear regression of the mean of the standard deviation of the COMEDIE forecast-AGNES observation ZPD differences. This yields to the following results. The standard deviation as function of the extrapolation time is

$$\sigma_{mean} = 0.6669 \cdot t + 1.6772 \quad (4.3.3.7.1)$$

and the R-squared value is

$$R^2 = 0.6710 \quad (4.3.3.7.2)$$

Therefore the mean extrapolation error growth rate for operational purposes or mean operational extrapolation EGR is

$$mean\ op.\ extrapolation\ EGR = 0.6669\ mm \cdot hr^{-1} \quad (4.3.3.7.3)$$

The mean op. extrapolation EGR is 35 % larger than the mean extrapolation EGR. The offset since the start of the extrapolation window is 1.6772 millimeters and thus approximately 25% less than for prediction purposes, c.f. eq. (4.3.3.6.1). Hence eq. (4.3.3.7.1) grows faster than eq. (4.3.3.6.1).

As far as the linear regression of the maximum of the standard deviation is concerned, one obtains

$$\sigma_{max} = 1.0233 \cdot t + 4.0583 \quad (4.3.3.7.4)$$

with an  $R^2$ -value of

$$R^2 = 0.5344 \quad (4.3.3.7.5)$$

Thence the maximum operational extrapolation error growth rate is

$$max.\ op.\ extrapolation\ EGR = 1.0233\ mm \cdot hr^{-1} \quad (4.3.3.7.6)$$

which is as much as 53 % larger than the mean op. extrapolation EGR and 73% bigger than the equivalent quantity of eq. (4.3.3.6.6) ! Therefore the extrapolation error increases maximal of 12.28 mm every twelve hours but only of 8.00 mm on average.

### 4.3.3.8.ZPD forecast and positioning

The primary purpose of the NAVSTAR GPS is navigation. Hence, it is possible to relate the ZPD error to the positioning error. Indeed, according to [Geiger, 1987] the error in altitude along the zenith of the GPS receiver is equal to 2.7 times the ZPD error. That is

$$\delta z = 2.7 \cdot \delta ZPD \quad (4.3.3.8.1)$$

where  $\delta ZPD$  is the Zenith Path Delay error for a given extrapolation time. The horizontal position error is given by

$$\begin{aligned} \delta x &= 4 \cdot \delta \delta ZPD \cdot \sin \varepsilon \cdot \cos \omega \\ \delta y &= 4 \cdot \delta \delta ZPD \cdot \sin \varepsilon \cdot \sin \omega \end{aligned} \quad (4.3.3.8.2a,b)$$

where  $\varepsilon$  is the elevation angle ( $\varepsilon = 90^\circ$  at zenith) and  $\omega$  is the azimuth angle.  $\delta \delta ZPD$  represents the influence of slanted atmospheric layers and is defined as

$$\delta \delta ZPD := \int \frac{\partial N}{\partial z} \cdot z \, dz \quad (4.3.3.8.3)$$

where  $N$  is the refractivity. Those slanted atmospheric layers induce horizontal gradients in the Path Delay. They however do not affect the horizontal position if one considers Zenith Path Delays and assumes that the atmosphere consists in a superposition of horizontal layers. Note that according to [Geiger, 1987]  $\delta x$  and  $\delta y$  are almost thousand times smaller than  $\delta z$ .

The ZPD extrapolation error is stated in Table 24 for a 6 hours, 12 hours, 18 hours and a one day forecast. This yields to a maximum of

$$\delta z = 2.56\ cm\ vertical\ error \quad (4.3.3.8.4)$$

for a 12 hours forecast.

## 4.4. Summary

In a first step the Zenith Hydrostatic Delay (ZHD), the Zenith Dry Delay (ZDD) and Zenith Wet Delay (ZWD) models derived in Chapter 3, i.e. eq. (3.4.9.20), eq. (3.4.9.23) and eq. (3.4.9.22) have been tested on reference values for the different parameters. Variations in each of the parameters of Table 10 have been studied. From a

point of view of the order of magnitude, the results obtained are in good agreement with observations made from the Automated GPS Network Switzerland (AGNES).

The least square collocation technique or Kriging algorithm is based around a design matrix  $\mathbf{A}$ , which entries are all partial derivatives of the functional models with respect to each model parameter. These partial derivatives are computed in Appendix B and then tested on the parameters of Table 10. The ZDD and ZWD partial derivatives show very different patterns as one varies the GPS receiver's altitude  $z_0$ .

The Zenith Path Delay (ZPD) is just the sum of the ZDD and ZWD. Hence its partial derivative with respect to one parameter is the sum of the partial derivatives of the ZDD and ZWD with respect to the same parameter.  $\partial ZPD/\partial T_1$ ,  $\partial ZPD/\partial z_1$  and  $\partial ZPD/\partial z'$  do not depend on  $z_0$ . It is thus expected that they would introduce singularities in the design matrix, hindering its pseudo-inversion. This is the source of concern as one intends to perform collocations with the system. Constrains on seven parameters of the ZPD model have been applied in order to make possible the inversion of the normal matrix  $\mathbf{N}$ .

The ZPD model has been implemented in the software package COMEDIE: Collocation of Meteorological Data for Interpolation and Estimation of Tropospheric Path Delays. It has then been validated on a virtual regional campaign in Switzerland starting on Monday 22 May 2000 at 00:00:00 UTC and ending on Tuesday 30 May 2000 at 00:00:00 UTC. GPS data for this observation window and for eleven AGNES GPS permanent stations at Andermatt, Davos, EPF Lausanne, ETH Zurich, FHBB Muttentz, Jungfrauoch, Locarno-Monti, Neuchatel, Payerne, Pfänder and Zimmerwald has been used.

Zenith Path Delays have been estimated at the eleven AGNES stations using the model of Chapter 3 and the COMEDIE software package. The differences between the COMEDIE ZPD estimates and the AGNES ZPD observations are evaluated when possible. Good agreements between estimates and observations are noted at all stations except Jungfrauoch and Locarno-Monti. This is probably due to the lack of data from stations at similar high altitudes for the former and due to the location South of the Swiss Alps mountains for the latter. The Alps mountainous chain represent a climatic barrier separating Tessin from the other parts of Switzerland. Further there appears to be no correlation between average, standard deviation and RMS of the ZPD differences with the altitude of the GPS receiver.

ZPD forecasts are performed at all eleven AGNES stations at disposals. The extrapolation starts on Saturday 27 May 2000 at 00:00:00 UTC and ends on Tuesday 30 May 2000 at 00:00:00 UTC. In the first 12 hours of the extrapolation time window some damped oscillations of the ZPD forecast are observed. Afterwards, the ZPD estimates seem to gradually stabilize around the ZPD value given by the functional model.

COMEDIE forecast-AGNES observation ZPD differences are computed and their average, standard deviation and RMS are calculated. For half of the AGNES stations surveyed it is possible to yield to a meaningful forecast during 9 hours after the last data were available. Both the standard deviation and RMS of the ZPD differences are less than 1 centimeter during the first 12 hours of the forecast. This implies that one can conduct a satisfactory prediction of the Zenith Path Delay twelve hours in advance! The ZPD extrapolation error evolves at an approximate velocity of half a millimeter per hour.

The evaluation has again been performed for operational ends. Anew both the standard deviation and RMS of the ZPD differences are less than 1 centimeter at 12 hours after the beginning of the forecast. Therefore one can undertake a good prevision for twelve hours in the future. The ZPD extrapolation error during operations evolves at an approximate velocity of two thirds of millimeter per hour.

Navigation, i.e. the determination of one's position as function of time is the primary purpose of the NAVSTAR Global Positioning System. The 1-cm error in ZPD estimate implies nearly as much as 2.50 cm vertical error in the user's position. One cannot evaluate the horizontal position error due to the ZPD error with a single ZPD measurement at one's location. Multiple observations at different sites are required.

## 5. Conclusions

### 5.1. Work summary

Insufficient knowledge on the atmosphere above the receiver has always been one of the main limitations to the accuracy of the United States Department of Defense's NAVSTAR (Navigation by Timing And Ranging) GPS (Global Positioning System). GPS is nowadays the most widely used satellite system for navigation purposes. The present study focused on modeling the atmospheric effects on the GPS signal and eventually applying it to path delay forecasting.

The L-band radio signals emitted by GPS satellites are slowed and bent as they cross the different layers of the Earth's atmosphere: the ionosphere and the neutral atmosphere (troposphere and stratosphere). By linearly combining the two GPS observables on both  $L_1$  and  $L_2$  carrier frequencies, the errors induced by the ionosphere can be removed to great extent. Double differences are then formed and thus the atomic clock ditherings are removed from the solution. Finally the carrier ambiguity is resolved. The major error remaining is purely due to atmospheric effects.

The total path delay induced by the presence of the atmosphere is computed from the phase differences observed in the phase pseudorange. This delay is then usually mapped to the zenith direction at the ground-based GPS receiver's location using so-called mapping functions. It therefore corresponds to a Zenith Path Delay.

A functional model for this Zenith Path Delays has been developed. Fermat's principle allows connecting the refractive index of a given atmospheric layer to the signal path. In atmospheric sciences, the refractivity is generally used instead of the refractive index. The Essen and Froome formula provides the relation between the refractivity and the three atmospheric fields, namely the atmospheric pressure  $p$ , the partial water vapor pressure  $e$  or its related relative humidity and the temperature  $T$ . The formula is split in three terms proportional to  $(p - e)/T$ ,  $e/T$  and  $e/T^2$ . While the first term corresponds to the dry atmosphere, the two latter generate the wet refractivity. Four-dimensional models for those fields have been conceived.

The spatial and temporal meteorological fields are inserted in the Essen and Froome formula, which is then integrated along the GPS satellite signal path. The analytical integration and the projection along the zenith direction delivers an expression of the Zenith Path Delay (ZPD) as function of ten parameters: the reference pressure  $p_{ref}$ , the reference humidity  $e_{ref}$ , the reference temperature  $T_{ref}$ , the temperature at tropopause  $T_1$ , the tropospheric temperature gradient or lapse rate  $\gamma$ , the GPS receiver's altitude  $z_0$ , the tropopause height  $z_1$ , the upper limit of integration  $z'$ , the pressure scale height  $H_p$  and the humidity scale height  $H_e$ .

The least-squares collocation technique or Kriging algorithm requires the calculation of a design matrix  $\mathbf{A}$ , which entries are all partial derivatives of the functional models with respect to each model parameter. These partial derivatives are computed and then tested on the default parameter values. The ZPD can be split into a Zenith Dry Delay (ZDD) and a Zenith Wet Delay (ZWD). Hence the ZPD partial derivative with respect to one parameter is the sum of the partial derivatives of the ZDD and ZWD with respect to the same parameter. Both partial derivatives show very different patterns as one varies the GPS receiver's altitude  $z_0$ .  $\partial ZPD/\partial T_1$ ,  $\partial ZPD/\partial z_1$  and  $\partial ZPD/\partial z'$  do not depend on  $z_0$ . It is thus expected that they would introduce rank deficiencies in the design matrix, hindering the inversion of the normal matrix  $\mathbf{N}$ . This is the source of concern as one intends to perform collocations with the system. Constrains on seven parameters of the ZPD model have been applied in order to make possible the pseudo-inversion of the design matrix  $\mathbf{A}$ .

The ZPD model has been implemented in the software package COMEDIE: Collocation of Meteorological Data for Interpolation and Estimation of Tropospheric Path Delays developed at the Geodesy and Geodynamics Lab at the Swiss Federal Institute of Technology at Zurich. It has then been validated on a regional campaign in Switzerland starting on Monday 22 May 2000 at 00:00:00 UTC and ending on Tuesday 30 May 2000 at 00:00:00 UTC. GPS data delivered by the Swiss Federal Office of Topography for this observation window and for eleven AGNES GPS permanent stations at Andermatt, Davos, EPF Lausanne, ETH Zurich, FHBB Muttentz, Jungfrauoch, Locarno-Monti, Neuchatel, Payerne, Pfänder and Zimmerwald has been used.

Zenith Path Delays have been estimated at the eleven AGNES stations using the ZPD model developed and the COMEDIE software package. The differences between the COMEDIE ZPD estimates and the AGNES ZPD observations are evaluated when possible. Good agreements between estimates and observations are noted at all stations except Jungfraujoch and Locarno-Monti. This is probably due to the lack of data from stations at similar high altitudes for the former and due to its location South of the Swiss Alps for the latter. The Alps mountains represent a climatic barrier stopping wet and cold air masses arriving from a North-western direction. Hence Locarno-Monti has a very different climate than the rest of the AGNES stations surveyed. Further there appears to be no correlation between average, standard deviation and RMS of the ZPD differences with the altitude of the GPS receiver.

ZPD forecasts are performed at all eleven AGNES stations at disposals. The extrapolation starts on Saturday 27 May 2000 at 00:00:00 UTC and ends on Tuesday 30 May 2000 at 00:00:00 UTC. In the first 12 hours of the extrapolation time window some damped oscillations of the ZPD forecast are observed. Afterwards, the ZPD estimates seem to gradually stabilize around the ZPD value given by the functional model.

COMEDIE forecast-AGNES observation ZPD differences are computed and their average, standard deviation and RMS are evaluated. For half of the AGNES stations surveyed it is possible to yield to a meaningful forecast during 9 hours after the last data were available. Both the standard deviation and RMS of the ZPD differences are less than 1 centimeter during the first 12 hours of the forecast. This implies that one can conduct a satisfactory prediction of the Zenith Path Delay twelve hours in advance! The ZPD extrapolation error evolves at an approximate velocity of half a millimeter per hour.

The evaluation has again been performed for operational ends. Anew both the standard deviation and RMS of the ZPD differences are less than 1 centimeter at 12 hours after the beginning of the forecast. Therefore one can undertake a good prevision for twelve hours in the future. The ZPD extrapolation error during operations evolves at an approximate velocity of two thirds of millimeter per hour.

Navigation, i.e. the determination of one's position as function of time is the primary purpose of the NAVSTAR Global Positioning System. The 1-cm error in ZPD estimate implies nearly as much as 2.50 cm vertical error in the user's position. One cannot evaluate the horizontal position error due to the ZPD error with a single ZPD measurement at one's location. Multiple observations at different sites are required.

## **5.2. Recommendations**

For practical purposes, the path delay has been analytically computed in the GPS space vehicle direction and then evaluated along the zenith axis. Further the atmosphere above the area of interest has been stacked in horizontal layers assumed as isotropic. For increased accuracy, one should proceed with computations taking the inclination of the atmospheric layers into account. The refractivity should also be integrated directly along the GPS receiver-space vehicle axis without being mapped to zenith. Thence one would obtain so-called slant path delays that take the elevation of the GPS space vehicle in consideration.

Seven out of the ten model parameters have been constrained around their default values in order to make possible the pseudo-inversion of design matrix and the inversion of the normal matrix. One should further investigate which parameters can be evaluated via collocation and which must be constrained.

The ZPD model presented in this study is one-dimensional as it depends explicitly only on the GPS receiver's altitude with respect to the mean sea level. Slant path delays do show an explicit dependence on the three dimensional position of the GPS receiver and should therefore deliver better results. The time aspect of the ZPD has been introduced solely through the covariance function. Letting the model parameters depend on time and on position would increase the sensibility of the slant path delay to atmospheric variations and thus improve the model accuracy.

ZPD estimates have been computed at just eleven AGNES stations. To date, the full AGNES network consists of 29 GPS permanent stations. Inserting data from the full AGNES ground receiver constellation would improve the reliability of the statistics that have been derived. Using such information over a year's period would put seasonal effects to light.

AGNES-derived path delays were available only for two hours time periods. A higher data processing rate would allow for more frequent ZPD estimates or ZPD forecasts and AGNES observations comparisons. This would enable better determination of the time threshold for the 1-centimeter precision. As of 1 March 2002, AGNES produces hourly path delays.

**Blank page**

**Blank page**



## Bibliography

- Barrel H. and Sears J.E. (1939)  
Phil. Trans. Royal Society, Part A., Vol. 238, Nr. I., 1939
- Bevis M., Businger S., Herring T.A., Rocken C., Anthes R.A. and Ware R.H. (1992)  
GPS Meteorology: Remote sensing of atmospheric water vapor using the global positioning system  
J. Geophys. Res., Vol. 97, No. D14, pp. 15,787-15,801, Oct. 20, 1992
- Bohren C.F. and Albrecht B.A. (1998)  
Atmospheric thermodynamics  
Oxford University Press, New York, 1998  
ISBN 0-19-509904-4
- Botton S. (1997)  
GPS, localisation et navigation.  
Hermès, Paris, 1997.
- Brockmann E., Grünig S., Schneider D., Wiget A. and Wild U. (2001)  
National report of Switzerland: Introduction and first applications of a real time precise positioning Service using the Swiss permanent Network AGNES  
In Torres J.A. and Hornik H. (Eds)  
Subcommission for the European Reference Frame (EUREF), Dubrovnik, January 2001
- Brockmann E. and Troller M. (2002)  
GPS Meteorology in the Swiss Alps: Interpolation Accuracy for different Alpine Areas and Near Real-time Results. Exploitation of Ground-Based GPS for Meteorology, COST Action 716 Workshop  
GeoForschungsZentrum Potsdam, January 28-29, 2002.
- Businger S., Chiswell S.R., Bevis M., Duan J., Anthes R.A., Rocken C., Ware R.H., Exner M., Van Hove T and Solheim F.S. (1996)  
The promise of GPS in atmospheric monitoring  
Bull. Amer. Meteor. Soc., Vol. 77, pp. 5-18, 1996
- CCIR (1986)  
Recommendations and reports of the CCIR, 1986  
Volume V, Propagation in non-ionized media.  
XVIth plenary assembly, Dubrovnik, 1986  
International Radio Consultative Committee – CCIR  
International Telecommunication Union, Geneva, Switzerland  
ISBN 92-61-02741-5
- Chen D. and Lachapelle G. (1994)  
A comparison of the Fast Ambiguity Search Filtering and least squares search algorithms for ambiguity resolution on the fly.  
Proceedings of the International Symposium on Kinematic Systems in Geodesy, Geomatics and Navigation.  
Banff, Canada, august 30 –September 2, 1994, pp. 241-253.
- Christensen R. (1991)  
Linear models for multivariate, time series and spatial data.  
Springer texts in statistics, Springer Verlag, 1991.  
ISBN 0-387-97413-X
- Cocard M. and Geiger A. (1992)  
Systematic search for all possible widelanes.  
Sixth International Symposium on Satellite Positioning, Ohio, March 1992.
- Davis J.L., Herring T.A., Shapiro I.I., Rogers A.E. and Elgered G. (1985)  
Geodesy by radiointerferometry: effects of atmospheric modelling errors on estimates of baseline length  
Radio Science, Vol. 20, pp. 1593-1607, 1985
- Davis J.L. and Elgered G. (1998)  
The spatio-temporal structure of GPS water vapor determinations  
Phys. Chem. Earth, Vol. 23, No. 1, pp. 91-96, 1998
- Davies K. (1990)  
Ionospheric Radio.  
IEE Electromagnetic Wave Series. Vol. 31, pp. 70-73. Peter Peregrinus (Ed.), London, 1990.  
ISBN 0-86341-186-X
- DoD (1995)  
Department of Defense, Office of the Assistant Secretary of Defense (Public Affairs), News release 384-95

- DoD-USCG (1993)  
Department of Defense, United States Coast Guards, Navigation Center, Global Positioning System, Standard Positioning Service, Signal Specification ICD-GPS-200, Revision C from 10 October 1993.  
Available on-line at <http://www.navcen.uscg.gov/pubs/gps/icd200/default.htm>
- Eckert V., Cocard M. and Geiger A. (1992)  
Collocation of meteorological data for interpretation and estimation of tropospheric path delays  
Institute of Geodesy and Photogrammetry, Swiss Federal Institute of Technology Zurich  
Technical report F194, 1992
- Elósegui P., Davis J.L., Gradinarsky L.P., Elgered G., Johansson J.M., Tahmoush D.A. and Rius A. (1999)  
Sensing atmospheric structure using small-scale space geodetic networks  
*Geophys. Res. Lett.*, Vol. 26, No. 16, pp. 2445-2448, Aug. 15, 1999
- Emardson T.R. (1998a)  
Studies of atmospheric water vapor using the Global Positioning System  
PhD thesis Nr 1404, Chalmers University of Technology. Published in technical report Nr. 339, 1998
- Emardson T.R., Elgered G and Johansson J.M. (1998b)  
Three months of continuous monitoring of atmospheric water vapor with a network of Global Positioning System receivers  
*J. Geophys. Res.*, Vol. 103, No. D2, pp. 1807-182065, Jan. 27, 1998
- Emardson T.R. and Derks H.J.P. (1998c)  
On the relation between the wet delay and the integrated precipitable water vapour in the European atmosphere  
Submitted to *Meteorological Applications*, 1998
- Emardson T.R. and Johansson J.M. (1998d)  
Spatial interpolation of the atmospheric water vapor content between sites in a ground-based GPS network  
Submitted to *Geophysical Research Letters*, 1998
- Essen L. and Froome K.D. (1951)  
The refractive indices and dielectric constants of air and its principal constituents at 24,000 Mc/s.  
*Proceedings of the Royal Society B*, Vol. 64, pp. 862-875, 1951
- Forssell B. (1991)  
Radionavigation systems  
New York [etc.] Prentice Hall 1991, ISBN: 0-13-751058-6
- Frei E. and Schubernigg M. (1992)  
GPS surveying technique using the Fast Ambiguity Resolution Approach (FARA).  
34<sup>th</sup> Australian Surveyors Congress and 18<sup>th</sup> National Surveying Conference, Cairne, Australia, May 23-29, 1992.
- Fridez P. Hugentobler and Schaer S. (Ed.) (2001)  
Bernese GPS Software, Version 4.2, February 2001.  
Astronomical Institute University of Berne, Switzerland.
- Fromm H.-H. and Lucas R. (1998)  
The European contribution to GNSS-2, a status report on the technical preparations.  
European Space Agency-ESTEC, Noordwijk, the Netherlands, ESA publications, 1998.
- Geiger A. (1987)  
Einfluss richtungsabhängiger Fehler bei Satellitenmessungen  
Institute of Geodesy and Photogrammetry, Swiss Federal Institute of Technology Zurich  
Technical report, Vol. 130, July 1987
- Geiger A. (1988)  
Einfluss und Bestimmung der Variabilität des Phasenzentrums von GPS-Antennen.  
Swiss Federal Institute of Technology at Zurich, Switzerland.  
*Institute of Geodesy and Photogrammetry, Mitteilungen* Vol. 43, 1988.
- Geiger A., Cocard M. and Hirter H. (1995)  
Dreidimensionale Modellierung des Refraktivitätsfeldes in der Atmosphäre.  
*Vermessung, Photogrammetrie, Kulturtechnik*, 4/95
- Gendt G. (2002)  
International GPS Service, GeoForschungsZentrum (GFZ) Potsdam, Dept.1  
<ftp://ftp.gfz-potsdam.de/pub/igstrop/>
- Goldberger A.S. (1962)  
Best linear unbiased prediction in the generalized regression model  
*Journal of the American Statistical Association*, Vol. 57, pp. 369-375, 1962
- Hatch R. (1989)  
Ambiguity resolution in the fast lane.  
*Proceedings of ION GPS-89, Second International Technical Meeting of the Satellite Division of the Institute of Navigation*, Colorado Springs, Colorado, September 27-29, 1989, pp. 45-50.

- Hatch R. (1991)  
Ambiguity resolution while moving – experimental results  
Proceedings of ION GPS-91, Fourth International Technical Meeting of the Satellite Division of the Institute of Navigation, Albuquerque, New Mexico, September 11-13, 1991, pp. 707-713.
- Herring T.A. (1992)  
Modeling atmospheric delays in the analysis of space geodetic data  
In: De Munck J.C. and Spoelstra T.A.T. (Eds.)  
Refraction of transatmospheric signals in geodesy.  
Netherlands Geodetic Commission, Delft, new series, Vol. 36, pp. 157-164, 1992
- Hirter H.A. (1998)  
Mehrdimensionale Interpolation von meteorologischen Feldern zur Berechnung der Brechungsbedingungen in der Geodäsie.  
PhD thesis ETH Nr. 11578, Swiss Federal Institute of Technology Zurich, 1998  
ISBN 3-906467-11-2
- Höflinger W. (1993)  
Entwicklung von 3D Meteo-Modellen zur Korrektur der troposphärischen Refraktion bei GPS-Messungen  
Geodesy and Geodynamics Lab, Institute of Geodesy and Photogrammetry  
Swiss Federal Institute of Technology, Zurich, Switzerland  
Report 216, 1993  
ISBN 3-906513-32-7
- Hofmann-Wellenhof R., Lichtenegger H. And Collins J. (1997)  
Global Positioning System, theory and practice.  
Fourth revised edition, Springer Verlag 1997.
- Hopfield H. (1969)  
Two-quartic tropospheric refractivity profile for correcting satellite data  
J. Geophys. Res., Vol. 74, No. 18, Aug. 20, 1969
- Jorgensen P.S. (1986)  
Relativity corrections in GPS user equipment.  
Record of the position location and navigation symposium, pp. 177-183.  
PLANS'86, Las Vegas, 4-7 September 1986.
- Kayton M. and Fried W.M. (1997)  
Avionics navigation systems  
Second edition, Wiley & Sons, New York, 1997  
ISBN 0-471-54795-6
- Krarup T. (1969)  
A contribution to the mathematical foundation of physical geodesy.  
Danish Geodetic Institute, Copenhagen, Publ. Nr. 44, 1969.
- Kruse L.P. (2000)  
Spatial and temporal distribution of atmospheric water vapor using space geodetic techniques.  
PhD thesis ETH Nr. 13639, Swiss Federal Institute of Technology Zurich, 2000
- Lertes E. (2000)  
Die Internationale Atmosphäre (ISA) als polytrope Zustandsbeschreibung.  
Fachhochschule Wiesbaden, AGAFE Mitteilungen, Vol. 1, pp. 26-29, 2000.  
Available on-line at  
[http://fbe4.e-technik.fh-wiesbaden.de/~agafe/AGAFE-Mitteilungen/Mitteilung\\_1\\_2000/mitteilung\\_1\\_2000.html](http://fbe4.e-technik.fh-wiesbaden.de/~agafe/AGAFE-Mitteilungen/Mitteilung_1_2000/mitteilung_1_2000.html)
- L+T (2002)  
Automatisches GPS Netz Schweiz - AGNES  
Federal Office of Topography, Wabern, Switzerland  
Update of 28-02-2002  
Available on-line at  
<http://www.swisstopo.ch/geoaktuell/de/geo/agnes.htm>
- Marini J.W. (1972)  
Correction of satellite tracking data for an arbitrary tropospheric profile  
Radio Science, Vol. 7, Nr. 2, pp. 223-231, 1972
- Matheron G. (1965)  
Les variables régionalisées et leur estimation.  
Une Application de la Théorie des Fonctions Aleatoires aux Sciences de la Nature  
Masson et Cie., Paris, 1965

- Matheron G. (1969)  
Le krigeage universel.  
Les cahiers du Centre de Morphologie Mathématique de Fontainebleau, Fascicule 1.  
Ecole Nationale Supérieure des Mines de Paris, 1969
- Melbourne W.G. (1985)  
The Case for Ranging in GPS Based Geodetic Systems.  
Proceedings First International Symposium on Precise Positioning with GPS, pp. 373-386, 1985.  
U.S. Department of Commerce, Rockville, Maryland.
- Moritz H. (1989)  
Advanced Physical Geodesy  
2<sup>nd</sup> edition, Herbert Wichmann Verlag, Karlsruhe, Germany, 1989  
ISBN 3-87907-106-3
- NATO (2001)  
Global Positioning System (GPS) Modernization  
NATO GPS Technical Workshop held on 29 June 2001 at the NAVSTA GPS Joint Program Office, Los Angeles AFB by Rita M. Lollock.  
Proceeding available on-line at  
[https://gps.losangeles.af.mil/gpslibrary/2000\\_Web\\_Library/2200\\_public/html/documents.html](https://gps.losangeles.af.mil/gpslibrary/2000_Web_Library/2200_public/html/documents.html)
- NAVCEN (2001a)  
GPS status message of 16 November 2001.  
Navigation Center, United States Coast Guards.  
Available on-line at <http://www.navcen.uscg.gov/ftp/GPS/status.txt>
- NAVCEN (2001b)  
GPS constellation history and status.  
Navigation Center, United States Coast Guards. GPS Status Message. Last Updated: 02 May 2001.  
Available on-line at <http://www.navcen.uscg.gov/gps/geninfo/constell.htm>
- NAVSTAR-JPO (2001)  
GPS overview and system principles.  
NAVSTAR GPS Joint Program Office, Los Angeles AFB, last revision on 2 October 2001.  
Available on-line at <http://gps.losangeles.af.mil/jpo/>
- Niell A.E. (1996)  
Global mapping functions for the atmosphere delay at radio wavelength  
J. Geophys. Res., Vol. 101, No. B2, pp. 3227-3246, Feb. 10, 1996
- NIMA (1997)  
Department of Defense World Geodetic System 1984: Its Definition and Relationship with Local Geodetic Systems. NIMA TR8350.2 Third Edition. 4 July 1997. Bethesda, MD: National Imagery and Mapping Agency.  
Available on-line from <http://164.214.2.59:80/GandG/wgs-84/>
- NSC (1996)  
National Security Council, Office of Science and Technology Policy, U.S. Global Positioning System Policy: Presidential Decision Directive of March 29, 1996.  
Available on-line at <http://www.spatial.maine.edu/~leick/news4.htm>
- NSC (2000)  
National Security Council, Office of Science and Technology Policy, U.S. Global Positioning System Policy: Presidential Decision Directive of May 1, 2000.  
Available on-line at [http://clinton4.nara.gov/WH/EOP/OSTP/html/0053\\_2.html](http://clinton4.nara.gov/WH/EOP/OSTP/html/0053_2.html)
- Remondi B.W. (1990)  
Pseudo-kinematic GPS results using the ambiguity function method.  
National Information Center, Rockville, Maryland, NOAA Technical Memorandum NOS NGS-52, 1990.
- Rocken C. and Meertens C. (1991)  
Monitoring selective availability dither frequencies and their effect on GPS data.  
Bull. Géod. N° 65, pp. 162-169, 1991.
- Rocken C., Ware R., Van Hove T., Solheim F., Alber C., Johnson J., Bevis M. and Businger S. (1993)  
Sensing atmospheric water vapor with the global positioning system  
Geophys. Res. Lett., Vol. 20, No. 23, pp. 2631-2634, Dec. 14, 1993
- Rocken C., Van Hove T. And Ware R. (1997)  
Near real-time GPS sensing of atmospheric water vapor  
Geophys. Res. Lett., Vol. 24, no. 24, pp. 3221-3224, Dec. 13, 1997
- Rödel W. (2000)  
Physik unserer Umwelt: die Atmosphäre  
Third edition, Springer, Berlin, 2000  
ISBN 3-540-67180-3

- Saastamoinen J. (1971)  
Atmospheric correction for the troposphere and stratosphere in radio ranging of satellites  
In: The use of artificial satellites for geodesy.  
Geophys. Monogr. Ser, Vol. 15, Amer. Geophys. Union, pp. 247-251, 1971
- Saastamoinen J. (1972)  
Introduction to practical computation of astronomical refraction  
Bull. Geod., Vol. 106, pp. 383-397, 1972
- Seeber G. (1993)  
Satellite Geodesy, Foundations, Methods and Applications.  
Walter de Gruyter Berlin 1993.
- Smith, E.K., and S. Weintraub (1953)  
The constants in the equation for atmospheric refractive index at radio frequencies  
Institute of Radio Engineering, Vol. 41, pp. 1035-1037, 1953
- Spilker J.J. (1978)  
GPS signal structure and performance characteristics – space segment.  
J. Inst. Navigation, Vol. 25, N° 2, pp. 121-146, 1978.
- Thayer D. (1974)  
An improved equation for the radio refractive index of air  
Radio Science, Vol. 9, pp. 803-807, 1974
- Tiemeyer, B. (1999)  
Global Navigation Satellite System-Aviation.  
European Organisation for the Safety of Air Navigation, Eurocontrol, Bretigny, France. Presentation made at the  
Swiss Federal Institute of Technology, Zurich in March 1999.
- Troller M. and Brockmann E. (2001)  
COMEDIE-Modellierung für die Kampagne GRTI00 - Vergleiche verschiedener Atmosphärenmodellierungen.  
Federal Office of Topography, Wabern, Switzerland, Vol. TB (B) 01-20, 2001
- Troller M., Cocard M and Geiger A. (2002)  
Software package Comedie: Collocation of Meteorological Data for Interpolation and Estimation of  
Tropospheric Path Delays.  
User Documentation, Version 1.1, GGL-ETHZ, 18 January 2002
- USAF (1999)  
United States Air Force, Space and Missile System Center (AFMC), Office of Public Affairs, *News Release No*  
99-22. Available on the web at <http://gps.losangeles.af.mil/y2000/EOW-news.html>
- USNO (2001)  
GPS Time vs. UTC via USNO Master Clock  
GPS Timing Data & Information, United States Naval Observatory, Update of 16 November 2001.  
Available on-line at [http://tycho.usno.navy.mil/gps\\_datafiles.html](http://tycho.usno.navy.mil/gps_datafiles.html)
- Wei M. (1987)  
Statistische Probleme bei der Kollokation  
PhD thesis, Mitteilungen der geodätischen Institute der Technischen Universität Graz, Folge 54, Technische  
Universität Graz, 1987
- Wirth B. (1990)  
Höhensysteme, Schwerepotentiale und Niveauflächen: systematische Untersuchung zur zukünftigen  
terrestrischen und GPS-gestützten Höhenbestimmung in der Schweiz.  
Geodätisch-geophysikalische Arbeiten in der Schweiz.  
Schweizerische Geodätische Kommission, Vol. 42, pp. 203, 1990
- WRC-2000 (2000)  
The European positions for the World Radio Communications Conference 2000 (WRC-2000).  
COM (2000), 86 final, 8 March 2000.  
Commission of the European Communities.
- Wübbena G. (1985)  
Software Developments for Geodetic Positioning with GPS using TI 4100 Code and Carrier Measurements.  
Proceedings First International Symposium on Precise Positioning with GPS, pp. 403-412, 1985.  
U.S. Department of Commerce, Rockville, Maryland.

**Blank page**

# Appendices

## Appendix A. Essen and Froome formula

The Essen and Froome formula, eq. (3.2.2.7), is given by

$$N(p, T, e) = (n-1) \times 10^6 = \frac{77.64}{T} \cdot (p-e) + \frac{64.68}{T} \cdot \left(1 + \frac{5748}{T}\right) \cdot e \quad (\text{A.1})$$

The refractivity  $N$  has been computed as function of the partial water vapor pressure  $e$  and of the temperature  $T$  in the range

$$200 \text{ K} \leq T \leq 325 \text{ K} \quad (\text{A.2})$$

The partial water vapor pressure varies between 5 hPa in summer and 15 hPa in winter at European latitudes. Hence eq. (A.1) has been evaluated for  $e=0$  hPa, 5 hPa, 10 hPa and 15 hPa. The case  $e=0$  hPa has been taken into consideration regardless of its physical meaning, as it represents the idealized situation where the atmosphere contains no water vapor, i.e. is absolutely dry. It is plotted on Figure A.1 below.

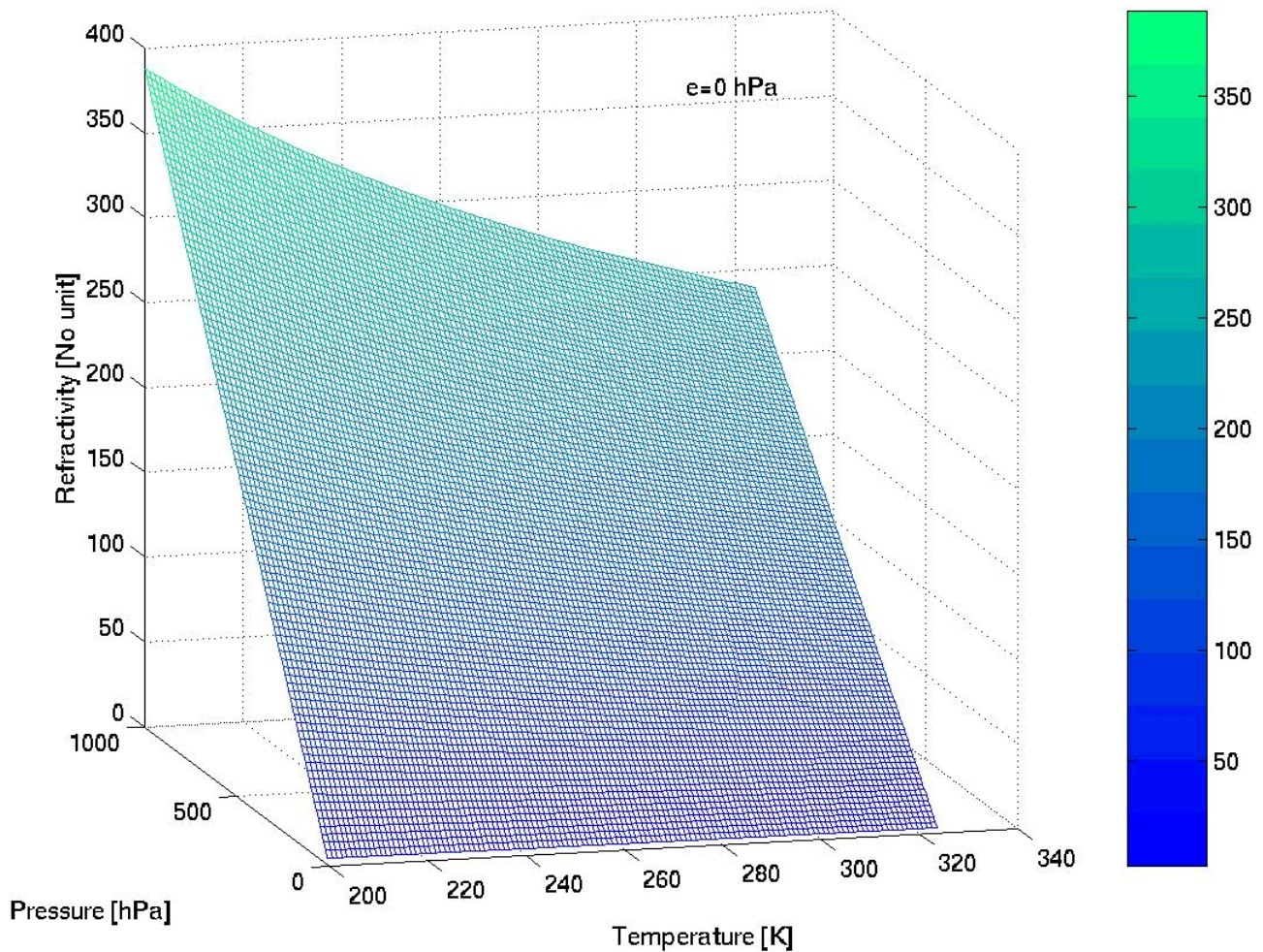


Figure A.1. Essen and Froome Formula.  $N(p, T)$  for  $e=0$  hPa

For  $e=0$  hPa and  $p=0$  hPa, the refractivity is constant and equal to zero. For a non-vanishing pressure, it varies as the inverse of the temperature of the atmosphere. The variations are in the range 0-400 with the maximum refractivity being reached at minimum temperature and maximum atmospheric pressure. According to the International Radio Consultative Committee of the International Telecommunication Union, c.f. [CCIR, 1986], the average value of the radio refractivity at the surface of the Earth is  $N=325$  for an average mid-latitude atmospheric profile. This is hardly achieved without any atmospheric humidity. Therefore consider the case where  $e \neq 0$  hPa.



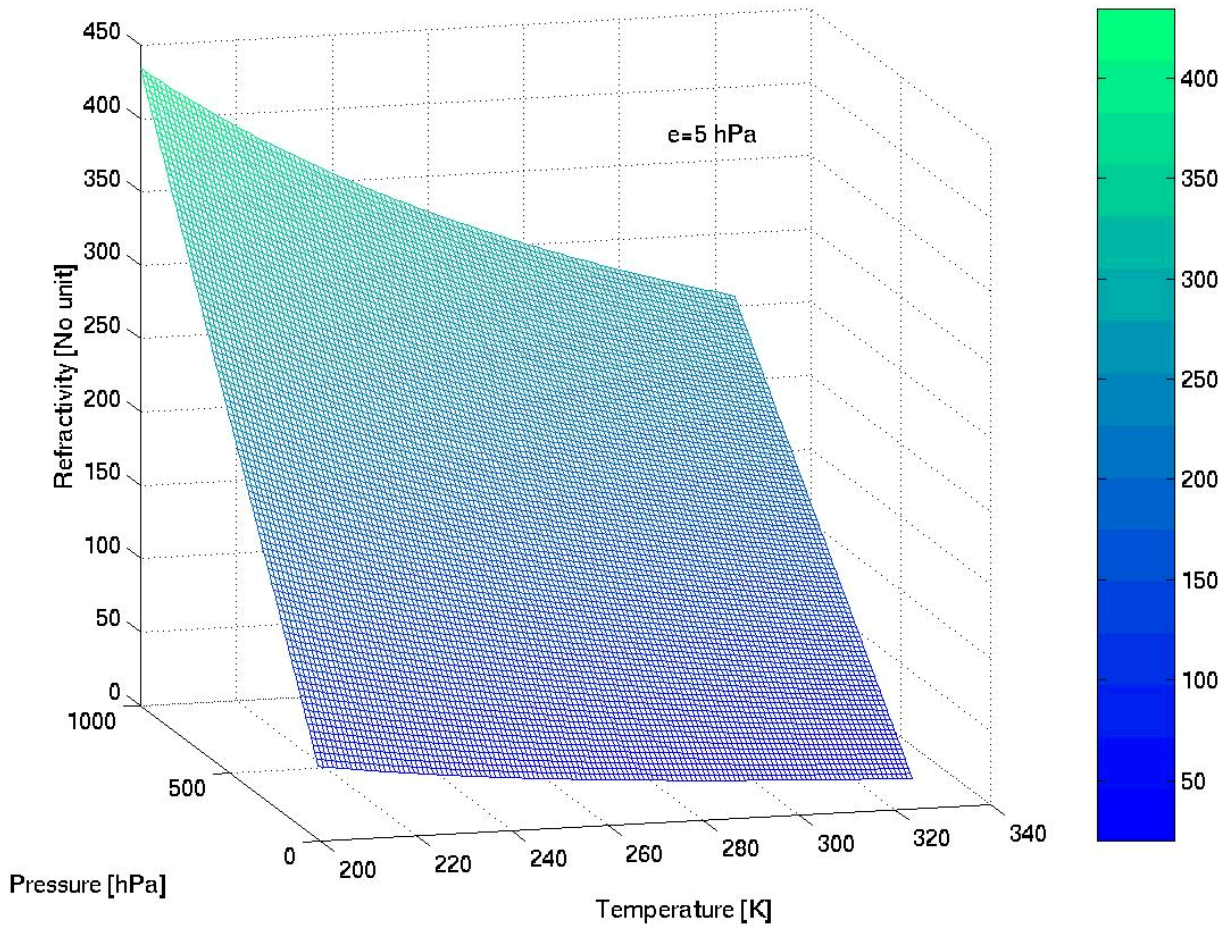


Figure A.2. Essen and Froome Formula.  $N(p, T)$  for  $e=5$  hPa

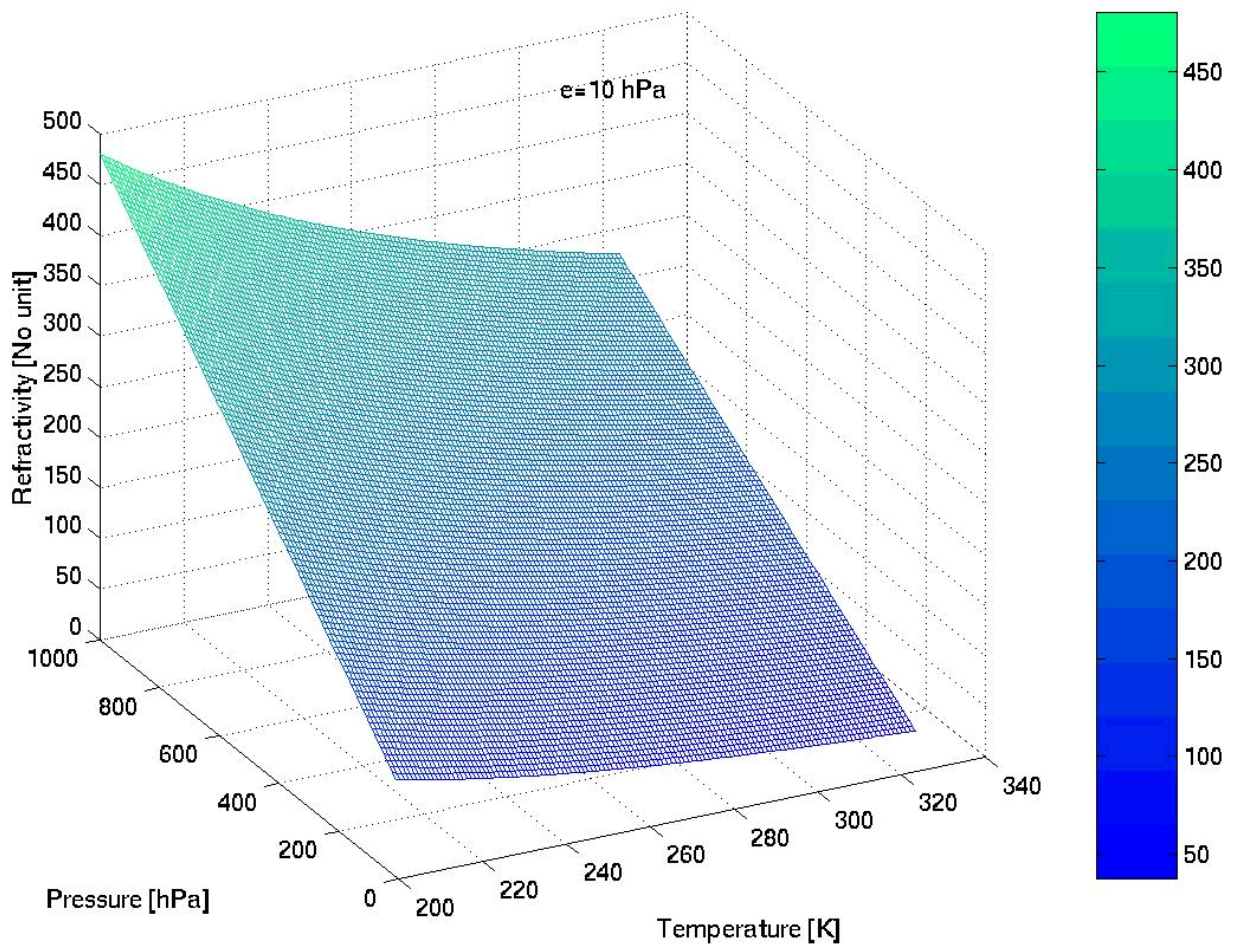


Figure A.3. Essen and Froome Formula.  $N(p, T)$  for  $e=10$  hPa



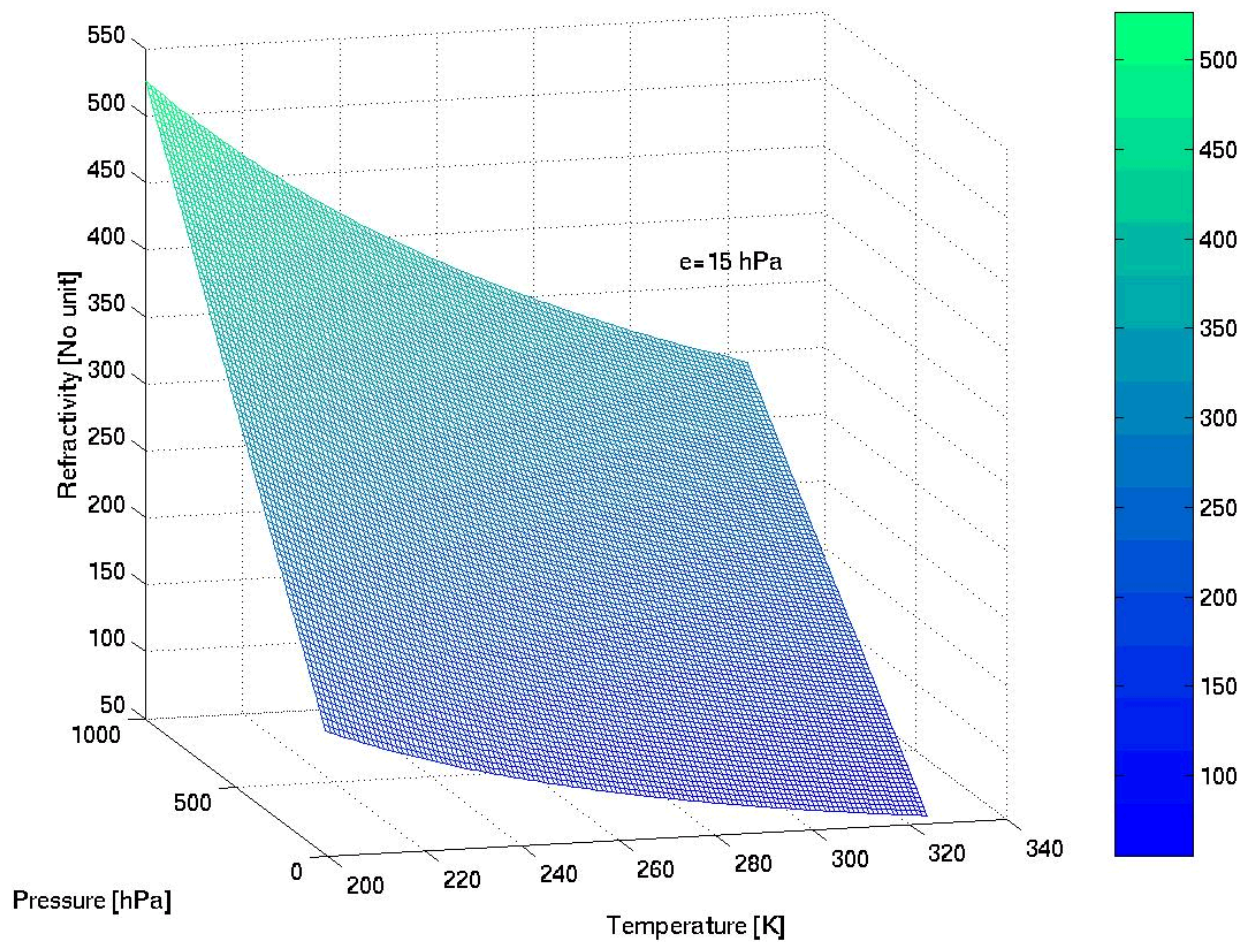


Figure A.4. Essen and Froome Formula.  $N(p, T)$  for  $e=5$  hPa

As can be seen on Figures A.2, A.3 and A.4, the general shape of the refractivity remains the same. However its amplitude increases by a fourth. Differences are mostly noted for low values of  $N$ , i.e. when  $p=0$  hPa. The isolines present node and saddle point-like shapes reflecting the curvature of the refractivity surface.

Referring to [CCIR, 1986], the average value of the radio refractivity at the surface of the Earth is  $N=315$ . This is in good agreement with the results obtained from eq. (A.1) for  $e=10$  hPa and a surface temperature of  $T=15^\circ\text{C}$  and atmospheric pressure of  $p=1000$  hPa. Furthermore, the atmospheric water vapor pressure is mostly centered around 10 hPa at all seasons in Switzerland. Therefore Figure A.3 is chosen as reference for further consideration.

**Blank page**

## Appendix B. Zenith path delay partial derivatives

Accordingly to paragraph 2.2, it is compulsory to compute the partial derivatives of the path delay along the zenith direction in order to fill the design matrix  $\mathbf{A}$  of the system.

### B.1. Introduction

Recall the main results of paragraph 3.4. The Zenith Path Delay (ZPD) can be split in a ‘dry’ term, the Zenith Dry Delay (ZDD) and a ‘wet’ term, the Zenith Wet Delay (ZWD). Eq. (3.4.9.16) states

$$ZPD := ZDD + ZWD \quad (\text{B.1.1})$$

Further the ZPD is a function of

$$ZPD = ZPD(p_{ref}, e_{ref}, T_{ref}, T_1, \gamma, z_0, z_1, z', H_p, H_e) \quad (\text{B.1.2})$$

and the ZDD depends on

$$ZDD = ZDD(p_{ref}, e_{ref}, T_{ref}, T_1, \gamma, z_0, z_1, z', H_p, H_e) \quad (\text{B.1.3})$$

while the ZWD is a function of

$$ZWD = ZWD(e_{ref}, T_{ref}, T_1, \gamma, z_0, z_1, z', H_e) \quad (\text{B.1.4})$$

From paragraph 2.2, it is known that the ZPD measurements  $\mathbf{l}$  are of the form

$$\mathbf{l} = \mathbf{A}\mathbf{x} + \mathbf{s} + \mathbf{n} \quad (\text{B.1.5})$$

where  $\mathbf{n}$  the noise part,  $\mathbf{s}$  the signal part and  $\mathbf{A}$  is the design matrix, derived from the linearization of  $\mathbf{l}$ . Hence  $\mathbf{A}$  is given by

$$\mathbf{A} = \frac{\partial \mathbf{l}}{\partial \mathbf{x}} \quad (\text{B.1.6})$$

where  $\mathbf{x}$  is the parameters vector. Combine eq. (B.1.2) and eq. (B.1.6) to obtain

$$\mathbf{x}^T = \{p_{ref}, e_{ref}, T_{ref}, T_1, \gamma, z_0, z_1, z', H_p, H_e\} \quad (\text{B.1.7})$$

It is more convenient to compute the partial derivatives of the ZDD and ZWD than to consider the ZPD as a sole entity. Such a move makes sense as the system is linearized.

### B.2. Mathematical background

It is intended here to provide a short summary of the mathematical laws that are used to compute the different partial derivatives.

**Convention 1.** Let denote the simple derivative of a smooth derivable function  $u$  on  $\mathbb{R}$  by  $u'$ , i.e.

$$u' = \frac{\partial u}{\partial x} \quad \text{where } u = u(x_i), x_i \in ]-\infty, +\infty[, i \in \mathbb{N} \quad (\text{B.2.1})$$

**Law B.1.** (Natural logarithm). Let  $u$  be a smooth derivable function on  $\mathbb{R}$ . Then the derivative of the natural logarithm is

$$\frac{\partial \ln(u)}{\partial x} = \frac{u'}{u} \quad (\text{B.2.2})$$

**Law B.2.** (Series differential). Let  $u$  be a smooth derivable function on  $[a, b]$  and  $S$  an uniformly converging series on the same interval. Then the series  $S$  can be derived termwise and it holds

$$\left( \sum_{n \geq 1} u_n(x) \right)' = \sum_{n \geq 1} u_n'(x) \quad (\text{B.2.3})$$

From Law B.2. follows the

**Corollary B. 1.** (Series with constant coefficients). Let  $u$  be a smooth derivable function on  $[a, b]$  and  $S$  a series with constant coefficients, uniformly converging on the same interval. Then the series  $S$  can be derived termwise and it holds

$$\left( \sum_{n \geq 1} a_n \cdot x^n \right)' = \sum_{n \geq 1} n \cdot a_n \cdot x^{n-1} \quad (\text{B.2.4})$$

**Law B. 3.** (Exponential) Let  $u$  be a smooth derivable function on  $\mathbb{R}$ . Then the exponential of  $u$  can be Taylor developed as

$$e^{u(x)} = \sum_{n \geq 0} \frac{[u(x)]^n}{n!} = 1 + \sum_{n \geq 1} \frac{[u(x)]^n}{n!} \quad (\text{B.2.5})$$

### B.3. Help functions

The partial derivatives with respect to the parameters of eq. (B.1.3) are computed in the following.

#### B.3.1. Logarithm $\ln(T_{ref}, \gamma, z_0, z_1)$

Define the following function

$$\ln(T_{ref}, \gamma, z_0, z_1) := \ln \left( \frac{T_{ref} + \gamma \cdot z_1}{T_{ref} + \gamma \cdot z_0} \right) \quad (\text{B.3.1.1})$$

Its partial derivatives are

$$\mathbf{B.3.1.1.} \quad \partial \ln(T_{ref}, \gamma, z_0, z_1) / \partial T_{ref}$$

Use Law B.1. and eq. (B.3.1.1) to obtain

$$\begin{aligned} \frac{\partial \ln(T_{ref}, \gamma, z_0, z_1)}{\partial T_{ref}} &= \left[ \frac{\partial}{\partial T_{ref}} \left( \frac{T_{ref} + \gamma \cdot z_1}{T_{ref} + \gamma \cdot z_0} \right) \right] \cdot \left( \frac{T_{ref} + \gamma \cdot z_1}{T_{ref} + \gamma \cdot z_0} \right)^{-1} \\ &= \frac{1 \cdot (T_{ref} + \gamma \cdot z_0) - (T_{ref} + \gamma \cdot z_1) \cdot 1}{(T_{ref} + \gamma \cdot z_0)^2} \cdot \left( \frac{T_{ref} + \gamma \cdot z_0}{T_{ref} + \gamma \cdot z_1} \right) \end{aligned} \quad (\text{B.3.1.1.1})$$

i.e.

$$\frac{\partial \ln(T_{ref}, \gamma, z_0, z_1)}{\partial T_{ref}} = \frac{\gamma \cdot (z_0 - z_1)}{(T_{ref} + \gamma \cdot z_0) \cdot (T_{ref} + \gamma \cdot z_1)} \quad (\text{B.3.1.1.2})$$

$$\mathbf{B.3.1.2.} \quad \partial \ln(T_{ref}, \gamma, z_0, z_1) / \partial \gamma$$

Use Law B.1. and eq. (B.3.1.1) to obtain

$$\begin{aligned} \frac{\partial \ln(T_{ref}, \gamma, z_0, z_1)}{\partial \gamma} &= \left[ \frac{\partial}{\partial \gamma} \left( \frac{T_{ref} + \gamma \cdot z_1}{T_{ref} + \gamma \cdot z_0} \right) \right] \cdot \left( \frac{T_{ref} + \gamma \cdot z_1}{T_{ref} + \gamma \cdot z_0} \right)^{-1} \\ &= \frac{z_1 \cdot (T_{ref} + \gamma \cdot z_0) - (T_{ref} + \gamma \cdot z_1) \cdot z_0}{(T_{ref} + \gamma \cdot z_0)^2} \cdot \left( \frac{T_{ref} + \gamma \cdot z_0}{T_{ref} + \gamma \cdot z_1} \right) \end{aligned} \quad (\text{B.3.1.2.1})$$

i.e.

$$\frac{\partial \ln(T_{ref}, \gamma, z_0, z_1)}{\partial \gamma} = \frac{T_{ref} \cdot (z_1 - z_0)}{(T_{ref} + \gamma \cdot z_0) \cdot (T_{ref} + \gamma \cdot z_1)} \quad (\text{B.3.1.2.2})$$

### B.3.1.3. $\partial \ln(T_{ref}, \gamma, z_0, z_1) / \partial z_0$

Use Law B.1. and eq. (B.3.1.1) to obtain

$$\frac{\partial \ln(T_{ref}, \gamma, z_0, z_1)}{\partial z_0} = \left[ \frac{\partial}{\partial z_0} \left( \frac{T_{ref} + \gamma \cdot z_1}{T_{ref} + \gamma \cdot z_0} \right) \right] \cdot \left( \frac{T_{ref} + \gamma \cdot z_1}{T_{ref} + \gamma \cdot z_0} \right)^{-1} = \frac{-(T_{ref} + \gamma \cdot z_1) \cdot \gamma}{(T_{ref} + \gamma \cdot z_0)^2} \cdot \left( \frac{T_{ref} + \gamma \cdot z_0}{T_{ref} + \gamma \cdot z_1} \right) \quad (\text{B.3.1.3.1})$$

i.e.

$$\frac{\partial \ln(T_{ref}, \gamma, z_0, z_1)}{\partial z_0} = \frac{-\gamma}{T_{ref} + \gamma \cdot z_0} \quad (\text{B.3.1.3.2})$$

### B.3.1.4. $\partial \ln(T_{ref}, \gamma, z_0, z_1) / \partial z_1$

Use Law B.1. and eq. (B.3.1.1) to obtain

$$\frac{\partial \ln(T_{ref}, \gamma, z_0, z_1)}{\partial z_1} = \left[ \frac{\partial}{\partial z_1} \left( \frac{T_{ref} + \gamma \cdot z_1}{T_{ref} + \gamma \cdot z_0} \right) \right] \cdot \left( \frac{T_{ref} + \gamma \cdot z_1}{T_{ref} + \gamma \cdot z_0} \right)^{-1} = \frac{\gamma}{(T_{ref} + \gamma \cdot z_0)} \cdot \left( \frac{T_{ref} + \gamma \cdot z_0}{T_{ref} + \gamma \cdot z_1} \right) \quad (\text{B.3.1.4.1})$$

i.e.

$$\frac{\partial \ln(T_{ref}, \gamma, z_0, z_1)}{\partial z_1} = \frac{\gamma}{T_{ref} + \gamma \cdot z_1} \quad (\text{B.3.1.4.2})$$

## B.3.2. $S_{11}$

Recall that the series  $S_{11}$  has been defined by eq. (3.4.9.25) as

$$S_{11} := \sum_{n \geq 1} \left( \frac{-1}{\gamma \cdot H_p} \right)^n \cdot \frac{1}{n \cdot n!} \cdot \left[ (T_{ref} + \gamma \cdot z_1)^n - (T_{ref} + \gamma \cdot z_0)^n \right] \quad (\text{B.3.2.1})$$

i.e.

$$S_{11} = S_{11}(T_{ref}, \gamma, z_0, z_1, H_p) \quad (\text{B.3.2.2})$$

Its partial derivatives are

### B.3.2.1. $\partial S_{11} / \partial T_{ref}$

$$\begin{aligned} \frac{\partial S_{11}}{\partial T_{ref}} &= \sum_{n \geq 1} \left( \frac{-1}{\gamma \cdot H_p} \right)^n \cdot \frac{1}{n \cdot n!} \cdot \left[ n \cdot (T_{ref} + \gamma \cdot z_1)^{n-1} - n \cdot (T_{ref} + \gamma \cdot z_0)^{n-1} \right] \\ &= \frac{1}{(T_{ref} + \gamma \cdot z_1)} \cdot \sum_{n \geq 1} \left( \frac{-1}{\gamma \cdot H_p} \right)^n \cdot \frac{1}{n!} \cdot (T_{ref} + \gamma \cdot z_1)^n - \frac{1}{(T_{ref} + \gamma \cdot z_0)} \cdot \sum_{n \geq 1} \left( \frac{-1}{\gamma \cdot H_p} \right)^n \cdot \frac{1}{n!} \cdot (T_{ref} + \gamma \cdot z_0)^n \end{aligned} \quad (\text{B.3.2.1.1})$$

It follows that

$$\frac{\partial S_{11}}{\partial T_{ref}} = \frac{1}{(T_{ref} + \gamma \cdot z_1)} \cdot \left[ e^{\frac{-(T_{ref} + \gamma \cdot z_1)}{\gamma \cdot H_p}} - 1 \right] - \frac{1}{(T_{ref} + \gamma \cdot z_0)} \cdot \left[ e^{\frac{-(T_{ref} + \gamma \cdot z_0)}{\gamma \cdot H_p}} - 1 \right] \quad (\text{B.3.2.1.2})$$

### B.3.2.2. $\partial S_{11}/\partial \gamma$

Compute first this expression

$$\frac{\partial}{\partial \gamma} (-\gamma \cdot H_p)^{-n} = (-n) \cdot (-H_p) \cdot (-\gamma \cdot H_p)^{-n-1} = n \cdot H_p \cdot \left( \frac{-1}{\gamma \cdot H_p} \right)^{n+1} \quad (\text{B.3.3.2.1})$$

It follows then

$$\begin{aligned} \frac{\partial S_{11}}{\partial \gamma} &= \sum_{n \geq 1} n \cdot H_p \cdot \left( \frac{-1}{\gamma \cdot H_p} \right)^{n+1} \cdot \frac{1}{n \cdot n!} \cdot \left[ (T_{ref} + \gamma \cdot z_1)^n - (T_{ref} + \gamma \cdot z_0)^n \right] \\ &+ \sum_{n \geq 1} \left( \frac{-1}{\gamma \cdot H_p} \right)^n \cdot \frac{1}{n \cdot n!} \cdot \left[ n \cdot z_1 \cdot (T_{ref} + \gamma \cdot z_1)^{n-1} - n \cdot z_0 \cdot (T_{ref} + \gamma \cdot z_0)^{n-1} \right] \end{aligned} \quad (\text{B.3.2.2.1})$$

This can be simplified to

$$\begin{aligned} \frac{\partial S_{11}}{\partial \gamma} &= \frac{-H_p}{\gamma \cdot H_p} \cdot \sum_{n \geq 1} \left( \frac{-1}{\gamma \cdot H_p} \right)^n \cdot \frac{1}{n!} \cdot \left[ (T_{ref} + \gamma \cdot z_1)^n - (T_{ref} + \gamma \cdot z_0)^n \right] \\ &+ \frac{z_1}{T_{ref} + \gamma \cdot z_1} \cdot \sum_{n \geq 1} \left( \frac{-1}{\gamma \cdot H_p} \right)^n \cdot \frac{1}{n!} \cdot (T_{ref} + \gamma \cdot z_1)^n \\ &- \frac{z_0}{T_{ref} + \gamma \cdot z_0} \cdot \sum_{n \geq 1} \left( \frac{-1}{\gamma \cdot H_p} \right)^n \cdot \frac{1}{n!} \cdot (T_{ref} + \gamma \cdot z_0)^n \end{aligned} \quad (\text{B.3.2.2.2})$$

i.e.

$$\begin{aligned} \frac{\partial S_{11}}{\partial \gamma} &= \frac{-1}{\gamma} \cdot \left[ \left( e^{\frac{-(T_{ref} + \gamma \cdot z_1)}{\gamma \cdot H_p}} - 1 \right) - \left( e^{\frac{-(T_{ref} + \gamma \cdot z_0)}{\gamma \cdot H_p}} - 1 \right) \right] \\ &+ \frac{z_1}{T_{ref} + \gamma \cdot z_1} \cdot \left( e^{\frac{-(T_{ref} + \gamma \cdot z_1)}{\gamma \cdot H_p}} - 1 \right) \\ &- \frac{z_0}{T_{ref} + \gamma \cdot z_0} \cdot \left( e^{\frac{-(T_{ref} + \gamma \cdot z_0)}{\gamma \cdot H_p}} - 1 \right) \end{aligned} \quad (\text{B.3.2.2.3})$$

and finally

$$\begin{aligned} \frac{\partial S_{11}}{\partial \gamma} &= \frac{-1}{\gamma} \cdot \left[ e^{\frac{-(T_{ref} + \gamma \cdot z_1)}{\gamma \cdot H_p}} - e^{\frac{-(T_{ref} + \gamma \cdot z_0)}{\gamma \cdot H_p}} \right] \\ &+ \frac{z_1}{T_{ref} + \gamma \cdot z_1} \cdot \left( e^{\frac{-(T_{ref} + \gamma \cdot z_1)}{\gamma \cdot H_p}} - 1 \right) - \frac{z_0}{T_{ref} + \gamma \cdot z_0} \cdot \left( e^{\frac{-(T_{ref} + \gamma \cdot z_0)}{\gamma \cdot H_p}} - 1 \right) \end{aligned} \quad (\text{B.3.2.2.4})$$

**B.3.2.3.**  $\partial S_{11}/\partial z_0$

$$\begin{aligned} \frac{\partial S_{11}}{\partial z_0} &= \sum_{n \geq 1} \left( \frac{-1}{\gamma \cdot H_p} \right)^n \cdot \frac{1}{n \cdot n!} \cdot [0 - n \cdot \gamma \cdot (T_{ref} + \gamma \cdot z_0)^{n-1}] \\ &= \frac{-\gamma}{(T_{ref} + \gamma \cdot z_0)} \cdot \sum_{n \geq 1} \left( \frac{-1}{\gamma \cdot H_p} \right)^n \cdot \frac{1}{n!} \cdot (T_{ref} + \gamma \cdot z_0)^n \end{aligned} \quad (\text{B.3.2.3.1})$$

that is

$$\frac{\partial S_{11}}{\partial z_0} = \frac{-\gamma}{(T_{ref} + \gamma \cdot z_0)} \cdot \left[ e^{\frac{-(T_{ref} + \gamma \cdot z_0)}{\gamma \cdot H_p}} - 1 \right] \quad (\text{B.3.2.3.2})$$

**B.3.2.4.**  $\partial S_{11}/\partial z_1$

$$\begin{aligned} \frac{\partial S_{11}}{\partial z_1} &= \sum_{n \geq 1} \left( \frac{-1}{\gamma \cdot H_p} \right)^n \cdot \frac{1}{n \cdot n!} \cdot [n \cdot \gamma \cdot (T_{ref} + \gamma \cdot z_1)^{n-1} - 0] \\ &= \frac{\gamma}{(T_{ref} + \gamma \cdot z_1)} \cdot \sum_{n \geq 1} \left( \frac{-1}{\gamma \cdot H_p} \right)^n \cdot \frac{1}{n!} \cdot (T_{ref} + \gamma \cdot z_1)^n \end{aligned} \quad (\text{B.3.2.4.1})$$

i.e.

$$\frac{\partial S_{11}}{\partial z_1} = \frac{\gamma}{(T_{ref} + \gamma \cdot z_1)} \cdot \left[ e^{\frac{-(T_{ref} + \gamma \cdot z_1)}{\gamma \cdot H_p}} - 1 \right] \quad (\text{B.3.2.4.2})$$

**B.3.2.5.**  $\partial S_{11}/\partial H_p$

$$\begin{aligned} \frac{\partial S_{11}}{\partial H_p} &= \sum_{n \geq 1} (-\gamma \cdot H_p)^{-n-1} \cdot (-n) \cdot (-\gamma) \cdot \frac{1}{n \cdot n!} \cdot [(T_{ref} + \gamma \cdot z_1)^n - (T_{ref} + \gamma \cdot z_0)^n] \\ &= \frac{\gamma}{-\gamma \cdot H_p} \cdot \sum_{n \geq 1} (-\gamma \cdot H_p)^{-n} \cdot \frac{1}{n!} \cdot [(T_{ref} + \gamma \cdot z_1)^n - (T_{ref} + \gamma \cdot z_0)^n] \\ &= \frac{-1}{H_p} \cdot \left[ \left( e^{\frac{-(T_{ref} + \gamma \cdot z_1)}{\gamma \cdot H_p}} - 1 \right) - \left( e^{\frac{-(T_{ref} + \gamma \cdot z_0)}{\gamma \cdot H_p}} - 1 \right) \right] \end{aligned} \quad (\text{B.3.2.5.1})$$

i.e.

$$\frac{\partial S_{11}}{\partial H_p} = \frac{-1}{H_p} \cdot \left[ e^{\frac{-(T_{ref} + \gamma \cdot z_1)}{\gamma \cdot H_p}} - e^{\frac{-(T_{ref} + \gamma \cdot z_0)}{\gamma \cdot H_p}} \right] \quad (\text{B.3.2.5.2})$$

### B.3.3. S<sub>12</sub>

Recall that the series  $S_{12}$  has been defined by eq. (3.4.9.27) as

$$S_{12} := \sum_{n \geq 1} \left( \frac{-1}{\gamma \cdot H_e} \right)^n \cdot \frac{1}{n \cdot n!} \cdot \left[ (T_{ref} + \gamma \cdot z_1)^n - (T_{ref} + \gamma \cdot z_0)^n \right] \quad (\text{B.3.3.1})$$

It differs from  $S_{11}$  only through one term, namely the first factor in eq. (B.3.3.1). Indeed  $H_e$  is replaced by  $H_p$ . Therefore both series depends on the same variable, except for  $H_e$  and  $H_p$ , i.e.

$$S_{12} = S_{12}(T_{ref}, \gamma, z_0, z_1, H_e) \quad (\text{B.3.3.2})$$

Their partial derivatives are similar. Hence retake the results from paragraph B.3.2.

#### B.3.3.1. $\partial S_{12} / \partial T_{ref}$

$$\frac{\partial S_{12}}{\partial T_{ref}} = \frac{1}{(T_{ref} + \gamma \cdot z_1)} \cdot \left[ e^{\frac{-(T_{ref} + \gamma \cdot z_1)}{\gamma \cdot H_e}} - 1 \right] - \frac{1}{(T_{ref} + \gamma \cdot z_0)} \cdot \left[ e^{\frac{-(T_{ref} + \gamma \cdot z_0)}{\gamma \cdot H_e}} - 1 \right] \quad (\text{B.3.3.1.1})$$

#### B.3.3.2. $\partial S_{12} / \partial \gamma$

$$\begin{aligned} \frac{\partial S_{12}}{\partial \gamma} = & \frac{-1}{\gamma} \cdot \left[ e^{\frac{-(T_{ref} + \gamma \cdot z_1)}{\gamma \cdot H_e}} - e^{\frac{-(T_{ref} + \gamma \cdot z_0)}{\gamma \cdot H_e}} \right] \\ & + \frac{z_1}{T_{ref} + \gamma \cdot z_1} \cdot \left( e^{\frac{-(T_{ref} + \gamma \cdot z_1)}{\gamma \cdot H_e}} - 1 \right) - \frac{z_0}{T_{ref} + \gamma \cdot z_0} \cdot \left( e^{\frac{-(T_{ref} + \gamma \cdot z_0)}{\gamma \cdot H_e}} - 1 \right) \end{aligned} \quad (\text{B.3.3.2.1})$$

#### B.3.3.3. $\partial S_{12} / \partial z_0$

$$\frac{\partial S_{12}}{\partial z_0} = \frac{-\gamma}{(T_{ref} + \gamma \cdot z_0)} \cdot \left[ e^{\frac{-(T_{ref} + \gamma \cdot z_0)}{\gamma \cdot H_e}} - 1 \right] \quad (\text{B.3.3.3.1})$$

#### B.3.3.4. $\partial S_{12} / \partial z_1$

$$\frac{\partial S_{12}}{\partial z_1} = \frac{\gamma}{(T_{ref} + \gamma \cdot z_1)} \cdot \left[ e^{\frac{-(T_{ref} + \gamma \cdot z_1)}{\gamma \cdot H_e}} - 1 \right] \quad (\text{B.3.3.4.1})$$



**B.3.3.5.**  $\partial S_{12}/\partial H_e$ 

$$\frac{\partial S_{12}}{\partial H_e} = \frac{-1}{H_e} \cdot \left[ e^{\frac{-(T_{ref} + \gamma \cdot z_1)}{\gamma \cdot H_e}} - e^{\frac{-(T_{ref} + \gamma \cdot z_0)}{\gamma \cdot H_e}} \right] \quad (\text{B.3.3.5.1})$$

**B.4. Zenith Dry Delay partial derivatives**

The partial derivatives of the ZDD with respect to the parameters of eq. (B.1.3) or eq. (B.1.7) are computed in the following.

**B.4.1.**  $\partial ZDD/\partial p_{ref}$ 

Note that the ZDD is linear in  $p_{ref}$ . Its partial derivative is then easy to compute.

$$\begin{aligned} \frac{\partial ZDD}{\partial p_{ref}} &= 10^{-6} \cdot 77.64 \cdot \frac{1}{\gamma} \cdot e^{\frac{T_{ref}}{\gamma \cdot H_p}} \cdot \left[ \ln \left( \frac{T_{ref} + \gamma \cdot z_1}{T_{ref} + \gamma \cdot z_0} \right) + S_{11} \right] \\ &+ 10^{-6} \cdot 77.64 \cdot \frac{1}{T_1} \cdot H_p \cdot \left[ e^{\frac{-z_1}{H_p}} - e^{\frac{-z'}{H_p}} \right] \end{aligned} \quad (\text{B.4.1.1})$$

**B.4.2.**  $\partial ZDD/\partial e_{ref}$ 

As remarked before, the ZDD is also linear in  $e_{ref}$ . Thus

$$\begin{aligned} \frac{\partial ZDD}{\partial e_{ref}} &= -10^{-6} \cdot 77.64 \cdot \frac{1}{\gamma} \cdot e^{\frac{T_{ref}}{\gamma \cdot H_e}} \cdot \left[ \ln \left( \frac{T_{ref} + \gamma \cdot z_1}{T_{ref} + \gamma \cdot z_0} \right) + S_{12} \right] \\ &- 10^{-6} \cdot 77.64 \cdot \frac{1}{T_1} \cdot H_e \cdot \left[ e^{\frac{-z'}{H_e}} - e^{\frac{-z_1}{H_e}} \right] \end{aligned} \quad (\text{B.4.2.1})$$

**B.4.3.**  $\partial ZDD/\partial T_{ref}$ 

To compute this partial derivative, use eq. (B.3.1.1.2). One has

$$\begin{aligned} \frac{\partial ZDD}{\partial T_{ref}} &= 10^{-6} \cdot 77.64 \cdot \frac{p_{ref}}{\gamma} \cdot \frac{1}{\gamma \cdot H_p} \cdot e^{\frac{T_{ref}}{\gamma \cdot H_p}} \cdot \left[ \ln \left( \frac{T_{ref} + \gamma \cdot z_1}{T_{ref} + \gamma \cdot z_0} \right) + S_{11} \right] \\ &+ 10^{-6} \cdot 77.64 \cdot \frac{p_{ref}}{\gamma} \cdot e^{\frac{T_{ref}}{\gamma \cdot H_p}} \cdot \left[ \frac{\gamma \cdot (z_0 - z_1)}{(T_{ref} + \gamma \cdot z_0) \cdot (T_{ref} + \gamma \cdot z_1)} + \frac{\partial S_{11}}{\partial T_{ref}} \right] \\ &- 10^{-6} \cdot 77.64 \cdot \frac{e_{ref}}{\gamma} \cdot \frac{1}{\gamma \cdot H_e} \cdot e^{\frac{T_{ref}}{\gamma \cdot H_e}} \cdot \left[ \ln \left( \frac{T_{ref} + \gamma \cdot z_1}{T_{ref} + \gamma \cdot z_0} \right) + S_{12} \right] \\ &- 10^{-6} \cdot 77.64 \cdot \frac{e_{ref}}{\gamma} \cdot e^{\frac{T_{ref}}{\gamma \cdot H_e}} \cdot \left[ \frac{\gamma \cdot (z_0 - z_1)}{(T_{ref} + \gamma \cdot z_0) \cdot (T_{ref} + \gamma \cdot z_1)} + \frac{\partial S_{12}}{\partial T_{ref}} \right] \\ &+ 0 - 0 \end{aligned} \quad (\text{B.4.3.1})$$

Insert eq. (B.3.2.1.2) and eq. (B.3.3.1.1) in eq. (B.4.3.1).

$$\begin{aligned}
\frac{\partial ZDD}{\partial T_{ref}} &= 10^{-6} \cdot 77.64 \cdot p_{ref} \cdot e^{\frac{T_{ref}}{\gamma \cdot H_p}} \cdot \left( \frac{1}{\gamma^2 \cdot H_p} \cdot \left[ \ln \left( \frac{T_{ref} + \gamma \cdot z_1}{T_{ref} + \gamma \cdot z_0} \right) + S_{11} \right] + \frac{(z_0 - z_1)}{(T_{ref} + \gamma \cdot z_0) \cdot (T_{ref} + \gamma \cdot z_1)} \right) \\
&+ 10^{-6} \cdot 77.64 \cdot \frac{p_{ref}}{\gamma} \cdot e^{\frac{T_{ref}}{\gamma \cdot H_p}} \cdot \left( \frac{1}{(T_{ref} + \gamma \cdot z_1)} \cdot \left[ e^{\frac{-(T_{ref} + \gamma \cdot z_1)}{\gamma \cdot H_p}} - 1 \right] - \frac{1}{(T_{ref} + \gamma \cdot z_0)} \cdot \left[ e^{\frac{-(T_{ref} + \gamma \cdot z_0)}{\gamma \cdot H_p}} - 1 \right] \right) \\
&- 10^{-6} \cdot 77.64 \cdot e_{ref} \cdot e^{\frac{T_{ref}}{\gamma \cdot H_e}} \cdot \left( \frac{1}{\gamma^2 \cdot H_e} \cdot \left[ \ln \left( \frac{T_{ref} + \gamma \cdot z_1}{T_{ref} + \gamma \cdot z_0} \right) + S_{12} \right] + \frac{(z_0 - z_1)}{(T_{ref} + \gamma \cdot z_0) \cdot (T_{ref} + \gamma \cdot z_1)} \right) \\
&- 10^{-6} \cdot 77.64 \cdot \frac{e_{ref}}{\gamma} \cdot e^{\frac{T_{ref}}{\gamma \cdot H_e}} \cdot \left[ \frac{1}{(T_{ref} + \gamma \cdot z_1)} \cdot \left[ e^{\frac{-(T_{ref} + \gamma \cdot z_1)}{\gamma \cdot H_e}} - 1 \right] - \frac{1}{(T_{ref} + \gamma \cdot z_0)} \cdot \left[ e^{\frac{-(T_{ref} + \gamma \cdot z_0)}{\gamma \cdot H_e}} - 1 \right] \right]
\end{aligned} \tag{B.4.3.2}$$

#### B.4.4. $\partial ZDD/\partial T_1$

$$\begin{aligned}
\frac{\partial ZDD}{\partial T_1} &= 0 - 0 + 10^{-6} \cdot 77.64 \cdot \left( \frac{-p_{ref}}{T_1^2} \right) \cdot H_p \cdot \left[ e^{\frac{-z_1}{H_p}} - e^{\frac{-z'}{H_p}} \right] \\
&- 10^{-6} \cdot 77.64 \cdot \left( \frac{-e_{ref}}{T_1^2} \right) \cdot H_e \cdot \left[ e^{\frac{-z'}{H_e}} - e^{\frac{-z_1}{H_e}} \right]
\end{aligned} \tag{B.4.4.1}$$

that is

$$\frac{\partial ZDD}{\partial T_1} = 10^{-6} \cdot 77.64 \cdot \frac{p_{ref}}{T_1^2} \cdot H_p \cdot \left[ e^{\frac{-z'}{H_p}} - e^{\frac{-z_1}{H_p}} \right] + 10^{-6} \cdot 77.64 \cdot \frac{e_{ref}}{T_1^2} \cdot H_e \cdot \left[ e^{\frac{-z'}{H_e}} - e^{\frac{-z_1}{H_e}} \right] \tag{B.4.4.2}$$

#### B.4.5. $\partial ZDD/\partial \gamma$

It holds

$$\frac{\partial}{\partial \gamma} e^{\frac{-T_{ref}}{\gamma \cdot H_p}} = \frac{0 - T_{ref} \cdot H_p}{(\gamma \cdot H_p)^2} \cdot e^{\frac{-T_{ref}}{\gamma \cdot H_p}} = \frac{-T_{ref}}{\gamma^2 \cdot H_p} \cdot e^{\frac{-T_{ref}}{\gamma \cdot H_p}} \tag{B.4.5.1}$$

Use eq. (B.3.1.2.2), (B.3.2.2.4) and eq. (B.3.3.2.1).

$$\begin{aligned}
\frac{\partial ZDD}{\partial \gamma} = & 10^{-6} \cdot 77.64 \cdot \left( \frac{-P_{ref}}{\gamma^2} \right) \cdot e^{\frac{T_{ref}}{\gamma \cdot H_p}} \cdot \left[ \ln \left( \frac{T_{ref} + \gamma \cdot z_1}{T_{ref} + \gamma \cdot z_0} \right) + S_{11} \right] \\
& + 10^{-6} \cdot 77.64 \cdot \frac{P_{ref}}{\gamma} \cdot \left( \frac{-H_p}{T_{ref}} \right) \cdot \left( \frac{T_{ref}}{\gamma \cdot H_p} \right)^2 \cdot e^{\frac{T_{ref}}{\gamma \cdot H_p}} \cdot \left[ \ln \left( \frac{T_{ref} + \gamma \cdot z_1}{T_{ref} + \gamma \cdot z_0} \right) + S_{11} \right] \\
& + 10^{-6} \cdot 77.64 \cdot \frac{P_{ref}}{\gamma} \cdot e^{\frac{T_{ref}}{\gamma \cdot H_p}} \cdot \left[ \frac{T_{ref} \cdot (z_1 - z_0)}{(T_{ref} + \gamma \cdot z_0) \cdot (T_{ref} + \gamma \cdot z_1)} + \frac{\partial S_{11}}{\partial \gamma} \right] \\
& - 10^{-6} \cdot 77.64 \cdot \left( \frac{-e_{ref}}{\gamma^2} \right) \cdot e^{\frac{T_{ref}}{\gamma \cdot H_e}} \cdot \left[ \ln \left( \frac{T_{ref} + \gamma \cdot z_1}{T_{ref} + \gamma \cdot z_0} \right) + S_{12} \right] \\
& - 10^{-6} \cdot 77.64 \cdot \frac{e_{ref}}{\gamma} \cdot \left( \frac{-H_e}{T_{ref}} \right) \cdot \left( \frac{T_{ref}}{\gamma \cdot H_e} \right)^2 \cdot e^{\frac{T_{ref}}{\gamma \cdot H_e}} \cdot \left[ \ln \left( \frac{T_{ref} + \gamma \cdot z_1}{T_{ref} + \gamma \cdot z_0} \right) + S_{12} \right] \\
& - 10^{-6} \cdot 77.64 \cdot \frac{e_{ref}}{\gamma} \cdot e^{\frac{T_{ref}}{\gamma \cdot H_e}} \cdot \left[ \frac{T_{ref} \cdot (z_1 - z_0)}{(T_{ref} + \gamma \cdot z_0) \cdot (T_{ref} + \gamma \cdot z_1)} + \frac{\partial S_{12}}{\partial \gamma} \right] \\
& + 0 - 0
\end{aligned} \tag{B.4.5.2}$$

Rewrite it by inserting (B.3.2.2.4) and eq. (B.3.3.2.1) in eq. (B.4.5.1).

$$\begin{aligned}
\frac{\partial ZDD}{\partial \gamma} = & 10^{-6} \cdot 77.64 \cdot \frac{P_{ref}}{\gamma} \cdot e^{\frac{T_{ref}}{\gamma \cdot H_p}} \cdot \left[ -\frac{1}{\gamma} \cdot \left( 1 + \frac{T_{ref}}{\gamma \cdot H_p} \right) \cdot \left[ \ln \left( \frac{T_{ref} + \gamma \cdot z_1}{T_{ref} + \gamma \cdot z_0} \right) + S_{11} \right] \right] \\
& + 10^{-6} \cdot 77.64 \cdot \frac{P_{ref}}{\gamma} \cdot e^{\frac{T_{ref}}{\gamma \cdot H_p}} \cdot \left[ \frac{T_{ref} \cdot (z_1 - z_0)}{(T_{ref} + \gamma \cdot z_0) \cdot (T_{ref} + \gamma \cdot z_1)} - \frac{1}{\gamma} \cdot \left[ e^{\frac{-(T_{ref} + \gamma \cdot z_1)}{\gamma \cdot H_p}} - e^{\frac{-(T_{ref} + \gamma \cdot z_0)}{\gamma \cdot H_p}} \right] \right] \\
& + 10^{-6} \cdot 77.64 \cdot \frac{P_{ref}}{\gamma} \cdot e^{\frac{T_{ref}}{\gamma \cdot H_p}} \cdot \left[ \frac{z_1}{T_{ref} + \gamma \cdot z_1} \cdot \left( e^{\frac{-(T_{ref} + \gamma \cdot z_1)}{\gamma \cdot H_p}} - 1 \right) - \frac{z_0}{T_{ref} + \gamma \cdot z_0} \cdot \left( e^{\frac{-(T_{ref} + \gamma \cdot z_0)}{\gamma \cdot H_p}} - 1 \right) \right] \\
& + 10^{-6} \cdot 77.64 \cdot \frac{e_{ref}}{\gamma} \cdot e^{\frac{T_{ref}}{\gamma \cdot H_e}} \cdot \left[ \frac{1}{\gamma} \cdot \left( 1 + \frac{T_{ref}}{\gamma \cdot H_e} \right) \cdot \left[ \ln \left( \frac{T_{ref} + \gamma \cdot z_1}{T_{ref} + \gamma \cdot z_0} \right) + S_{12} \right] \right] \\
& - 10^{-6} \cdot 77.64 \cdot \frac{e_{ref}}{\gamma} \cdot e^{\frac{T_{ref}}{\gamma \cdot H_e}} \cdot \left[ \frac{T_{ref} \cdot (z_1 - z_0)}{(T_{ref} + \gamma \cdot z_0) \cdot (T_{ref} + \gamma \cdot z_1)} - \frac{1}{\gamma} \cdot \left[ e^{\frac{-(T_{ref} + \gamma \cdot z_1)}{\gamma \cdot H_e}} - e^{\frac{-(T_{ref} + \gamma \cdot z_0)}{\gamma \cdot H_e}} \right] \right] \\
& - 10^{-6} \cdot 77.64 \cdot \frac{e_{ref}}{\gamma} \cdot e^{\frac{T_{ref}}{\gamma \cdot H_e}} \cdot \left[ \frac{z_1}{T_{ref} + \gamma \cdot z_1} \cdot \left( e^{\frac{-(T_{ref} + \gamma \cdot z_1)}{\gamma \cdot H_e}} - 1 \right) - \frac{z_0}{T_{ref} + \gamma \cdot z_0} \cdot \left( e^{\frac{-(T_{ref} + \gamma \cdot z_0)}{\gamma \cdot H_e}} - 1 \right) \right]
\end{aligned} \tag{B.4.5.3}$$

#### B.4.6. $\partial ZDD / \partial z_0$

Use eq. (B.3.1.3.2), (B.3.2.3.4) and eq. (B.3.3.3.1). It holds

$$\begin{aligned}
\frac{\partial ZDD}{\partial z_0} &= 10^{-6} \cdot 77.64 \cdot \frac{P_{ref}}{\gamma} \cdot e^{\frac{T_{ref}}{\gamma \cdot H_p}} \cdot \left[ \frac{-\gamma}{T_{ref} + \gamma \cdot z_0} + \frac{\partial S_{11}}{\partial z_0} \right] \\
&\quad - 10^{-6} \cdot 77.64 \cdot \frac{e_{ref}}{\gamma} \cdot e^{\frac{T_{ref}}{\gamma \cdot H_e}} \cdot \left[ \frac{-\gamma}{T_{ref} + \gamma \cdot z_0} + \frac{\partial S_{12}}{\partial z_0} \right] \\
&\quad + 0 - 0
\end{aligned} \tag{B.4.6.1}$$

That is

$$\begin{aligned}
\frac{\partial ZDD}{\partial z_0} &= 10^{-6} \cdot 77.64 \cdot \frac{P_{ref}}{\gamma} \cdot e^{\frac{T_{ref}}{\gamma \cdot H_p}} \cdot \left[ \frac{-\gamma}{T_{ref} + \gamma \cdot z_0} + \frac{-\gamma}{(T_{ref} + \gamma \cdot z_0)} \cdot \left[ e^{\frac{-(T_{ref} + \gamma \cdot z_0)}{\gamma \cdot H_p}} - 1 \right] \right] \\
&\quad - 10^{-6} \cdot 77.64 \cdot \frac{e_{ref}}{\gamma} \cdot e^{\frac{T_{ref}}{\gamma \cdot H_e}} \cdot \left[ \frac{-\gamma}{T_{ref} + \gamma \cdot z_0} + \frac{-\gamma}{(T_{ref} + \gamma \cdot z_0)} \cdot \left[ e^{\frac{-(T_{ref} + \gamma \cdot z_0)}{\gamma \cdot H_e}} - 1 \right] \right]
\end{aligned} \tag{B.4.6.2}$$

This reduces to

$$\begin{aligned}
\frac{\partial ZDD}{\partial z_0} &= -10^{-6} \cdot 77.64 \cdot \frac{P_{ref}}{T_{ref} + \gamma \cdot z_0} \cdot e^{\frac{T_{ref}}{\gamma \cdot H_p}} \cdot \left[ 1 + \left[ e^{\frac{-(T_{ref} + \gamma \cdot z_0)}{\gamma \cdot H_p}} - 1 \right] \right] \\
&\quad + 10^{-6} \cdot 77.64 \cdot \frac{e_{ref}}{T_{ref} + \gamma \cdot z_0} \cdot e^{\frac{T_{ref}}{\gamma \cdot H_e}} \cdot \left[ 1 + \left[ e^{\frac{-(T_{ref} + \gamma \cdot z_0)}{\gamma \cdot H_e}} - 1 \right] \right]
\end{aligned} \tag{B.4.6.3}$$

or

$$\frac{\partial ZDD}{\partial z_0} = -10^{-6} \cdot 77.64 \cdot \frac{P_{ref}}{T_{ref} + \gamma \cdot z_0} \cdot e^{\frac{-z_0}{H_p}} + 10^{-6} \cdot 77.64 \cdot \frac{e_{ref}}{T_{ref} + \gamma \cdot z_0} \cdot e^{\frac{-z_0}{H_e}} \tag{B.4.6.4}$$

that is

$$\frac{\partial ZDD}{\partial z_0} = \frac{10^{-6} \cdot 77.64}{T_{ref} + \gamma \cdot z_0} \cdot \left[ -P_{ref} \cdot e^{\frac{-z_0}{H_p}} + e_{ref} \cdot e^{\frac{-z_0}{H_e}} \right] \tag{B.4.6.5}$$

#### B.4.7. $\partial ZDD/\partial z_1$

Use eq. (B.3.1.4.2), (B.3.2.4.2) and eq. (B.3.3.4.1). It holds

$$\begin{aligned}
\frac{\partial ZDD}{\partial z_1} &= 10^{-6} \cdot 77.64 \cdot \frac{P_{ref}}{\gamma} \cdot e^{\frac{T_{ref}}{\gamma \cdot H_p}} \cdot \left[ \frac{\gamma}{T_{ref} + \gamma \cdot z_1} + \frac{\partial S_{11}}{\partial z_1} \right] \\
&\quad - 10^{-6} \cdot 77.64 \cdot \frac{e_{ref}}{\gamma} \cdot e^{\frac{T_{ref}}{\gamma \cdot H_e}} \cdot \left[ \frac{\gamma}{T_{ref} + \gamma \cdot z_1} + \frac{\partial S_{12}}{\partial z_1} \right] \\
&\quad + 10^{-6} \cdot 77.64 \cdot \frac{P_{ref}}{T_1} \cdot H_p \cdot \left[ \frac{-1}{H_p} \cdot e^{\frac{-z_1}{H_p}} - 0 \right] \\
&\quad - 10^{-6} \cdot 77.64 \cdot \frac{e_{ref}}{T_1} \cdot H_e \cdot \left[ 0 - \frac{-1}{H_e} \cdot e^{\frac{-z_1}{H_e}} \right]
\end{aligned} \tag{B.4.7.1}$$

This is

$$\begin{aligned}
\frac{\partial ZDD}{\partial z_1} &= 10^{-6} \cdot 77.64 \cdot \frac{P_{ref}}{\gamma} \cdot e^{\frac{T_{ref}}{\gamma \cdot H_p}} \cdot \left[ \frac{\gamma}{T_{ref} + \gamma \cdot z_1} + \frac{\gamma}{(T_{ref} + \gamma \cdot z_1)} \cdot \left[ e^{\frac{-(T_{ref} + \gamma \cdot z_1)}{\gamma \cdot H_p}} - 1 \right] \right] \\
&\quad - 10^{-6} \cdot 77.64 \cdot \frac{e_{ref}}{\gamma} \cdot e^{\frac{T_{ref}}{\gamma \cdot H_e}} \cdot \left[ \frac{\gamma}{T_{ref} + \gamma \cdot z_1} + \frac{\gamma}{(T_{ref} + \gamma \cdot z_1)} \cdot \left[ e^{\frac{-(T_{ref} + \gamma \cdot z_1)}{\gamma \cdot H_e}} - 1 \right] \right] \\
&\quad - 10^{-6} \cdot 77.64 \cdot \frac{P_{ref}}{T_1} \cdot e^{\frac{-z_1}{H_p}} \\
&\quad - 10^{-6} \cdot 77.64 \cdot \frac{e_{ref}}{T_1} \cdot e^{\frac{-z_1}{H_e}}
\end{aligned} \tag{B.4.7.2}$$

Eq. (B.4.7.2) can be rewritten as

$$\begin{aligned}
\frac{\partial ZDD}{\partial z_1} &= 10^{-6} \cdot 77.64 \cdot \frac{P_{ref}}{T_{ref} + \gamma \cdot z_1} \cdot e^{\frac{-z_1}{H_p}} \\
&\quad - 10^{-6} \cdot 77.64 \cdot \frac{e_{ref}}{T_{ref} + \gamma \cdot z_1} \cdot e^{\frac{-z_1}{H_e}} \\
&\quad - 10^{-6} \cdot 77.64 \cdot \frac{P_{ref}}{T_1} \cdot e^{\frac{-z_1}{H_p}} \\
&\quad - 10^{-6} \cdot 77.64 \cdot \frac{e_{ref}}{T_1} \cdot e^{\frac{-z_1}{H_e}}
\end{aligned} \tag{B.4.7.3}$$

or

$$\begin{aligned}
\frac{\partial ZDD}{\partial z_1} &= 10^{-6} \cdot 77.64 \cdot \frac{1}{T_{ref} + \gamma \cdot z_1} \cdot \left[ p_{ref} \cdot e^{\frac{-z_1}{H_p}} - e_{ref} \cdot e^{\frac{-z_1}{H_e}} \right] \\
&\quad - 10^{-6} \cdot 77.64 \cdot \frac{1}{T_1} \cdot \left[ p_{ref} \cdot e^{\frac{-z_1}{H_p}} + e_{ref} \cdot e^{\frac{-z_1}{H_e}} \right]
\end{aligned} \tag{B.4.7.4}$$

#### B.4.8. $\partial ZDD/\partial z'$

$$\begin{aligned}
\frac{\partial ZDD}{\partial z'} &= 0 - 0 \\
&\quad + 10^{-6} \cdot 77.64 \cdot \frac{P_{ref}}{T_1} \cdot H_p \cdot \left[ 0 - \left( \frac{-1}{H_p} \right) \cdot e^{\frac{-z'}{H_p}} \right] \\
&\quad - 10^{-6} \cdot 77.64 \cdot \frac{e_{ref}}{T_1} \cdot H_e \cdot \left[ \left( \frac{-1}{H_e} \right) \cdot e^{\frac{-z'}{H_e}} - 0 \right]
\end{aligned} \tag{B.4.8.1}$$

that is

$$\frac{\partial ZDD}{\partial z'} = 10^{-6} \cdot 77.64 \cdot \frac{P_{ref}}{T_1} \cdot e^{\frac{-z'}{H_p}} + 10^{-6} \cdot 77.64 \cdot \frac{e_{ref}}{T_1} \cdot e^{\frac{-z'}{H_e}} \tag{B.4.8.2}$$

or

$$\frac{\partial ZDD}{\partial z'} = 10^{-6} \cdot 77.64 \cdot \frac{1}{T_1} \cdot \left( p_{ref} \cdot e^{\frac{-z'}{H_p}} + e_{ref} \cdot e^{\frac{-z'}{H_e}} \right) \quad (\text{B.4.8.3})$$

#### B.4.9. $\partial ZDD/\partial H_p$

Remark that it holds

$$\frac{\partial}{\partial H_p} e^{\pm \frac{z}{H_p}} = (\pm z) \cdot \left( \frac{-1}{H_p^2} \right) \cdot e^{\pm \frac{z}{H_p}} = \mp \frac{z}{H_p^2} \cdot e^{\pm \frac{z}{H_p}} \quad (\text{B.4.9.1})$$

Use the fact that  $S_{12}$  does not depend on  $H_p$ .

$$\begin{aligned} \frac{\partial ZDD}{\partial H_p} &= 10^{-6} \cdot 77.64 \cdot \frac{p_{ref}}{\gamma} \cdot \left( \frac{-T_{ref}}{\gamma \cdot H_p^2} \right) \cdot e^{\frac{T_{ref}}{\gamma \cdot H_p}} \cdot \left[ \ln \left( \frac{T_{ref} + \gamma \cdot z_1}{T_{ref} + \gamma \cdot z_0} \right) + S_{11} \right] \\ &+ 10^{-6} \cdot 77.64 \cdot \frac{p_{ref}}{\gamma} \cdot e^{\frac{T_{ref}}{\gamma \cdot H_p}} \cdot \left[ 0 + \frac{\partial S_{11}}{\partial H_p} \right] \\ &- 0 \\ &+ 10^{-6} \cdot 77.64 \cdot \frac{p_{ref}}{T_1} \cdot 1 \cdot \left[ e^{\frac{-z_1}{H_p}} - e^{\frac{-z'}{H_p}} \right] \\ &+ 10^{-6} \cdot 77.64 \cdot \frac{p_{ref}}{T_1} \cdot H_p \cdot \left[ \frac{z_1}{H_p^2} \cdot e^{\frac{-z_1}{H_p}} - \frac{z'}{H_p^2} \cdot e^{\frac{-z'}{H_p}} \right] \\ &- 0 \end{aligned} \quad (\text{B.4.9.2})$$

that is

$$\begin{aligned} \frac{\partial ZDD}{\partial H_p} &= 10^{-6} \cdot 77.64 \cdot \frac{p_{ref}}{\gamma} \cdot e^{\frac{T_{ref}}{\gamma \cdot H_p}} \cdot \left[ \left( \frac{-T_{ref}}{\gamma \cdot H_p^2} \right) \cdot \left[ \ln \left( \frac{T_{ref} + \gamma \cdot z_1}{T_{ref} + \gamma \cdot z_0} \right) + S_{11} \right] + \frac{\partial S_{11}}{\partial H_p} \right] \\ &+ 10^{-6} \cdot 77.64 \cdot \frac{p_{ref}}{T_1} \cdot \left[ \left( 1 + \frac{z_1}{H_p} \right) \cdot e^{\frac{-z_1}{H_p}} - \left( 1 + \frac{z'}{H_p} \right) \cdot e^{\frac{-z'}{H_p}} \right] \end{aligned} \quad (\text{B.4.9.3})$$

With eq. (B.3.2.5.2) it follows that

$$\begin{aligned} \frac{\partial ZDD}{\partial H_p} &= 10^{-6} \cdot 77.64 \cdot \frac{p_{ref}}{\gamma} \cdot e^{\frac{T_{ref}}{\gamma \cdot H_p}} \cdot \left[ \left( \frac{-T_{ref}}{\gamma \cdot H_p^2} \right) \cdot \left[ \ln \left( \frac{T_{ref} + \gamma \cdot z_1}{T_{ref} + \gamma \cdot z_0} \right) + S_{11} \right] + \frac{-1}{H_p} \cdot \left( e^{\frac{-(T_{ref} + \gamma \cdot z_1)}{\gamma \cdot H_p}} - e^{\frac{-(T_{ref} + \gamma \cdot z_0)}{\gamma \cdot H_p}} \right) \right] \\ &+ 10^{-6} \cdot 77.64 \cdot \frac{p_{ref}}{T_1} \cdot \left[ \left( 1 + \frac{z_1}{H_p} \right) \cdot e^{\frac{-z_1}{H_p}} - \left( 1 + \frac{z'}{H_p} \right) \cdot e^{\frac{-z'}{H_p}} \right] \end{aligned} \quad (\text{B.4.9.4})$$

i.e.

$$\begin{aligned} \frac{\partial ZDD}{\partial H_p} = & -10^{-6} \cdot 77.64 \cdot \frac{p_{ref}}{\gamma \cdot H_p} \cdot e^{\frac{T_{ref}}{\gamma \cdot H_p}} \cdot \left[ \left( \frac{T_{ref}}{\gamma \cdot H_p} \right) \cdot \left[ \ln \left( \frac{T_{ref} + \gamma \cdot z_1}{T_{ref} + \gamma \cdot z_0} \right) + S_{11} \right] + e^{\frac{-(T_{ref} + \gamma \cdot z_1)}{\gamma \cdot H_p}} - e^{\frac{-(T_{ref} + \gamma \cdot z_0)}{\gamma \cdot H_p}} \right] \\ & + 10^{-6} \cdot 77.64 \cdot \frac{p_{ref}}{T_1} \cdot \left[ \left( 1 + \frac{z_1}{H_p} \right) \cdot e^{\frac{-z_1}{H_p}} - \left( 1 + \frac{z'}{H_p} \right) \cdot e^{\frac{-z'}{H_p}} \right] \end{aligned} \quad (\text{B.4.9.5})$$

#### B.4.10. $\partial ZDD/\partial H_e$

Remark that it holds

$$\frac{\partial}{\partial H_e} e^{\pm \frac{z}{H_e}} = (\pm z) \cdot \left( \frac{-1}{H_e^2} \right) \cdot e^{\pm \frac{z}{H_e}} = \mp \frac{z}{H_e^2} \cdot e^{\pm \frac{z}{H_e}} \quad (\text{B.4.10.1})$$

Now use eq. (B.3.3.5.1) and the fact that  $S_{11}$  does not depend on  $H_e$ .

$$\begin{aligned} \frac{\partial ZDD}{\partial H_e} = & 0 - 10^{-6} \cdot 77.64 \cdot \frac{e_{ref}}{\gamma} \cdot \left( \frac{-T_{ref}}{\gamma \cdot H_e^2} \right) \cdot e^{\frac{T_{ref}}{\gamma \cdot H_e}} \cdot \left[ \ln \left( \frac{T_{ref} + \gamma \cdot z_1}{T_{ref} + \gamma \cdot z_0} \right) + S_{12} \right] \\ & - 10^{-6} \cdot 77.64 \cdot \frac{e_{ref}}{\gamma} \cdot e^{\frac{T_{ref}}{\gamma \cdot H_e}} \cdot \left[ 0 + \frac{\partial S_{12}}{\partial H_e} \right] \\ & + 0 - 10^{-6} \cdot 77.64 \cdot \frac{e_{ref}}{\gamma} \cdot e^{\frac{T_{ref}}{\gamma \cdot H_e}} \cdot \left[ e^{\frac{-z'}{H_e}} - e^{\frac{-z_1}{H_e}} \right] \\ & - 10^{-6} \cdot 77.64 \cdot \frac{e_{ref}}{T_1} \cdot H_e \cdot \left[ \left( \frac{z'}{H_e^2} \right) \cdot e^{\frac{-z'}{H_e}} - \left( \frac{-z_1}{H_e^2} \right) \cdot e^{\frac{-z_1}{H_e}} \right] \end{aligned} \quad (\text{B.4.10.2})$$

i.e.

$$\begin{aligned} \frac{\partial ZDD}{\partial H_e} = & -10^{-6} \cdot 77.64 \cdot \frac{e_{ref}}{\gamma} \cdot e^{\frac{T_{ref}}{\gamma \cdot H_e}} \cdot \left[ \left( \frac{-T_{ref}}{\gamma \cdot H_e^2} \right) \cdot \left[ \ln \left( \frac{T_{ref} + \gamma \cdot z_1}{T_{ref} + \gamma \cdot z_0} \right) + S_{12} \right] + \frac{\partial S_{12}}{\partial H_e} \right] \\ & - 10^{-6} \cdot 77.64 \cdot \frac{e_{ref}}{T_1} \cdot \left[ \left( 1 + \frac{z'}{H_e} \right) \cdot e^{\frac{-z'}{H_e}} - \left( 1 + \frac{z_1}{H_e} \right) \cdot e^{\frac{-z_1}{H_e}} \right] \end{aligned} \quad (\text{B.4.10.3})$$

that is

$$\begin{aligned} \frac{\partial ZDD}{\partial H_e} = & -10^{-6} \cdot 77.64 \cdot \frac{e_{ref}}{\gamma} \cdot e^{\frac{T_{ref}}{\gamma \cdot H_e}} \cdot \left[ \left( \frac{-T_{ref}}{\gamma \cdot H_e^2} \right) \cdot \left[ \ln \left( \frac{T_{ref} + \gamma \cdot z_1}{T_{ref} + \gamma \cdot z_0} \right) + S_{12} \right] + \frac{-1}{H_e} \cdot \left( e^{\frac{-(T_{ref} + \gamma \cdot z_1)}{\gamma \cdot H_e}} - e^{\frac{-(T_{ref} + \gamma \cdot z_0)}{\gamma \cdot H_e}} \right) \right] \\ & - 10^{-6} \cdot 77.64 \cdot \frac{e_{ref}}{T_1} \cdot \left[ \left( 1 + \frac{z'}{H_e} \right) \cdot e^{\frac{-z'}{H_e}} - \left( 1 + \frac{z_1}{H_e} \right) \cdot e^{\frac{-z_1}{H_e}} \right] \end{aligned} \quad (\text{B.4.10.4})$$

or simpler

$$\begin{aligned} \frac{\partial ZDD}{\partial H_e} = & 10^{-6} \cdot 77.64 \cdot \frac{e_{ref}}{\gamma \cdot H_e} \cdot e^{\frac{T_{ref}}{\gamma \cdot H_e}} \cdot \left[ \left( \frac{T_{ref}}{\gamma \cdot H_e} \right) \cdot \left[ \ln \left( \frac{T_{ref} + \gamma \cdot z_1}{T_{ref} + \gamma \cdot z_0} \right) + S_{12} \right] + e^{\frac{-(T_{ref} + \gamma \cdot z_1)}{\gamma \cdot H_e}} - e^{\frac{-(T_{ref} + \gamma \cdot z_0)}{\gamma \cdot H_e}} \right] \\ & - 10^{-6} \cdot 77.64 \cdot \frac{e_{ref}}{T_1} \cdot \left[ \left( 1 + \frac{z'}{H_e} \right) \cdot e^{\frac{-z'}{H_e}} - \left( 1 + \frac{z_1}{H_e} \right) \cdot e^{\frac{-z_1}{H_e}} \right] \end{aligned} \quad (B.4.10.5)$$

## B.5. Zenith Wet Delay partial derivatives

The partial derivatives of the ZWD with respect to the parameters of eq. (B.1.3) or eq. (B.1.7) are computed in the following.

### B.5.1. $\partial ZWD / \partial e_{ref}$

Note that the ZWD is linear in  $e_{ref}$ . Its partial derivative is then easy to compute.

$$\begin{aligned} \frac{\partial ZWD}{\partial e_{ref}} = & -10^{-6} \cdot 64.68 \cdot \frac{1}{\gamma} \cdot e^{\frac{T_{ref}}{\gamma \cdot H_e}} \cdot \left[ \ln \left( \frac{T_{ref} + \gamma \cdot z_1}{T_{ref} + \gamma \cdot z_0} \right) + S_{12} \right] \\ & + 10^{-6} \cdot 5748 \cdot 64.68 \cdot \frac{1}{\gamma} \cdot e^{\frac{T_{ref}}{\gamma \cdot H_e}} \cdot \left[ \frac{-e^{\frac{-(T_{ref} + \gamma \cdot z_1)}{\gamma \cdot H_e}}}{T_{ref} + \gamma \cdot z_1} + \frac{e^{\frac{-(T_{ref} + \gamma \cdot z_0)}{\gamma \cdot H_e}}}{T_{ref} + \gamma \cdot z_0} - \frac{1}{\gamma \cdot H_e} \cdot \left[ \ln \left( \frac{T_{ref} + \gamma \cdot z_1}{T_{ref} + \gamma \cdot z_0} \right) + S_{12} \right] \right] \\ & + 10^{-6} \cdot 64.68 \cdot \frac{H_e}{T_1} \cdot \left[ e^{\frac{-z'}{H_e}} - e^{\frac{-z_1}{H_e}} \right] \\ & - 10^{-6} \cdot 5748 \cdot 64.68 \cdot \frac{H_e}{T_1^2} \cdot \left[ e^{\frac{-z'}{H_e}} - e^{\frac{-z_1}{H_e}} \right] \end{aligned} \quad (B.5.1.1)$$

### B.5.2. $\partial ZWD / \partial T_{ref}$

First compute this expression

$$\begin{aligned} \frac{\partial}{\partial T_{ref}} \left[ \frac{e^{\frac{-(T_{ref} + \gamma \cdot z_1)}{\gamma \cdot H_e}}}{T_{ref} + \gamma \cdot z_1} \right] = & \left[ \frac{-1}{\gamma \cdot H_e} \cdot e^{\frac{-(T_{ref} + \gamma \cdot z_1)}{\gamma \cdot H_e}} \cdot (T_{ref} + \gamma \cdot z_1) - e^{\frac{-(T_{ref} + \gamma \cdot z_1)}{\gamma \cdot H_e}} \cdot 1 \right] \cdot [T_{ref} + \gamma \cdot z_1]^{-2} \\ = & \left( -\frac{1}{T_{ref} + \gamma \cdot z_1} \right) \cdot \left[ \frac{1}{\gamma \cdot H_e} + \frac{1}{T_{ref} + \gamma \cdot z_1} \right] \cdot e^{\frac{-(T_{ref} + \gamma \cdot z_1)}{\gamma \cdot H_e}} \end{aligned} \quad (B.5.2.1)$$

It follows that



$$\begin{aligned}
\frac{\partial ZWD}{\partial T_{ref}} = & -10^{-6} \cdot 64.68 \cdot \frac{e_{ref}}{\gamma} \cdot \left( \frac{1}{\gamma \cdot H_e} \right) \cdot e^{\frac{T_{ref}}{\gamma \cdot H_e}} \cdot \left[ \ln \left( \frac{T_{ref} + \gamma \cdot z_1}{T_{ref} + \gamma \cdot z_0} \right) + S_{12} \right] \\
& -10^{-6} \cdot 64.68 \cdot \frac{e_{ref}}{\gamma} \cdot e^{\frac{T_{ref}}{\gamma \cdot H_e}} \cdot \left[ \frac{\gamma \cdot (z_0 - z_1)}{(T_{ref} + \gamma \cdot z_0) \cdot (T_{ref} + \gamma \cdot z_1)} + \frac{\partial S_{12}}{\partial T_{ref}} \right] \\
& +10^{-6} \cdot 5748 \cdot 64.68 \cdot \frac{e_{ref}}{\gamma} \cdot \left( \frac{1}{\gamma \cdot H_e} \right) \cdot e^{\frac{T_{ref}}{\gamma \cdot H_e}} \cdot \left[ -\frac{e^{-\frac{(T_{ref} + \gamma \cdot z_1)}{\gamma \cdot H_e}}}{T_{ref} + \gamma \cdot z_1} + \frac{e^{-\frac{(T_{ref} + \gamma \cdot z_0)}{\gamma \cdot H_e}}}{T_{ref} + \gamma \cdot z_0} - \frac{1}{\gamma \cdot H_e} \cdot \left[ \ln \left( \frac{T_{ref} + \gamma \cdot z_1}{T_{ref} + \gamma \cdot z_0} \right) + S_{12} \right] \right] \\
& +10^{-6} \cdot 5748 \cdot 64.68 \cdot \frac{e_{ref}}{\gamma} \cdot e^{\frac{T_{ref}}{\gamma \cdot H_e}} \cdot \left[ \left( \frac{1}{T_{ref} + \gamma \cdot z_1} \right) \cdot \left[ \frac{1}{\gamma \cdot H_e} + \frac{1}{T_{ref} + \gamma \cdot z_1} \right] \cdot e^{-\frac{(T_{ref} + \gamma \cdot z_1)}{\gamma \cdot H_e}} \right] \\
& +10^{-6} \cdot 5748 \cdot 64.68 \cdot \frac{e_{ref}}{\gamma} \cdot e^{\frac{T_{ref}}{\gamma \cdot H_e}} \cdot \left[ -\left( \frac{1}{T_{ref} + \gamma \cdot z_0} \right) \cdot \left[ \frac{1}{\gamma \cdot H_e} + \frac{1}{T_{ref} + \gamma \cdot z_0} \right] \cdot e^{-\frac{(T_{ref} + \gamma \cdot z_0)}{\gamma \cdot H_e}} \right] \\
& +10^{-6} \cdot 5748 \cdot 64.68 \cdot \frac{e_{ref}}{\gamma} \cdot e^{\frac{T_{ref}}{\gamma \cdot H_e}} \cdot \left[ -\frac{1}{\gamma \cdot H_e} \cdot \left[ \frac{\gamma \cdot (z_0 - z_1)}{(T_{ref} + \gamma \cdot z_0) \cdot (T_{ref} + \gamma \cdot z_1)} + \frac{\partial S_{12}}{\partial T_{ref}} \right] \right] \\
& +0-0
\end{aligned} \tag{B.5.2.2}$$

Introduce eq. (B.3.3.1.1.) in eq. (B.5.2.2)

$$\begin{aligned}
\frac{\partial ZWD}{\partial T_{ref}} = & -10^{-6} \cdot 64.68 \cdot \frac{e_{ref}}{\gamma} \cdot \left( \frac{1}{\gamma \cdot H_e} \right) \cdot e^{\frac{T_{ref}}{\gamma \cdot H_e}} \cdot \left[ \ln \left( \frac{T_{ref} + \gamma \cdot z_1}{T_{ref} + \gamma \cdot z_0} \right) + S_{12} \right] \\
& -10^{-6} \cdot 64.68 \cdot \frac{e_{ref}}{\gamma} \cdot e^{\frac{T_{ref}}{\gamma \cdot H_e}} \cdot \left[ \frac{\gamma \cdot (z_0 - z_1)}{(T_{ref} + \gamma \cdot z_0) \cdot (T_{ref} + \gamma \cdot z_1)} + \frac{1}{(T_{ref} + \gamma \cdot z_1)} \cdot \left[ e^{-\frac{(T_{ref} + \gamma \cdot z_1)}{\gamma \cdot H_e}} - 1 \right] \right] \\
& -10^{-6} \cdot 64.68 \cdot \frac{e_{ref}}{\gamma} \cdot e^{\frac{T_{ref}}{\gamma \cdot H_e}} \cdot \left[ -\frac{1}{(T_{ref} + \gamma \cdot z_0)} \cdot \left[ e^{-\frac{(T_{ref} + \gamma \cdot z_0)}{\gamma \cdot H_e}} - 1 \right] \right] \\
& +10^{-6} \cdot 5748 \cdot 64.68 \cdot \frac{e_{ref}}{\gamma} \cdot \left( \frac{1}{\gamma \cdot H_e} \right) \cdot e^{\frac{T_{ref}}{\gamma \cdot H_e}} \cdot \left[ -\frac{e^{-\frac{(T_{ref} + \gamma \cdot z_1)}{\gamma \cdot H_e}}}{T_{ref} + \gamma \cdot z_1} + \frac{e^{-\frac{(T_{ref} + \gamma \cdot z_0)}{\gamma \cdot H_e}}}{T_{ref} + \gamma \cdot z_0} - \frac{1}{\gamma \cdot H_e} \cdot \left[ \ln \left( \frac{T_{ref} + \gamma \cdot z_1}{T_{ref} + \gamma \cdot z_0} \right) + S_{12} \right] \right] \\
& +10^{-6} \cdot 5748 \cdot 64.68 \cdot \frac{e_{ref}}{\gamma} \cdot e^{\frac{T_{ref}}{\gamma \cdot H_e}} \cdot \left[ \left( \frac{1}{T_{ref} + \gamma \cdot z_1} \right) \cdot \left[ \frac{1}{\gamma \cdot H_e} + \frac{1}{T_{ref} + \gamma \cdot z_1} \right] \cdot e^{-\frac{(T_{ref} + \gamma \cdot z_1)}{\gamma \cdot H_e}} \right] \\
& +10^{-6} \cdot 5748 \cdot 64.68 \cdot \frac{e_{ref}}{\gamma} \cdot e^{\frac{T_{ref}}{\gamma \cdot H_e}} \cdot \left[ -\left( \frac{1}{T_{ref} + \gamma \cdot z_0} \right) \cdot \left[ \frac{1}{\gamma \cdot H_e} + \frac{1}{T_{ref} + \gamma \cdot z_0} \right] \cdot e^{-\frac{(T_{ref} + \gamma \cdot z_0)}{\gamma \cdot H_e}} \right] \\
& +10^{-6} \cdot 5748 \cdot 64.68 \cdot \frac{e_{ref}}{\gamma} \cdot e^{\frac{T_{ref}}{\gamma \cdot H_e}} \cdot \left[ -\frac{1}{\gamma \cdot H_e} \cdot \left[ \frac{\gamma \cdot (z_0 - z_1)}{(T_{ref} + \gamma \cdot z_0) \cdot (T_{ref} + \gamma \cdot z_1)} \right] \right] \\
& +10^{-6} \cdot 5748 \cdot 64.68 \cdot \frac{e_{ref}}{\gamma} \cdot e^{\frac{T_{ref}}{\gamma \cdot H_e}} \cdot \left[ -\frac{1}{\gamma \cdot H_e} \cdot \left( \frac{1}{(T_{ref} + \gamma \cdot z_1)} \cdot \left[ e^{-\frac{(T_{ref} + \gamma \cdot z_1)}{\gamma \cdot H_e}} - 1 \right] - \frac{1}{(T_{ref} + \gamma \cdot z_0)} \cdot \left[ e^{-\frac{(T_{ref} + \gamma \cdot z_0)}{\gamma \cdot H_e}} - 1 \right] \right) \right]
\end{aligned} \tag{B.5.2.3}$$

and simplify the expression

$$\begin{aligned}
\frac{\partial ZWD}{\partial T_{ref}} = & -10^{-6} \cdot 64.68 \cdot \frac{e_{ref}}{\gamma^2 \cdot H_e} \cdot e^{\frac{T_{ref}}{\gamma \cdot H_e}} \cdot \left[ \ln \left( \frac{T_{ref} + \gamma \cdot z_1}{T_{ref} + \gamma \cdot z_0} \right) + S_{12} \right] \\
& - 10^{-6} \cdot 64.68 \cdot \frac{e_{ref}}{\gamma \cdot (T_{ref} + \gamma \cdot z_1)} \cdot e^{\frac{T_{ref}}{\gamma \cdot H_e}} \cdot \left[ \frac{\gamma \cdot (z_0 - z_1)}{(T_{ref} + \gamma \cdot z_0)} + \left( e^{\frac{-(T_{ref} + \gamma \cdot z_1)}{\gamma \cdot H_e}} - 1 \right) \right] \\
& + 10^{-6} \cdot 64.68 \cdot \frac{e_{ref}}{\gamma \cdot (T_{ref} + \gamma \cdot z_0)} \cdot e^{\frac{T_{ref}}{\gamma \cdot H_e}} \cdot \left[ e^{\frac{-(T_{ref} + \gamma \cdot z_0)}{\gamma \cdot H_e}} - 1 \right] \\
& + 10^{-6} \cdot 5748 \cdot 64.68 \cdot \frac{e_{ref}}{\gamma^2 \cdot H_e} \cdot e^{\frac{T_{ref}}{\gamma \cdot H_e}} \cdot \left[ -e^{\frac{-(T_{ref} + \gamma \cdot z_1)}{\gamma \cdot H_e}} + e^{\frac{-(T_{ref} + \gamma \cdot z_0)}{\gamma \cdot H_e}} - \frac{1}{\gamma \cdot H_e} \cdot \left[ \ln \left( \frac{T_{ref} + \gamma \cdot z_1}{T_{ref} + \gamma \cdot z_0} \right) + S_{12} \right] \right] \\
& + 10^{-6} \cdot 5748 \cdot 64.68 \cdot \frac{e_{ref}}{\gamma \cdot (T_{ref} + \gamma \cdot z_1)} \cdot e^{\frac{-z_1}{H_e}} \cdot \left[ \frac{1}{\gamma \cdot H_e} + \frac{1}{T_{ref} + \gamma \cdot z_1} \right] \\
& - 10^{-6} \cdot 5748 \cdot 64.68 \cdot \frac{e_{ref}}{\gamma \cdot (T_{ref} + \gamma \cdot z_0)} \cdot e^{\frac{-z_0}{H_e}} \cdot \left[ \frac{1}{\gamma \cdot H_e} + \frac{1}{T_{ref} + \gamma \cdot z_0} \right] \\
& - 10^{-6} \cdot 5748 \cdot 64.68 \cdot \frac{e_{ref}}{\gamma \cdot H_e} \cdot e^{\frac{T_{ref}}{\gamma \cdot H_e}} \cdot \left[ \frac{(z_0 - z_1)}{(T_{ref} + \gamma \cdot z_0) \cdot (T_{ref} + \gamma \cdot z_1)} \right] \\
& - 10^{-6} \cdot 5748 \cdot 64.68 \cdot \frac{e_{ref}}{\gamma^2 \cdot H_e} \cdot e^{\frac{T_{ref}}{\gamma \cdot H_e}} \cdot \left[ \frac{1}{(T_{ref} + \gamma \cdot z_1)} \cdot \left( e^{\frac{-(T_{ref} + \gamma \cdot z_1)}{\gamma \cdot H_e}} - 1 \right) - \frac{1}{(T_{ref} + \gamma \cdot z_0)} \cdot \left( e^{\frac{-(T_{ref} + \gamma \cdot z_0)}{\gamma \cdot H_e}} - 1 \right) \right]
\end{aligned} \tag{B.5.2.4}$$

### B.5.3. $\partial ZWD / \partial T_1$

Remark that both  $S_{11}$  and  $S_{12}$  do not depend on  $T_1$ .

$$\begin{aligned}
\frac{\partial ZWD}{\partial T_1} = & -0 + 0 \\
& + 10^{-6} \cdot 64.68 \cdot \left( \frac{-e_{ref}}{T_1^2} \right) \cdot H_e \cdot \left[ e^{\frac{-z'}{H_e}} - e^{\frac{-z_1}{H_e}} \right] \\
& - 10^{-6} \cdot 5748 \cdot 64.68 \cdot \left( \frac{-2 \cdot e_{ref}}{T_1^3} \right) \cdot H_e \cdot \left[ e^{\frac{-z'}{H_e}} - e^{\frac{-z_1}{H_e}} \right]
\end{aligned} \tag{B.5.3.1}$$

i.e.

$$\frac{\partial ZWD}{\partial T_1} = -10^{-6} \cdot 64.68 \cdot \frac{e_{ref}}{T_1^2} \cdot H_e \cdot \left[ e^{\frac{-z'}{H_e}} - e^{\frac{-z_1}{H_e}} \right] + 10^{-6} \cdot 5748 \cdot 64.68 \cdot \frac{2 \cdot e_{ref}}{T_1^3} \cdot H_e \cdot \left[ e^{\frac{-z'}{H_e}} - e^{\frac{-z_1}{H_e}} \right] \tag{B.5.3.2}$$

or

$$\frac{\partial ZWD}{\partial T_1} = 10^{-6} \cdot 64.68 \cdot \frac{e_{ref}}{T_1^2} \cdot H_e \cdot \left( -1 + 5748 \cdot \frac{2}{T_1} \right) \cdot \left[ e^{\frac{-z'}{H_e}} - e^{\frac{-z_1}{H_e}} \right] \tag{B.5.3.3}$$

**B.5.4.**  $\partial ZWD/\partial\gamma$ 

First compute this

$$\begin{aligned} \frac{\partial}{\partial\gamma} e^{-\frac{(T_{ref} + \gamma \cdot z_1)}{\gamma \cdot H_e}} &= \left[ \frac{\partial}{\partial\gamma} \frac{-(T_{ref} + \gamma \cdot z_1)}{\gamma \cdot H_e} \right] \cdot e^{-\frac{(T_{ref} + \gamma \cdot z_1)}{\gamma \cdot H_e}} \\ &= - \left[ \frac{z_1 \cdot \gamma \cdot H_e - (T_{ref} + \gamma \cdot z_1) \cdot H_e}{(\gamma \cdot H_e)^2} \right] \cdot e^{-\frac{(T_{ref} + \gamma \cdot z_1)}{\gamma \cdot H_e}} \\ &= \left[ \frac{(T_{ref} + \gamma \cdot z_1) - z_1 \cdot \gamma}{\gamma^2 \cdot H_e} \right] \cdot e^{-\frac{(T_{ref} + \gamma \cdot z_1)}{\gamma \cdot H_e}} \end{aligned} \quad (B.5.4.1)$$

i.e.

$$\frac{\partial}{\partial\gamma} e^{-\frac{(T_{ref} + \gamma \cdot z_1)}{\gamma \cdot H_e}} = \frac{T_{ref}}{\gamma^2 \cdot H_e} \cdot e^{-\frac{(T_{ref} + \gamma \cdot z_1)}{\gamma \cdot H_e}} \quad (B.5.4.2)$$

Therefore it holds

$$\frac{\partial}{\partial\gamma} \frac{e^{-\frac{(T_{ref} + \gamma \cdot z_1)}{\gamma \cdot H_e}}}{T_{ref} + \gamma \cdot z_1} = \left[ \frac{T_{ref}}{\gamma^2 \cdot H_e} \cdot e^{-\frac{(T_{ref} + \gamma \cdot z_1)}{\gamma \cdot H_e}} \cdot (T_{ref} + \gamma \cdot z_1) - e^{-\frac{(T_{ref} + \gamma \cdot z_1)}{\gamma \cdot H_e}} \cdot z_1 \right] \cdot [T_{ref} + \gamma \cdot z_1]^{-2} \quad (B.5.4.3)$$

that is

$$\frac{\partial}{\partial\gamma} \frac{e^{-\frac{(T_{ref} + \gamma \cdot z_1)}{\gamma \cdot H_e}}}{T_{ref} + \gamma \cdot z_1} = \frac{1}{T_{ref} + \gamma \cdot z_1} \cdot \left[ \frac{T_{ref}}{\gamma^2 \cdot H_e} - \frac{z_1}{T_{ref} + \gamma \cdot z_1} \right] \cdot e^{-\frac{(T_{ref} + \gamma \cdot z_1)}{\gamma \cdot H_e}} \quad (B.5.4.4)$$

Thus the partial derivative of the ZWD with respect to  $\gamma$  is

$$\begin{aligned} \frac{\partial ZWD}{\partial\gamma} &= -10^{-6} \cdot 64.68 \cdot \left( \frac{-e_{ref}}{\gamma^2} \right) \cdot e^{\frac{T_{ref}}{\gamma \cdot H_e}} \cdot \left[ \ln \left( \frac{T_{ref} + \gamma \cdot z_1}{T_{ref} + \gamma \cdot z_0} \right) + S_{12} \right] \\ &\quad - 10^{-6} \cdot 64.68 \cdot \frac{e_{ref}}{\gamma} \cdot \left( \frac{-T_{ref}}{\gamma^2 \cdot H_e} \right) \cdot e^{\frac{T_{ref}}{\gamma \cdot H_e}} \cdot \left[ \ln \left( \frac{T_{ref} + \gamma \cdot z_1}{T_{ref} + \gamma \cdot z_0} \right) + S_{12} \right] \\ &\quad - 10^{-6} \cdot 64.68 \cdot \frac{e_{ref}}{\gamma} \cdot e^{\frac{T_{ref}}{\gamma \cdot H_e}} \cdot \left[ \frac{T_{ref} \cdot (z_1 - z_0)}{(T_{ref} + \gamma \cdot z_0) \cdot (T_{ref} + \gamma \cdot z_1)} + \frac{\partial S_{12}}{\partial\gamma} \right] \\ &\quad + 10^{-6} \cdot 5748 \cdot 64.68 \cdot \left( \frac{-e_{ref}}{\gamma^2} \right) \cdot e^{\frac{T_{ref}}{\gamma \cdot H_e}} \cdot \left[ -e^{-\frac{(T_{ref} + \gamma \cdot z_1)}{\gamma \cdot H_e}} + e^{-\frac{(T_{ref} + \gamma \cdot z_0)}{\gamma \cdot H_e}} - \frac{1}{\gamma \cdot H_e} \cdot \left[ \ln \left( \frac{T_{ref} + \gamma \cdot z_1}{T_{ref} + \gamma \cdot z_0} \right) + S_{12} \right] \right] \\ &\quad + 10^{-6} \cdot 5748 \cdot 64.68 \cdot \frac{e_{ref}}{\gamma} \cdot \left( \frac{-T_{ref}}{\gamma^2 \cdot H_e} \right) \cdot e^{\frac{T_{ref}}{\gamma \cdot H_e}} \cdot \left[ -e^{-\frac{(T_{ref} + \gamma \cdot z_1)}{\gamma \cdot H_e}} + e^{-\frac{(T_{ref} + \gamma \cdot z_0)}{\gamma \cdot H_e}} - \frac{1}{\gamma \cdot H_e} \cdot \left[ \ln \left( \frac{T_{ref} + \gamma \cdot z_1}{T_{ref} + \gamma \cdot z_0} \right) + S_{12} \right] \right] \end{aligned}$$

**P.T.O.**

$$\begin{aligned}
& +10^{-6} \cdot 5748 \cdot 64.68 \cdot \frac{e_{ref}}{\gamma} \cdot e^{\frac{T_{ref}}{\gamma \cdot H_e}} \cdot \left[ \frac{-1}{T_{ref} + \gamma \cdot z_1} \cdot \left[ \frac{T_{ref}}{\gamma^2 \cdot H_e} - \frac{z_1}{T_{ref} + \gamma \cdot z_1} \right] \cdot e^{\frac{-(T_{ref} + \gamma \cdot z_1)}{\gamma \cdot H_e}} \right] \\
& +10^{-6} \cdot 5748 \cdot 64.68 \cdot \frac{e_{ref}}{\gamma} \cdot e^{\frac{T_{ref}}{\gamma \cdot H_e}} \cdot \left[ \frac{1}{T_{ref} + \gamma \cdot z_0} \cdot \left[ \frac{T_{ref}}{\gamma^2 \cdot H_e} - \frac{z_0}{T_{ref} + \gamma \cdot z_0} \right] \cdot e^{\frac{-(T_{ref} + \gamma \cdot z_0)}{\gamma \cdot H_e}} \right] \\
& +10^{-6} \cdot 5748 \cdot 64.68 \cdot \frac{e_{ref}}{\gamma} \cdot e^{\frac{T_{ref}}{\gamma \cdot H_e}} \cdot \left[ -\left( \frac{-1}{\gamma^2 \cdot H_e} \right) \cdot \left[ \ln \left( \frac{T_{ref} + \gamma \cdot z_1}{T_{ref} + \gamma \cdot z_0} \right) + S_{12} \right] \right] \\
& +10^{-6} \cdot 5748 \cdot 64.68 \cdot \frac{e_{ref}}{\gamma} \cdot e^{\frac{T_{ref}}{\gamma \cdot H_e}} \cdot \left[ -\frac{1}{\gamma \cdot H_e} \cdot \left[ \frac{T_{ref} \cdot (z_1 - z_0)}{(T_{ref} + \gamma \cdot z_0) \cdot (T_{ref} + \gamma \cdot z_1)} + \frac{\partial S_{12}}{\partial \gamma} \right] \right] \\
& +0-0
\end{aligned} \tag{B.5.4.5}$$

Insert eq. (B. 3.3.2.1) in eq. (B.5.4.5). It reduces to

$$\begin{aligned}
\frac{\partial ZWD}{\partial \gamma} &= 10^{-6} \cdot 64.68 \cdot \frac{e_{ref}}{\gamma} \cdot e^{\frac{T_{ref}}{\gamma \cdot H_e}} \cdot \left[ \frac{1}{\gamma} \cdot \left( 1 + \frac{T_{ref}}{\gamma \cdot H_e} \right) \cdot \left[ \ln \left( \frac{T_{ref} + \gamma \cdot z_1}{T_{ref} + \gamma \cdot z_0} \right) + S_{12} \right] - \frac{T_{ref} \cdot (z_1 - z_0)}{(T_{ref} + \gamma \cdot z_0) \cdot (T_{ref} + \gamma \cdot z_1)} \right] \\
& -10^{-6} \cdot 64.68 \cdot \frac{e_{ref}}{\gamma} \cdot e^{\frac{T_{ref}}{\gamma \cdot H_e}} \cdot \left[ \frac{-1}{\gamma} \cdot \left[ e^{\frac{-(T_{ref} + \gamma \cdot z_1)}{\gamma \cdot H_e}} - e^{\frac{-(T_{ref} + \gamma \cdot z_0)}{\gamma \cdot H_e}} \right] + \frac{z_1}{T_{ref} + \gamma \cdot z_1} \cdot \left( e^{\frac{-(T_{ref} + \gamma \cdot z_1)}{\gamma \cdot H_e}} - 1 \right) \right] \\
& -10^{-6} \cdot 64.68 \cdot \frac{e_{ref}}{\gamma} \cdot e^{\frac{T_{ref}}{\gamma \cdot H_e}} \cdot \left[ -\frac{z_0}{T_{ref} + \gamma \cdot z_0} \cdot \left( e^{\frac{-(T_{ref} + \gamma \cdot z_0)}{\gamma \cdot H_e}} - 1 \right) \right] \\
& -10^{-6} \cdot 5748 \cdot 64.68 \cdot \frac{e_{ref}}{\gamma^2} \cdot \left( 1 + \frac{T_{ref}}{\gamma \cdot H_e} \right) \cdot e^{\frac{T_{ref}}{\gamma \cdot H_e}} \cdot \left[ \frac{-e^{\frac{-(T_{ref} + \gamma \cdot z_1)}{\gamma \cdot H_e}}}{T_{ref} + \gamma \cdot z_1} + \frac{e^{\frac{-(T_{ref} + \gamma \cdot z_0)}{\gamma \cdot H_e}}}{T_{ref} + \gamma \cdot z_0} - \frac{1}{\gamma \cdot H_e} \cdot \left[ \ln \left( \frac{T_{ref} + \gamma \cdot z_1}{T_{ref} + \gamma \cdot z_0} \right) + S_{12} \right] \right] \\
& -10^{-6} \cdot 5748 \cdot 64.68 \cdot \frac{e_{ref}}{\gamma \cdot (T_{ref} + \gamma \cdot z_1)} \cdot \left[ \frac{T_{ref}}{\gamma^2 \cdot H_e} - \frac{z_1}{T_{ref} + \gamma \cdot z_1} \right] \cdot e^{\frac{-z_1}{H_e}} \\
& +10^{-6} \cdot 5748 \cdot 64.68 \cdot \frac{e_{ref}}{\gamma \cdot (T_{ref} + \gamma \cdot z_0)} \cdot \left[ \frac{T_{ref}}{\gamma^2 \cdot H_e} - \frac{z_0}{T_{ref} + \gamma \cdot z_0} \right] \cdot e^{\frac{-z_0}{H_e}} \\
& +10^{-6} \cdot 5748 \cdot 64.68 \cdot \frac{e_{ref}}{\gamma^3 \cdot H_e} \cdot e^{\frac{T_{ref}}{\gamma \cdot H_e}} \cdot \left[ \ln \left( \frac{T_{ref} + \gamma \cdot z_1}{T_{ref} + \gamma \cdot z_0} \right) + S_{12} \right] \\
& -10^{-6} \cdot 5748 \cdot 64.68 \cdot \frac{e_{ref}}{\gamma^2 \cdot H_e} \cdot e^{\frac{T_{ref}}{\gamma \cdot H_e}} \cdot \left[ \frac{T_{ref} \cdot (z_1 - z_0)}{(T_{ref} + \gamma \cdot z_0) \cdot (T_{ref} + \gamma \cdot z_1)} - \frac{1}{\gamma} \cdot \left[ e^{\frac{-(T_{ref} + \gamma \cdot z_1)}{\gamma \cdot H_e}} - e^{\frac{-(T_{ref} + \gamma \cdot z_0)}{\gamma \cdot H_e}} \right] \right] \\
& -10^{-6} \cdot 5748 \cdot 64.68 \cdot \frac{e_{ref}}{\gamma^2 \cdot H_e} \cdot e^{\frac{T_{ref}}{\gamma \cdot H_e}} \cdot \left[ \frac{z_1}{T_{ref} + \gamma \cdot z_1} \cdot \left( e^{\frac{-(T_{ref} + \gamma \cdot z_1)}{\gamma \cdot H_e}} - 1 \right) - \frac{z_0}{T_{ref} + \gamma \cdot z_0} \cdot \left( e^{\frac{-(T_{ref} + \gamma \cdot z_0)}{\gamma \cdot H_e}} - 1 \right) \right]
\end{aligned} \tag{B.5.4.6}$$

### B.5.5. $\partial ZWD/\partial z_0$

First compute this

$$\begin{aligned} \frac{\partial}{\partial z_0} \frac{e^{-\frac{(T_{ref} + \gamma \cdot z_0)}{\gamma \cdot H_e}}}{T_{ref} + \gamma \cdot z_0} &= \left[ \frac{-1}{H_e} \cdot e^{-\frac{(T_{ref} + \gamma \cdot z_0)}{\gamma \cdot H_e}} \cdot (T_{ref} + \gamma \cdot z_0) - e^{-\frac{(T_{ref} + \gamma \cdot z_0)}{\gamma \cdot H_e}} \cdot \gamma \right] \cdot [T_{ref} + \gamma \cdot z_0]^{-2} \\ &= \frac{-1}{(T_{ref} + \gamma \cdot z_0)} \cdot \left[ \frac{1}{H_e} + \frac{\gamma}{(T_{ref} + \gamma \cdot z_0)} \right] \cdot e^{-\frac{(T_{ref} + \gamma \cdot z_0)}{\gamma \cdot H_e}} \end{aligned} \quad (\text{B.5.5.1})$$

With eq. (B.3.1.3.2) one has

$$\begin{aligned} \frac{\partial ZWD}{\partial z_0} &= -10^{-6} \cdot 64.68 \cdot \frac{e_{ref}}{\gamma} \cdot e^{\frac{T_{ref}}{\gamma \cdot H_e}} \cdot \left[ \frac{-\gamma}{T_{ref} + \gamma \cdot z_0} + \frac{\partial S_{12}}{\partial z_0} \right] \\ &+ 10^{-6} \cdot 5748 \cdot 64.68 \cdot \frac{e_{ref}}{\gamma} \cdot e^{\frac{T_{ref}}{\gamma \cdot H_e}} \cdot \left[ 0 + \frac{-1}{(T_{ref} + \gamma \cdot z_0)} \cdot \left[ \frac{1}{H_e} + \frac{\gamma}{(T_{ref} + \gamma \cdot z_0)} \right] \cdot e^{-\frac{(T_{ref} + \gamma \cdot z_0)}{\gamma \cdot H_e}} \right] \\ &+ 10^{-6} \cdot 5748 \cdot 64.68 \cdot \frac{e_{ref}}{\gamma} \cdot e^{\frac{T_{ref}}{\gamma \cdot H_e}} \cdot \left[ -\frac{1}{\gamma \cdot H_e} \cdot \left( \frac{-\gamma}{T_{ref} + \gamma \cdot z_0} + \frac{\partial S_{12}}{\partial z_0} \right) \right] \\ &+ 0 - 0 \end{aligned} \quad (\text{B.5.5.2})$$

Insert eq. (B.3.3.3.1) in eq. (B.5.5.2)

$$\begin{aligned} \frac{\partial ZWD}{\partial z_0} &= -10^{-6} \cdot 64.68 \cdot \frac{e_{ref}}{\gamma} \cdot e^{\frac{T_{ref}}{\gamma \cdot H_e}} \cdot \left[ \frac{-\gamma}{T_{ref} + \gamma \cdot z_0} + \frac{-\gamma}{(T_{ref} + \gamma \cdot z_0)} \cdot \left[ e^{-\frac{(T_{ref} + \gamma \cdot z_0)}{\gamma \cdot H_e}} - 1 \right] \right] \\ &+ 10^{-6} \cdot 5748 \cdot 64.68 \cdot \frac{e_{ref}}{\gamma} \cdot e^{\frac{T_{ref}}{\gamma \cdot H_e}} \cdot \left[ 0 + \frac{-1}{(T_{ref} + \gamma \cdot z_0)} \cdot \left[ \frac{1}{H_e} + \frac{\gamma}{(T_{ref} + \gamma \cdot z_0)} \right] \cdot e^{-\frac{(T_{ref} + \gamma \cdot z_0)}{\gamma \cdot H_e}} \right] \\ &+ 10^{-6} \cdot 5748 \cdot 64.68 \cdot \frac{e_{ref}}{\gamma} \cdot e^{\frac{T_{ref}}{\gamma \cdot H_e}} \cdot \left[ -\frac{1}{\gamma \cdot H_e} \cdot \left( \frac{-\gamma}{T_{ref} + \gamma \cdot z_0} + \frac{-\gamma}{(T_{ref} + \gamma \cdot z_0)} \cdot \left[ e^{-\frac{(T_{ref} + \gamma \cdot z_0)}{\gamma \cdot H_e}} - 1 \right] \right) \right] \end{aligned} \quad (\text{B.5.5.3})$$

Eq. (B.5.5.3) reduces to

$$\begin{aligned} \frac{\partial ZWD}{\partial z_0} &= 10^{-6} \cdot 64.68 \cdot \frac{e_{ref}}{T_{ref} + \gamma \cdot z_0} \cdot e^{\frac{-z_0}{H_e}} - 10^{-6} \cdot 5748 \cdot 64.68 \cdot \frac{e_{ref}}{\gamma \cdot (T_{ref} + \gamma \cdot z_0)} \cdot \left[ \frac{1}{H_e} + \frac{\gamma}{(T_{ref} + \gamma \cdot z_0)} \right] \cdot e^{\frac{-z_0}{H_e}} \\ &+ 10^{-6} \cdot 5748 \cdot 64.68 \cdot \frac{e_{ref}}{(\gamma \cdot H_e) \cdot (T_{ref} + \gamma \cdot z_0)} \cdot e^{\frac{-z_0}{H_e}} \end{aligned} \quad (\text{B.5.5.4})$$

i.e.

$$\frac{\partial ZWD}{\partial z_0} = 10^{-6} \cdot 64.68 \cdot \frac{e_{ref}}{(T_{ref} + \gamma \cdot z_0)} \cdot \left[ 1 - \frac{5748}{(T_{ref} + \gamma \cdot z_0)} \right] \cdot e^{\frac{-z_0}{H_e}} \quad (\text{B.5.5.5})$$

### B.5.6. $\partial ZWD / \partial z_1$

With eq. (B.5.5.1) for  $z_1$  and eq. (B.3.1.4.2), it holds

$$\begin{aligned}
\frac{\partial ZWD}{\partial z_1} = & -10^{-6} \cdot 64.68 \cdot \frac{e_{ref}}{\gamma} \cdot e^{\frac{T_{ref}}{\gamma \cdot H_e}} \cdot \left[ \frac{\gamma}{T_{ref} + \gamma \cdot z_1} + \frac{\partial S_{12}}{\partial z_1} \right] \\
& + 10^{-6} \cdot 5748 \cdot 64.68 \cdot \frac{e_{ref}}{\gamma} \cdot e^{\frac{T_{ref}}{\gamma \cdot H_e}} \cdot \left[ \frac{1}{(T_{ref} + \gamma \cdot z_1)} \cdot \left[ \frac{1}{H_e} + \frac{\gamma}{(T_{ref} + \gamma \cdot z_1)} \right] \cdot e^{\frac{-(T_{ref} + \gamma \cdot z_1)}{\gamma \cdot H_e}} \right] \\
& + 10^{-6} \cdot 5748 \cdot 64.68 \cdot \frac{e_{ref}}{\gamma} \cdot e^{\frac{T_{ref}}{\gamma \cdot H_e}} \cdot \left[ 0 - \frac{1}{\gamma \cdot H_e} \cdot \left[ \frac{\gamma}{T_{ref} + \gamma \cdot z_1} + \frac{\partial S_{12}}{\partial z_1} \right] \right] \\
& + 10^{-6} \cdot 64.68 \cdot \frac{e_{ref}}{T_1} \cdot H_e \cdot \left[ 0 - \left( \frac{-1}{H_e} \right) \cdot e^{\frac{-z_1}{H_e}} \right] \\
& - 10^{-6} \cdot 5748 \cdot 64.68 \cdot \frac{e_{ref}}{T_1^2} \cdot H_e \cdot \left[ 0 - \left( \frac{-1}{H_e} \right) \cdot e^{\frac{-z_1}{H_e}} \right]
\end{aligned} \tag{B.5.6.1}$$

Insert eq. (B.3.3.4.1) in eq. (B.5.6.1)

$$\begin{aligned}
\frac{\partial ZWD}{\partial z_1} = & -10^{-6} \cdot 64.68 \cdot \frac{e_{ref}}{\gamma} \cdot e^{\frac{T_{ref}}{\gamma \cdot H_e}} \cdot \left[ \frac{\gamma}{T_{ref} + \gamma \cdot z_1} + \frac{\gamma}{(T_{ref} + \gamma \cdot z_1)} \cdot \left[ e^{\frac{-(T_{ref} + \gamma \cdot z_1)}{\gamma \cdot H_e}} - 1 \right] \right] \\
& + 10^{-6} \cdot 5748 \cdot 64.68 \cdot \frac{e_{ref}}{\gamma \cdot (T_{ref} + \gamma \cdot z_1)} \cdot e^{\frac{T_{ref}}{\gamma \cdot H_e}} \cdot \left[ \frac{1}{H_e} + \frac{\gamma}{(T_{ref} + \gamma \cdot z_1)} \right] \cdot e^{\frac{-(T_{ref} + \gamma \cdot z_1)}{\gamma \cdot H_e}} \\
& + 10^{-6} \cdot 5748 \cdot 64.68 \cdot \frac{e_{ref}}{\gamma} \cdot e^{\frac{T_{ref}}{\gamma \cdot H_e}} \cdot \left[ -\frac{1}{\gamma \cdot H_e} \cdot \left( \frac{\gamma}{T_{ref} + \gamma \cdot z_1} + \frac{\gamma}{(T_{ref} + \gamma \cdot z_1)} \cdot \left[ e^{\frac{-(T_{ref} + \gamma \cdot z_1)}{\gamma \cdot H_e}} - 1 \right] \right) \right] \\
& + 10^{-6} \cdot 64.68 \cdot \frac{e_{ref}}{T_1} \cdot e^{\frac{-z_1}{H_e}} - 10^{-6} \cdot 5748 \cdot 64.68 \cdot \frac{e_{ref}}{T_1^2} \cdot e^{\frac{-z_1}{H_e}}
\end{aligned} \tag{B.5.6.2}$$

and simplify eq. (B.5.6.2)

$$\begin{aligned}
\frac{\partial ZWD}{\partial z_1} = & -10^{-6} \cdot 64.68 \cdot \frac{e_{ref}}{T_{ref} + \gamma \cdot z_1} \cdot e^{\frac{-z_1}{H_e}} \\
& + 10^{-6} \cdot 5748 \cdot 64.68 \cdot \frac{e_{ref}}{\gamma \cdot (T_{ref} + \gamma \cdot z_1)} \cdot \left[ \frac{1}{H_e} + \frac{\gamma}{(T_{ref} + \gamma \cdot z_1)} \right] \cdot e^{\frac{-z_1}{H_e}} \\
& - 10^{-6} \cdot 5748 \cdot 64.68 \cdot \frac{e_{ref}}{(H_e \cdot \gamma) \cdot (T_{ref} + \gamma \cdot z_1)} \cdot e^{\frac{-z_1}{H_e}} \\
& + 10^{-6} \cdot 64.68 \cdot \frac{e_{ref}}{T_1} \cdot \left( 1 - \frac{5748}{T_1} \right) \cdot e^{\frac{-z_1}{H_e}}
\end{aligned} \tag{B.5.6.3}$$

i.e.

$$\begin{aligned}
\frac{\partial ZWD}{\partial z_1} &= -10^{-6} \cdot 64.68 \cdot \frac{e_{ref}}{T_{ref} + \gamma \cdot z_1} \cdot e^{\frac{-z_1}{H_e}} \\
&+ 10^{-6} \cdot 5748 \cdot 64.68 \cdot \frac{e_{ref}}{(T_{ref} + \gamma \cdot z_1)^2} \cdot e^{\frac{-z_1}{H_e}} \\
&+ 10^{-6} \cdot 64.68 \cdot \frac{e_{ref}}{T_1} \cdot \left(1 - \frac{5748}{T_1}\right) \cdot e^{\frac{-z_1}{H_e}}
\end{aligned} \tag{B.5.6.4}$$

### B.5.7. $\partial ZWD/\partial z'$

Remark that  $S_{12}$  is independent of  $z'$ . Thus

$$\begin{aligned}
\frac{\partial ZWD}{\partial z'} &= -0 + 0 \\
&+ 10^{-6} \cdot 64.68 \cdot \frac{e_{ref}}{T_1} \cdot H_e \cdot \left[ \left( \frac{-1}{H_e} \right) \cdot e^{\frac{-z'}{H_e}} - 0 \right] \\
&- 10^{-6} \cdot 5748 \cdot 64.68 \cdot \frac{e_{ref}}{T_1^2} \cdot H_e \cdot \left[ \left( \frac{-1}{H_e} \right) \cdot e^{\frac{-z'}{H_e}} - 0 \right]
\end{aligned} \tag{B.5.7.1}$$

Eq. (B.5.7.1) can be rewritten as

$$\frac{\partial ZWD}{\partial z'} = -10^{-6} \cdot 64.68 \cdot \frac{e_{ref}}{T_1} \cdot \left(1 - \frac{5748}{T_1}\right) \cdot e^{\frac{-z'}{H_e}} \tag{B.5.7.2}$$

### B.5.8. $\partial ZWD/\partial H_e$

Remind that

$$\begin{aligned}
\frac{\partial}{\partial H_e} e^{\frac{-(T_{ref} + \gamma \cdot z_1)}{\gamma \cdot H_e}} &= -\frac{\partial}{\partial H_e} \left[ \frac{(T_{ref} + \gamma \cdot z_1)}{\gamma \cdot H_e} \right] \cdot e^{\frac{-(T_{ref} + \gamma \cdot z_1)}{\gamma \cdot H_e}} = -\frac{0 - (T_{ref} + \gamma \cdot z_1) \cdot \gamma}{(\gamma \cdot H_e)^2} \cdot e^{\frac{-(T_{ref} + \gamma \cdot z_1)}{\gamma \cdot H_e}} \\
&= \frac{(T_{ref} + \gamma \cdot z_1)}{\gamma \cdot H_e^2} \cdot e^{\frac{-(T_{ref} + \gamma \cdot z_1)}{\gamma \cdot H_e}}
\end{aligned} \tag{B.5.8.1}$$

Therefore

$$\begin{aligned}
\frac{\partial ZWD}{\partial H_e} = & -10^{-6} \cdot 64.68 \cdot \frac{e_{ref}}{\gamma} \cdot \left( \frac{-T_{ref}}{\gamma \cdot H_e^2} \right) \cdot e^{\frac{T_{ref}}{\gamma \cdot H_e}} \cdot \left[ \ln \left( \frac{T_{ref} + \gamma \cdot z_1}{T_{ref} + \gamma \cdot z_0} \right) + S_{12} \right] \\
& -10^{-6} \cdot 64.68 \cdot \frac{e_{ref}}{\gamma} \cdot e^{\frac{T_{ref}}{\gamma \cdot H_e}} \cdot \left[ 0 + \frac{\partial S_{12}}{\partial H_e} \right] \\
& +10^{-6} \cdot 5748 \cdot 64.68 \cdot \frac{e_{ref}}{\gamma} \cdot \left( \frac{-T_{ref}}{\gamma \cdot H_e^2} \right) \cdot e^{\frac{T_{ref}}{\gamma \cdot H_e}} \cdot \left[ \frac{-e^{-\frac{(T_{ref} + \gamma \cdot z_1)}{\gamma \cdot H_e}}}{T_{ref} + \gamma \cdot z_1} + \frac{e^{-\frac{(T_{ref} + \gamma \cdot z_0)}{\gamma \cdot H_e}}}{T_{ref} + \gamma \cdot z_0} \right] \\
& +10^{-6} \cdot 5748 \cdot 64.68 \cdot \frac{e_{ref}}{\gamma} \cdot \left( \frac{-T_{ref}}{\gamma \cdot H_e^2} \right) \cdot e^{\frac{T_{ref}}{\gamma \cdot H_e}} \cdot \left[ -\frac{1}{\gamma \cdot H_e} \cdot \left[ \ln \left( \frac{T_{ref} + \gamma \cdot z_1}{T_{ref} + \gamma \cdot z_0} \right) + S_{12} \right] \right] \\
& +10^{-6} \cdot 5748 \cdot 64.68 \cdot \frac{e_{ref}}{\gamma} \cdot e^{\frac{T_{ref}}{\gamma \cdot H_e}} \cdot \left[ \frac{T_{ref} + \gamma \cdot z_1}{\gamma \cdot H_e^2} \cdot \frac{-e^{-\frac{(T_{ref} + \gamma \cdot z_1)}{\gamma \cdot H_e}}}{T_{ref} + \gamma \cdot z_1} + \frac{T_{ref} + \gamma \cdot z_0}{\gamma \cdot H_e^2} \cdot \frac{e^{-\frac{(T_{ref} + \gamma \cdot z_0)}{\gamma \cdot H_e}}}{T_{ref} + \gamma \cdot z_0} \right] \\
& +10^{-6} \cdot 5748 \cdot 64.68 \cdot \frac{e_{ref}}{\gamma} \cdot e^{\frac{T_{ref}}{\gamma \cdot H_e}} \cdot \left[ -\left( \frac{-1}{\gamma \cdot H_e^2} \right) \cdot \left[ \ln \left( \frac{T_{ref} + \gamma \cdot z_1}{T_{ref} + \gamma \cdot z_0} \right) + S_{12} \right] \right] \\
& +10^{-6} \cdot 5748 \cdot 64.68 \cdot \frac{e_{ref}}{\gamma} \cdot e^{\frac{T_{ref}}{\gamma \cdot H_e}} \cdot \left[ \frac{-1}{\gamma \cdot H_e} \cdot \left[ 0 + \frac{\partial S_{12}}{\partial H_e} \right] \right] \tag{B.5.8.2} \\
& +10^{-6} \cdot 64.68 \cdot \frac{e_{ref}}{T_1} \cdot 1 \cdot \left[ e^{\frac{-z'}{H_e}} - e^{\frac{-z_1}{H_e}} \right] \\
& +10^{-6} \cdot 64.68 \cdot \frac{e_{ref}}{T_1} \cdot H_e \cdot \left[ \left( \frac{z'}{H_e^2} \right) \cdot e^{\frac{-z'}{H_e}} - \left( \frac{z_1}{H_e^2} \right) \cdot e^{\frac{-z_1}{H_e}} \right]
\end{aligned}$$

This can be simplified to



$$\begin{aligned}
\frac{\partial ZWD}{\partial H_e} = & +10^{-6} \cdot 64.68 \cdot \frac{e_{ref} \cdot T_{ref}}{\gamma^2 \cdot H_e^2} \cdot e^{\frac{T_{ref}}{\gamma \cdot H_e}} \cdot \left[ \ln \left( \frac{T_{ref} + \gamma \cdot z_1}{T_{ref} + \gamma \cdot z_0} \right) + S_{12} \right] \\
& -10^{-6} \cdot 64.68 \cdot \frac{e_{ref}}{\gamma} \cdot e^{\frac{T_{ref}}{\gamma \cdot H_e}} \cdot \left[ \frac{\partial S_{12}}{\partial H_e} \right] \\
& -10^{-6} \cdot 5748 \cdot 64.68 \cdot \frac{e_{ref} \cdot T_{ref}}{\gamma^2 \cdot H_e^2} \cdot e^{\frac{T_{ref}}{\gamma \cdot H_e}} \cdot \left[ -e^{\frac{-(T_{ref} + \gamma \cdot z_1)}{\gamma \cdot H_e}} + e^{\frac{-(T_{ref} + \gamma \cdot z_0)}{\gamma \cdot H_e}} \right] \\
& +10^{-6} \cdot 5748 \cdot 64.68 \cdot \frac{e_{ref} \cdot T_{ref}}{\gamma^3 \cdot H_e^3} \cdot e^{\frac{T_{ref}}{\gamma \cdot H_e}} \cdot \left[ \ln \left( \frac{T_{ref} + \gamma \cdot z_1}{T_{ref} + \gamma \cdot z_0} \right) + S_{12} \right] \\
& -10^{-6} \cdot 5748 \cdot 64.68 \cdot \frac{e_{ref}}{\gamma^2 \cdot H_e^2} \cdot e^{\frac{T_{ref}}{\gamma \cdot H_e}} \cdot \left[ e^{\frac{-(T_{ref} + \gamma \cdot z_1)}{\gamma \cdot H_e}} - e^{\frac{-(T_{ref} + \gamma \cdot z_0)}{\gamma \cdot H_e}} \right] \\
& +10^{-6} \cdot 5748 \cdot 64.68 \cdot \frac{e_{ref}}{\gamma^2 \cdot H_e^2} \cdot e^{\frac{T_{ref}}{\gamma \cdot H_e}} \cdot \left[ \ln \left( \frac{T_{ref} + \gamma \cdot z_1}{T_{ref} + \gamma \cdot z_0} \right) + S_{12} \right] \\
& -10^{-6} \cdot 5748 \cdot 64.68 \cdot \frac{e_{ref}}{\gamma^2 \cdot H_e} \cdot e^{\frac{T_{ref}}{\gamma \cdot H_e}} \cdot \left[ \frac{\partial S_{12}}{\partial H_e} \right] \\
& +10^{-6} \cdot 64.68 \cdot \frac{e_{ref}}{T_1} \cdot \left[ \left( 1 + \frac{z'}{H_e} \right) \cdot e^{\frac{-z'}{H_e}} - \left( 1 + \frac{z_1}{H_e} \right) \cdot e^{\frac{-z_1}{H_e}} \right] \\
& -10^{-6} \cdot 5748 \cdot 64.68 \cdot \frac{e_{ref}}{T_1^2} \cdot \left[ \left( 1 + \frac{z'}{H_e} \right) \cdot e^{\frac{-z'}{H_e}} - \left( 1 + \frac{z_1}{H_e} \right) \cdot e^{\frac{-z_1}{H_e}} \right]
\end{aligned} \tag{B.5.8.3}$$

Insert eq. (B.3.3.5.1) in eq. (B.5.8.3)

$$\begin{aligned}
\frac{\partial ZWD}{\partial H_e} = & +10^{-6} \cdot 64.68 \cdot \frac{e_{ref} \cdot T_{ref}}{\gamma^2 \cdot H_e^2} \cdot e^{\frac{T_{ref}}{\gamma \cdot H_e}} \cdot \left[ \ln \left( \frac{T_{ref} + \gamma \cdot z_1}{T_{ref} + \gamma \cdot z_0} \right) + S_{12} \right] \\
& -10^{-6} \cdot 64.68 \cdot \frac{e_{ref}}{\gamma} \cdot e^{\frac{T_{ref}}{\gamma \cdot H_e}} \cdot \left[ \frac{-1}{H_e} \cdot \left[ e^{\frac{-(T_{ref} + \gamma \cdot z_1)}{\gamma \cdot H_e}} - e^{\frac{-(T_{ref} + \gamma \cdot z_0)}{\gamma \cdot H_e}} \right] \right] \\
& -10^{-6} \cdot 5748 \cdot 64.68 \cdot \frac{e_{ref} \cdot T_{ref}}{\gamma^2 \cdot H_e^2} \cdot e^{\frac{T_{ref}}{\gamma \cdot H_e}} \cdot \left[ -e^{\frac{-(T_{ref} + \gamma \cdot z_1)}{\gamma \cdot H_e}} + e^{\frac{-(T_{ref} + \gamma \cdot z_0)}{\gamma \cdot H_e}} \right] \\
& +10^{-6} \cdot 5748 \cdot 64.68 \cdot \frac{e_{ref} \cdot T_{ref}}{\gamma^3 \cdot H_e^3} \cdot e^{\frac{T_{ref}}{\gamma \cdot H_e}} \cdot \left[ \ln \left( \frac{T_{ref} + \gamma \cdot z_1}{T_{ref} + \gamma \cdot z_0} \right) + S_{12} \right] \\
& -10^{-6} \cdot 5748 \cdot 64.68 \cdot \frac{e_{ref}}{\gamma^2 \cdot H_e^2} \cdot e^{\frac{T_{ref}}{\gamma \cdot H_e}} \cdot \left[ e^{\frac{-(T_{ref} + \gamma \cdot z_1)}{\gamma \cdot H_e}} - e^{\frac{-(T_{ref} + \gamma \cdot z_0)}{\gamma \cdot H_e}} \right]
\end{aligned} \tag{B.5.8.4}$$

$$\begin{aligned}
& +10^{-6} \cdot 5748 \cdot 64.68 \cdot \frac{e_{ref}}{\gamma^2 \cdot H_e^2} \cdot e^{\frac{T_{ref}}{\gamma \cdot H_e}} \cdot \left[ \ln \left( \frac{T_{ref} + \gamma \cdot z_1}{T_{ref} + \gamma \cdot z_0} \right) + S_{12} \right] \\
& -10^{-6} \cdot 5748 \cdot 64.68 \cdot \frac{e_{ref}}{\gamma^2 \cdot H_e} \cdot e^{\frac{T_{ref}}{\gamma \cdot H_e}} \cdot \left[ \frac{-1}{H_e} \cdot \left[ e^{\frac{-(T_{ref} + \gamma \cdot z_1)}{\gamma \cdot H_e}} - e^{\frac{-(T_{ref} + \gamma \cdot z_0)}{\gamma \cdot H_e}} \right] \right] \\
& +10^{-6} \cdot 64.68 \cdot \frac{e_{ref}}{T_1} \cdot \left[ \left( 1 + \frac{z'}{H_e} \right) \cdot e^{\frac{-z'}{H_e}} - \left( 1 + \frac{z_1}{H_e} \right) \cdot e^{\frac{-z_1}{H_e}} \right] \\
& -10^{-6} \cdot 5748 \cdot 64.68 \cdot \frac{e_{ref}}{T_1^2} \cdot \left[ \left( 1 + \frac{z'}{H_e} \right) \cdot e^{\frac{-z'}{H_e}} - \left( 1 + \frac{z_1}{H_e} \right) \cdot e^{\frac{-z_1}{H_e}} \right]
\end{aligned}$$

that is

$$\begin{aligned}
\frac{\partial ZWD}{\partial H_e} = & +10^{-6} \cdot 64.68 \cdot \frac{e_{ref} \cdot T_{ref}}{\gamma^2 \cdot H_e^2} \cdot e^{\frac{T_{ref}}{\gamma \cdot H_e}} \cdot \left[ \ln \left( \frac{T_{ref} + \gamma \cdot z_1}{T_{ref} + \gamma \cdot z_0} \right) + S_{12} \right] \\
& +10^{-6} \cdot 64.68 \cdot \frac{e_{ref}}{\gamma \cdot H_e} \cdot e^{\frac{T_{ref}}{\gamma \cdot H_e}} \cdot \left[ e^{\frac{-(T_{ref} + \gamma \cdot z_1)}{\gamma \cdot H_e}} - e^{\frac{-(T_{ref} + \gamma \cdot z_0)}{\gamma \cdot H_e}} \right] \\
& -10^{-6} \cdot 5748 \cdot 64.68 \cdot \frac{e_{ref} \cdot T_{ref}}{\gamma^2 \cdot H_e^2} \cdot e^{\frac{T_{ref}}{\gamma \cdot H_e}} \cdot \left[ \frac{-e^{\frac{-(T_{ref} + \gamma \cdot z_1)}{\gamma \cdot H_e}}}{T_{ref} + \gamma \cdot z_1} + \frac{e^{\frac{-(T_{ref} + \gamma \cdot z_0)}{\gamma \cdot H_e}}}{T_{ref} + \gamma \cdot z_0} \right] \\
& +10^{-6} \cdot 5748 \cdot 64.68 \cdot \frac{e_{ref} \cdot T_{ref}}{\gamma^3 \cdot H_e^3} \cdot e^{\frac{T_{ref}}{\gamma \cdot H_e}} \cdot \left[ \ln \left( \frac{T_{ref} + \gamma \cdot z_1}{T_{ref} + \gamma \cdot z_0} \right) + S_{12} \right] \\
& -10^{-6} \cdot 5748 \cdot 64.68 \cdot \frac{e_{ref}}{\gamma^2 \cdot H_e^2} \cdot e^{\frac{T_{ref}}{\gamma \cdot H_e}} \cdot \left[ e^{\frac{-(T_{ref} + \gamma \cdot z_1)}{\gamma \cdot H_e}} - e^{\frac{-(T_{ref} + \gamma \cdot z_0)}{\gamma \cdot H_e}} \right] \\
& +10^{-6} \cdot 5748 \cdot 64.68 \cdot \frac{e_{ref}}{\gamma^2 \cdot H_e^2} \cdot e^{\frac{T_{ref}}{\gamma \cdot H_e}} \cdot \left[ \ln \left( \frac{T_{ref} + \gamma \cdot z_1}{T_{ref} + \gamma \cdot z_0} \right) + S_{12} \right] \\
& +10^{-6} \cdot 5748 \cdot 64.68 \cdot \frac{e_{ref}}{\gamma^2 \cdot H_e^2} \cdot e^{\frac{T_{ref}}{\gamma \cdot H_e}} \cdot \left[ e^{\frac{-(T_{ref} + \gamma \cdot z_1)}{\gamma \cdot H_e}} - e^{\frac{-(T_{ref} + \gamma \cdot z_0)}{\gamma \cdot H_e}} \right] \\
& +10^{-6} \cdot 64.68 \cdot \frac{e_{ref}}{T_1} \cdot \left( 1 - \frac{5748}{T_1} \right) \cdot \left[ \left( 1 + \frac{z'}{H_e} \right) \cdot e^{\frac{-z'}{H_e}} - \left( 1 + \frac{z_1}{H_e} \right) \cdot e^{\frac{-z_1}{H_e}} \right]
\end{aligned} \tag{B.5.8.5}$$

or

$$\begin{aligned}
\frac{\partial ZWD}{\partial H_e} = & 10^{-6} \cdot 64.68 \cdot \frac{e_{ref}}{\gamma^2 \cdot H_e^2} \cdot e^{\frac{T_{ref}}{\gamma \cdot H_e}} \cdot \left[ T_{ref} \cdot \left( 1 + \frac{5748}{\gamma \cdot H_e} \right) + 5748 \right] \cdot \left[ \ln \left( \frac{T_{ref} + \gamma \cdot z_1}{T_{ref} + \gamma \cdot z_0} \right) + S_{12} \right] \\
& + 10^{-6} \cdot 64.68 \cdot \frac{e_{ref}}{\gamma \cdot H_e} \cdot e^{\frac{T_{ref}}{\gamma \cdot H_e}} \cdot \left[ e^{\frac{-(T_{ref} + \gamma \cdot z_1)}{\gamma \cdot H_e}} - e^{\frac{-(T_{ref} + \gamma \cdot z_0)}{\gamma \cdot H_e}} \right] \\
& - 10^{-6} \cdot 5748 \cdot 64.68 \cdot \frac{e_{ref} \cdot T_{ref}}{\gamma^2 \cdot H_e^2} \cdot e^{\frac{T_{ref}}{\gamma \cdot H_e}} \cdot \left[ \frac{-e^{\frac{-(T_{ref} + \gamma \cdot z_1)}{\gamma \cdot H_e}}}{T_{ref} + \gamma \cdot z_1} + \frac{-e^{\frac{-(T_{ref} + \gamma \cdot z_0)}{\gamma \cdot H_e}}}{T_{ref} + \gamma \cdot z_0} \right] \\
& + 10^{-6} \cdot 64.68 \cdot \frac{e_{ref}}{T_1} \cdot \left( 1 - \frac{5748}{T_1} \right) \cdot \left[ \left( 1 + \frac{z'}{H_e} \right) \cdot e^{\frac{-z'}{H_e}} - \left( 1 + \frac{z_1}{H_e} \right) \cdot e^{\frac{-z_1}{H_e}} \right]
\end{aligned} \tag{B.5.8.6}$$

## B.6. Parameter dependencies of the partial derivatives

In order to clarify which term computed above depends on which parameters, a summary of the parameter dependency of the different partial derivatives of the Zenith Dry Delay and of the Zenith Wet Delay is approached in Table B.1 hereunder.

Parameters											
Function	$p_{ref}$	$e_{ref}$	$T_{ref}$	$T_1$	$\gamma$	$z_0$	$z_1$	$z'$	$H_p$	$H_e$	Eq. Nr.
ZDD	×	×	×	×	×	×	×	×	×	×	(3.4.9.23)
ZWD		×	×	×	×	×	×	×		×	(3.4.9.22)
$\partial ZDD / \partial p_{ref}$			×	×	×	×	×	×	×		(B.4.1.1)
$\partial ZDD / \partial e_{ref}$			×		×	×	×	×		×	(B.4.2.1)
$\partial ZDD / \partial T_{ref}$	×	×	×		×	×	×		×	×	(B.4.3.2)
$\partial ZDD / \partial T_1$	×	×		×			×	×	×	×	(B.4.4.2)
$\partial ZDD / \partial \gamma$	×	×	×		×	×	×		×	×	(B.4.5.3)
$\partial ZDD / \partial z_0$	×	×	×		×	×			×	×	(B.4.6.5)
$\partial ZDD / \partial z_1$	×	×	×		×		×		×	×	(B.4.7.4)
$\partial ZDD / \partial z'$				×				×	×	×	(B.4.8.3)
$\partial ZDD / \partial H_p$	×		×	×	×	×	×		×		(B.4.9.5)
$\partial ZDD / \partial H_e$		×	×	×	×	×	×	×		×	(B.4.10.5)
$\partial ZWD / \partial p_{ref}$											—
$\partial ZWD / \partial e_{ref}$			×	×	×	×	×	×		×	(B.5.1.1)
$\partial ZWD / \partial T_{ref}$		×	×		×	×	×			×	(B.5.2.3)
$\partial ZWD / \partial T_1$		×		×			×	×		×	(B.5.3.3)
$\partial ZWD / \partial \gamma$		×	×	×	×	×	×			×	(B.5.4.6)
$\partial ZWD / \partial z_0$		×	×		×	×				×	(B.5.5.5)
$\partial ZWD / \partial z_1$		×	×	×	×		×			×	(B.5.6.4)
$\partial ZWD / \partial z'$		×		×				×		×	(B.5.7.2)
$\partial ZWD / \partial H_p$											—
$\partial ZWD / \partial H_e$		×	×	×	×	×	×			×	(B.5.8.6)

Table B.1. Parameter dependencies of the partial derivatives

Two rows have been added in order to explicitly show that the ZWD does not depend on  $p_{ref}$  and on  $H_p$ . The equation number has been introduced to ease fast referencing.

## Appendix C. COMEDIE software

Accordingly to paragraph 4.3.1, the different program parts are presented hereunder. The ZPD functional model is first introduced. Then the main programs that are the core of the COMEDIE software are visualized and finally a short introduction on the data input is provided.

### C.1. *m\_herschke*

The routine `m_herschke.c` contains the Zenith Dry Delay (ZDD) and Zenith Wet Delay (ZWD) functional models, i.e. eq. (3.4.9.23) and (3.4.9.22).

```

/*
 * FILE:          m_herschke
 *
 * PROJECT:       COMEDIE
 *
 * PURPOSE:       ZPD model
 *
 * COPYRIGHT:     © 2002 Geodesy and Geodynamics Lab,
 *               Swiss Federal Institute of Technology Zurich
 *
 * AUTHORS:       Philippe Herschke
 *
 * HISTORY :      dd-mm-yyyy -- description
 *               07-02-2002 -- created
 *               15-02-2002 -- constrains applied to parameters
 */

#ifndef M_HERSCHKE
#define M_HERSCHKE

/* -----
 * param  0  1  2  3  4  5  6
 *         tref gamma z1  z' t1 eref He
 */
double zwd_herschke(double *param, double h);

/* -----
 * param  0  1  2  3
 *         pref eref tref gamma
 */
double zpd_herschke(double *param, double h);

#endif

```

Table C.1. `m_herschke.h` library

The corresponding main routine is

```

/*
 * FILE:          m_herschke
 *
 * PROJECT:       COMEDIE
 *
 * PURPOSE:       ZPD and ZWD modeling
 *
 * COPYRIGHT:     © 2002 Geodesy and Geodynamics Lab,
 *               Swiss Federal Institute of Technology Zurich
 *
 * AUTHOR:        Philippe Herschke
 *
 * HISTORY:       see corresponding header file

```

```

*/

#include <stdio.h>
#include <stdlib.h>
#include <common.h>

/* ----- */
double s_term(double x, double eps)
{
    int i=1;
    double x1 = x;
    double x2 = 1;
    double result = x;
    double x3;

    do
    {
        i++;
        x1 *= x;
        x2 *= i;
        x3 = x1/x2/i;
        result += x3;
    }
    while (fabs(x3)>eps);
    return result;
}

/* ----- */
* param0    1      2  3  4  5  6
*           tref gamma z1 z' t1 eref He
*/
double zwd_herschke(double *param, double h)
{
    double e0_div_gamma = param[5]/param[1];
    double div_gammaH = 1/param[1]/param[6];
    double t1 = param[0] + param[1]*param[2];
    double t = param[0] + param[1]*h;
    double cte = 64.68 * e0_div_gamma * exp(param[0]*div_gammaH);

    double s12, x;
    double term1, term2, term3, term4;

    s12=s_term(-t1*div_gammaH, 1.0e-10) - s_term(-t*div_gammaH, 1.0e-10);
    x = log(t1/t) + s12;

    term1 = -cte * x;
    term2 = cte * 5748.0 * (-exp(-t1*div_gammaH)/t1 + exp(-t*div_gammaH)/t - div_gammaH*x);

    x = exp(-param[3]/param[6]) - exp(-param[2]/param[6]);

    term3 = 64.68 * param[5]/param[4] * param[6] * x;
    term4 = -term3*5748/param[4];

    return (term1 + term2 + term3 + term4)*1.0e-6;
}

/* ----- */
* param0    1      2  3
*           pref eref tref gamma
*/
double zpd_herschke(double *param, double h)
{
    double t1 = 216.64;
    double z1 = 11000.0;
    double z_prime = 15000.0;

```

```

double Hp = 9000.0;
double He = 3000.0;
double gamma = -0.006501;
double pref_div_gamma = param[0]/gamma;
double eref_div_gamma = param[1]/gamma;
double div_gammaHp = 1/gamma/Hp;
double div_gammaHe = 1/gamma/He;
double div_t1 = 1/t1;
double div_t1_square = 1/t1/t1;

// double t1 = param[2] + gamma*z1;

double t = param[2] + gamma*h;

double cte = 64.68*eref_div_gamma*exp(param[2]*div_gammaHe);

double s11, s12, x11, x12, y12;
double term1, term2, term3, term4, term5, term6, term7, term8;

s11 = s_term(-t*div_gammaHp, 1.0e-10) - s_term(-t*div_gammaHp, 1.0e-10);
x11 = log(t1/t) + s11;

s12 = s_term(-t*div_gammaHe, 1.0e-10) - s_term(-t*div_gammaHe, 1.0e-10);
x12 = log(t1/t) + s12;

y12 = exp(-z_prime/He) - exp(-z1/He);
term1 = 77.64*pref_div_gamma*exp(param[2]*div_gammaHp)*x11;
term2 = 77.64*eref_div_gamma*exp(param[2]*div_gammaHe)*x12;
term3 = 77.64*param[0]*div_t1*Hp*(exp(-z1/Hp) - exp(-z_prime/Hp) );
term4 = 77.64*param[1]*div_t1*He*y12;
term5 = cte*x12;
term6 = cte*5748.0*( -exp(-t*div_gammaHe)/t1 + exp(-t*div_gammaHe)/t - div_gammaHe*x12 );
term7 = 64.68* param[1]*div_t1* He*y12;
term8 = 5748.0*64.68*param[1]*div_t1_square*He*y12;

return (term1 - term2 + term3 - term4 - term5 + term6 + term7 - term8)*1.0e-6;

}

```

Table C.2. m\_herschke.c routine for ZPD functional model

## C.2. m\_model

The m\_model.c routine contains all functional model available in the COMEDIE software. The serial number 1000 has been attributed to the ZPD model of Chapter 3. This calls the m\_herschke.c routine.

```

/*
 * FILE:          m_model.c
 *
 * PROJECT:       COMEDIE
 *
 * PURPOSE:       contains all functional models and partial derivatives
 *
 * COPYRIGHT:     © 2002 Geodesy and Geodynamics Lab,
 *                Swiss Federal Institute of Technology Zurich
 *
 * AUTHORS:       Cocard Marc
 *                Troller Marc
 *                Herschke Philippe (model serial # 1000)
 *
 * HISTORY:       see corresponding header file
 */

#include <stdio.h>
#include <stdlib.h>
#include <string.h>

```

```

#include <common.h>
#include "m_general.h"
#include "m_herschke.h"
#include "m_point.h"
#include "m_model.h"

/* ----- */
double heavy(double height, double maxheight)
{
    int a = 1;
    double value;

    value = 1/PI*atan2(a*(height-maxheight), 1)+0.5;
    return value;
}

/* ----- */
struct Model * init_model(int type, int count, int sigma)
{
    struct Model * model;
    int i;

    if ((model = (struct Model *) malloc(sizeof(struct Model))) == NULL) return NULL;
    memset(model, 0, sizeof(struct Model));
    model->type = type;
    model->count = count;

    if ((model->param = (double *) malloc(sizeof(double)*count)) == NULL) return NULL;
    memset(model->param, 0, sizeof(double)*count);

    if ((model->name = (char **) malloc(sizeof(char *)*count)) == NULL) return NULL;
    memset(model->name, 0, sizeof(char *)*count);

    if ( sigma
        {
            if ((model->sigma = (double *) malloc(sizeof(double)*count)) == NULL) return NULL;
            for (i=0; i<count; i++) model->sigma[i] = -99.9;
        }
    return model;
}

/* ----- */
struct Model * copy_model(struct Model *old)
{
    struct Model * model;
    int i;

    if ((model = init_model(old->type, old->count, old->sigma==NULL?0:1)) == NULL)
    return NULL;
    memcpy(model->param, old->param, sizeof(double)*old->count);
    for (i=0; i<old->count; i++)
        if (old->name[i] != NULL &&
            (model->name[i]=strdup(old->name[i])) == NULL) return NULL;
    if (old->sigma != NULL) memcpy(model->sigma, old->sigma, sizeof(double)*old->count);
    return model;
}

/* ----- */
void free_model(struct Model *model)
{
    int i;
    if (model->param != NULL) free(model->param);
    if (model->name != NULL)
    {
        for (i=0; i<model->count; i++)
            if (model->name[i] != NULL) free(model->name[i]);
    }
}

```



```

    free(model->name);
}
if (model->sigma != NULL) free(model->sigma);
free(model);
}

/* ----- */
int check_model(struct Model *model)
{
extern char * pgname;

/* here are the known model types with their corresponding dimension */
const int known_model_type[] = { 1, 2, 3, 100, 101, 200, 201, 202, 203, 300, 301, 1000};
const int known_model_count[] = { 5, 6, 6, 2, 5, 2, 5, 6, 3, 2, 5, 3};

int i;

for (i=0; i<sizeof(known_model_count)/sizeof(int); i++)
    if (model->type == known_model_type[i])
    {
        if (model->count == known_model_count[i]) return 0;
        fprintf(stderr,"%s: ***ERROR: model %d requires %d parameters\n",
                pgname, model->type, known_model_count[i]);
        return -1;
    }

fprintf(stderr,"%s: ***ERROR: model type %d not supported\n", pgname, model->type);
return -1;
}
/* ----- */
int filename_model(struct Model *model, char **measunit)
{
switch (model->type)
{
case 1: /* covariance without attenuation factor */
{
    if ((model->name[0] = strdup("sigma signal")) == NULL) return -1;
    if ((model->name[1] = strdup("delta-x [km]")) == NULL) return -1;
    if ((model->name[2] = strdup("delta-y [km]")) == NULL) return -1;
    if ((model->name[3] = strdup("delta-height [km]")) == NULL) return -1;
    if ((model->name[4] = strdup("delta-time [hour]")) == NULL) return -1;
    return 0;
}

case 2: /* covariance with attenuation factor */
{
    if ((model->name[0] = strdup("sigma signal")) == NULL) return -1;
    if ((model->name[1] = strdup("delta-x [km]")) == NULL) return -1;
    if ((model->name[2] = strdup("delta-y [km]")) == NULL) return -1;
    if ((model->name[3] = strdup("delta-height [km]")) == NULL) return -1;
    if ((model->name[4] = strdup("delta-time [hour]")) == NULL) return -1;
    if ((model->name[5] = strdup("attenuation factor")) == NULL) return -1;
    return 0;
}

case 3: /* covariance with attenuation factor & Heavyside function */
{
    if ((model->name[0] = strdup("sigma signal")) == NULL) return -1;
    if ((model->name[1] = strdup("delta-x [km]")) == NULL) return -1;
    if ((model->name[2] = strdup("delta-y [km]")) == NULL) return -1;
    if ((model->name[3] = strdup("delta-height [km]")) == NULL) return -1;
    if ((model->name[4] = strdup("delta-time [hour]")) == NULL) return -1;
    if ((model->name[5] = strdup("attenuation factor")) == NULL) return -1;
    return 0;
}

case 100: /* pressure simple model */
{

```

```

    if ((*measunit = strdup("hPa")) == NULL) return -1;
    if ((model->name[0] = strdup("pressure at sea level [hPa]")) == NULL) return -1;
    if ((model->name[1] = strdup("scaling height [m]")) == NULL) return -1;
    return 0;
}
case 101 : /* pressure with horizontal gradients */
{
    if ((*measunit = strdup("hPa")) == NULL) return -1;
    if ((model->name[0] = strdup("pressure at sea level [hPa]")) == NULL) return -1;
    if ((model->name[1] = strdup("scaling height [m]")) == NULL) return -1;
    if ((model->name[2] = strdup("horizontal gradient x-direction [hPa/100km]")) == NULL) return -1;
    if ((model->name[3] = strdup("horizontal gradient y-direction [hPa/100km]")) == NULL) return -1;
    if ((model->name[4] = strdup("time gradient [hPa/hour]")) == NULL) return -1;
    return 0;
}
case 200 : /* temperature simple model */
{
    if ((*measunit = strdup("oCel")) == NULL) return -1;
    if ((model->name[0] = strdup("temperature at sea level [oCel]")) == NULL) return -1;
    if ((model->name[1] = strdup("temperature gradient [oCel/km]")) == NULL) return -1;
    return 0;
}
case 201 : /* temperature with horizontal gradients */
{
    if ((*measunit = strdup("oCel")) == NULL) return -1;
    if ((model->name[0] = strdup("temperature at sea level [oCel]")) == NULL) return -1;
    if ((model->name[1] = strdup("temperature gradient [oCel/km]")) == NULL) return -1;
    if ((model->name[2] = strdup("horizontal gradient x-direction [oCel/100km]")) == NULL) return -1;
    if ((model->name[3] = strdup("horizontal gradient y-direction [oCel/100km]")) == NULL) return -1;
    if ((model->name[4] = strdup("time gradient[oCel/hour]")) == NULL) return -1;
    return 0;
}
case 202 : /* temperature with horizontal gradients - two functions */
{
    if ((*measunit = strdup("oCel")) == NULL) return -1;
    if ((model->name[0] = strdup("temperature at sea level [oCel]")) == NULL) return -1;
    if ((model->name[1] = strdup("temperature gradient [oCel/km]")) == NULL) return -1;
    if ((model->name[2] = strdup("horizontal gradient x-direction [oCel/100km]")) == NULL) return -1;
    if ((model->name[3] = strdup("horizontal gradient y-direction [oCel/100km]")) == NULL) return -1;
    if ((model->name[4] = strdup("time gradient[oCel/hour]")) == NULL) return -1;
    if ((model->name[5] = strdup("constant temperature in the higher area [oCel]")) == NULL) return -1;
    return 0;
}

case 203 : /* temperature without horizontal gradients - two functions */
{
    if ((*measunit = strdup("oCel")) == NULL) return -1;
    if ((model->name[0] = strdup("temperature at sea level [oCel]")) == NULL) return -1;
    if ((model->name[1] = strdup("temperature gradient [oCel/km]")) == NULL) return -1;
    if ((model->name[2] = strdup("constant temperature in the higher area [oCel]")) == NULL) return -1;
    return 0;
}

case 300 : /* humidity simple model */
{
    if ((*measunit = strdup("hPa")) == NULL) return -1;
    if ((model->name[0] = strdup("humidity at sea level")) == NULL) return -1;
    if ((model->name[1] = strdup("scaling height")) == NULL) return -1;
    return 0;
}
case 301 : /* humidity with horizontal gradients */
{
    if ((*measunit = strdup("hPa")) == NULL) return -1;
    if ((model->name[0] = strdup("humidity at sea level")) == NULL) return -1;
    if ((model->name[1] = strdup("scaling height")) == NULL) return -1;
    if ((model->name[2] = strdup("horizontal gradient x-direction")) == NULL) return -1;
    if ((model->name[3] = strdup("horizontal gradient y-direction")) == NULL) return -1;
    if ((model->name[4] = strdup("time gradient")) == NULL) return -1;
}

```

```

    return 0;
}

case 1000 : /* zenith path delay (ZPD) */
{
    if ((*measunit = strdup("m")) == NULL) return -1;
    if ((model->name[0] = strdup("reference pressure [hPa]")) == NULL) return -1;
    if ((model->name[1] = strdup("reference humidity [hPa]")) == NULL) return -1;
    if ((model->name[2] = strdup("reference temperature [K]")) == NULL) return -1;
//    if ((model->name[3] = strdup("tropospheric temperature gradient [K/m]")) == NULL) return -1;
    return 0;
}

} /* end switch */

return -1; /* model->type not supported */
}

/* ----- */
void write_model(FILE *fp, struct Model *model, int withsigma)
{
    int i;
    if (model != NULL)
    {
        fprintf(fp, "%21d  type\n", model->type);
        fprintf(fp, "%21d  param count\n", model->count);
        for (i=0; i<model->count; i++)
        {
            if (withsigma) fprintf(fp, "%12.5f %8.2f", model->param[i], model->sigma[i]);
            else fprintf(fp, "%21.5f", model->param[i]);

            if (model->name[i] == NULL) fprintf(fp, " parameter %2d\n", i+1);
            else fprintf(fp, " %s\n", model->name[i]);
        }
    }
}

/* ----- */
struct Model * read_model(FILE *fp, int *linenr, int withsigma)
{
    char line[MAXLINELENGTH];
    int type, count, i, offset;
    struct Model *model;

    if (readnextline(fp, line, linenr) != 0 || sscanf(line, "%d", &type) != 1) return NULL;
    if (readnextline(fp, line, linenr) != 0 || sscanf(line, "%d", &count) != 1) return NULL;

    if ((model=init_model(type, count, withsigma)) == NULL) return NULL;

    for (i=0; i<count; i++)
    {
        if (readnextline(fp, line, linenr) != 0) return NULL;
        if (sscanf(line, "%lf %n", &(model->param[i]), &offset) != 1) return NULL;

        if (withsigma && sscanf(line+offset, "%lf", &(model->sigma[i])) != 1) return NULL;
    }
    return model;
}

/* ----- */
int calc_covariance(struct Model *cov, struct Point *p1, struct Point *p2, double *covvalue)
{
    /* CAUTION: correlation length unit is km resp. hours !!! Conversions directly performed in routine itself */

    double dx2, dy2, dh2, dt2;
    double damping;

```

```

dx2 = SQR((p1->xcoord - p2->xcoord)/1000.0/cov->param[1]);
dy2 = SQR((p1->ycoord - p2->ycoord)/1000.0/cov->param[2]);
dh2 = SQR((p1->height - p2->height)/1000.0/cov->param[3]);
dt2 = SQR((p1->mjd - p2->mjd)*24.0/cov->param[4]);

switch (cov->type)
{
case 1: /* without damping factor */
{
(*covvalue) = SQR(cov->param[0])/(1 + dx2+dy2+dh2+dt2);
return 0;
}
case 2: /* with damping factor */
{
damping=-(p1->height + p2->height)/2/cov->param[5]/1000;
damping=exp(damping);
(*covvalue) = SQR(cov->param[0])/(1 + (dx2+dy2+dh2+dt2)*damping);
return 0;
}
case 3: /* with damping factor & additional time-correlation (Heavyside function) */
{
damping=-(p1->height + p2->height)/2/cov->param[5]/1000;
damping=exp(damping)
(*covvalue) = SQR(cov->param[0])/(1 + (dx2+dy2+dh2+dt2*heavy(p1->height, 5000))*damping);
return 0;
}
}
return -1; /* cov->type not supported */
}

/* ----- */
int calc_model(struct Model *model, struct Point *p, double *value, struct Point *refpoint)
{
switch (model->type)
{
case 100 : /* pressure simple model */
{
*value = model->param[0]*exp(-p->height/model->param[1]);
return 0;
}

case 101 : /* pressure with horizontal gradients */
{
*value = ( model->param[0]
+ model->param[2] * (p->xcoord-refpoint->xcoord)*1.0e-5
+ model->param[3] * (p->ycoord-refpoint->ycoord)*1.0e-5
+ model->param[4] * (p->mjd-refpoint->mjd) * 24.0)
* exp(-p->height/model->param[1]);
return 0;
}

case 200 : /* temperature simple model */
{
*value = model->param[0] + model->param[1] * p->height * 1.0e-3;
return 0;
}

case 201 : /* temperature with horizontal gradients */
{
*value = ( model->param[0]
+ model->param[2] * (p->xcoord - refpoint->xcoord)*1.0e-5
+ model->param[3] * (p->ycoord - refpoint->ycoord)*1.0e-5
+ model->param[4] * (p->mjd - refpoint->mjd) * 24.0
+ model->param[1] * p->height * 1.0e-3);
return 0;
}

case 202 : /* temperature with horizontal gradients - two functions */

```

```

    {
        *value = ( model->param[2] * (p->xcoord - refpoint->xcoord)*1.0e-5
                + model->param[3] * (p->ycoord - refpoint->ycoord)*1.0e-5
                + model->param[4] * (p->mjd - refpoint->mjd) * 24.0
                + (model->param[0] + model->param[1] * p->height *1.0e-3)
                * (1 - heavy(p->height, 11000))
                + model->param[5] *heavy(p->height, 11000));
        return 0;
    }

case 203 : /* temperature without horizontal gradients - two functions */
{
    *value = (( model->param[0] + model->param[1] * p->height +1.0e-3)
            * (1 - heavy(p->height, 11000))
            + model->param[2] *heavy(p->height, 11000));
    return 0;
}

case 300 : /* humidity simple model */
{
    *value = model->param[0] * exp(-p->height/model->param[1]);
    return 0;
}

case 301 : /* humidity with horizontal gradients */
{
    *value = ( model->param[0]
            + model->param[2] * (p->xcoord - refpoint->xcoord)*1.0e-5
            + model->param[3] * (p->ycoord - refpoint->ycoord)*1.0e-5
            + model->param[4] * (p->mjd - refpoint->mjd) *24.0 )
            * exp(-p->height/model->param[1]);
    return 0;
}

case 1000 : /* zenith path delay (ZPD) model Herschke */
{
    /* compute zenith path delay */
    *value = zpd_herschke(model->param, p->height);
    return 0;
}
}
return -1; /* model->type not supported */
}

/* ----- */
int calc_derivation(struct Model *model, struct Point *p, double *deriv, struct
Point *refpoint)
{
    double *paramdummy;
    double dparam;
    double value0;
    int i;

#define LN10 (log(10))

    switch(model->type)
    {
        case 100 : /* pressure simple model */
            {
                deriv[0] = exp(-p->height/model->param[1]);
                deriv[1] = model->param[0] * deriv[0] * p->height / SQR(model->param[1]);
                return 0;
            }

        case 101 : /* pressure with horizontal gradients */
            {
                deriv[0] = exp(-p->height/model->param[1]);

```

```

    deriv[1] = ( model->param[0]
                + model->param[2] * (p->xcoord - refpoint->xcoord) * 1.0e-5
                + model->param[3] * (p->ycoord - refpoint->ycoord) * 1.0e-5
                + model->param[4] * (p->mjd - refpoint->mjd) * 24.0 )
                * deriv[0]*p->height/SQR(model->param[1]);
    deriv[2] = (p->xcoord - refpoint->xcoord) * deriv[0] * 1.0e-5;
    deriv[3] = (p->ycoord - refpoint->ycoord) * deriv[0] * 1.0e-5;
    deriv[4] = (p->mjd - refpoint->mjd) * deriv[0] * 24.0;
    return 0;
}

case 200 : /* temperature simple model */
{
    deriv[0] = 1;
    deriv[1] = p->height * 1.0e-3;
    return 0;
}

case 201 : /* temperature with horizontal gradients */
{
    deriv[0] = 1;
    deriv[1] = p->height * 1.0e-3;
    deriv[2] = (p->xcoord - refpoint->xcoord)*1.0e-5;
    deriv[3] = (p->ycoord - refpoint->ycoord)*1.0e-5;
    deriv[4] = (p->mjd - refpoint->mjd) * 24.0;
    return 0;
}

case 202 : /* temperature with horizontal gradients - two functions */
{
    deriv[0] = 1 - heavy(p->height, 11000);
    deriv[1] = (p->height - p->height * heavy(p->height, 11000)) * 1.0e-3;
    deriv[2] = (p->xcoord - refpoint->xcoord)*1.0e-5;
    deriv[3] = (p->ycoord - refpoint->ycoord)*1.0e-5;
    deriv[4] = (p->mjd - refpoint->mjd) * 24.0;
    deriv[5] = heavy(p->height, 11000);
    return 0;
}

case 203 : /* temperature with horizontal gradients - two functions */
{
    deriv[0] = 1 - heavy(p->height, 11000);
    deriv[1] = (p->height - p->height * heavy(p->height, 11000)) * 1.0e-3;
    deriv[2] = heavy(p->height, 11000);
    return 0;
}

case 300 : /* humidity simple model */
{
    deriv[0] = exp(-p->height/model->param[1]);
    deriv[1] = model->param[0]*deriv[0]*LN10*p->height/SQR(model->param[1]);
    return 0;
}

case 301 : /* humidity with horizontal gradients */
{
    deriv[0] = exp(-p->height/model->param[1]);
    deriv[1] = ( model->param[0]
                + model->param[2] * (p->xcoord - refpoint->xcoord) * 1.0e-5
                + model->param[3] * (p->ycoord - refpoint->ycoord) * 1.0e-5
                + model->param[4] * (p->mjd - refpoint->mjd) * 24.0 )
                * deriv[0]*p->height/SQR(model->param[1]);
    deriv[2] = (p->xcoord - refpoint->xcoord) * deriv[0]*1.0e-5;
    deriv[3] = (p->ycoord - refpoint->ycoord) * deriv[0]*1.0e-5;
    deriv[4] = (p->mjd - refpoint->mjd) * deriv[0] * 24.0;
    return 0;
}

```

```

case 1000 : /* zenith path delay (ZPD) */
{
  value0 = zpd_herschke(model->param, p->height);
  paramdummy = (double *) malloc(model->count*sizeof(double));
  for (i=0; i<model->count; i++)
  {
    memcpy(paramdummy, model->param, model->count*sizeof(double));
    dparam = fabs(model->param[i]/1000);
    paramdummy[i]+=dparam;
    deriv[i] = (zpd_herschke(paramdummy, p->height) - value0)/dparam;
  }
  free(paramdummy);

  return 0;
}

} /* end switch */
return -1; /* model->type not supported */
}

```

Table C.3. m\_model.c routine containing the COMEDIE functional models

### C.3. Collocation and prediction programs

As these programs are extensive, it is not of interest to provide here an output of those. Instead it is referred to [Troller et al., 2002].

### C.4. Input files

There are two input files. The first, `colloc_input` is structured in blocks that call a functional model and a covariance function. In addition, the functional parameters are initialized with their default values.

```

#-----
#  VERSION 1          INPUT FILE M_COLCPREP
#-----
#
# all blank lines and lines starting with a pound-sign (#)
# are comment lines.
#
# The first non-comment line must start with the string "VERSION"
# followed by the version number.
#
# The file may contain more than 1 model. All models must have
# a unique identification number (greater than zero) in the
# first input field.
#
# The char ">" is used as delimiter. Comment before ">" is
# overread.

##### UNITS #####

nr.                > 0
name               > text appears in output file
funct.model.type   > regular model number
funct.model.number.of.parameters > 2 or 5
funct.model.parameters > hPa, °C, m
funct.model.sigma.a.priori > hPa, °C, m
covariance.type    > 1 or 2
covariance.number.of.parameters > 5 or 6
covariance.parameters > no unit, km/[hPa °C], km/hPa, km/°C, h/[hPa, °C], km
.
.
.

##### ZENITH PATH DELAY MODELS #####

```

nr.	> 1000
name	> zpd
funct.model.type	> 1000
funct.model.number.of.parameters	> 3
funct.model.parameters	> 1013.25 10.0 288.15
funct.model.sigma.a.priori	>
covariance.type	> 1
covariance.number.of.parameters	> 5
covariance.parameters	> 2 100 100 1 6

Table C.4. Example of colloc\_input file

The second, input\_main determines the observation window for the data extraction as well as the time period for the collocation and for the prediction.

```
#-----
#          GENERAL INPUTFILE FOR PROGRAM COMEDIE
#-----

block.keyword          > GENERAL
start.time             > 2000 05 22 00 00 00
end.time               > 2000 05 30 00 00 00
interval.for.1.collocation.(hour) > 12
project name           > pd_estimation
comedie main path      > /home/logvert/herschke/daten/pathdelay/
working directory      > work
subdirectory.extracted.datafiles > extract
subdirectory.collocated.files > colloc
subdirectory.interpolated.files > interpol
subdirectory.pathdelay.files > pathdelay
subdirectory.per.station.pathdelay.files > pd_station

#-----

block.keyword          > DATAEXTRACT
prefix.of.files        > ext
#---- AGNES ----
station.file           > agnes.st
offset.(before and after time interval.in hour) > 12
path.to.database       > /home/logvert/herschke/COMEDIE/daten/pathdelay/work
ZPD: std.dev.of.meas.values > 0.50

.
.
.

#-----

block.keyword          > COLCPREP
prefix.of.files        > coll
name.of.the.colcprep.optionfile > colloc_input
ZPD model.nr.         > 1000

.
.
.

#-----

block.keyword          > INTERPOL
prefix.of.files        > ip
file.of.interpolation.points > work/station.st
variables.to.interpolate > zpd
interpolation.start.time > 2000 05 22 00 00 00
interpolation.end.time > 2000 05 30 00 00 00
```



```
interpolation.interval(hour)          > 0.017  
#-----
```

Table C. 5. Example of input\_main file for observation window and routine execution